JOURNAL OF ATMOSPHERIC AND TERRESTRIAL PHYSICS

EDITORIAL ADVISORY BOARD

H. O. G. ALFVÉN-STOCKHOLM · **J. BARTELS**-GÖTTINGEN · **W. J. G. BEYNON**-SWANSEA · **P. M. S. BLACKETT**-LONDON · **E. G. BOWEN**-SYDNEY · **SIR DAVID BRUNT**-LONDON · **R. BUREAU**-BAGNEUX · **S. CHAPMAN**-ALASKA · **J. EGEDAL**-COPENHAGEN · **V. F. HESS**-NEW YORK · **E. O. HULBURT**-WASHINGTON, D.C. **H. ISRAEL**-AACHEN · **D. K. MENZEL**-CAMBRIDGE, MASS. · **S. K. MITRA**-CALCUTTA · **M. NICOLET**-UCCLE · **E. H. NORINDER**-UPSALA · **B. van der POL**-GENEVA · **N. V. PUSHKOV**-MOSCOW · **J. A. RATCLIFFE**-CAMBRIDGE · **O. E. H. RYDBECK**-GOTHENBURG · **SIR GEORGE SIMPSON**-LONDON · **H. SOLBERG**-OSLO · **J. VELDKAMP**-DE BILT · **M. WALDMEIER**-ZÜRICH · **J. ZENNECK**-ALTHEGNENBERG

EDITOR-IN-CHIEF

SIR EDWARD APPLETON, F.R.S.

EDINBURGH

VOLUME 12

1958

PERGAMON PRESS

LONDON · NEW YORK · PARIS · LOS ANGELES

OL.
12
958

J. Atmosph. Terr. Phys.

VOL.
12
1958

CONTENTS

No. 1.

F. HEPBURN: Classification of atmospheric waveforms 1
E. R. SCHMERLING: An easily applied method for the reduction of *h-f* records to *N-h* profiles including the effects of the earth's magnetic field 8
G. V. GROVES: Trajectory determination of a supersonic body by acoustical observations 17
J. W. KING: The fading of radio waves reflected at oblique incidence 26
B. H. BRIGGS: A study of the ionospheric irregularities which cause spread-*F* echoes and scintillations of radio stars 34
J. O. THOMAS, JENIFER HASELGROVE and AUDREY ROBBINS: The electron distribution in the ionosphere over Slough—I. Quiet days 46
G. H. MUNRO and L. H. HEISLER: Ionospheric records of solar eclipses 57
I. L. JONES: The height variation of drift in the *E*-region 68

Research Notes

J. O. THOMAS and AUDREY ROBBINS: Ionospheric true height and M. U. F. calculations 77
B. LANDMARK: Echoes from the lower ionosphere during Polar blackouts 79
H. A. MIRANDA: On the de-emanation of a radium solution 80

K-indices of geomagnetic activity of the observatories at Hartland, Eskdalemuir and Lerwick for September, October and November 1957 84

Book Reviews

"The Planet Earth" edited by D. R. BATES, F.R.S. (Reviewed by E. V. APPLETON) 87
"Die Sonnenkorona-Struktur und Variationen der Korona" by M. WALDMEIER (Reviewed by M. A. ELLISON) 87

Books Received 88

Nos. 2/3.

B. H. BRIGGS: The diurnal and seasonal variations at spread-*F* ionospheric echoes and the scintillations of a radio star 89
J. R. KOSTER: Radio star scintillations at an equatorial station 100
D. D. CROMBIE: Differences between the east–west and west–east propagation of VLF signals over long distances 110
V. A. BAILEY: Some methods for studying wave-propagation in a uniform magneto-ionic medium 118
HERMANN POEVERLEIN: Low frequency reflection in the ionosphere—I 126
V. C. A. FERRARO and I. ÖZDOGAN: The effect of diffusion on the vertical distribution of ionization in a quiet *F*-region 140
J. D. WHITEHEAD: The distance attenuation of radio waves reflected at vertical incidence from the ionosphere 150
J. W. CHAMBERLAIN, D. M. HUNTEN and J. E. MACK: Resonance scattering by atmospheric sodium —IV. Abundance of sodium in twilight 153
A. VALLANCE JONES and D. H. MCPHERSON: The seasonal variation of the intensity ratio of the *D*-lines in twilight 166
F. E. ROACH, L. R. MEGILL, M. H. REES and E. MAROVICH: The height of nightglow 5577 . 171
GERHARD ELWERT: Die Verteilung der Röntgenstrahlung der sonnenkorona über die emittierende Fläche und die Restintensität bei totalen sonnenfinsternissen 187
F. L. ROESLER, C. Y. FAN and J. W. CHAMBERLAIN: Interpretation of rotational temperatures at auroral N_2^+ bands—I. Proton impact at intermediate energies 200
M. SMIDDY and J. A. CHALMERS: The double field-mill 206

Research Notes

R. W. NICHOLLS: Relative vibrational transition probabilities and *r*-centroids for the Meinel ($A^2\Pi X^2\Sigma$) band system of N_2^+ 211
M. A. ELLISON: Magnetic activity following a solar flare 214
V. A. BAILEY and L. GOLDSTEIN: Control of the ionosphere by means of radio waves . . 216
A. A. WEISS and J. W. SMITH: A radar record of an aurora at Adelaide 217

Letters to the Editor

A. DALGARNO: Ambipolar diffusion in the *F2*-layer 219
G. L. ROGERS: Diffraction microscope and the ionosphere; use of a satellite 220

Book Reviews

"Hygrometry" by H. SPENCER-GREGORY and E. ROURKE (reviewed by C. HINKEL) . . 222
"Artificial Stimulation of Rain" Edited by HELMUT WEICKMANN and WALDO SMITH (reviewed by P. M. SAUNDERS) 222
"The Ionosphere" by KARK RAWER: (reviewed by E. V. APPLETON) 223

Papers to be published in future issues 224

R. E. Houston, Jr.: The effect of certain solar radiations on the lower ionosphere 225
Hermann Poeverlein: Low-frequency reflection in the ionosphere—II 236
R. B. Banerji: Method of measuring ionospheric winds by fading at spaced receivers . . 248
H. Volland and J. Taubenheim: On the ionospheric current system of the geomagnetic solar flare effect (s.f.e.) 258
C. M. Minnis: Non-uniformity in the brightness of the sun's disk during the eclipse of 30 June 1954 266
C. M. Minnis: The interpretation of changes in the *E*- and *F1*-layers during solar eclipses . . 272
G. J. Romick and C. T. Elvey: Variations in the intensity of the hydrogen emission line H_β during auroral activity 283
G. A. Faucher: A study of air flow in a large-ion chamber 288
M. Srirama Rao and B. Ramachandra Rao: Investigation of magneto-ionic fading in oblique incidence medium-wave transmissions 293
D. Lal, P. K. Malhotra and B. Peters: On the production of radioisotopes in the atmosphere by cosmic radiation and their application to meteorology 306
K. Endresen, T. Hagfors, B. Landmark and J. Rödsrud: Observations of angle of arrival of meteor echoes in v.h.f. forward scatter propagation 329

Research Notes
K. Weekes: On the interpretation of the Doppler effect from senders in an artificial satellite . 335
F. H. Hibberd: The effect of the ionosphere on the Doppler shift of radio signals from an artificial satellite 338
Tor Hagfors: Preliminary results of studies of the angular distribution of a VHF ionospheric forward scatter signal 340
B. Landmark: The fading of long duration meteor bursts in forward scatter propagation . 341

K-indices of geomagnetic activity from the observatories at Hartland, Eskdalemuir and Lerwick for December 1957 and January and February 1958 343

Book Reviews
"Polar Atmosphere Symposium: Part II Ionospheric Section" (reviewed by E. V. Appleton) . 346
"The Exploration of Space" by R. Hanbury Brown and A. C. B. Lovell (reviewed by E. V. Appleton) 346
"The Physics of Clouds" by B. J. Mason (reviewed by J. R. Atkinson) 347
"Proceedings of the Third Berkeley Symposium on Mathematical Statistics and Probability. Vol. III: Astronomy and Physics" Edited by J. Neyman (reviewed by L. Rosenfeld) . . 347
"Exploring the Atmosphere's First Mile" Edited by H. H. Lettau and B. Davidson (reviewed by F. Pasquill) 348
"Cloud Study: a Pictorial Guide" by F. J. Ludlam and R. S. Scorer (reviewed by James Paton) 349
"Advances in Geophysics. Vol. III" Edited by H. S. Landsberg (reviewed by S. K. Runcorn) . 349

Papers to be published in future issues 351
Erratum 352

VOL. 12 1958

AUTHOR INDEX

(B) denotes a book review

Appleton, E. V. pp. 87(B), 223(B), 346(B)
Atkinson, J. R. p. 347(B)
Bailey, V. A. pp. 118, 216
Banerji, R. B. p. 248
Brandt, J. C. p. 288
Briggs, B. H. pp. 34, 89
Chalmers, J. A. p. 206
Chamberlain, J. W. pp. 153, 200, 288
Crombie, D. D. p. 110
Dalgarno, A. p. 219
Ellison, M. A. pp. 87(B), 214
Elvey, C. T. p. 283
Elwert, Gerhard p. 187
Endresen, K. p. 328
Fan, C. Y. p. 200
Faucher, G. A. p. 288
Ferraro, V. C. A. p. 140
Goldstein, L. p. 216
Groves, G. V. p. 17
Hagfors, Tor pp. 328, 340
Haselgrove, Jenifer p. 46
Heisler, L. H. p. 57
Hepburn, F. p. 1
Hibberd, F. H. p. 338
Hinkel, C. p. 222(B)
Houston, R. E., Jr. p. 225
Hunten, D. M. p. 153
Jones, A. Vallance p. 166
Jones, I. L. p. 166
King, J. W. p. 26
Koster, J. R. p. 100
Lal, D. p. 306
Landmark, B. pp. 79, 328, 341
Mack, J. E. p. 153
Malhotra, P. K. p. 316
Marovich, E. p. 171
McPherson, D. H. p. 166
Megill, L. R. p. 171
Minnis, C. M. pp. 266, 272
Miranda, H. A. p. 80
Munro, G. H. p. 57
Nicholls, R. W. p. 211
Özdoğan, I. p. 140
Pasquill, F. p. 348(B)
Paton, James p. 348(B)
Peters, B. p. 316
Poeverlein, Hermann pp. 126, 236
Rao, B. Ramachandra p. 293
Rao, M. Srirama p. 293
Rees, M. H. p. 171
Roach, F. E. p. 171
Robbins, Audrey pp. 46, 79
Rödsrud, J. p. 328
Roesler, F. L. p. 200
Rogers, G. L. p. 220
Romick, G. J. p. 283
Rosenfeld, L. p. 347(B)
Runcorn, H. S. p. 349(B)
Saunders, P. M. p. 222
Schmerling, E. R. p. 8
Smiddy, M. p. 206
Smith, J. W. p. 217
Thomas, J. O. pp. 46, 77
Weekes, K. p. 337
Weiss, A. A. p. 217
Whitehead J. D. p. 150

Journal of Atmospheric and Terrestrial Physics, 1958, Vol. 12, pp. 1 to 7. Pergamon Press Ltd., London

Classification of atmospheric waveforms

F. HEPBURN
Physics Department, University of Nottingham

(*Received* 19 *August* 1957)

Abstract—The desirability and requirements of a systematic classification of atmospheric waveforms are discussed. An observational scheme is suggested and interpreted in terms of known properties of the discharge and propagation mechanisms. This data is reviewed to clarify application of the scheme to individual waveforms. The relationship of the classification to previous inadequate groupings is indicated.

1. INTRODUCTION

THE study of atmospheric waveforms has revealed great variety in the electromagnetic disturbances resulting from the generation and subsequent propagation of radio waves from lighting discharges. Several previous classifications, attempted for convenient reference, are felt to be deficient because of incomplete investigation of the relevant parameters and limited or misleading grouping. Such investigation is now well developed and the more recent classifications have successfully related features of the waveforms to known occurrences in the discharge channel, although in a piecemeal manner. The surprising absence of a formal and systematic classification which is reasonably comprehensive has provoked this attempt in the hope that an explicit statement of what is probably tacitly accepted by several workers may prove useful and stimulating. It is based upon the results of several years' recording of atmospheric waveforms by the author in England and a critical investigation of the classifications suggested by previous workers.

It is very desirable that any grouping be based upon observational material for convenient and rational application to individual waveforms and also be unambiguous and compatible with theoretical considerations. In some cases both the general appearance and finer detail of the waveform depend simultaneously upon several parameters, none of which is dominant under all circumstances, so that even a sequential classification on a theoretical basis is not straightforward or directly obvious from the recorded waveforms. However, there is no valid reason why theoretical considerations should not be borne in mind when deciding the type and limits of a grouping, which may otherwise be ambiguous or lose significance. Classification essentially emphasizes differences, initially ignoring borderline cases where transitions are not abrupt, and tends to suggest different "mechanisms" for the resulting waveforms. Sometimes the implication is justified, but on other occasions a differentiating nomenclature obscures the underlying uniformity. Some years ago (HEPBURN, 1952) a classification was derived from purely observational material, which it is believed satisfied the requirements mentioned above, and a systematized version is suggested in the present paper. The phenomena are well enough understood to justify the use of descriptive titles and the classification is easily intelligible, without losing its observational basis, if one remembers the reasons for variations of waveform in terms of the relevant parameters. Appreciation of this should prevent possible criticism of the grouping on the grounds of an

apparently hypothetical basis. As the observational grouping is most easily presented in terms of acknowledged source and propagation phenomena, the effects of various parameters are first outlined. To maintain a relatively simple scheme, some variables are conveniently although somewhat arbitrarily considered as principal determinants of the waveform. Unfortunately, the wealth of previous classifications has exhausted the appropriate and very desirable descriptive vocabulary and it must be remembered that use of familiar terminology in the present context does not necessarily imply identity with the attributions of previous authors.

2. SOURCE EFFECTS

The effects of propagation are limited by the occurrences at the source, where sudden current surges produce radiation field pulses observable at great distances. The largest surges occur in the return stroke of a discharge to earth at intervals from 5 to 100 or more msec in a multiple discharge (SCHONLAND, MALAN and COLLENS, 1935) and last about 50 μsec. Comparable radiation pulses having higher frequency content are generated by the smaller but more rapid movements of charge taking place in the stepped leader process of an air discharge, which may reach the earth and be the precursor of a return stroke. Air discharges of two kinds have been reported from photographic studies (SCHONLAND *et al.*, 1935) and deduced from direct observation and waveform records (RIVAULT, 1945). Stepped leader discharges have been shown by SCHONLAND to be a method of propagation of a charged ionization channel usually directed downwards from a charged region of a cloud to a lower charged region (cloud discharge) or to the earth (precursor). The occasional association with a positive very low-frequency component is a confirmation of the direction of the discharge, since the leader is most frequently negatively charged. The steps occur at irregular intervals of about 70 μsec and this discharge lasts several msec. The other much simpler kind of air discharge shows evidence, particularly in its later stages, of very few steps, well spaced in time, designated as dart discharges by analogy with the dart-stepped leader phenomenon of subsequent strokes in a multiple discharge to earth. These darts occur at intervals of up to 1–2 msec, and their association with negative net field changes (LUTKIN, 1939) and negative slow tails (HEPBURN, 1952) is in agreement with the concept of an upwardly directed leader, which at least in its later stages can propagate with less frequent steps. Examples of the waveforms from "close" discharges are shown in Fig. 1. Three widely separate and easily distinguishable source effects are thus: return stroke pulses occurring singly (trace 1) or at intervals of about 30 msec, dart discharges having pulses roughly each msec (trace 3) and stepped discharges showing pulses at 70 μsec intervals (trace 2).

3. GEOGRAPHICAL AND TEMPORAL EFFECTS

Propagation modifies the initial radiated pulse in the same manner whether it be of isolated return-stroke origin or one step of the sequence in a dart or stepped-cloud discharge. The modification is determined by a combination of geographical location and time of occurrence of the discharge. By day and night for storms

VOL. 12 1958

beyond 1700 km to the south-west of the British Isles a single pulse is transformed into a short train of about seven smooth oscillations, which increase in period from 80 to very nearly 250 μsec throughout the waveform and have maximum amplitude after two or three oscilllations (cf. LUTKIN, 1939; RIVAULT 1945; CATON and PIERCE, 1952; HEPBURN, 1952). The onset of night-time conditions has remarkably little effect upon the waveforms, producing only slight increase in amplitude, duration and final period. However, within the transition range and to great distances to the south and east, time of day has a major effect. At night the waveforms have an extended series of pulses or oscillations, the peak separation increasing from 100 to 600 μsec throughout the waveform. These long trains of pulses are most directly explained in terms of successive reflections of the primary radiation pulse between the earth and ionosphere. By day the successive reflected pulse amplitudes decay extremely rapidly after the first couple of oscillations and the separation of the last detectable pair of rather angular peaks is variable. At short range the small amount of dispersion is insufficient to differentiate the source and propagation effects and at greater distances the heavy daytime attenuation makes interpretation of these waveforms ambiguous.

Examples of the modification of dart discharge and return-stroke pulses are shown in Fig. 2. The time and position of a discharge are very evidently responsible for three principal resultants of a primary pulse: a short extremely smooth oscillation (trace 4), a short peaked waveform (trace 6) and the more extended version of reflection waveform having a long train of pulses (trace 5). For return-stroke and some dart-air discharge the resultant waveforms are easily distinguishable, but for stepped discharges the rapid sequence of the pulses confuses the waveform and the distinctions may be difficult or impossible.

4. Distance and Individuality of the Discharges

Minor changes within the above scheme depend upon the distance and individual current variation of the discharge. The increase along the waveform of the interval between successive maxima of the oscillations or pulses varies systematically with distance, conforming broadly with reflection theory predictions (SCHONLAND *et al.*, 1939; HALES, 1948; HEPBURN and PIERCE, 1954; HORNER and CLARKE, 1954). With increasing distance the long train waveforms (Fig. 3, column 3) show a transition from peaky to sinusoidal character (HEPBURN and PIERCE, 1954) associated with the proportionately greater attenuation of the higher order mode responses of the propagation process.

Similar small modifications are due to the precise current variation in the particular discharge responsible for the wave form. Depending upon the rate of decay of the discharge current, the radiated pulse may be double or single, yielding symmetrical or unsymmetrical long train waveforms. Similarly, smooth waveforms (Fig. 3, column 1) frequently show an obvious irregularity in the otherwise steady increase of oscillation period (HEPBURN, 1957a). The occurrence of a very low-frequency or slow-tail component on the waveform trace and its dependence upon the discharge current has been the subject of a previous paper (HEPBURN, 1957b) and will not be considered in the present context. Traces illustrating the effects upon the three types of waveform due to distance and current variation are given in Fig. 3.

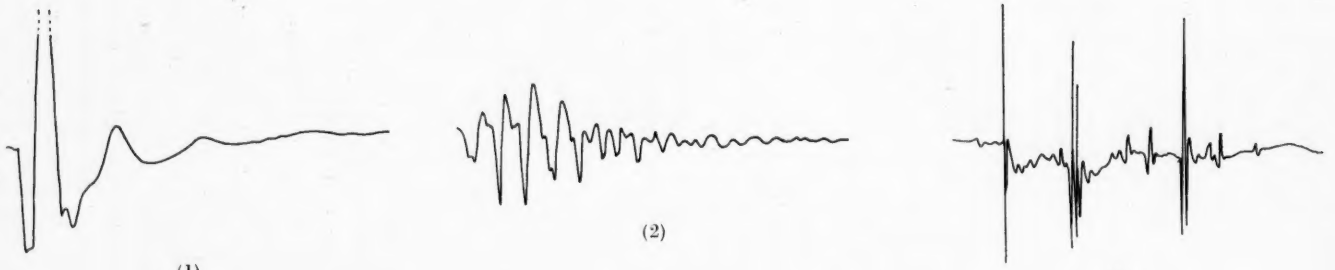

(1) (2) (3)

Fig. 1. Source effects. Return stroke, stepped and dart discharge kinds of waveform.

(4) (5) (6)

Fig. 2. Major geographical and temporal effects. Smooth, peaked and long train types of waveform.

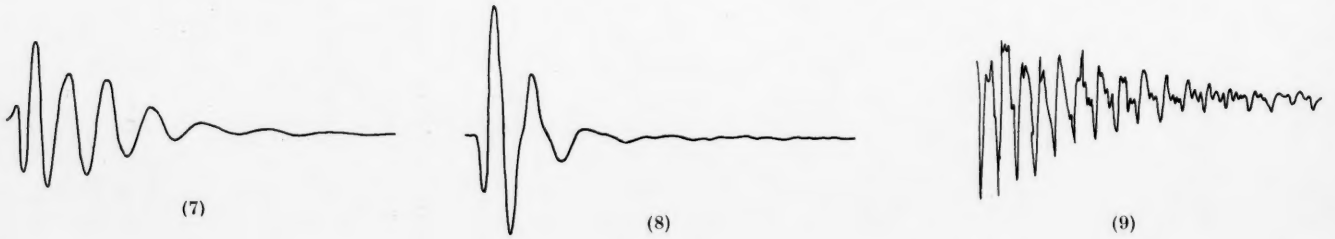

(7) (8) (9)

VOL. 12
1958

OL.
12
958

Fig. 3. Distance and discharge current modifications of smooth, peaked and long train return stroke waveforms. Rows 1 and 3 from closer discharges; 2 and 4 from greater distances; Rows 1 and 2 are regular or symmetrical waveforms; rows 3 and 4 are irregular or unsymmetrical traces.

Waveform data

Waveform 4 and all in column 3 have 10 msec duration; the others last 1 msec.

Tracings are given as the large range in writing speed on some of the waveform traces made satisfactory reproduction of the originals impossible. Notes on individual examples give recording date and time in hours GMT and the Sferics fix for the individual discharge or storm centre in terms of range in kilometres and azimuth in degrees from north.

1. 22.3.55, 1430. 450,150	2. 22.3.55, 1430. 450,150	3. 27.5.51, 1930. 900, 85
4. 4.12.50, 1925. 1400,220	5. 22.3.55, 2015. 1600,244	6. 27.5.51, 1800. 2000,270
7. 11.5.55, 1130. 2200,250	8. 29.3.55, 1430. 1100,170	9. 28.5.51, 0050. 900, 85
10. 19.4.56, 1430. 3400,275	11. 5.11.56, 1330. 2000,133	12. 28.5.51, 0120. 4000,194
13. 11.5.55, 1130. 2100,250	14. 29.3.55, 1530. 1100,170	15. 28.5.51, 0120. 900, 85
16. 19.4.56, 1430. 3400,275	17. 29.3.55, 1930. 1900,129	18. 12.12.50, 1800. 3000,160

5. THE CLASSIFICATION SCHEME

Using the foregoing outline, it is found convenient to classify waveforms by appearance, and the resulting analysis gives considerable information concerning the current variation, location and time of the discharge. Firstly, the kind of discharge (1—return stroke, 2—stepped or 3—dart) is noted from the isolation or repetition interval of very similar components of the waveform. The type of waveform (1—smooth, 2—peaked or 3—long train) is then distinguishable from the modification of each initial pulse. Subsequent investigation of the variety of waveform (1—symmetrical or regular, 2—unsymmetrical or irregular) reveals characteristics of the discharge and measurement gives the distance of origin from peak time intervals. The only point of difficulty in principle lies in distinguishing the varieties of stepped discharge and the long-train dart waveforms, which are very similar for the reasons indicated.

6. RELATIONSHIP TO PREVIOUS GROUPINGS

Previous classifications are due to LUTKIN, RIVAULT and CATON and PIERCE (*loc. cit.*). LUTKIN's groups referring to daytime observation are identifiable with waveforms from the three kinds of discharge. Further subdivision was not attempted, but the carefully reported differences of return-stroke waveforms from sources to the east and west corresponds exactly with the present distinction between smooth and peaked traces. RIVAULT extended the observations to night-time and partially discovered the corresponding geographical limitations on smooth and long train waveforms. He acceptably attributes the short bursts of oscillation at msec intervals to air discharges, but surprisingly suggested that they may also be of multiple return-stroke origin, although the time intervals involved make this suggestion untenable. CATON and PIERCE in common with earlier workers recognize stepped discharge waveforms as a separate group and acknowledge a slight variation in form, but attribute it to a purely diurnal effect. The methods of distinguishing regular peaked and long oscillatory train types are not clear and the regular peaked category appears to be introduced arbitrarily to bridge the gap between the peaked and long train types of the present terminology (i.e. day and night variants of reflection waveforms). However, they make questionable distinction between day and night waveforms from beyond 1600 km to the south-west and only slight reference to the differences shown by daytime waveforms, which are implied to be of solely directional origin. The bursts of small waveforms appearing as a further subdivision of their regular smooth type, associated with "hook" components of the return stroke (MALAN and SCHONLAND, 1947), may very probably be of dart discharge origin.

CONCLUSION

It is believed that the classification suggested is a rational synthesis of the previous fragmentary attempts and it is hoped that it will prove a more convenient and comprehensive basis of reference for future work than has been hitherto available.

Acknowledgements—This study of atmospheric waveforms obviously owes much to the careful observation of previous workers. The author's experimental work

VOL. 12 1958

has been pursued at the Observatories and Cavendish Laboratory, Cambridge, and latterly at the Physics Department of the University of Nottingham. I am grateful to the Directors of these establishments and of the Meteorological Office for the provision of suitable facilities and in particular to Dr. T. W. WORMELL for his introduction to the subject.

REFERENCES

CATON P. G. F. and PIERCE E. T.	1952	*Phil. Mag.* **43,** 393.
HALES A. L.	1948	*Proc. Roy. Soc.* A**193,** 60.
HEPBURN F.	1952	Thesis, University of Cambridge.
	1957a	*J. Atmosph. Terr. Phys.* **10,** 121.
	1957b	*J. Atmosph. Terr. Phys.* **10,** 266.
HEPBURN F. and PIERCE E. T.	1954	*Phil. Mag.* **45,** 917.
HORNER F. and CLARKE C.	1955	*J. Atmosph. Terr. Phys.* **7,** 1.
LUTKIN F.	1939	*Proc. Roy. Soc.* A**171,** 285.
MALAN D. J. and SCHONLAND B. F. J.	1947	*Proc. Roy. Soc.* A**191,** 485.
RIVAULT R.	1945	*C. R. Acad. Sci. Paris* **221,** 540.
SCHONLAND B. F. J., MALAN D. J. and COLLENS H.	1935	*Proc. Roy. Soc.* A**152,** 595.
SCHONLAND B. F. J., ELDER J. S., VAN WYK J. W. and CRUIKSHANK G. A.	1939	*Nature, Lond.* **143,** 893.

L.
2
58

Journal of Atmospheric and Terrestrial Physics, 1958, Vol. 12, pp. 8 to 16. Pergamon Press Ltd., London

An easily applied method for the reduction of *h-f* records to *N-h* profiles including the effects of the earth's magnetic field*

E. R. SCHMERLING
Ionosphere Research Laboratory, The Pennsylvania State University,
University Park, Pennsylvania

(*Received* 18 *August* 1957)

Abstract—A method is presented by means of which experimental h'-f records may be readily reduced to electron-density-height profiles without the use of computing aids during the final reduction process. No special assumptions are made concerning profile shapes, account is taken of the earth's magnetic field, and collisions are neglected.

This method depends on sampling h' at fixed sub-multiples of the frequencies f_n at which true heights are required: true heights being then simply obtained by averaging these values. The sampling frequencies depend on the parameters of the earth's magnetic field, and must be computed for the magnetic co-ordinates of each station from which records are to be analysed. This computation, in its entirety, is quite complex; but once performed, the results are available for use on any number of records. The method is, therefore, especially suitable for the rapid routine reduction of large numbers of records.

Complete computations are presented for one station, and the results are checked against an analysis of h'-f curves for known profiles.

1. INTRODUCTION

SEVERAL methods are at present available for the reduction of h'-f records to electron-density-height profiles. Of these, one of the most rapid and convenient is the method of KELSO (1952), particularly when applied in the form described by SCHMERLING and THOMAS (1956). This method has, however, the important disadvantage that no account is taken of the earth's magnetic field, so that considerable errors are introduced when records are analysed from stations located well away from the magnetic equator.

Other methods have more recently been described which take account of the earth's magnetic field. In general, these all require, at some stage, calculations of great numerical complexity. In the method of BUDDEN (1955), which is discussed more fully by SCHMERLING (1957), the computations are performed by a digital computer. The computer handles all the numerical work, leaving to the operator only the simple task of reading about thirty values of h' from each record, and feeding this information to the computer. Other methods have also been described which do not require the use of a digital computer. These are considerably more lengthy in execution, as the work must then be performed by the operator, who has to go through a lengthy procedure for each record to be reduced. The methods of JACKSON (1956) and KELSO (1954, 1957) fall into this latter category.

The purpose of this work is to describe a method which does not require any computing aids for the actual reductions, and is quick and convenient to use. In essence, the procedure is closely similar to the original Kelso method, which is modified to include automatically the effect of the earth's magnetic field. The inherent numerical complexity of the computation is entirely absorbed into the

* The research reported in this paper was supported by the Geophysics Research Directorate of the Air Force Cambridge Research Center, Air Research and Development Command, under Contract AF19(604)-1304.

VOL.
12
1958

preliminary calculation of a set of frequencies at which the h'-f records are to be sampled. These sampling frequencies must be computed specifically for the magnetic co-ordinates of each station from which records are to be analysed. A computer is used for this initial stage of the process; once the sampling frequencies are found, however, they are available for the reduction of any number of h'-f records from that station.

This method should prove useful where a digital computer is not available, provided that the initial set of sampling frequencies can be supplied. It is thus eminently suitable for field use, and for the routine reduction of large numbers of records.

2. General Principles

The present method was suggested by an examination of the no-field Kelso method. This will accordingly be first discussed, albeit from a different viewpoint to that originally used in its derivation. The theory is based on the use of ray-optics, and electronic collisions are neglected.

Without making special assumptions as to the shape of the electron-density-height profiles, Appleton (1930) and de Groot (1930) showed that, neglecting the magnetic field, the true height of reflection $h(f_n)$ at a frequency f_n is given by

$$h(f_n) = \int_0^{f_n} G(f_n, f) h'(f)\, df \tag{1}$$

where

$$G(f_n, f) = \frac{2}{\pi \sqrt{f_n^2 - f^2}} \tag{2}$$

On making the substitution

$$\theta(f_n, f) = \frac{2}{\pi} \arcsin (f/f_n) \tag{3}$$

equation (1) reduces to

$$h(f_n) = \int_0^1 h'(\theta)\, d\theta \tag{4}$$

θ is here considered as a function of f at a fixed value of f_n.

The integration in (4) may be performed numerically without actually transforming the h'-f curves. If the area under each h'-θ curve is imagined to be divided up into k equal strips, the trapezium rule gives, approximately,

$$h(f_n) = \frac{1}{k}\left\{h'(\theta_0) + h'(\theta_1) + \ldots + h'(\theta_r) + \ldots + h'(\theta_{k-1})\right\} \tag{5}$$

where

$$\theta_r = \frac{2r + 1}{2k} \tag{6}$$

and r is an integer, ranging from 0 to $k - 1$.

Equation (5) states that the true height is obtained by averaging k values of h', read off the h'-f curve at particular frequencies, given by the solution of equations (6) and (3). These particular frequencies will be called the sampling frequencies;

they clearly correspond to the mid-ordinates of the strips in the h'-θ plane. The accuracy of the approximation obviously increases with k; experience shows that five or ten values are quite adequate in practice, depending on the smoothness of the h'-f curve.

From the considerations of the previous paragraph it is seen how a table of sampling frequencies may be built up for each value of f_n. Inspection of equation (3) reveals that an independent computation for each f_n is unnecessary, since the ratio of sampling frequency to f_n is independent of f_n. This ratio will be called the sampling ratio, and denoted by R.

If the effect of the earth's magnetic field is included, h may still be expressed in terms of h', for the ordinary ray, by an equation of the form (1). In what follows, attention will be devoted exclusively to the ordinary ray. With the inclusion of the magnetic field, $G(f_n, f)$ can no longer be expressed in any simple analytical form, but must be evaluated numerically. No discontinuities are introduced for the ordinary ray, so that the new function G may be considered as a somewhat distorted version of the no-field function. To establish the sampling frequencies, we shall proceed by taking a known relation between h and h', evaluating $G(f_n, f)$, transforming to a function θ which satisfies (4) (but not, of course, (3)), and dividing this up into equal intervals as before.

In the no-field case the sampling ratio R is independent of f_n. This is no longer strictly true when the field is included; fortunately, however, it will be seen that R varies quite slowly with f_n, so that we may divide f_n up into several ranges of frequency, in each of which R may be considered independent of f_n.

VOL. 12 1958

3. Evaluation of the Function $\theta(f_n, f)$

The Budden matrix provides a relation between h and h' which includes the effect of the earth's magnetic field. Taking one row of the matrix, we have

$$h(f_n) = A_{nn}h'(n\Delta f + f_0) + A_{n,n-1}h'([n-1]\,\Delta f + f_0) + \ldots \tag{7}$$

The coefficients A, unequal in magnitude, are the coefficients of the Budden matrix, and refer to n values of h' sampled at equal increments, Δf, of frequency, above the cut-off frequency f_0. A detailed discussion of the matrix method has been given by SCHMERLING (1957). The problem is now to find k values of sampling frequency, unequally spaced, which result in all the A's becoming equal to $1/k$.

We now define a continuous function, $a(f_n, f)$, such that

$$h(f_n) = \frac{}{\Delta f}\int_0^{f_n} a(f_n, f)h'(f)\,df \tag{8}$$

This is the analogue of equation (1). We then interpret equation (7) as an approximate expanded form of (8). Expanding equation (8) by the trapezium rule, we have,

$$\begin{aligned} h(f_n) = \tfrac{1}{2}\{&[a(f_n, n\Delta f + f_0)h'(n\Delta f + f_0) + a(f_n, [n-1]\Delta f + f_0)h'([n-1]\Delta f + f_0)] \\ &+ [a(f_n, [n-1]\Delta f + f_0)h'([n-1]\Delta f + f_0) + a(f_n, [n-2] \\ &\times \Delta f + f_0)h'([n-2]h'\ \Delta f + f_0) + \ldots\} \end{aligned} \tag{9}$$

Comparing coefficients with (7), we obtain the following relations:

$$\left.\begin{aligned} a(f_n, n\Delta f + f_0) &= 2A_{nn} \\ a(f_n, r\Delta f + f_0) &= A_{nr} \quad \text{for} \quad 0 < r < n \end{aligned}\right\} \tag{10}$$

We now have to determine a function $\theta(f_n, f)$ such that

$$h(f_n) = \frac{1}{\Delta f}\int_0^{f_n} a(f_n, f)h'(f)\, df \equiv \int_0^1 h'(\theta)\, d\theta \tag{11}$$

This implies that

$$\frac{\partial\theta(f_n, f)}{\partial f} = \frac{1}{\Delta f}a(f_n, f)$$

i.e.

$$\theta(f_n, f_r) = \frac{1}{\Delta f}\int_0^{f_r} a(f_n, x)\, dx \tag{12}$$

Expanding (12) by the trapezium rule, in strips of width Δf, we obtain

$$\theta(f_n, r\Delta f + f_0) = \tfrac{1}{2}a(f_n, r\Delta f + f_0) + a(f_n, [r-1]\Delta f + f_0) + a(f_n, [r-2]\Delta f + f_0) + \dots$$

Substituting from (10), we then have

$$\left.\begin{aligned} \theta(f_n, r\Delta f + f_0) &= \tfrac{1}{2}A_{nr} + \sum_{m=1}^{r-1} A_{nm} + P_n \quad \text{for} \quad 0 < r < n \\ \theta(f_n, n\Delta f + f_0) &= \sum_{m=1}^{n} A_{nm} + P_n = 1 \end{aligned}\right\} \tag{13}$$

The term P_n is the residual of the Budden matrix, and takes account of the portion below the low-frequency cut-off, f_0, which cannot be observed on experimental h'-f records. The function θ is not, therefore, directly evaluated below f_0. Consideration of (11) and (12) indicates that θ, as here defined, becomes zero at zero frequency. Values between $f = 0$ and $f = f_0$ may thus be obtained, if required, by interpolation. High accuracy is clearly not needed in this range.

The function θ is readily obtained from the Budden matrix coefficients by use of the relations (13). On dividing θ into k equal increments, a table of sampling frequencies may be built up. The sampling ratios, R, are then obtained by dividing these sampling frequencies by f_n.

4. Procedure for Reduction

The table of sampling frequencies may be used directly to read values of h' from the h'-f curves. h is obtained as the average of these values, in accordance with equation (5). Repetition of the process for several values of f_n enables the entire electron-density-height or N-h profile to be determined. This procedure suffers from the disadvantage that a table of sampling frequencies must be available for each value of f_n which is ever likely to be required. A very considerable simplification can be effected by the use of sampling ratios.

The sampling ratio, R, is defined as the ratio of the sampling frequency to f_n, and may be readily obtained from a relatively small set of tables of sampling

frequency. Unlike the no-field case, R is a function of f_n, but varies so slowly that it may be considered constant over a fairly large range of f_n.

The simplest procedure is to plot each h'-f curve on a logarithmic scale of frequency. Many ionospheric sounding equipments already produce records on such a scale, so that replotting may be unnecessary. The sampling ratios are then marked on a slider, on the same scale, with a datum corresponding to f_n. Within the range of validity of the slider, it is then only necessary to align the datum with the frequency on the record for which h is required, to read off h' at the ordinates indicated by the marks on the slider, and to average these values. This gives h. The process must be repeated for every point desired on the N-h profile. f_n in Mc/s is related to N in electrons per cm^3 by

$$N = 1{\cdot}24 \times 10^4 f_n{}^2.$$

The sampling technique just described is relatively rapid in application, and requires an absolute minimum of equipment. The foregoing results can also be applied to a continuous integration technique, which may have some advantages for the accurate reduction of records containing fine structure. A continuous integration technique has been described by WHALE (1951). This is unduly cumbersome, and the magnetic field correction is erroneous. A simplified analogue machine for performing the same process has been suggested by SCHMERLING (1957). The function θ discussed here must be normalized to $\theta(f_n, f/f_n)$ and considered as a function of f/f_n only, over a restricted range of f_n. This information is sufficient to cut the cams according to the outline presented in the above reference. The machine will then perform the reduction of h'-f curves by continuous sampling; equivalent to the sampling method discussed here as $k \to \infty$.

VOL. 12 1958

5. COMPUTATIONS FOR WASHINGTON, D.C.

A complete set of computations has been carried through for Washington, D.C. (gyrofrequency 1·48 Mc/s, magnetic dip angle = 71·5°). Two Budden 30 × 30 matrices were computed for the ranges 1·6 to 7·6 Mc/s in 0·2 Mc/s steps, and from 1 to 16 Mc/s in 0·5 Mc/s steps These computations were performed on the PENNSTAC digital computer at this Institution, by the procedure described in SCHMERLING (1957). The function θ was then calculated from (13), and is shown in Fig. 1.

Sampling frequencies were then found by inverse interpolation from the curves. For $k = 10$ (10-point sampling method), the sampling frequencies are given by

$$\theta = 0{\cdot}95,\ 0{\cdot}85,\ 0{\cdot}75,\ 0{\cdot}65,\ 0{\cdot}55,\ 0{\cdot}45,\ 0{\cdot}35,\ 0{\cdot}25,\ 0{\cdot}15, \text{ and } 0{\cdot}05.$$

The sampling ratios R, found on division by f_n, are shown as functions of f_n in Fig. 2. For comparison, the zero-field values obtained from equation (3) are also indicated.

It was judged that R varies sufficiently slowly for mean values over the three frequency ranges 1–4, 4–8 and 8–16 Mc/s to be adequate in practice. Three sliders thus suffice for the reduction of h'-f records from any one station. These

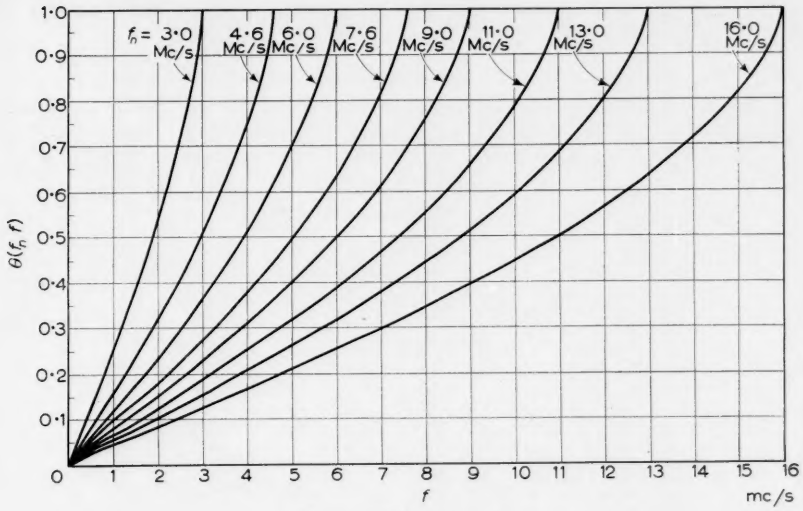

Fig. 1. Washington θ curves

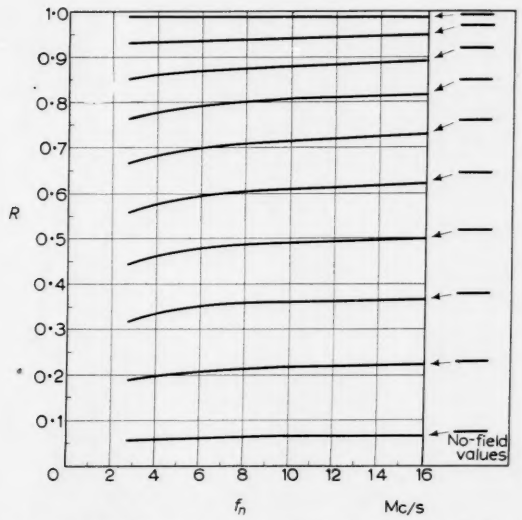

Fig. 2. Sampling ratios, R, for Washington; 10-point method.

mean values of R, computed for 5- and 10-point methods, are given in Tables 1 and 2 for Washington, D.C.

6. Test Reductions

The sampling frequencies (or ratios) which form the basis of the present method are derived, by a series of transformations, from the coefficients of the Budden matrix. The accuracy of these transformations may, therefore, be tested by comparing the results obtained, from the same h'-f curve, by (a) the new method, and (b) the matrix method.

Such a comparison is shown in Fig. 3, for a profile as indicated by the solid line. The solid line actually shows the profile obtained by the matrix method, and stops slightly short of the true peak, since this falls between the fixed sampling intervals of the matrix. The results of reducing the same h'-f curve by the 5- and 10-point slider methods are indicated by the crosses and circles, respectively.

Table 1. Sampling ratios for Washington, D.C.: 5-point method
(dip angle = 71·5°, gyrofrequency = 1·48 Mc/s)

1–4 Mc/s	4–8 Mc/s	8–16 Mc/s
0·967	0·966	0·969
0·813	0·833	0·856
0·623	0·652	0·677
0·387	0·418	0·436
0·127	0·137	0·148

Table 2. Sampling ratios for Washington, D.C.: 10-point method
(dip angle = 71·5°, gyrofrequency = 1·48 Mc/s)

1–4 Mc/s	4–8 Mc/s	8–16 Mc/s
0·990	0·990	0·990
0·935	0·939	0·949
0·862	0·872	0·884
0·776	0·793	0·812
0·680	0·702	0·720
0·575	0·596	0·616
0·458	0·480	0·496
0·330	0·352	0·354
0·196	0·208	0·220
0·060	0·063	0·067

The profile obtained by ignoring the magnetic field is shown dotted. It is seen that both 5- and 10-point methods agree well with the matrix method. Any residual error is very much less than when the no-field approximation is used.

To test the method further, h'-f curves were computed for three given profiles for Washington D.C. Chapman-shaped profiles were taken, truncated at the lower end at frequencies between 1 and 2 Mc/s for the different curves. This was done to obtain test results independent of any confusion from errors due to the choice of low-frequency cut-off. The h'-f curves were computed on PENNSTAC as described in the SCHMERLING (1957) reference, and are shown in Fig. 4.

In Figs. 5, 6 and 7 the original profiles are shown, together with the results obtained by reducing the h'-f curves using 5- and 10-point slider methods. It is seen that the agreement is everywhere quite good. In some cases, the 10-point method gives somewhat better agreement near the critical frequency.

VOL. 12 1958

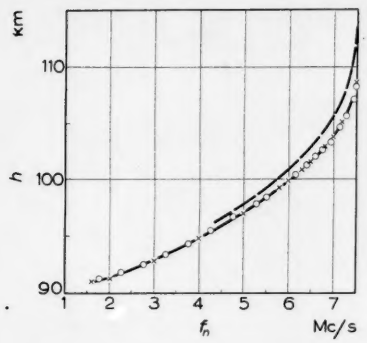

Fig. 3. Comparison of results.
——— Matrix method
— — — No-field method
○ 10-point method
× 5-point method.

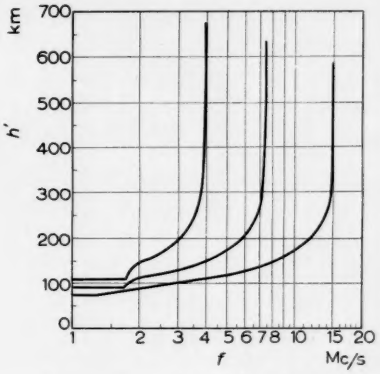

Fig. 4. Computed h'-f curves for Washington, D.C.

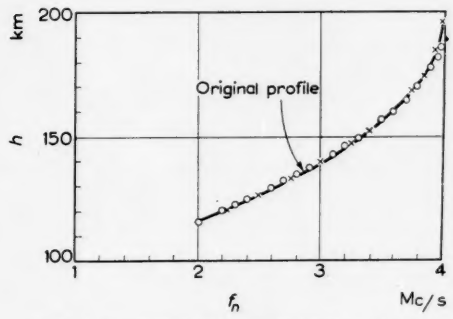

Fig. 5. Test results for Washington, D.C.
○ 5-point method
× 10-point method.

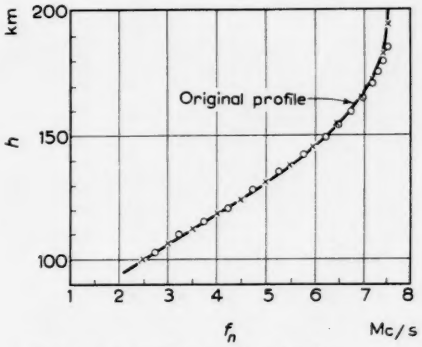

Fig. 6. Test results for Washington, D.C.
○ 5-point method
× 10-point method.

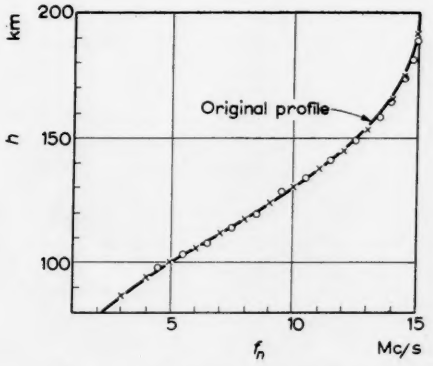

Fig. 7. Test results for Washington, D.C.
○ 5-point method
× 10-point method.

This suggests that the 5-point method is adequate when the h'-f curve is smooth and slowly varying below f_n, but that the 10-point method should be used near the critical frequency, and in all cases when retardation cusps are seen below f_n.

7. CONCLUSIONS

It has been shown how the preliminary computations may be performed for a method of reducing h'-f records to N-h profiles which requires no further computing aids, and yet takes full account of the earth's magnetic field. This method is quite simple and rapid in application, thus affording a good means for the routine reduction of many h'-f records.

The initial computations have been performed for one station, and tested against theoretical h'-f curves from known profiles. The excellent agreement found establishes the essential soundness of the method.

The work described here should be regarded as a preliminary investigation, or pilot study. The starting point consisted of the calculation of matrix coefficients on a digital computer. These were then transformed by relatively crude semi-graphical methods to obtain the required sampling ratios. It would clearly be more satisfactory to perform all stages of the process on a digital computer, and this is currently being investigated.

Apart from the fact that no computing aids are necessary for the actual reduction of records, this method has one further advantage over the matrix method. In the latter method, h can only be computed at predetermined values of f, leaving, in general, a small gap between the last computed value of h and the value of h at the critical frequency. For a critical frequency of 15·4 Mc/s, for example, using a 30×30 matrix in the range 1 to 16 Mc/s in 0·5 Mc/s steps, the last computed value would be at 15 Mc/s. By using the slider technique, it is possible to evaluate h up to 15·4 Mc/s, since the slider can be placed anywhere on the curve.

VOL. 12 1958

REFERENCES

APPLETON E. V.	1930	*Proc. Phys. Soc.* **42,** 321.
BUDDEN K. G.	1955	*Cambridge Conf. on Ion. Physics* (Physical Society.) p. 332.
DE GROOT W.	1930	*Phil. Mag.* **10,** 521.
JACKSON J. E.	1956	*J. Geophys. Res.* **61,** 107.
KELSO J. M.	1952	Sci. Report No. 19 Ionosphere Research Lab. Penn State University. *Ibid.* **57,** 357.
KELSO J. M.	1954	Sci. Report No. 55 Ionosphere Research Lab. Penn. State University. *J. Atmosph. Terr. Phys.* **5,** 11.
KELSO J. M.	1957	*Ibid.* **10,** 103.
SCHMERLING E. R.	1957	Sci. Report No. 94 Ionosphere Research Lab. Penn. State University.
SCHMERLING E. R. and THOMAS J. O.	1956	*Phil. Trans. Roy. Soc.* **248,** 75.
WHALE H. A.	1951	*J. Atmosph. Terr. Phys.* **1,** 244.

Journal of Atmospheric and Terrestrial Physics, 1958, Vol. 12, pp. 17 to 25. Pergamon Press Ltd., London

Trajectory determination of a supersonic body by acoustical observations

G. V. Groves
Department of Physics, University College, London

(*Received* 20 *September* 1957)

Abstract—A theory is developed for deriving the trajectory of a body moving at supersonic speeds through the atmosphere from observations on the times of arrival of its shock wave at a number of microphones at known points on the ground, wind and temperature effects being taken into account.

It is shown that with $3n + 4$ microphones, the position, velocity, acceleration, etc., up to the nth derivative of the spatial co-ordinates of the body with respect to time can be found at some determined instant of time. Hence with 7 microphones, the position and velocity of the body at a certain instant of time can be found, although 4 microphones are seen to be adequate for a more approximate determination of these quantities. Particular consideration is given to the method of solution in the 7 microphone case.

1. Introduction

The propagation of sound through the atmosphere is being utilized by this department as a means of determining winds and temperatures in the upper atmosphere by the so-called rocket-grenade experiment. The writer has already given a solution to the problem of deriving winds and temperatures from the travel times of sound waves between grenades exploding at known points in the atmosphere and microphones on the ground (Groves, 1956). From the results of that paper, it has been found possible to treat the problem of determining the trajectory of a supersonic body by acoustical observations. In this case, the atmospheric structure is known, while the origin of the sound needs to be determined.

The writer's interest in the problem of trajectory determination by acoustical observations has arisen from its possible application to a high-altitude rocket and its recovery after flight. This aspect of the problem is discussed in a current paper.

2. General Conditions Determined by Reception of Shock-Wave at ith Microphone at Time t_i

Let O be a point on the earth's surface and $Oxyz$ mutually perpendicular axes with Oz in the vertical direction (Fig. 1). Microphones are located at various points on the ground, the co-ordinates of the ith microphone at H_i being (x_i, y_i, z_i).

Let $(\xi(\tau), \eta(\tau), \zeta(\tau))$ be the co-ordinates of a moving body at time τ. The atmospheric disturbance that it produces will be taken to originate from a continuous distribution of small disturbances along its flight path: let $t_i(\tau)$ be the time at which the disturbance produced at time τ reaches H_i. When the body is moving with supersonic speed, $t_i(\tau)$ has a minimum with respect to τ; the minimum value being the time of arrival of the shock-wave. If τ_i is the time at which the shock-wave received at H_i was generated by the body, then τ_i satisfies

$$[dt_i(\tau)/d\tau]_{\tau=\tau_i} = 0; \tag{1}$$

and the shock-wave is received at time $t_i = t_i(\tau_i)$.

It is assumed that within the region of the Oxy-plane over which observations are made, the wind velocity components $u(z)$, $v(z)$, $w(z)$ and the speed of sound $c(z)$ depend only on height. Under this assumption, the passage of a wavefront

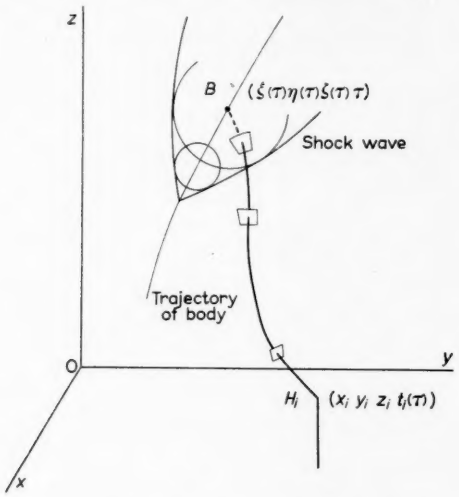

Fig. 1. Diagram showing passage of wavefront element of small disturbance produced at time τ to microphone at H_i. The shock wave is the envelope of such wavelets.

element along an unreflected path in the atmosphere such as BH_i has been considered previously in connection with the rocket-grenade experiment (GROVES, 1956). From equations (27) and (16) of that paper, the relationship between $\xi(\tau)$, $\eta(\tau)$, $\zeta(\tau)$, τ and x_i, y_i, z_i, $t_i(\tau)$ is

$$[U_i(\zeta) + X_i(\tau)Z_i(\tau)/T_i(\tau)]^2 + [V_i(\zeta) + Y_i(\tau)Z_i(\tau)/T_i(\tau)]^2 + [W_i(\zeta) + Z_i^2(\tau)/T_i(\tau)]^2 - C_i^2(\zeta) = 0, \tag{2}$$

where

$$X_i(\tau) = \xi(\tau) - x_i \qquad Y_i(\tau) = \eta(\tau) - y_i \qquad Z_i(\tau) = \zeta(\tau) - z_i \tag{3}$$

and (with Mach number $M = 1$)

$$T_i(\tau) = t_i(\tau) - \tau \tag{4}$$

and from equations (28), (29) (with Mach number $M = 1$)

$$U_i(\zeta) = \int_{z_i}^{\zeta} u(z)\,dz - U_{ei} \qquad V_i(\zeta) = \int_{z_i}^{\zeta} v(z)\,dz - V_{ei}$$

$$W_i(\zeta) = \int_{z_i}^{\zeta} w(z)\,dz - W_{ei} \qquad C_i(\zeta) = \int_{z_i}^{\zeta} c(z)\,dz - C_{ei}. \tag{5}$$

It has been shown that U_{ei}, V_{ei}, W_{ei}, C_{ei} can be expressed as integrals of products of the variations in $u(z)$, $v(z)$, $w(z)$ and $c(z)$, and are usually small compared with $C_i(\zeta)$. They are expected to contribute amounts of the order of one per cent,

VOL. 12 1958

provided the ray BH_i does not come too near to being totally reflected. Throughout this paper, $U_{\varepsilon i}$, $V_{\varepsilon i}$, $W_{\varepsilon i}$, $C_{\varepsilon i}$ will be neglected in (5).

From (1) and (2), the condition satisfied by τ_i is

$$\left\{[U_i(\zeta) + X_i(\tau)Z_i(\tau)/T_i(\tau)]\frac{d}{d\tau}[U_i(\zeta) + X_i(\tau)Z_i(\tau)/T_i(\tau)] + \ldots + \ldots - \ldots\right\}_{\tau=\tau_i} = 0 \quad (6)$$

with $T_i(\tau)$ redefined as

$$T_i(\tau) = t_i - \tau. \quad (7)$$

equation (7) replaces equation (4) from now onwards.

Introducing

$$\begin{aligned} P_i(\tau) &= U_i(\zeta(\tau)) + X_i(\tau)Z_i(\tau)/T_i(\tau) \\ Q_i(\tau) &= V_i(\zeta(\tau)) + Y_i(\tau)Z_i(\tau)/T_i(\tau) \\ R_i(\tau) &= W_i(\zeta(\tau)) + Z_i^2(\tau)/T_i(\tau) \end{aligned} \quad (8)$$

the two conditions determined by the arrival of the shock wave at H_i at time t_i can be written, from equation (2) and equation (6), as

$$P_i^2(\tau_i) + Q_i^2(\tau_i) + R_i^2(\tau_i) - C_i^2(\tau_i) = 0 \quad (9)$$

$$P_i(\tau_i)\dot{P}_i(\tau_i) + Q_i(\tau_i)\dot{Q}_i(\tau) + R_i(\tau_i)\dot{R}_i(\tau_i) - C_i(\tau_i)\dot{C}_i(\tau) = 0, \quad (10)$$

where a dot denotes differentiation with respect to τ.

3. Method of Deriving Trajectory from Observations with m Microphones

To determine the unknown functions $\xi = \xi(\tau)$, $\eta = \eta(\tau)$, $\zeta = \zeta(\tau)$, it is assumed that they can be expressed as

$$\begin{aligned} \xi &= \xi_0 + \dot{\xi}_0(\tau - \tau_0) + \ddot{\xi}_0(\tau - \tau_0)^2/2! + \ldots \\ \eta &= \eta_0 + \dot{\eta}_0(\tau - \tau_0) + \ddot{\eta}_0(\tau - \tau_0)^2/2! + \ldots \\ \zeta &= \zeta_0 + \dot{\zeta}_0(\tau - \tau_0) + \ddot{\zeta}_0(\tau - \tau_0)^2/2! + \ldots \end{aligned} \quad (11)$$

for values of τ under consideration.

Substituting equation (11) into equations (9) and (10) and expanding in powers of $\tau_i - \tau_0$ gives

$$f_i(\tau_0) + \dot{f}_i(\tau_0)(\tau_i - \tau_0) + \ddot{f}_i(\tau_0)(\tau_i - \tau_0)^2/2! + \ldots = 0 \quad (12)$$

$$\dot{f}_i(\tau_0) + \ddot{f}_i(\tau_0)(\tau_i - \tau_0) + \dddot{f}_i(\tau_0)(\tau_i - \tau_0)^2/2! + \ldots = 0, \quad (13)$$

where

$$f_i(\tau) = \tfrac{1}{2}[P_i^2(\tau) + Q_i^2(\tau) + R_i^2(\tau) - C_i^2(\tau)]. \quad (14)$$

With m microphones, i takes the values $i = 1 \ldots m$, and the unknowns in equations (12) and (13) are (ξ_0, η_0, ζ_0), $(\dot{\xi}_0, \dot{\eta}_0, \dot{\zeta}_0) \ldots \tau_0$ and τ_i $(i = 1 \ldots m)$. If $(\xi_0^{(n+1)}, \eta_0^{(n+1)}, \zeta_0^{(n+1)})$ and all higher derivatives are zero, the unknowns number $3(n + 1) + m + 1$, whereas the number of equations is $2m$. Hence, a complete solution is possible if

$$m = 3n + 4$$

For example if $n = 1$, then $m = 7$, i.e. the position and velocity of a body can be found at a certain time using 7 microphones by assuming that its acceleration is zero (over that part of the trajectory from which elements of its shock wave are received). This case appears to be particularly worthy of consideration because it provides a set of initial conditions from which the remainder of the trajectory could be calculated by dynamics.

2. Method of Solution with 7 Microphones

It is now assumed that $\ddot{\xi}_0$, $\ddot{\eta}_0$, $\ddot{\zeta}_0$ and higher derivatives are zero, and a solution is sought for ξ_0, η_0, ζ_0, $\dot{\xi}_0$, $\dot{\eta}_0$, $\dot{\zeta}_0$, τ_0.

The method of solution to be followed is one of successive approximation based on the assumption that the time intervals

$$\varepsilon_i = \tau_i - \tau_0 \tag{15}$$

are small. Let ξ_{0k} etc., denote the values of the unknowns ξ_0 etc., which satisfy equations (12) and (13) when terms in ε_i^{k+1} and higher powers of ε_i are neglected. Let f_{ik}, $\dot{f}_{ik}$, ... denote the corresponding values of $f_i(\tau_0)$, $\dot{f}_i(\tau_0)$, ... Then from equations (12) and (13)

$$f_{i0} = 0 \tag{16}$$

$$\dot{f}_{i0} = 0 \tag{17}$$

$$f_{i1} + \dot{f}_{i1}\varepsilon_{i1} = 0 \tag{18}$$

$$\dot{f}_{i1} + \ddot{f}_{i1}\varepsilon_{i1} = 0 \tag{19}$$

$$f_{i2} + \dot{f}_{i2}\varepsilon_{i2} + \tfrac{1}{2}\ddot{f}_{i2}\varepsilon_{i2}^2 = 0 \tag{20}$$

$$\dot{f}_{i2} + \ddot{f}_{i2}\varepsilon_{i2} + \tfrac{1}{2}\dddot{f}_{i2}\varepsilon_{i2}^2 = 0. \tag{21}$$

From equations (16) and (17), ξ_{00}, η_{00}, ζ_{00}, τ_{00}, $\dot{\xi}_{00}$, $\dot{\eta}_{00}$, $\dot{\zeta}_{00}$ can be obtained. The solution is undertaken in the next two sections.

Eliminating $\dot{f}_{i1}$ from equations (18) and (19), f_{i1} is seen to be zero to the first order in ξ_i; and hence $\xi_{01} = \xi_{00}$, $\eta_{01} = \eta_{00}$, $\zeta_{01} = \zeta_{00}$, $\tau_{01} = \tau_{00}$.

Eliminating $\dot{f}_{i2}$ from equations (20) and (21) gives

$$f_{i2} = \tfrac{1}{2}\ddot{f}_{i2}\varepsilon_{i2}^2;$$

and squaring equation (21) gives

$$\dot{f}_{i2}^2 = \ddot{f}_{i2}^2\varepsilon_{i2}^2$$

on neglecting terms in ε_{i2}^3 and ε_{i2}^4. Hence

$$2f_{i2}\ddot{f}_{i2} - \dot{f}_{i2}^2 = 0\,. \tag{22}$$

The solution of equation (22) ($i = 1, \ldots, 7$) for ξ_{02}, η_{02}, ζ_{02}, τ_{02}, $\dot{\xi}_{02}$, $\dot{\eta}_{02}$, $\dot{\zeta}_{02}$, is undertaken in section 7.

Elimination of $\ddot{f}_{i2}$ from equations (20) and (21) gives

$$\varepsilon_{i2} = -2f_{i2}/\dot{f}_{i2} \tag{23}$$

VOL. 12 1958

Having obtained approximate values for the ε_i as well as the other unknowns, one could solve

$$f_{iK} + \dot{f}_{iK}\varepsilon_{iK} + \ldots + f_{iK}^{(K)}\varepsilon_{iK}{}^{K}/K! = 0$$
$$\dot{f}_{iK} + \ddot{f}_{iK}\varepsilon_{iK} + \ldots + f_{iK}^{(K+1)}\,\varepsilon_{iK}{}^{K}/K! = 0$$

for $\xi_{0K}, \eta_{0K}, \zeta_{0K}, \tau_{0K}, \dot{\xi}_{0K}, \dot{\eta}_{0K}, \dot{\zeta}_{0K}, \xi_{iK}$ $(i = 1, \ldots, 7)$ by successive approximation.

4. Solution of $f_i = 0$ for $\xi_{01}, \eta_{01}, \zeta_{01}, \tau_{01}$

By equations (3) and (7), equation (8) can be written

$$\begin{aligned} P_i &= [(\xi - u_0\tau) - (x_i - u_0 t_i) + (\bar{u}_i - u_0)T_i]Z_i/T_i \\ Q_i &= [(\eta - v_0\tau) - (y_i - v_0 t_i) + (\bar{v}_i - v_0)T_i]Z_i/T_i \\ R_i &= [\zeta - z_i + \bar{w}_i T_i]Z_i/T_i \end{aligned} \tag{24}$$

and

$$C_i = [c_0(t_i - \tau) + (\bar{c}_i - c_0)T_i]Z_i/T_i,$$

where

$$\bar{u}_i = U_i/Z_i \qquad \bar{v}_i = V_i/Z_i$$
$$\bar{w}_i = W_i/Z_i \qquad \bar{c}_i = C_i/Z_i \tag{25}$$

and u_0, v_0, w_0, c_0 are arbitrary values, whose choice is considered below.

In terms of

$$\theta_1 = (\xi - u_0\tau)/d_0 \qquad \theta_2 = (\eta - v_0\tau)/d_0$$
$$\theta_3 = c_0\tau/d_0 \qquad \theta_4 = \tfrac{1}{2}(\zeta^2 + \theta_1{}^2 + \theta_2{}^2 - \theta_3{}^2) \tag{26}$$

$$\alpha_i = (u_0 t_i - x_i)/d_0 \qquad \beta_i = (v_0 t_i - y_i)/d_0 \qquad \gamma_i = c_0 t_i/d_0, \tag{27}$$

where d_0 is a scaling factor with the dimensions of length, the equation $f_i = 0$ becomes

$$(\theta_1 + \alpha_i + \Delta_{ui})^2 + (\theta_2 + \beta_i + \Delta_{vi})^2 + [(2\theta_4 + \theta_3{}^2 - \theta_2{}^2 - \theta_1{}^2)^{\frac{1}{2}} + \Delta_{wi}]^2 = (\gamma_i - \theta_3 + \Delta_{ci})^2, \tag{28}$$

where

$$\Delta_{ui} = (\bar{u}_i - u_0)T_i/d_0 \qquad \Delta_{vi} = (\bar{v}_i - v_0)T_i/d_0 \tag{29}$$

$$\Delta_{wi} = (\bar{w}_i T_i - z_i)/d_0 \qquad \Delta_{ci} = (\bar{c}_i - c_0)T_i/d_0 \tag{30}$$

Hence equation (28) can be written

$$[\theta_1 \quad \theta_2 \quad \theta_3 \quad \theta_4]\boldsymbol{M} = \boldsymbol{\delta} + \boldsymbol{\delta}_\Delta \tag{31}$$

where

$$\boldsymbol{M} = \begin{bmatrix} \alpha_1 \ldots \alpha_4 \\ \beta_1 \ldots \beta_4 \\ \gamma_1 \ldots \gamma_4 \\ 1 \quad \ldots 1 \end{bmatrix} \tag{32}$$

$$\boldsymbol{\delta} = [\delta_1 \ldots \delta_4] \qquad \boldsymbol{\delta}_\Delta = [\delta_{\Delta 1} \ldots \delta_{\Delta 4}] \tag{33}$$

$$\delta_i = \tfrac{1}{2}(\gamma_i{}^2 - \beta_i{}^2 - \alpha_i{}^2) \tag{34}$$

$$\delta_{\Delta i} = -\{(\alpha_i + \theta_1 + \tfrac{1}{2}\Delta_{ui})\Delta_{ui} + (\beta_i + \theta_2 + \tfrac{1}{2}\Delta_{vi})\Delta_{vi} + [(2\theta_4 + \theta_3{}^2 - \theta_2{}^2 - \theta_1{}^2)^{\frac{1}{2}} + \tfrac{1}{2}\Delta_{wi}]\Delta_{wi} - (\gamma_i - \theta_3 + \tfrac{1}{2}\Delta_{ci})\Delta_{ci}\} \tag{35}$$

In practice, microphone heights z_i will be only slightly different, and hence $\bar{u}_i$, $\bar{v}_i$, $\bar{w}_i$ and $\bar{c}_i$ are almost independent of i. Let u_0, v_0, c_0 be chosen as the means of $\bar{u}_i$, $\bar{v}_i$, $\bar{c}_i$, then $|\bar{u}_i - u_0|$, $|\bar{v}_i - v_0|$, $|\bar{c}_i - c_0|$ are small. In order to do this an initial guess at ζ needs to be made. It is assumed that the origin is chosen so that z_i are small and that $|\bar{w}_i|$, $|z_i/T_i|$ are of the same order of smallness. δ_Δ can then be neglected in equation (31), and a first approximate solution for ξ, η, ζ, τ obtained. By successive approximations, ξ_{01}, η_{01}, ζ_{01}, τ_{01} are obtained.

In practice, the vertical wind speed and the differences in microphone heights will usually be so small that the first approximation is adequate. Differences in microphone heights would be expected to influence Δ_{wi} more than Δ_{ui}, Δ_{vi} or Δ_{ci}, and this term could be included in the first approximate solution by taking

$$\delta_{\Delta i} = -(\zeta/d_0)\Delta_{wi} = \zeta z_i/d_0^2.$$

(6) Solution of $\dot{f}_i = 0$ for $\dot{\xi}_{00}$, $\dot{\eta}_{00}$, $\dot{\zeta}_{00}$

From equation (14)

$$\dot{f}_i \equiv P_i\dot{P}_i + Q_i\dot{Q}_i + R_i\dot{R}_i - C_i\dot{C}_i, \tag{36}$$

while from equation (8)

$$\begin{aligned}
\dot{P}_i &= u(\zeta)\dot{\zeta} + (Z_i/T_i)\dot{\xi} + (X_i/T_i)\dot{\zeta} + X_iZ_i/T_i^2 \\
\dot{Q}_i &= v(\zeta)\dot{\zeta} + (Z_i/T_i)\dot{\eta} + (Y_i/T_i)\dot{\zeta} + Y_iZ_i/T_i^2 \\
\dot{R}_i &= w(\zeta)\dot{\zeta} + 2(Z_i/T_i)\dot{\zeta} + Z_i^2/T_i^2 \\
\dot{C}_i &= c(\zeta)\dot{\zeta}
\end{aligned} \tag{37}$$

Hence $\dot{f}_i = 0$ becomes

$$\begin{aligned}
&P_i\dot{\xi} + Q_i\dot{\eta} + Z_i^{-1}[(X_i + u(\zeta)T_i)P_i + (Y_i + v(\zeta)T_i)Q_i \\
&\quad + (2Z_i + w(\zeta)T_i)R_i - c_i(\zeta)T_iC_i]\dot{\zeta} + (P_iX_i + Q_iY_i + R_iZ_i)/T_i = 0.
\end{aligned} \tag{38}$$

The coefficients of $\dot{\xi}$, $\dot{\eta}$, $\dot{\zeta}$ in this equation can be evaluated using the solutions of section (5), and $\dot{\xi}_{00}$, $\dot{\eta}_{00}$, $\dot{\zeta}_{00}$ obtained using the data from 3 microphones.

For the purpose of numerical solution, equation (38) can be written

$$\lambda_i\dot{\xi} + \mu_i\dot{\eta} + \omega_i\dot{\zeta} = P_i \tag{39}$$

where, by equations (24), (26) and (29)

$$\begin{aligned}
\lambda_i &= P_iT_i/d_0Z_i = \alpha_i + \theta_1 + \Delta_{ui} \\
\mu_i &= Q_iT_i/d_0Z_i = \beta_i + \theta_2 + \Delta_{vi} \\
\nu_i &= R_iT_i/d_0Z_i = (2\theta_4 + \theta_3^2 - \theta_2^2 - \theta_1^2)^{\frac{1}{2}} + \Delta_{wi}
\end{aligned} \tag{40}$$

$$\sigma_i = \gamma_i - \theta_3 + \Delta_{ci} \tag{41}$$

$$\omega_i = [(X_i + u(\zeta)T_i)\lambda_i + (Y_i + v(\zeta)T_i)\mu_i + (2Z_i + w(\zeta)T_i)\nu_i - c(\zeta)T_i\sigma_i]/Z_i \tag{42}$$

$$\rho_i = -(\lambda_iX_i + \mu_iY_i + \nu_iZ_i)/T_i \tag{43}$$

(7) Solution of $2f_i\ddot{f}_i = \dot{f}_i^2$ ($i = 1, \ldots 7$) for ξ_{02}, η_{02}, ζ_{02}, τ_{02}, $\dot{\xi}_{02}$, $\dot{\eta}_{02}$, $\dot{\zeta}_{02}$,

Let ξ_{0a}, η_{0a}, ζ_{0a}, τ_{0a}, $\dot{\xi}_{0a}$, $\dot{\eta}_{0a}$, $\dot{\zeta}_{0a}$, be an approximate solution obtained, for example,

VOL. 12 1958

by the methods of sections (5) and (6). Let $f_{ia}, \dot{f}_{ia}, \ddot{f}_{ia}$ be the corresponding values of $f_i, \dot{f}_i, \ddot{f}_i$, and write $\xi_0 = \xi_{0a} + \Delta\xi$ etc., and $f_i = f_{ia} + \Delta f_i$ etc.

To solve $2\, f_i \ddot{f}_i = \dot{f}_i^2$ by successive approximation, second order terms are neglected leaving

$$[f_{ia}\ j\dot{f}_{ia}\ \ddot{f}_{ia}][\Delta\ddot{f}_{ia}\ j\Delta\dot{f}_{ia}\ \Delta f_{ia}]' = \tfrac{1}{2}\dot{f}_{ia}^2 - f_{ia}\ddot{f}_{ia}, \qquad j = \sqrt{-1}. \tag{44}$$

This can be written in dimensionless form as (suffixes i and a are omitted in the rest of this section)

$$[\phi_0\ j\phi_1\ \phi_2][\Delta\phi_2\ j\Delta\phi_1\ \Delta\phi_0]^1 = \tfrac{1}{2}\phi_1^2 - \phi_0\phi_2, \tag{45}$$

where

$$\begin{aligned} \phi_0 &= f/a_0^2\, d_0^2 \\ \phi_1 &= \dot{f}t_0/a_0^2 d_0^2 \\ \phi_2 &= \ddot{f}t_0^2/a_0^2 d_0^2 \end{aligned} \tag{46}$$

and t_0 and d_0 are arbitrary units of time and distance. a_0 will be taken as d_0/t_0.

From equation (14)

$$\begin{aligned} \phi_0 &= \tfrac{1}{2}\boldsymbol{\alpha}_0 \cdot \boldsymbol{\alpha}_0' \\ \phi_1 &= \boldsymbol{\alpha}_0 \cdot \boldsymbol{\alpha}_1' \\ \phi_2 &= \boldsymbol{\alpha}_1 \cdot \boldsymbol{\alpha}_1' + \boldsymbol{\alpha}_0 \cdot \boldsymbol{\alpha}_2', \end{aligned} \tag{47}$$

where

$$\begin{aligned} \boldsymbol{\alpha}_0 &= [P\ Q\ R\ jC]/a_0 d_0 \\ \boldsymbol{\alpha}_1 &= [\dot{P}\ \dot{Q}\ \dot{R}\ j\dot{C}]t_0/a_0 d_0 \\ \boldsymbol{\alpha}_2 &= [\ddot{P}\ \ddot{Q}\ \ddot{R}\ j\ddot{C}]t_0^2/a_0 d_0. \end{aligned} \tag{48}$$

From equations (8) and (25)

$$\boldsymbol{\alpha}_0 = n[\bar{u}T + X\ \ \bar{v}T + Y\ \ \bar{w}T + Z\ \ j\bar{c}T]/d_0 \tag{49}$$

and from equation (37)

$$\boldsymbol{\alpha}_1 = [u + l\ \ v + m\ \ w + n\ \ jc]\dot{\zeta}_0/a_0 + (Z/d_0)[p\ q\ r\ 0] \tag{50}$$

$$\boldsymbol{\alpha}_2 = [u'\ v'\ w'\ jc']\dot{\zeta}_0/a_0 + 2(T/t_0)r[p\ q\ r\ 0], \tag{51}$$

where

$$u = u(\zeta_0)/a_0 \quad \text{etc} \tag{52}$$

$$u' = (\dot{\zeta}_0/a_0)u'(\zeta_0)d_0/a_0 \quad \text{etc}$$

$$p = (l + \dot{\xi}_0/a_0)t_0/T \qquad q = (m + \dot{\eta}_0/a_0)t_0/T \qquad r = (n + \dot{\zeta}_0/a_0)t_0/T \tag{53}$$

$$l = X/a_0 T \qquad m = Y/a_0 T \qquad n = Z/a_0 T \tag{54}$$

From equation (47)

$$\begin{bmatrix} \Delta\phi_2 \\ j\Delta\phi_1 \\ \Delta\phi_0 \end{bmatrix} = \begin{bmatrix} \boldsymbol{\alpha}_2 & 2\boldsymbol{\alpha}_1 & \boldsymbol{\alpha}_0 \\ j\boldsymbol{\alpha}_1 & j\boldsymbol{\alpha}_0 & 0 \\ \boldsymbol{\alpha}_0 & 0 & 0 \end{bmatrix} \begin{bmatrix} \Delta\boldsymbol{\alpha}_0' \\ \Delta\boldsymbol{\alpha}_1' \\ \Delta\boldsymbol{\alpha}_2' \end{bmatrix} \tag{55}$$

From equation (8), it is found that to the first order in small quantities

$$[\Delta\boldsymbol{\alpha}_0\ \Delta\boldsymbol{\alpha}_1\ \Delta\boldsymbol{\alpha}_2]' = \boldsymbol{L}[\Delta\xi/d_0\ \Delta\eta/d_0\ \Delta\zeta/d_0\ \Delta\tau/t_0]' + \boldsymbol{M}[\Delta\dot{\xi}\ \Delta\dot{\eta}\ \Delta\dot{\zeta}]'/a_0 \tag{56}$$

where

$$\boldsymbol{L} = \begin{bmatrix} n & 0 & u+l & ln \\ 0 & n & v+m & mn \\ 0 & 0 & w+2n & n^2 \\ 0 & 0 & jc & 0 \\ r & 0 & u'+p & pn+rl \\ 0 & r & v'+q & qn+rm \\ 0 & 0 & w'+2r & 2rn \\ 0 & 0 & jc' & 0 \\ r' & 0 & u''+p' & 2rp+np'+lr' \\ 0 & r' & v''+q' & 2rq+nq'+mr' \\ 0 & 0 & w''+2r' & 2r^2+2nr' \\ 0 & 0 & jc'' & 0 \end{bmatrix} \tag{57}$$

$$\boldsymbol{M} = \begin{bmatrix} 0 & 0 & 0 \\ 0 & 0 & 0 \\ 0 & 0 & 0 \\ 0 & 0 & 0 \\ n & 0 & u+l \\ 0 & n & v+m \\ 0 & 0 & w+2n \\ 0 & 0 & jc \\ 2r & 0 & 2(u'+p) \\ 0 & 2r & 2(v'+q) \\ 0 & 0 & 2(w'+2r) \\ 0 & 0 & 2jc'' \end{bmatrix} \tag{58}$$

$$u'' = (\ddot{\zeta}_0/a_0)^2\ u''(\zeta_0)d_0^2/a_0^2 \qquad \text{etc.} \tag{59}$$

$$p' = 2pt_0/T \qquad q' = 2qt_0/T \qquad r' = 2rt_0/T. \tag{60}$$

VOL. 12 1958

By equations (55) and (56), equation (45) becomes

$$\boldsymbol{l}[\Delta\xi/d_0\ \Delta\eta/d_0\ \Delta\zeta/d_0\ \Delta\tau/t_0]' + \boldsymbol{m}[\dot{\Delta}\xi\ \dot{\Delta}\eta\ \dot{\Delta}\zeta]'/a_0 = \tfrac{1}{2}\phi_1^2 - \phi_0\phi_2, \tag{61}$$

where

$$\boldsymbol{l} = \boldsymbol{s}\,.\,\boldsymbol{L} \qquad \boldsymbol{m} = \boldsymbol{s}\,.\,\boldsymbol{m} \tag{62}$$

$$\boldsymbol{s} = [\phi_0\ j\phi_1\ \phi_2] \begin{bmatrix} \alpha_2 & 2\alpha_1 & \alpha_0 \\ j\alpha_1 & j\alpha_0 & 0 \\ \alpha_0 & 0 & 0 \end{bmatrix} \tag{63}$$

Using the data from 7 microphones, equation (61) can be solved for $\Delta\xi$, $\Delta\eta$, $\Delta\zeta$, $\Delta\tau$, $\dot{\Delta}\xi$, $\dot{\Delta}\eta$, $\dot{\Delta}\zeta$ and improved values obtained for ξ_{0a} etc. With successive approximations, these values will tend to ξ_{02} etc.

8. Discussion

The complexity of determining the trajectory of a body by acoustical observations arises from the fact that the shock-wave elements received at various microphones originate, in general, from different points of the trajectory. A point of the trajectory cannot, therefore, be determined without considering the velocity, acceleration, etc. of the body. When the points of the trajectory from which the received shock waves originate are sufficiently close together, a solution by successive approximation is possible. In the case of 7 microphones, this method of solution has been formulated in a form ready for numerical calculation.

An attempt has been made to test the theory using data obtained from the shock wave of a shell fired at an elevation of about 30° (and fused to explode at 10,000 ft altitude). From the arrival times of the shock wave at 4 microphones, spaced some 5000–10,000 ft apart, the position of the shell was calculated by the theory of section (5) and its velocity by that of section (6). The values obtained were not unreasonable, accuracies being about 1000 ft in position and a few hundred feet per second in velocity. The positions of the microphones had been selected for other reasons than that of observing the shock wave and were not ideally situated, lying some 15,000 ft away from the part of the trajectory where the shock waves originated and all in the same general direction from it. If the microphones had been nearer the trajectory much better accuracy could have been expected. The arrival times at three further microphones were used to carry through the 7 microphone solution of section (7). The numerical computation was found to be practicable, but the incremental adjustments of position and velocity were obtained with doubtful accuracy due, it is thought, to the unsatisfactory location of the microphones.

Reference

Groves G. V. 1956 *J. Atmosph. Terr. Phys.* **8**, 189.

Journal of Atmospheric and Terrestrial Physics, 1958, Vol. 12, pp. 26 to 33. Pergamon Press Ltd., London

The fading of radio waves reflected at oblique incidence

J. W. KING
Cavendish Laboratory, Cambridge

(*Received* 13 *August* 1957)

Abstract—Previous experimental results on the reflection of radio waves from the ionosphere at near-vertical incidence have been extended to include the case of waves incident obliquely. It is shown that the radio diffraction pattern formed at the ground by a medium frequency wave reflected at oblique incidence is very much larger than expected and is, on the average, roughly circular. It is concluded that the ionospheric irregularities responsible for the fading have much greater extent in the horizontal than in the vertical plane. It is found, in general, that the speed of fading of a wave of frequency f is proportional to $f \cos i$, where i is the angle of incidence on the ionosphere, and that the probability distribution of amplitude tends to be log normal rather than of the type discussed by RICE (1947).

(1) *Introduction*

Studies (MITRA, 1949; MCNICOL, 1949; MILLMAN, 1952; and BOWHILL, 1956) of radio waves reflected from the ionosphere near vertical incidence indicate that the speed of fading is roughly proportional to the radio frequency of the wave over a range from 16 kc/s to 2000 kc/s. BOWHILL (1956) has suggested that the situation is complicated by the occurrence of two different speeds of fading on frequencies near 100 kc/s, and that for frequencies less than this the fading speed is constant. The previous studies have also shown (BRIGGS and PHILLIPS, 1950; BRAMLEY, 1951; BOWHILL, 1956; and HARWOOD, 1951) that when fading occurs an irregular radio diffraction pattern is formed over the ground, and that the pattern is on the whole symmetrical, with an auto-correlation function which falls to 0·5 in a distance of about one and a half wavelengths.

VOL. 12 1958

It is the purpose of this paper to extend the experimental results to include waves incident obliquely on the ionosphere.

In an important paper FEJER (1953) has examined the form of the diffraction pattern which would be formed by the passage of a wave obliquely through an ionosphere containing irregularities. He has shown (Par. 4 (iv a), p. 468) that if the ionospheric irregularities were, on the average, spherically symmetrical, then the diffraction pattern on a plane normal to the emerging beam would have circular symmetry, while that on a plane making an angle ψ with the emerging beam would be, on the average, elliptical, with its long axis in the plane of incidence and equal to sec ψ times its short axis. If, however, the ionospheric irregularities were in the form of flat discs with small extent vertically, and, on the average, with circular symmetry in the horizontal plane, then the diffraction pattern on a plane parallel to the discs would be circular. These results of FEJER apply also to the shapes of shadows cast by large spherical or disc-like objects and can be simply visualized in terms of such shadows, as indicated in Fig. 1. Experiments, designed to measure the size and shape of the diffraction pattern on the ground, are described in Par. 2, and are discussed in terms of FEJER's theory in Par. 5(a) of this paper.

Observations of the rates of fading on different radio frequencies, f, transmitted

over different distances are discussed in Par. 3, and it is shown that the rate of fading is fairly closely proportional to $f \cos i$, where i is the angle of incidence on the ionosphere.

Studies (McNicol, 1949; Mitra, 1949) of the amplitude probability distributions for the fading of waves reflected at vertical incidence have shown that they agreed with the expression given by Rice (1947) for the case where a specularly reflected wave of power b, which could vary with different conditions, was added to a random component of power 1. A more detailed investigation of the amplitude distribution is described in Par. 4, where it is suggested that a log-normal distribution more accurately represents the results.

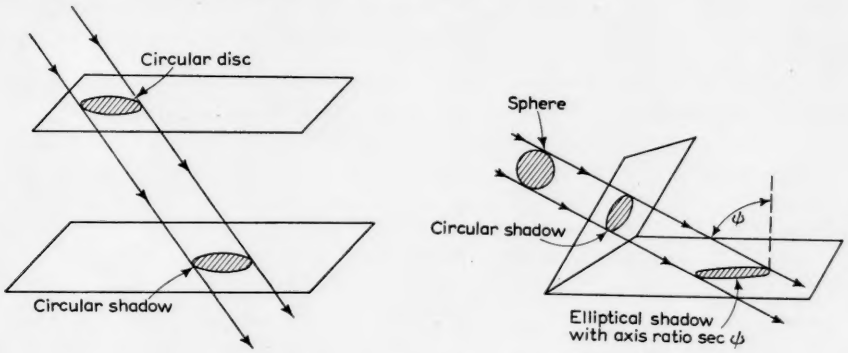

Fig. 1. To illustrate the results of Fejer's theory.

(2) *The size of the diffraction pattern*

A measure of the size of the diffraction pattern at the ground is given by the distance at which the correlation of the amplitudes at two separated points falls to 0·5. The previous published results, all of which are for vertical or near vertical incidence, are listed in Table 1. In order to investigate waves reflected at oblique

Table 1

Frequency	Observer	Distance for ρ to fall to 0·5 km	number of λ
16 kc/s	Harwood (1951)	30	1·6
70 kc/s	Bowhill (1953)	7·9	1·8
85 kc/s	Bowhill (1953)	5·3	1·5
2·4 Mc/s	Briggs and Phillips (1950)	0·20	1·6
4·8 Mc/s	Briggs and Phillips (1950)	0·20	3·2
4·7 Mc/s (mean)	Bramley (1951)	0·55	8·7

incidence the signals received at night from a transmitter at Rome (845 kc/s, $\lambda = 335$ m, distant 1496 km) were recorded near Cambridge. One receiver of a pair was situated at Cambridge and the other at a succession of places which were chosen

so that the line joining the receivers was either very nearly in or perpendicular to the plane of incidence. Table 2 contains the details of the positions selected.

If $a_1, a_2, \ldots, a_n$ and $b_1, b_2, \ldots, b_n$ represent the values of the amplitude recorded at the two places at corresponding times and if

$$\bar{a} = \sum_1^n a_x/n \qquad \text{and} \qquad \bar{b} = \sum_1^n b_x/n,$$

then values of the correlation coefficient

$$\rho = \frac{\sum_1^n (a_x - \bar{a})(b_x - \bar{b})}{\sqrt{\sum_1^n (a_x - \bar{a})^2 \sum_1^n (b_x - \bar{b})^2}}$$

were computed with the aid of the EDSAC digital computer in the Mathematical Laboratory, Cambridge. Altogether 168 values of ρ were computed, the average value of n being 180 and the average duration of the records analysed being 90 min. The results are given in Table 2. The most comprehensive set of results

Table 2

Date	Separation between spaced receivers (km)		Number of periods analysed	Mean value of cross-correlation coefficient
	Perpendicular to plane of propagation	Along plane of propagation		
22–23 December 54	0·45	1·95	9	0·83 ± 0·03
4–8 January 55	1·38	0·87	12	0·80 ± 0·05
11–20 February 55	4·33	0·32	12	0·62 ± 0·04
14–15 March 55	0·39	21·20	3	0·43 ± 0·18
20–29 March 55	0·20	14·08	44	0·68 ± 0·02
20–29 March 55	7·68	0·25	44	0·63 ± 0·03
20–29 March 55	7·68	14·08	44	0·56 ± 0·03

are those for the equinox period 20–29 March 1955, from which the following deductions are made:—

(a) In the plane of propagation the correlation coefficient has a value 0·68 for a receiver separation of 40 wavelengths. If it is assumed that the spatial correlogram is gaussian, then the distance in which the correlation would fall to 0·5 in the plane of incidence would be 53 wavelengths.

(b) With the same assumption, the distance in which the correlation falls to 0·5 in a direction perpendicular to the plane of incidence is found to be 26 wavelengths.

These results are considered more fully in Par. 5.

(3) *The night-time rate of fading*

The fading speed, defined as the number of maxima which occur on the amplitude record in 1 hr, was determined for as many different frequencies as

VOL. 12 1958

possible, with a wide range of values of sec i. The results are given in Table 3. Some of these are taken from records made by the author, or his colleagues in Cambridge; others are taken from the published literature. In nearly every case the entry represents several hundred hours of recording.

Table 3

Frequency (kc/s)	sec i	Reference	Observed fading speed (night) (max./h)
16	1·13	Bowhill (1953)	8·5
16	1·13	Harwood (1951)	5·0
30	1·05	Bowhill (1953)	8·6
43	1·23	Bowhill (1953)	9·4
65	1·23	Harwood (1951)	8·6
70	1·16	Bowhill (1953)	12·7
70	4·39		8·6
85	4·11		8·8
113	4·39		11·2
113	1·13	Bowhill (1953)	24·2
127	1·06	Bowhill (1953)	103·3
127	3·52		10·0
150	1·00	Jones (1953)	34·2
164	3·24		13·1
185	4·52		14·1
191	5·34		13·7
200	1·03	Bowhill (1953)	43·8
200	1·33		49·4
233	2·98		15·2
245	4·11		14·3
845	5·78		32·4
1765	1·00	Pawsey (1935)	413 (F region)
2000	1·00		614 (F region)

In calculating the values of sec i it has been assumed that the height of reflection was 85 km, and the curvature of the earth has been allowed for. The two highest frequencies, both at vertical incidence, were reflected from the F region.

In Fig. 2 the fading speed is plotted against the radio frequency multiplied by cos i. The points are found to lie scattered about a straight line represented by the expression

$$\text{fading speed} = 0{\cdot}30 \times f \cos i \quad \text{max./hr}$$

where f is the frequency in kc/s.

The evidence of Fig. 2 does not appear to support the contention of Bowhill (1956) that the fading speed was substantially constant for frequencies less than 100 kc/s. Further information on this point is obtained from the analysis of the fading records in terms of their temporal auto-correlation functions. The results are listed in Table 4, and appear to show that the fading speed is substantially decreased for the lower frequencies.

In order to see whether, in the scatter about the straight line of Fig. 2, there was any systematic dependence on sec i, the departures of the points from the straight line were plotted against sec i in Fig. 3. The amount of scatter is similar for the cases of both vertical and oblique incidence, and it seems reasonable to conclude that the fading speed at oblique incidence is proportional to $f \cos i$.

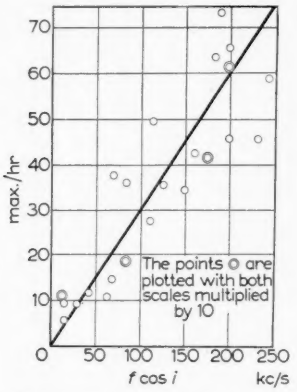

Fig. 2. Fading speed (max./hr) related to $f \cos i$, where i is the angle of incidence on the ionosphere.

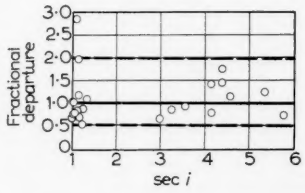

Fig. 3. The fractional departure of the points in Fig. 2 from the straight line, plotted against sec i.

VOL. 12 1958

It should be mentioned that for all the nine different frequencies for which records have been analysed throughout a complete year or more (thus removing any possible sunspot cycle effect) there appears to be a seasonal variation of fading speed such that the fading is approximately 1·5 times faster at midwinter than at midsummer.

Table 4

Frequency (kc/s)	$f \cos i$ (kc/s)	Reference	Time (min) in which the autocorrelogram falls to 0·5
16	14	HARWOOD (1951)	4·5
65	53	HARWOOD (1951)	2·2
845	146		1·5
150	150	MILLMAN (1952)	0·3 to 1·3

(4) *The probability distribution of the amplitude*

If the downcoming wave is produced partly by a process of "specular" reflection and partly by scattering from a randomly-distributed series of irregularities, then its amplitude at the ground will vary in a way which was discussed by MCNICOL (1949). The amplitude will have a probability distribution of a type discussed by RICE (1947), which depends on the ratio b of the power in the specular

portion to that in the randomly scattered portion. When $b = 0$, the "Rice" distribution is the same as a Rayleigh distribution.

Table 5 lists apparent values of b calculated from night-time observations made with vertically incident waves. For frequencies greater than about 150 kc/s, $b = 0$ and the amplitude has a Rayleigh distribution. For frequencies less than 150 kc/s, b becomes greater as the frequency becomes smaller.

Table 5

Frequency (kc/s)	Reference	Mean apparent value of b
16	Bowhill (1953)	$\approx 10{\cdot}0$
16	Harwood (1951)	4·5
43	Harwood (1951)	5·0
65	Harwood (1951)	4·3
70	Bowhill (1953)	3·6
127	Bowhill (1953)	2·2
150	Millman (1952)	$\approx 0{\cdot}0$
200		0·3
844	Pawsey (1935)	0·0
2000		0·1

If the probability distribution is examined in detail for frequencies less than 150 kc/s it is found to be more nearly "log-normal" than Rayleigh. (Distributions which may be inspected are given by the Decca Navigator Company, 1950; Harwood, 1951; and Millman, 1952.) This difference is also particularly noticeable for the case of Rome (845 kc/s) received at Cambridge, for which 250 amplitude distributions have been plotted from records lasting over a total of 300 hr. A typical example is shown in Fig. 4.

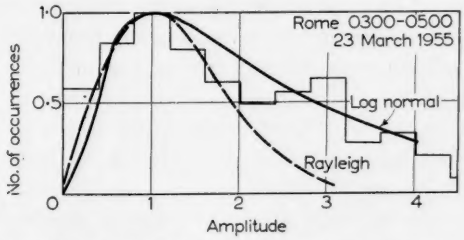

Fig. 4. Amplitude probability distribution of the signal received at Cambridge from Rome (distance 1496 km, frequency 845 kc/s) 0300–0500 GMT. 23 March 55.

(5) *Discussion of results*

(a) *The size and shape of the radio diffraction pattern.* In Par. 2 it was shown that the radio diffraction pattern formed at the ground by a wave of frequency 845 kc/s incident very obliquely on the ground (sec $\psi = 10{\cdot}5$, sec $i = 5{\cdot}8$)* was, on the average, roughly circular, and that the correlation fell to 0·5 in about 40 wavelengths. Other experiments would lead us to expect that for the same frequency

* Here ψ represents the angle of incidence on the ground, and i the angle of incidence on the ionosphere.

incident vertically the corresponding distance would be about 1·5 wavelengths.

If the same ionospheric irregularities had been responsible for the fading of the downcoming wave in the two cases and if they were on the average spherical, it would have been expected from the theory of FEJER that the correlation distance perpendicular to the plane of oblique incidence would be the same as the correlation distance at vertical incidence, and that in the plane of oblique incidence it would be sec ψ times greater where ψ is the angle of incidence on the ground. Since neither of these results is observed it must be concluded that some other irregularities are responsible for the fading at oblique incidence. Since the diffraction pattern on the ground has roughly circular symmetry FEJER's theory suggests that the ionospheric irregularities must approximate to flat circular discs with small extent in the vertical plane. If they produce changes of amplitude, their average size must be half the average "size" of the diffraction pattern which they produce, so that their auto-correlation function must fall to 0·5 in a distance of about 20 wavelengths, i.e. 7 km. If, however, they produce changes of phase of r.m.s. magnitude $\Delta\phi$, then they must have a size $\Delta\phi$ times as great (RATCLIFFE (1956)).

Since the part of the ionosphere which reflects waves at oblique incidence is below that which reflects them at vertical incidence, it is presumably only in the lower ionosphere that the large-scale disc-like irregularities occur. Evidence of a different kind (LANDMARK, 1957; SHRAG, 1955) has suggested that in the lower ionosphere there may be irregular distortions of the planes of constant electron density, of a kind which produce effective "concave mirrors" of radius 20 km or so, capable of focussing waves reflected from them. It might be that oblique reflection from distortions of this kind could account for the results described here.

(b) *The speed of fading.* It has been suggested in Par. 3 that for waves incident obliquely on the ionosphere, the fading speed is proportional to $f \cos i$. If the fading were produced by a radio diffraction pattern drifting over the ground with a constant speed, we should have to conclude that the size of the pattern was proportional to $\lambda \sec i$. But the results of (a) show that the size of the radio diffraction pattern produced by the wave from Rome is considerably greater than this, and the speed of fading cannot therefore be accounted for by a constant drift speed. Moreover, experiments conducted by BOWHILL (1956) appear to show that, at the lower equivalent frequencies, the fading is accounted for to a large extent by irregular changes in the diffraction pattern, and not by the drift of a relatively constant pattern.

All these considerations lead to the conclusion that the relation between the speeds of fading at vertical and oblique incidence is not yet understood.

(c) *The probability distribution of amplitude.* The fact that the probability distribution of amplitude is more nearly log-normal than Rayleigh implies that the amplitude assumes large values more often than would be expected on the Rayleigh distribution. At vertical incidence it has been shown (WHITEHEAD, 1956) that these large values could be caused by "focusing" from effective concave mirrors in the ionosphere and it is perhaps possible that they could be produced in the same way at oblique incidence.

VOL. 12 1958

Another mechanism which might produce the observed distribution is one in which "clouds" producing greater and smaller absorption moved overhead in the ionosphere. If the electron density in these were normally distributed the amplitude would be log normally distributed, provided the clouds were large enough for ray optics to be applicable. With a radio diffraction pattern of the size discussed in Par. 2 this condition would be fulfilled.

Acknowledgements—The author wishes to thank Mr. J. A. RATCLIFFE for his invaluable advice in connection with this work, and Rhodes University for a Scholarship which enabled him to work in the Cavendish Laboratory.

REFERENCES

BOOKER H. G., RATCLIFFE J. A. and SHINN D. H.	1950	*Phil. Trans. Roy. Soc. Lond.* **242,** 579.
BOWHILL S. A.	1953	Ph.D. Thesis, University of Cambridge.
BOWHILL S. A.	1956	*J. Atmosph. Terr. Phys.* **8,** 129.
BRAMLEY E. N.	1951	*Proc. Instn. Elect. Engrs.* 98 Pt. III, 19.
BRIGGS B. H. and PHILLIPS G. J.	1950	*Proc. Phys. Soc.* B **63,** 907.
Decca Navigator Company	1950	*Memo Plans* 125.
FEJER J. A.	1953	*Proc. Roy. Soc.* A **220,** 455.
HARWOOD J.	1951	Ph.D. Thesis, University of Cambridge.
JONES R. E.	1953	Penn. State College, Scientific Report No. 48
LANDMARK B.	1957	*J. Atmosph. Terr. Phys.* **10,** 288.
MCNICOL R. W. E.	1949	*Proc. Instn. Elect. Engrs.* **96,** Pt III, 517.
MILLMAN G. H.	1952	*Ann. Geophys.* **8,** 365.
MITRA S. N.	1949	*Proc. Instn. Elect. Engrs.* **96,** Pt III, 505.
PAWSEY J. L.	1935	*Proc. Camb. Phil. Soc.* **31,** 125.
RATCLIFFE J. A.	1956	*Rep. Prog. Phys.* **19,** 188.
RICE S. O.	1947	*Bell Syst. Tech. J.* **27,** 109.
SHRAG R. L.	1955	*Phys. Soc. Cambridge Conf. Report* p. 202.
WHITEHEAD J. D.	1956	*J. Atmosph. Terr. Phys.* **9,** 269.

Journal of Atmospheric and Terrestrial Physics, 1958, Vol. 12, pp. 34 to 45. Pergamon Press Ltd., London

A study of the ionospheric irregularities which cause spread-*F* echoes and scintillations of radio stars

B. H. Briggs
Cavendish Laboratory, Cambridge

(*Received* 13 *August* 1957)

Abstract—A study is made of the correlation between the occurrence of spread-*F* echoes at Slough, Inverness and Oslo. It is concluded that the ionospheric irregularities which cause the spreading occur in patches which have dimensions of the order of 500 km in a NS direction, and considerably greater in the EW direction. There is an indication that these "bands" of irregularities may lie along lines of magnetic latitude, and that they tend to occur in the same geographical position on successive nights. The correlation of the scintillations of the radio star in Cassiopeia with the occurrence of spread-*F* echoes at two places is investigated. The results are found to be consistent with the same picture of the spatial distribution of the irregularities. Some indirect arguments suggest that the irregularities causing the scintillations are at heights near 300 km.

1. Introduction

In this paper we shall be concerned with the phenomena of "spread-*F*" echoes, the scintillations of a radio star, and with the relation between them. We begin with a brief description of the two phenomena.

Spread-*F* echoes are observed at certain times in vertical incidence soundings of the ionosphere. The phenomenon is best seen on records of the virtual height as a function of frequency ($h'(f)$ records), as obtained at ionospheric observatories. There are several different kinds of spread-*F*, but the most common in medium latitudes takes the form of a thickening of the trace which becomes more marked as the critical frequency of the *F* region is approached (Fig. 1). The occurrence and nature of this phenomenon have been studied by various workers for different stations (e.g. Booker and Wells, 1938; Wells, 1954; Reber, 1954, 1956; Wright, Koster and Skinner, 1956). It is mainly a night-time phenomenon. Generally, spread-*F* echoes appear at sunset and the spreading increases throughout the night until layer sunrise, when there is a rapid decrease. In medium latitudes, the spreading is much more prevalent on winter nights than on summer nights. The spreading is generally believed to be due to the presence of pronounced irregularities in the ionization near the maximum of the *F*-region.

Scintillations of a radio star take the form of irregular fluctuations in the strength and apparent position of the source. We shall here be concerned only with the amplitude variations of the radio waves as observed at a single point on the ground. These scintillations have been studied by many workers (e.g. Ryle and Hewish, 1950; Little and Maxwell, 1951; Hewish, 1952; Hartz, 1955; Wright, Koster and Skinner, 1956; Dagg, 1957). At most places, the scintillations are found to be a night-time phenomenon, with a maximum of occurrence near midnight, and they are found to be correlated with spread-*F* echoes. It is therefore generally assumed that they are caused by the passage of the radio waves from the star through irregularities of ionization in the *F* region of the ionosphere, that these are the same as those which cause the spread-*F* echoes, and that they are present mainly by night.

VOL. 12 1958

If observations are made when the star is at very low angles of elevation, a different type of scintillation is observed, which appears to be correlated with irregularities in the *E* region (Bolton, Slee and Stanley, 1953; Wild and Roberts, 1956). Also, for stations where there is considerable auroral activity the scintillations can occur at all times of day and vary as a function of sidereal rather than solar time (Hartz, 1955). We shall not, however, be concerned with either of these effects in the present paper. We shall use scintillation data only for the source in Cassiopeia as observed at Cambridge, for which the scintillations are a night-time phenomenon, and are correlated with the occurrence of spread-*F* echoes.

In previous work on this subject, the occurrence of scintillations was compared with the occurrence of spread-*F* echoes at a single ionospheric station. The region of the ionosphere effective for the production of scintillations was usually at a distance of several hundred kilometres from this station. The fact that a correlation was found between the two phenomena showed, therefore, that the irregularities occurred in patches of considerable horizontal extent. It was not possible, however, to determine the size of the patches. In the present paper we shall make use of observations at three ionospheric stations separated by about 800 km. In this way it is possible to determine the approximate size and shape of the patches of irregularities. It is also possible by some indirect arguments to make deductions about their height.

In section 2 we begin by defining a "spread-*F* index" as a measure of the amount of spreading of the ionospheric echoes. We then study the correlation between the values of this index at the three ionospheric stations, and also the correlation between its mean value for one night and the next. Then in section 3 we define a "scintillation index" to represent the degree of variability of the waves from the radio star. We then study the correlation between the scintillation index and the spread-*F* index for two of the ionospheric stations. The significance of the results obtained is discussed in section 4.

2. A Study of the Occurrence of Spread-*F* Echoes at Three Ionospheric Stations

(a) *Definition of the "spread-*F *index"*

The three stations used for this study were Slough (52°N, 1°W), Inverness (57°N, 4°W) and Oslo (60°N, 11°E). At these stations hourly $h'(f)$ records are made as a routine, and the main parameters deduced from the records are published as monthly bulletins of ionospheric characteristics. For Slough and Inverness, the actual $h'(f)$ records were available for study, but for Oslo only the monthly bulletins were available. A different measure of spread-*F* was used in the two cases.

When the $h'(f)$ records were available, an index in the range 0–3 was assigned to each hourly record according to the conventions illustrated in Fig. 1. An index of zero was given to records which showed no spreading, and an index of 1 to records which showed a very slight spreading near the critical frequency of the *F* region (Fig. 1(a) and (b)). An index of 2 was given to records which showed

considerable spreading but which still showed separated traces for the ordinary and extraordinary rays (Fig. 1(c)). An index of 3 was given when the spreading was so great that the traces for the ordinary and extraordinary rays were completely joined up (Fig. 1(d)).

There were some unusual records which did not fit well into this classification. Some records showed "spurs" or diffuse echoes at a fairly constant height which extended above the normal critical frequency. These were usually associated with considerable spreading near the critical frequency, and were given an index of 3. Any spreading at levels well below the F region was ignored.

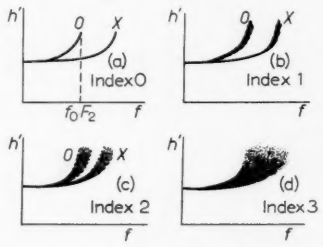

Fig. 1. Diagrams which illustrate the development of spread-F echoes, and the index on a scale 0–3 used to measure the intensity of the phenomenon.

For Oslo, where only the monthly bulletins were available, use was made of the symbol "F" which is used in the bulletins to qualify the values of critical frequency when spreading is present. An index in the range 0–3 was obtained from the bulletins as shown in Table 1.

Table 1

Typical published f_0F_2	8·9	8·9 F	(8·9) F	F
Spread-F index	0	1	2	3

It is believed that the indices obtained by the two methods measure essentially the same phenomenon, and are similar to the index used by other workers (e.g. Wright, Koster and Skinner, 1956). The index obtained from the records is, however, more reliable than that obtained from the bulletins.

The present paper is based mainly on a detailed study of results for the following four months: September 1954, December 1954, March 1955, and June 1955.

(b) *The correlation between the occurrence of spread-*F *echoes on one night and the next*

Before we investigate the correlation between the values of the spread-F index at different stations, it is of interest to examine some features of the results for a single station.

The figures obtained show at once the usual night-time increase. It can also be seen from the figures that if the index is high for any particular night, it tends to remain so for the whole of the night, or at any rate for a large part of it. Also, when the index is high, the spreading tends to start earlier and end later.

VOL. 12 1958

The question then arises: do nights of high or low spread-*F* occurrence occur in groups? To investigate this the mean value of the spread-*F* index for each night (1800–0600 G.M.T.) was evaluated. The series of figures obtained was subjected to an autocorrelation analysis for time shifts of 24 hr (i.e. one night) and 48 hr (i.e. two nights). This was done separately for the four months, and the results for Slough and Inverness are given in Table 2.* The spread-*F* figures for Oslo were less reliable and were not analysed in this way, but an inspection of the figures suggests that the results would have been similar.

Table 2

Time shift		24 hr	48 hr
Slough	Sep. 1954	0 ± 0·19	0 ± 0·19
	Dec. 1954	+0·40 ± 0·16	+0·11 ± 0·20
	Mar. 1955	+0·20 ± 0·18	+0·05 ± 0·19
	June 1955	+0·54 ± 0·13	0 ± 0·19
Inverness	Sep. 1954	+0·29 ± 0·17	+0·13 ± 0·19
	Dec. 1954	+0·08 ± 0·19	+0·16 ± 0·18
	Mar. 1955	+0·65 ± 0·15	+0·57 ± 0·15
	June 1955	+0·26 ± 0·18	−0·07 ± 0·19
Mean		+0·30 ± 0·06	+0·11 ± 0·07

The results show that for both stations there is a significant positive correlation between the mean spread-*F* index for one night and the next. The correlation coefficient between the mean spread-*F* index for nights separated by 48 hr is slightly positive, but is barely significant when the error is taken into account.

Table 3

Time shift		24 hr	48 hr	72 hr
Slough	June–Aug. 1950	+0·43 ± 0·08	+0·13 ± 0·10	0 ± 0·10

In view of the importance of this effect for any theory of the origin of spread-*F* echoes, a longer and independent series of results was analysed in a similar way. Records from Slough for the period 1 June 1950 to 31 August 1950 were used, and the results are shown in Table 3.

* Throughout the present paper, the correlation coefficient ρ between n pairs of values of two variables x and y has been calculated from the equation

$$\rho = \frac{\Sigma xy - \frac{(\Sigma x)(\Sigma y)}{n}}{\sqrt{\left(\Sigma x^2 - \frac{(\Sigma x)^2}{n}\right)\left(\Sigma y^2 - \frac{(\Sigma y)^2}{n}\right)}}$$

The error σ in ρ has been calculated from the equation $\sigma = (1 - \rho^2)/\sqrt{n}$

These results agree quite well with the mean results in Table 2. We conclude that, at any one place, there is a tendency for nights of high spread-*F* index to occur in groups.

(c) *The correlation between the occurrence of spread-*F *echoes at three ionospheric stations*

In order to investigate the correlation between the occurrence of spread-*F* echoes at the three stations the figures for the mean spread-*F* index for the whole night at each station were used. The object now was to see whether the nights for which the spread-*F* index was above the monthly average for one station coincided with those for which it was above the average for the others.

The correlation coefficient between the nightly figures was evaluated for each of the four months, and for the three pairs of stations Slough–Inverness, Inverness–Oslo, and Slough–Oslo. The results are shown in Table 4.

It will be seen that the correlation between Slough and Inverness and between Slough and Oslo is zero within the limits of the error. For Inverness and Oslo,

Table 4

	Correlation coefficient Slough–Inverness	Correlation coefficient Inverness–Oslo	Correlation coefficient Slough–Oslo
Sep. 1954	$-0{\cdot}08 \pm 0{\cdot}19$	$+0{\cdot}58 \pm 0{\cdot}13$	$+0{\cdot}04 \pm 0{\cdot}18$
Dec. 1954	$-0{\cdot}22 \pm 0{\cdot}17$	$+0{\cdot}05 \pm 0{\cdot}19$	$+0{\cdot}19 \pm 0{\cdot}15$
March 1955	$+0{\cdot}16 \pm 0{\cdot}19$	$+0{\cdot}35 \pm 0{\cdot}17$	$+0{\cdot}12 \pm 0{\cdot}18$
June 1955	$+0{\cdot}21 \pm 0{\cdot}18$	$+0{\cdot}43 \pm 0{\cdot}17$	$+0{\cdot}05 \pm 0{\cdot}18$
Mean	$+0{\cdot}02 \pm 0{\cdot}09$	$+0{\cdot}35 \pm 0{\cdot}08$	$+0{\cdot}10 \pm 0{\cdot}08$

however, there is a significant positive correlation. As previously explained, the index used for Oslo was of a different kind from that used for Inverness. This difference could reduce the correlation between the two places, but it could not increase it. If the original records had been available from Oslo, so that the same kind of index could have been used, it is possible that the positive correlation would have been greater.

It is of interest to consider the geographical positions of these stations; they are shown in Fig. 2. The distance between Slough and Inverness is 720 km and the line joining them lies approximately north-south. The distance between Inverness and Oslo is 920 km, and these stations have nearly the same geomagnetic latitude. (The dotted line marked "60°M" in Fig. 2 is the parallel of 60°N magnetic latitude.) Their geographic latitudes differ by about 3°. (The solid line marked "57°G" is the parallel of 57°N geographic latitude.)

The significance of these results requires some discussion. In the first place, it should be pointed out that by using the mean value of the spread-*F* index for the whole night we have eliminated the effect of the diurnal variation. If we had evaluated the correlation coefficient between the hourly figures, we would have

VOL. 12 1958

found a positive correlation in all cases, because the diurnal variation is similar at the three stations. Secondly, it should be noted that a lack of correlation between two stations does not necessarily imply that if spread-*F* echoes are present at one station they are absent at the other. The correlation coefficient takes account only of deviations from the monthly mean value, and it is these deviations which are uncorrelated.

We shall now attempt to interpret these results in terms of the spatial structure of the irregularities. If we had available a measure of the degree of irregularity at every point in the horizontal plane, we might expect to find that it would have the form of a two-dimensional function, which had a certain mean value together with random variations around the mean. Our results place certain limits on the horizontal scale of this random pattern. The lack of correlation between Slough and Inverness shows that the scale in the north–south direction is less than 720 km. The positive correlation between Inverness and Oslo shows that the scale measured in that direction is of the order of 920 km, and possibly much larger. We conclude that the pattern has a structure which is elongated in a roughly east–west direction. It is possible that the direction of elongation coincides with the parallels of geomagnetic latitude, though this cannot be decided with certainty from the present results. Such a pattern could be imagined to be built up by the superposition of "bands" of irregularities, each band lying along a parallel of latitude. The fact that there is a correlation at any one station between the spread-*F* index for one night and the next suggests that the structure of the pattern tends to recur, and the bands appear in similar geographical positions on successive nights.

3. A Study of the Correlation Between the Scintillations of a Radio Star and the Spread-*F* Index at Two Ionospheric Stations

(a) *Definition of the "scintillation index"*

Ryle and Hewish (1950) defined in "index of fluctuation" of the waves from a radio star as the ratio of the mean deviation of the intensity to the mean intensity. For the present purposes it was sufficient to estimate the value of this quantity from an inspection of the records without actual measurements, and an index on a scale of 0–5 was used. We shall call this quantity the "scintillation index." The records used were for the source in Cassiopeia (23.01) as observed at Cambridge (52°N, 0°E). A scintillation index was assigned to the records for each hour of the four months previously considered for which records were available. In general there were appreciable scintillations only at night; the daytime records were in any case difficult to use owing to the presence of interference.

A comparison of the scintillation results with the spread-*F* index at Slough and Inverness is made in the next two sections. The spread-*F* results for Oslo were not considered sufficiently reliable to justify their use in a detailed comparison.

(b) *The correlation between the scintillation index at Cambridge and the spread-*F *index at Slough*

A line from Cambridge to the source in Cassiopeia intersects the ionosphere in a point whose position depends on time as shown in Fig. 2. Three curves are shown

for irregularities at three different heights. The figures on the curves are the time measured in hours after the upper culmination of the source (i.e. the hour angle). It will be seen that the effective region of the ionosphere for the production of scintillations is sometimes near Slough and sometimes hundreds of kilometres away. We have seen in section 2(c) that the spatial distribution of the irregularities is such that there is no correlation between points separated by distances of this order. We should, therefore, expect to find that near upper culmination the scintillation index would be correlated with the spread-*F* index at Slough, but at several hours away from upper culmination there should be no correlation.

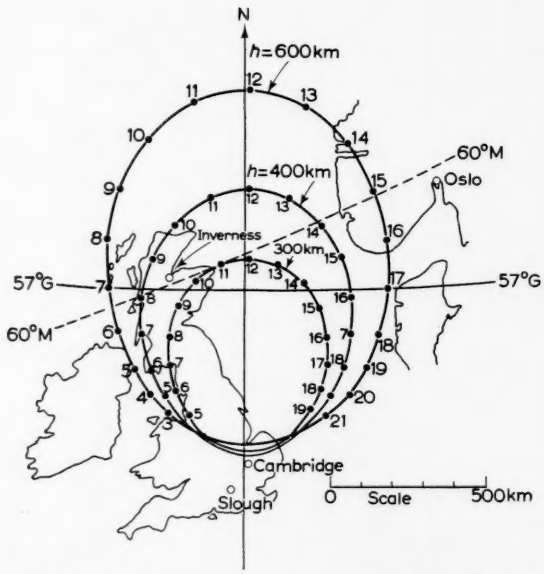

Fig. 2. Map showing the three ionospheric observatories at Slough, Inverness and Oslo. The curves show the locus of the point of intersection with the ionosphere of a line from Cambridge to the source in Cassiopeia.

The correlation coefficients were calculated as follows. A particular hour was chosen and the series of scintillation figures for successive days of the month were compared with the corresponding spread-*F* figures. Each of the four months was analysed separately. By evaluating the correlation coefficient at a fixed time, the effect of the diurnal variation of the two quantities was removed. Any seasonal trend in the two quantities over one month was believed to be negligible. Thus the correlation coefficients refer only to the random variations of the two quantities, and are unaffected by diurnal or seasonal variations.

A correlation coefficient is obtained in this way for each hour, and can be plotted as a function of local solar time or of the hour angle of the source. A given solar time corresponds to a different hour angle at different times of year. It was considered to be sufficiently accurate to use a mean value for the difference between solar time and hour angle for each month.

VOL. 12 1958

In Fig. 3 the correlation coefficient between the scintillation index observed at Cambridge and the spread-*F* index at Slough is plotted as a function of the hour angle of the source. A mean line has been drawn by eye through the points, which all lie within $\pm 0{\cdot}2$ of the line. As this is the error in the value of the correlation coefficients, the scatter around the mean line is no greater than would be expected

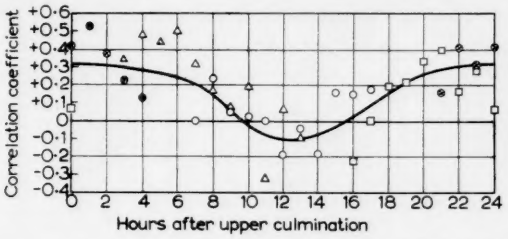

Fig. 3. The variation with hour angle of the correlation coefficient between the scintillation index at Cambridge and the spread-*F* index at Slough.
⊗ September 1954 △ December 1954
○ March 1955 □ June 1955

by chance. The result shows that the correlation is highest near upper culmination, and it is zero, or even slightly negative, near lower culmination.

The line joining the effective region to Slough does not depart very much from the north–south direction. We can therefore investigate the size of the patches of irregularities in a north–south direction in the following way. From Fig. 2 we see that a given hour after upper culmination corresponds to a certain distance of the effective region from Slough. We can therefore replot the results of Fig. 3 to show

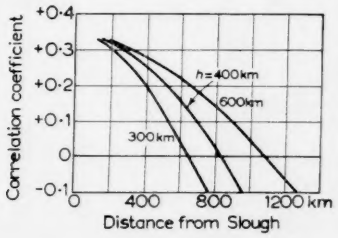

Fig. 4. The correlation coefficient between the scintillation index and the spread-*F* index at Slough plotted as a function of the horizontal distance between the effective region of the ionosphere and the observing station at Slough.

how the correlation varies with the horizontal distance of the effective region from Slough. This is done in Fig. 4 for three different assumed heights of the irregularities.

The correlation coefficient does not approach unity at zero distance as might at first sight be expected. The reasons for this may be any or all of the following:— (i) inaccuracies in the scintillation and the spread-*F* indices, which have been assigned to the records without quantitative measurements, (ii) variations in the heights of the irregularities which, if above the maximum of the *F*-region, may cause scintillation but no spread-*F* echoes, (iii) variations of the vertical thickness

of the irregular region, which would affect the scintillation index more than the spread-*F* index. For these reasons, one would not expect to find perfect correlation even if the two phenomena were measured at the same place in the ionosphere. In spite of these difficulties, the curves of Fig. 4 serve to show the horizontal scale of the patches of irregularities. For example, if the height of 600 km is assumed, the correlation coefficient falls to one-half of its value at zero separation in a distance of about 800 km, and if 400 km is assumed, in a distance of about 600 km.

We can use the results of Fig. 4 to make some deductions about the height of the irregularities. We have seen in section 2(c) that there is zero correlation

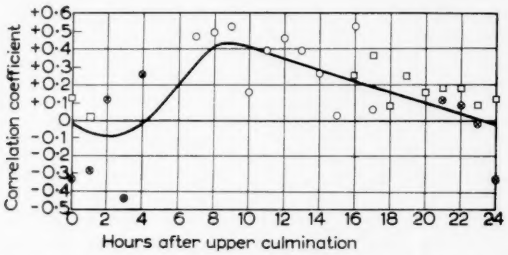

Fig. 5. The variation with hour angle of the correlation coefficient between the scintillation index at Cambridge and the spread-*F* index at Inverness.
⊗ September 1954
○ March 1955 □ June 1955

between the values of the spread-*F* index at points separated by 720 km in a north–south direction. This would be inconsistent with the curves of Fig. 4 unless the irregularities were situated at heights below about 300 km. We shall give other reasons later for rejecting a height much below 300 km, and we therefore adopt this figure as the most probable height. We then see from Fig. 4 that the correlation coefficient would drop to one-half of its value at zero separation in a distance of 450 km. We adopt this figure as the best estimate of the "size" of the patches in a north–south direction.

(c) *The correlation between the scintillation index at Cambridge and the spread-*F *index at Inverness*

In Fig. 5 the correlation coefficient between the scintillation index at Cambridge and the spread-*F* index at Inverness is plotted as a function of the hour angle.

During December 1954, the correlation coefficient was found to be small at all times. It is suggested that this results from the fact that spread-*F* echoes were so prevalent at Inverness in this month that an index of 3 was obtained for most of the night, so that the variations were not reproduced in the index. For this reason no points have been plotted in Fig. 3 for December.*

It will be seen from Fig. 2 that the effective region of the ionosphere for the

* It will be noted also that in Table 4, December is the only month which shows zero correlation between Inverness and Oslo. This is again believed to be due to the unreliability of the Inverness figures for this month.

VOL. 12 1958

production of scintillations is nearest to Inverness at about nine hours after upper culmination; the exact time of closest approach depends on the height assumed for the irregularities. The experimental curve of Fig. 5 shows an observed maximum of correlation near this time. The accuracy is not great enough to permit an exact determination of the time and hence of the height of the irregularities. We can, however, make some deductions about the height from the shape of the experimental curve. If the irregularities were at 600 km, the appropriate curve of Fig. 2 shows that the correlation should rise to a maximum seven hours after upper culmination, i.e. at the time of closest approach to Inverness, and should then fall off again quite rapidly, owing to the rapid increase in the distance from Inverness. This is not oberved in the experimental curve, which is asymmetrical around the maximum, and maintains a positive correlation for many hours after the maximum. This is readily explained if the irregularities are near 300 km; for Fig. 2 then shows that after passing Inverness, the effective region moves approximately along a line of magnetic latitude. Similar arguments rule out a height much below 300 km.

These conclusions are somewhat uncertain with the present data, owing to the large scatter of the experimental points, but they could be made more precise if more results were analysed in a similar way. The method could be extended by the use of data from more ionospheric stations. It is hoped that this type of analysis will be applied to the large amount of data on scintillations and spread-*F* echoes which will be accumulated during the International Geophysical Year.

Curves similar to those of Fig. 4 cannot usefully be plotted for Inverness. This is because the line joining the effective region to Inverness varies greatly in direction; sometimes it is north–south and sometimes east–west.

4. Discussion

The results of section 2 and section 3 have shown that the irregularities which cause spread-*F* echoes and scintillations are not distributed uniformly in the horizontal plane, but occur in bands which lie along parallels of latitude. The dimensions of these bands are of the order of 450 km at right angles to the parallels of latitude, and considerably greater along the parallels of latitude.

There appears to have been no previous work on the correlation of spread-*F* echoes at separated stations. There have been simultaneous observations of scintillations at two separated stations, and the results are consistent with the conclusions of the present paper. Thus Smith, Little and Lovell (1950) compared the occurrence of scintillations at Jodrell Bank and Cambridge, a separation of 210 km in a roughly north–south direction. The observations were made near upper culmination of the sources in Cygnus and Cassiopeia. It was found that the records were generally *either* steady at both sites *or* fluctuating at both sites on a given night. There were, however, approximately 10 per cent significant exceptions when the records were fluctuating at one place but not at the other. We concluded in section 3(b) that the correlation coefficient in a north–south line falls to one-half in a distance of 450 km. We should therefore expect a good but not perfect correlation at 210 km, which is consistent with the results obtained. Again F. G. Smith (private communication) compared the occurrence of scintillations at Cambridge, England and Washington, D.C., U.S.A., during six months of 1954

and found zero correlation. This result is again consistent with the sizes of the irregular regions deduced in the present paper.

We will consider next the significance of the fact that the irregular regions tend to follow parallels of latitude. In connection with this fact we should also note that Spencer (1955) concluded that the individual irregularities were elongated along the direction of the earth's magnetic field. Both results indicate a marked magnetic control. They are also very similar to results of experiments on radio reflections from aurorae. The auroral echoes are found to be aspect sensitive in a way which could be explained if they were returned from ionized columns aligned along the direction of the earth's field (Booker, Gartlein and Nichols, 1955). The reflecting regions also occur in bands along parallels of geomagnetic latitude, as, indeed, do some types of visible aurorae (Bullough and Kaiser, 1954, 1955; Kaiser, 1957). Aspect-sensitive radio echoes have also been obtained from both the *E* and *F* regions at lower latitudes, where ordinary auroral echoes would not normally be expected (Peterson, Villard, Leadabrand and Gallagher, 1955). Peterson *et al.* described the echoes as rather like a weak southerly extension of the auroral-type echoes. It now seems likely that the irregularities which cause these echoes also cause spread-*F* echoes and scintillations. The similarity of all these phenomena has also been pointed out by Kaiser (1956) and Booker (1956).

If spread-*F* echoes are produced by irregularities aligned along the earth's magnetic field, it seems probable that the mean direction of arrival of the scattered waves would be at an angle to the vertical. Such directional effects would be worth looking for.

The *height* of the irregularities deduced in section 3(b) and (c) was 300 km. Hewish (1952) obtained a value of about 400 km from a diffraction argument. He also compared the scintillation results with the fading of waves reflected at vertical incidence, and found that on some occasions scintillations were present when the ionosphere behaved as a perfectly smooth reflector. From this he concluded that the irregularities were, on these occasions, above the level of reflection. This again led to a height of 400 km or above. It now seems likely that these observations could be explained differently. The effective region for the production of scintillations was at a considerable horizontal distance from the point of reflection, so that in view of the results of the present paper, a close correlation with the fading of the reflected wave would not be expected. The argument therefore loses its force. Booker (1956) rejected a height as great as 400 km on theoretical grounds, if the irregularities were due to turbulence. Kaiser (1956) considered that the existence of stable irregularities with linear dimensions less than the mean free path was unlikely. With the dimensions given by Spencer (1955) this sets an upper limit to the height at about 250 km. It should, however, be pointed out that Spencer's figure of 3 km for the size of an individual irregularity relates only to the size across the direction of the earth's magnetic field. Owing to the inhibiting effect of the field on diffusion, an irregularity could persist for some time even if its size measured across the field was smaller than the mean free path.

We conclude that there is no valid objection, experimental or theoretical, to a height of 300 km. There is, of course, no reason why the irregularities should not be spread over a considerable range of heights centred on this value.

VOL. 12 1958

Acknowledgements—This work has been carried out during the tenure of an Imperial Chemical Industries Fellowship. I am indebted to the Director of Radio Research, D.S.I.R., for making available the $h'(f)$ records for Slough and Inverness, and to my wife for help with the calculation of the correlation coefficients.

References

Bolton J. G., Slee O. B. and Stanley G. J.	1953	*Aust. J. Phys.* **6,** 434.
Booker H. G.	1956	*J. Geophys. Res.* **61,** 673.
Booker H. G., Gartlein C. W. and Nichols B.	1955	*Ibid.* **60,** 1.
Booker H. G. and Wells H. W.	1938	*Terr. Mag. Atmosph. Elect.* **43,** 249.
Bullough K. and Kaiser T. R.	1954	*J. Atmosph. Terr. Phys.* **5,** 189.
Bullough K. and Kaiser T. R.	1955	*Ibid.* **6,** 198.
Dagg M.	1957	*J. Atmosph. Terr. Phys.* **10,** 194.
Dagg M.	1957	*Ibid.* **10,** 204.
Hartz T. R.	1955	*Canad. J. Phys.* **33,** 476.
Hewish A.	1952	*Proc. Roy. Soc.* A **214,** 494.
Kaiser T. R.	1956	*The Airglow and the Aurorae* p. 156 Pergamon Press, London.
Kaiser T. R.	1957	*J. Geophys. Res.* **62,** 297.
Little C. G. and Maxwell A.	1951	*Phil. Mag.* **42,** 267.
Peterson A. M., Villard O. G. Jr., Leadabrand R. L. and Gallagher P. B.	1955	*J. Geophys. Res.* **60,** 497.
Reber G.	1954	*Ibid.* **59,** 257.
Reber G.	1956	*Ibid.* **61,** 157.
Ryle M. and Hewish A.	1950	*Mon. Not. R. Ast. Soc.* **110,** 381.
Smith F. G., Little C. G. and Lovell A. C. B.	1950	*Nature, Lond.* **165,** 422.
Spencer M.	1955	*Proc. Phys. Soc.* B **68,** 493.
Wells H. W.	1954	*J. Geophys. Res.* **59,** 273.
Wild J. P. and Roberts J. A.	1956	*J. Atmosph. Terr. Phys.* **8,** 55.
Wright R. W., Koster J. R. and Skinner N. J.	1956	*Ibid.* **8,** 240.

Journal of Atmospheric and Terrestrial Physics, 1958, Vol. 12, pp. 46 to 56. Pergamon Press Ltd., London

The electron distribution in the ionosphere over Slough—I. Quiet days

J. O. Thomas, Jenifer Haselgrove and Audrey Robbins
Cavendish Laboratory, Cambridge

(*Received* 24 *August* 1957)

Abstract—A method of calculating the distribution of electron density with height from experimental virtual height-frequency records using an electronic digital computer is outlined. The method assumes that the $N(h)$ curve is monotonically increasing but makes no other *a priori* assumptions about the shape of the layer. It allows for the effect of the earth's magnetic field.

The method has been applied to a representative selection of $h'(f)$ records taken at Slough and the *F2* layer results for the International Quiet Days are presented and compared with previous work. The height of maximum electron density in the *F2* layer is found to be considerably lower than previously supposed, particularly in the summer and equinox months. Results for the *F1* layer show that the peak of the layer (h_mF1) is lower than previously supposed and that the seasonal variation of h_mF1 is the opposite to that expected for a Chapman layer.

VOL. 12 1958

1. Introduction

It is well known that, from observations of how the equivalent height h' depends on the radio-wave frequency, f, (the $h'(f)$ curve), it is possible to deduce, with certain reservations, how the electron density N varies with height h (the $N(h)$ curve). This paper describes the calculation of $N(h)$ curves from $h'(f)$ data obtained at Slough once every hour on all days of 6 months chosen to represent three seasons at two epochs in the solar cycle.

The results are an improvement on those previously given (Schmerling and Thomas, 1955, 1956), because the calculation (section 2) includes the effect of the earth's magnetic field and because the whole of the observed $h'(f)$ curve is used.

The outstanding features of the new results for ionospherically "quiet" days are reviewed in section 5 and those for "disturbed" days are presented in a companion paper (Thomas and Robbins, 1958). Full details of the results of the calculations are available to all interested workers in the form of a book of tables (Thomas, Haselgrove and Robbins, 1957) from the Radio Section, Cavendish Laboratory, Cambridge.

2. The Method of Computation

The method of calculation makes no *a priori* assumptions about the shape of the layer, other than that the electron density increases monotonically with height, and is a development of the matrix inversion method given by Budden (1954). Using the notation of section 2 of the paper by Budden (1954) (but writing h for z), we have

$$\underline{h'} = \underline{M}\,\underline{D}\underline{h} \tag{1}$$

where

$$\underline{M} = \begin{bmatrix} M_{11} & 0 & 0 & 0 \ldots\ldots\ldots \\ M_{21} & M_{22} & 0 & 0 \ldots\ldots\ldots \\ M_{31} & M_{32} & M_{33} & 0 \ldots\ldots\ldots \\ \vdots & & & \\ M_{n1} & \ldots\ldots\ldots\ldots & M_{nm} & \ldots\ldots \end{bmatrix} \quad \text{and} \quad \underline{D} = \begin{bmatrix} 1 & 0 & 0 & 0 \ldots\ldots \\ -1 & 1 & 0 & 0 \ldots\ldots \\ 0 & -1 & 1 & 0 \ldots\ldots \\ \vdots & & & \end{bmatrix}$$

and

$$M_{nm} = \frac{1}{\Delta f} \int_{(m-1)\Delta f}^{m\Delta f} \mu'(n\Delta f, f_0)\, df_0 \qquad m \leqslant n \qquad (2)$$

$$M_{nm} = 0 \qquad m > n$$

$\underline{h}'$ and $\underline{h}$ are regarded as vectors (column matrices) whose elements h'_n and h_n are the virtual and true heights respectively for reflection of a wave of frequency $n\Delta f$.

In forming equation (1) the assumption is made that the gradient dh/df of the $h(f)$ curve is approximately constant in any interval $((n-1)\Delta f, n\Delta f)$. The error caused by making this assumption is greatest near the maximum of a layer where the effect is to reduce the curvature of the layer profile. The error is however negligibly small.

The required true height h may be found from the equation

$$\underline{h} = (\underline{M}\,\underline{D})^{-1}\underline{h}' = \underline{A}^{-1}\underline{h}' \quad \text{where} \quad \underline{A} = \underline{M}\,\underline{D}$$

The elements of the inverted matrix $\underline{A}^{-1}$ were given by BUDDEN, *loc. cit.*, with values of the earth's field and dip angle appropriate to south-east England for a height of 300 km.

It is possible, however, to solve equation (1) for $\underline{h}$, given $\underline{h}'$, without inverting the matrix $\underline{A}$.* We have from (1)

$$\begin{aligned} h'_1 &= A_{11}h_1 \\ h'_2 &= A_{21}h_1 + A_{22}h_2 \\ h'_3 &= A_{31}h_1 + A_{32}h_2 + A_{33}h_3 \\ &\text{etc.} \end{aligned} \qquad (3)$$

* We are grateful to Mr. D. T. CAMINER of Messrs Leo Computers Ltd., for making this suggestion. It is interesting to note that JACKSON (1956) has recently published details of a step-by-step technique for obtaining $N(h)$ curves which is in principle the same as that outlined here.

These equations can be solved one by one to give

$$\begin{aligned} h_1 &= \frac{1}{A_{11}} h'_1 \\ h_2 &= -\frac{A_{21}}{A_{22}} h_1 + \frac{1}{A_{22}} h'_2 \\ h_3 &= -\frac{A_{31}}{A_{33}} h_1 - \frac{A_{32}}{A_{33}} h_2 + \frac{1}{A_{33}} h'_3 \\ &\text{etc.} \end{aligned} \tag{4}$$

Thus a matrix $\underline{B}$ may be formed, defined by

$$\begin{aligned} B_{nm} &= -\frac{A_{nm}}{A_{nn}}, \qquad m \neq n \\ B_{nn} &= \frac{1}{A_{nn}} \end{aligned} \tag{5}$$

The values of $h_1, h_2, \ldots$ can then be found in succession, obtaining h_{n+1} from the formula

$$h_{n+1} = \sum_{r=1}^{n} B_{n+1,r}\, h_r + B_{n+1,n+1}\, h'_{n+1} \tag{6}$$

The calculation was programmed for the EDSAC, the electronic digital computer in the Mathematical Laboratory of the University of Cambridge. A frequency interval $\Delta f = 0{\cdot}1$ Mc/s was found to be adequate even for curves with sharp cusps and for the distorted $h'(f)$ curves often found on ionospherically disturbed days. The method is extremely rapid to use, the complete calculation taking about 1 min./curve. It can be used for any observing station if the appropriate matrix $\underline{B}$ is calculated using three constants (magnetic dip, field strength and the lower frequency limit of the recorder) suitably stored in the machine.

The $h'(f)$ records were read at intervals of 0·1 Mc/s (or under certain conditions of 0·5 Mc/s) down to the minimum virtual height on the record ($h'F2$ by night, $h'E$ by day).

The virtual heights at or near the discontinuities in the $h'(f)$ curves corresponding to the critical frequencies are discussed in section 4.

3. Assumptions and Approximations

In the analysis the effects of collisions are neglected. This neglect is not considered to be of importance. There are two additional assumptions which may introduce discrepancies between the $N(h)$ curve deduced from the data and the true profile.

(1) The electron density is assumed to increase monotonically with height.

(2) It is assumed that at the lowest frequency recorded, the virtual height is equal to the true height for the corresponding electron density.

These assumptions will now be discussed in detail.

VOL. 12 1958

It is well known (DE GROOT, 1930) that it is not possible to deduce the electron distribution uniquely over any range of heights where N passes through a minimum. MANNING (1949) has shown that a direct integral analysis (as in this paper) of the experimental $h'(f)$ curve will give an electron distribution which is monotonically increasing with height and therefore in which there is no valley between the various electron density peaks. If our assumption is incorrect, it will produce the greatest error in the region just above the maximum of the E layer and its effect has therefore been illustrated by numerical examples, as follows.

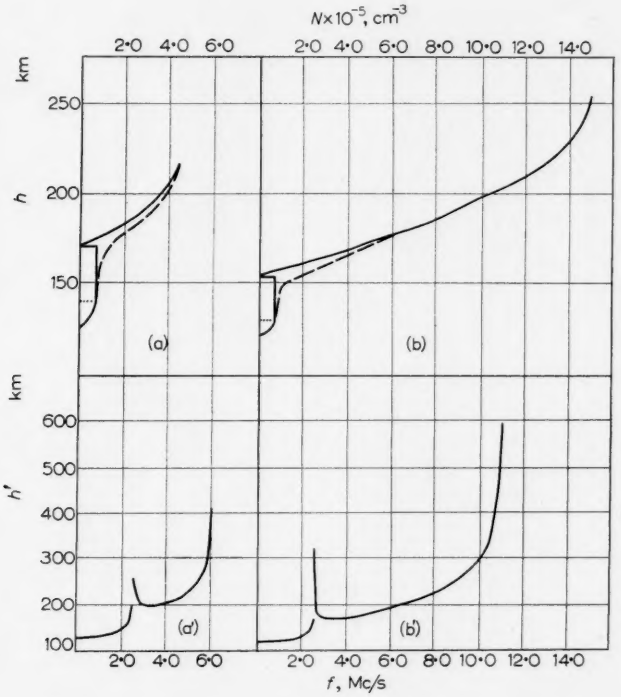

Fig. 1. Assumed $N(h)$ curves and corresponding $h'(f)$ curves (continuous lines). The broken lines are the computed $N(h)$ curves.

It was supposed that the actual $N(h)$ curves had the form shown by the continuous lines in Fig. 1(a,b). The E and F layers are represented by semi-parabolae with parameters chosen to correspond approximately to conditions at noon above Slough in December 1953 and January 1950 respectively. Data given by SHINN (1953, 1954) and BECKER (1957) were used to deduce what the observed $h'(f)$ curves would be like in the presence of the earth's magnetic field (a′ and b′, Fig. 1). These $h'(f)$ curves were then analysed by the method described in this paper and the resulting $N(h)$ curves are shown by broken lines in Fig. 1(a,b). The differences between the continuous and broken lines give an idea of the errors which might be expected to result from our assumption.

It should be emphasized that the results given correspond to the lowest possible height for the electron density profiles and that the actual $N(h)$ curve might lie anywhere within a zone of possible true heights. The lower limit of the zone corresponds to the broken lines in Fig. 1(a,b) and the upper limit to the $N(h)$ curve for the case when there is no ionization between the E and F layers. It is important to note, however, that rocket results show little or no decrease in the electron

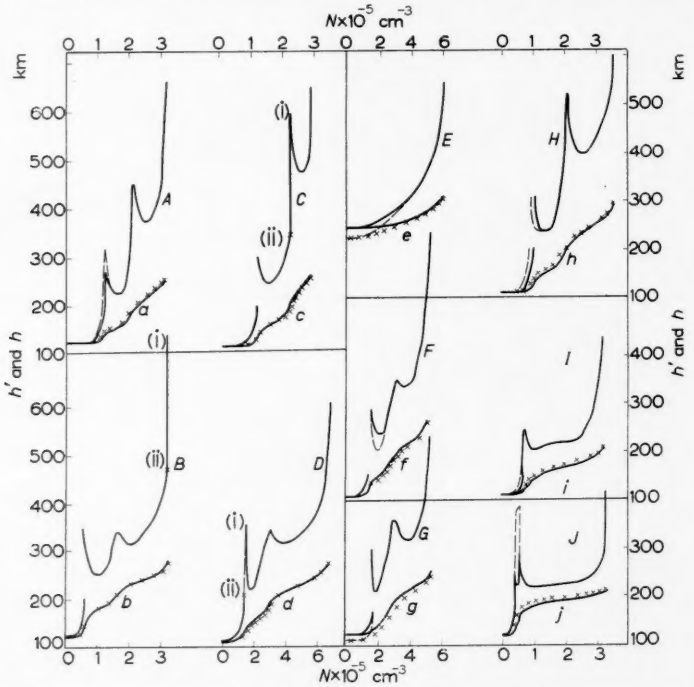

Fig. 2. Test $h'(f)$ curves (drawn as $h'(N)$ curves) and corresponding $N(h)$ curves. The crosses show the $N(h)$ curves corresponding to the alternative $h'(f)$ curves. For details see Table 1.

density above h_mE and that there is similar evidence from other sources (Landmark and Lied, 1957).

The $h'(f)$ curves were analysed down to the minimum virtual height ($h'F2$ by night, $h'E$ by day) and these were taken to be the height of the bottom of the layer concerned (h_0F2 by night, h_0E by day). Failure to allow for the ionization below $h'E$ by day affects the E layer electron density profiles but produces a negligible error in the $F1$ and $F2$ layers.

At night the lowest recorded virtual height for the Slough recorder is $h'F2$ and failure to allow for the effect of ionization below $h'F2$ may introduce serious errors.

There is some evidence that ionization persists throughout the night in the E region with a density corresponding to a critical frequency of about 0·5 Mc/s (Watts and Brown, 1954). An estimate of the group retardation produced by this ionization below the F layer may be made by supposing that the region between

VOL. 12 1958

100 and 250 km is filled with a uniform electron density having a critical frequency f_c. Thus if $f_c = 0{\cdot}5$ Mc/s and the lowest observable frequency was 1 Mc/s, then the group retardation, including the effect of the earth's magnetic field, would be 7 km, and since the observed value of h' at 1Mc/s would determine the lower edge of the $N(h)$ curve, that edge itself would be too high by this amount. At a frequency of 2 Mc/s the extra retardation would be 3 km.

Table 1

Source of reading error	See Fig. 2		Magnitude of the assumed error	True height error			Direction of probable error
	Assumed $h'(N)$	Corresponding $N(h)$		Lower $F1$	Upper $F1$ Lower $F2$	Upper $F2$	
Interpolation of h' near f_0E*	A	a	See Fig. 2	5	4	2	low
Difficulty in measuring a steep $h'(f)$ curve†							
(a) Curve steep at f_0F2	B	b	h' at the critical frequency	0	0	5	low
(b) ,, ,, f_0F1	C	c	given by points (i) and (ii)	0	5	3	low
(c) ,, ,, f_0E	D	d	in Fig. 2	8	5	3	low
Error in measurement of the minimum virtual height (e.g. due to presence of E_s)							
(a) $h'F2$ at night	E	e	$h'F2$ wrong by 15 km (Fig. 2)		15	6 ($f_0F2 = 7{\cdot}0$ Mc/s)	random
(b) $h'F1$	F	f	error of 20 km in $h'F1$	10	6	5	random
(c) $h'E$	G	g	10 km	10	5	4	random
Error in measurement of f_0E	H	h	0·2 Mc/s	15	6	3	random
$h'(f)$ trace not visible near f_0E; presence of $E2$‡	J	j	Trace not visible for 0·3 Mc/s (Fig. 2)	10	6	3	random
Shape of E layer $h'(f)$ curve	I	i	See Fig. 2	5	3	1	random
Error due to reading h' at nearest 0·1 Mc/s below f_0F2§				0	0	10	low

* PEKERIS (1940) has shown that the assumption of finite, instead of infinite, values of h' at the critical frequency does not cause large errors. When it was necessary to interpolate, h' was given values roughly mid-way between the curves (A) with a maximum value at the E-$F1$ cusp of about 300 km. The average error likely to arise is about one-half of the difference between the true heights shown in Fig. 2(a).

† The trace appears so steep as to be almost vertical over a large range of virtual height at f_0F2 in about 1 record in 2. In these cases, we have read the virtual height at the mid-point of the vertical portion. An alternative might be to read to the cross on the $h'(N)$ curve in Fig. 2. It seems probable that if a higher frequency sensitivity had been available, h' would have been greater (corresponding to the top height in Fig. 2(B)) and our true heights in these cases are therefore probably on the low side.

‡ In these cases the normal interpolation would correspond to an $h'(N)$ curve mid-way between the two shown and the true height errors are about one half the difference between the two extreme $N(h)$ curves shown (Fig. 2 (j)).

§ In the calculation, readings of h' must be given at all integral multiples of 0·1 Mc/s. If the critical frequency is not an integral multiple of 0·1 Mc/s, the first height read is that corresponding to the nearest multiple of 0·1 Mc/s below the true critical frequency. For this reason h_mF2 may be too small. During storms when f_0F2 may only be 0·2 Mc/s above f_0F1, this effect will of course be very important. Even then, however; the error is unlikely to be greater than 20 km.

The importance of this underlying ionization is, however, greatest near sunrise and sunset when f_0E may be only just below the lowest frequency of the recorder. If f_c were 0·8 Mc/s, the corresponding extra group retardation would be 10 km at 1·5 Mc/s and 6 km at 2 Mc/s.

When the lowest frequency recorded is from the E layer, lack of measurements on lower frequencies will affect the form of the E layer seriously, but the effect on the form of the F layer is slight. Accurate measurements on the E layer now in progress at this laboratory suggest that the E layer heights quoted here may be up to 10 km too high; the variations of these heights are, however, qualitatively correct.

4. Accuracy of the Results

Good records can usually be read to an accuracy of ± 5 km in h' and of $\pm 0{\cdot}1$ Mc/s in f. In order to examine the effect of errors in reading the $h'(f)$ curves a series of extreme values were read off a number of test curves and the corresponding $N(h)$ curves deduced (Fig. 2). The errors which can arise are shown in Fig. 2 and summarized in Table 1.

It should be noted that these reading errors are not all likely to occur on the same record and that many are of a random kind which if present together will not be additive.

Table 2

Possible errors	$N(h)$ curve error		
	Night ($F2$)	Day	
		E and $F1$	$F2$
(1) Monotonically increasing $N(h)$		low <20 km near bottom of $F1$ layer <5 km near h_mF1	low <5 km
(2) Neglect of ionization below minimum virtual height recorded			
(a) $h'F$ (night)	high (see Thomas, Haselgrove & Robbins (1957)) $\geqslant 20$ km low down $\geqslant 10$ km at h_mF2 for $f_0F2 = 2$ Mc/s		
(b) $h'E$ (day)		high <5 km at h_mE	high <1 km
(3) Reading errors (see Table 1)	$\geqslant 10$ km	$\geqslant 15$ km probably low	$\geqslant 10$ km probably low
(4) Linear variation of h with f		high <5 km	high <5 km

An attempt to summarize the effect of all the errors which may arise is made in Table 2. It is interesting to note that errors (1) and (3) (Table 2) are in a direction such that they tend to cancel errors (2) and (4).

Due regard to the considerations mentioned above leads us to suppose that at night the heights in the electron distributions deduced for the F layer are accurate to ± 10 km, except, possibly, low down if there is considerable ionization below the F layer. By day the heights for the $F2$ layer and the upper part of the $F1$ layer

VOL. 12 1958

are also accurate to ± 10 km. The heights in the lower part of the *F1* layer may be less accurate than this.

The major inaccuracies mentioned above are of a random type and when averages are taken the error is reduced. The rest of the paper is concerned with averages of this kind.

5. Discussion of Results

The electron distribution has been determined for the ionosphere above Slough (lat. 51·5°N, long. 0·5°W) for every hour in each day of 6 months chosen to represent summer, equinox and winter in a year of high and a year of low sunspot

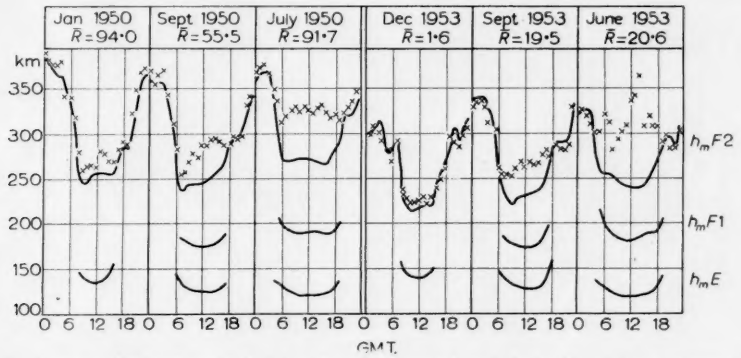

Fig. 3. Average diurnal variation for the 10 International Quiet Days in each month of the heights of the electron density maxima h_mF2, h_mF1 and h_mE. The crosses show the variation of h_mF2 for the same days from the Slough bulletins. $\bar{R}$ is the average relative Zürich sunspot number for the International Quiet Days.

number (January, September, July 1950; December, September, June 1953) when the record could be analysed by the method described here. Out of 4,392 records, 3,883 were analysed. The results have been published (Thomas, Haselgrove and Robbins, 1957) as a book of tables of electron density against height and time and may be obtained from the Radio Section, Cavendish Laboratory, Cambridge.

A discussion of the results will here be confined to the averages obtained for the 10 International Quiet Days in each month.

We consider first the heights h_mE, h_mF1 and h_mF2 of the electron density maxima in the *E*, *F1* and *F2* layers. These are plotted as continuous lines in Fig. 3 and should be compared with the crosses which represent the mean values of h_mF2 for the 10 International Quiet Days from the Slough Bulletin *B*.

These latter results, deduced by a method which approximates to the electron distribution with a parabola, agree well with those deduced by Schmerling and Thomas (1955, 1956), using a Kelso (1952) type of analysis and making no *a priori* assumption about the form of the electron distribution. Both methods neglected the effect of the earth's magnetic field and of group retardation produced by ionization below the *F* region. Fig. 3 shows that the new results are consistently lower than the old.

The lines in Fig. 3 have been drawn in such a way that no individual hourly average value differs from that given by the line by more than 5 km. Values of

h_mF2 on individual quiet days may vary from the mean value at any hour by up to about 30 km at night and 15 km by day. The values of h_mF1 may vary by up to about 12 km from the mean.

When the effect of the earth's magnetic field is included, the heights of the calculated electron profiles are lower than when it is neglected. The magnitude of the systematic error due to neglecting the earth's magnetic field depends on the magnetic latitude (or dip) of the station concerned, the field strength, the frequency of the radio wave and the critical frequency of the layer. For a given critical frequency, the error decreases with decreasing frequency. The error decreases with increasing critical frequency.

During the daytime, the method of analysis, which yields a monotonically increasing $N(h)$ curve from $h'E$, inevitably gives lower heights for the F region compared with the old analysis.

Both of these factors will have their greatest effect on h_mF2 when f_0F2 is relatively low (causing the field correction to be relatively larger) and when the ratio f_0F2/f_0F1 is least (causing the group retardation correction to be relatively larger). Thus the greatest difference between h_mF2 in the present and the previous results occurs in summer in sunspot minimum years. The importance of this alteration is seen in June 1953 (Fig. 3) where the new curve of h_mF2 follows a more reasonable course than the old one.

The values of h_mF1 given in Fig. 3 are of particular interest because they are lower than has usually been supposed; for example, the average midday heights are:

June 1953 180 km	July 1950 190 km
Sept. 1953 175 km	Sept. 1950 175 km

It is interesting to note that a number of rocket flights at White Sands, New Mexico (32·4°N, 106·3°W) gave values of h_mF1 slightly lower still.

The seasonal behaviour of h_mF1 (unlike that of E and the diurnal variation of h_mF1) is the inverse of that expected for a Chapman layer, h_mF1 being greater in summer than in the equinoxes.

There is some slight indication that in summer the sunspot variation of h_mF1 is similar to that of h_mF2, namely that the heights are lower in sunspot minimum than in sunspot maximum, but the effect is not large.

The average total electron content (n_T) of the ionosphere up to the level of h_mF2 for each hour on the International Quiet Days in each month was calculated from the $N(h)$ curves using the trapezium rule and is considered to be correct to ± 5 per cent. A comparison of the N_mF2 and n_T curves for each month (Fig. 4) indicates that the well known bite-out effect in N_mF2 in the summer and equinox is not so marked on the n_T results, but is not entirely removed.

The midday value of N_mF2 is greater in winter than in summer (the winter

VOL. 12 1958

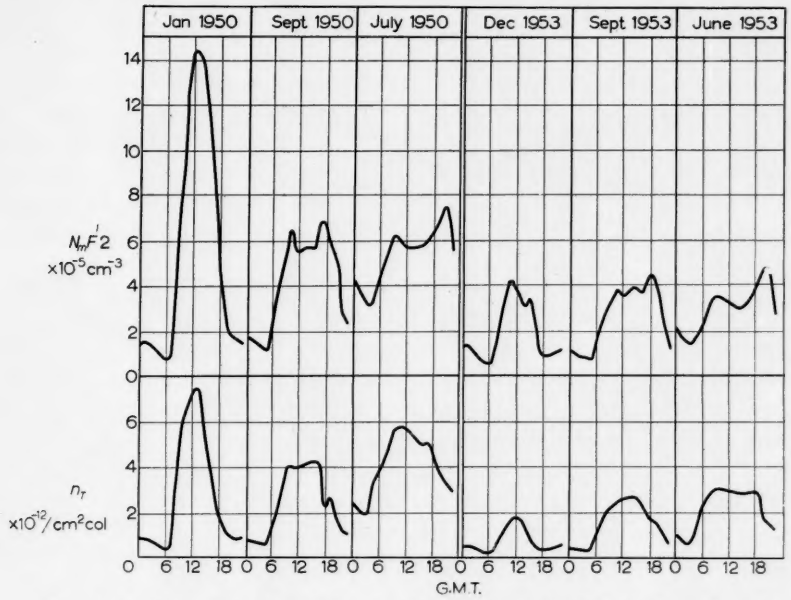

Fig. 4. Average diurnal variation for the 10 International Quiet Days in each month of N_mF2 and n_T (the total electron content up to h_mF2).

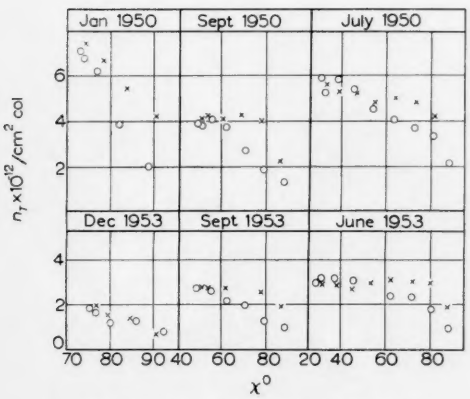

Fig. 5(a). Variation of the total electron content, n_T, with the sun's zenith angle χ. The circles are for morning values and the crosses for afternoon values.

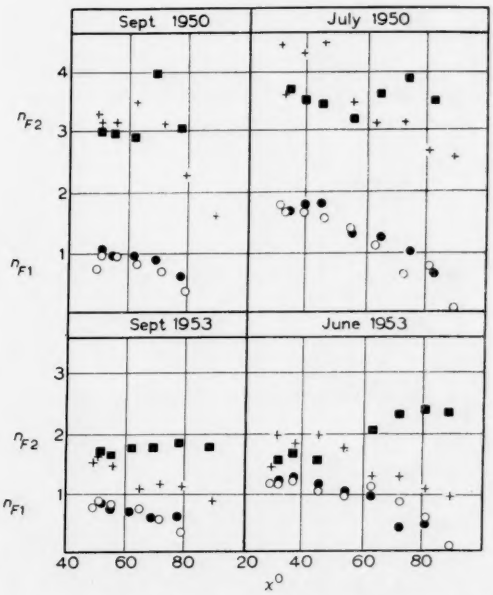

5(b). Variation of the total electron content of the *F1* layer (morning values ○, afternoon values ●) and *F2* layer (morning values ■, afternoon values ×) with χ. The ordinates are total electron content in units of 10^{12} electrons/cm² col.

anomaly) and this effect is much more marked in sunspot maximum than in sunspot minimum years. Fig. 4 shows that in sunspot maximum years this anomaly is repeated in the total electron content, n_T. It cannot therefore be explained simply in terms of a different distribution of the electrons below the peak of the layer.

Fig. 5(a) shows how the average n_T for the International Quiet Days varies with χ, the sun's zenith angle, and Fig. 5(b) shows how the total electron content of the *F1* and *F2* layers varies with χ in summer and equinox.

Acknowledgements—This work was carried out with the assistance of a grant from the Department of Scientific and Industrial Research. We are much indebted to Dr. R. L. Smith-Rose, Director of Radio Research of the Department of Scientific and Industrial Research, London, for the loan of records from Slough. We also wish to thank Dr. M. V. Wilkes, F.R.S., Director of the Mathematical Laboratory in the University of Cambridge for granting permission to use the EDSAC. We are grateful to Dr. K. G. Budden and Dr. K. Weekes of the Radio Group of the Cavendish Laboratory, with whom we have had useful discussion. The authors also wish to thank the computing staff of the Radio Group and in particular Miss D. Mills and Mrs. D. Sargent, who were responsible for the reading, coding and punching of the vast number of records used in the calculations.

References

Becker W.	1957	*Arch. Elektr. Übertr.* **11,** 166.
Budden K. G.	1954	The Physics of the Ionosphere. *Proc. Camb. Ionosph. Conf.* p. 332. Physical Society, Lond.
De Groot W.	1930	*Phil. Mag.* **10,** 521.
Kelso J. M.	1952	*J. Geophys. Res.* **57,** 357.
Landmark B. and Lied F.	1957	*J. Atmosph. Terr. Phys.* **10,** 114.
Manning L. A.	1949	*Proc. Inst. Radio Engrs. N.Y.* **37,** 599.
Pekeris C. L.	1940	*Terr. Magn. Atmos. Elect.* **45,** 205.
Schmerling E. R. and Thomas J. O.	1955	*Tables of F2 Layer Electron Density* (*Series A Number* 1). Cavendish Laboratory, Cambridge.
Schmerling E. R. and Thomas J. O.	1956	*Phil. Trans.* A **248,** 609.
Shinn D. H.	1953	*J. Atmosph. Terr. Phys.* **4,** 240.
Shinn D. H.	1954	The Physics of the Ionosphere. *Proc. Camb. Ionosph. Conf.* p. 402. Physical Society, London.
Thomas J. O., Haselgrove J. and Robbins A. R.	1957	*Tables of Ionospheric Electron Density, Slough* (*England*) (*Series B Number* 1). Cavendish Laboratory, Cambridge.
Thomas J. O. and Robbins A. R.	1958	In Press.
Watts J. M. and Brown J. N.	1954	*J. Geophys. Res.* **59,** 71.

VOL. 12 1958

Journal of Atmospheric and Terrestrial Physics, 1958, Vol. 12, pp. 57 to 67. Pergamon Press Ltd., London

Ionospheric records of solar eclipses

G. H. Munro and L. H. Heisler
Radio Research Laboratories (Sydney Laboratory),
Commonwealth Scientific and Industrial Research Organization
c/o Electrical Engineering Department, University of Sydney

(*Received* 13 *August* 1957)

Abstract—Interpretations of radio observations of solar eclipses are reviewed on the basis of experience gained in the study of travelling ionospheric disturbances.

It is shown that the passage of an eclipse introduces horizontal gradients of ionization which distort the ionospheric reflecting surfaces. This implies that ionosonde soundings are no longer truly vertical and their interpretation as such must introduce errors in deduced ion distributions. In addition, the varying obliquity of the returned rays will distort the apparent variation of ion density with time, and focussing may cause inaccuracies in deduced reflection coefficients.

It is emphasized that during eclipses incidental travelling disturbances will cause additional complications, which further confuse interpretation, and it is shown how they may be detected on ionosonde records.

Confirmation of the presence of curvature is provided by actual records of the 1940 eclipse taken in South Africa by A. J. Higgs.

It is found difficult to estimate the actual errors in past observations, and supplementary observations during future eclipses are suggested to facilitate such corrections and make more precise deductions possible.

1. Introduction

In a paper entitled *Cusp Type Disturbances on Ionospheric Records* (Munro and Heisler, 1956) it was pointed out that a solar eclipse would produce in the *F* region of the ionosphere, transient conditions very similar to those resulting from the passage of a Travelling Ionospheric Disturbance. The fundamental feature is that any temporary localized change in ion distribution results in curvature of the reflecting surfaces effective for radio rays, thereby varying their paths from transmitter to receiver via the ionosphere, and introducing changes in intensity of the returned rays.

There has recently been published *Solar Eclipses and the Ionosphere*, a book which summarizes proceedings at a conference held under the auspices of the Mixed Commission for the Ionosphere at Cambridge in August 1955. Throughout this conference no consideration was given to the geometrical optics of reflection at curved surfaces. Where this is taken into account it is found to contribute materially to the satisfactory interpretation of such controversial features as apparent *F1* stratification, and the disagreement of observed ionization changes with theoretical deductions.

It seems desirable therefore to indicate more specifically where in the interpretation of ionospheric eclipse records it is important to consider the results of curvature, and to indicate how future observations may be designed to permit more accurate deductions.

2. Comparison of Travelling Ionospheric Disturbances (T.I.D.s) and Eclipse Ionospheric Disturbances (E.I.D.s)

Both Travelling Disturbances and Eclipse Disturbances, as they pass overhead, cause the ionization density at any height to be first reduced and then increased.

In an eclipse this is due to the gradual removal and subsequent restoration of the ionizing radiation from the sun. During a travelling disturbance it is mainly due to a redistribution of existing ionization. A typical eclipse perturbation has been shown diagrammatically by Ratcliffe (1956) as deduced from theoretical considerations; and also by various authors (Savitt, 1950) as deduced from actual observations. The T.I.D. perturbation has been described by Munro (1950) from actual observations. In these latter studies it was, however, found more revealing to represent the spatial distribution of ionization by lines (or contours) of equal ionization (isoionic contours) in the vertical plane of propagation of the

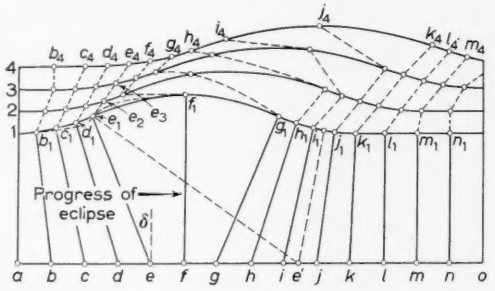

Fig. 1. Diagrammatical representation of reflection points during an eclipse.

disturbance. When the distribution during an eclipse is considered in the same way, as shown diagrammatically in Fig. 1, it is found that the two cases have much in common.

In both the most obvious feature is the curvature of these contours, each of which is the effective reflecting surface for a particular frequency. A ray projected vertically will not in general return to the sender, while a ray which does return to that location (hereafter called the "returned ray") will have been reflected at a point not directly overhead. This can be clearly seen in Fig. 1, which shows the returned rays from contour 1 for a series of equally spaced observing points from a to o. It will be observed that if we proceed at uniform speed from a to e the deviation of the ray from the vertical increases and the reflection point moves along the surface more slowly than does the observing point along the ground. e_1 is the transition point where the curvature of the contour changes from convex to concave; the obliquity of the returned ray (indicated by the deviation angle δ) is here a maximum. As we continue from e to f the reflection point sweeps rapidly from e_1 to f_1 and the ray returns equally rapidly to the vertical. The process then reverses as we continue from f to o. At a fixed observing point therefore, the reflection point will tend to linger at the "shoulders" of the curve as between c_1 and e_1, and g_1 and l_1 where the deviation is greatest.

This diagram shows another feature which is common to both E.I.D.s and T.I.D.s. If several such contours are drawn, the point of inflection on each has a progressive displacement with height, which may be expressed as a tilt of the vertical axis of the disturbance. In the case of T.I.D.s this tilt is forward in the direction of travel, a fundamental feature of these disturbances. However, in the case of the eclipse its slope is backward in the direction of travel of the eclipse,

VOL. 12 1958

due to some extent to the angle of incidence of the ionizing radiation from the sun (or the axis of the eclipse shadow), but mainly to the decrease in recombination rate with height, which is also responsible for the reduction of curvature in the higher isoionic contours as shown in Fig. 1.

The returned ray reflection points for each observing site a to n are indicated on the contours and connected by dotted lines. These lines will therefore represent approximately the loci of the reflection points as the observing frequency is varied between the limits corresponding with reflecting surfaces 1 and 4.

From this diagram we may make two important deductions: firstly, that for a given location the obliquity of the returned ray varies with height of reflection and therefore with frequency (this implies that an ionosonde record is not a truly vertical sounding); and secondly, that retardation (which is a function of the distance between the contours along the ray path) will vary with time for a particular frequency, and that the height, and therefore the frequency, at which it is a maximum will vary with time.

3. Interpretation of Eclipse Records

On first consideration from simple theoretical examination of ion density variation, it might be thought that the curvatures during an eclipse would be too small to cause appreciable retardation or deviation. However, there is ample evidence that such effects exist, and closer examination shows how they may come about. To an observer on the ground the ionosphere rarely presents a plane reflecting surface, as a number of factors contribute to the production of tilts, or introduce curvature, which is the major cause of large deviations of the returned ray from the vertical. Owing to the latitude variations of ionization, tilt and curvature will occur in the north–south direction; in particular, the equatorial anomaly should have quite an appreciable influence. The diurnal variation of ionization will introduce curvature in the east–west direction that will be particularly marked near sunrise and sunset. The perturbation resulting from the passage of the eclipse will be superimposed on these normal variations and, furthermore, the combination of all these factors will tend to magnify the curvature resulting from travelling disturbances which we consider to be present to some extent most of the time in the ionosphere. For example, in Fig. 1 if a perturbation is superimposed on contour 1 as shown by the dotted line, complexities will be observed between points g and j, as for example at e'.

It should be borne in mind that the appearance and disappearance of "stratification," which implies irregularities in the vertical gradient of ionization, must result in curvature of isoionic surfaces; and that this curvature will be greatest where the vertical gradient of ionization is least, as occurs, normally, between the *F1* and *F2* regions and possibly in parts of the region between *E* and *F1*. The change in vertical gradient due to non-uniform recombination will be greatest, in the eclipse case, near the time of maximum obscuration in the appropriate region at the particular observing site.

Thomas and Robbins (1956) discuss vertical movements in the *F* region observed during an eclipse and suggest that modified dynamo currents may result in electrostatic polarization fields being built up in the *F* region as

described by Martyn (1955). This vertical transport of electrons would further distort isoionic contours.

It is important to remember also that for assessing deviation the height or path to be considered is the virtual and not the actual one, by analogy with virtual image in the optical case. We have had practical confirmation of this from phase path observations of travelling disturbances taken by a method previously described (Munro, 1953). This is the probable explanation of Bramley's observation (1956) that the recorded tilt during a partial eclipse (70 per cent totality) was 5°, while that deduced theoretically for a "true height" surface was 2·5°. Taking all these contributions into consideration, the occurrence of serious deviations of returned rays from the vertical during an eclipse becomes probable, particularly at heights where there is normally a small rate of change of ion density.

It is not possible to determine actual curvatures from virtual height records, but it has been found that the simultaneous recording of phase path and group height changes does permit reconstruction of the actual curvature, and estimation of the deviation angle δ shown in Fig. 1. Since past eclipse records seem to consist entirely of group path records, it is difficult to estimate the actual (quantitative) curvature and its resultant effects; but in the following sections the above considerations are applied qualitatively in the examination of the main features of such records.

(a) *Apparent stratification.* The so-called $F1\frac{1}{2}$ is an eclipse occurrence which has been described by Minnis (1955), Ledig *et al.* (1946), Delobeau (1953), and Estrabaud (1953, 1954). The phenomenon as observed on an ionosonde record consists of a retardation peak which generally, in the sequence of records, moves progressively up the $h'f$ curve. We would expect such an effect from consideration of Fig. 1. Ratcliffe (1956) suggested it would occur even if the ionosonde soundings were truly vertical; since in progressing from f to the right of the diagram a retardation peak occurs first at low frequencies between contours 1 and 2, and gradually moves to higher frequencies. The effect of non-vertical reflection is to make this peak more pronounced, because of rapid changes in the ray paths from a region of high retardation to one of low retardation as the frequency increases. This retardation peak will be superimposed on the undisturbed $h'f$ curve and will therefore accentuate any existing *F1* peak when the two are nearly at the same frequency. This explains the problem referred to by Ratcliffe (1956) as to why an eclipse always makes the *F1* layer appear more prominent. It will be noticed also from Fig. 1 that increase in retardation at low frequencies does not occur until the observer is at point g. This would be after totality; and it is observed that $F1\frac{1}{2}$ always occurs at this phase of an eclipse.

The degree of curvature of isoionic surfaces in a finite cone above the observing point will depend upon the zenith angle of the sun at the time of the eclipse. Since for a given time of day this is always smaller in lower latitudes the distortion of isoionic surfaces will be greater. The occurrence of $F1\frac{1}{2}$ is therefore probably related to geographical latitude rather than to geomagnetic latitude as suggested by Ratcliffe (1956).

Sequences similar to $F1\frac{1}{2}$ occurrence during an eclipse are observed as a result

VOL. 12 1958

of T.I.D.s. However, as expected, due to the forward tilt of the wavefront, they progress *down* the *h'f* curve. An example is shown in Fig. 2. The sequence in this case is very similar, but in reverse, to that shown in Fig. 9 of a paper by LEJAY and DURAND (1956). Notice the accentuation of the *F1* trace at 1135.

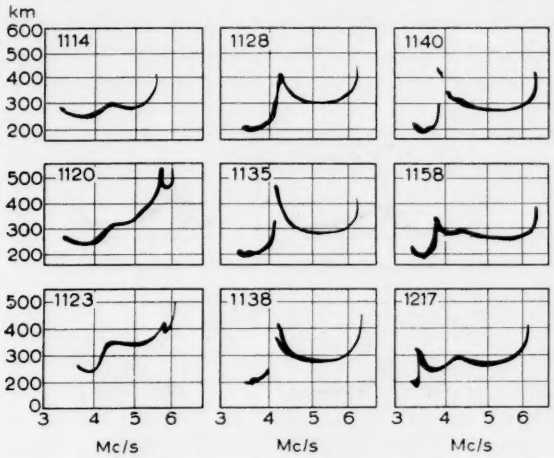

Fig. 2. Travelling disturbance affecting both *F1* and *F2* ordinary ray traces. Camden, 16 May 1954.

We have, by courtesy of A. J. HIGGS, the Ionospheric Prediction Service, and the Commonwealth Observatory, been able to examine the original ionosonde records taken by Mr. HIGGS at Victoria West in South Africa during the total eclipse of 1 October 1940. Fig. 3 is a tracing of the record at 1630, 20 min after

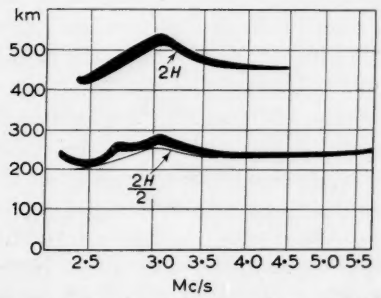

Fig. 3. Eclipse ionosonde record showing "$F1\frac{1}{2}$" on first reflection only of the ordinary ray. Victoria West, 1630 hr 30° E.M.T., 1 October 1940.

totality, and shows very clearly the double peak in the *F* region associated with "$F1\frac{1}{2}$" phenomena as already discussed. It is interesting to note, however, that only a single peak occurs in the second reflection. Moreover, it is found that the apparent height of the second reflection is less than twice that of the first reflection only over the range where the peaks occur (see Fig. 3, in which the line $2H/2$ represents half the apparent height of the second reflection.) This seems to be

conclusive evidence of oblique reflection at frequencies near these peaks. The deviation necessary to produce the maximum discrepancy in the observed virtual heights of F and $2F$ is of the order of 5°.

(b) *Complex reflections.* It has been shown in considering T.I.D.s (Munro and Heisler, 1956) that for a given percentage change in ionization due to a disturbance, the curvature and retardation will be a function of the initial gradient of ionization as well as the rate of change of ionization, and will therefore tend to reach a maximum in the *F1* region. In an eclipse this tendency is further

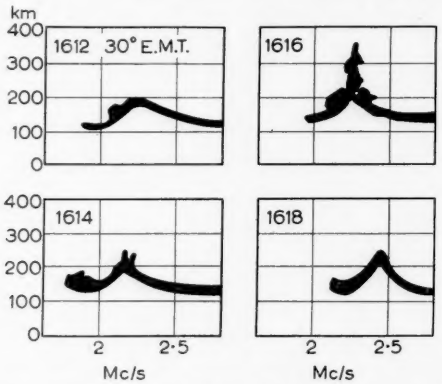

Fig. 4. Complexities on eclipse ionosonde records (ordinary ray). Victoria West, 1 October 1940.

VOL. 12 1958

increased by the rate of recombination being relatively more rapid in the lower F region than at greater heights. We should therefore expect complex reflection, such as that appearing at 1138 in Fig. 2, to be a feature of records when the two retardation peaks are superimposed or close together; and, in fact, the existence of complex reflections is a criterion of non-vertical reflection. Fig. 4, a series of tracings of records taken at Victoria West, shows the rapid development of complex reflections at 1614 and 1616. Notice the similarity between the 1614 record on this figure, and the record for 1138 on Fig. 2 which is due to a T.I.D.; also the remarkable difference between the records for 1616 and 1618. These features emphasize the necessity for ionosonde observations at short intervals, preferably supplemented by $h't$ records, to make possible a complete analysis of an E.I.D. There seems to be some indication of complexities in published records, for example, at 0920 in Fig. 9 of a paper by Lejay and Durand (1956); and a plot (Fig. 3) in a paper by Bibl and Delobeau (1955) of *F1* height against time during an eclipse shows definite complex reflections at and after totality. It is considered likely that such complexities occur frequently in eclipse records but have hitherto been neglected because of the difficulty of their interpretation.

(c) *Anomalies in variation of ionization.* Much consideration has been given to non-uniformity in changes of ionization as deduced from ionosonde records, and efforts have been made to explain them as due to irregularities in the radiation from different parts of the sun's disc or the chromosphere (Minnis, 1955). Consideration of Fig. 1 will show that serious errors can be introduced by assuming

that an ionosonde record gives a truly vertical sounding. For a given ionosonde observing point, the ionization minimum (i.e. the apex of the curve) can be overhead only for a very short period for each particular frequency successively. Moreover, we must realize that, unlike a T.I.D., the eclipse shadow has an approximately circular horizontal section, and also generally has an inclination to the vertical across, as well as along, its track. The case of a circular disturbance was considered by MUNRO (1953) for a single frequency, and it was shown that a returned ray could be vertical only if the apex of curvature passed directly overhead; so that in the case of an eclipse, unless the axis of the shadow cone is vertical it will never be possible to make a truly vertical multifrequency sounding. Moreover, it can be seen in Fig. 1 that as the disturbance passes overhead the reflection point for a given frequency makes an oscillation about the vertical and tends to linger at the "shoulders" of the curve. Therefore a plot of observed critical frequency against time on a linear scale would not correctly represent the change of ionization with time. This will mean that during the eclipse the ionization will appear to decay at first more slowly and then more rapidly than is actually the case, the actual variation depending upon the shape of isoionic contour. This would therefore give the impression of non-uniform radiation from the sun of just the type observed. RATCLIFFE (1956) in a criticism of non-uniform radiation hypothesis discusses the relationship $(N_1^2/N_0^2) = (I_1/I_0)$ where N_1 and N_0, I_1 and I_0 are the electron densities and the rate of production of ions at times t_1 and t_0 respectively. He points out that in most eclipse cases the observed value of $(N_1^2/N_0^2) < (I_1/I_0)$ and that this is particularly noticeable when t_0 occurs during totality so that I_1/I_0 is infinite, suggesting that at, or slightly after, totality the value of I_0 is greater than expected. On the above hypothesis this would be so, as an ionosonde sounding at or near totality is never vertical, and would record the higher ion density of those regions each side of eclipse centre. These considerations will apply most markedly in the F region. For the *E1*, if it is a thin layer, there will be less curvature; but its effects may still be appreciable. Phase-path recording would be particularly useful in estimating its amount and significance. LANDMARK (1957) using this technique has since shown tilts in the E region of the order of 5°.

(d) *Absorption.* In measuring absorption during an eclipse effects of curvature must be taken into account also. In Fig. 1 it is apparent that towards the beginning and end of the eclipse the curvature of reflecting surfaces is convex downward, and there will therefore be some loss of the returned ray due to divergence on reflection. In the middle portion, however, the curvature is concave downward, and there will be an increase in the recorded intensity of the returned ray due to focusing. Where the curvature approaches the critical value, as just before and after the complex reflection, this increase will be very great. These effects will be additional to those resulting from non-vertical reflection of the returned ray; and the combination must introduce errors in interpretation of absorption measurements made during an eclipse, particularly of F-layer absorption (PIGGOTT, 1956).

(e) *True height estimation.* It is not valid to determine vertical ionization distributions from eclipse ionosonde records by integration processes such as MANNING's (1947) or KELSO's (1952), as the path of the returned ray varies

considerably with frequency. Any such analysis must lead to error in estimating distributions of ionization.

(f) *Travelling ionospheric disturbances.* There is little doubt that pronounced *F2*-layer stratification and appearance of "*G* layer" on control days, mentioned by Hennessey and Torres (1956) and more recently Minnis (1957), are due to T.I.D.'s of the type described by Munro and Heisler (1956); and the possibility must not be overlooked of presence of T.I.D.'s on eclipse days. Higgs' records of the 1940 eclipse are particularly suitable for the detection of travelling disturbances, as they were taken at 2 min intervals. Moreover, Higgs was very conscious of the prevalence of such "pulsations," as he termed them, since he had been studying them in Australia (Munro, 1950 *loc. cit.*); and in his paper (Higgs, 1942) emphasizes their disturbing effect. In Fig. 5 we have plotted the variations in virtual height at three discrete frequencies during the eclipse period.

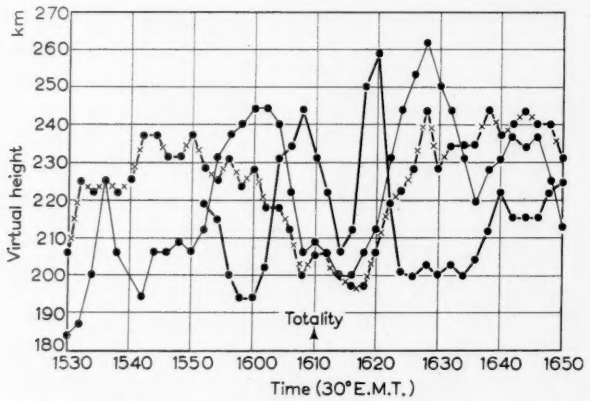

Fig. 5. Variation of virtual height at three different frequencies during the eclipse at Victoria West, 1 October 1940. (—●— 2·5 Mc/s, —●— 3·0 Mc/s, —×— 3·5 Mc/s.)

It will be seen that each curve shows a series of peaks with an approximate symmetrical distribution about the time of eclipse totality, but with a difference in time distribution of the peaks which seems to be progressive with frequency, the corresponding peaks being closer to totality at the lowest frequency. It may appear therefore that this is entirely an eclipse phenomenon, but it is necessary to make a closer examination for other influences.

It has already been mentioned that whereas a T.I.D. anomaly progresses down the *h'f* curve, the comparable eclipse perturbation moves up the curve; so we may use this criterion to distinguish between the two. In Fig. 6 we have plotted, for all virtual height peaks observed, the frequency at which the peak appears against the time of the recording. It will be seen that before totality there are three successive peaks progressing to lower frequencies, and after totality one main peak moving up to higher frequencies. Bearing in mind that in this presentation decreasing ionization will accelerate the downward trend of T.I.D.s and increasing ionization will reduce it, it seems very probable that only the peak designated by crosses is a genuine eclipse effect and the others are T.I.D.s. Any

VOL. 12 1958

doubt in a case like this could be resolved if observations were made at suitably spaced sites; as in general T.I.D.s tend to travel from north to south, or vice versa, and eclipses from west to east. It is also of interest in Fig. 4 that the falling and rising retardation peaks coincide at the same frequency at 1616, which is the time when the complexity first appears, thus confirming our prediction in Section 3(b). It should be noted that the two peaks in Fig. 3 can be identified in Fig. 6.

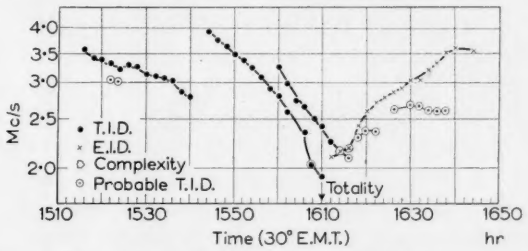

Fig. 6. Movements of virtual height peaks during a solar eclipse (1 October 1940).

The higher one appears to be the true eclipse peak but the lower one could be a travelling disturbance peak modified by the eclipse perturbation. In considering distortion of reflecting surfaces it must be borne in mind that where T.I.D.s are present during an eclipse the effect of the elongated T.I.D. front moving north and south will be superimposed on the circular perturbation due to the eclipse moving from east to west, so that the resulting distortion will be very complex.

It seems to be clearly established therefore that for the accurate interpretation of eclipse records under each of the headings (a) to (f) the effects of curvature must be taken into account.

4. Applications

Knowing the factors introducing uncertainties into the interpretation of records it is possible to plan future observations so that the required corrections can be applied more accurately. The following broad principles are suggested as a guide for this purpose.

(1) Observing sites should be selected if possible so that the middle of the eclipse path will be directly overhead at the required ionospheric height and not at ground level. Central lines of I.G.Y. eclipse paths for ionospheric heights of 100, 200 and 300 kms are published in U.R.S.I. Information Bulletin No. 90.

(2) Observations should be as frequent as possible to record adequately the rapid changes in E.I.D. phenomena.

(3) It would be very useful to take angle of reflection observations on fixed frequencies to supplement the $h'f$ records.

(4) It would be of particular value to record phase path changes as well as virtual height changes on selected fixed frequencies in conjunction with $h'f$ and reflection angle observations.

(5) Finally, comparison of records at different sites some tens of kilometres apart would facilitate corrections for deviation and enable detection of the presence of T.I.D.'s.

The I.G.Y. affords excellent opportunity for co-operative observations of this kind and a planned grouping of stations over a limited area would provide records of far greater value than those from scattered stations at many localities. In particular, organization along these lines during the total eclipse in October 1958 should permit more accurate interpretation of eclipse results, and possibly enhance the value of previous records also.

5. Conclusion

It has been shown that many abnormalities which occur in eclipse records can be explained in terms of oblique reflections. It is to be stressed that this is the rule rather than the exception in most ionospheric measurements, and that the term "vertical incidence" record is a misnomer and is seldom true of actual records, at least of those made during the daylight hours. Any change in stratification is enough to cause curvature of isoionic contours and hence oblique reflection; while any change in ionization which is progressing horizontally must give rise to reflections other than vertical.

It is thus necessary in examining any progressive phenomenon in the ionosphere, such as sunrise and sunset effects, eclipses, and travelling disturbances of any type, to consider effects of deviation.

Acknowledgements—This investigation is part of the research programme sponsored by the Radio Research Board. The authors express their appeciation to the Commonwealth Observatory and the Ionospheric Prediction Service for making available the records of the 1940 eclipse in South Africa and to Mr. A. J. Higgs for permission to use the extracted information; to the University of Sydney, in paticular to Professor D. M. Myers, for provision of facilities in the Department; and to Dr. D. F. Martyn, F.R.S., the Chief Officer-in-Charge of the Radio Research Laboratories, for helpful discussions during the preparation of this paper.

VOL. 12 1958

References

Bibl L. and Delobeau F.	1955	*Z. Geophysik* **21,** 215.
Bramley E. N.	1956	*J. Atmosph. Terr. Phy.* **8,** 98.
Delobeau F.	1953	*Ann. Géophys.* **9,** 317.
Estrabaud S.	1953	*C. R. Acad. Sci. Paris* **236,** 833.
Estrabaud S.	1954	*Note Prélim. Lab. Nat. Radio Électr.* No. 174.
Hennessey J. J. and Torres J. S.	1956	*Solar Eclipses and the Ionosphere* p. 65. Pergamon Press, London.
Higgs A. J.	1942	*Mon. Not. R. Astr. Soc.* **102,** 24.
Kelso J. M.	1952	*J. Geophys. Res.* **57,** 357.
Landmark B.	1957	*J. Atmosph. Terr. Phys.* **10,** 288.
Ledig P. G., Jones M. W., Gresecke A. A. and Chernosky E. J.	1946	*Terr. Magn. Atmosph. Elect.* **51,** 411.
Lejay R. P. and Durand J.	1956	*Solar Eclipses and the Ionosphere* p. 85. Pergamon Press, London.
Manning L. A.	1947	*Proc. Inst. Radio Engrs. N.Y.* **35,** 1203.
Martyn D. F.	1955	*Report Camb. Ionosph. Conf.* p. 254. Physical Society, London.
Minnis C. M.	1955	*J. Atmosph. Terr. Phys.* **6,** 91.

Minnis C. M.	1957	*J. Atmosph. Terr. Phys.* **10,** 229.
Munro G. H.	1950	*Proc. Roy. Soc.* A **202,** 208.
Munro G. H.	1953	*Proc. Roy. Soc.* A **219,** 447.
Munro G. H. and Heisler L. H.	1956	*Aust. J. Phys.* **9,** 343.
Piggot W. R.	1956	*Solar Eclipses and the Ionosphere* p. 106. Pergamon Press, London.
Ratcliffe J. A.	1956	*Solar Eclipses and the Ionosphere* p. 1. Pergamon Press, London.
Savitt J.	1950	*J. Geophys. Res.* **55,** 385.
Thomas J. O. and Robbins A. R.	1956	*Solar Eclipses and the Ionosphere* p. 94. Pergamon Press, London.

DL.
12
958

Journal of Atmospheric and Terrestrial Physics, 1958, Vol. 12, pp. 68 to 76. Pergamon Press Ltd., London

The height variation of drift in the *E* region

I. L. Jones
Cavendish Laboratory, Cambridge

(*Received* 13 *August* 1957)

Abstract—Observations of drift velocities in the *E* region of the ionosphere have been made simultaneously with waves of frequency about 2·0 and 2·5 Mc/s, by means of the Mitra method. Since the observed velocities were significantly different, it is deduced that the important scattering occurs near the level of reflection, so that the observations on the two frequencies provide information about the drift velocities at two different heights. The velocities rotated through 360° in the course of the daylight hours, and during the winter months the rotation corresponding to reflection at the smaller height lagged behind that corresponding to the greater.

The rotation of the velocity was not uniform during the day, and this non-uniformity is explained by considering how the height of reflection varies during the day.

When the results were compared with those deduced from radio observation of meteor trails made by Greenhow and Neufeld (1956), it was found that the time lag between the rotating drifts observed by the two methods could be satisfactorily explained if proper account was taken of the different heights to which the observations refer. Rapid changes in the drifts were observed in September and October by both methods.

1. Introduction

This paper gives an account of measurements, made by the Mitra* (1949) method, of the velocity of drift of ionospheric irregularities in the *E* region. The measurements were made simultaneously on two frequencies reflected from different levels separated by about 4 km. The measured drift velocities differed significantly from each other, both in their instantaneous values and also in their variation throughout the day. The conclusion is reached that the fading, which is the phenomenon observed in the Mitra method, is imposed mainly near the level of reflection, and that the regular movements in the *E* region are appreciably different at heights separated by about 4 km. These results, and the experimental arrangements used in obtaining them are discussed in sections 2 and 3.

Briggs and Spencer (1954) discussed the results available at that time and showed that the drift velocity in the *E* region had an important component which rotated through 360° during the daylight hours. In the present series of observations this component was found to be clearly marked, particularly in the winter months, and its average daily variation could be determined with some precision. It was then found that the rotation observed on the smaller frequency, reflected from the lower height, lagged behind that observed on the greater frequency reflected from the greater height. This lag may be described by saying that the "phase" of the rotating component advances with increasing height. These results are discussed in section 4.

Throughout the day the height of reflection changes in a regular way, and because the phase changes with height, the observed drift direction will rotate non-uniformly in a way that can be calculated, as shown in section 5.

* The fading of a radio wave reflected by the ionosphere is observed at the three corners of a right-angled triangle of sides about one wavelength. Time delays between similarities at the three points are measured, and the velocity of drift deduced.

VOL. 12 1958

Greenhow and Neufeld (1956) described measurements of drift velocities made by observing radio waves reflected from meteor trails, and they also found a component of velocity which rotated twice in 24 hr, with a phase which increased with height. Their results are compared with the present ones in section 6, and it is shown that they are consistent when due allowance is made for the different heights to which the observations refer. In section 7 it is shown that a rapid change in the phase of the rotating component of the velocity, which Greenhow and Neufeld had observed to occur in September and October, is also observable at the different height explored by the Mitra method.

Irregularities of electron density need not, in general, move with the neutral air molecules. For meteor trails, however, Clemmow, Johnson and Weekes (1955) have shown that the movement is the same as that of the neutral air, so that the good agreement between the phase of the semi-diurnal component observed by the meteor method and by the Mitra method, suggests that in the E region the electron density irregularities and the air move together.

2. Experimental Arrangement

The Mitra method (1948) of observing drifts was used simultaneously on frequencies of about 2 and 2·5 Mc/s. Three circularly polarized loop aerials were arranged so as to make two pairs, one in the north–south, and one in the east–west direction, and two pairs of receivers were switched every $7\frac{1}{2}$ min so as to record in succession first on one pair of aerials and then on the other. Thus the mean drift for 15 min could be determined on each frequency. The method of Phillips (1955) was used to record the time intervals between the occurrence of minima in the fading from one pair of aerials. A record of this type is shown and explained in Fig. 1.

No attempt was made to determine the difference of the equivalent heights on the two frequencies, but some of the experiments were conducted at the time when a colleague, Mr. B. J. Robinson, was taking accurate $h'(f)$ records from which he could deduce the true height of reflection on the two frequencies in use. In general, the difference between these heights was about 3–4 km. The details are discussed later in section 4.

Measurements were made for periods of about one week on several occasions between March 1955 and October 1956. The north–south and east–west components of the drift velocity were calculated for each 15 min period, and were averaged for the week. The results are discussed below.

3. The Height at Which the Fading Is Imposed on the Reflected Wave

Experiments of the kind described here measure the drift of a radio diffraction pattern over the ground. If this drift is to be related to that in the ionosphere it is necessary to decide at what height in the ionosphere the fading is imposed on the wave.

Three separate pieces of evidence suggest, as follows, that the fading is predominantly imposed near the level of reflection.

(a) On some days an almost continuous record of reliable time delays was

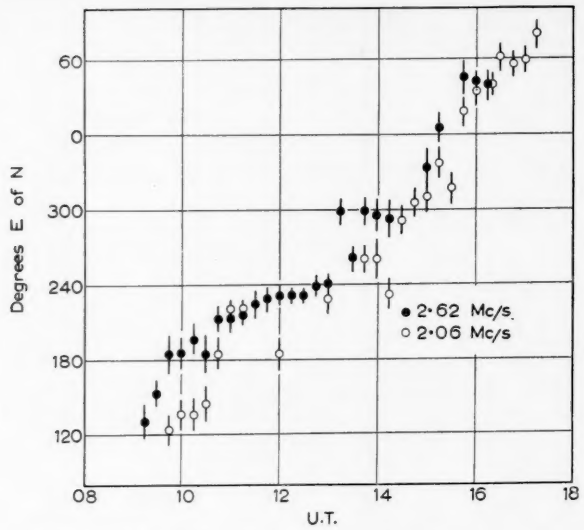

Fig. 2. The direction of drift measured simultaneously on two frequencies on 18 March 1956

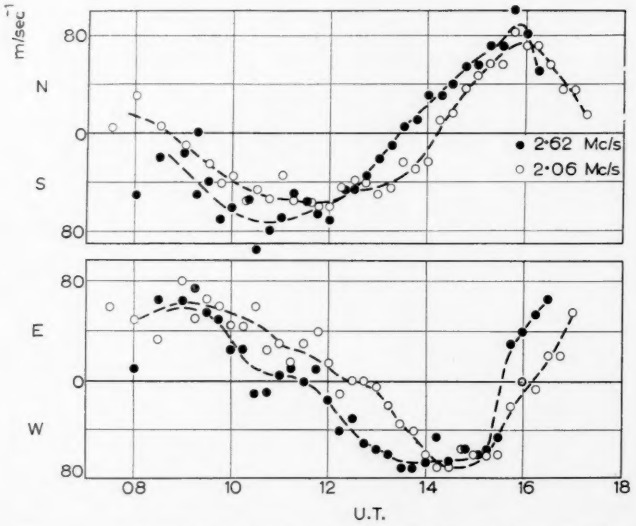

Fig. 3. The mean N–S and E–W component of drift observed from 15 March to 20 March 1956

obtained, when the type of fading on the two frequencies was similar. Fig. 2 shows how, on one of these days, the directions of drift varied with time. The limits shown are for an estimated error of $\pm 0{\cdot}1$ sec in the time delay. These results show that on some occasions the direction of drift measured simultaneously on the two frequencies was quite different. Fig. 1 shows a section of the Phillips record made between 0930 and 1130 U.T. on the day to which Fig. 2 refers. The E–W time delays are quite different on the two frequencies from 0945 to about 1045

VOL. 12 1958

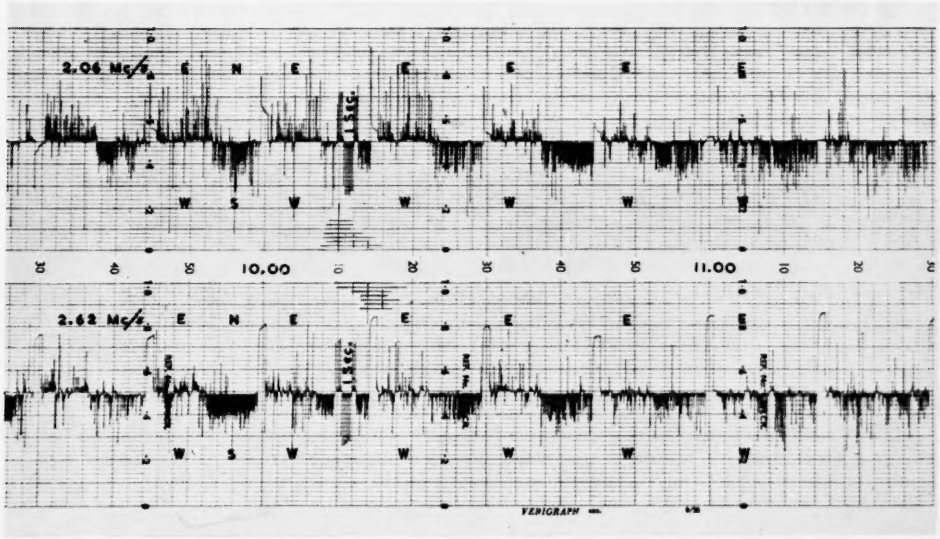

Fig. 1. The time delays between the minima of two fading records measured by the Phillips recorder on two frequencies, taken on 18 March 1956. The apparatus is switched every $7\frac{1}{2}$ min from the E–W to the N–S pair of aerials. The time delays are given by the length of the spikes, while an indication of the fading speed is given by the number of spikes occurring in unit time.

VOL.
12
1958

U.T., the E–W component on the high frequency changing from east to west before that on the low frequency.

(b) When the mean direction of drift, averaged over several days, is compared on the two frequencies it is found that it varies through the day in the same kind of regular way, but that the regular change of direction at the lower height lags behind that at the greater height as shown in Fig. 3.

(c) It is shown in section 5 that lack of uniformity in the rotation of the drift direction can be explained through regular daily variations in the height of reflection. The height changes involved are of the order of 5–10 km.

Each of these observations seems to show that the drift measured by the Mitra method is characteristic of a level which is near the level of reflection of the waves; if it were not, then in (a) and (b) the two frequencies could not exhibit the differences mentioned, while in (c) the effect of the height change would be unimportant. Booker (1955) has given reasons which suggest that the fading is imposed on the wave near the level of reflection, where the wave-length in the medium is large.

4. The Height Variation of Drift Direction

The results of Fig. 3 have been replotted in Fig. 4 to show how the mean direction of drift varies with time on the two frequencies. The approximate linearity of the curves indicates an approximately uniform rotation during the daylight hours.

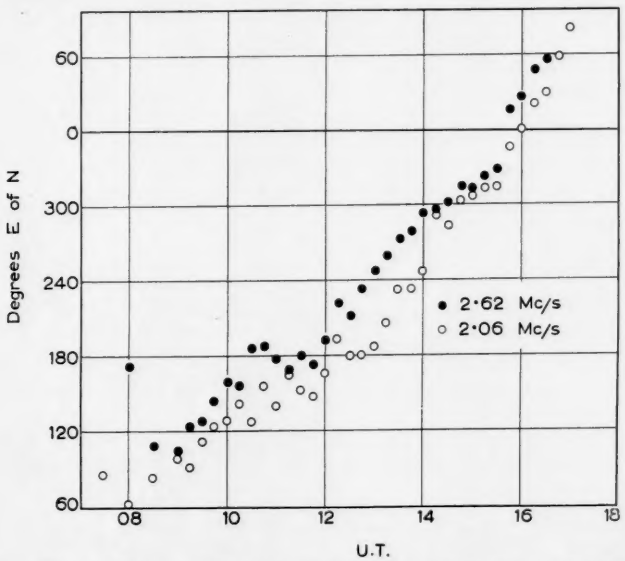

Fig. 4. The mean direction of drift derived from the results of Fig. 3.

Although the scatter of points on curves like Figs. 3 and 4 was greater for some of the other months, it was nearly always possible to measure the mean difference $\Delta\phi$ in the directions of drift on the two frequencies, and the results are given in Table 1. The standard deviation of the mean values shows their significance.

The last column shows the height gradient of the direction of drift on the assumption that the two frequencies were reflected from heights which differed by 3·5 km.

During the summer months the semi-diurnal component was small, and the results obtained were unreliable. During the winter months, the difference in direction of drift on the two frequencies was consistent, the direction of drift corresponding to the greater height leading that at the lower height.

In discussing the direction of drift of the rotating component it is important to consider the effect of a superimposed steady drift. A polar plot of the drift velocity showed that during the winter months the steady component was small. Therefore, during this time the direction of drift was that of the semi-diurnal rotating component. During the summer, there was a large steady E–W component.

Table 1

Month	Low frequency	High frequency	Mean $\Delta\phi$ (standard deviations are shown in brackets)	$\Delta\phi$ deg. km^{-1}
March 1955	2·01 Mc/s	2·5–2·9 Mc/s	26° ± (5)	7·5
May ..	2·01	3·00	Unreliable	
June ..	2·01	3·00	..	
July ..	2·01	3·00	..	
November ..	2·03	2·47	15° ± (4)	4·0
December ..	2·03	2·50	26° (doubtful)	
February 1956	2·05	2·62	33° ± (7)	9·5
March ..	2·05	2·62	29° ± (3)	8·5
September ..	2·27	3·00	H. F. Unreliable	
October ..	2·27	3·00	30° ± (7)	8·5

The height separation for the two frequencies reflected from the *E* region was calculated, for the results of October 1956, from experimental results obtained by Mr. B. J. Robinson. He made accurate $h'(f)$ records while the drift experiment was in progress, and from these deduced the electron distributions by methods which he will describe separately. His results show that the two frequencies were separated by a distance of about 3–4 km. From the results of all his measurements so far as have been analysed, he considers that on the average over the year, the two frequencies used were reflected from heights which differed by about 3–4 km, because during the greater part of the observing time both frequencies were away from the critical frequency of the *E* region.

VOL. 12 1958

From all these results, the overall conclusion is that during the winter, the direction of the semi-diurnal rotating component of drift velocity varies with height in such a way that the drift at the greater height leads that at the lower, by about 7 deg. km^{-1}. This agrees well with the conclusion of GREENHOW and NEUFELD (1956) who found a change in direction of the same magnitude during the winter months.

5. The Effect of the Diurnal Variation of Reflection Height

During the day, the height of reflection on a constant frequency changes in a regular way, and is least at midday. In the previous section it has been shown that the direction of drift at the lower height lags behind that at the greater height. Thus, in the morning as the height of reflection decreases, the temporal rate of change of direction should decrease, while in the afternoon, as the height of reflection increases, the temporal rate of change of direction should increase.

The way in which the direction would be expected to vary throughout the day, when these height changes were allowed for, was computed as follows. The diurnal variation of height of reflection in the *E* region was obtained by Mr. B. J. ROBINSON, and the results for October, November, February and March were

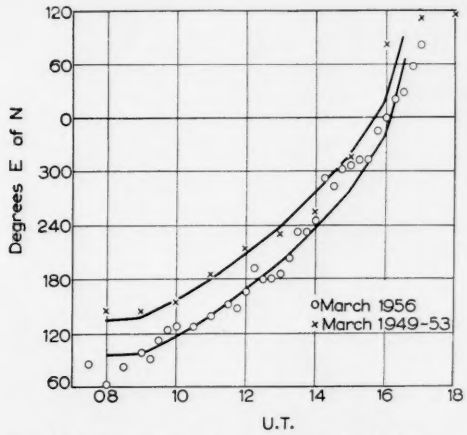

Fig. 5. The effect of the diurnal variation of reflection height on the direction of drift. The line shows the expected variation of drift direction with time, calculated for hourly periods.

made available to the author. It was assumed that the gradient of phase was 7 deg. km^{-1} and that for a constant height of reflection, the period of rotation of the semi-diurnal component has a constant value of 12 hr.

Fig. 5 shows the good agreement that exists between the experimental variation for March 1956 and the variation computed on the above assumptions. Also shown in Fig. 5 is the mean variation in direction of drift during March for the years 1949–1953. This again fits the expected variation. During the four months mentioned above, the same kind of agreement was obtained.

There is some evidence that reflection often occurs from E_s near sunset, so that the height of reflection changes very slowly, and the temporal rate of change of

direction might be expected to be reduced. This reduction can be seen on the mean curve for 1949–1953 in Fig. 5. If, near sunset, reflection is from E_s then the height difference on the two frequencies will be small, and the difference in direction of drift will be reduced.

Thus the departure from a uniform rotation during the day can be explained by taking into account the change in height of reflection, and the way in which the drift direction changes with height.

6. Comparison of Drifts Obtained by the Mitra Method with Those Obtained by Radio Observations of Drifting Meteor Trails

Greenhow and Neufeld (1956) made observations on meteors and deduced drifts at four heights in which there was a component which rotated through 360° in 12 hr. It is interesting to compare their results with ours. For this purpose we

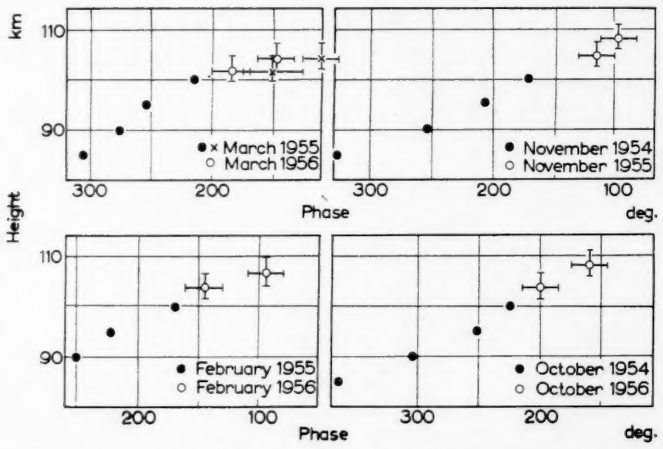

Fig. 6. Comparison of the phase of the semi-diurnal component obtained by the Mitra method, with that obtained by the meteor method. ● Meteor method, ○ Mitra method

shall compare the phase of the semi-diurnal component obtained by the two methods.

The meteor results were obtained during the period September 1954 to August 1955 and those of the Mitra method during the period March 1955 to October 1956. It was, however, found that for each method separately the phase was approximately the same in the same months in different years, so that it seemed reasonable to compare the results of the two methods month by month, even if the observations were made in different years. The results are plotted in Fig. 6.

The phase of the meteor results is the mean obtained from the N–S and E–W components, while the phase of the semi-diurnal component obtained by the Mitra method is that appropriate to the period near midday, when the height of reflection was constant. During October 1956, the height, and the height difference was obtained from the analysis of simultaneous $h'(f)$ records by Mr. B. J. Robinson. For the other months, the heights were obtained from records taken during the following year. Estimated errors in both the height and phase are shown on the curves.

VOL. 12 1958

The results of the two types of experiment seem to show that there is a roughly constant gradient of phase between 85 and 110 km. The results obtained by the Mitra method for March 1955 were less reliable than the others, and it is seen that these agree less well with the results of the Meteor method.

7. Drift Results during September and October

Greenhow and Neufeld (1955) show that during September and October the phase of the semi-diurnal component of drift changes by nearly 360°. This is a very marked and rapid change, and if, as we have shown in the previous Section, the results of the two experiments agree, we should expect this same variation in the phase of the drift observed by the Mitra method.

Briggs and Spencer (1954) gave average drifts for the four seasons of the year, and any rapid change in the autumn would have been smoothed out. Thus, in order to see if the effect was present, the individual monthly records for September and October were investigated.

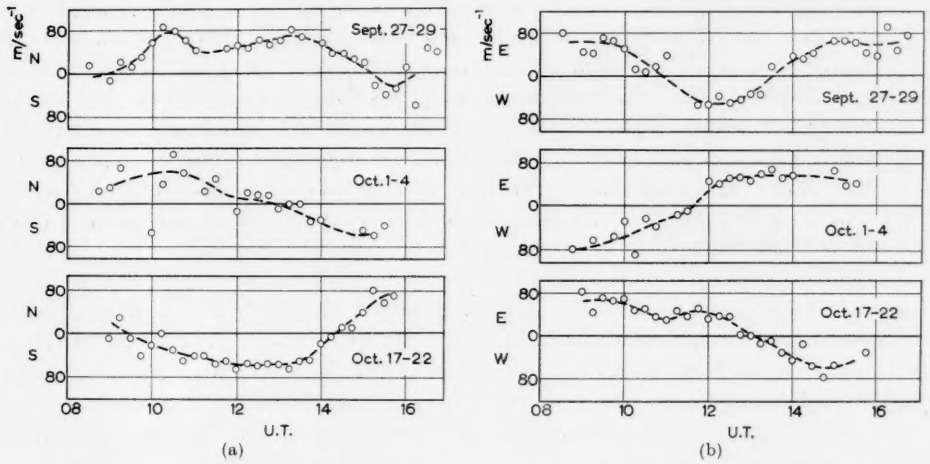

Figs. 7a, b. The mean N–S and E–W components of drift for September and October 1956

Observations were made during September and October 1956 and the results are shown in Figs. 7a and 7b. These results show that large changes of phase occurred during this period of observation of less than one month. The two periods, September 27–29, and October 1–4, show a phase change of about 2·5 hr (75°) in five days. Greenhow and Neufeld (1955) published similar curves for September 1954, which showed a phase change of 2·5 hr in six days. Observations made by Dr. G. J. Phillips, in 1949, 1950 and 1951 are shown in Figs. 8a and 8b, and the change over from S to N, in the N–S component, and from W to E, in the E–W component, takes place at about the same time as for the results of September 1956.

This September and October effect is very marked on the results of both methods, and of the same magnitude, so that we can conclude that the same movement is observed by both methods.

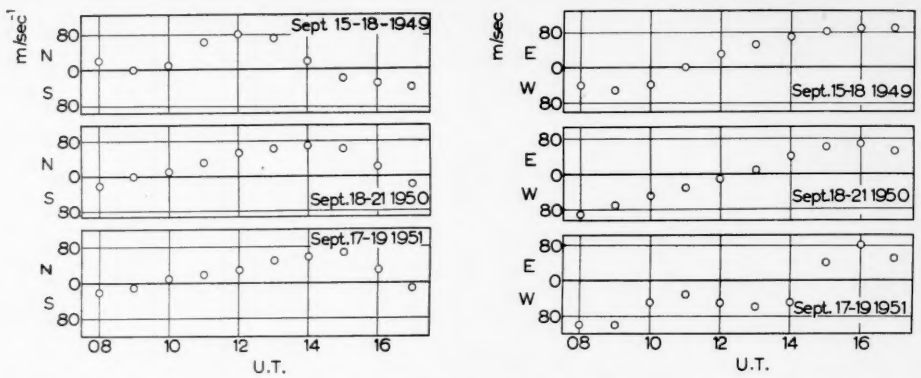

Figs. 8a, b. The mean N–S and E–W components of drift for September 1949, 1950 and 1951.

8. CONCLUSIONS

We conclude that for a wave reflected in the *E* region by day, the fading is imposed near the level of reflection, so that the measured drift refers to a region near that level. In winter, the direction of drift at two heights in the *E* region rotates fairly uniformly, the rotation at the greater height leading that at the lower height. The change in direction of drift with height is about 7 or 8 deg. km^{-1}.

Comparison with the meteor observations of drift shows good agreement when due allowance is made for the height difference involved. This agreement suggests that the semi-diurnal component of drift measured by the Mitra method is the drift of the neutral air.

Acknowledgements—I am indebted to the Gassiot Committee of the Royal Society for a grant which enabled me to do this work. I also wish to express my thanks to Mr. B. J. ROBINSON for providing the results of true height analysis in the *E* region and for discussion concerning the diurnal behaviour of the *E* region.

I have benefited much from discussion with Mr. J. A. RATCLIFFE and Dr. B. H. BRIGGS.

REFERENCES

BRIGGS B. H. and SPENCER M.	1954	*Rep. Prog. Phys.* **17,** 254.
BOOKER H. G.	1955	*J. Atmosph. Terr. Phys.* **6,** 124.
CLEMMOW P. C., JOHNSON M. A. and WEEKES K.	1955	*The Physics of the Ionosphere.* Physical Society, London.
GREENHOW J. S. and NEUFELD E. L.	1955	*Phil. Mag.* **46,** 549.
GREENHOW J. S. and NEUFELD E. L.	1956	*Phil. Mag.* **1,** 1157.
MITRA S. N.	1949	*Proc. Inst. Elect. Engrs.* **96,** Part III, 441.
PHILLIPS G. J.	1955	*J. Atmosph. Terr. Phys.* **6,** 124.

VOL. 12 1958

RESEARCH NOTES

Ionospheric true height and M.U.F. calculations

(*Received* 24 *August* 1957)

In a recent paper (Thomas, Haselgrove and Robbins, 1957a,b), new and more accurate determinations of the electron density distribution in the ionosphere over Slough (lat. 51·5°N, long. 0·5°W) were made and the results compared with those obtained using methods which neglected the effect of the earth's magnetic field and of group retardation produced by ionization in the low ionosphere (Schmerling and Thomas, 1955, 1956; see also Slough Bulletins—Series B). The height at which a given electron density was found was consistently lower in the new results than in the old ones, particularly in the day time in summer and in sunspot minimum years (Table 1).

Table 1

Month and year	h_mF2 (km) at 0000 G.M.T.		Difference (km) (b − a)	h_mF2 (km) at 1200 G.M.T.		Difference (km) (d − c)
	Slough bulletins (a)	T.H.R. (b)		Slough bulletins (c)	T.H.R. (d)	
Jan. 1950	385	377	−8	270	257	−13
Sept. ,,	380	375	−5	295	249	−46
July ,,	375	368	−7	340	276	−64
Dec. 1953	300	308	+8	225	216	− 9
Sept. ,,	340	349	+9	270	231	−39
June ,,	320	322	+2	320	243	−77

The table shows the monthly mean values of h_mF2. The values in the columns marked T.H.R. were calculated using the heights published in Thomas, Haselgrove and Robbins (1957b).

It is interesting to consider the effect of these new results on the calculation of the maximum usable frequency (M.U.F.) of radio waves in oblique incidence transmission. It is known that the larger deviations from the predicted values of M.U.F. occur in summer (Appleton and Beynon, 1944, 1947) and in sunspot minimum years (Wilkins and Minnis, 1951), the predicted M.U.F. being too low.

Appleton and Beynon (1944), for example, have made a careful study of data supplied by the B.B.C. Engineering Division relating to long-distance broadcasting from Daventry to Gibraltar and Algiers. The main results they found from such data for 1943 are quoted, as follows: "... it is clear that satisfactory reception was often accomplished at noon, on frequencies 1–6 Mc/s higher than the mean calculated value for the particular month. Further communication data have shown that the divergence becomes progressively more marked from January to June, being most pronounced during the daytime period of May, June and July. Furthermore, it appears that no appreciable divergence from mean calculated values is recorded at night."

The method used in this country for calculating the M.U.F., $f_{\max}$, is that due to APPLETON and BEYNON (1940, 1947) in which the M.U.F. factor x is calculated from a knowledge of the height h_0 of the lower edge, and the semi-thickness y_m of the parabola approximating to the shape of the *F2* layer near the maximum, and the distance D of transmission. The M.U.F. is then equal to xf_0 where f_0 is the vertical incidence critical frequency. The vertical incidence parameters y_m and h_m are calculated from $h'(f)$ records assuming a parabolic distribution and no correction is made for the effect of the earth's field. The M.U.F. predictions are based on values of h_m and y_m (calculated in the same way) published in the Slough bulletins.

With the new values of h_mF2 and "thicknesses," x was calculated using Fig. 1 of the paper by APPLETON and BEYNON (1947). Fig. 2 of the same paper showed that changes of thickness hardly affected the values of x. These values are compared in Table 2 with the Slough bulletin values of x for a distance of transmission of 3000 km, (M3000)*F2*. In this table the M.U.Fs. derived from the two sets of data are also compared using $f_{\max} = xf_0$ and taking f_0 to be the monthly median noon value of f_0F2 from the Slough bulletins.

The main point of interest is that the M.U.F. factor (which is independent of the critical frequency) obtained from the new results is always greater than the Slough bulletin value.

The values of h_mF2 calculated near the equator are not as greatly affected by neglect of the earth's magnetic field or of group retardation produced by underlying layers and thus the predicted M.U.Fs. for transmission paths centred on, or near, the equator should be more accurate, as seems to be suggested by Table 2 of the paper by WILKINS and MINNIS (1951).

Table 2

Month and year	Noon (M3000)*F2*		Noon M.U.F. in Mc/s	
	Slough bulletins	T.H.R.	Slough bulletins	T.H.R.
Jan. 1950	3·3	3·4	34·4	35·4
Sept. ,,	3·1	3·5	18·9	21·4
July ,,	2·8	3.25	18·5	21·5
Dec. 1953	3·65	3·75	21·2	21·8
Sept. ,,	3·25	3·7	16·9	19·2
June ,,	2·9	3·55	14·5	17·8

The numbers in the columns labelled T.H.R. were calculated using the heights published in THOMAS, HASELGROVE and ROBBINS (1957b).

It should be noted that it seems likely that the transmission of abnormally high frequencies, often usable over long distances in summer, involves reflection from the abnormal *E* layer and that this largely accounts for the fact that the predicted values of M.U.F. at these times are too low. However, as we have shown it may well be that some of the apparent differences (~3 Mc/s) in the prediction of oblique incidence propagation frequencies can be explained when the true heights of reflection are used.

VOL. 12 1958

An important publication on oblique ray paths in the ionosphere has recently appeared (HASELGROVE, 1957). In this paper, Mrs HASELGROVE has modified the original M.U.F. calculation for north–south transmission of the ordinary ray by taking into account the effect of the earth's magnetic field. Her results were that "for dip angles less than about 30°, predicted skip distances will be much less than the true ones and predicted M.U.Fs. will be too high. For a dip of 67½°, however, which is the value for south-east England, the errors are negligible."

This means that near the equator, at any rate for north–south transmissions, the use of a theory which neglects the earth's field for calculating M.U.Fs. tends to compensate for using, in those calculations, values of ionospheric true heights which were themselves obtained by neglecting the field. That is, the present predicted M.U.Fs. would be decreased by allowing for the field in their calculation and increased by using the (lower) true heights obtained when the effect of the earth's field is taken into account. It should be remembered, however, that the latter error decreases as the equator is approached so that one might expect on the whole that M.U.Fs. for paths centred on the equator might be slightly lower than those predicted. Mrs. HASELGROVE'S new work does not, however, affect our conclusions about the Slough M.U.Fs.

J. O. THOMAS
AUDREY ROBBINS

Cavendish Laboratory, Cambridge

REFERENCES

APPLETON E. V. and BEYNON W. J. G.	1940	*Proc. Phys. Soc.* **92,** 518.
APPLETON E. V. and BEYNON W. J. G.	1944	*D.S.I.R. Report Paper No. R.R.B.*/C102.
APPLETON E. V. and BEYNON W. J. G.	1947	*Proc. Phys. Soc.* **59,** 58.
HASELGROVE J.	1957	*Proc. Phys. Soc.* B **70,** 653.
SCHMERLING E. R. and THOMAS J. O.	1955	*Phil. Trans. Roy. Soc. London* **248,** 609.
SCHMERLING E. R. and THOMAS J. O.	1956	*Tables of Ionospheric Electron Density,* Series A No. 1, Cavendish Laboratory, Cambridge.
THOMAS J. O., HASELGROVE J. and ROBBINS A. R.	1957a	*J. Atmosph. Terr. Phys.* **13,** 46.
THOMAS J. O., HASELGROVE J. and ROBBINS A. R.	1957b	*Tables of Ionospheric Electron Density,* Series B No. 1, Cavendish Laboratory, Cambridge.
WILKINS A. F. and MINNIS C. M.	1951	*Proc. Inst. Elec. Engrs.* **98,** 209.

Echoes from the lower ionosphere during Polar blackouts

(*Received* 19 *August* 1957)

IN connection with an ionospheric scatter circuit between Southern and Northern Norway, special pulse soundings were carried out near the mid-point of the path in the period 15 June to 31 July 1957. It is the purpose of this note to present some results obtained at this station, which may have some bearing on problems in connection with conditions of radio-fade outs in the Polar region.

The measurements consisted of simple pulse soundings on a fixed frequency of 2·3 Mc/s, and either $h'(t)$-recordings or photographic records of the oscillographic Class-A display (range-amplitude) were made. The station was set up at Nordli (65°N, 14°E), a

place removed from power lines and electrical machinery of any kind, and it was hoped that during daytime the noise level would be so low that weak reflections from the lower part of the E-layer would be detectable.

The most important parameters for the experimental system are given below:

Transmitted power:	10 kW peak power
Aerials:	Horizontal dipoles mounted 10 m above ground
Receiver noise factor:	1 dB

Observations

During normal conditions weak reflections were always observed down to heights of the order of 85 km, and in some cases down to heights of the order of 75 km. A typical example of an $h'(t)$-recording as obtained during quiet conditions is shown in Fig. 1. The low echo seems to be of a filamentary structure. This is not a real effect, but is due to the method of recording. In fact, closer observations showed that the echo was present all the time.

When an absorption effect occurred, the low echoes were first found to be undetectable, and in the major phase of the storm, a complete blackout was often observed. This result seems to indicate that the absorption effect must be produced at least partly below say 85 km. In three cases it was found that during conditions of excessive absorption, echoes were formed in the height range 65–70 km. Such echoes were only observed in periods when the strength of the main E-echo was increasing.

In Fig. 2 various phases of an absorption effect occurring in the morning of 30 June 1957 are illustrated. Before 0900 MET, E-echoes and low echoes down to heights of the order of 90 km were observed. The echoes then became gradually weaker, and the low echoes became first undetectable. After 1035 no echoes were observed on the $h'(t)$-recording with the setting used. When increasing the receiver setting, it was found that the echoes were almost in the noise level. In the period 1115–1130 no echoes were observed. In the period 1130–1145 the strength of the echoes increased rapidly, and at the same time echoes were formed at heights of the order of 65–70 km. These echoes are interpreted as reflections from the lower boundary of the layer producing the absorption effect.

The observations were made in a period when great solar disturbances occurred. Only in three cases were echoes observed in the 65–70 km level, but these were all in periods when an absorption effect was in the decreasing phase.

Acknowledgements—The author is indebted to his collegues at the NDRE for helpful co-operation.

B. Landmark

Norwegian Defence Research Establishment
Kjeller, Norway

VOL. 12 1958

On the de-emanation of a radium solution

(*Received* 5 *October* 1957)

There have been some indications in recent years that low-level radon determinations are becoming increasingly more applicable in a variety of fields of study. These include large-volume water-flow measurements (Hess, 1943; Bullen and O'Connor, 1954) large scale uranium prospecting (Payot and Jaquerod, 1953), and meteorological studies of air-mass movements (Damon and Kuroda, 1954).

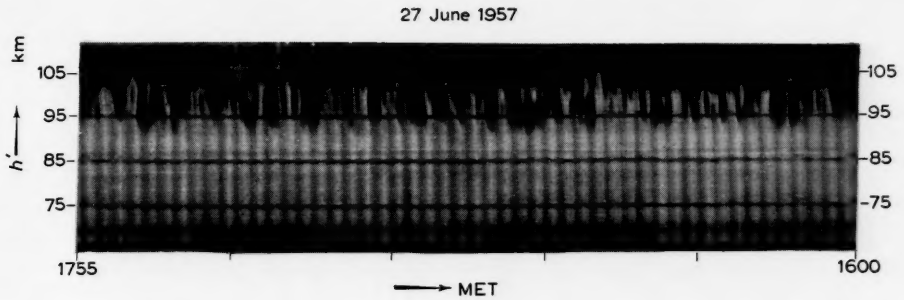

Fig. 1. A typical $h'(t)$-recording obtained during quiet ionospheric conditions.

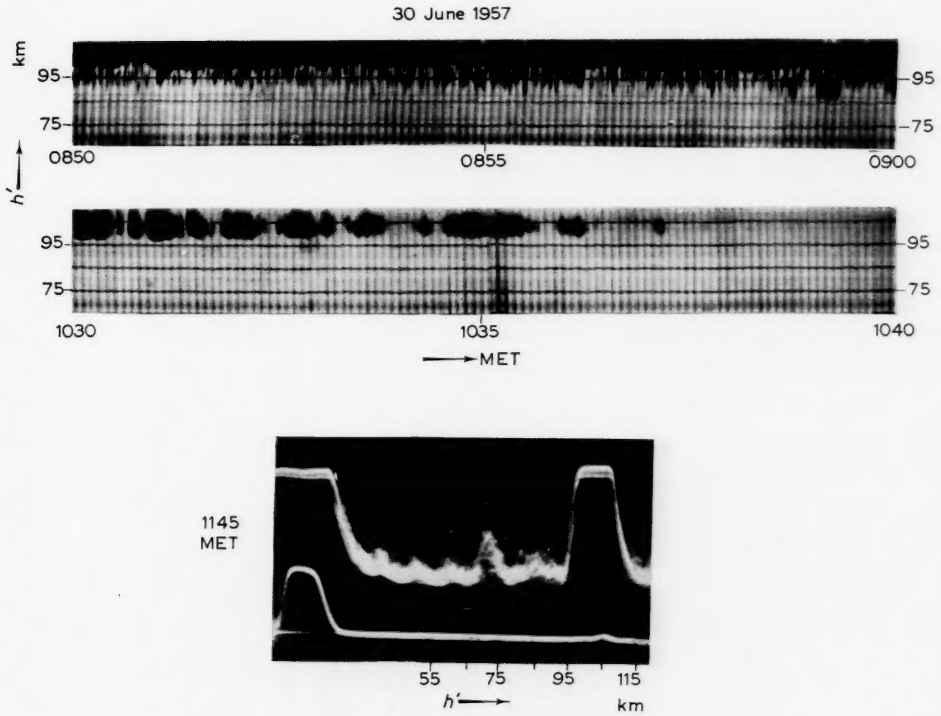

Fig. 2. Records obtained in a period when excessive absorption occurred.

VOL.
12
1958

In all such studies, the problem of removing radon from solution for subsequent analysis appears either during the direct determinations, or during the process of calibration. In this connection, some controversy has arisen in the literature concerning the necessity of boiling the solution at reduced pressure in order to remove all of the radon from solution (HESS, 1943; BULLEN and O'CONNOR, 1954; EVANS, 1935; DAVIS, 1947).

DAVIS (1947), for example, has shown that by boiling a radium standard solution at reduced pressure, and by bubbling nitrogen through the solution at a rate of about $\frac{1}{4}$ l./min, more than 99·99 per cent of the radon is released from solution after 16 min of bubbling.

If one bubbles nitrogen through the solution directly into an ionization chamber, the amount of nitrogen to be used is naturally restricted by the volume of the chamber.

It is to be noted that those investigators who have maintained that boiling, etc., is necessary have used ionization chambers of volume 8 l. or less, while Hess (1943), who reported virtually complete removal without boiling and without operating at reduced pressure, worked with chambers of about 30 l. volume.

It was felt that a quantitative study of the de-emanation procedure might possibly shed some further light on the apparent discrepancy. A series of de-emanations of a 400 cm^3 radium solution was therefore carried out. Nitrogen free of radon was forced through the solution (contained in a standard 1 l. de-emanating flask) at the rate of 1 l./min; the bubbles rose through the solution from a depth of about 2 in. The process was at all times carried out at atmospheric pressure and room temperature. A measured period of build-up time was allowed to elapse between each successive de-emanation.

In one experiment, the first 6 l. of nitrogen bubbled through the solution were discarded, and the seventh to the tenth litres were directed into a 4 l. ionization chamber through a drying agent; its activity was measured. In a subsequent experiment, the first 10 litres were discarded, and the eleventh to the fourteenth litres were directed into a chamber, etc. This was repeated four times, each time with a different portion of the bubbling gas selected.

Table 1. Activity of different portions of bubbling gas during de-emanation

Amount of bubbling gas discarded previous to passing into ionization chamber (litres)	Portion of bubbling gas passed into ionization chamber (litres)	Activity at time of de-emanation, corrected for infinite build-up time* (in arbitrary units)	(n)
6	7th–10th	167	2·5
10	11th–14th	131	3·5
14	15th–18th	102	4·5
35	36th–39th	21·2	9·75
0	0–36th	2730†	

* Corrected also for generation of radon during sampling period (4 min).

† Used charcoal trap as concentrating agent; then, outgassed into chamber. This value includes not only the amount of radon in solution, but also that quantity which remains undissolved within the storage flask.

In every case, bubbling was continued until about 35 l. of nitrogen had been passed through the solution. Also, the total activity was determined by bubbling 36 l. of nitrogen through the solution and a charcoal trap. Table 1 shows the results of these experiments.

In order to analyse the data of Table 1, we first assume that for every 4 l. portion of

bubbling gas, a given fraction (f) of the radon *in solution* is removed* (f being assumed independent of the concentration).

Letting Y_0 be the amount of radon in solution at the start of a de-emanation,
Y_1 be the amount of radon remaining in solution at the end of the first 4 l. portion of bubbling,
Y_n be the amount of radon remaining in solution at the end of the nth 4 l. portion of bubbling, and
letting Z_1 be the amount of radon removed (from solution) during the first 4 l. portion of bubbling,
Z_2 be the amount of radon removed (from solution) during the second 4 l. portion of bubbling,
Z_n be the amount removed during the nth portion,

then,

$$Z_1 = fY_0$$
$$Z_n = fY_{n-1}$$
$$Z_{n+1} = fY_n \tag{1}$$

and,

$$Y_1 = Y_0 - Z_1 = Y_0(1-f)$$
$$Y_2 = Y_1 - Z_2 = Y_0(1-f)^2$$
$$Y_{n-1} = Y_0(1-f)^{n-1}$$
$$Y_n = Y_0(1-f)^n \tag{2}$$

Eliminating Y from equations (1) and (2),

$$\frac{Z_{n+1}}{Z_n} = (1-f) \tag{3}$$

and, in general,

$$\frac{Z_n}{Z_m} = \frac{(1-f)^{n-1}}{(1-f)^{m-1}} = (1-f)^{n-m} \tag{4}$$

or,

$$\log Z_n = \log Z_m + (n-m)\log(1-f)$$

Letting $n = 0$, and leaving Z_0 unspecified, we see that, provided the assumptions are correct, a plot of $\log Z_n$ as a function of (n) yields a straight line with slope equal to $\log(1-f)$.

The data of Table 1, plotted in the above manner in Fig. 1, indicates the correctness of the assumptions. From the graph in Fig. 1, an average value of (f) was found to be 0·252.

The author has recently developed an improved technique for measuring the radon content of the atmosphere, employing coconut charcoal as a concentrating agent (MIRANDA, 1957). The charcoal trap described in this report can be used equally well for de-emanating a radium solution. The procedure is quite simple. Nitrogen gas is bubbled through the standard solution at a rate of 1 l./min at atmospheric pressure and room temperature. The emerging gas is allowed to pass over a drying agent, and then through the charcoal trap. It will be seen that this procedure allows an unlimited amount of nitrogen to be bubbled through the solution.

In particular, more than 50 l. of nitrogen gas was used for the de-emanations. As will be shown directly, this amounts to greater than 99·1 per cent extraction.

* This amounts to asserting that Henry's law holds for the bubbles as they rise through the solution (subject, of course, to the condition that the bubbles are small enough, and/or are in contact with the liquid for a sufficiently long period of time for equilibrium to be established).

VOL. 12 1958

By extrapolating to $n = 13$ (which corresponds to bubbling 52 l. of nitrogen through the solution), we see from Fig. 1 that $Z_{13} = 8{\cdot}2$.

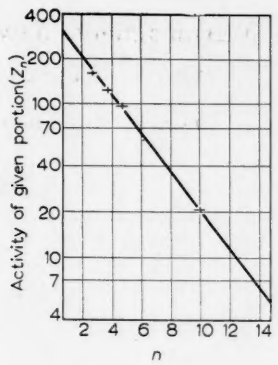

Fig. 1. Activity of different portions of bubbling gas during de-emanation.

In order to determine the amount of radon still remaining after 52 l. of bubbling, a relationship between Z_n and Y_n is required.

One notes from equations (1), that $Z_n = fY_{n-1}$, and from equations (2), that

$$Y_{n-1} = Y_n(1 - f)^{-1} \tag{5}$$

Eliminating Y_{n-1} from equations (1) and (5) above, one obtains

$$Y_n = Z_n(1 - f)/f,$$

and, inserting the value of (f) found from the graph,

$$Y_{13} = 24{\cdot}3$$

Thus, the fraction of radon remaining in the storage flask after 52 l. of bubbling is 24·3/2730, or 0·89 per cent. This corresponds to better than 99·1 per cent extraction.

Since the value 2730 was obtained with only 36 l. of bubbling, it is a bit low. Therefore, the value 99·1 per cent can be considered a lower limit for 52 l. of bubbling gas.

The work reported herein was supported by a grant from the Geophysics Research Directorate of the Air Force Cambridge Research Center, under contract No. AF 19(122)–409.

H. A. Miranda*

Physics Dept., Fordham University
New York 58, *New York*

References

Bullen T. G. and O'Connor W. F.	1954	*Sewage Industr. Wastes* **26,** 497.
Damon P. E. and Kuroda P. K.	1954	*Trans. Amer. Geophys. Union* **35,** 208.
Davis F. J.	1947	*J. Res. Nat. Bur. Stand., Wash.* **39,** 545.
Evans R. D.	1935	*Rev. Sci. Instrum.* **6,** 99.
Hess V. F.	1943	*Trans. Amer. Geophys. Union* **24,** 587.
Miranda, Jr., H. A.	1957	*J. Atmosph. Terr. Phys.* To be published.
Payot R. and Jaquerod A.	1953	*Mem. Soc. Phys. Hist. Nat. Genève* **42,** 257.

* Now at Columbia University, Hudson Laboratories, Dobbs Ferry, New York.

Journal of Atmospheric and Terrestrial Physics, 1958, Vol. 12, pp. 84 to 86. Pergamon Press Ltd., London

Indices of geomagnetic activity

of the Observatories HARTLAND (*Ha*), ESKDALEMUIR (*Es*) and LERWICK (*Le*)

September, October and November 1957

THE K-indices etc. for October and November are derived from the new Magnetic Observatory at Hartland (Lat. 50° 59·7′ N; Long. 4° 29′ W) following the closing of the Abinger Magnetic Observatory on 18 April, 1957.

In estimating the K-indices the Abinger Sq curves have been used as a guide.

The figures given on pages 84 to 86 represent the *K*-indices for three-hour intervals, beginning with 00–03 hrs for the first and ending with 21–24 hrs for the eighth figure.

September 1957

Day	*Ha* Range for $K = 9 : 500\gamma$			*Es* Range for $K = 9 : 750\gamma$			*Le* Range for $K = 9 : 1000\gamma$			*Day*
	K-Indices		*Sum*	*K-Indices*		*Sum*	*K-Indices*		*Sum*	
1	5433	3223	25	4433	3222	23	6533	3212	25	1
2	3554	5467	39	2554	6577	41	2654	7587	44	2
3	6556	7864	47	5556	7964	47	7756	7853	48	3
4	3422	7967	40	3423	7879	43	3433	8979	46	4
5	7754	5455	42	9854	5446	45	8954	4447	45	5
6	4323	4542	27	4324	4542	28	4424	4462	30	6
7	2323	3322	20	2323	2322	19	2222	2211	14	7
8	1113	3223	16	1012	2313	13	1122	2213	14	8
9	2232	2321	17	2233	2221	17	2332	2220	16	9
10	1122	2331	15	1122	2321	14	1122	2322	15	10
11	1122	2113	13	1222	2222	15	2122	2122	14	11
12	2122	2323	17	2222	3223	18	1121	2213	13	12
13	6678	6634	46	7778	6634	48	9988	5534	51	13
14	2345	4334	28	2245	4334	27	2245	5435	30	14
15	3322	3233	21	3322	2233	20	3332	2234	22	15
16	4312	2342	21	4322	2132	19	4422	2232	21	16
17	2123	3331	18	1112	3333	17	1112	3331	15	17
18	3212	2233	18	3222	2333	20	3321	2332	19	18
19	1122	2101	10	1122	2210	11	0112	2100	7	19
20	1012	1232	12	1022	2332	15	1012	1321	11	20
21	3115	5556	31	3115	5666	33	3115	6778	38	21
22	4543	6847	41	4543	6757	41	7554	8868	51	22
23	7766	6664	48	7776	7664	50	9986	6686	58	23
24	5434	4332	28	4333	4332	25	5334	4332	27	24
25	3243	3212	20	3343	3212	21	3233	3212	19	25
26	1122	2321	14	2112	3311	14	2113	3330	16	26
27	0021	3222	12	0022	2212	11	1021	2211	10	27
28	1332	3231	18	0332	2231	16	1331	1121	13	28
29	3443	6877	42	3343	6987	43	3333	8989	46	29
30	6554	4435	36	7434	5535	36	6644	5435	37	30

VOL. 12 1958

October 1957

Day	*Ha* Range for $K = 9 : 500\gamma$		*Sum*	*Es* Range for $K = 9 : 750\gamma$		*Sum*	*Le* Range for $K = 9 : 1000\gamma$		*Sum*	*Day*
	K-Indices			*K-Indices*			*K-Indices*			
1	4333	3243	25	3332	4244	25	4431	3255	27	1
2	3323	3223	21	2211	3323	17	4411	2214	19	2
3	3213	4443	24	3213	3443	23	3112	3553	23	3
4	3223	3333	22	3223	2333	21	3222	3233	20	4
5	3212	2333	19	3222	2332	19	3212	2332	18	5
6	2010	1011	06	2011	0011	6	2001	0000	3	6
7	1122	3122	14	1122	2122	13	1111	2111	9	7
8	1022	0100	06	2011	0100	5	1011	0101	5	8
9	1133	3123	17	0122	2223	14	1122	2223	15	9
10	3332	2343	23	3332	2343	23	3332	3343	24	10
11	3434	2322	23	3323	2222	19	3323	4333	24	11
12	2222	3324	20	2222	2324	19	2322	2324	20	12
13	5523	3254	29	4422	3244	25	6432	2244	27	13
14	3543	4535	32	3543	4535	32	4553	4546	36	14
15	3123	3343	22	2122	2233	17	4211	2343	20	15
16	2002	2221	11	1011	2221	10	1011	1210	7	16
17	1123	3211	14	1222	3211	14	1112	2211	11	17
18	2023	2222	15	1121	1222	12	1011	1222	10	18
19	0023	2332	15	0113	1232	13	0023	1222	12	19
20	2222	2334	20	2212	2334	19	1212	1235	17	20
21	3222	3336	24	3222	2435	23	3221	2337	23	21
22	4233	3324	24	4233	3323	23	5232	2213	20	22
23	4233	2244	24	4232	2243	22	5232	1244	23	23
24	2222	2240	16	2122	2241	16	2122	2140	14	24
25	2222	2223	17	2222	2223	17	2122	1123	14	25
26	3233	3112	18	3212	2112	14	3112	1112	12	26
27	2223	3323	20	1112	3322	15	1112	2312	13	27
28	3133	2332	20	3123	2331	18	3222	1321	16	28
29	3333	3333	24	3322	3233	21	3222	3234	21	29
30	2343	3231	21	2343	2231	20	3332	1132	18	30
31	1122	3121	13	1122	3221	14	1112	2111	10	31

OL.
12
958

November 1957

Day	*Ha* *Range for* $K = 9 : 500\gamma$			*Es* *Range for* $K = 9 : 750\gamma$			*Le* *Range for* $K = 9 : 1000\gamma$			*Day*
	K-Indices		*Sum*	*K-Indices*		*Sum*	*K-Indices*		*Sum*	
1	1322	2222	16	1322	2212	15	1322	1222	15	1
2	1222	2214	16	1112	2114	13	1112	1113	11	2
3	3233	3331	21	3122	3321	17	3022	2321	15	3
4	2011	1222	11	2011	1222	11	1011	0221	8	4
5	1102	2211	10	1111	2221	11	1011	1211	8	5
6	0022	2365	20	0011	2356	18	1011	1257	18	6
7	6433	3331	26	8433	3221	26	8423	3221	25	7
8	1232	3335	22	1233	3334	22	0122	3235	18	8
9	4333	3444	28	4342	3334	26	4432	3345	28	9
10	5333	3333	26	4333	3333	25	5432	3334	27	10
11	3233	4233	23	3233	3234	23	3333	3225	24	11
12	3223	3323	21	3222	3313	19	3223	3323	21	12
13	3222	3233	20	2121	2223	15	3112	2223	16	13
14	3223	4443	25	3223	3333	22	4323	3333	24	14
15	3334	3323	24	3333	3323	23	4432	2223	22	15
16	2222	3221	16	2222	2321	16	2112	2231	14	16
17	1223	2103	14	1111	2103	10	1112	1103	10	17
18	4433	4332	26	3333	4332	24	3333	4422	24	18
19	2333	3222	20	1222	2122	14	1222	2122	14	19
20	2223	3333	21	1112	2333	16	1111	2233	14	20
21	0012	2113	10	1000	1113	7	0011	1113	8	21
22	3122	2220	14	2101	2220	10	2101	2220	10	22
23	0123	3313	16	0111	3313	13	0001	2212	8	23
24	3323	3322	21	3221	2222	16	2221	2222	15	24
25	3354	3444	30	2343	3433	25	2343	2546	29	25
26	4443	4666	37	4343	4665	35	5333	4777	39	26
27	5444	4434	32	5534	3434	31	7734	3334	34	27
28	3443	4343	28	3333	3244	25	4433	3344	28	28
29	3324	3323	23	3323	3323	22	3222	2323	19	29
30	2233	3321	19	2212	3221	15	2212	2110	11	30

VOL. 12 1958

Book reviews

The Planet Earth. *Edited by* D. R. BATES, F.R.S. Pergamon Press, London, 1957. 312 pp. 35s.

THIS collection of geophysical essays deals with our planet, the earth, from its inner core to its outer atmospheric fringe. Its appearance is as timely as it is welcome, for there could be no more authoritative commentary on the work of the International Geophysical Year 1957–1958 which is now in progress. Professor D. R. Bates, the editor of the volume, has assembled a distinguished group of specialists to write the various essays, all of whom seem, by editorial instruction or otherwise, to have addressed themselves to the same type of reader. The result is that the volume exhibits a remarkable homogeneity, each author starting at the beginning and yet managing to lead his reader to his own section of the frontier of knowledge.

The volume contains seventeen essays in all, the subjects and authors being as follows:—The International Geophysical Year: S. CHAPMAN; Origin, age, and possible Ultimate Fate of the Earth: GERARD P. KUIPER; The Deep Interior: K. E. BULLEN; The Crust: J. TUZO WILSON; The Oceans: G. E. R. DEACON; Geomagnetic Field: E. H. VESTINE; Composition and Structure of the Atmosphere: D. R. BATES; Climate: E. T. EADY; The General Circulation of the Atmosphere and Oceans: E. T. EADY; Ice Ages: E. J. ÖPIK; Meteorology: B. J. MASON; The Ionosphere: J. A. RATCLIFFE; The Airglow: D. R. BATES; Aurorae and Magnetic Storms: V. C. A. FERRARO; Meteors: A. C. B. LOVELL; Cosmic Radiation: J. G. WILSON; and Genesis of Life: J. B. S. HALDANE.

The whole volume can be recommended as providing the general reader with friendly guidance in understanding the problems being attacked during the intensified activity of the I.G.Y. And there is little doubt that, as forecast by the editor himself, the book will even provide the specialist with useful introductions to those branches of geophysics he has not himself studied.

It only remains to add one word of mild criticism. While undoubtedly the essays are devoted to subjects, rather than to the *experimental methods* by which those subjects are being advanced, one might have expected greater reference to instrumented-satellites and instrumented-rockets than is found here.

E. V. APPLETON

M. WALDMEIER: **Die Sonnenkorona-Struktur und Variationen der Korona**, Band 11. Birkhäuser Verlag, Basel und Stuttgart, 1957. 353 pp., 299 diagrams, 68.50 SFr.

THIS is the second of a series of volumes which the author has planned to treat comprehensively all aspects of coronal research. When he began his observational work at the Arosa high-altitude station in 1938, the corona was still a mysterious phenomenon whose physical constitution was little understood. Almost nothing was known about its density, temperature or chemical composition. All this has been altered by astonishing developments in coronal research during the past 20 years. The great puzzle of the origin of the emission lines has been resolved; and the temperature—one million degrees—shows it to be the hottest gas accessible to observation. Its high temperature leads to the emission of ultra-violet light, X-rays and

to solar radio waves. Our understanding of the corona has thus become of paramount importance to astrophysics, on the one hand, and to the study of solar–terrestrial relations, on the other.

The first volume (1951) was mainly a compilation of the observations made over one 11-year cycle (1938–49). The present work brings the observations up to 1954 and discusses the behaviour of the principal emission lines over the 16-year period. Much space is devoted to the rare and interesting appearances of the yellow line, 5694 Å. This originates in the ion Ca (XV), which has the highest ionization potential (814 eV) of any coronal line. Waldmeier's maps show that these appearances are closely confined to the regions above the giant F-type sunspots. The same regions are characterized by special activity in flares and sunspot prominences, and they must be regarded as the hottest spots within the corona.

Numerous isophotal maps, tables and solid models are made use of to illustrate the intensity distributions with latitude of the lines 5303, 6374 Å and their variations throughout the cycle. Other chapters deal with coronal condensations and isophotal contours, and the book contains large numbers of heliographic maps of the corona for comparison with those of the photosphere.

One can only marvel at the vast amount of observational material which is here so uniformly presented and discussed. The format and printing are both of the highest standard. The future volumes, which are designed to cover the physical aspects of the problem, will be awaited with interest.

M. A. Ellison

Books received

H. E. Landsberg (edited by) *Advances in Geophysics, Vol. III.* 378 pp. (Academic Press Inc., New York, 1957) $8.80.

H. Israël *Luftelektrizität und Radioaktivität* (Verständliche Wissenschaft 62nd volume). 125 pp. (Springer Verlag, 1957) D.M. 7.80.

J. Allan Chalmers *Atmospheric Electricity.* 327 pp. (Pergamon Press, 1957) 63s. ($10).

The United Kingdom Contribution to the I.G.Y. 1957–58. 72 pp. (The Royal Society, 1957) 10s. net.

S. H. Gould *Variational Methods for Eigenvalue Problems.* 179 pp. (University of Toronto Press, 1957) 48s.

D. Pedoe *International Series of Monographs in Pure and Applied Mathematics.* Vol. 2: Circles. 78 pp. (Pergamon Press, 1957) 20s.

H. Weickmann and Waldo Smith (edited by) *Artificial Stimulation of Rain* 427 pp. (Pergamon Press, 1957) £5. 5s.

Karl Rawer *The Ionosphere* (Frederick Ungar Publishing Co. New York, 1957) $7.50.

B. J. Mason *The Physics of Clouds* 481 pp. (Oxford University Press, 1957) 70s.

D. R. Bates *The Planet Earth.* 312 pp. (Pergamon Press, 1957) 35s.

A. C. B. Lovell and R. Hanbury Brown *The Exploration of Space by Radio.* 207 pp. (Chapman and Hall, 1957) 35s.

F. H. Ludlam and R. S. Scorer *Cloud Study. A Pictorial Guide.* 80 pp. (John Murray, 1957) 12s. 6d.

M. Zelikoff (edited by) *The Threshold of Space.* 342 pp. (Pergamon Press, 1957) £5. 5s.

Heinz H. Lettau and Ben Davidson (edited by) *Exploring the Atmosphere's First Mile Volume I: Instrumentation and Data Evaluation. Volume II: Site Description and Data Tabulation.* 578 pp. (Pergamon Press on behalf of Geophysics Research Directorate, Air Force Cambridge Research Center, Air Research and Development Command, 1957.) £7. 0s per set.

VOL. 12 1958

Journal of Atmospheric and Terrestrial Physics, 1958, Vol. 12, pp. 89 to 99. Pergamon Press Ltd., London

The diurnal and seasonal variations of spread-*F* ionospheric echoes and the scintillations of a radio star

B. H. Briggs
Cavendish Laboratory, Cambridge

(*Received* 9 *November* 1957)

Abstract—A comparison is made of the spread-*F* ionospheric echoes observed at Slough (52°N) and Inverness (57°N). It is found that the degree of spreading is greater at the station of higher latitude. The diurnal and seasonal variations are similar at the two stations. The diurnal and seasonal variations of the scintillation index of the radio star in Cassiopeia are explained in terms of measured ionospheric parameters (spread-*F* index and critical frequency) together with the change of zenith angle of the source. A large seasonal anomaly which was previously thought to exist is found to be much reduced when all the relevant factors are taken into account.

1. Introduction

The close association of the scintillations of radio stars with the occurrence of "spread-*F*" ionospheric echoes has been described by several workers (Ryle and Hewish, 1950; Little and Maxwell, 1951; Hewish, 1951 and 1952; Wells, 1954; Hartz, 1955; Wright *et al.*, 1956; Dagg, 1957; Singleton, 1957; Briggs, 1958). It has been generally supposed that both phenomena are caused by the same ionospheric irregularities in the upper part of the *F*-region. If this is so, it would be expected that the diurnal and seasonal variations of the two phenomena would be similar. This is not found to be the case, and it is the object of the present paper to examine some possible reasons for the differences.

The main facts about the diurnal and seasonal variations are as follows. The spreading of the echoes from the *F*-region at Slough begins at sunset and increases throughout the night. It reaches a maximum just before sunrise, and then decreases rapidly. The scintillation index of the source in Cassiopeia as observed at Cambridge is a maximum near midnight and decreases to a small value several hours before sunrise (Ryle and Hewish, 1950). Spread-*F* echoes occur much more frequently, and with a greater extent of spreading, in winter than in summer. The scintillations of the radio star show little seasonal change (Hewish, 1952). We therefore have to explain both a *diurnal anomaly* and a *seasonal anomaly*.

An explanation of these anomalies which has been suggested is that the ionospheric irregularities may sometimes be "blanketed" by uniform ionization below them. They would then still affect the waves from the radio star and cause scintillations, but they would not cause spread echoes. In fact, if they were above the maximum of the *F*-region, they would be completely unobservable by reflected waves. Booker and Wells (1938) first suggested that the rapid disappearance of the spread echoes at sunrise was due to the formation of new ionization lower down. They suggested that the irregularities were present all the time and that the observed diurnal variation was due entirely to blanketing. If this were true, however, the observed maximum of the scintillation index at midnight would be even more difficult to explain. The blanketing hypothesis has more success in

reconciling the differences in the seasonal variations. The greater ionization density of the F-region by night in summer might prevent the observation of the irregularities by reflected waves and could explain the marked seasonal variation of spread-F echoes. It is, however, unsatisfactory to invoke the hypothesis to explain the seasonal anomaly when it makes the diurnal anomaly even more serious. We shall therefore reject the blanketing hypothesis, and try to find some other explanation of the anomalies.

A more careful consideration of the spread-F and scintillation phenomena suggests that the relation between them would not be expected to be simple. The following points suggest themselves as being worthy of further examination.

(a) *Geographical variations*

The observations of spread-F echoes at a single ionospheric station refer to conditions at a fixed point in the ionosphere. In the observation of scintillations, however, we are concerned with a region of the ionosphere which moves about in the horizontal plane as the position of the source changes in elevation and in azimuth. It may be that the degree of irregularity of the ionosphere changes from point to point in the horizontal plane. If this is so, the variation must be allowed for before the diurnal variation of the scintillation index can be related to that of the spread-F index. In Section 2 we shall consider this point in more detail and shall attempt to allow for variations in the horizontal plane by making use of observations from two ionospheric stations.

VOL. 12 1958

(b) *The effect of the ionized background*

It might be expected that the effect of the ionosphere on the waves from the star would depend on the mean ionization density as well as the intensity of the irregularities. This point is examined in Section 3. It is shown that the critical frequency of the F-region must be introduced as another parameter before the variations of the scintillation index can be predicted. The critical frequency has its own diurnal, seasonal, and geographical variations.

(c) *The effect of the zenith angle of the source*

The ionospheric irregularities produce irregular phase variations across the wavefront arriving from the star. The magnitude of the phase variations depends upon the thickness of the irregular region which is traversed, and this thickness varies with the zenith angle of the source. Further, the observed scintillation index depends upon the depth of the *amplitude fluctuations*, and Hewish (1952) has shown that these increase in depth as the wave travels downwards from the ionosphere. The distance travelled by the wave from the ionosphere to the point of observation varies with the zenith angle of the source. Both these effects mean that a given degree of irregularity of the ionosphere will produce the largest scintillation index when the source is at lower culmination and the zenith angle is a maximum. The way in which the scintillation index would be expected to vary with zenith angle is examined quantitatively in Section 4.

After a discussion of these three points we consider in Section 5 how far it is possible to account for the diurnal and seasonal variations of the scintillation index

in terms of observed ionospheric parameters together with the apparent motion of the source. The scintillation results which will be used are those of DAGG (1957) which relate to the source in Cassiopeia as observed at Jodrell Bank (53°N, 2°W).* The ionospheric data have been obtained from the stations at Slough (52°N, 1°W) and Inverness (57°N, 4°W).

2. GEOGRAPHICAL VARIATIONS

It is of some interest to compare the occurrence of spread-*F* echoes at two ionospheric stations of different latitudes. We shall therefore discuss this point separately before considering its application to scintillations. The two stations mentioned above differ in latitude by 5°, and the more northerly one, at 57°N, is not very far from the auroral zone.

A study has been made of the occurrence of spread-*F* echoes at the two stations for the following months: September 1954, December 1954, March 1955, and June 1955. These are the same months which were studied in another connexion in an earlier paper (BRIGGS, 1958). As explained in the earlier paper, a measure of the spreading of the echoes can be obtained in two ways. The published "Bulletins of Ionospheric Characteristics" can be used, in which the presence of spread-*F* echoes is indicated by the symbol "*F*". Alternatively, the hourly $h'(f)$ records themselves can be studied. In either case, a "spread-*F* index" in the range 0–3 can be defined. As we wish to compare the values of the spread-*F* index at the two stations, it is important to use a consistent method of analysis. The published Bulletins are compiled at the stations themselves by different persons, and there is the danger that a systematic error may arise due to a different use of the symbol "*F*" at the two stations. This point can be investigated by comparing the index obtained from the Bulletins with the index obtained from the records, as analysed by the same person.

In Fig. 1 the monthly mean spread-*F* index obtained by the author from the records for Slough is compared with that obtained from the Bulletins. While in general the forms of the diurnal curves are similar, the actual value of the index obtained from the records is much higher than that from the Bulletins. The month of June 1955 is an extreme case, where an index of zero was obtained from the Bulletins at all hours, though the index from the records reached a mean value of slightly over unity. This difference would not be serious in itself, since the definitions of the indices are somewhat arbitrary, and there is no reason to expect the actual values to agree. It is clear, however, that the index obtained from the Bulletins is not useful in the summer months, as it is zero for most of the time.

In Fig. 2, similar curves are plotted for Inverness. For this station there is much better agreement between the values obtained by the two methods. This shows that the symbol "*F*" in the Bulletins is *not* used consistently by the two stations.

If Figs. 1 and 2 are compared it will be seen that if the Bulletins alone had been used the erroneous conclusion would have been reached that the spread-*F*

* The reason for using the results for Jodrell Bank was that these were the most complete results which were available. The scintillation records obtained at Cambridge are usually spoilt in the daytime by interference, so that results are available for the night-time only.

index is much greater at Inverness than at Slough. The results obtained from the records show that the real difference is not very large.

No further use will be made of the results obtained from the Bulletins. The results obtained from the records will now be discussed in more detail in order to

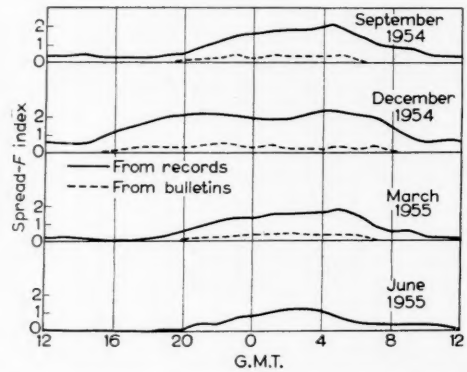

Fig. 1. The diurnal variation of the spread-F index at Slough for 4 different months. The results obtained from the published Bulletins are compared with the results obtained from the $h'(f)$ records themselves.

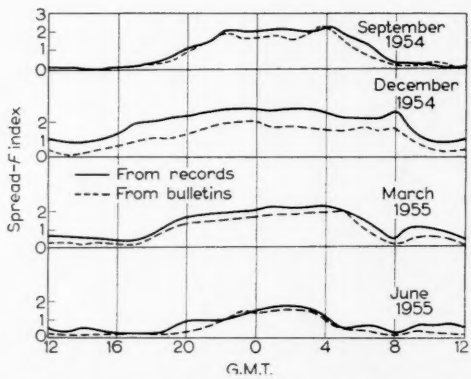

Fig. 2. The diurnal variation of the spread-F index at Inverness for 4 different months. The results obtained from the published Bulletins are compared with the results obtained from the $h'(f)$ records themselves.

bring out the real differences between the two stations. These can be seen more clearly in Figs. 3–6. The top curves in these figures show the monthly mean diurnal variation of the spread-F index at the two stations. The differences between the curves is greatest in the early part of the night, when the spread-F index at Inverness may be double that at Slough. As sunrise approaches, the curves come closer together. There is, however, no marked difference between the two stations either in the form of the diurnal variation or in the seasonal changes. If any special effects occur near the auroral zone, it appears that Inverness is not close enough to the zone to show them.

VOL. 12 1958

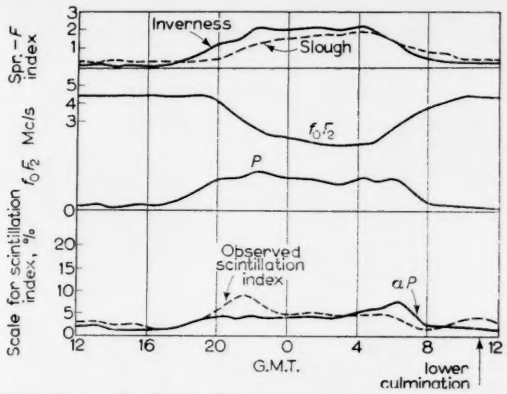

Fig. 3. Results for September 1954. The curves show the diurnal variations of the spread-F index, the critical frequency of the F-region, the quantities P and αP and the observed scintillation index (from DAGG, 1957).

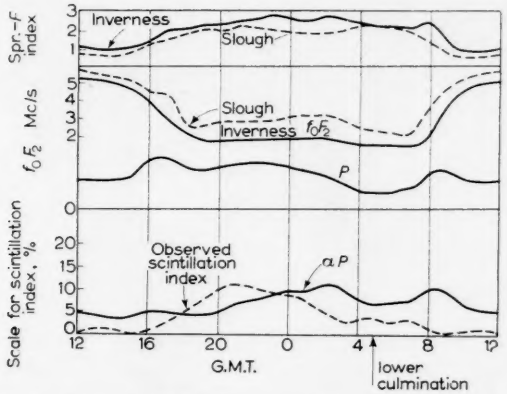

Fig. 4. Results for December 1954. The curves show the diurnal variations of the spread-F index, the critical frequency of the F-region, the quantities P and αP and the observed scintillation index (from DAGG, 1957).

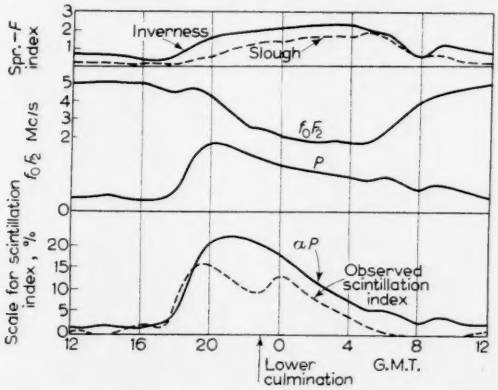

Fig. 5. Results for March 1955. The curves show the diurnal variations of the spread-F index, the critical frequency of the F-region, the quantities P and αP and the observed scintillation index (from DAGG, 1957).

We now return to the problem of the stellar scintillations, and consider how the diurnal variation of the scintillation index will be related to that of the spread-*F* index. It will first be necessary to consider how the effective region of the ionosphere moves about in the horizontal plane.

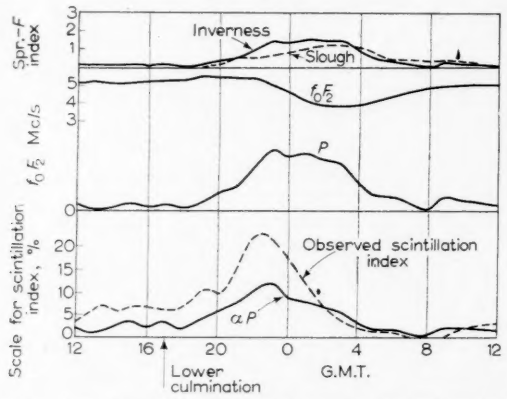

Fig. 6. Results for June 1955. The curves show the diurnal variations of the spread-*F* index, the critical frequency of the *F*-region, the quantities P and αP and the observed scintillation index (from Dagg, 1957).

If a height is assumed for the ionospheric irregularities, the latitude and longitude of the effective region can be determined at any time. For the purposes of this calculation, a height of 400 km was assumed. It was then found that the *longitude* of the region did not differ at any time by more than 8° from the longitude of either ionospheric station. This corresponds to $\frac{1}{2}$ hr in time, and as the diurnal curves show little change in a time as short as this, it was not necessary to make any correction for the longitude variations. The way in which the *latitude* of the effective region varies with the hour angle of the Cassiopeia source is shown in Table 1.

Table 1

A	0	1	2	3	4	5	6
B	53·7	53·8	54·0	54·2	54·5	55·0	55·8
A	7	8	9	10	11	12	
B	56·8	57·9	59·0	60·0	60·6	61·0	

A Hours before or after upper culmination of the Cassiopeia source.
B Latitude of the effective region of the ionosphere. The irregularities were assumed to be at 400 km, and the values were calculated for Jodrell Bank.

It will be seen from the table that the latitude is sometimes intermediate between the latitudes of Slough (52°N) and Inverness (57°N) and sometimes it is north of Inverness. When the latitude was between that of the two stations, linear interpolation was used to determine the monthly mean spread-*F* index from its known values at the two stations. Similarly, when the latitude was north of Inverness,

linear extrapolation was used. This procedure is justifiable at most times, because the differences between the two stations are not large. It may, however, require further consideration at the times when the effective region is at its most northerly position, which is quite close to the auroral zone. It was not possible to make any further investigation of effects near the auroral zone with the ionospheric data which were available.

When the interpolation or extrapolation procedure had been carried out according to the position of the ionospheric region at each hour, a new diurnal curve for the spread-F index was obtained. This new curve was different from the curves at either ionospheric station, and it is the one which is relevant to a discussion of the diurnal variation of the scintillation index.

3. The Effect of the Ionized Background

Let the ionospheric irregularities be situated in a region where the mean ionization density is N, and let the perturbations due to the irregularities be of magnitude ΔN. It can be shown that the magnitude of the irregular phase variations produced across the wavefront from the star will be proportional to $\sqrt{n}\,\Delta N$, where n is the number of irregularities traversed (Ratcliffe, 1956, p. 221). In this section we consider only the magnitude of ΔN; the other factor $\sqrt{n}$ is discussed in Section 4.

Let f_0 be the critical frequency of the region, and Δf_0 be the spread in critical frequency. Then N is proportional to f_0^2, and therefore ΔN is proportional to $f_0\,\Delta f_0$. Now, the spread-F index used in this paper, and defined in an earlier paper (Briggs, 1958), is roughly proportional to the spread in the critical frequency Δf_0. Thus the value of ΔN will be proportional to the product of the critical frequency and the spread-F index.

In this way the critical frequency of the F-region enters as another parameter which has its own diurnal, seasonal, and geographical variations. The values of the critical frequency at Slough and Inverness were obtained from the published Bulletins. Changes in the latitude of the effective region of the ionosphere were allowed for in the same way as for the spread-F index. However, in practice this procedure was found to be necessary only for the month of December. For the other months, the critical frequencies at the two stations were so nearly equal that the interpolation procedure was unnecessary.

The monthly mean values of critical frequency are plotted in Figs. 3–6. For December the curves for Slough and Inverness are shown separately. The interpolated curve is not shown.

The curves marked "P" in Figs. 3–6 were obtained by multiplying the interpolated values of the spread-F index by the monthly mean values of the critical frequency at each hour. The quantity P is proportional to the magnitude of ΔN, with due allowance for the changes in geographical position of the effective region of the ionosphere.

4. The Effect of the Zenith Angle of the Source

As the position of the source changes, the angle of incidence i of the waves on the ionosphere changes. This angle of incidence is a function of the zenith angle of

the source. If we assume that the thickness of the irregular region is constant, the thickness actually traversed by the obliquely incident wave is proportional to sec i. The number of irregularities along the line of sight is also proportional to sec i. If a number of irregularities are traversed successively, the r.m.s. phase deviation produced is increased in proportion to the square root of the number. It follows that the root-mean-square phase deviation is proportional to $\Delta N \sqrt{\sec i}$.

We have considered so far only the irregular phase variations produced across the wavefront. When the wave leaves the ionosphere there will be little or no amplitude variations across the wavefront. As the wave travels, the amplitude variations

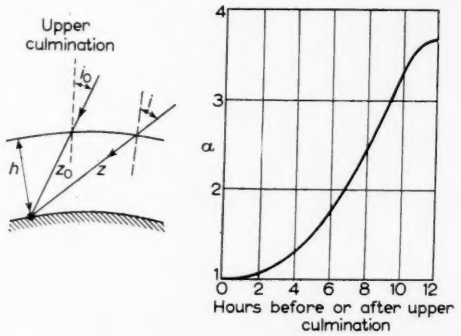

Fig. 7. The curve shows how the quantity $\alpha = (z\sqrt{\sec i})/(z_0\sqrt{\sec i_0})$ varies as a function of the hour angle of the source. The meaning of the symbols is shown in the diagram on the left.

will increase in depth in a manner which has been discussed by Hewish (1952). Now, the distance travelled by the wave from the ionosphere to the point of observation depends upon the zenith angle of the source in a way which can easily be calculated. Thus the zenith angle enters into the calculations in these two different ways.

Hewish (1952) has shown that the depth of the amplitude variations, and therefore the scintillation index, is approximately proportional to the r.m.s. phase deviation and to the distance z travelled by the wave from the ionosphere to the point of observation. This is not a general result, but the curves given by Hewish show that it holds quite accurately for the conditions with which we are concerned in the study of scintillations.

We conclude that the effect of the zenith angle of the source can be allowed for by multiplying the curve P already obtained by the quantity $z\sqrt{\sec i}$. In this expression, both z and i are functions of the zenith angle of the source and therefore of its hour angle. As we are not concerned with absolute values, but only with diurnal and seasonal changes, it is sufficient to consider the ratio

$$\alpha = \frac{z\sqrt{\sec i}}{z_0\sqrt{\sec i_0}}$$

where the values z_0 and i_0 refer to upper culmination. The quantity α is then unity at upper culmination, and it is found to reach a maximum value of 3·7 at lower culmination. The way in which α varies with the hour angle is shown in Fig. 7. This

VOL. 12 1958

curve is almost independent of the height assumed for the irregularities.*

We are now in a position to compare the results of the present calculations with the observed variation of the scintillation index. The lowest solid curves in Figs. 3–6 show the diurnal variation of the quantity αP. The results of DAGG (1957) are plotted for comparison as dotted curves.

5. DISCUSSION

The success or failure of the present ideas is to be judged by the extent to which the diurnal and seasonal changes of the quantity αP agree or disagree with the diurnal and seasonal changes of the scintillation index. The absolute value of αP has no direct significance, but in Figs. 3–6 the same scales have been used throughout so that the seasonal as well as the diurnal changes can be studied. We shall give a brief discussion of the results for each month. The times mentioned are all GMT.

September 1954 (*Fig.* 3)

The spread-F index is high from 2000 to 0600, with a broad maximum in between. The curve for P does not differ greatly in shape from the curves for the spread-F index. For this month, lower culmination is near 1100, so that α is largest at this time, and smallest at 2300. The curve for αP agrees fairly well with the curve for the scintillation index. The scale used to plot αP was chosen in such a way as to obtain the best fit with the scintillation curve, and the same scale was then used for the other months.

December 1954 (*Fig.* 4)

The spread-F index is high from 1600 to 0800 with a sharp decrease at 0900. The quantity P is large at all times, with a minimum near 0600. The value of α is high near this time, as lower culmination is at 0500. The final result is a curve for αP with a broad maximum from 2200 to 1000. This does not agree well with the observed scintillation curve, but the general level of the curve is of the right order of magnitude.

March 1955 (*Fig.* 5)

The variations of the spread-F index are very similar to those for the other equinoctial month of September (Fig. 3). The variation of critical frequency, however, is considerably different, and the variation of P is therefore also different. It has a maximum at 2000 and decreases throughout the night. For this month, lower culmination is at 2300, and so αP reaches very high values between 2000 and 0000, and is low in the daytime. This variation agrees well with the observed scintillation index.

* It will be seen from the diagram in Fig. 7 that if the earth were flat, the ratio z/z_0 would be independent of the height h of the irregularities. A small correction arises from the curvature of the earth. The curve of Fig. 7 was calculated for a height of 400 km, but it would not change very much for any height in the range 0–600 km.

June 1955 (*Fig.* 6)

There is little spreading of F-region echoes in this month; the mean index rises to 1·5 for a short period between 2200 and 0400. The night-time critical frequency, however, is high, and as a result the quantity P reaches values as high as those for the other months. Lower culmination is at 1700, so that αP tends to be large before midnight and small after midnight. It is found to have a maximum at 2300. The *variation* of αP agrees well with the variation of the scintillation index, but the actual values of αP are too small by a factor of about 2. This factor of 2 is what remains of the seasonal anomaly mentioned in Section 1 of the paper.

On the whole, the results are satisfactory. It will be seen that, in general, the variations of the scintillation index agree better with the calculated variations of αP than with the spread-F index at either station. The remaining discrepancies could be explained by the blanketing hypothesis. It should, however, be pointed out that the data used were obtained by allocating an index to each record by inspection, and not by actual measurement. The possible errors, therefore, are quite large, and it may be that the agreement is as good as can be expected. It is particularly difficult to obtain reliable values for the spread-F index in the winter, because the spreading is so great that any variations are no longer apparent.

It would be useful to repeat the calculations described in this paper for observations made in different parts of the world. The method could be extended and made more precise if ionospheric observations were available from several suitably situated stations. It would be particularly interesting to apply the methods to the scintillation results obtained at Ottawa (Hartz, 1955), because these differ considerably from those obtained at most other places. Hartz found little variation of the scintillation index with solar time; the main effect was a variation with sidereal time, with a maximum at lower culmination of the source. It is possible that this could be explained along the lines suggested in this paper, but it would be necessary to have results from ionospheric stations near the auroral zone. It is not certain that a reliable spread-F index can be defined for such stations, owing to the large amount of spreading which is nearly always present.

Another possible extension of the work would be to the study of the sunspot cycle variations. It would be of interest to see whether the same sort of considerations could be used to relate the sunspot cycle variation of the scintillation index to the sunspot cycle variations of the spread-F index and of the critical frequency of the F-region.

6. Conclusions

The main conclusions of this paper may be summarized as follows:

(1) In a comparison of the occurrence of spread-F echoes at different ionospheric stations, the published Bulletins should be used with care.

(2) The spreading of the F-region echoes at Inverness (57°N) is somewhat greater than at Slough (52°N), but there are no marked differences between the diurnal and seasonal variations at the two stations.

(3) The diurnal and seasonal variations of the scintillation index for the

VOL. 12 1958

source in Cassiopeia can be explained fairly well in terms of measured ionospheric parameters together with the apparent motion of the source. In particular, the seasonal anomaly, which was previously thought to be very large, is reduced to a factor of the order of 2.

(4) The methods used in the present paper should be applied to more extensive measurements. The sunspot cycle variations of the scintillation index and the spread-*F* index would also repay further study.

Acknowledgements—This work was carried out during the tenure of an Imperial Chemical Industries Fellowship. I am indebted to the Director of Radio Research, D.S.I.R., for making available the $h'(f)$ records for Slough and Inverness.

References

Booker H. G. and Wells H. W.	1938	*Terr. Mag.* **43,** 249.
Briggs B. H.	1958	*J. Atmosph. Terr. Phys.*
Dagg M.	1957	*J. Atmosph. Terr. Phys.* **10,** 204.
Hartz T. R.	1955	*Canad. J. Phys.* **33,** 476.
Hewish A.	1951	*Proc. Roy. Soc.* A **209,** 81;
	1952	*Proc. Roy. Soc.* A **214,** 494.
Little C. G. and Maxwell A.	1951	*Phil. Mag.* **42,** 267.
Ratcliffe J. A.	1956	*Reports on Progress in Physics* Vol. 19, p. 188. Physical Society, London.
Ryle M. and Hewish A.	1950	*Mon. Not. R. Astr. Soc.* **110,** 381.
Singleton D. G.	1957	*Aust. J. Phys.* **10,** 60.
Wells H. W.	1954	*J. Geophys. Res.* **59,** 273.
Wright R. W., Koster J. R. and Skinner N. J.	1956	*J. Atmosph. Terr. Phys.* **8,** 240.

Journal of Atmospheric and Terrestrial Physics, 1958, Vol. 12, pp. 100 to 109. Pergamon Press Ltd., London

Radio star scintillations at an equatorial station

J. R. KOSTER
Department of Physics, University College of Ghana, W. Africa

(*Received* 24 *September* 1957)

Abstract—Radio star scintillations have been observed at a frequency of 45 Mc/s over a period of 4 years at an equatorial station with a phase switching interferometer. Scintillation effects are found to be very severe, the output from even intense radio stars often dropping to zero. Scintillation occurs only at night, and is of nearly daily occurrence near sunspot maximum, correlating positively with the sunspot cycle. It correlates highly with the occurrence of spread-*F* echoes, but with no other geophysical phenomena. It is as yet unclear whether the observed results are due to absorption of the signal or can be accounted for by the impression of a much larger phase deviation on the emergent wave front by the diffracting screen responsible for scintillation. The phenomenon correlates highly with the trans-equatorial scatter of radio signals observed near sunspot maximum.

VOL.
12
1958

INTRODUCTION

AN interferometer for the observation of radio stars has been in continuous operation at the University College of Ghana, Achimota, (6°N, 0°W) since April of 1953. An analysis of the records for scintillation effects shows some significant differences between scintillation as observed at an equatorial station and that observed at higher latitudes.

1. EQUIPMENT

The receiving equipment is a phase switching interferometer of the type described by RYLE (1952). The aerials are broadside arrays, each made up of eight full-wave dipoles spaced a half wavelength apart and fixed a quarter wavelength above a reflecting screen. The axis of each array is along an E–W line, and the two arrays are at the ends of an E–W baseline 200 m (30 wavelengths) in length. This gives a beam width of 46° between half-power points in a N–S direction, and of 14·5° in an E–W direction, with a lobe spacing of nearly 2°. The frequency used is 45 Mc/s. The receivers are similar to those described by RYLE (1952) and the phase switch is of the stub type, but fully electronic, with the rotating condensers replaced by germanium diodes. Switching frequencies of 30 c/s and 5 kc/s were employed for some time before the present rate of 7·5 kc/s was adopted. The receiver is normally operated with an output time-constant of 3 sec. The records are made with an Evershed and Vignoles 0–1 mA recording milliammeter at a chart speed of 3 in/hr.

2. RADIO SOURCES USED

The seven radio stars which appear in the records with an amplitude sufficiently large to be of use in the analysis are listed in the table given below. The star numbers followed by (*R*) are those given by RYLE, SMITH and ELSMORE (1950);

those followed by (*M*) are given by MILLS (1952). The International Astronomical Union Number is that given by PAWSEY (1955).

The radio stars in the constellations of Taurus, Virgo, Cygnus and Cassiopeia are relatively intense, and give records which are always useful. The small source in Hydra has been observed quite consistently, even though it has a relatively low flux density. The amplitude of the trace produced by this source is so small that it is sometimes difficult to determine from it an accurate value of the fluctuation number, although it does indicate the presence or absence of scintillations.

Table 1

Constellation	Number	R.A.	Decl.	I.A.U. No.
		H. M.		
Taurus	05:01(*R*)	05 31	22°	05N2A
Hydra	09–1A(*M*)	09 20	−11°	09S1A
Virgo	12:01(*R*)	12 28	13°	12N1A
Hercules	16–0(*M*)	16 45	6°	16N0A
Ophiuchus	18–0(*M*)	18 10	−6°	18S0A
Cygnus	19:01(*R*)	19 57	40°	19N4A
Cassiopeia	23:01(*R*)	23 21	58°	23N5A

The trace recorded during the meridian transit of the portion of the sky from R.A. 16:30 to R.A. 19:00 certainly contains the radio stars in Hercules and Ophiuchus, but shows some evidence of several other sources as well.

Most of these sources remain in the aerial pattern for approximately one hour at upper culmination. Both Cygnus and Cassiopeia, however, because of their higher declination and their much greater intensity, can be observed for almost 2 hr at transit.

This group of observable sources yields useful records over 10 hr of each day. Thus there are long periods during which no observations of scintillation are obtainable with this equipment, even though the available radio sources are quite well distributed over the 24 hr. This is not a serious limitation as far as differentiating between quiet and disturbed nights is concerned, since it is found that the disturbances generally last for a period of 2 or 3 hr if they occur at all. It is therefore unlikely that a disturbance would be missed entirely. Neither does it prevent one from getting the mean diurnal curve, since one can get a large number of readings for any given hour in the course of a year. But it does severely restrict the study of the actual changes in fluctuation number during the course of a single night, and makes the detection of genuine seasonal variations difficult.

3. METHOD OF REDUCING RECORDS

In analysing records of this kind it is customary to represent the degree of variability in terms of a "fluctuation index", which is defined as the ratio of the mean deviation of the intensity to the mean intensity. On this scale a fully developed Rayleigh distribution of amplitude corresponds to an absolute fluctuation index of 0·52. The Cambridge radio astronomers have developed a more

convenient comparison scale, according to which an index number ranging from 0 to 5 is assigned to the scintillation. On this scale an index F-number is equivalent to an absolute fluctuation index of $F/10$. It was the original intention to adopt the same scale for the analysis of the present records, but this proved impossible, since it was found that the scintillation of radio stars in Ghana manifests itself not only by the rapid fluctuations in the amplitude of the sinusoidal trace produced as the radio star passes through the interferometer pattern, but is often accompanied by the partial or total disappearance of the trace itself. The scale finally adopted is given in Fig. 1. It is an entirely arbitrary one, derived by setting

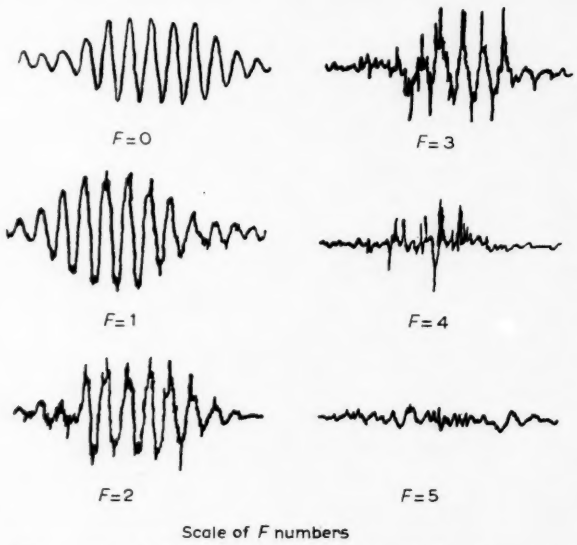

Fig. 1. The arbitrary scale of F-numbers used in the analysis. These are all recordings of the radio star in the constellation of Cygnus.

zero fluctuation as $F = 0$, complete disappearance of the source as $F = 5$, and then filling in the intermediate values with intermediate degrees of fluctuation and disappearance of the source. Values of fluctuation number on this scale are not directly comparable with those on the Cambridge scale. Changes in the rate of fluctuation, which are known to occur elsewhere, undoubtedly occur here as well, and they may influence to some extent the value assigned on this scale, although it is intended to show amplitude changes only.

4. The Diurnal Curve

In the analysis of the records the practice was adopted of assigning an F-number to each 20 min interval on the charts. Since a typical radio star was in the aerial pattern for approximately 1 hr per day, advancing 4 min in 24 hr, it is possible to get a series of 15 consecutive daily observations for each 20 min interval on the solar time scale. From these it is easy to plot mean F-number against local time for a given radio star. Fig. 2 shows two composite diurnal curves, the mean F-number from 3 sources being plotted against time of observation. The

VOL. 12 1958

upper curve was obtained near sunspot maximum, the lower one at sunspot minimum. Because of variations in the size of the diurnal curve for different radio stars, it was first necessary to normalize the values before combining them to give the above resultant curves.

The composite curves indicate the main features of the diurnal distribution of radio star scintillation in Ghana. It is, first of all, a strictly night-time phenomenon. Scintillation has never been observed before sunset, but frequently sets in between 1900 and 2000 local (GMT) time. The onset is often extremely abrupt, the F-number sometimes changing from $F = 0$ to $F = 5$ within a period

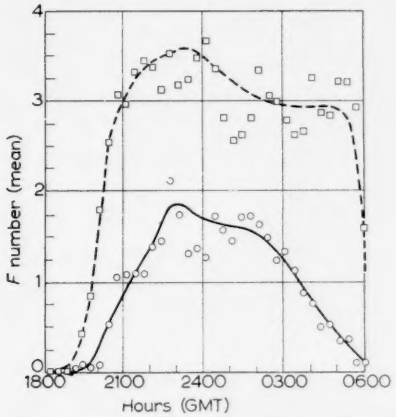

Fig. 2. Composite mean diurnal curves for sunspot minimum (○) and near sunspot maximum (□).

of from 5 to 10 min. The curve rises rapidly to a maximum at about 2220 hr, and then drops off more slowly, reaching a point near zero by sunrise. On only a few rare occasions, and these during magnetic disturbances, has scintillation been observed to extend into the hours of daylight.

5. The Frequency of Occurrence of Scintillations

The scintillation of radio stars is by no means an unusual or rare occurrence at the equator. The result of all records obtained from 1 April 1953 till 1 April 1957 can be summarized as in Table 2:

Table 2

Year	Number of nights	Number quiet	Number disturbed	% disturbed
1953	212	84	128	60
1954	310	169	141	45
1955	313	102	211	67
1956	272	33	239	86
1957	84	13	71	85
Total	1191	401	790	66

In the above table a "quiet" night is one on which all F-numbers were less than or equal to 2: a "disturbed" night is one on which at least one value of F was greater than 2. Severe scintillation effects were thus observed on two-thirds of all the nights on which observations were made. Inasmuch as there are many hours during which scintillation could have occurred without having been observed, since there may have been no star culminating at the time, the above must be taken as a minimum value, and the actual percentage of nights on which severe scintillation occurred may have been appreciably higher than the figure quoted here. It is extremely rare to find a night free from scintillation near sunspot maximum.

6. Scintillation and the Sunspot Cycle

Fig. 3 shows a plot of average fluctuation number (normalized) against time for various radio stars over the four year period covered by the present survey. A plot of sunspot number for the same period of time is given for comparison

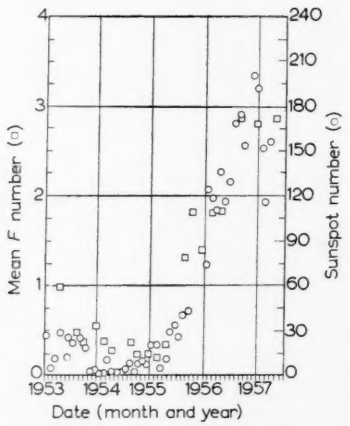

Fig. 3. The correlation of mean F-number (□) with sunspot number (○) for the four year period.

purposes. The plot shows conclusively that there is a very close positive correlation between fluctuation number and sunspot number. This result is worthy of note, since, as was pointed out by SINGLETON (1957), the literature shows that there is in general an inverse correlation between spread-F and sunspot number for low latitudes, the correlation changing to direct for latitudes greater than about 40°. Radio star scintillations correlate closely with spread-F echoes, as will be shown in the following paragraphs, and one would therefore expect an inverse correlation of scintillation with sunspot number.

7. The Correlation of Scintillation with Spread-F Echoes

A general feature of radio star scintillations is the positive correlation of the phenomenon with the occurrence of spread-F ionospheric echoes. Equatorial

VOL. 12 1958

scintillation is no exception in this regard, and an analysis of data available in 1953 and 1954 by WRIGHT, KOSTER and SKINNER (1956) showed that the correlation coefficient for 165 pairs of values representing the two phenomena was 0·46, a result which is highly significant even on the 0·1 per cent level. The ionospheric recordings for this comparison were made at the University College of Ibadan, Nigeria, some 450 km to the east of Achimota. Because several rather limited periods in the previous comparison showed a small correlation coefficient, and one of them even a negative one, it is desirable to make further comparisons using the newer data. The results are summarized in Table 3.

Table 3

Radio star	Number of observations	Date of observations	Correlation coefficient
Taurus	121	Oct. 1955–Mar. 1956	0·64
Hydra	111	Nov. 1955–Apr. 1956	0·58
Virgo	108	Jan. 1956–June 1956	0·51
Cygnus	72	May 1956–Sept. 1956	0·67
Cassiopeia	48	Oct. 1955–Dec. 1955	0·78
Cygnus	57	May 1955–Aug. 1955	0·54

Further comparisons could have been made with the data available from the latter part of 1956 and the early part of 1957, but by that time the occurrence of both phenomena became so nearly continuous as to make the correlation coefficient virtually meaningless. Further confirmation of the relationship seems quite unnecessary in any case.

The close correlation between scintillation at Achimota and spread-F echoes at Ibadan enables one to set a lower limit to the extent of the irregularities giving rise to both conditions. This extent is surely substantially greater than 500 km in an E–W direction. An upper limit to the extent in a N–S direction is provided by comparison of the Achimota scintillation results with those obtained at Cambridge. An early comparison of results from the two places by Smith (unpublished) showed that there was no significant correlation between the occurrence of scintillation at the two places. In the first several months' data examined, simultaneous observations were made at the two places on 22 different nights. These were divided into quiet and disturbed nights on a basis similar to that given above. A correlation coefficient of 0·08 was found between the two sets of values. This is deemed statistically insignificant, and leads to the conclusion that the extent of the ionospheric disturbances giving rise to scintillation must be less than 5000 km in a N–S direction.

It has been suggested by DAGG (1957) that it would be of interest to investigate the variations of the above correlation coefficient with time of night. He regards it as probable that the correlation would improve during the hours after midnight, when the masking effect of the F-layer would be less effective in screening the radio pulses from the irregularities which give rise to scintillation, these being thought of as distributed above the maximum electron density in the F-layer.

With this in mind, the data were divided into groups of 20 days each, and the corresponding correlation coefficients computed. The results are shown in Table 4.

Table 4

Time	Cass.	Taurus	Hydra	Virgo	Cygnus	Cygnus
04:20	—	0·11	0·57	0·34	0·60	—
03:00	—	0·22	0·57	0·49	0·55	0·76
01:40	—	0·73	0·45	0·53	0·60	0·25
00:20	—	0·96	0·52	0·77	0·29	0·58
23:00	—	0·53	0·70	0·45	—	0·66
21:40	—	0·87	0·42	0·52	—	0·71
20:20	0·80	0·81	0·65	0·51	—	—
19:00	0·75	0·43	—	0·53	0·58	—

One must conclude from the above that there is no significant increase in the value of the correlation coefficient during the hours after midnight for these two widely separated stations. This does not necessarily imply that DAGG's suggestion is untrue for equatorial results, however. The above results could only be considered as conclusive if they were derived from comparisons of records made at the same place and with sources sufficiently near the zenith to make it certain that both measurements are affected by the same portion of the ionosphere.

VOL. 12 1958

8. The Correlation of Scintillations with Other Phenomena

In the course of these investigations the correlation of scintillation with a number of other geophysical phenomena was investigated. These included solar flares, pulsational or polar sudden commencements, the planetary 3 hr range indices. No statistically significant correlations were found. Since no magnetic data were available from the vicinity, no comparison could be made with local magnetic variations. A rather extensive investigation led to the conclusion that there is no evidence for a lunar effect in the scintillation data.

9. Difference Between Scintillation at Achimota and That Observed at Higher Latitudes

When scintillation was first observed at Achimota, attention was drawn to the fact that it seemed to differ markedly in character from that observed elsewhere (HUNTLEY, 1953). Very frequently the sinusoidal trace from even an intense radio source such as Cygnus or Cassiopeia is entirely absent, as can be seen in Fig. 1. In order to investigate this effect further, an interferometer of much lower resolving power was constructed, each aerial being a single-folded dipole with a corner reflector, the two aerials being separated by a distance of 5 wavelengths. This gives a lobe separation of some 12°, about 6 times larger than that realized with the original instrument. The rest of the equipment is similar to that described above. Quite a number of simultaneous records were obtained with the two interferometers. In some cases the fluctuations bear a

marked resemblance to those recorded at higher latitudes with similar instruments. But it is very common for the amplitude of the trace even from the low-resolution interferometer to be reduced as much as 50 per cent of its normal value during times of scintillation, and quite frequently the trace disappears entirely. Examples ranging from zero scintillation through mild and severe cases are shown in Fig. 4. In each of the four examples given the upper trace

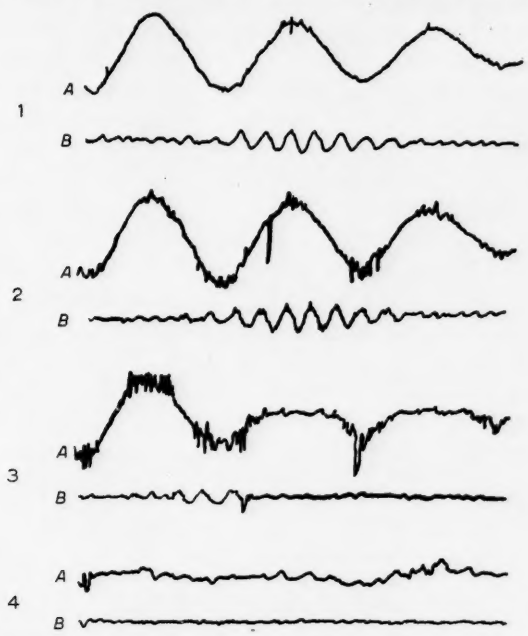

Fig. 4. Simultaneous records showing the diminution in amplitude of the trace of the radio star in Cassiopeia using a low-resolution interferometer (A) and the higher-resolution instrument (B).

(A) is that from the low-resolution interferometer and the lower trace (B) is that from the higher-resolution instrument used in the previous work. The second example in Fig. 4 and the first half of the third are very similar to the scintillation records obtained at Cambridge with a similar instrument. The last half of example 3 and the whole of example 4 are quite different, showing a great deal of diminution in the amplitude of the trace due to the radio star. These examples are all records of the radio star in Cassiopeia.

10. Possible Explanations of These Differences

The effects observed in the Ghana records could be accounted for in several ways. There is, first of all, the possibility that the incident radiation never actually reaches the ground at all during times of severe scintillation, but is absorbed or scattered in the ionosphere. The observed effects would also occur if the scale of the diffraction pattern across the ground were to become small compared to the aerial spacing. The signals in the two aerials would then become

completely incoherent and the amplitude of the output from a phase-switching interferometer would drop to zero. It follows from the theory developed by HEWISH (1951) that if the phase-changing screen responsible for scintillation effects introduces a much larger phase deviation at the equator than it does at higher latitudes this would give rise to a fine structure in the diffraction pattern which, especially if accompanied by a high drift velocity, could account for the observed effects. But a reduction of the scale of the diffraction pattern of the order of 100 is required to account for the observed effects. Further experiments are now in progress to determine whether the observed effects are the result of absorption or of a change of scale in the diffraction pattern across the ground.

Further evidence for unusual F-region conditions in equatorial regions was reported by FERRELL (1952) at a meeting of U.R.S.I. in Washington. The research data gathering project known as Radio Amateur Scientific Observations (R.A.S.O.) has collected information indicating a hitherto unreported post-sunset equatorial propagation effect. It was shown that during sunspot maximum frequencies in the 50–54 Mc/s amateur band were scattered across the equatorial regions of the western hemisphere to distances in excess of 4000 miles. The effects appear to be related to spread-F. The signals are often garbled and weak, and appear to result from F-region scattering. A similar effect, to be described elsewhere, has frequently been observed in Ghana during the past year, and seems to indicate very unusual night-time conditions in the F-region at the equator. It correlates so closely with the occurrence of scintillation that there seems to be little doubt of their common origin.

VOL. 12 1958

CONCLUSION

In conclusion, it can be stated that scintillation of unusual intensity occurs frequently at the equator. Its effects are so great that the observation of radio stars at longer wavelengths is extremely difficult during the hours of darkness except during the years near sunspot minimum. The evidence points to the F-region as the source of the disturbances. The same theory which has been successfully applied to scintillation at higher latitudes can be used here, but it is possible to explain the effects observed in the light of the theory only by postulating that the phase changing screen responsible for the phenomenon introduces a much larger deviation in phase at the equator than it does at higher latitudes. Unusual propagation effects observed at the equator indicate a considerable enhancement of the ability of the night-time F-layer to scatter radio waves. The origin of this enhancement is unknown.

Acknowledgements—Thanks are due to Professor H. E. HUNTLEY of the University College of Ghana for invaluable help in establishing the radio astronomy observatory and continued interest in the progress of the work; to Mr. MARTIN RYLE, F.R.S., of the Cavendish Laboratory and his research team for very useful advice on numerous occasions; to Dr. F. G. SMITH of the Cavendish Laboratory for permission to quote from his unpublished work; and to Mr. P. W. J. BLACK of the science workshops, University College of Ghana, for developing part of the electronic phase switch used in this work.

References

Dagg M.	1957	*J. Atmosph. Terr. Phys.* **10,** 204.
Ferrell O. P.	1952	*URSI, Proceedings of the General Assembly* Vol. IX, p. 100.
Hewish A.	1951	*Proc. Roy. Soc.* A **209,** 81.
Huntley H. E.	1953	*Nature, Lond.* **172,** 108.
Mills B. Y.	1952	*Aust. J. Sci. Res.* A **5,** 266.
Ryle M.	1952	*Proc. Roy. Soc.* A **211,** 351.
Ryle M., Smith F. G., and Elsmore B.	1950	*Mon. Not. R. Astr. Soc.* **101,** 381.
Pawsey J. L.	1955	*Astrophys. J.* **121,** 1
Singleton D. G.	1957	*Aust. J. Phys.* **10,** 60.
Wright R. W., Koster J. R. and Skinner N. J.	1956	*J. Atmosph. Terr. Phys.* **8,** 240.

OL.
2
958

Journal of Atmospheric and Terrestrial Physics, 1958, Vol. 12, pp. 110 to 117. Pergamon Press Ltd., London

Differences between the east–west and west–east propagation of VLF signals over long distances

D. D. CROMBIE
Dominion Physical Laboratory, Department of Scientific and Industrial Research, Lower Hutt, New Zealand

(*Received* 2 *October* 1957)

Abstract—An early suggestion by ROUND, ECKERSLEY, TREMELLEN and LUNNON that VLF signals received from the west are less attenuated than those from the east is investigated. The original evidence, together with further experimental data, give strong support to the hypothesis. The outline of a possible explanation of the effect is given.

1. INTRODUCTION

IN 1925, ROUND, ECKERSLEY, TREMELLEN and LUNNON, while discussing the results of a comprehensive series of VLF signal strength measurements made during a trip round the world, suggested that VLF signals which had travelled long distances were less attenuated if they had travelled from west to east instead of from east to west.

AUSTIN (1928), while reviewing unsolved radio problems, drew attention to this suggestion. There seems to have been nothing further reported in the literature until 1950, when TREMELLEN in a condensation of the data used by ROUND *et al.* (1925) considered that it was still not certain whether such an effect did exist.

In 1954, BUDDEN showed that propagation between two similar antennae along the direction of the earth's magnetic field must be reciprocal. He also stated that for certain angles of incidence of the waves on the ionosphere, the reciprocity condition was not satisfied if the direction of propagation was across the earth's field. No indication of the magnitude of the discrepancy, or its dependence on frequency, was given.

A recent attempt (CROMBIE *et al.*, 1957) to explain the diurnal phase variations observed in New Zealand on the highly frequency-stable transmissions from Rugby, suggested that the signals are received predominantly by the short great circle path of 18,700 km, both by night and by day, rather than by the long path of 21,300 km. Subsequent measurements (which will be discussed later) show that the signal over the short NNW path is 5–10 dB greater than that over the long SSE path. The relation between signal amplitude E and distance d can be written as

$$E \propto \exp(-dA) \tag{1}$$

where A is the attenuation constant. The antipodal focusing is necessarily the same on both the paths. The paths differ in length by about 2600 km, and if the difference in signal strength is to be attributed merely to the difference in length, it is necessary to assume an attenuation with a value between 2 and 4 dB/1000 km. These values are unreasonably large. Thus, WAIT (1957) has predicted an attenuation rate of 0·9 dB/1000 km for 16 kc/s (see Fig. 1).

VOL. 12 1958

This seems to be another example of the kind discussed by ROUND *et al.* The short path approaches New Zealand from NNW and propagation on this path seems to be unexpectedly favoured. The present paper reviews the available literature on the topic. It is concluded that the evidence strongly supports the hypothesis of ROUND *et al.* (1925).

2. EXPERIMENTAL EVIDENCE

In the paper by ROUND *et al.*, a large quantity of data on the measured field intensities of several VLF transmitters situated in Europe and the U.S.A. was given. A great deal of this was obtained on board ship during a trip round the world, and is not directly applicable to the present discussion. This is because the ship could not follow great circles through all the transmitters, and because the relative amounts of the paths in daylight and dark are unknown.

Much more important for the present discussion, however, are two series of measurements of the diurnal variation of field strength, and of azimuthal direction of arrival, which were made at Perth and Melbourne upon the European and North American transmissions. These measurements are particularly valuable because Perth is close to the antipodes of the North American transmitters, while Melbourne is relatively close to the antipodes of those in Europe. Thus, in the event of the path attenuation being independent of direction, the signals over the short and long great circles should be of comparable strength.

These two sets of measurements showed that the signal was received over both the short and long great-circle paths, and that the attenuation over a particular path was greater when that path was daylit than when it was dark. In general, the diurnal variation of signal strength showed two maxima, corresponding to the time at which each of the paths had its maximum length in darkness. This is particularly true for the higher-frequency signals.

It was also found that, in general the two maxima had different values. Particularly at the lower frequencies, this difference could be explained by supposing that apart from the effects of daylight and darkness, the signal which came from the west was less attenuated than that from the east. This was true even for the measurements made at Melbourne on the North American transmissions, where the path from west to east is the longer by a factor of 1·35.

The relevant data from ROUND *et al.* have been summarized in Tables 1 and 2. These show the ratios of the maximum signal strengths over the two paths. The observations of transmissions from Europe to Perth have not been included, partly because the west to east path between these points is much shorter than the east to west path, and partly because the original data are somewhat ambiguous. For the purpose of determining the lengths of the paths in Tables 1 and 2, Paris has been taken as the "centre of gravity" of the European transmitters, and New York as that of the North American transmitters. The resultant errors should be less than 1000 km.

In what follows, an attempt is made to estimate the difference in rates of minimum attenuation of signals from the west and of signals from the east. If the signals from the east are attenuated at the rate of $(A + \frac{1}{2}\Delta A)$ dB/1000 km,

Table 1. Ratios of the maximum signals from the west and east. European transmitters measured at Melbourne

Transmitter	Frequency (kc/s)	Ratio of signal strengths $\frac{\text{W–E}}{\text{E–W}}$
LY Bordeaux	12·8	>12·0
YN Lyons	19·4	>5·0
OUI Hanover	20·4	3·4
UFT Paris	20·7	3·4
MUU Caernarvon	21·2	2·1
POZ Nauen	23·8	6·8

Long path Paris–Melbourne ~23,200 km (E–W)
Short path Paris–Melbourne ~16,800 km (W–E)

Table 2. Ratios of the maximum signals from the west and east. North American transmitters, measured at Perth and Melbourne

Transmitter	Frequency (kc/s)	Ratio of signal strengths $\frac{\text{W–E}}{\text{E–W}}$ at Perth	at Melbourne
WQL	17·0	8·15	3·1
WQK	18·3	10·0	1·0
WGG	18·75	2·4	1·0
WII	22·1	0·37	0·31
WSO	26·0	—	0·38

Long path from New York (W–E)	21,000	23,000 km
Short path from New York (E–W)	19,000	17,000 km

and the length of path in units of 1000 km is d_E, while the corresponding values for signals from the west are $(A - \frac{1}{2}\Delta A)$ and d_W, the difference in signal level D, is

$$D = (A - \tfrac{1}{2}\Delta A)d_W - d_E(A + \tfrac{1}{2}\Delta A)$$

Thus

$$\Delta A = -\frac{D - A(d_W - d_E)}{\frac{1}{2}(d_W + d_E)} \qquad (2)$$

and the difference ΔA in attenuation rate can be estimated if A is known. The values of A that have been used are shown in Fig. 1. They were obtained from the work of Wait (1957) and Eckersley (1925), which does not take into account the presence of the earth's magnetic field.

The data from Tables 1 and 2 have been treated in accordance with equation (2),

VOL. 12 1958

using the values of A from Fig. 1; the resulting values of ΔA are shown in Fig. 2. It would seem from this that there may indeed be a difference in the rate of attenuation of signals from the west and from the east. The difference is larger at the lower frequencies and propagation from the west is favoured. The figure also suggests that above 20 kc/s, propagation from the east is favoured. The reasons for

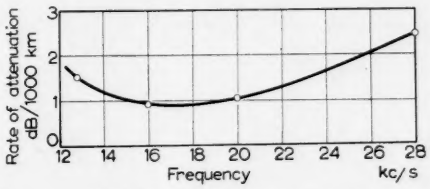

Fig. 1. Attenuation rate adopted for the purposes of this paper. The figures are based on the work of WAIT (1957) and ECKERSLEY (1932).

this apparent reversal are not clear. Apart from experimental errors, it may be due to the use of wrong values, for A, or possibly due to the fact that the long path is never completely dark. Alternatively the apparent reversal may be due to the presence of more land under the W–E paths, as discussed later.

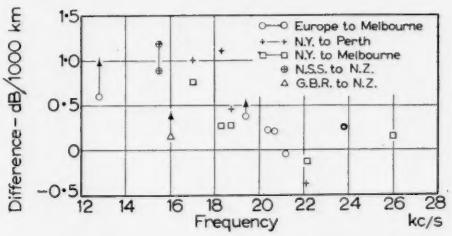

Fig. 2. Difference between attenuation rates of E–W and W–E paths. A positive difference gives the W–E path a smaller attenuation constant. The vertical lines denote uncertainty in the data.

2.1. *Recent measurements in New Zealand*

As pointed out in Section 1, there is reason to suspect that of the two great-circle paths between Rugby and Wellington, the signals from GBR are received predominantly by the short path which has a small west to east component. Observations have been made recently to elucidate this matter.

A loop aerial (one screened turn, 10 ft^2) and a vertical aerial were so connected through a gain and phase adjusting network that a cardioid polar diagram was obtained whose direction of maximum gain could be reversed by reversing the loop connexions. This was done automatically every half-hour, and the output of the receiver recorded.

The loop orientation and the network were initially adjusted for maximum front-to-back ratio by making use of the strong 16·6 kc/s signals from NPM in Hawaii, whose bearing is about 35° east of Rugby. After this was done, the loop was rotated through 35° to the west, on to the direction of maximum signal from Rugby.

The results of three sets of measurements each lasting 24 hr and taken at weekly intervals are shown in Fig. 3.

The reasons for the rather large differences between the signals recorded from the SSE on these three occasions are not understood, but it may be connected with the fact that the observations unfortunately coincided with IGY alerts.

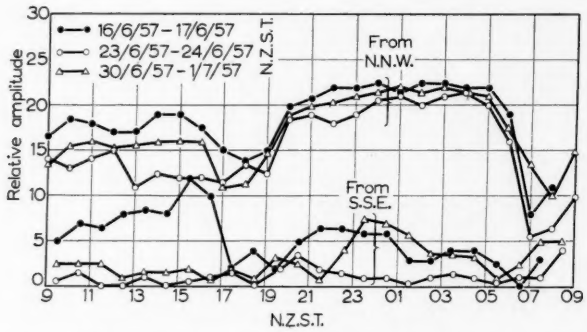

Fig. 3. Comparison of signal strengths of GBR received in New Zealand over the long and short paths.

Further observations have not been possible, because GBR has ceased transmission for the present and the date of its resumption is not known.

However, it can be seen from Fig. 3 that the difference between the maximum signals from the SSE and from the NNW is between 5 dB and approximately 10 dB. Application of the procedure outlined in the previous section indicates that the difference in rates of attenuation of the two paths is between 0·15 and 0·4 dB/1000 km. These points are shown on Fig. 2.

Observations have also been made at this Laboratory on transmissions from NSS, situated at Annapolis, U.S.A., and operating on 15·5 kc/s. These have been made with the same aerial system as before, but it has been necessary to rectify the output of the receiver before recording, instead of using the coherent integrator system used on GBR. Consequently, it has been difficult to separate the weak signals received over the short path (from the east) from noise. Over a large portion of the day, the signal from the west (the long path of about 26,000 km) is at least 6–12 dB above the apparent maximum signal from the east. The difference between the rates of attenuation of the E–W and W–E paths is between 0·8 and 1·05 dB/km, and these points are also shown on Fig. 2.

By contrast, it may be remarked that station NPG at 18·6 kc/s near San Diego is always received most strongly by the short path from the east and is barely detectable from the west. Station NPG is somewhat nearer to New Zealand than is NSS, but it will also be noticed that its frequency is higher than that of NSS and in consequence, judging from the trend of points in Fig. 2, one may expect its transmission from the west to be less strongly favoured than that of NSS.

2.2. *VLF signals from lightning*

Hepburn (1957) has reported that atmospherics received in the U.K. from

VOL. 12 1958

the south-west and from the south-east have different waveforms. Those from the south-west are more frequently of the "smooth" type, having a quasi-sinusoidal waveform, while those from the south-east are of the "reflection" type, and are much less smooth in character. CHAPMAN and PIERCE (1957) have also published similar data. It seems that these observations might be explained if the lower frequencies suffered less attenuation in travelling from the west than from the east. They might then be dominant in the south-west signal, giving it a smooth waveform, but be absent in signals from the south-east.

Whether this explanation is the correct one might be decided by a repetition of the experiments of HEPBURN, or of CHAPMAN and PIERCE, on the east coast of a continent such as North America, or an island surrounded by sea to considerable distances. If the results from such an experiment were similar to those of HEPBURN, etc., it would be strong evidence for a frequency-selective east–west effect.

3. DISCUSSION

All the relevant data discussed above are shown in Fig. 2. A study of this suggests two main features:

(1) The rate of attenuation of signals received from the west is less than that of signals received from the east.

(2) This difference decreases as the frequency increases and probably disappears above about 20 kc/s.

These results refer to signals which are received over paths that are not illuminated by the sun.

Three possible causes of these effects will be discussed, but it will be seen that none of the three afford a consistent explanation of the data.

(a) *The assumed attenuation rates*

If the assumed rate of attenuation shown in Fig. 1 were larger at the lower frequencies, then the results for the cases in which the west-east path is shorter than the east–west path could be explained. However, the results for the cases in which the west–east path is the longer could not be explained on this basis; moreover, for these paths the difference in rate of attenuation shown in Fig. 2 would be increased.

(b) *Seasonal effects*

The data on which Fig. 2 is based may simply indicate a seasonal effect in the ionosphere so that signals travelling by paths through the Southern and Northern Hemispheres are attenuated differently. Observations over the course of a year would confirm or deny this possibility. However, the observations of ROUND *et al.* (1925) at Melbourne and Perth were made over the periods from 15 May 1922 to 15 September 1922 and from 15 December 1922 to 22 January 1923, respectively. That these two sets of data are consistent, supports the view that the above conclusions are not entirely due to seasonal variations. It is not known whether the results of HEPBURN, etc. show seasonal variations.

(c) *Effect of land*

Different paths may show different attenuations because one traverses more land than the others. A brief investigation of this possibility has been made, the results being given in Table 3, which shows the relative amounts of land for each path. The total attenuation, based on average rates of 1 dB/1000 km for sea, and 2 dB/1000 km for land (WAIT, 1957), is also given for each path. In only two cases—New York to Perth and Rugby to Wellington—does the calculation predict that the east–west path should have the higher attenuation, and in the path from New York to Perth the predicted difference is only 3 dB. While the presence of land might account for the Rugby–Wellington result in Fig. 2, it could not account for the others. Indeed, if allowance were made for the different attenuations over land and over sea, the difference in attenuation rates for signals from the west and from the east would be greater than that indicated in Fig. 2.

Table 3. Effect of land on path attenuation

			New York to Wellington	New York to Melbourne	New York to Perth	Paris to Melbourne	Rugby to Wellington
Path lengths (km)	W–E	Land	4500	7250	0	12,300	2300
		Sea	21,500	16,000	21,500	4500	16,400
	E–W	Land	3500	4500	7000	2000	8000
		Sea	10,500	12,250	11,000	20,250	13,300
Total attenuation 1 dB/1000 km for sea 2 dB/1000 km for land	W–E		31	31	22	29	21
	E–W		18	21	25	24	29

4. INFLUENCE OF THE EARTH'S MAGNETIC FIELD

Possible simple explanations of the effects shown in Fig. 2 have been discussed above, and are shown to be unlikely. The basis of a more probable explanation will now be outlined.

If it is considered that VLF signals are propagated by *TM* modes (CROMBIE *et al.*, 1957; WAIT, 1957) in an ionosphere–earth waveguide, then it can be shown that in general the electric field will be elliptically polarized in the *vertical plane of propagation*. Moreover, the direction of rotation of the electric field will be reversed if the direction of propagation is reversed. If there are free electrons in the elliptically polarized field, then in the presence of a transverse horizontal magnetic field the refractive index of the region containing electrons will depend on the direction of propagation. Thus, a reversal of the direction of propagation will alter the propagation constant of the ionosphere–earth waveguide.

VOL. 12 1958

4.1. *Effect of direction of propagation*

The above hypothesis suggests that propagation in the direction of the earth's horizontal magnetic field will be reciprocal, but that propagation in directions inclined to the earth's horizontal field will be non-reciprocal. The non-reciprocity will be greater, the greater the component of magnetic field at right angles to the path. The effects observed on the Rugby–Wellington path are comparatively small, and this is probably due to the small angle that the path makes with the direction of the earth's magnetic field.

The hypothesis suggests that the magnetic field would not affect the propagation along paths that lie magnetically north or south. For such paths it is appropriate to adopt the attenuation constants predicted by WAIT and quoted in Fig. 1.

A fuller account of the possible influence of a transverse magnetic field on VLF propagation is being prepared.

CONCLUSIONS

While the results discussed in this paper can hardly be regarded as conclusive, they show that considerable weight must be given to the hypothesis that VLF signals are less attenuated in travelling from the west than from the east. Thus it seems desirable that further investigations of the effect should be made. In this connexion, the proposal of the National Bureau of Standards (GEORGE, 1957) to establish a standard frequency transmission on 10 kc/s is of considerable interest. If this proposal becomes fact, the transmissions will provide a valuable opportunity for further work.

L.
2
58

Acknowledgements—The writer wishes to express his appreciation for the valuable assistance given him in the writing of this paper, by his colleagues and, in particular, by Mr. N. F. BARBER.

REFERENCES

AUSTIN L. W.	1928	*Proc. Inst. Radio Engrs.* **16,** 348.
BUDDEN K. G.	1954	*Proc. Camb. Phil. Soc.* **50,** 604.
CHAPMAN F. W. and PIERCE E. T.	1957	*Proc. Inst. Radio Engrs.* **45,** 804.
CROMBIE D. D., ALLAN A. H. and NEWMAN M.	1957	Submitted to *Proc. Inst. Elec. Engrs.*
ECKERSLEY T. L.	1932	*J. Inst. Elec. Engrs.* **71,** 451.
GEORGE W. D.	1957	Paper 41. VLF Propagation Symposium, N.B.S., Boulder.
HEPBURN F.	1957	*J. Atmosph. Terr. Phys.* **10,** 121.
ROUND H. J., ECKERSLEY T. L., TREMELLEN K. and LUNNON F. C.	1925	*J. Inst. Elec. Engrs.* **63,** 933.
TREMELLEN K.	1950	*Marconi Rev.* **13,** 153.
WAIT J. R.	1957	*Proc. Inst. Radio Engrs.* **45,** 760.

Journal of Atmospheric and Terrestrial Physics, 1958, Vol. 12, pp. 118 to 125. Pergamon Press Ltd., London

Some methods for studying wave-propagation in a uniform magneto-ionic medium

V. A. BAILEY
University of Sydney

(*Received* 14 *November* 1957)

Abstract—The difficulty in using the classical general formulae of APPLETON, for determining the refractive and absorption indices and the polarization of each of the two wave-modes, is primarily due to the presence of the radical term $\rho = \sqrt{\gamma_T{}^4\delta^2 + \gamma_L{}^2}$ where δ is the reciprocal of a given complex number. This difficulty has been overcome by means of each of four methods of calculation developed in the School of Physics of the University of Sydney. The first three, although previously published, are here presented again but briefly.

The fourth method makes use of the following approximations:

$$\sqrt{1 + s^2} \text{ equals } \frac{4 + 3s^2}{4 + s^2} \text{ or } s.\frac{4s^2 + 3}{4s^2 + 1}$$

according as $|s| \lesssim 1$ (except when $s^2 \doteqdot -1$).

On applying them to Appleton's formulae, by taking $s = 2\gamma_L\gamma_T{}^{-2}(1 + \alpha + i\beta)$, we obtain the good approximate formulae (32) and (33) for M^2 (square of the complex refractive index) which, in effect, cover all possible situations with an error not exceeding about 1 per cent. Other applications of these approximations to $\sqrt{1 + s^2}$ can be made: for example to the polarization numbers R, for, with the same value of s,

$$R = is^{-1}\{1 \mp \sqrt{1 + s^2}\}.$$

VOL. 12 1958

THE classical problem of determining the refractive index μ, the absorption index χ and the polarization number R of each of the two modes of wave-propagation in a uniform magneto-ionic medium depends, as is known, on the following two formulae due to APPLETON (1927).

$$\left.\begin{aligned} M^2 \equiv (\mu - i\chi)^2 &= 1 + \{\alpha + i\beta - \gamma_T{}^2\delta \pm \sqrt{\gamma_T{}^4\delta^2 + \gamma_L{}^2}\}^{-1} \\ \text{where} \qquad \delta &= \tfrac{1}{2}(1 + \alpha + i\beta)^{-1}, \end{aligned}\right\} \quad (1)$$

and

$$R = i\gamma_L{}^{-1}\{\alpha + i\beta - (M^2 - 1)^{-1}\}, \quad (2)$$

where α, β, γ_T, γ_L are defined in the Appendix I.

The general discussion of equations (1) and (2) under different physical circumstances and even their computation in specified numerical instances are much handicapped by the presence of the radical term

$$\rho = \sqrt{\gamma_T{}^4\delta^2 + \gamma_L{}^2}, \quad (3)$$

since the quantity under the square-root sign is a complicated, complex function of α, β, γ_T and γ_L.

This difficulty has led BOOKER and other workers to restrict the general discussion of equations (1) and (2) to the following two extreme situations and their associated nomenclature:

$|\gamma_T{}^4\delta^2| \gg \gamma_L{}^2$, $\rho \doteqdot \gamma_T{}^2\delta$, Quasi-transverse (Q.T.) propagation.

$|\gamma_T{}^4\delta^2| \ll \gamma_L{}^2$, $\rho \doteqdot \gamma_L$, Quasi-longitudinal (Q.L.) propagation.

Besides excluding many important situations in which $\gamma_T{}^4\delta^2$ and $\gamma_L{}^2$ are of the same order of magnitude, this procedure is usually associated in the literature of the subject with an erroneous approximation for the absorption coefficient $\kappa_e(=\chi w/c)$ of an extraordinary mode in Q.L. propagation, namely

$$\kappa_e = \frac{\nu p_0{}^2}{2c\{(w - \Omega_L)^2 + \nu^2\}} \tag{4}$$

where $\Omega_L = \Omega \cos\theta$ and $\Omega/2\pi$ is the gyrofrequency (Booker, 1935).

The error in this approximation has misled some workers into the conclusion that theoretically there is no resonance in the phenomenon of wave-interaction as the frequency of the disturbing wave varies about the local gyrofrequency.

The difficulty due to the presence of the radical ρ, defined under equation (3), has been largely overcome by means of each of the four methods of calculation given below, which have been developed in the School of Physics of the University of Sydney.

The first three methods depend on the following pair of equations which are equivalent to the pair of equations (1) and (2):

$$R + R^{-1} = i\gamma_T{}^2\gamma_L{}^{-1}(1 + \alpha + i\beta)^{-1} = 2(x + iy)^{-1} \tag{5}$$

$$(M^2 - 1)(\alpha + i\beta + iR\gamma_L) = 1, \tag{6}$$

where $x = 2\gamma_T{}^{-2}\gamma_L\beta, \quad y = -2\gamma_T{}^{-2}\gamma_L(1 + \alpha)$.

These equations yield R and M in succession as follows.

Method 1 (Bailey, 1934)

We introduce the complex numbers z, ζ, w defined by

$$\left.\begin{aligned} z &= x + iy = -2i\gamma_T{}^{-2}\gamma_L(1 + \alpha + i\beta) \\ \zeta &= \xi + i\eta = z^{-1} \\ w &= u + iv = -i \log R \end{aligned}\right\} \tag{7}$$

in which the values of x and y are given by the formulae

$$x = 2\gamma_T{}^{-2}\gamma_L\beta, \qquad y = -2\gamma_T{}^{-2}\gamma_L(1 + \alpha). \tag{8}$$

Then $R = \exp(iw)$ and so (5) yields the equation

$$\cos w = \zeta \tag{9}$$

where

$$z\zeta = 1. \tag{10}$$

We now represent w and z conformally in the complex ζ-plane. The u-curves and v-curves then turn out to be given by a system of confocal hyperbolae and ellipses and the x-curves and y-curves turn out to be given by a system of co-axial circles.

If a chart is drawn beforehand with such circles and ellipses and with the auxiliary circles of the ellipses (to serve in the place of the hyperbolae), then it allows any pair of values of x and y given by (8) to determine two pairs of values

of u and v. The corresponding values of exp $(iu - v)$ then give the two values of the polarization number R corresponding to the two modes of propagation.

We next introduce the numbers Z, ζ_1 defined by

$$\left.\begin{aligned} Z &= X + iY = \alpha + i\beta + iR\gamma_L \\ \zeta_1 &= \xi_1 + i\eta_1 = (\mu - i\chi)^2 - 1 \end{aligned}\right\} \tag{11}$$

and express the polarization number R in the form

$$R = r + is \tag{12}$$

where r and s are now known quantities.

Consequently the values of X and Y are given by the formulae

$$X = \alpha - s\gamma_L, \qquad Y = \beta + r\gamma_L, \tag{13}$$

and the following relations must hold true:

$$\xi_1 = \mu^2 - \chi^2 - 1 \qquad \eta_1 = -2\mu\chi. \tag{14}$$

The equation (6) may now be written in the form

$$Z\zeta_1 = 1 \tag{15}$$

which is similar to that of (10).

We now represent Z and $M\,(=\mu - i\chi)$ conformally in the ζ_1-plane. The X-curves and Y-curves are given by a system of co-axial circles and the μ-curves and χ-curves are given by a system of confocal parabolas.

If a second chart is drawn beforehand with such circles and parabolas, it allows any pair of values of X and Y given by (13) to determine a pair of values of μ and χ.

We thus see how to determine the values of R, μ and χ for each of the two modes in a numerically specified situation by inspection of two simple charts. This method has been successfully applied in Australia and India.

Method 2 (Bailey and Somerville, 1938)

This method uses only algebraic processes for the derivation of R, μ and χ from the pair of equations (5) and (6).

From the definition $\zeta = z^{-1}$ in (7) we see that the values of ξ and η are given by the formulae

$$\xi = x/(x^2 + y^2) \qquad \eta = -y/(x^2 + y^2). \tag{16}$$

On writing (5) in the form

$$R + R^{-1} = 2(\xi + i\eta),$$

substituting for R from equation (12) and introducing in succession the new variables F and K by means of the substitutions

$$\tau = \xi(1 \pm F) \qquad s = \eta(1 \pm F^{-1}), \tag{17}$$

$$F = (1 - K/\xi)^{\frac{1}{2}}, \tag{18}$$

VOL. 12 1958

we obtain the following quadratic equation in K:

$$K + K^{-1} = J^{-1} \tag{19}$$

where the value of J is given by the formula

$$J = x/(1 + x^2 + y^2) \tag{20}$$

Since (17) requires F to be real, we may use only the smaller root of (19), i.e. we must have

$$0 \leqslant K \leqslant 1. \tag{21}$$

For use with numerical examples a table of values of K corresponding to different values of J has been constructed and the graphs of K and $(K - J)$ as functions of J have also been published (BAILEY and SOMERVILLE, 1938).

Thus, from any pair of values of x and y given by equation (8) we can derive in succession the values of J, K, F, r, s and R.

The values of the quantities X and Y can now be derived by means of the formulae (13).

From equations (15) and (14) we easily obtain the formulae

$$\mu^2, \chi^2 = \tfrac{1}{2}(a \pm b) \tag{22}$$

where

$$\left.\begin{aligned} a &= \{1 + (1 + 2X)/(X^2 + Y^2)\}^{\frac{1}{2}}, \\ b &= 1 + X/(X^2 + Y^2) \end{aligned}\right\} \tag{23}$$

Thus the values of μ^2 and χ^2 can now be derived by means of the formulae (23) and (22).

This method has been used in the U.S.A., to prepare extensive tables of R, μ and χ.

METHOD 3 (BAILEY and SOMERVILLE, 1938)

In this method the solutions R_1, R_2 of equation (5) in numerical instances can be obtained rapidly by means of a special linkage. Then the corresponding values of μ and χ can be obtained by means of another linkage or by means of one of the methods described above.

For many purposes it is desirable, or even necessary, to simplify the general discussion of wave-propagation under different physical conditions by using approximations to the algebraic expressions for μ, χ and R.

The most commonly used approximations are based on a partial expansion of the radical term ρ, defined under (3), by means of the binomial theorem. It is in this way that the classification into Q.T. and Q.L. propagation has arisen. But the methods 1, 2 and 3 described above show that this procedure and classification are not essential for calculating μ, χ and R, however convenient they may be for certain purposes.

We shall now introduce a simple method for approximating to any radical r which is not subject to the limitations imposed on the usual partial expansion by the binomial theorem.

METHOD 4

It is shown in Appendix II that if r_1 is an approximation to the square root r of a given number a, i.e.

$$r = \sqrt{a}, \tag{24}$$

then a much closer approximation to r is r_2, where

$$r_2 = r_1 \cdot \frac{3a + r_1^2}{a + 3r_1^2}. \tag{25}$$

This fact is illustrated by the following numerical examples:

$$a = 4, \qquad r = 2,$$

$$r_1 = 1, \qquad r_2 = 13/7 \doteq 1{\cdot}86,$$

$$r_1 = 2, \qquad r_2 = 2,$$

$$r_1 = 3, \qquad r_2 = 63/31 \doteq 2{\cdot}032.$$

$$a = 2i, \qquad r = 1 + i,$$

$$r_1 = 1, r_2 = \frac{6i + 1}{2i + 3} = \frac{15 + 16i}{13} \doteq 1{\cdot}15 + 1{\cdot}23i.$$

In passing, it may be mentioned that formula (25) can be used as an iterative formula to yield a sequence of approximations $r_2, r_3, r_4, \ldots$ which converges with great rapidity on a square root of any given real or complex number a. The convergence is of order 3.*

This formula (25) can now be applied to any of the formulae given above which involve a radix, such as (1), (18), a root of (19), (22) and (23).

Here we shall consider in detail only the application of equation (25) to APPLETON's formula (1) for M^2, i.e. to the radical ρ defined under (3).

Since
$$\rho = \gamma_T^2 \delta r, \tag{26}$$

where
$$r = \sqrt{1 + s^2} \tag{27}$$

and
$$s = 2\gamma_L \gamma_T^{-2}(1 + \alpha + i\beta), \tag{28}$$

we have here

$$a = 1 + s^2.$$

If we now take $r_1 = 1$, then (25) yields

$$r_2 = f(s) \equiv \frac{4 + 3s^2}{4 + s^2}.$$

In order to find the conditions under which $f(s)$ is a good approximation, we make use of the exact relation

$$\sqrt{1 + s^2} = f(s)(1 + t^2)^{\frac{1}{2}}$$

* It may be added here that an iteration with convergence of order 5 is

$$r_{n+1} = r_n \cdot \frac{5a^2 + 10ar_n^2 + r_n^4}{a^2 + 10ar_n^2 + 5r_n^4}.$$

VOL. 12 1958

where

$$t^2 \equiv t^2(s) \equiv s^6/(4 + 3s^2)^2.$$

Then $f(s)$ is a good approximation, within 5 per cent, when

$$|t(s)| \equiv |s^3/(4 + 3s^2)| < 0{\cdot}3. \tag{29}$$

When s is real, the condition $|s| < 1{\cdot}5$ satisfies (29) and so $f(s)$ is then a good approximation; when $|s| = 1$ the error is only about 1 per cent. On the other hand, when $|s| > 1$ the binomial series is divergent and so inapplicable, while with $s = 1$ the partial expansion $1 + \frac{1}{2}s^2$ is in error by about 6 per cent.

When $s^2 \doteqdot -1$, $a \doteqdot 0$, and then both $f(s)$ and the binomial series are inapplicable. But in such a situation we need (in general) only omit the radical term from equation (1) in order to obtain a good approximation to M^2.

When $|s^2| > 1$ we may use $sf(s^{-1})$ as an approximation to $\sqrt{1 + s^2}$, since

$$\sqrt{1 + s^2} = s\sqrt{1 + s^{-2}} \doteqdot sf(s^{-1}).$$

In this way we arrive at the following conclusion:

$$\left.\begin{aligned} &\sqrt{1 + s^2} \doteqdot \frac{4 + 3s^2}{4 + s^2} \quad \text{or} \quad s \cdot \frac{4s^2 + 3}{4s^2 + 1} \\ &\text{according as } |s| \lesseqgtr 1, \\ &\text{except when } s^2 \doteqdot -1. \end{aligned}\right\} \tag{30}$$

The error in (30) is within 5 per cent under the condition (29) when $|s| < 1$ and under the condition $|t(s^{-1})| < 0{\cdot}3$ when $|s| > 1$.

Another approximation can be derived from equation (25) by taking $r_1 = 1 + s$. In this way we can establish the following result:

$$\left.\begin{aligned} &\text{For all numbers } s = u + iv \text{ where } u > |v|, \\ &\sqrt{1 + s^2} \doteqdot (1 + s) \cdot \frac{2 + s + 2s^2}{2 + 3s + 2s^2} \\ &\text{within } 3{\cdot}2 \text{ per cent.} \end{aligned}\right\} \tag{31}$$

In order to test the approximations given under (30) we may introduce the ratios $F_1(s)$ and $F_2(s)$ defined by

$$F_1(s) = \sqrt{1 + s^2}\,(4 + s^2)/(4 + 3s^2),$$

$$F_2(s) = \sqrt{1 + s^2}\,(4s^2 + 1)/s(4s^2 + 3),$$

and examine how closely $F_1(s)$ and $F_2(s)$ approximate to 1 when $|s| \lesseqgtr 1$ respectively.

We obtain the following table of numerical results

Table 1

s	$\frac{3}{4}$	1	4/3	$-0{\cdot}4 + 1{\cdot}2i$
$\lvert s\rvert$	<1	1	>1	>1
$F_1(s)$	$\frac{365}{364}$	$\frac{7{\cdot}07}{7}$		
$F_2(s)$		$\frac{7{\cdot}07}{7}$	$\frac{365}{364}$	$\frac{693 - 124i}{682 - 126i}$

These examples strikingly illustrate the closeness of the approximations under (30).

On applying these approximations with s given by (28) and using equations (26), (3) and (1), we obtain the following approximations for M^2:

For $|s| \leqslant 1$,

$$1 + \left[\alpha + i\beta - \frac{{\gamma_T}^2}{2(1 + \alpha + i\beta)}\left\{1 \mp \frac{{\gamma_T}^4 + 3{\gamma_L}^2(1 + \alpha + i\beta)^2}{{\gamma_T}^4 + {\gamma_L}^2(1 + \alpha + i\beta)^2}\right\}\right]^{-1} \tag{32}$$

For $|s| \geqslant 1$,

$$1 + \left[\alpha + i\beta - \frac{{\gamma_T}^2}{2(1 + \alpha + i\beta)} \pm \gamma_L \cdot \frac{16{\gamma_L}^2(1 + \alpha + i\beta)^2 + 3{\gamma_T}^4}{16{\gamma_L}^2(1 + \alpha + i\beta)^2 + {\gamma_T}^4}\right]^{-1} \tag{33}$$

These are correct within about 1 per cent except when $s^2 \doteqdot -1$, i.e. when

$$\omega \doteqdot p_0 \quad \text{and} \quad \nu \doteqdot \nu_c = \Omega \cos^2 \theta/2 \sin \theta \tag{34}$$

where $\Omega/2\pi$ is the gyrofrequency.

The "double event" specified by (34) is likely to occur only rarely in the ionosphere, and so in general need not be provided for; even when it does occur it need not cause trouble, since then (as remarked earlier) we need only neglect the radical in equation (1).

It will be noted that the extreme condition $|s| \ll 1$ which comes under (32) corresponds to Q.T. propagation and the extreme condition $|s| \gg 1$ which comes under (33) corresponds to Q.L. propagation.

We may therefore extend the use of these terms by relating them to (32) and (33) respectively.

Approximations to M, and so to μ and χ, may now be obtained by applying the formula (25) to these approximations to M^2.

In conclusion, it may be remarked that the formula (25) could be of service in other problems in physics and mathematics in which the presence of radicals causes difficulties. For example, its use could give valuable approximations to elliptic integrals.

Similarly, (31) can be used to derive other good approximations in physics and mathematics.

Appendix I

The following notation includes the symbols α, β, γ_T, γ_L used in this paper.

VOL. 12 1958

e, m, electronic charge and mass, in e.s.u.
N number density of electrons.
ν collision frequency of an electron (with molecules).
H intensity of constant magnetic field present, in gauss.
ω angular frequency of a wave.
θ angle between H and the direction of propagation.
$p_0^2 = 4\pi Ne^2/m = 3{\cdot}19 \times 10^9 N$; $(p_0/2\pi$ = plasma-frequency).
$\Omega = -He/mc = 1{\cdot}77 \times 10^7 H$; $(\Omega/2\pi$ = gyrofrequency).
μ refractive index.
χ absorption index.
R polarization number.
$M = \mu - i\chi$, complex refractive index.
$\alpha = -\omega^2/p_0^2$
$\beta = \nu\omega/p_0^2$
$\gamma = \Omega\omega/p_0^2$
$\gamma_L = \gamma \cos\theta$
$\gamma_T = \gamma \sin\theta$

Appendix II

If e_1 is the error in r_1 and e_2 the error in r_2 as approximations to $r = \sqrt{a}$, then

$$e_1 = r - r_1, \qquad e_2 = r - r_2.$$

Hence, on using the relation $r^2 = a$ we obtain

$$e_1^3 = (r - r_1)^3 = r(a + 3r_1^2) - r_1(3a + r_1^2) = e_2(a + 3r_1^2) \qquad (2.1)$$

on account of the relation (25).

When e_1 is small enough, then $a + 3r_1^2 \doteqdot 4a$, and so we obtain the relation

$$e_2 \doteqdot e_1^3/4a. \qquad (2.2)$$

This shows that the error in the approximation r_2 is of a much higher order of smallness than the error in r_1.

Thus the sequence of interates $r_1, r_2, r_3, \ldots$ rapidly converges on r, and the convergence is of order 3.

It is not difficult to prove also, by means of (2.1), the remarkable fact that when a is a positive number, the sequence $r_1, r_2, r_3, \ldots$ will converge when the first approximation r_1 is taken to be *any* positive number whatever.

References

Appleton E. V.	1927	*U.R.S.I. Washington Proceedings.*
Bailey V. A.	1934	*Phil. Mag.* **18,** 516.
Bailey V. A. and Somerville J. M.	1938	*Phil. Mag.* **26,** 888.
Booker H. G.	1935	*Proc. Roy. Soc.* A **150,** 283.

Journal of Atmospheric and Terrestrial Physics, 1958, Vol. 12, pp. 126 to 139. Pergamon Press Ltd., London

Low-frequency reflection in the ionosphere—I

HERMANN POEVERLEIN
Propagation Laboratory, Electronics Research Directorate, Air Force Cambridge Research Center, Air Research and Development Command, Bedford, Mass.

(*Received* 28 *October* 1957)

Abstract—A theory of low-frequency reflection in the ionosphere is developed. At wavelengths long compared to the layer thickness, the ionospheric layer is considered as a thin conductive sheet, that leads to a discontinuity of the electromagnetic field. A thicker layer is subdivided into many thin (or differential) sublayers. The field is then thought of as a superposition of many partial waves, each of which is reflected by an individual sublayer. An additional penetrating wave must be assumed.

At the lowest frequencies—that is, in the case of thin-sheet reflection—the currents in the layer are horizontal and the reflection is of the metallic type, always showing reversal of the horizontal E-component. Dielectric-type reflection with sign or phase transition at the Brewster angle is obtained at somewhat higher frequencies, if vertical and horizontal current density components are of comparable magnitude.

The present first part of the paper deals with the thin-sheet reflection theory and the fundamentals of the general theory. Specialized cases of the general theory and some consequences will be discussed in the second part. The frequencies under consideration are roughly 1–100 kc/s.

1. INTRODUCTION

THE ionosphere is a medium varying continuously with height. At high frequencies, where the change of the medium over a few wavelengths is small, the theory of propagation and reflection can be based on geometric optics. At low frequencies, however, the thickness of the layer may be comparable to the wavelength. Various authors gave a mathematical treatment of wave propagation under this condition, often with the end of numerical evaluation or of developing a method for computation (RYDBECK, 1944, 1948; MALLINCKRODT, 1954; BUDDEN, 1955; DAVIDS and PARKINSON, 1955; BUTLER, GIBBONS, LEVY and MAY, 1956). In the present paper a rather physical concept shall be taken as basis of a theory. It will be attempted to obtain a crude systematic survey of the reflection characteristics (in Part II of the paper, which will appear soon). The formulations have some relationship to BUDDEN's theory (see also Part II of this paper).

An ionospheric layer is considered as the combination of a large number of thin sublayers, which are finally made differentials. Partial waves are assumed, each of them being reflected in a certain sublayer. Appropriate superposition of all partial waves, together with an additional penetrating wave, yields the total field. The currents in the sublayers, which cause the reflection of the partial waves, are themselves due to the total field.

A layer thin in the scale of wavelengths needs no subdivision and offers the possibility of a very simple theoretical treatment. The currents in such a thin layer flow in the plane of the layer. In the case of a thicker layer a differential sublayer acts as a thin layer on the partial wave attributed to it, but vertical current density components have to be taken into account.

DARWIN (1924) and HARTREE (1929), in a theory of ionospheric propagation, considered the single electrons as re-radiating and superimposed all their

VOL. 12 1958

re-radiations. In the present theory it can be thought that the re-radiations are already summed up over horizontal planes. The re-radiation of the complete planes is considered, but the summation in the vertical direction appears in the formulae.

The W.K.B. method (BREMMER, 1949, 1951) is an approach from the side of geometric optics, which is also based on the idea of partial reflections (but of a different kind). In contrast to the present method, its rigorous performance must include multiple reflections. The solutions are then series developments with respect to the number of multiples, which do not always converge well.

2. THIN-SHEET REFLECTION

At vertical incidence and without terrestrial magnetic field only horizontal currents would arise in the ionospheric layer. In general, horizontal and vertical currents are to be expected. If the layer is thin compared to the wavelength, however, a vertical current as extending only over a short height interval (the thickness of the layer) will produce a much stronger polarization than a horizontal current. This polarization tends to cancel the vertical electric field-strength component and thus to suppress the vertical current. In the limit case of negligible layer thickness the vertical current density component disappears. Only this case of negligible vertical current density will be considered in the present section.

2.1. *Vertical incidence without terrestrial magnetic field*

The simplest possibility is vertical incidence in absence of a constant magnetic field. Maxwell's equations under these conditions read

$$\left.\begin{aligned} -\frac{\partial}{\partial z} H_y &= i\omega\varepsilon E_x + J_x \\ -\frac{\partial}{\partial z} E_x &= i\omega\mu H_y \end{aligned}\right\} \qquad (1)$$

with z as vertical co-ordinate and x and y as the directions of the electric and magnetic field. The time dependence assumed is exp $(i\omega t)$. The dielectric constant ε is always that of vacuum.

The current density J_x is supposed to be different from zero only in an extremely thin layer (compared to the wavelength). This means that J_x as a function of z might be considered as a δ function: it disappears everywhere except at one level, where it becomes infinitely large; the integral of J_x over the height is finite.

Outside of the layer the field can be divided into an up-going and a down-going wave, each being propagated as a wave in vacuum. Up-going and down-going waves appear throughout the paper, later also within the layer. Therefore, notations for them may be introduced: F will be the electric field-strength of the up-going wave alone and G that of the down-going wave alone.* The total

* The definition of F and G will be modified later (Section 3.3).

electric and magnetic fields, then, below the layer are

$$\left.\begin{aligned} E_1 &= F_1 + G_1 \\ H_1 &= \sqrt{\frac{\varepsilon}{\mu}}\,(F_1 - G_1) \end{aligned}\right\} \tag{2}$$

and above the layer, where only an up-going wave exists,

$$\left.\begin{aligned} E_2 &= F_2 \\ H_2 &= \sqrt{\frac{\varepsilon}{\mu}}\,F_2 \end{aligned}\right\} \tag{3}$$

Only the magnitudes of the vectors are now considered. The fields below and above the layer obey Maxwell's equations (1) with $J_x = 0$.

In the layer, where the current density becomes the predominant quantity, Maxwell's equations can be simplified

$$\left.\begin{aligned} -\frac{\partial}{\partial z} H_y &= J_x \\ -\frac{\partial}{\partial z} E_x &= i\omega\mu H_y \end{aligned}\right\} \tag{4}$$

In penetrating the layer, H will jump in consequence of the infinite J_x. E, however, has to be continuous, i.e. constant within the infinitely thin layer, if H is not to become infinite. Thus

$$\left.\begin{aligned} E &= E_1 = E_2 \\ H_2 - H_1 &= -\int J dz \end{aligned}\right\} \tag{5}$$

Subscripts x and y are omitted now.

Introduction of F and G [equations (2) and (3)] yields

$$\left.\begin{aligned} F_2 - (F_1 + G_1) &= 0 \\ F_2 - (F_1 - G_1) &= -\sqrt{\frac{\mu}{\varepsilon}}\int J\,dz \end{aligned}\right\} \tag{6}$$

The current density may be expressed by the conductivity σ, which is a function of height z, and the electric field-strength E, which stays constant within the layer:

$$J = \sigma E = \sigma E_2 = \sigma F_2 \tag{7}$$

Hence

$$\left.\begin{aligned} F_2 - F_1 - G_1 &= 0 \\ F_2 - F_1 + G_1 &= -\sqrt{\frac{\mu}{\varepsilon}}\int \sigma\,dz\,.\,F_2 \end{aligned}\right\} \tag{8}$$

VOL. 12 1958

Equations (8) allow us to calculate reflection and transmission coefficients of the layer. The reflection coefficient becomes

$$\frac{G_1}{F_1} = -\frac{M}{M+2} \tag{9}$$

with

$$M = \sqrt{\frac{\mu}{\varepsilon}} \int \sigma \, dz = \frac{1}{c\varepsilon} \int \sigma \, dz \tag{10}$$

The transmission coefficient is

$$\frac{F_2}{F_1} = \frac{2}{M+2} \tag{11}$$

The conductivity σ as derived from the equation of motion of the electrons is

$$\sigma = N \frac{e^2}{m} \cdot \frac{1}{\nu + i\omega} \tag{12}$$

N is the electron concentration, ν the collision frequency. Replacing N by the angular plasma frequency ω_0 as a measure of the electron concentration [equation (37)] leads to

$$\sigma = \varepsilon \frac{{\omega_0}^2}{\nu + i\omega} \tag{13}$$

Parameter M with this σ becomes

$$M = \frac{1}{c} \int \frac{{\omega_0}^2}{\nu + i\omega} \, dz \tag{14}$$

In the denominator, ω might be neglected compared with ν.

Equation (10) shows that the integral of the conductivity over the layer thickness regardless of the structure of the layer determines the reflection coefficient. $|M| \gg 1$ yields almost perfect reflection, $|M| \ll 1$ almost perfect transmission. With large $|M|$ the reflection coefficient [equation (9)] is close to -1. That means, that in the case of good reflection, **E** is reversed.

2.2. *Oblique incidence without magnetic field*

At oblique incidence there are vertical field-strength and current density components in the layer, but as previously explained they are negligible if the layer is sufficiently thin or, in other words, if the wavelength is sufficiently long. An estimation of the wavelength required will not be given now. It could be made with the aid of the rigorous theory (Section 3).

The (x, z) plane will be the plane of incidence. All quantities (**E, H, J** and so on) are supposed to be the same functions of the horizontal co-ordinate x. Therefore $x = 0$ can be assumed generally.

The whole derivations are not much different from those for vertical incidence. It is the horizontal component of **H** which jumps, whereas the horizontal **E**-component is continuous.

In the equations which connect the horizontal **E**- and **H**-components there appears now a factor $\cos\varphi$ (φ is the angle of incidence). It appears on either side of the equation, depending on the polarization of the wave (**E** parallel or perpendicular to the plane of incidence). The reflection and transmission coefficients, then, become

for **E** *in the plane of incidence*

$$\frac{G_1}{F_1} = -\frac{M\cos\varphi}{M\cos\varphi + 2} \tag{15}$$

$$\frac{F_2}{F_1} = \frac{2}{M\cos\varphi + 2}\ , \tag{16}$$

for **E** *perpendicular to the plane of incidence*

$$\frac{G_1}{F_1} = -\frac{\dfrac{M}{\cos\varphi}}{\dfrac{M}{\cos\varphi} + 2} \tag{17}$$

$$\frac{F_2}{F_1} = \frac{2}{\dfrac{M}{\cos\varphi} + 2} \tag{18}$$

M was the quantity determining the degree of reflection in the case of vertical incidence. Now $M\cos\varphi$ or $M/\cos\varphi$ replaces it. For **E** in the plane of incidence the reflection becomes poor at shallow angles and complete transmission is found at grazing incidence. For **E** perpendicular the reflection is the better the shallower the angle and becomes perfect at grazing incidence.

In cases of good reflection the reflection coefficient [equations (15) and (17)] again approaches -1. The sign of the horizontal **E**-component, consequently, is reversed in reflection. For **E** in the plane of incidence and not too steep angles this is the characteristic of reflection from a conductor, but not from a dielectric.

2.3. *Introduction of the terrestrial magnetic field*

The derivations resemble the previous ones, but the two cases of polarization can no longer be separated. The formulae for the two horizontal components of the electric field-strengths—equations (6) with a factor $\cos\varphi$ or $1/\cos\varphi$ as mentioned in the last section—must be written down simultaneously:

$$\left.\begin{aligned} F_{2x} - (F_{1x} + G_{1x}) &= 0 \\ F_{2y} - (F_{1y} + G_{1y}) &= 0 \\ F_{2x} - (F_{1x} - G_{1x}) &= -\sqrt{\frac{\mu}{\varepsilon}}\cos\varphi \int J_x\, dz \\ F_{2y} - (F_{1y} - G_{1y}) &= -\sqrt{\frac{\mu}{\varepsilon}}\frac{1}{\cos\varphi} \int J_y\, dz \end{aligned}\right\} \tag{19}$$

VOL. 12 1958

The current density is not now simply proportional to the electric field-strength. Its vertical component is again assumed to disappear. The equation of motion of the electrons [equation (35)], then, leads to

$$\left.\begin{aligned}(\nu + i\omega)J_x - \omega_z J_y &= \varepsilon\omega_0{}^2 E_x \\ \omega_z J_x + (\nu + i\omega)J_y &= \varepsilon\omega_0{}^2 E_y,\end{aligned}\right\} \tag{20}$$

where

$$\omega_z = \frac{e}{m}\mu H_z \tag{21}$$

is the angular gyrofrequency corresponding to the vertical component of the terrestrial magnetic field.

From equations (20) the current density components are derived as

$$\left.\begin{aligned}J_x &= \frac{\varepsilon\omega_0{}^2}{\nu^2 - \omega^2 + \omega_z{}^2}[(\nu + i\omega)\,E_x + \omega_z E_y] \\ J_y &= \frac{\varepsilon\omega_0{}^2}{\nu^2 - \omega^2 + \omega_z{}^2}[-\omega_z E_x + (\nu + i\omega)E_y]\end{aligned}\right\} \tag{22}$$

The conductivity now is a two-dimensional tensor, consisting of four factors or components.

The reflection and transmission coefficients are obtained from equations (19) and (22), again with the assumption of continuous horizontal **E**-components. Two parameters appear now in place of M [equation (14)]:

$$\left.\begin{aligned}M_\nu &= \frac{1}{c}\int \frac{\omega_0{}^2}{\nu^2 - \omega^2 + \omega_z{}^2}\,(\nu + i\omega)\,dz \\ M_H &= \frac{1}{c}\int \frac{\omega_0{}^2}{\nu^2 - \omega^2 + \omega_z{}^2}\,\omega_z\,dz\end{aligned}\right\} \tag{23}$$

The reflection coefficient in terms of these parameters is

for **E** *in the plane of incidence*

$$\left.\begin{aligned}{}_{\parallel}R_{\parallel} &= -1 + \frac{2\left(\dfrac{1}{\cos\varphi}\,M_\nu + 2\right)}{M_H{}^2 + \left(\dfrac{1}{\cos\varphi}\,M_\nu + 2\right)(\cos\varphi\,M_\nu + 2)} \\ &\text{for } \mathbf{E} \text{ perpendicular to the plane of incidence} \\ {}_{\perp}R_{\perp} &= -1 + \frac{2(\cos\varphi\,M_\nu + 2)}{M_H{}^2 + \left(\dfrac{1}{\cos\varphi}\,M_\nu + 2\right)(\cos\varphi\,M_\nu + 2)}\end{aligned}\right\} \tag{24}$$

These reflection coefficients express the re-radiation of the unchanged polarization.

Besides, a component of the other polarization is re-radiated, corresponding to*

$$ {}_{\parallel}R_{\perp} = -{}_{\perp}R_{\parallel} = \frac{2M_H}{M_H{}^2 + \left(\frac{1}{\cos\varphi}M_v + 2\right)(\cos\varphi\, M_v + 2)} \tag{25} $$

If one of the two parameters M_H and M_v is large, reflection with unchanged polarization is almost perfect. An exception is again grazing incidence with **E** in the plane of incidence, in which case no reflection of unchanged or changed polarization occurs.

In nearly perfect reflection the horizontal **E**-component is again in general reversed and the field-strength of the changed polarization becomes very small. Thus the reflection is of the metallic type, as before.

3. General Theory

In this section consideration will no longer be restricted to extremely low frequencies or negligible layer thicknesses. The ratio of the layer thickness to the wavelength is now assumed to be of any value. All quantities within the layer may be functions of height. In general, vertical current density components must be included.

The incident waves are plane homogeneous waves and the layer is stratified horizontally. Therefore the dependence on the horizontal co-ordinates (x, y) is again the same for all field-strengths and currents and needs no attention.

VOL. 12 1958

3.1. *Fundamental equations*

The wave equation derived from Maxwell's equations with any current density distribution is (cf. Appendix)

$$ \nabla^2\mathbf{E} + k^2\mathbf{E} = \frac{i}{\varepsilon\omega}[k^2\mathbf{J} + \nabla(\nabla \cdot \mathbf{J})] \tag{26} $$

∇^2 is the Laplace operator, ε the dielectric constant of vacuum, and $k = \omega/c$ the wave number in vacuum.

The (x, z) plane (z vertical) will be taken as plane of incidence. For the dependence on the horizontal co-ordinates there may be written

$$ \left.\begin{aligned} \frac{\partial}{\partial x} &= -ik_x \\ \frac{\partial}{\partial y} &= 0 \end{aligned}\right\} \tag{27} $$

with constant k_x. A constant k_z may be introduced from

$$ k^2 = k_x{}^2 + k_z{}^2 \tag{28} $$

$\partial/\partial z$ of course cannot be replaced by the constant factor $-ik_z$.

* ${}_{\parallel}R_{\perp}$ means incident **E**-component in the plane of incidence, re-radiated **E**-component perpendicular. The directions $\parallel, \perp$ and the direction of incidence are taken in the sense of a right-hand co-ordinate system.

The wave equation in components becomes now

$$\left.\begin{aligned}
\frac{\partial^2 E_x}{\partial z^2} + k_z^2 E_x &= \frac{i}{\varepsilon\omega}\left(k_z^2 J_x - ik_x \frac{\partial J_z}{\partial z}\right) \\
\frac{\partial^2 E_y}{\partial z^2} + k_z^2 E_y &= \frac{i}{\varepsilon\omega} k^2 J_y \\
\frac{\partial^2 E_z}{\partial z^2} + k_z^2 E_z &= \frac{i}{\varepsilon\omega}\left(k^2 J_z - ik_x \frac{\partial J_x}{\partial z} + \frac{\partial^2 J_z}{\partial z^2}\right)
\end{aligned}\right\} \qquad (29)$$

An attempt to solve these equations will be made by means of the following ideas. The ionospheric layer is subdivided into many thin sublayers (finally considered as differentials). Each sublayer reflects partially. It is assumed, instead, that the entire field consists of many partial waves, one of which is reflected in each sublayer. The propagation of a partial wave up to and down from its reflecting sublayer is supposed to be undisturbed vacuum propagation (with vacuum k_z).

A partial wave, thus, behaves like a totally reflected wave in the preceding theory of thin layers. It is reflected in a certain thin sublayer. This reflection means a discontinuity of its electromagnetic field, by which account is taken of the current in the sublayer.

The partial wave contains a wave going up to the reflecting sublayer and a reflected down-going wave, but it needs not contain a wave propagated beyond the reflecting sublayer. An additional wave, which passes through the entire layer without reflection, must then be superimposed on all partial waves.

The currents in a sublayer, in contrast to those in a single thin layer, have horizontal and vertical components. Therefore two types of partial waves might be deemed possible, one type being reflected with sign reversal and the other without sign reversal of the field-strength component under consideration.

An expression, which combines the two types of partial waves and a penetrating wave, is

$$f(z) = \int_{\zeta=z}^{\infty} [A(\zeta) \,.\, (e^{-ik_z(z-\zeta)} - e^{ik_z(z-\zeta)}) + B(\zeta) \,.\, (e^{-ik_z(z-\zeta)} + e^{ik_z(z-\zeta)})]d\zeta + Ce^{-ik_z z} \qquad (30)$$

The variable z is the height, for which $f(z)$ is a field-strength component, whereas ζ is the reflection level of the partial waves. The coefficient k_z is constant. The exponential terms represent up- or down-going waves. The partial waves reflected below z do not contribute to the field in z.

The second derivative of the expression, equation (30), is

$$\frac{d^2 f}{dz^2} = -k_z^2 f(z) + 2ik_z A(z) - 2\frac{dB(z)}{dz} \quad ; \qquad (31)$$

hence

$$\frac{d^2 f}{dz^2} + k_z^2 f = 2ik_z A(z) - 2\frac{dB(z)}{dz} \qquad (32)$$

A comparison of this formula with the wave equation in component representation, equations (29), leads to (see remarks in the Appendix)

$$\left.\begin{aligned} E_x &= C_x e^{-ik_z z} + \frac{1}{2\varepsilon\omega}\int_{\zeta>z} [k_z J_x(\zeta)\,(e^{-ik_z(z-\zeta)} - e^{ik_z(z-\zeta)}) - \\ &\qquad - k_x J_z(\zeta)(e^{-ik_z(z-\zeta)} + e^{ik_z(z-\zeta)})]\,d\zeta \\ E_y &= C_y e^{-ik_z z} + \frac{1}{2\varepsilon\omega}\int_{\zeta>z} \frac{k^2}{k_z} J_y(\zeta)\,(e^{-ik_z(z-\zeta)} - e^{ik_z(z-\zeta)})\,d\zeta \\ E_z - \frac{i}{\varepsilon\omega} J_z &= -\frac{k_x}{k_z} C_x e^{-ik_z z} + \frac{1}{2\varepsilon\omega}\int_{\zeta>z} [-k_x J_x(\zeta)\,(e^{-ik_z(z-\zeta)} + e^{ik_z(z-\zeta)}) \\ &\qquad + \frac{k_x^2}{k_z} J_z(\zeta)\,(e^{-ik_z(z-\zeta)} - e^{ik_z(z-\zeta)})]\,d\zeta. \end{aligned}\right\} \quad (33)$$

The expressions for the field-strength components given by these equations* actually fulfil the differential equations (29) and might be considered as their solution. However, the current density components are (linear) functions of the field-strength components and equations (33), therefore, are still integral equations for the field-strength components. The factors k, k_x and k_z are the vacuum propagation constants. The left-hand side of the third equation is the vertical component of the displacement vector divided by ε (with $\mathbf{J}$ as polarization current),

$$\frac{D_z}{\varepsilon} = E_z - \frac{i}{\varepsilon\omega} J_z \quad (34)$$

The dependence on x was omitted in equations (33). After its introduction it can be seen that the various terms represent waves propagated either in the direction of the incident waves (up-going waves) or in the direction of reflected waves (down-going waves).

3.2. *Current density and effect of its various components*

The current density $\mathbf{J}$ as a function of $\mathbf{E}$ is obtained from the equation of motion of the electrons

$$(\nu + i\omega)m\mathbf{v} = e(\mathbf{E} + \mathbf{v} \times \mu\mathbf{H}) \quad (35)$$

with

$$\mathbf{J} = Ne\mathbf{v} \quad (36)$$

The plasma frequency ω_0 according to

$$\omega_0^2 = \frac{1}{\varepsilon} \cdot \frac{e^2}{m} N \quad (37)$$

will be taken as a measure of the electron concentration N and the gyrofrequency

$$\boldsymbol{\omega}_H = \frac{e}{m}\mu\mathbf{H} \quad (38)$$

as measure of the terrestrial magnetic field $\mathbf{H}$. The gyrofrequency $\boldsymbol{\omega}_H$ is considered

* Designations sin and cos were intentionally not introduced.

VOL. 12 1958

as a vector with the components ω_x, ω_y, ω_z. The equations for $\mathbf{J}$ derived from equations (35) and (36) are then

$$\left.\begin{aligned} (\nu + i\omega)J_x \quad & -\omega_z J_y & & +\omega_y J_z = \omega_0^2 \varepsilon E_x \\ \omega_z J_x + (\nu + i\omega)J_y \quad & & & -\omega_x J_z = \omega_0^2 \varepsilon E_y \\ -\omega_y J_x \quad & +\omega_x J_y + \left(\nu + i\omega - i\frac{\omega_0^2}{\omega}\right) J_z = \omega_0^2 D_z \end{aligned}\right\} \tag{39}$$

D_z, equation (34), has been introduced in place of εE_z.

The above integral equations (33) require the $\mathbf{J}$-components as functions of the field-strength components (E_x, E_y, D_z), i.e. the solutions of the linear equations (39). These solutions will not be written down for the general case. Some typical approximations for them will be given in the discussion of various specialized cases in Part II of the paper.

The integral equations (33) exhibit two different types of reflection due to the different current density components. Horizontal current densities lead to reflection with sign reversal of the horizontal field-strength component and with sign conservation of the vertical field-strength component. A vertical current density component has just the opposite effect (sign conservation of the horizontal component and sign reversal of the vertical component). According to equations (33), vertical current density components lose their influence at vertical incidence ($k_x = 0$); horizontal current density components at grazing incidence ($k_z = 0$) for $\mathbf{E}$ in the plane of incidence. The phase in these two cases, hence, must behave oppositely. Phase transition must be expected in an intermediate range of angles of incidence (for $\mathbf{E}$ in the plane of incidence). The reflection coefficient in the transition range is probably diminished due to the combined effect of the two current density components and may even disappear at a definite angle. These characteristics are known for reflection from a dielectric, where minimum (or zero) reflection and phase transition occur at the Brewster angle. They are now obtained in the case where J_x and J_z are of comparable magnitude. Numerical evaluations of very low-frequency theory (BUDDEN, 1955) actually show minimum reflection at a certain angle.

In Section 2 it was found that at the lowest frequencies the sign of the horizontal field-strength component is always reversed (metallic-type reflection). Therefore a transition must take place not only with changing angle, but also with changing frequency.

3.3. *Differential equations for the up-going and down-going wave*

The various terms in the integral equations (33) were ascribed to up-going and down-going waves respectively. It is possible, therefore, to write separately field strengths of the complete up-going and the complete down-going wave. If they are denoted $\mathbf{F}$ and $\mathbf{G}$, there is

$$\left.\begin{aligned} E_x &= F_x + G_x \\ E_y &= F_y + G_y \\ \frac{D_z}{\varepsilon} &= F_z + G_z \end{aligned}\right\} \tag{40}$$

The z components of **F** and **G** are taken as the two parts of D_z/ε (z-component of displacement vector divided by ε).

F and **G** are obtained from equations (33) as

$$\left.\begin{aligned}
F_x &= \frac{1}{2\varepsilon\omega}\int_{\zeta>z}(k_zJ_x - k_xJ_z)e^{-ik_z(z-\zeta)}\,d\zeta \qquad + C_xe^{-ik_zz}\\
F_y &= \frac{1}{2\varepsilon\omega}\int_{\zeta>z}\frac{k^2}{k_z}J_ye^{-ik_z(z-\zeta)}\,d\zeta \qquad + C_ye^{-ik_zz}\\
F_z &= \frac{1}{2\varepsilon\omega}\int_{\zeta>z}\left(-k_xJ_x + \frac{k_x^2}{k_z}J_z\right)e^{-ik_z(z-\zeta)}\,d\zeta - \frac{k_x}{k_z}C_xe^{-ik_zz}\\
G_x &= \frac{1}{2\varepsilon\omega}\int_{\zeta>z}(-k_zJ_x - k_xJ_z)e^{ik_z(z-\zeta)}\,d\zeta\\
G_y &= \frac{1}{2\varepsilon\omega}\int_{\zeta>z}\left(-\frac{k^2}{k_z}J_y\right)e^{ik_z(z-\zeta)}\,d\zeta\\
G_z &= \frac{1}{2\varepsilon\omega}\int_{\zeta>z}\left(-k_xJ_x - \frac{k_x^2}{k_z}J_z\right)e^{ik_z(z-\zeta)}\,d\zeta
\end{aligned}\right\} \tag{41}$$

The z-components are proportional to the x-components,

$$\left.\begin{aligned}
F_z &= -\frac{k_x}{k_z}F_x\\
G_z &= \frac{k_x}{k_z}G_x
\end{aligned}\right\} \tag{42}$$

They need therefore no consideration.

Equations (41) actually *define* the up-going and the down-going wave, but in such a way that the two waves in combination satisfy Maxwell's equations or the wave equation (26). In a current-free area, e.g. below the ionospheric layer, the lower boundary of integration may be replaced by a fixed boundary. The vectors **F** and **G** represent then an up-going and down-going wave in the common sense.

Differentiation of equations (41) leads to the following differential equations for **F** and **G**:

$$\left.\begin{aligned}
\frac{\partial F_x}{\partial z} + ik_zF_x &= \frac{1}{2\varepsilon\omega}(-k_zJ_x + k_xJ_z)\\
\frac{\partial F_y}{\partial z} + ik_zF_y &= \frac{1}{2\varepsilon\omega}\left(-\frac{k^2}{k_z}J_y\right)\\
\frac{\partial G_x}{\partial z} - ik_zG_x &= \frac{1}{2\varepsilon\omega}(k_zJ_x + k_xJ_z)\\
\frac{\partial G_y}{\partial z} - ik_zG_y &= \frac{1}{2\varepsilon\omega}\frac{k^2}{k_z}J_y
\end{aligned}\right\} \tag{43}$$

VOL. 12 1958

This set of four first-order differential equations governs the fields **F** and **G**. The components of **J** are linear functions of E_x, E_y, D_z/ε [equations (39)]. These field-strength components may be replaced by the components of **F** and **G** [equations (40)]. Equations (42) yield

$$\frac{D_z}{\varepsilon} = \frac{k_x}{k_z}(-F_x + G_x) \tag{44}$$

Hence only x- and y-components can be assumed to stay finally in the differential equations. The angular frequency ω might be replaced by ck. The constants ε, k, k_x, and k_z are still those for vacuum.

The set of differential equations looks simple. It could be used for approximate numerical calculation, provided the data involved are given as functions of height. Solutions in terms of known functions are not expected under general conditions. Even theoretical studies of wave propagation in stratified media, which were based on simplifying assumptions (e.g. no terrestrial magnetic field, refractive index being a mathematically proper function of height) resulted in rather intricate solutions (GANS, 1915; EPSTEIN, 1930; RAWER, 1939; RYDBECK, 1944 and WILKES, 1947). Surprisingly, however, elementary functions are obtained as solutions of equations (43) under certain conditions which include the existence of the terrestrial magnetic field. Section 1.3 of Part II will deal with this case.

The differential equations (43) lead to the thin-sheet reflection theory of the preceding section, if the terms with $\pm ik_z$ on the left side and J_z are considered negligible.

APPENDIX

Derivation of wave equation (26)

From Maxwell's equations

$$\left.\begin{aligned} \nabla \times \mathbf{H} &= i\omega\varepsilon\mathbf{E} + \mathbf{J} \\ \nabla \times \mathbf{E} &= -i\omega\mu\mathbf{H} \end{aligned}\right\} \tag{45}$$

one obtains the wave equation first in the form

$$\left.\begin{aligned} \nabla \times (\nabla \times \mathbf{E}) &= \omega^2\varepsilon\mu\mathbf{E} - i\omega\mu\mathbf{J} \\ &= k^2\mathbf{E} - i\frac{k}{c\varepsilon}\mathbf{J} \end{aligned}\right\} \tag{46}$$

The well-known relationship of vector analysis

$$\nabla \times (\nabla \times \mathbf{E}) = -\nabla^2\mathbf{E} + \nabla(\nabla \cdot \mathbf{E}) \tag{47}$$

together with the divergence condition following from the first Maxwell equation

$$\nabla \cdot \mathbf{E} = \frac{i}{\varepsilon\omega}\nabla \cdot \mathbf{J} \tag{48}$$

yields

$$\nabla \times (\nabla \times \mathbf{E}) = -\nabla^2\mathbf{E} + \frac{i}{\varepsilon\omega}\nabla(\nabla \cdot \mathbf{J}) \tag{49}$$

This substitution transforms equation (46) into wave equation (26).

Equations (33)

Equations (33) are not the only possible representation of the field-strength components as sums or integrals of reflected partial waves in combination with a penetrating wave, but they are probably the only representation of this kind in which the amplitudes are functions of the current density components only and not of their derivatives. The second derivative of J_z in the wave equations (29) is taken into account by the term containing J_z, on the left side of the third equation. This avoids having a derivative in the amplitudes of partial waves.

The expressions for the field-strength components must fulfil not only the wave equation but also the divergence condition [equation (48)]. The expressions given by equations (33) actually fulfil the divergence condition. Quite generally it can be said: If the boundary conditions are chosen so narrow as to admit only one solution of the wave equation, then this solution fulfils the divergence condition unless the boundary conditions are unreasonable, i.e. contradictory to the divergence condition.* The assumption of transverse plane homogeneous waves (up-going and down-going) outside the layer implies such narrow boundary conditions.

The fact that the partial waves had to be derived from E_x, E_y and D_z rather than E_z is no accident, but a consequence of the continuity of E_x, E_y and D_z at any horizontal boundary. An interpretation of $\mathbf{F}$ and $\mathbf{G}$ to be given in the second part of this paper (Section 3) will show that $\mathbf{F}$ and $\mathbf{G}$ must be continuous at a horizontal boundary, and therefore also $\mathbf{F} + \mathbf{G}$. The sum $\mathbf{F} + \mathbf{G}$ represents the actual field. Its components, therefore, must be components of some vector describing the field. The only components in question which are continuous at a boundary are E_x, E_y, D_z (the latter perhaps divided by vacuum ε).

Acknowledgements—I wish to express my thanks to Mr. RODNEY A. BROOKS, Mr. LEONARD C. HUMPHREY, Dr. EDWARD A. LEWIS and Dr. FRIEDRICH VILBIG for stimulating discussions and to Miss ALMA GANIO for help in preparing the manuscript.

* I owe this statement to RODNEY A. BROOKS.

REFERENCES

BREMMER H.	1949	*Terrestrial Radio Waves* p. 310. Elsevier, New York.
BREMMER H.	1951	*The Theory of Electromagnetic Waves.* Proceedings of a Symposium, New York University. p. S169. Interscience, New York.
BUDDEN K. G.	1955	*Proc. Roy. Soc.* A **227,** 516.
BUTLER S. R., GIBBONS J. J., LEVY G. S. and MAY J. J.	1956	Solutions of the coupled wave equations for vertical ionospheric propagation at 75 and 150 kc/s. *Ionospheric Res. Sci. Rep. No.* 84, Penn. State University, University Park, Pennsylvania.
DARWIN C. G.	1924	*Trans. Camb. Phil. Soc.* **23,** 137.
DAVIDS N. and PARKINSON R. W.	1955	*J. Atmosph. Terr. Phys.* **7,** 173.
EPSTEIN P. S.	1930	*Proc. Nat. Acad. Sci. U.S.A.* **16,** 627.

VOL. 12 1958

Gans R.	1915	*Ann. Phys.* **47,** 709.
Hartree D. R.	1929	*Proc. Camb. Phil. Soc.* **25,** 97.
Mallinckrodt A. J.	1954	The boundary problem in ionospheric wave propagation. *Tech. Rep. No.* 2, Radio Prop. Lab. Stanford University, Stanford, California.
Rawer K.	1939	*Ann. Phys.* **35,** 385.
Rydbeck O. E. H.	1944	*Chalmers tek. Högsk. Handl. No.* 34.
Rydbeck O. E. H.	1948	*Chalmers tek. Högsk. Handl. No.* 74.
Wilkes M. V.	1947	*Proc. Roy. Soc.* A **189,** 130.

OL.
12
958

Journal of Atmospheric and Terrestrial Physics, 1958, Vol. 12, pp. 140 to 149. Pergamon Press Ltd., London

The effect of diffusion on the vertical distribution of ionization in a quiet *F*-region

V. C. A. FERRARO and I. ÖZDOĞAN*
Department of Mathematics, Queen Mary's College, London E.1

(*Received* 30 *November* 1957)

Abstract—The vertical distribution of ions in a quiet *F*-region is calculated on the assumption that electrons disappear by attachment to neutral molecules and by diffusion. The coefficient of attachment, K, is assumed to be constant and the value of the coefficient of diffusion, D, adopted is that calculated according to the classical theory of gases. Adopting numerical values of the molecular air density and temperature in the *F*-region inferred from rocket data, it is found that diffusion produces a diurnal oscillation in the level of maximum ionization characterized by a rapid rise soon after sunrise followed by a slower fall of level which continues till dawn. It is suggested that since this is at variance with the observed behaviour of the height of the *F2*-region, the adopted value of the coefficient of diffusion may be too large by a factor of 10. It is also inferred that the value of K is likely to be smaller than the value suggested in recent work of RATCLIFFE *et al.* (1956) and that its value is probably somewhat smaller than 10^{-4}sec^{-1} at levels lower than 300 km.

1. INTRODUCTION

THIS paper is a continuation of earlier papers by one of us (FERRARO, 1945, 1946) on the effect of diffusion of ions in the ionosphere. In these papers it was assumed that electrons disappeared according to a quadratic law of recombination; whilst this is certainly the case for the *E*- and *F1*-regions, recent work by RATCLIFFE *et al.* (1956) indicates that in the *F*-region, above 240 km, the rate of loss of electrons is more consistent with a linear law of recombination. They find that if this is the case, the coefficient of attachment K between the levels of 250 and 350 km decreases exponentially with the layer h according to the law

$$K = 10^{-4} \exp\left(\frac{300 - h}{50}\right) \text{sec}^{-1} \qquad (1)$$

This value is derived mainly from observations at night-time made by SCHMERLING and THOMAS (1956).

If the molecular density of the *F2*-region is as low as rocket data indicate, ionic diffusion may well be the dominant factor in determining the vertical distribution of ions.

RATCLIFFE *et al.* have, in fact, suggested that the peak level of the *F2*-region seems likely to be determined mainly by diffusion processes, and it is of interest in this connexion to calculate the vertical distribution of ionization in the *F*-region on the assumption that electrons disappear by attachment to neutral air molecules and ionic diffusion. As was shown by FERRARO, diffusion tends to lower the level of maximum ionization below the level which would be attained if there were no diffusion.

We have not been entirely successful as yet in integrating the equations of diffusion when K decreases exponentially upwards according to the law (1). In this paper we give the solution when K is constant and in numerical illustrations we shall adopt a mean value of the order of 10^{-4}sec^{-1}. This overestimates the rate of loss of electrons in the higher levels, say from 300 to 400 km, as compared

* University of Istanbul.

VOL. 12 1958

with equation (1), and underestimates it below 300 km. We have also neglected oscillatory movements in the ionosphere as a whole.

2. The Equations of the Problem

The relevant equation of the problem was derived by Ferraro (1945) and the derivation will not be repeated here. Let N be the electron density, n the density of the neutral molecules at a height x above a reference level, H the scale height, D the coefficient of diffusion of the ions in the ionosphere, q the rate of ion-production and K the coefficient of attachment. Then the equation satisfied by N is

$$\frac{\partial N}{\partial t} = q - KN + D\left(\frac{\partial^2 N}{\partial x^2} + \frac{3}{2H}\frac{\partial N}{\partial x} + \frac{N}{2H^2}\right) \tag{2}$$

The coefficient of diffusion, D, may be written in the form b/n, where b is a function of n and the temperature of air, T. For temperatures of the order obtaining in the F-region, b is practically constant, but its value is subject to some uncertainty. The value of b derived from classical kinetic theory (Ferraro, 1957) is of the order of 10^{18} at room temperature and 10^{19} at temperature of the order 1000°. At a temperature of 500° the value of $b = 5 \times 10^{18}$. Because of the neglect of the effect of electron transfer, this value may well be too large by a factor of order unity.

The density and temperature of the neutral molecules in the $F2$-region is also uncertain, though the density seems likely to decrease exponentially with height. Accordingly we shall write

$$n = n_0 \exp\left(-\frac{x - x_0}{H}\right) \tag{3}$$

where x_0 will be taken to be the height of the level of maximum ion-production. It will be convenient to measure the time of day in radians φ, so that we write

$$t = 1{\cdot}37 \times 10^4 \varphi = k\varphi \tag{4}$$

and to introduce the quantity q_0, the value of q for the overhead sun. If χ denotes the sun's zenith distance, we have, for a Chapman region,

$$q = q_0 \exp\left[1 - \frac{x - x_0}{H} - \exp\left(-\frac{x - x_0}{H}\right)\sec\chi\right] \tag{5}$$

Introducing a new independent variable ζ and a new dependent variable M defined by

$$\zeta^2 = \exp\left(-\frac{x - x_0}{H}\right), \qquad N = M\zeta^{3/2} \tag{6}$$

we obtain from (2) the following equation for M, viz.

$$\frac{\partial M}{\partial \varphi} = kq\zeta^{-3/2} - kKM + \frac{1}{4\gamma}\left(\frac{\partial^2 M}{\partial \zeta^2} + \frac{1}{\zeta}\frac{\partial M}{\partial \zeta} - \frac{M}{4\zeta^2}\right) \tag{7}$$

where

$$\gamma = n_0 H^2/(kb) \tag{8}$$

Furthermore, equation (5) may be written

$$q = q_0 e \zeta^2 \exp\left(-\zeta^2 \sec\chi\right) \tag{9}$$

We have to find a periodic solution of (7) with period 2π for this special form of q.

3. A Particular Solution

We shall restrict the solution to the particular case of the equator at the equinoxes; in this case $\chi = \frac{1}{2}\pi - \varphi$. Let $\bar{M}$ denote the Hankel transform of M defined by the equation

$$\bar{M}(\xi) = \int_0^\infty \zeta M(\zeta) J_{1/2}(\xi\zeta)\, d\zeta \tag{10}$$

Multiplying (7) by $\zeta J_{\frac{1}{2}}(\xi\zeta)$ and integrating with respect to ζ from 0 to ∞, we find

$$\frac{\partial \bar{M}}{\partial \varphi} + [kK + \xi^2/(4\gamma)]\bar{M} = \int_0^\infty kq\zeta^{-1/2} J_{1/2}(\xi\zeta)\, d\zeta, \tag{11}$$

since (Sneddon, 1951)

$$\int_0^\infty \zeta\left(\frac{\partial^2 M}{\partial \zeta^2} + \frac{1}{\zeta}\frac{\partial M}{\partial \zeta} - \frac{M}{4\zeta^2}\right) J_{1/2}(\xi\zeta)\, d\zeta = -\xi^2 \bar{M}(\xi) \tag{12}$$

For a Chapman region defined by equation (9) the infinite integral occurring in (11) is convergent and its value is

$$\frac{keq_0 \xi^{1/2}}{(2 \operatorname{cosec} \varphi)^{3/2}} \exp\left(-\tfrac{1}{4}\xi^2 \sin \varphi\right) \tag{13}$$

Equation (11) can now be solved, and on taking the inverse transform of this solution we obtain the particular solution valid in the range $0 \leqslant \varphi \leqslant 2\pi$ in the form

$$M_0 = \int_0^\varphi \mathcal{G}(\zeta, \varphi, \alpha)\, d\alpha \tag{14}$$

where

$$\mathcal{G}(\zeta, \varphi, \alpha) = \frac{keq_0 \zeta^{1/2} e^{-kK(\varphi - \alpha)}}{\left[1 + \frac{1}{\gamma}(\varphi - \alpha) \operatorname{cosec} \alpha\right]^{3/2}} \exp\left[-\frac{\zeta^2 \operatorname{cosec} \alpha}{1 + \frac{1}{\gamma}(\varphi - \alpha) \operatorname{cosec} \alpha}\right] \tag{15}$$

Then from (6) the corresponding value N_0 of N is

$$N_0 = \int_0^\varphi \zeta^{3/2} \mathcal{G}(\zeta, \varphi, \alpha)\, d\alpha \tag{16}$$

This solution can be interpreted very simply as follows: in (15) write

$$x'_0 = x_0 - H \log\left[1 + \frac{1}{\gamma}(\varphi - \alpha) \operatorname{cosec} \alpha\right] \tag{17}$$

and replace ζ^2 by $\exp\left(-\dfrac{x - x_0}{H}\right)$. Then the integrand in (16) may be written

$$\frac{kq_0 e^{-kK(\varphi - \alpha)}}{\left[1 + \frac{1}{\gamma}(\varphi - \alpha) \operatorname{cosec} \alpha\right]^{1/2}} \exp\left[1 - \frac{x - x'_0}{H} - \exp\left(-\frac{x - x'_0}{H}\right) \operatorname{cosec} \alpha\right]$$

A comparison with (5) shows that this is a Chapman region whose level of maximum ion-concentration occurs at a depth $x_0 - x'_0$ or $H \log\left[1 + \dfrac{1}{\gamma}(\varphi - \alpha) \operatorname{cosec} \alpha\right]$

VOL. 12 1958

below that for a Chapman region and which is diluted by the factor

$$f = e^{-kK(\varphi-\alpha)}\left[1 + \frac{1}{\gamma}(\varphi - \alpha)\operatorname{cosec}\alpha\right]^{-1/2}.$$

Thus the integral (14) may be interpreted as the ionization produced by a continuous succession of bursts of radiation emitted at times $\varphi = \alpha$, $0 \leqslant \alpha \leqslant \varphi$, which are diluted partly by recombinations and partly by diffusion in the ratio $f : 1$ and whose level of maximum ionization is lowered to a depth $H \log\left[1 + \frac{1}{\gamma}(\varphi - \alpha)\operatorname{cosec}\alpha\right]$ below that for a Chapman region. We note that if γ is large compared with unity, this depth is small. Thus this effect of diffusion may be expected to become important when γ becomes comparable with, or is smaller than, unity.

4. The Periodic Solution

We now determine the solution of equation (2), which is periodic in φ with period 2π. Consider the series

$$N = N_0 + \sum_{r=1}^{\infty} N_r \tag{18}$$

where N_0 is given by (16) and $N_r = M_r\zeta^{3/2}$ with

$$M_r = \int_0^{\pi} \mathcal{G}(\zeta, \varphi + 2r\pi, \alpha)\, d\alpha \tag{19}$$

in the range $0 \leqslant \varphi \leqslant 2\pi$. It is readily verified that (19) is a solution of (7) when $q \equiv 0$. Since $0 < \mathcal{G} < keq_0\left[1 + \frac{2r\pi}{\gamma}\operatorname{cosec}\alpha\right]^{-3/2}$ it follows that the series (18) is uniformly convergent. Moreover

$$\begin{aligned} M_{\varphi=2\pi} &= \int_0^{2\pi} \mathcal{G}(\zeta, 2\pi, \alpha)\, d\alpha + \sum_{r=1}^{\infty}\int_0^{\pi} \mathcal{G}(\zeta, 2r\pi + 2\pi, \alpha)\, d\alpha \\ &= \int_0^{\pi} \mathcal{G}(\zeta, 2\pi, \alpha)\, d\alpha + \sum_{r=1}^{\infty}\int_0^{\pi} \mathcal{G}(\zeta, 2(r+1)\pi, \alpha)\, d\alpha \end{aligned} \tag{20}$$

since $q = 0$ for $\varphi \geqslant \pi$; thus

$$M_{\varphi=2\pi} = \sum_{r=1}^{\infty}\int_0^{\pi} \mathcal{G}(\zeta, 2r\pi, \alpha)\, d\alpha = M_{\varphi=0} \tag{21}$$

Whence it follows that $N_{\varphi=2\pi} = N_{\varphi=0}$ since $N = M\zeta^{3/2}$. The solution is therefore periodic in φ with period 2π, and since (18) is the solution of the equation (7) it is the required solution.

It is clear from the interpretation of the function $\mathcal{G}$ given in Section 4 that N_0 represents the contribution to the electron density from the ionization produced on the first day, and N_r the contribution from the rth day previously. Because of the presence of the exponential $\exp[-kK(\varphi - \alpha)]$ in (15), in general, the contribution from ionization produced two or more days previously can be neglected.

5. Numerical Illustrations

In numerical illustrations of our results, we have taken $b = 5 \times 10^{18}$ in the formula for D, $n_0 = 1{\cdot}37 \times 10^9$ mol/cm^3 and $H = 50$ km. These values are those inferred by Heavens, Friedman and Hulburt (1955) from rocket data for a

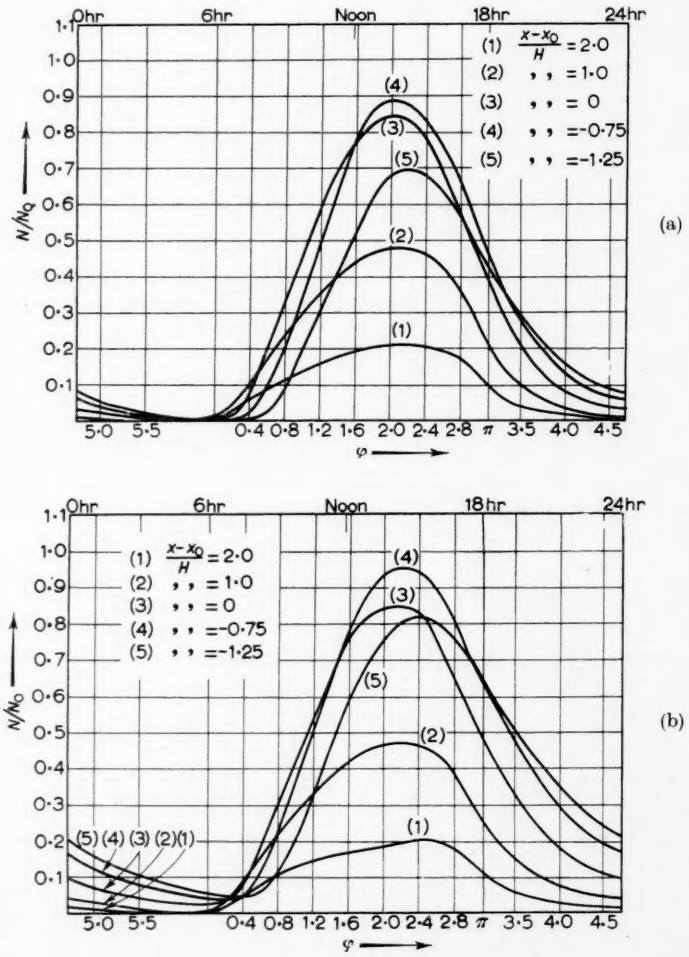

Fig. 1. Illustrating the diurnal variation of N/N_m at different heights for the cases when $kK = 1$ (curve (a)) and $kK = \frac{1}{2}$ (curve (b)) at the equator at the equinoxes. (N represents the electron density and N_m the electron density at noon.)

height of about 250 km. We have considered two values of K corresponding to $kK = 1$ and $\frac{1}{2}$, that is, $K = 0{\cdot}7 \times 10^{-4}$ and $0{\cdot}37 \times 10^{-4}$, which, according to equation (1), are the values of K at heights of 317 km and 350 km respectively. We have furthermore supposed that the level of maximum ion-production to occur at about 250 km. The result of our calculations are shown in Figs. 1–4. In these diagrams N is expressed as a fraction of the maximum electron density N_m at

VOL. 12 1958

mid-day (at the equator at the equinoxes) and the curves corresponding to $kK = 1$ are marked (a), those for $kK = \frac{1}{2}$ are marked (b).

Fig. 1 illustrates the daily variation of N/N_m at different heights. It will be

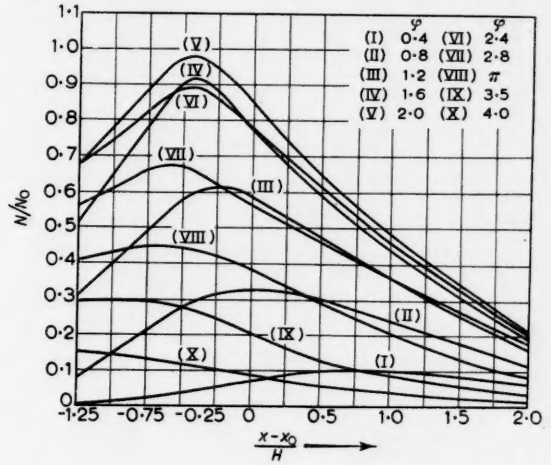

(a)

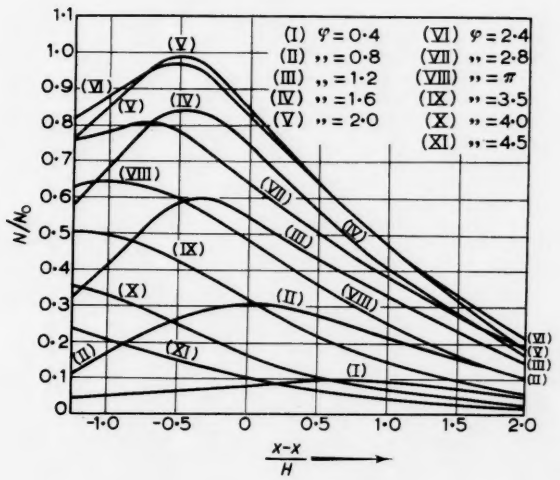

(b)

Fig. 2. Illustrating the vertical distribution of N/N_m at different times of the day for $kK = 1$ (curve (a)) and $KK = \frac{1}{2}$ (curve (b)) at the equator at the equinoxes. (N represents the electron density and N_m the electron density at noon.)

seen that for both values of the coefficients K, the level of maximum ionization is lower than the level of maximum ion-production, $x = x_0$, though by not more than about three-quarters of a scale height or, say, 40 km. The maximum ionization occurs later in the afternoon for levels above or below the level of maximum ionization, which occurs at about a little over 1 hr after mid-day.

Fig. 2 illustrates the vertical variation of N/N_m at different times of the day; in both cases it will be seen that the level of maximum ionization slowly descends as the day advances into night, being lowest just before sunrise. Thereafter it rises quickly to about one scale height above the level of maximum ion production 1 hr after sunrise. This is also illustrated in Fig. 3 which indicates the variation of the level of maximum ionization with time. Fig. 4 illustrates the daily variation of the maximum electron ionization density $(N/N_m)_{\max}$. It will be seen that there

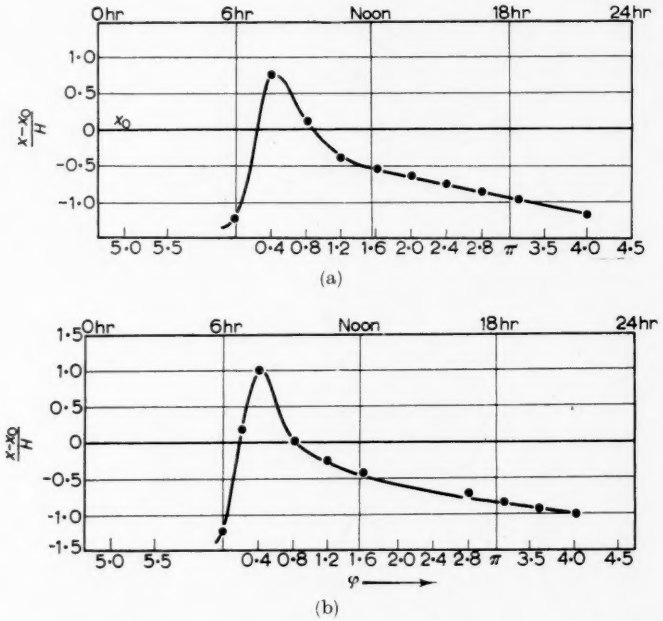

Fig. 3. Illustrating the diurnal variation of the level of maximum electron density for the cases when $kK = 1$ (curve (a)) and $kK = \frac{1}{2}$ (curve (b)) at the equator at the equinoxes.

is a general, though not detailed, agreement with the corresponding (mean) curve for Watheroo for March, 1939. The divergence between the two curves is most marked during the morning.

One unexpected result is that the values of $(N/N_m)_{\max}$ appear to be vanishingly small just before sunrise for case (a), for which $K = 0{\cdot}7 \times 10^{-4}s^{-1}$, and rather small for the case (b) for which $K = 0{\cdot}37 \times 10^{-4}s^{-1}$; these values of K are considerably lower than the values derived from (1) at the level of about 200 km, which is two scale heights below the level at which $K = 10^{-4}s^{-1}$ according to (1). For this reason we have also integrated equation (2) ignoring diffusion but assuming that K varies according to the law given by (1) instead of being constant. The results are shown in Fig. 5. It will be seen that N/N_m tends to a definite limit at great heights. This can be seen from the equation for N in this case, viz.

$$\frac{\partial N}{\partial t} = q - KN \tag{22}$$

VOL. 12 1958

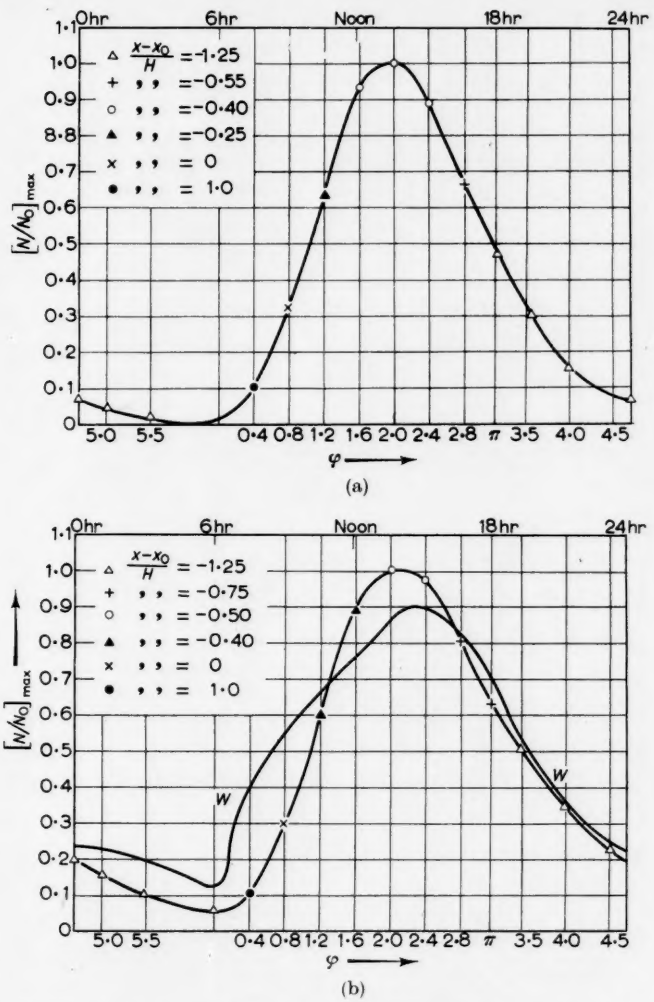

Fig. 4. Showing the daily variation of the maximum electron density, $(N/N_m)_{max}$, for the two cases $kK = 1$ (curve (a)) and $kK = \frac{1}{2}$ (curve (b)). The curve marked (W) in (b) gives corresponding mean curve for Watheroo for March 1939.

In this equation, q is the Chapman function given by equation (9), viz.

$$q = eq_0\zeta^2 \exp(-\zeta^2 \sec \chi)$$

K is given by (1). If the level of maximum ion-production x_0 is assumed to be at 250 km, then (1) may be rewritten

$$K = 10^{-4}e\zeta^2$$

Also at great height, where ζ is small, the curves in Fig. 5 indicate that $\partial N/\partial t \sim 0$; thus the limiting value N_{ma} of N for ζ small is given by $q_0/10^{-4}$ or $10^4 q_0$. According to RATCLIFFE *et al.* (1956), the value of q_0 in the $F2$-region may vary between

300 and 600. For these values of q_0 the values of N_{ma} range from 3×10^6 to 6×10^6 electrons/cm^3. These values are of the same order of magnitude as that obtaining in the *F2*-region. It will be seen from Fig. 5 that at a depth of one

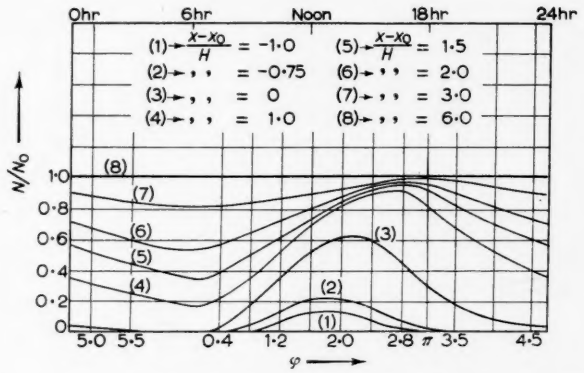

Fig. 5. Illustrating the diurnal variation of N/N_m for various heights on the supposition that there is no diffusion and that the rate of disappearance of electrons at height H km is given by $K = 10^{-4} \exp\left[\frac{300 - h}{50}\right] \text{sec}^{-1}$.

scale height below the level x_0 (= 200 km), the electron density calculated on the assumption that K is given by equation (1) is negligible.

Thus, it seems likely that the value of K below 250 km must be of the order of $10^{-4} s^{-1}$ at most and that the formula (1) gives values of K which may be too large by a factor of order unity.

6. Discussion

The results of this paper show, firstly, that if the coefficient of diffusion in the *F*-region is as large as the classical theory indicates, then diffusion will tend to produce an anharmonic oscillation in the level of maximum ionization in this region. This is characterized by a rapid rise of this level just after sunrise to a height of about one scale height (50 km) above the level of maximum ion production (250 km) followed by a steady fall to a minimum height which may exceed one and a quarter scale heights, or say 70 km, just before sunrise. This is quite unlike the observed diurnal variation of the height of the *F2*-level of maximum ionization and it suggests that either diffusion is less marked and that the value of the coefficient of diffusion, D, adopted here is too large by as much as a factor of 10, or else that diffusion is offset by other factors. It is possible that a quantal calculation may reduce the value of D.

Secondly, the results are somewhat at variance with the value of K deduced by Ratcliffe *et al.* (1956) in the *F*-region. For their estimated values our calculations give electron densities just before sunrise which are too low compared with the observed values. This second conclusion is, moreover, likely to be independent of any vertical motion of ions which may obtain in the ionosphere and

VOL. 12 1958

this suggests that the coefficient of attachment, K, may be somewhat smaller than the value adopted here.

Undoubtedly, vertical motions of ions are important in the F-region, and we hope to consider this effect in a later paper.

References

Ferraro V. C. A.	1945	*Terr. Mag.* **50,** 215.
	1946	*Terr. Mag.* **51,** 427.
	1957	*J. Atmosph. Terr. Phys.* In press.
Heavens R. J., Friedmann H. and Hulburt E. O.	1955	*The Physics of the Ionosphere* p. 237. Report of the Physical Society Conference
Ratcliffe J. A., Schmerling E. R., Setty C. S. G. K. and Thomas J. O.	1956	*Phil. Trans.* **248,** 621.
Schmerling E. R. and Thomas J. O.	1956	*Phil. Trans.* **248,** 609.
Sneddon I. N.	1951	*Fourier Transforms.* McGraw-Hill, New York.

OL.
12
958

Journal of Atmospheric and Terrestrial Physics, 1958, Vol. 12, pp. 150 to 152. Pergamon Press Ltd., London

The distance attenuation of radio waves reflected at vertical incidence from the ionosphere

J. D. WHITEHEAD
Otago University, Dunedin, N.Z.

(*Received* 21 *October* 1957)

Abstract—It is shown that the assumption that the amplitude of radio waves propagated from a point source falls off inversely as the group path P' leads to a value of apparent reflection coefficient of the ionosphere which may be seriously in error, and in particular to a large error in the measurement of the electronic collision frequency in the F-region.

INTRODUCTION

WHEN the reflection coefficient of the ionosphere is measured, consideration has to be given to the effect of refraction on the distance attenuation of the waves. It is often assumed that the amplitude of radio waves propagated from a point source falls off inversely as the group path P', whereas the correct expression is $\int ds/\mu$, where μ is the refractive index and the integral is taken over the path of length s.

If the effect of the earth's magnetic field is neglected, the group refractive index μ' is equal to $1/\mu$, so that $\int \mu' ds = P' = \int ds/\mu$. It is the purpose of this note to point out that because of the presence of the earth's magnetic field the assumption that P' is approximately equal to $\int ds/\mu$ leads to serious errors in the measurement of the reflection coefficient. Only waves propagated at vertical incident in the ordinary mode and having a frequency greater than the longitudinal gyrofrequency, are considered. The notation is that explained in APPLETON's paper (1932).

It has been shown (WHITEHEAD, 1952) that near the level where the electron density is such that $X = 1$, the refractive index for the ordinary ray is given by $\mu = \operatorname{cosec}\theta\sqrt{1 - X}$, where θ is the angle between the imposed magnetic field and the direction of propagation. We then find that the group refractive index is

$$\mu' = \frac{\operatorname{cosec}\theta}{\sqrt{(1 - X)}} = \frac{\operatorname{cosec}^2\theta}{\mu}$$

so that μ' is always greater than $1/\mu$.

The exact values of $\int ds/\mu$ and $\int \mu' ds$ depend on the particular $N{:}h$ profile of the ionosphere. However, because both $1/\mu$ and μ' are large only near $X = 1$, it is sufficient for our purpose to assume an $N{:}h$ profile in which the electron density N is zero up to a certain level and increases linearly from that level upwards. Even so, the integration can only be done approximately, but provided that $Y_L \ll 1$, it may be shown that, at vertical incidence,

$$\int \frac{ds}{\mu} = P' \sin^2\theta + P\cos^2\theta$$

VOL. 12 1958

where P is the actual path length. Thus we see that in high latitudes, where $\theta < 45°$, $\int ds/\mu$ is more nearly equal to P than P'.

Measurement of the Reflection Coefficient of the Ionosphere

If the reflection coefficient of the ionosphere is found by measuring the amplitude of the first echo and the apparatus has been correctly calibrated, it is easy to show from the above equation that the correct value for the reflection coefficient is given by $\rho = \{1 - [(P' - P)/P'] \cos^2 \theta\}\rho_M$ or $-\log \rho = -\log \rho_M - \log \{1 - [(P' - P)/P'] \cos^2 \theta\}$ where ρ_M is the apparent reflection coefficient found by assuming that the distance attenuation is proportional to P'.

The term $(-\log \rho_M)$ corresponds to the published values. The order of magnitude of the correction $-\log \{1 - [(P' - P)/P'] \cos^2 \theta\}$, is given in the following table.

The values of P' correspond to those well away from critical frequencies and for F-region reflections are the average values observed on twelve quiet days, one from each month of the year. The F-region data* have been derived from P': f curves taken at Christchurch, where $\theta = 21{\cdot}9°$.

Table 1

	P' (km)	P (km)	$-\log \{1 - [(P' - P)/P'] \cos^2 \theta\}$
Reflections from:			
E-region at noon	240	220	0·07 neper
F-region at noon	530	330	0·39 neper
F-region at midnight	600–800	550–600	0·07–0·25 neper

The correction on disturbed days will generally be greater than that given in the last column of Table 1. The correction also becomes greater at lower working frequencies for which Y_L is not small.

It should be pointed out that if the reflection coefficient is found by comparing the amplitude of the first and second echoes (as during the calibration of the equipment), the correct value is obtained, but that the constant of the apparatus calculated from this measurement and used when only the first echo is present, is incorrect. The full expression for the correct value of the reflection coefficient is then

$$\rho = \left\{ \frac{1 - \left(\frac{P' - P}{P'}\right) \cos^2 \theta}{1 - \left[\frac{P' - P}{P}\right]_{\text{cal}} \cos^2 \theta} \right\} \rho_M$$

where the values of P' and P in the square brackets refer to the group and actual paths during the absolute calibration. However, the absolute calibration is usually performed during the night, using reflections from either sporadic E- or F-region. Under these conditions $[P' - P/P]_{\text{cal}} \cos^2 \theta$ is usually much less than

* I am indebted to Mr. G. A. M. King of the Geophysical Observatory, Christchurch, for these data.

unity. We may conclude that the present measurements of the reflection coefficient ρ_M of E-region and F-region at night are not greatly in error, but that those of F-region during the day may be in error by more than 0·3 neper. Because the correction has a marked diurnal and seasonal variation, our present conclusions about the diurnal and seasonal variation of $-\log \rho$ might be markedly altered.

The Measurement of the Collision Frequency of Electrons in F-Region

A further error introduced by taking the incorrect distance attenuation is apparent when the electronic collision frequency is measured by finding the change in $-\log \rho$ corresponding to a change in P' minus the phase path. The phase path is very nearly equal to the actual path and the formula for calculating the collision frequency was given by Appleton (1928) and is

$$-\Delta \log \rho = \frac{\nu}{2c} \Delta(P' - P)$$

where ν = electronic collision frequency,
c = velocity of light.

This formula is only correct when the effect of the earth's magnetic field is neglected, but is sufficiently accurate in the presence of the earth's field provided the extra absorption occurs very near the reflecting level. If $-\log \rho$ is measured by assuming that the distance attenuation is proportional to P', an incorrect value of ν, ν_M is calculated. This value is the one usually given in the literature. The correct value of ν can be shown to be approximately

$$\nu = \nu_M + \frac{2c \cos^2 \theta}{P}$$

In New Zealand, the correction $(2c \cos^2 \theta)/P$ is equal to about $2{\cdot}5 \times 10^3$ per sec for E-region reflections and about $1{\cdot}5 \times 10^3$ per sec for F-region reflections. As the measured values of ν, ν_M for F-region are about 10^3 per sec, it is seen that the correct value of ν is considerably higher than has been supposed.

Conclusion

The present published noon values of $-\log \rho$ for reflections from the F-region of the ionosphere are too low by about 0·3 nepers, because the distance attenuation has been incorrectly taken to be proportional to the group path. The correction has a diurnal and seasonal variation which introduces additional variations in the values of $-\log \rho$.

Previous measurements of the collision frequency in F-region give values which are too low by an amount equal to about $1{\cdot}5 \times 10^3$ per sec.

Acknowledgements—I am indebted to my colleagues in the Physics Department of Otago University for many helpful discussions.

References

Appleton E. V. 1932 *J. Inst. Elect. Engrs.* **71,** 430.
Appleton E. V. 1928 *Int. Union Sci. Rad. Tel.* **1,** Part I.
Whitehead J. D. 1952 *J. Atmosph. Terr. Phys.* **2,** 361.

VOL. 12 1958

Journal of Atmospheric and Terrestrial Physics, 1958, Vol. 12, pp. 153 to 165. Pergamon Press Ltd., London

Resonance scattering by atmospheric sodium—IV

Abundance of sodium in twilight*

J. W. CHAMBERLAIN, D. M. HUNTEN and J. E. MACK
Yerkes Observatory, University of Chicago; University of Saskatchewan;
and University of Wisconsin

(*Received* 23 *October* 1957)

Abstract—The theory of Part I is extended to take account of the hyperfine structure of the D-lines. The absolute intensity of $D_1 + D_2$ and the ratio D_2/D_1 are computed as functions of total Na abundance for an angle of solar depression, β, of 6·5°. Observations made in Saskatoon are discussed in terms of the seasonal variation of Na. Abundance determinations from the D_2/D_1 ratio in twilight and from the terrestrial component of D-line absorption in the solar spectrum are in good accord with abundances deduced from the absolute twilight intensity.

1. INTRODUCTION

THEORETICAL calculations recently made by HUNTEN (1956b) of the absolute intensity of the sodium D-lines in twilight, on the basis of resonance scattering of sunlight, first revealed an intriguing discrepancy. It is known that when the theoretical intensity (for a particular angle of solar depression, β) is plotted against assumed sodium abundance, the curve goes through a maximum. This characteristic of the curve is readily understandable when we consider that for small abundances the intensity increases as the number of atoms, but for large amounts of sodium the incident solar flux is seriously diminished through resonance absorption (BRICARD and KASTLER, 1944; DONAHUE and RESNICK, 1955). But the puzzling feature of HUNTEN's results was that the maximum computed emission, reduced to the zenith, was about 4·1 kilorayleighs (kR)† (which occurred for a total abundance in a vertical column of $N \approx 10^{10}$ Na atoms/cm^2), whereas he frequently observed intensities in excess of this maximum. Moreover, there were inconsistencies between the observed and computed D_2/D_1 ratio.

HUNTEN suggested that secondary scatterings, which had been neglected in the theory, might increase the computed intensity significantly. Discussion of these problems between HUNTEN and CHAMBERLAIN in July 1955 led to the present series of papers in which CHANDRASEKHAR's theory of radiative transfer in finite atmospheres has been applied to the sodium layer.

* The research reported in this paper was supported in part by the Geophysics Research Directorate of the Air Force Cambridge Research Center, Air Research and Development Command, under Contract AF 19(122)-480 with the University of Chicago and Contract AF 19(604)-1831 with the University of Saskatchewan; by the Office of Ordnance Research under contract with the University of Wisconsin; and by the Wisconsin Alumni Research Foundation. One of us (J. E. M.) did part of this work during a summer consultantship with General Atomic Division of General Dynamics, San Diego, California, to whom he wishes to express his appreciation for the facilities and the working environment provided there.

† If $\mathcal{I}$, the integrated intensity in a given direction, is measured in units of 10^6 quanta/cm^2 sec sterad, then $4\pi\mathcal{I}$ is the *apparent* rate of emission in rayleighs (1 R = 10^6 quanta/cm^2 sec) in a column along the line of sight. See HUNTEN, ROACH and CHAMBERLAIN (1956) for further explanation.

In Part I (Chamberlain, 1956) it was found that secondary scatterings could raise the maximum intensity by only 16 per cent or so. However, there was some uncertainty in the adopted parameters (for example, the central intensity of the D-lines in the solar spectrum) and, further, it was suggested that irregularities in the horizontal distribution of sodium might increase the maximum expected intensity.

Secondary scatterings have a more profound effect on the computed D_2/D_1 ratio, which was brought into fair accord with the observations of Harrison and Vallance Jones (1956). Galperin (1956a, b) independently applied the transfer theory to the problem of the D_2/D_1 ratio for a single assumed sodium abundance, and his results are in good agreement with those of Part I.

At a conference on *Sodium in the Twilight Airglow* held at Yerkes Observatory in February 1957, a number of workers* in this subject discussed these topics and related problems in detail. It was pointed out by Mack that since some of the hyperfine splitting of the D-lines is larger than the Doppler width at temperatures around 200°K, resonance absorption would have less importance in diminishing the observed intensity than the theory predicted; or, for a given sodium abundance, the layer of sodium is thinner optically than had been supposed. The hyperfine structure seems to have been universally overlooked in previous work in this subject, which means that all published computations must be appropriately modified.

In this paper it is shown that allowance for the hyperfine structure leads to theoretical intensities that are no longer inconsistent with the observations. Moreover, the sodium abundances deduced from these measurements are in reasonable agreement with determinations by other means.

To a first approximation, we may consider the hyperfine structure as splitting the D_1- and D_2-lines into two components each, with these component lines having Doppler profiles characteristic of the kinetic temperature (see Section 2). The ratio of the f-values (integrated absorption coefficients) of these two components is 5/3. Hence an approximate correction to the total $D_1 + D_2$ intensities of Parts I and II may be made as follows. For a given abundance N, read the $D_1 + D_2$ intensity from the published graphs for $\frac{5}{8}N$ and for $\frac{3}{8}N$. Add these intensities to find the corrected value for abundance N.

The D_2/D_1 ratios in twilight and nightglow and the zenith-horizon variation of intensity in the nightglow (Chamberlain and Negaard, 1956, Part II) may be corrected approximately by using the computations for one-half the actual Na abundance.

The problems of the absolute intensity and ratio of the D-lines in twilight, at a particular angle of solar depression, are of fundamental importance in ascertaining the Na abundance. Hence in this paper the effect of hyperfine structure on the deduced abundance is examined in more detail. The calculations are then applied to observations made in Saskatoon.

---

* Participants included J. E. Blamont, J. Hirschberg, J. E. Mack, D. P. McNutt, University of Wisconsin; T. M. Donahue, University of Pittsburgh; D. M. Hunten, University of Saskatchewan; L. R. Megill, F. E. Roach, Boulder Laboratories of the National Bureau of Standards; J. W. Chamberlain, C. Y. Fan, A. Omholt, Yerkes Observatory.

VOL. 12 1958

2. Hyperfine Structure and Broadening of the *D*-Lines

The ground level of neutral sodium, $3s\ ^2S_{1/2}$, consists of two hyperfine-structure components at $-36{\cdot}9341$ mK ($F = 1$), $+22{\cdot}1604$ mK ($F = 2$) relative to the centroid (Kusch and Taub, 1949). Here the unit is the millikayser (mK), or 10^{-3} cm^{-1}, and the plus sign denotes a positive increment in total energy. The $3p\ ^2P_{1/2}$ level has two components at $-4{\cdot}0$ mK ($F = 1$), $+2{\cdot}4$ mK ($F = 2$) (Jackson and Kuhn, 1938) and the $3p\ ^2P_{3/2}$ level, four components at approximately $-2{\cdot}43$ mK ($F = 0$), $-1{\cdot}76$ mK ($F = 1$), $-0{\cdot}54$ mK ($F = 2$), and $+1{\cdot}49$ mK ($F = 3$) (Sagalyn, 1954).

The corresponding line structure is shown in Fig. 1. The main body of the figure shows the influence of temperature upon the shapes of the components, with the neighbourhoods of the minima plotted at intervals of 20 deg., in the

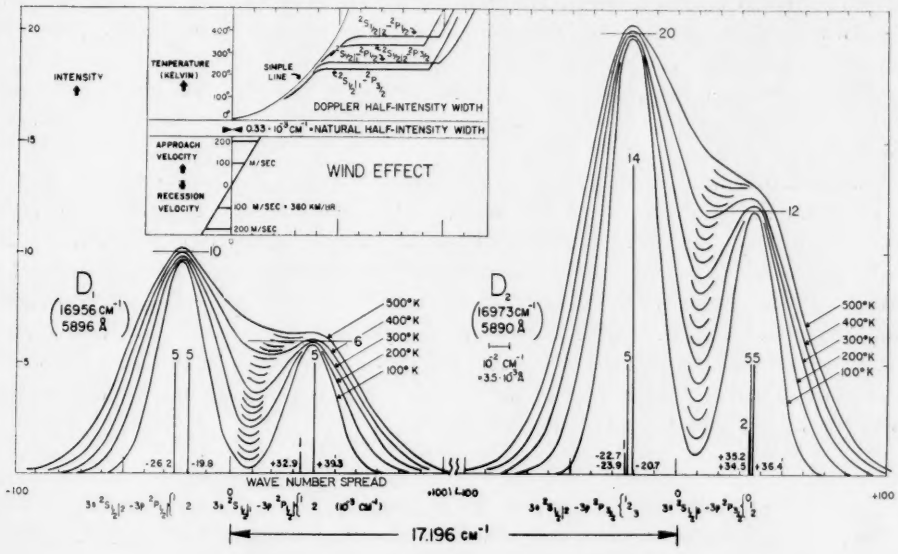

Fig. 1. Line profiles for D_1- and D_2-emission at various temperatures. The inserts show the Doppler half-intensity widths, the natural half-intensity width, and the broadening due to winds. See Section 2 of text for discussion.

region 100–500°K. Each of the ten simple line components is shown as a vertical line with a length proportional to the intensity of the component; this array shows how the lines would appear at 0°K. The intensity scale for each temperature is chosen so that the peak of the Gaussian for each component coincides with the top of the vertical line. For any temperature greater than about 5·7°K, blending occurs; then each of the two complexes, D_1 and D_2, has not more than two peaks. Hereafter in this paper the term *component* will be used to denote the blend of two (for D_1) or three (for D_2) simple Gaussian distributions contributing to one of these peaks. For upper-atmosphere studies each of these blended components may be treated approximately as a Gaussian (cf. Section 3), although Fig. 1 was calculated without any such approximation. The complex D_1 loses

its minimum at about 460°K and D_2 at about 510°K, but the assymmetry remains marked to a somewhat higher temperature. At much higher temperatures, D_1 and D_2 approach single Gaussians with peak intensities of 16 and 32, respectively, each centred about the zero shown for its wave-number scale.

The upper part of the insert in Fig. 1 shows the half-intensity width of an ideal simple line and of each of the four components as functions of temperature. At low temperatures the components exhibit half-intensity widths characteristic of single lines at slightly greater temperatures (cf. Appendix). But in the upper part of the temperature range that is interesting in upper-atmosphere studies, the concept of half-intensity width becomes almost useless as the minimum between the two components reaches half the height of the peak in question.

The middle of the insert gives an idea of the magnitude of the natural half-intensity breadth arising from the limited lifetime of the upper states. This breadth is seen to be negligible compared with that arising from the temperature. Zeeman and Stark broadening in the upper atmosphere are likewise negligible. A magnetic field of several oersteds or an electric field of several thousand V/cm would be required to contribute separation or displacement as great as the natural breadth.

On the other hand, the effect of winds cannot be neglected, as the lower part of the insert in Fig. 1 shows. A radial wind component of 100 m sec^{-1} changes the wave number by 5·66 mK. Huxley (1957) has found over Adelaide (latitude 35° south) prevailing winds from the west up to about 65 m sec^{-1}, at about 80 km altitude in the Australian winter and at 100 km in the summer, and periodic components of the same order of magnitude. While pure translation would only shift the line pattern, turbulence with velocity differences of 100 m sec^{-1} could contribute as much width to the line components as a temperature increase of about 60 deg. at 200°K or 100 deg. at 300°K.

VOL. 12 1958

3. Total Intensity and Ratio of the *D*-lines

It is evident from Fig. 1 that for temperatures in the neighbourhood of 200°K, we may regard each of the *D*-lines as composed of two *components*, with absorption coefficients at the centers of these components in the ratio of about 5/3. Also each of these components may be represented approximately by a Doppler profile characteristic of some effective temperature, T_e. In the Appendix we derive an expression for the effective temperature of a component (composed of two *close* fine-structure lines) in terms of the kinetic temperature. In Table 1 are presented the values of the effective temperatures for a kinetic temperature of 220°K, with no broadening from turbulent winds.

The effective values of α_0, the absorption coefficients at the centre of the various components, were obtained by imposing the condition

$$\int_0^\infty \alpha_\nu \, d_\nu = \alpha_0 \frac{U\nu_0}{c} \int_{-\infty}^{\infty} \exp(-x^2)\, dx = \frac{\pi e^2}{mc} f \tag{1}$$

where

$$x = \frac{c(\nu - \nu_0)}{\nu_0 U} \tag{2}$$

and $U = (2\,kT/M)^{1/2}$. Hence the effective α_0 varies at $T_e^{-1/2}$.

Table 1. Components of the D-lines for $T = 220°\text{K}$

Component	D_{1a}	D_{1b}	D_{2a}	D_{2b}
Transitions $(3s\ ^2S)\,J \mid F -$ $(3p\ ^2P)\,J \mid F$	$\frac{1}{2} \mid 2 - \frac{1}{2} \mid 2$ $\frac{1}{2} \mid 2 - \frac{1}{2} \mid 1$	$\frac{1}{2} \mid 1 - \frac{1}{2} \mid 2$ $\frac{1}{2} \mid 1 - \frac{1}{2} \mid 1$	$\frac{1}{2} \mid 2 - \frac{3}{2} \mid 3$ $\frac{1}{2} \mid 2 - \frac{3}{2} \mid 2$ $\frac{1}{2} \mid 2 - \frac{3}{2} \mid 1$	$\frac{1}{2} \mid 1 - \frac{3}{2} \mid 2$ $\frac{1}{2} \mid 1 - \frac{3}{2} \mid 1$ $\frac{1}{2} \mid 1 - \frac{3}{2} \mid 0$
T_e (°K)	235	228	221	221
α_0 (10^{-12} cm^2)	4·35	2·65	8·97	5·37

In Part I, equation (11), we obtained an expression for the integrated intensity of a single line that is scattered in twilight. This equation may be written

$$\mu 4\pi \mathscr{I}(\tau_0, +\mu) = r\pi F_c \frac{\mu\mu_0}{\mu + \mu_0} \cdot \frac{U\nu_0}{c} \int_{-\infty}^{\infty} \Phi\,(\tau_0, x)\, dx, \tag{3}$$

where $\mu_0 = \sin\beta$, $\mu = \cos\theta$, θ is the angle of emergence of the observed emission from the sodium layer, πF_c is the solar photon flux per unit frequency interval in the continuum at the earth, and r is the residual intensity (relative to the continuum) at the centre of the Fraunhofer Na line. Also in equation (3),

$$\Phi(\tau_0, x) = \exp\left(\frac{-\tau_0 e^{-x^2}}{\mu_0}\right)\Big[X^*(\mu)X^*(\mu_0) - Y^*(\mu)Y^*(\mu_0)\Big]. \tag{4}$$

The X^*- and Y^*-functions in equation (4) are functions of $\tau_\nu = \tau_0 \exp(-x^2)$. CHANDRASEKHAR and ELBERT (1952) tabulate these functions vs. τ_ν and μ.

For any adopted set of parameters μ, μ_0, and τ_0, the functions Φ in equation (4) may be computed for any value of x. The integral in equation (3), and the integrated intensity $\mathscr{I}$, may then be evaluated numerically by SIMPSON's rule. By changing τ_0 and repeating the calculations, we derive a complete curve for a particular μ and μ_0.

In Fig. 2 we present the computations of $\mu 4\pi\mathscr{I}$ vs. τ_0 for $\beta = 6{\cdot}5°$, $T = 200°\text{K}$, and $r_1 = 0{\cdot}0590$ (for the Fraunhofer D_1-line). As in Part I, we adopt the value $F_c = 205$ quanta/cm^2 sec sec^{-1}. To derive the intensity for a line with an effective temperature T_e, but with the same τ_0, the values read from Fig. 2 should be multiplied by $(T_e/200)^{1/2}$. For a line excited by the Fraunhofer D_2 residual intensity, the values from the figure should be multiplied by $r_2/r_1 = 0{\cdot}0506/0{\cdot}0590 = 0{\cdot}858$. These residual intensities, taken from the recent work of SCRIMGER and HUNTEN (1957), are slightly different from the values adopted in Part I.

They should be very suitable for twilight calculation, since they were measured by a method which very nearly duplicates in the laboratory the natural scattering by atmospheric sodium. Thus, the hyperfine components and the details of the

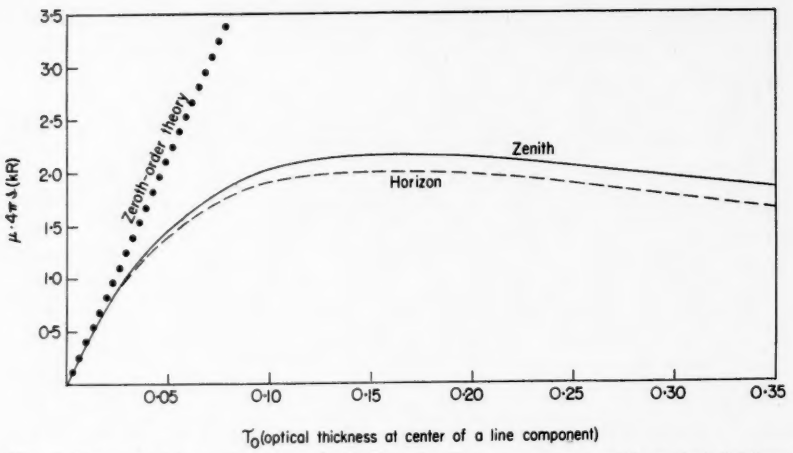

Fig. 2 Integrated intensity for a single Doppler line-component, with optical thickness τ_0 at the centre of the component. Excitation is by the residual intensity in the Fraunhofer D_1-line for $T = 200°$K and $\beta = 6{\cdot}5°$. See Section 3 of text for discussion.

structure of the Fraunhofer lines are automatically taken into account. However, the probable error in the measurement of r_2/r_1 is estimated to be 10 per cent. Hence it should be borne in mind that sodium abundances obtained from D_2/D_1 intensity ratios are uncertain to that extent.

The straight line in Fig. 2 is given by

$$\mu 4\pi \mathscr{J}^{(0,0)} = r_1 \pi F_c \frac{\sqrt{\pi} U \nu_0}{c} \tau_0 = 43{\cdot}3\tau_0 \,, \tag{5}$$

Table 2. Intensity tables, single Doppler component*
($\mu \,.\, 4\pi\mathscr{J}$ in kilorayleighs)

Zenith ($\mu = 1{\cdot}0$)

τ_0/μ_0	0·04	0·08	0·12	0·16	0·32
0·04	0·701	0·694	0·612	0·549	0·447
0·06	0·940	1·110	1·062	0·979	0·765
0·08	1·099	1·447	1·499	1·442	1·147
0·10	1·210	1·722	1·887	1·893	1·589
0·12	1·293	1·944	2·226	2·314	2·071
0·15	1·383	2·202	2·649	2·869	2·821

Horizon ($\mu = 0{\cdot}3$)

τ_0/μ_0	0·04	0·08	0·12	0·16	0·32
0·04	0·685	0·671	0·591	0·530	0·433
0·06	0·916	1·061	1·010	0·928	0·725
0·08	1·068	1·381	1·411	1·349	1·069
0·10	1·175	1·636	1·765	1·753	1·452
0·12	1·255	1·843	2·073	2·127	1·862
0·15	1·341	2·083	2·456	2·618	2·487

* Computed from equation (3) for $T = 200°$K and $r_1 = 0{\cdot}0590$.

VOL. 12 1958

where the numerical value applies to $T = 200°\text{K}$ and $4\pi\mathscr{I}$ is in kilorayleighs. Clearly, for a given value of N, the total intensity does not depend on T in this approximation, as τ_0 varies as $T^{1/2}$. In the figure we plot $\mu \cdot 4\pi\mathscr{I}$, which is not very sensitive to μ. Two curves are given: One computed for $\mu = 1$ (applicable near the zenith) and the other for $\mu = 0{\cdot}3$ (applicable for observations near the horizon).

Table 2 presents the numerical results of similar calculations for a variety of combinations of μ, μ_0 and τ_0. To obtain final values that are accurate to three

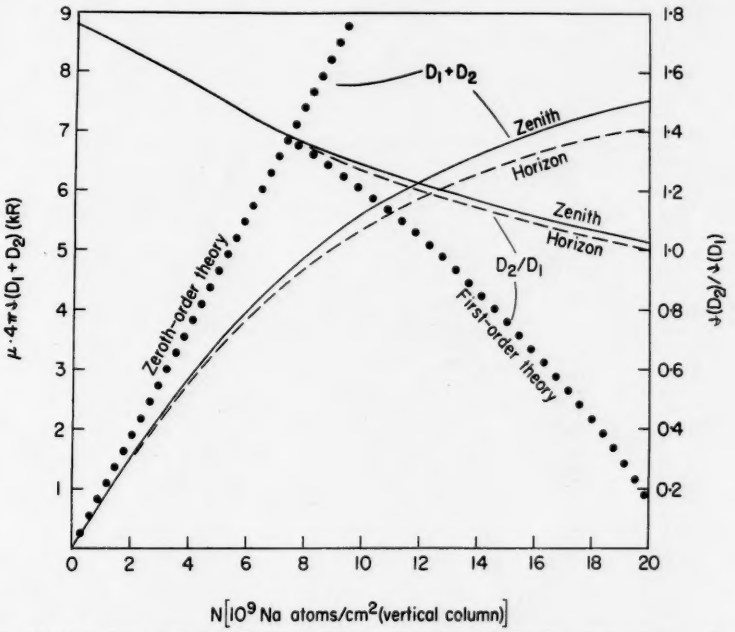

Fig. 3. Absolute intensity and D_2/D_1 ratio as a function of Na abundance for a solar depression of $\beta = 6{\cdot}5°$ (measured at the observed point) and a kinetic temperature of 220°K in the scattering layer. The $D_1 + D_2$ ordinate gives intensities "reduced to the zenith". Solid curves should be used for observations near the zenith; dashed curves near the horizon. The dotted curve gives the intensity without scattering in the first passage through the Na layer and without any secondary scatterings. Similar curves for other angles β may be readily computed from the data in Table 2, as these curves have been obtained from those in Fig. 2.

significant figures it was necessary to compute a number of X^*- and Y^*-functions (for $\tau_\nu < 0{\cdot}05$) in addition to those given by CHANDRASEKHAR and ELBERT. These calculations were carried out by Mr. JOHN C. BRANDT and will soon be published in Part V.

Fig. 3 gives the predicted total intensities and D_2/D_1 ratio as a function of Na abundance. These curves follow directly from those in Fig. 2 (or the values in Table 2) combined with the data in Table 1. In Fig. 3 the straight, broken line (total intensity for no secondary scattering) is computed from equation (I.7), slightly modified for the new values of r_1 and r_2. The revised equation is

$$\mu 4\pi\mathscr{I}^{(0,0)}\,(D_1 + D_2) = 0{\cdot}888 \times 10^{-9}N, \tag{6}$$

with $4\pi\mathscr{I}^{(0,0)}$ expressed in kR.

The other broken line in Fig. 3 gives the ratio from an approximate computation that is valid for small abundances. Such an asymptotic relation is useful for small N, as the *relative* errors in the intensities computed from the X- and Y-functions are greater at small τ, where the errors in the D_2/D_1 ratios therefore become appreciable. With an effective optical thickness (HUNTEN 1956c, Part III) of $\tau_{\text{eff}} = \tau_0/\sqrt{2}$, equations (I.3) and (I.4) lead to a ratio for small τ_0 of

$$\frac{\mathscr{I}(D_2)}{\mathscr{I}(D_1)} = \frac{r_2\{\alpha_0(D_{2a})[1 - \tau_0(D_{2a})/\sqrt{2}\mu_0] + \alpha_0(D_{2b})[1 - \tau_0(D_{2b})/\sqrt{2}\mu_0]\}}{r_1\{\alpha_0(D_{1a})[1 - \tau_0(D_{1a})/\sqrt{2}\mu_0] + \alpha_0(D_{1b})[1 - \tau_0(D_{1b})/\sqrt{2}\mu_0]\}} \tag{7}$$

In equation (7), $\tau_0 = N\alpha_0$ and the various values of α_0 are found in Table 1.

4. THE Na ABUNDANCE AND SEASONAL VARIATION

Although a good many measurements of intensities and intensity ratios in twilight have been made in the past, lack of a reliable theory has prevented their confident interpretation in terms of abundances. Since we feel that this deficiency

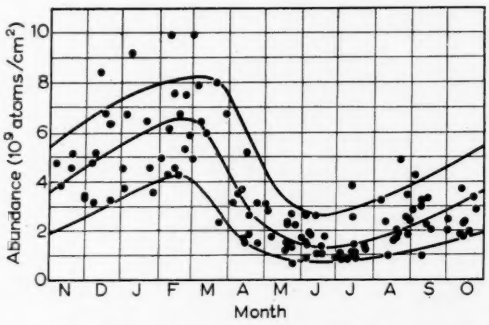

Fig. 4. Abundances derived from the measurements of HUNTEN (1956a, and unpublished data). The "average" curve was derived by eye; the "extreme" curves include nearly all, but not all, the points.

has now been remedied, we proceed to derive abundances from published results and to discuss briefly a few more recent measurements that have not previously been published. It would obviously be valuable to make simultaneous measurements of both the intensity and the ratio; although a few attempts at this have been made, no good results are yet available. Day-time observations of the absorption of sunlight by atmospheric sodium give an abundance that does not depend on the radiative-transfer theory and thus provide a useful check. All the methods are in substantial agreement.

Absolute intensity. An approximate measurement of the total $D_1 + D_2$ intensity was made by BRICARD and KASTLER (1944); their result is equivalent to $\mu 4\pi\mathscr{I} = 7{\cdot}2$ kR. The abundance of nearly 20×10^9 atoms/cm^2 is considerably larger than any in Fig. 4, but it is satisfactory as an estimate. A series of measurements covering several years was reported by HUNTEN (1956a); the corresponding abundances appear in Fig. 4, along with others based on more recent data. These data were obtained at an angle of solar depression of $\beta \approx 6°$ to $6\frac{1}{2}°$. No attempt

VOL. 12 1958

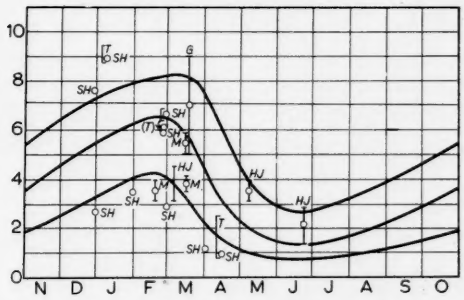

Fig. 5. Abundances derived from ratio measurements and from absorption. The three curves have been transferred from Fig. 4 for comparison. The initials *G*, *HJ*, and *M* may be interpreted with the help of Table 3. *SH* refers to the absorption measurements; and *T* bracketed with it represents a twilight intensity measurement made the same day.

has been made to distinguish the points belonging to different years, but there are some differences in the months from June to September: Nearly all these results from 1953 and 1954 fall below the "average" line, and nearly all the more recent ones fall above. Winter and spring results, although widely scattered, show no such tendency. The three curves were sketched by eye; it should be noted that the "maximum" and "minimum" curves do not include all the points, but only the general mass. The "average" curve varies between $6{\cdot}5 \times 10^9$ atoms/cm^2 at the end of February and $1{\cdot}3 \times 10^9$ near the end of June, a range of 5–1. The extremes of the curves are in the ratio 10–1, and the extreme points about 12–1. The seasonal variation is undoubtedly associated with a latitude variation, and there is little point in trying to explain it until absolute measurements have been made at other latitudes.

Intensity ratio. Several workers have recently measured the intensity ratio D_2/D_1; the results are summarized in Table 3 and Fig. 5. The three curves in Fig. 4 have been transferred to Fig. 5 to aid in the comparison. It must be emphasized again that the lines do not include all the points. Although the measurements were made at three different places (Moscow, Churchill, and Saskatoon), the range of latitude is only about 8°, so that the various observations

Table 3. Available measurements of the intensity ratio, with abundances derived from Fig. 3

Reference	Dates	Ratio	Abundance (10^9 atoms/cm^2)
Galperin (1956a, b)	Mar. 15–18	$1{\cdot}30 \pm 0{\cdot}04$	$7{\cdot}0 \pm 2{\cdot}0$
Harrison and Vallance Jones (1956)	Mar. 4–15	$1{\cdot}45 \pm 0{\cdot}05$	$3{\cdot}8 \pm 0{\cdot}7$
	May 1–9	$1{\cdot}47 \pm 0{\cdot}03$	$3{\cdot}5 \pm 0{\cdot}4$
	June 27–30	$1{\cdot}57 \pm 0{\cdot}05$	$2{\cdot}1 \pm 0{\cdot}7$
Montalbetti (1957)	Feb. 1956	$1{\cdot}49 \pm 0{\cdot}02$	$3{\cdot}4 \pm 0{\cdot}3$
	Mar. 1956	$1{\cdot}37 \pm 0{\cdot}02$	$5{\cdot}4 \pm 0{\cdot}4$
	Mar. 1957	$1{\cdot}46 \pm 0{\cdot}02$	$3{\cdot}8 \pm 0{\cdot}3$

should be comparable. Galperin's (1956a,b) result does not appear to have been corrected for the presence of the Fraunhofer lines in the white light, which appears to some extent as a background on the spectrum plate, but this correction probably has only a slight effect. The zenith angle of observation was 65°, rather than the 75° used in the calculations, so that a small interpolation on Fig. 3 was necessary. The result falls just in the region where the small slope of the curve exaggerates the error the most, but in any case large probable errors are to be expected in this method because of the great experimental difficulties. (It is certainly not claimed that the intensity measurements are free of appreciable errors, but there is no way of estimating them; a figure of ± 10 per cent may be reasonable.)

The observations of Harrison and Vallance Jones (1956) were made by following the shadow line over a large range of zenith angles. Therefore, an average of the theoretical zenith and horizon curves has been used to derive abundances. Agreement with the results from the absolute intensity is generally very good, although the March result is a little lower than expected. The programme has been continued by Vallance Jones and McPherson (1957); as reported by them, excellent agreement is found. A large number of photoelectric measurements in the zenith have been made at Churchill, Canada, by Montalbetti (1957). Only preliminary results are available; each of the numbers given is an average for several nights. Again, substantial agreement with abundances from Fig. 4 is obtained, although the value for February is slightly low. It may be concluded that the ratio and intensity measurements agree as well as can be expected. A much better comparison could be made if simultaneous measurements of both were available.

Terrestrial absorption. A series of abundance measurements by an entirely different method have been reported by Scrimger and Hunten (1957). Here the absorption of sunlight by the sodium is observed directly during the day. The results are shown in Fig. 5 along with three found in twilight on the same days. The agreement is excellent; it should be noted that the absorption measurements for April were very inaccurate. The probable errors could not be shown in the figure without confusing it. The agreement of the absorption and twilight measurements not only demonstrate a consistency in the observations, but suggest, indeed, that the theoretical basis for the abundance determinations is correct.

5. Summary

We have assumed throughout that the mechanism responsible for exciting the *D*-lines in twilight is resonance scattering. In the past there has been some dispute on this matter, with some investigators favouring dissociation of a sodium compound by ultra-violet light.

The investigations of Bricard and Kastler (1944, 1950), however, established resonance scattering as the most likely mechanism: They showed that zenith-horizon comparisons, when properly interpreted, indicated a screening height too low to be applicable to ultra-violet light. This result has been verified at Saskatoon (Hunten, 1954; Hunten and Shepherd, 1954). Also, Bricard and Kastler found a small polarization in the *D*-lines, which would be expected for resonance scattering but not for dissociation.

VOL. 12 1958

In this paper we have extended calculations made in Part I. The results in Table 2 should be accurate to within a few units in the third significant figure, for a single, Doppler-broadened line in an atmosphere composed of two plane-parallel sections, adjusted to approximate a spherical atmosphere, as sketched in Fig. 1 of Part I. The main errors in the theoretical values will lie in departures in the real atmosphere from this model and in departures of the *D*-lines from a representation in terms of superimposed Doppler profiles for effective temperatures.

The corrections for ground albedo in Table 1 of Part I were derived with an approximate formulation (HUNTEN, 1956c, Part III). To this accuracy, the corrections in that table may be applied to the individual line components to which the present Fig. 2 and Table 2 apply.

It is comforting that the abundances derived here from the three different types of observation are in such good agreement. In fact, this agreement may be considered as still further evidence that resonance scattering is the excitation mechanism. It is most unlikely that such consistency could be obtained from three completely different observational techniques were the theory based on an utterly false premise.

With the practicability of ascertaining sodium abundances rather accurately, two problems present themselves for further study. Firstly, there is the long-standing problem of the origin of atmospheric sodium: Does it arise from the sea or extraterrestrial space? Continued observations may disclose small abundance changes at the passage of meteor streams, if the sodium enters through meteoritic bombardment.

L.
2
58

At present, however, there is no compelling reason to invoke extraterrestrial sources to explain the abundance. MOYERMAN and SHULER (1953) find that inland air contains on the average about $1{\cdot}15 \times 10^{11}$ atoms of sodium/cm^3, mostly in the form NaCl. Thus approximately one atom in 5×10^8 is sodium at sea-level. In the free sodium layer the density of Na probably does not exceed 10^4 atoms/cm^3, or one atom in 10^{10}. There is reason to believe that there is little "hidden" sodium in chemical combination above the height of the maximum concentration of Na, but it is likely that a considerable amount of sodium is ionized at these altitudes. Nevertheless, the relative abundance of sodium (in all forms) may fall by a factor of 10 or 20 between sea-level and the sodium layer. Small particles of salt will have a smaller scale height than the atmospheric gases, but it is still not unreasonable that enough sodium would be transported to 85 km to provide the observed Na.

The second major problem is the seasonal variation of Na. Several discussions of the photochemistry and ionization equilibrium of sodium have appeared in recent years. We may simply state here that the great amplitude of the seasonal variation, as demonstrated with some confidence in this paper, seems to defy all explanation in terms of a transformation of Na into ions or molecular compounds in a static atmosphere. Perhaps further consideration should be given to dynamic effects in the atmosphere, consisting of either vertical transport or exchange of air between different latitudes (HUNTEN, 1956a). If these motions are important, sodium may be an almost ideal tracer with which to study them.

Acknowledgements—Thanks are due Mr. JOHN C. BRANDT at Yerkes Observatory for assistance with numerical calculations.

APPENDIX

Effective Doppler profile for two close lines

If the separation of two lines is $\Delta\nu$, we define $d = c\Delta\nu/\nu_0 U$, where ν_0 is the frequency of the centroid of the two lines. If α_1 and α_2 are the values of the absorption coefficient at the centre of these lines, then the distances, in these dimensionless units, of the line centres from the centroid are $d_1 = d\alpha_2/(\alpha_1 + \alpha_2)$ and $d_2 = d\alpha_1/(\alpha_1 + \alpha_2)$.

The absorption coefficient for the combined lines is

$$\alpha_\nu = \alpha_1 \exp\left[-(x - d_1)^2\right] + \alpha_2 \exp\left[-(x + d_2)^2\right], \tag{A.1}$$

where x is given by equation (2). For $d^2 \ll 1$, we have $\exp(-d_1^2) \ll \exp(-d_2^2) \approx 1$, and expanding the terms linear in d_1 and d_2 in power series, we find

$$\alpha_\nu \approx (\alpha_1 + \alpha_2) \exp(-x^2)\left[1 + 2\alpha_1\alpha_2\left(\frac{xd}{\alpha_1 + \alpha_2}\right)^2 + \ldots.\right]. \tag{A.2}$$

Again, for $d^2 \ll 1$, the term in square brackets can be closely represented by an exponential, so that

$$\alpha_\nu \approx (\alpha_1 + \alpha_2) \exp\left\{-x^2\left[1 - 2\alpha_1\alpha_2\left(\frac{d}{\alpha_1 + \alpha_2}\right)^2\right]\right\} \tag{A.3}$$

This equation is in the form $\alpha_\nu = \alpha_e \exp(-x_e^2)$, where α_e and x_e are *effective* values for the combined lines. Let x_e define an effective temperature T_e. Then

$$\frac{x^2}{x_e^2} = \frac{T_e}{T} \approx 1 + 2\alpha_1\alpha_2\left(\frac{d}{\alpha_1 + \alpha_2}\right)^2 \tag{A.4}$$

Equation (A.4) was used to compute T_e in Table 1. However, α_e was not taken simply as $\alpha_1 + \alpha_2$; but by imposing equation (1), which allows for the fact that as the combined *component* becomes broader (or the separate lines more widely spaced) the absorption coefficient at the centre decreases. This effect is not allowed for in the approximation used here.

REFERENCES

BRICARD J. and KASTLER A.	1944	*Ann. Géophys.* **1,** 53.
	1950	*Ann. Géophys.* **6,** 286.
CHAMBERLAIN J. W.	1956	*J. Atmosph. Terr. Phys.* **9,** 73 (Part I).
CHAMBERLAIN J. W. and NEGAARD B. J.	1956	*J. Atmosph. Terr. Phys.* **9,** 169 (Part II).
CHANDRASEKHAR S. and ELBERT D.	1952	*Astrophys. J.* **115,** 269.
DONAHUE T. M. and RESNICK R.	1955	*Phys. Rev.* **98,** 1622.
GALPERIN G. I.	1956a	*Astron. Zh.* **33,** 173.
	1956b	*The Airglow and Aurorae.* (Edited by ARMSTRONG E. B. and DALGARNO A.) p. 91. Pergamon Press, London.
HARRISON A. W. and VALLANCE JONES A.	1956	*The Airglow and Aurorae.* (Edited by ARMSTRONG E. B. and DALGARNO A.) p. 95. Pergamon Press, London.

VOL. 12 1958

HUNTEN D. M.	1954	*J. Atmosph. Terr. Phys.* **5,** 44.
	1956a	*The Airglow and Aurorae.* (Edited by ARMSTRONG E. B. and DALGARNO A.) p. 114. Pergamon Press, London.
	1956b	*The Airglow and Aurorae.* (Edited by ARMSTRONG E. B. and DALGARNO A.) p. 183. Pergamon Press, London.
	1956c	*J. Atmosph. Terr. Phys.* **9,** 179 (Part III).
HUNTEN D. M., ROACH F. E. and CHAMBERLAIN J. W.	1956	*J. Atmosph. Terr. Phys.* **8,** 345.
HUNTEN D. M. and SHEPHERD G. G.	1956	*J. Atmosph. Terr. Phys.* **5,** 57.
HUXLEY L. G. H.	1957	*Aus. J. Phys.* In press.
JACKSON D. A. and KUHN H.	1938	*Proc. Roy. Soc.* A **167,** 205.
KUSCH P. and TAUB H.	1949	*Phys. Rev.* **75,** 1477.
MONTALBETTI R.	1957	Private communication.
MOYERMAN R. M. and SHULER K. E.	1953	*Science* **118,** 612.
SAGALYN P. L.	1954	*Phys. Rev.* **94,** 885.
SCRIMGER J. A. and HUNTEN D. M.	1957	*Canad. J. Phys.* **35,** 918.
VALLANCE JONES A. and MCPHERSON D. H.	1957	*J. Atmosph. Terr. Phys.* **13,** 178.

L.
2
58

Journal of Atmospheric and Terrestrial Physics, 1958, Vol. 12, pp. 166 to 170. Pergamon Press Ltd., London

The seasonal variation of the intensity ratio of the *D*-lines in twilight*

A. Vallance Jones and D. H. McPherson
University of Saskatchewan, Saskatoon, Sask.

(*Received* 20 *September* 1957)

Abstract—The intensity ratio of the sodium *D*-lines in twilight has been measured over the period from May 1955 to July 1956 from photographic spectra obtained with an auroral spectrograph having a dispersion of 30 Å/mm. Significant variations of the D_2/D_1 line ratio were found, ranging from a mean value of 1·40 ± 0·08 for the period from December to February to a value of 1·67 ± 0·20 for the period from May to June. The abundances of sodium calculated from these ratios are in agreement with abundances calculated from the absolute brightness and the direct absorption methods. The measurements are in good agreement with the theoretical calculations of Chamberlain, Hunten and Mack (1957).

1. Introduction

It has been shown by Hunten (1956) and Chamberlain (1956) that the intensity ratio of the sodium *D*-lines of the twilight airglow is a sensitive indicator of the abundance of sodium in the upper atmosphere for abundances between 2×10^9 atoms/cm^2 (column) and 10×10^9 atoms/cm^2 (column). Recently a more refined analysis of this dependence has been made by Chamberlain, Hunten and Mack (1957). The results of a series of measurements of the ratio have been published by Harrison and Vallance Jones (1956). These results gave an indication of seasonal increase in the ratio from March to June. In an attempt to confirm this seasonal variation, a longer series of measurements has been made with a spectrograph of higher dispersion. Measurements were made also of the ratio for the *D*-lines of the night airglow, partly to obtain further data on this quantity and partly as a check on the experimental method.

2. Experimental

A 9 in. *f*/0·8 Schmidt spectrograph with a linear dispersion of 30 Å/mm was employed. The width of the geometrical image of the slit at the plate corresponded to 0·98 Å. The linear dispersion of this spectrograph was about twice as great as that of the instrument used by Harrison and Vallance Jones (1956). Kodak 103a-D spectroscopic plates were used.

The twilight exposures were programmed, as described in the previous paper, in such a way that the line of sight of the spectrograph intersected the geometrical shadow line of the earth at a height of 65 km. No correction was made for atmospheric refraction. The duration of the exposures varied from 22 to 330 min.

The photometric procedure employed was the second of the two methods described by Harrison and Vallance Jones. The larger plates ($1\frac{1}{4}$ in. × $2\frac{1}{2}$ in.) of the 9 in. spectrograph made it possible to place the step-sector intensity calibration and the twilight exposure well away from the edges of the plate where development is sometimes uneven. The calibration exposure was lengthened to

* The research reported in this paper has been sponsored by the Geophysics Research Directorate of the Air Force Cambridge Research Center, Air Research and Development Command under Contract AF 19(604)–1831.

VOL. 12 1958

30 min to make it comparable with the twilight exposure and so free the calibration from errors due to reciprocity failure. A sodium lamp was used as the calibrating source. As a result of these improvements in the procedure, systematic errors should be reduced to a minimum.

A Jarell-Ash Model JA203 microphotometer was used in the measurement of the plate densities. The equivalent slit width of the microphotometer was 0·05 Å;

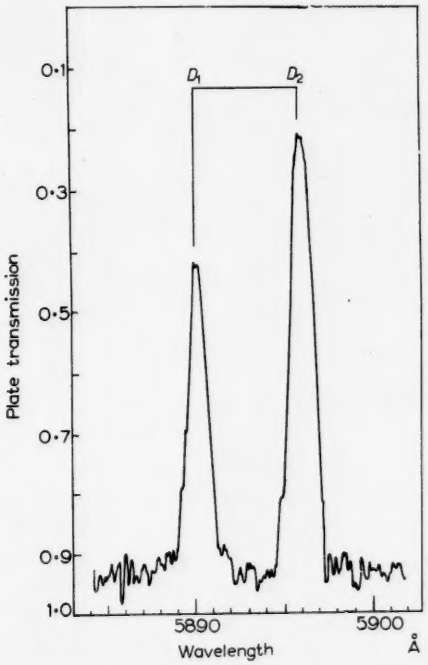

Fig. 1. Microphotometer tracing of twilight Na lines for 1 July and 2 July 1956. The ordinate is transmission expressed as a percentage of clear plate transmission.

consequently, it was considerably narrower than the spectral slit width of the spectrograph. A typical microphotometer tracing is shown in Fig. 1. Four microphotometer tracings were made across different segments of the lines on each plate; in this way an estimate could be made of the error of the mean intensity ratio for each plate. The deviations among these four tracings arose mostly from the graininess of the emulsion.

The night airglow measurements were made in the same way as the twilight measurements, except that the exposures were carried out at fixed zenith distances.

3. Results

The results of the measurements of the D_2/D_1 ratio are shown graphically in Fig. 2. The small solid circles on this graph give the mean D_2/D_1 ratio for individual plates; the length of the vertical line through each small circle represents twice the standard deviation of the D_2/D_1 ratios as determined from the different

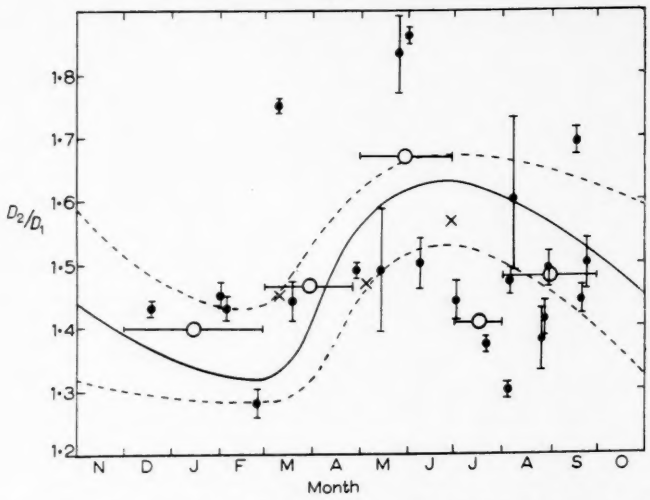

Fig. 2. Measured D_2/D_1 ratios for twilight airglow. ● Values from individual plates; ○ mean values for periods indicated by horizontal lines; × mean values of HARRISON and VALLANCE JONES (1956).

segments of each plate. Only plates of density satisfactory for measurement were considered.

The results of the measurements for the night airglow are given in Table 1.

Table 1. D_2/D_1 intensity ratios for night airglow

Date	Zenith distance	Exposure time	Intensity ratio
	deg.	hr	
1955			
30 Nov.–6 Dec.	0°	9·5	2·02 ± 0·02
11 Dec.–17 Dec.	0°	8·5	1·85 ± 0·19
18 Dec.	0°	8·9	2·18 ± 0·18
1956			
30 Jan.–1 Feb.	0°	15	1·78 ± 0·23
1 Feb.–7 Feb.	0°	20	1·80 ± 0·26
8 Feb.–20 Feb.	75°	21	1·86 ± 0·22
25 Feb.–26 Feb.	45°	16	1·93 ± 0·44
Mean ratio			1·92 ± 0·11

VOL.
12
1958

The accuracy of the results from the individual plates must be considered carefully. For most plates, at least two entirely separate determinations of the D_2/D_1 ratio were made. The average differences between these duplicate determinations show that the accuracy of the results is not in general better than ± 7 per cent. This conclusion is confirmed by the deviations among the results for the determinations of D_2/D_1 for the night airglow (see Table 1).

4. Discussion of Results

The calculations of Chamberlain, Hunten and Mack (1957) provide a connexion between the abundance of sodium in the upper atmosphere and the twilight D_2/D_1 ratio. Measurements of the seasonal variation of the brightness of the sodium emission interpreted according to this theory provide very good evidence for a seasonal variation in the abundance of sodium. There should consequently be a corresponding seasonal variation in the D_2/D_1 ratio. Since the points in Fig. 2 show considerable scatter, mean values of the ratio were calculated

Table 2

Period	Observed mean ratio	Na abundance 10^9 atoms/cm^2 (column)	
		From D_2/D_1 ratio	From absolute brightness
August–September	1·48 ± 0·12	3·4 ± 1·8	2·5 ± 1·0
December–February	1·40 ± 0·08	5·0 ± 2·0	5·5 ± 2·3
May–June	1·67 ± 0·20	0·7 ± 1·0	1·8 ± 0·6
Mean for year	1·50 ± 0·10		

for the periods set out in Table 2. These were periods in which the greatest numbers of plates had been obtained in the shortest time and in which the absolute brightness of the Na emission is fairly constant. The precision indices in Tables 1 and 2 are standard deviations. These mean values are shown in Fig. 2 by the large circles; the horizontal lines through these circles indicate the period over which the mean was computed. Mean values are given on the graph also for the remaining periods of the year for which there are only two plates each. Student's t-test for small samples was applied to the above mean ratios to determine whether they were significantly different. On the basis of Fisher's 5 per cent level of significance, the difference between the December–February and May–June means is "significant" since the probability of this difference occurring by chance is less than 5 per cent (Kenney and Keeping, 1951); on the other hand, the probability for the chance occurrence of the difference between the August–September and May–June means is 10 per cent. Consequently, the latter difference is not "significant" in the above sense, although there is a strong indication that the difference is real.

The sodium abundances were obtained from the mean D_2/D_1 ratios by means of the theoretical curves of CHAMBERLAIN, HUNTEN and MACK; the values obtained are tabulated in the third column of Table 2. Values of the mean sodium abundances for the same periods obtained from the measurements of absolute brightness are given in the fourth column of Table 2. The figures given in Table 2 show that the sodium abundances calculated from the mean D_2/D_1 ratios are in very satisfactory agreement with the values obtained from absolute brightness measurements. On the other hand, the individual values of the D_2/D_1 ratios show greater fluctuations than would be expected on the basis of the observed fluctuations in absolute brightness. In Fig. 2 the solid curve drawn among the points corresponds to the seasonal variation of the D_2/D_1 ratio expected on the basis of the seasonal variation of the absolute brightness and the curves given by CHAMBERLAIN, HUNTEN and MACK. The broken lines give approximately the limits of the fluctuations in the ratio corresponding to the fluctuations in the absolute brightness for the period 1953–1956. It will be seen that some of the observed values of the ratio lie outside the expected limits; however, in view of the possibilities of errors as large as 7 per cent in the ratio measurement, these deviations cannot be considered serious. The values reported by HARRISON and VALLANCE JONES are plotted in Fig. 2; these values also follow the expected trend.

CONCLUSIONS

These measurements confirm the reality of the seasonal variation of the D_2/D_1 ratio. The mean values of this ratio provide a quantitative measure of the variation of the abundance of sodium in the upper atmosphere, and lead to results in agreement with the abundances measured by direct absorption (SCRIMGER and HUNTEN, 1957) and from absolute brightnesses. The measurements support the theory of CHAMBERLAIN, HUNTEN and MACK.

Acknowledgement—We should like to acknowledge the great value of discussions with Dr. D. M. HUNTEN.

REFERENCES

CHAMBERLAIN J. W.	1956	*J. Atmosph. Terr. Phys.* **9,** 73.
CHAMBERLAIN J. W., HUNTEN D. M., and MACK J. E.	1957	To be submitted to *J. Atmosph. Terr. Phys.*
HARRISON A. W. and VALLANCE JONES A.	1956	*The Airglow and the Aurorae* p. 95. Pergamon Press, London and New York.
HUNTEN D. M.	1956	*The Airglow and the Aurorae* p. 183. Pergamon Press, London and New York.
KENNEY J. F. and KEEPING E. S.	1951	*The Mathematics of Statistics* (2nd Ed.) p. 175. Van Nostrand, New York and London.
SCRIMGER J. A. and HUNTEN D. M.	1957	*Canad. J. Phys.* **35,** 918.

VOL. 12 1958

Journal of Atmospheric and Terrestrial Physics, 1958, Vol. 12, pp. 171 to 186. Pergamon Press Ltd., London

The height of nightglow 5577

F. E. Roach, L. R. Megill, M. H. Rees and E. Marovich
National Bureau of Standards, Boulder Laboratories

(*Received* 25 *October* 1957)

Abstract—An analysis is given of observations of nightglow 5577 during twelve nights at Fritz Peak, Colorado. A new photometer with a birefringent filter effectively eliminates light of astronomical origin. The heights deduced from the systematic increase of the nightglow intensity toward the horizon depend critically on the scattering and extinction of the lower atmosphere. It is found that, if a constant extinction coefficient is used in the reductions for all the nights, the spread in deduced heights is from 51 to 136 km with 100 km as the mean value. A more probable interpretation is that the actual height is 100 km and that the extinction coefficient varies from night to night. For an entire night of data the uncertainty in the extinction coefficient produces the largest error in the deduced height. On the other hand, at a given instant the spottiness of the sky is the predominant source of error.

1. Introduction

Recent night firings of rockets give evidence that 5577 nightglow originates in a region between 90 and 100 km above the earth's surface (Berg *et al.*, 1956; Koomen *et al.*, 1956; Heppner *et al.*, 1957). Estimates of height from the analysis of ground observations have, over the years, given widely divergent results, the principal reason being that the deduced height is extremely sensitive to a number of uncertainties that enter into the interpretation of the observations. These uncertainties are: (1) the contamination of the observations by light of astronomical origin, (2) the "spottiness" of the airglow over the sky as seen by an observer on the ground, (3) the extinction of the lower atmosphere and ozonosphere, and (4) the scattered light in the lower atmosphere. All are significant, but the most difficult to evaluate has been the first. The relative contributions of the airglow and the astronomical components vary systematically with zenith distance and sporadically with the positions of the Milky Way and Zodiacal Light. Approximate methods for eliminating the astronomical light have been utilized with only partial success (Roach and Meinel, 1955; Barbier *et al.*, 1957).

Recently we have put into operation at Fritz Peak, Colorado (latitude 39° 55′ N; longitude 105° 29′ W; elevation 9000 feet), a nightglow photometer which eliminates the photometric effect of the astronomical light. Although the other uncertainties remain in the analysis, it is a significant improvement to be rid of the one which has probably been the chief source of systematic error in the past determinations of nightglow heights.

During the last quarter of the calendar year 1956 we obtained observations of 5577 nightglow with this new photometer during twelve nights. In this paper we give the results of an analysis of these observations.

2. The Photometer

The basically new component of the photometer is a birefringent filter of the modified Lyot type designed by R. B. Dunn of the High Altitude Observatory (Sacramento Peak, New Mexico) of the Air Force Cambridge Research Center.

The prototype photometer using a filter of Dunn's design is described by Dunn and Manring (1955) and some results with the instrument at Sacramento Peak are given by Manring and Pettit (1955). Similar photometers have been used by Blamont and Kastler (1951) and Koomen *et al.* (1955).

The birefringent filter has the property that an emission line source appears at the output of a photomultiplier as an alternating current signal (80 c/s in our case), whereas a continuous light source yields a direct current signal. Thus the nightglow signal is alternating and the background (integrated star light and zodiacal light) is, to a high approximation, unmodulated.

The signal from the photomultiplier (Dumont 6291) is amplified by a conventional r.c. coupled amplifier whose frequency response cuts off rapidly above 100 c/s so that the dark current pulses from the photomultiplier are largely averaged out.

A phase-sensitive rectifier is used to discriminate against pick-up signals in the system, the phase signal being obtained from the same shaft as that rotating the polaroid in the birefringent filters.*

The linearity of the entire system is better than 1 per cent over a range of about twice that used in practice. The time constant of the system including the recorder is about 0·25 sec.

The photometer telescope is mounted on an alt-azimuth base. In the present study the sky is covered in a series of five almucantars (zenith distances 80, 75, 70, 60 and 40°) and the zenith. The sweep speed is 10°/sec, and about 3½ min are consumed in a single sky survey. A timer schedules a survey on each quarter hour.

VOL. 12 1958

3. The Observations

Table 1 shows a log of the nights included in this study. A portion of a record is shown in Fig. 2. The records are read at sixteen equally spaced azimuths starting at the north. The three digit readings are recorded on punched cards with the help of an oscillogram reader. One card includes the sixteen azimuth readings for a given almucantar plus the zenith, and the necessary identification information.† Five cards are sufficient for an entire sky survey (81 readings). The data for a night of fifty surveys are on 250 cards. In the present study there is a total of 536 sky surveys (43,416 readings on 2680 cards).

4. Determination of Height: Theory

If the nightglow is due to a uniformly bright emitting layer of constant thickness at a constant height, then, in the absence of a lower atmosphere, an observer on the surface of the earth will see an increase in brightness from the zenith toward the horizon according to equation (1):

$$V_z = \frac{I_z}{I_0} = \frac{1}{\sqrt{[1 - \{(R/(R+h)\}^2 \sin^2 z]}} \qquad (1)$$

* The reader should refer to the paper by Dunn and Manring (1955) for the details of the construction of the birefringent filter. In this paper we give only a general description.

† We have standardized a punched-card system of recording airglow data for the International Geophysical Year. Details are given in IGY operating bulletins.

L.
2
58

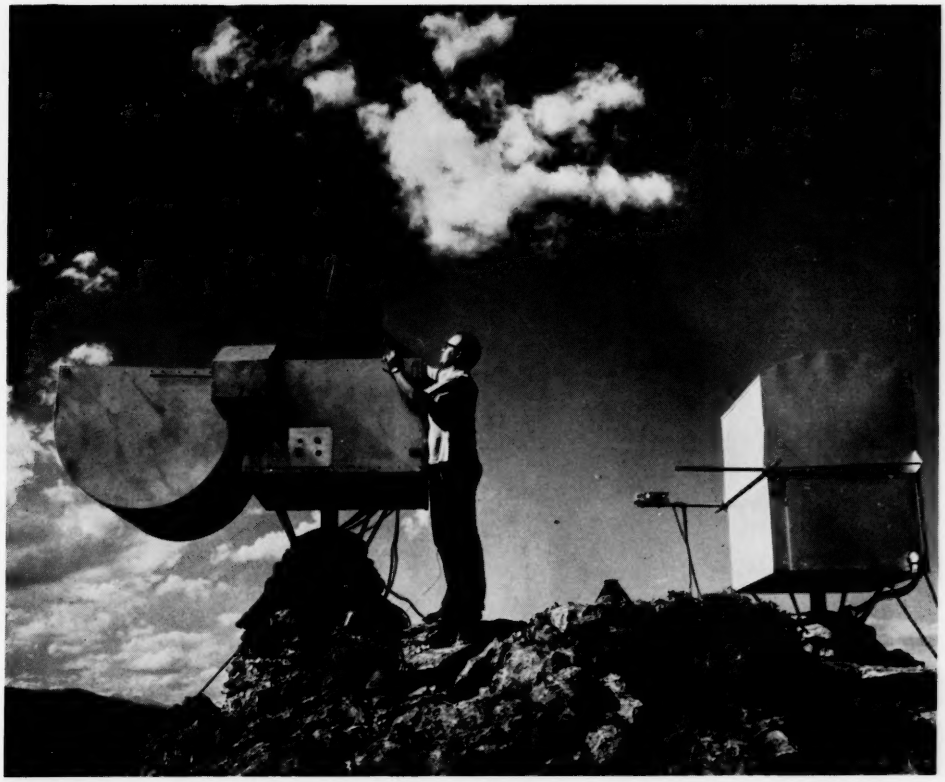

Fig. 1. Airglow photometer with birefringent filter at Fritz Peak.

VOL.
12
1958

Table 1. Log of observations

Night		Number of surveys	Observers*	Quality of sky
Number	Date (1956)			
1	1 and 2 October	41	Ro, C	Excellent
2	3 and 4 October	38	Ro, M	Excellent
3	6 and 7 October	41	C, H	Excellent
4	30 and 31 October	44	Me, Re	Good
5	29 and 30 November	47	Me, H	Excellent
6	30 November and 1 December	50	C, Me	Good
7	1 and 2 December	29	Re, H	Fair
8	3 and 4 December	51	Re, C	Excellent
9	8 and 9 December	45	Me, Re	Fair
10	28 and 29 December	50	Ro, Ro′, C	Good
11	29 and 30 December	51	Re, C	Excellent
12	31 December and 1 January	49	Re, M	Fair

*C = J. E. Cruz
H = H. H. Hardy
M = E. Marovich
Me = L. R. Megill
Re = M. H. Rees
Ro = F. E. Roach
Ro′ = Gerard Roach

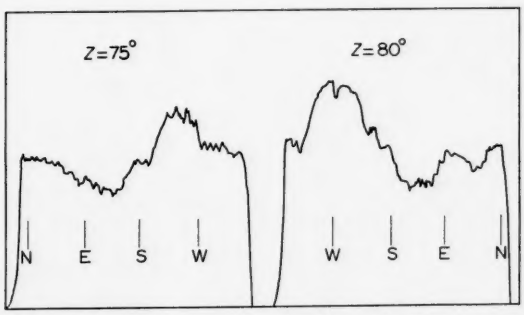

Fig. 2. Record made with photometer at Fritz Peak at 1800 M.S.T. on 28 December 1956.

where I_z and I_0 are brightness at zenith distances z and 0, R is the radius of the earth, and h is the height of the emitting layer (VAN RHIJN, 1924). If there were no lower atmosphere, it would be convenient to solve equation (1) for h, giving

$$h = R\left\{\frac{V_z \sin z}{\sqrt{(V_z^2 - 1)}} - 1\right\} \tag{2}$$

from which

$$\frac{\partial h}{\partial V_z} = -\frac{R \sin z}{(V_z^2 - 1)^{3/2}}. \tag{3}$$

Table 2

From equations (1) and (3)
For $h = 100$ km

Z	40	60	70	75	80
V_z	1·292	1·914	2·635	3·234	4·085
$-\partial h/\partial V_z$	7484	1269	413	212	92
Δh in km for 5% error in V_z	483	121	54	34	19
% Accuracy in V_z for $\Delta h = 10$ km	0·10	0·41	0·92	1·5	2·7

In Table 2 we show for $h = 100$ km, values of V_z and $\partial h/\partial V_z$ for the zenith distances included in the present study.

In Table 2 we also show some numerical quantities from equations (1) and (3) for a height of 100 km. It is seen that if there is an error of 5 per cent in V_{80} the resulting error in deduced height is 19 km (or 19 per cent). This sensitive dependence of the deduced height on the observed intensity ratio is a major reason for the wide divergence in the heights (based on the VAN RHIJN method) reported in the literature.

In this paper we shall adopt the procedure of correcting the direct observations to outside the lower atmosphere for deduction of heights from equations (1) or (2). The reverse procedure is frequently followed of referring the theory to inside the atmosphere. In either case it is necessary to correct for scattered light and extinction by the lower atmosphere.

For scattering we have used the tables given by ASHBURN (1954). In our calculations we have used a scattering coefficient of 0·064, corresponding to Rayleigh scattering at Fritz Peak for 5577 Å (ALLEN, 1955). Allowance was made for weakening of the original light by the ozonosphere (0·25 cm of ozone assumed). The numerical values used by us are shown in Table 3.

The extinction correction is shown in Table 4. Values of the extinction coefficients from 0·12 to 0·20 (referred to sea-level are included.

VOL. 12 1958

Table 3. Scattering function

Unit = Zenith intensity (inside atmosphere) for Fritz Peak
h = 100 km

Ground Albedo \ Z	0	40	60	70	75	80
0·00	0·064	0·086	0·137	0·200	0·259	0·370
0·25	0·075	0·101	0·160	0·230	0·294	0·427
0·50	0·087	0·115	0·181	0·265	0·336	0·480
0·80	0·102	0·132	0·208	0·298	0·387	0·552

Table 4. Correction for extinction of lower atmosphere, $e^{\tau m}$
Fritz Peak (m_{zen} = 0·708)

τ (sea-level) \ Z	0	40	60	70	75	80
0·12	1·089	1·117	1·185	1·279	1·383	1·609
0·13	1·096	1·127	1·202	1·306	1·421	1·674
0·14	1·104	1·137	1·219	1·333	1·460	1·742
0·15	1·112	1·148	1·237	1·361	1·500	1·813
0·16	1·120	1·158	1·254	1·389	1·542	1·886
0·17	1·128	1·169	1·272	1·418	1·584	1·962
0·18	1·136	1·180	1·290	1·447	1·627	2·042
0·19	1·144	1·191	1·309	1·477	1·672	2·124
0·20	1·152	1·202	1·327	1·508	1·718	2·210

5. The Mean Values of V_z'

In Table 5 are shown mean values of V_z' for each of the twelve nights. The prime indicates that the observations are as observed at the earth's surface inside the lower atmosphere without extinction and scattering corrections.

For purposes of discussing heights we shall break down the data into smaller

and smaller groups in the following order: (1) the grand averages of V_z' for all the data (last row in Table 5), (2) the mean values for each night (principal entries of Table 5), and (3) the mean values by survey during each night. Each value of V_z' entering into the analysis includes 8576 (536 × 16) observations in the

Table 5. V_z' (mean for entire night)

Night \ Z	0	40	60	70	75	80
1	1·000	1·262	1·793	2·249	2·496	2·525
2	1·000	1·283	1·809	2·259	2·499	2·512
3	1·000	1·269	1·786	2·146	2·436	2·587
4	1·000	1·296	1·888	2·267	2·638	2·959
5	1·000	1·259	1·759	2·090	2·371	2·577
6	1·000	1·282	1·787	2·114	2·422	2·605
7	1·000	1·317	1·847	2·231	2·506	2·710
8	1·000	1·294	1·810	2·171	2·520	2·770
9	1·000	1·265	1·752	2·069	2·321	2·490
10	1·000	1·273	1·784	2·139	2·407	2·586
11	1·000	1·275	1·789	2·101	2·445	2·747
12	1·000	1·280	1·818	2·193	2·492	2·683
Grand Average	1·000	1·280	1·802	2·169	2·463	2·646

grand average, about 700 observations for the nightly averages, and 16 observations for the average by survey.

6. Mean Height as a Function of Extinction and Albedo

We wish to examine the manner in which the grand averages of V_z' (Table 5) yield different values for the deduced height, depending on the assumed extinction coefficient and ground albedo. Calculations have been made of V_z from V_z' for τ varying from 0·12 to 0·20 in steps of 0·01 and for albedos of 0·0, 0·25, 0·5 and 0·8. The height has been determined by solution of equation (2) from V_{70}, V_{75} and V_{80}. The final adopted height (Table 6) is the weighted mean of the three, weights

VOL. 12 1958

being assigned as follows: 1 for V_{70}, 2 for V_{75} and 3 for V_{80}, corresponding roughly to the reciprocal of $\partial h/\partial V_z$.*

A plot of the deduced height (from Table 6) vs. assumed τ (extinction) for four values of ground albedo is shown in Fig. 3. In Table 7 we show the values of the extinction coefficient from Fig. 3 corresponding to heights 90, 95, 100,

Table 6. Height (km) from mean of 12 nights

τ(Extinction)	λ(albedo) = 0·00	λ = 0·25	λ = 0·50	λ = 0·80
0·12	163	170	174	182
0·13	146	150	157	164
0·14	130	134	140	147
0·15	115	120	124	130
0·16	101	105	110	116
0·17	87	91	96	102
0·18	75	79	82	88
0·19	63	67	73	76
0·20	51	55	59	64

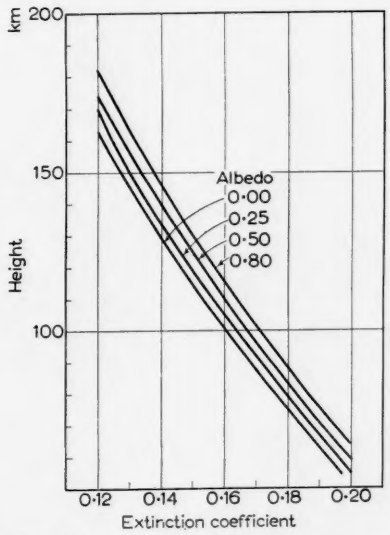

Fig. 3. Deduced height of nightglow 5577 for the mean of twelve nights vs. assumed extinction coefficient for four assumed albedos. From Table 6.

105 and 110 km, again for four assumed values of ground albedo. In order to evaluate the results it is necessary to consider the probable values of the extinction and albedo at our observing station.

The minimum value of the extinction coefficient can be given with some

* This method of weighting has been compared with a least-squares solution for the height in which all the data for all zenith distances are utilized. The two methods yield results agreeing within 2 km.

certainty. Its maximum value depends on the extent to which dust, haze and water-vapour are present above the observer. In general, we select good quality nights for observation. There has not been any visible evidence of dust on any

Table 7. Extinction coefficient (sea-level) from Fig. 3

h (km) \ λ	0	0·25	0·5	0·8
110	0·154	0·157	0·160	0·164
105	0·157	0·160	0·164	0·168
100	0·161	0·164	0·168	0·172
95	0·165	0·168	0·171	0·175
90	0·168	0·172	0·175	0·179

Table 8. Extinction coefficient (5577 Å) referred to sea-level

Source	Minimum	Probable	Maximum
Molecular scattering	0·091	0·091	0·091
Ozone	0·028	0·033	0·033
Water-vapour	—	0·001	0·002
Dust	—	0·032	0·064
Total	0·119	0·157	0·190

VOL. 12 1958

occasion during the observing period in question. In Table 8 are given estimates of maximum, minimum and probable extinction coefficients for 5577 Å, which should include all cases encountered by us at Fritz Peak.*

Recently, Penndorf (1956) has made a compilation of the literature on the ground albedo, and we give here some typical measurements quoted by Penndorf at 5600 Å from the work of Krinov (1947).

Water	0·05
Snow	0·77
Limestone, clay	0·63
Sand, desert, mountain outcrops	0·24
Coniferous forests in winter	0·03

During the last quarter of 1956 there was very little snow in the vicinity of Fritz Peak, and we have adopted 0·25 for our working value of albedo, λ, in the present investigation.

Referring to Table 7, it is seen that for $\lambda = 0{\cdot}25$ an extinction coefficient range from 0·157 to 0·172 corresponds to heights between 90 and 110 km for the

* The entries in Table 8 and the extinction coefficients throughout this paper refer to sea-level rather than the 9000 ft of Fritz Peak. In applications to Fritz Peak we use its actual air mass (0·708 in the zenith).

mean observations of our twelve nights. This range of extinction values is well within the uncertainty indicated by Table 8. On the other hand, if τ really varies between 0·12 and 0·19, then the height is uncertain between 67 and 170 km (Table 6).

If we accept the height reported by the rocket firings ($\sim$100 km), then the value of the extinction coefficient (corresponding to $\lambda = 0{\cdot}25$) is 0·164. We shall adopt this combination of constants in the next section.

7. The Height from Night to Night

From the selected values of τ (0·164) and λ(0·25) we have calculated $\bar{V}_z$ for each night separately from the values of $\bar{V}_z'$ in Table 5 by the formula

$$V_z = \frac{(V_z' - S_z') \exp(\tau m_z)}{(V_0' - S_0') \exp(\tau m_0)} = \frac{(V_z' - S_z') \exp(\tau m_z)}{(1{\cdot}000 - S_0') \exp(\tau m_0)} \tag{4}$$

where S_0' and S_z' are the scattered light in the zenith and at zenith distance z in units of the observed total brightness of the zenith (from Table 3); and m_0

Table 9. V_z(mean for entire night)

$\tau = 0{\cdot}164 \qquad \lambda = 0{\cdot}25$

Night \ Z	0	40	60	70	75	80	Height (km)
1	1·000	1·299	1·982	2·721	3·302	3·869	112
2	1·000	1·323	1·991	2·734	3·306	3·845	113
3	1·000	1·307	1·973	2·581	3·212	3·984	110
4	1·000	1·338	2·097	2·745	3·515	4·669	51
5	1·000	1·296	1·940	2·506	3·115	3·964	118
6	1·000	1·322	1·975	2·539	3·191	4·016	109
7	1·000	1·361	2·047	2·696	3·317	4·210	86
8	1·000	1·335	2·003	2·615	3·338	4·321	79
9	1·000	1·303	1·933	2·478	3·039	3·805	136
10	1·000	1·312	1·971	2·573	3·168	3·982	111
11	1·000	1·314	1·977	2·521	3·225	4·278	87
12	1·000	1·320	2·013	2·645	3·295	4·160	92
Mean	1·000	1·319	1·992	2·613	3·252	4·092	100

and m_z are the air masses (referred to unity in the zenith at sea-level) at Fritz Peak in the zenith and at zenith distance z. The results are shown in Table 9.

In the last column are shown the heights deduced from a least-squares solution of equation (2) utilizing the values of V_z from all five zenith distances.

The range of heights deduced is from 51 km to 136 km. The mean height is found to be

$$100 \pm 4 \text{ (p.e.) km}$$

Table 10. Standard deviations

Standard deviation	Category	Defining equation	Measure of scatter for
s_1	Between nights	$s_1^2 = \frac{1}{k-1}\sum_{i=1}^{k}(\overline{V}_i - \overline{V})^2$	A single night if there are the same number of surveys, n_i, for each night
$\bar{s}_1$	Between nights	$\bar{s}_1^2 = \frac{1}{\overline{n}_i}\cdot\frac{1}{k-1}\sum_{i=1}^{k} n_i(\overline{V}_i - \overline{V})^2$	A single night weighted according to the number of surveys for each night
s_2	Between nights	$s_2^2 = \frac{1}{k(k-1)}\sum_{i=1}^{k}(\overline{V}_i - \overline{V})^2$	Mean of k nights if there are the same number of surveys for each night
$\bar{s}_2$	Between nights	$\bar{s}_2^2 = \frac{1}{\overline{n}_i}\cdot\frac{1}{k(k-1)}\sum_{i=1}^{k} n_i(\overline{V}_i - \overline{V})^2$	Mean of k nights, each night weighted according to the number of surveys
s_3	Within nights	$s_3^2 = \frac{1}{n_i - 1}\sum_{j=1}^{n_i}(V_{ij} - \overline{V}_i)^2$	A single survey during a given night (spottiness)
$\bar{s}_3$	Within nights	$\bar{s}_3^2 = \frac{1}{N-k}\sum_{i=1}^{k}\sum_{j=1}^{n_i}(V_{ij} - \overline{V}_i)^2$	A single survey based on all the data from all nights
s_4	Within nights	$s_4^2 = \frac{1}{n_i(n_i-1)}\sum_{j=1}^{n_i}(V_{ij} - \overline{V}_i)^2$	Mean of n_i surveys during a given night
$\bar{s}_4$	Within nights	$\bar{s}_4^2 = \frac{1}{\overline{n}_i}\cdot\frac{1}{N-k}\sum_{i=1}^{k}\sum_{j=1}^{n_i}(V_{ij} - \overline{V}_i)^2$	Mean of n_i surveys (one night) based on all the data from all the nights
s_r	Between nights	$\bar{s}_r^2 = \bar{s}_1^2 - \bar{s}_4^2$	Residual between nights after removal of effect of spottiness
		$F = \bar{s}_1^2/\bar{s}_4^2$	

V_{ij} = Value of V for the j th survey on the i th night.
V_i = Mean value of V for the i th night (principal entries of Table 9).
V = Mean value of V for all the data (last row of Table 9).
$N = \sum_{i=1}^{k} n_i$

The constants used predetermine a height of 100 km, so the significant figure is the probable error of the mean. Also of some significance is the probable error of a height deduced for a single night, ± 15 km.

We wish next to consider the factors that may contribute to the scatter of the determined heights: (1) scatter due to spottiness of the airglow and (2) scatter due to variable extinction from night to night.

8. Scatter Due to Spottiness of the Airglow

In order to study the extent to which the determination of height is influenced by the spottiness of the airglow, we shall examine the quantity V_z rather than the derived height. The nature of the observing programme is such that the entire sky is surveyed every 15 min in a series of almucantars at zenith distances 80, 75, 70, 60 and 40°. Each almucantar is measured at sixteen azimuths. We have calculated the average values of V_z for each of the 536 surveys of the present study and for each zenith distance.

The problem we wish to solve is the following: Is the scatter in the values of V_z among the several surveys during a night able to account for the scatter among the values of V_z between nights? In other words, is the spottiness of the sky during the night the cause of the variability between nights? This is a standard problem in statistics.* Referring to Table 10, the solution depends on whether $\bar{s}_1 \approx \bar{s}_4$ or $\bar{s}_1 \gg \bar{s}_4$. If the two deviations are sensibly equal to each other, then the spottiness of the sky is adequate to account for the variation from night to night. If on the other hand $\bar{s}_1 \gg \bar{s}_4$, then it is indicated that there is a significant "between night" variance in addition to that due to the spottiness of the sky.

In Table 11 is a summary of calculations of several of the standard deviations.

Table 11. Numerical values of standard deviations

	40	60	70	75	80
$\bar{s}_2$	0·003	0·013	0·027	0·036	0·071
$\bar{s}_1$	0·016	0·044	0·093	0·123	0·248
$\bar{s}_4$	0·013	0·026	0·045	0·061	0·093
$\bar{s}_3$	0·089	0·176	0·298	0·404	0·623
F	1·5	2·8	4·3	4·1	7·0
s_r	0·010	0·035	0·082	0·107	0·229

It is noted that in all cases $\bar{s}_1 > \bar{s}_4$. Whether the difference between $\bar{s}_4$ and $\bar{s}_1$ is significant can be estimated by the numerical value of the ratio $\bar{s}_1^2/\bar{s}_4^2 = F$. For the size of sample that we have ($N - k = 524$; $k - 1 = 11$), the probability that F would exceed the value 1·8 simply by chance is only 0·05. In our case $F > 1{\cdot}8$ for all values of z except 40°, which forces on us the conclusion that

* See for example: *Techniques of Statistical Analysis*, Section 5.2 Chapter 8. Eisenhart, Hastay and Wallis McGraw-Hill, New York.

the spottiness of the sky cannot account for the variation of V_z between nights. It is thus necessary to look for some other physical cause for the residual standard deviation, s_r. It is noted, however, that $\bar{s}_3$ is in all cases very much larger than $\bar{s}_1$, from which it follows that, *for a single survey*, height determinations are predominantly controlled by the airglow spottiness.

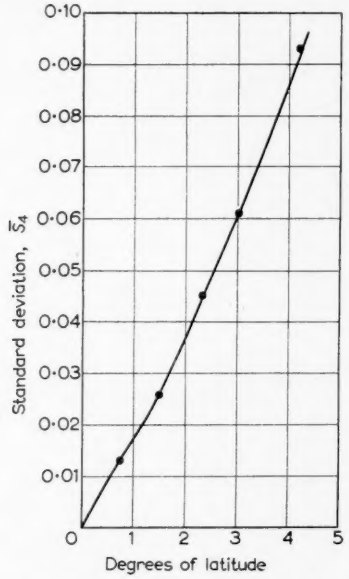

Fig. 4. Standard deviation due to spottiness of nightglow vs. distance in degrees of latitude to the intersection of the line of sight and an upper atmosphere layer at 100 km.

In Fig. 4 the values of $\bar{s}_4$ are plotted against the distance along the earth's surface to the line-of-sight intersection with an emitting layer at a height of 100 km. It is noted that $\bar{s}_4$ increases with distance. Thus, the larger the circle (geographically speaking) that includes the sixteen readings of an almucantar, the larger is the scatter of the data. This is consistent with the idea that the spottiness is, to a first approximation, proportional to the geographical separation of the individual observations.

9. Scatter Due to Variable Extinction

In this section we shall examine the consequences of the assumption that the residual scatter, s_r, in V_z is due to a variation in the extinction from night to night. That this is a plausible assumption is indicated by Fig. 5, where it is noted that s_r is proportional to the extinction term, $e^{\tau m}$, and that it goes to zero at $e^{\tau m} = 1{\cdot}12$, which is the zenith value for $\tau = 0{\cdot}16$ (Table 4).

From equation (4) we find

$$\tau = \frac{2{\cdot}303}{m_z - m_0} \log \frac{V_z(1{\cdot}000 - S_0')}{V_z' - S_z'} \tag{7}$$

We have deduced numerical values of τ from equation (7) for each of the twelve

VOL. 12 1958

nights, on the assumption that the true height of the airglow is 100 km, with the results shown in Table 12. The weight in the last column is 1 (for V_{70}), 2 (V_{75}) and 3 (V_{80}).

The conclusion to be drawn is that the data are consistent with a constant

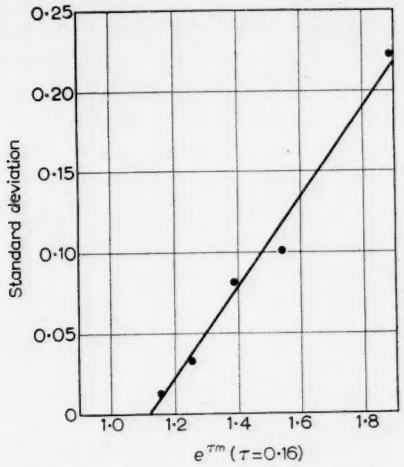

Fig. 5. Standard deviation (residual) vs. extinction correction, $e^{\tau m}$.

Table 12. Extinction coefficient from equation (7)
Assumed height = 100 km

Night	V_{70}	V_{75}	V_{80}	Mean	
				Unweighted	Weighted
1	0·140	0·153	0·180	0·158	0·164
2	0·136	0·152	0·182	0·157	0·164
3	0·179	0·167	0·172	0·173	0·172
4	0·133	0·122	0·123	0·126	0·124
5	0·201	0·183	0·173	0·186	0·181
6	0·192	0·171	0·169	0·177	0·174
7	0·147	0·151	0·155	0·151	0·152
8	0·169	0·148	0·147	0·155	0·151
9	0·209	0·195	0·185	0·196	0·192
10	0·182	0·174	0·172	0·176	0·174
11	0·197	0·165	0·150	0·171	0·163
12	0·161	0·154	0·158	0·158	0·157
Mean	0·170	0·161	0·164	0·165	0·164

height (100 km) for the airglow and a variation of extinction from a minimum of 0·12 to a maximum of 0·19, which is just the range which might be expected (Table 8).

10. Remarks on Possible Systematic Errors

A small systematic correction to the observed values of V'_z should be applied because of the effect of the finite field of view. This point was discussed by Roach and Meinel (1955). An examination of their Fig. 7 indicates that, for a 5° diameter field, the correction is trivial for $z = 70°$, less than $+0{\cdot}005$ for $z = 75°$ and approximately 0·01 for $z = 80°$. In the present paper we have not included this correction for our photometer, which has a 4° field, with the consequence that a small systematic effect remains in our value, especially for V_z' from $z = 80°$. A convenient test of the importance that should be attached to our omission of this correction in the present study is obtained by an application of equation (7).

The extinction coefficient for $z = 80°$ would be lowered by 0·001 for a systematic increase in V'_z of 0·01, which is seen to be small compared with the observed difference between τ (from 70°) and τ from (80°). Other errors seem to overshadow that due to the finite field.

Another possible source of systematic error is the setting of the zenith distance of the photometer. We have measured these settings and find they are within 0·5° of their rated values.

Attention is called to the fact that our birefringent filter is actually a polarimeter, and if the airglow should have a change of polarization with zenith distance this would have an effect on the deduced heights. Any such effect would be thrown into our empirical determinations of the extinction coefficient.

VOL.
12
1958

11. Conclusions

In Fig. 6 we show a plot of the two alternative solutions of this paper for the individual nights. Our data for twelve nights are consistent with two extreme possibilities, either:

(1) The heights vary from 51 to 136 km (mean value of 100 km) with a constant extinction coefficient of 0·164, or

(2) The height is fixed at 100 km and the extinction varies from 0·12 to 0·19.

We believe that the second is the more probable approximation. A range of heights from night to night over 85 km (from 51 to 136 km) is not likely, since the physical conditions in the upper atmosphere are so vastly different between these limits.

The question arises: what is the necessary accuracy required in our knowledge of τ in order that the uncertainty in the deduced height shall be the same as that which is inherent in the spottiness of the sky itself. The uncertainty in height for one night from spottiness is given by $\bar{s}_4(\partial h/\partial V_z) = 0{\cdot}093 \times 92 = 9$ km (for $z = 80°$). An examination of Fig. 3 shows that the uncertainty in τ leading to an uncertainty in h of 9 km is 0·007. To determine the effective extinction coefficient over the entire sky and throughout a night with such finesse would be a major undertaking. It seems obvious that other methods of airglow height determination (rockets, triangulation) are more likely to yield data that can be relied on to within 10 km. This is true when data for an entire night are included in an analysis but much more forcefully so if heights are desired for smaller amounts of data, say every hour during a night.

In Table 13 we give a summary of the height uncertainty for various amounts of data based on the results of the present study.

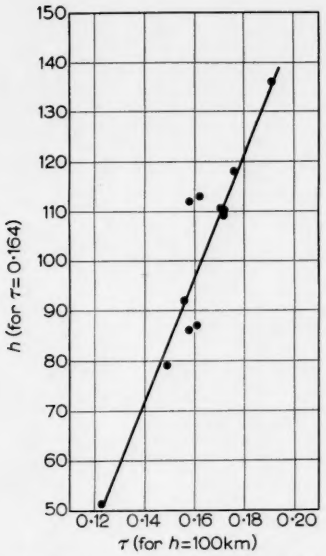

Fig. 6. Range of solutions for a variable height (fixed extinction) or a variable extinction (fixed height).

Table 13. Summary of height uncertainties

Quantity of data	Standard deviation				Δh corresponding to the standard deviation		
	s	V_{70}	V_{75}	V_{80}	70	75	80
One survey	$\bar{s}_3$	0·298	0·404	0·623	123	85	57
Mean of 44 surveys during one night	$\bar{s}_4$	0·045	0·061	0·093	19	13	9
One night	$\bar{s}_1$	0·093	0·123	0·248	38	26	23
Mean of 12 nights	$\bar{s}_2$	0·027	0·036	0·071	11	8	7

Acknowledgements—We are indebted to our associates for assistance in the preparation of this study: to Mr. J. E. Cruz and Mr. H. H. Hardy as observers and to Miss Pauline Jamnick for help with the computing and scaling of the records.

References

Allen C. W.	1955	*Astrophysical Quantities* p. 116. The Athlone Press, London.
Ashburn E. V.	1954	*J. Atmosph. Phys.* **5,** 83.
Barbier D. Dufay J. and Williams D. R.	1951	*Ann. Astrophys.* **14,** 399.
Berg O. E., Koomen M., Meredith L. and R. Scolnik R.	1956	*J. Geophys. Res.* **61,** 302.

Blamont J. and Kastler A.	1951	*Ann. Geophys.* **7,** 73.
Dunn R. B. and Manring E. R.	1955	*J. Opt. Soc. Amer.* **45,** 899.
Heppner J. P., Stolarik J. D. and Meredith L. H.	1957	*Trans. Amer. Geophys. Un.* **38,** 394.
Koomen M. J., Packer D. M. and Tousey R.	1955	*The Airglow and the Aurorae* (Edited by Dalgarno A. and Armstrong E.) p.355. Pergamon Press, London
Koomen M., Scolnik R. and Tousey R.	1956	*J. Geophys.Res* **61,** 304.
Krinov E. L.	1947	*Spectral Reflectance Properties of Natural Formations* (in Russian 1947). National Research Council of Canada Technical Translation TT-439, Ottawa (1953).
Manring E. R. and Pettit H. B.	1955	*The Airglow and the Aurorae* (Edited by Dalgarno A. and Armstrong E.) p. 29. Pergamon Press, London.
Penndorf R.	1956	Geophysical Research Paper number 44. Geophysics Research Directorate, Air Force Cambridge Research Center.
Roach F. E. and Meinel A. B.	1955	*Astrophys. J.* **122,** 530.
van Rhijn P. J.	1924	*Bull. Astr. Insts. Netherlds.* **2,** 75.

VOL.
12
1958

Journal of Atmospheric and Terrestrial Physics, 1958, Vol. 12, pp. 187 to 199. Pergamon Press Ltd., London

Die Verteilung der Röntgenstrahlung der Sonnenkorona über die emittierende Fläche und die Restintensität bei totalen Sonnenfinsternissen

The distribution of X-rays emitted by the solar corona and the residual intensity during solar eclipses

GERHARD ELWERT
Astronomisches Institut der Universität, Tübingen, Germany

(*Received* 8 *October* 1957)

Zussammenfassung—Während bei der Deutung des zeitlichen Verlaufs der Elektronendichte in der E-Schicht bei totalen Sonnenfinsternissen gewöhnlich angenommen wird, dass die Intensität der ionisierenden Strahlung proportional zur Fläche der optisch sichtbaren Sonnenscheibe ist, hat sich neuerdings gezeigt, dass bei der Totalität ein Restbetrag ΔJ der Intensität J übrigbleibt. Da es wahrscheinlich ist, dass der wesentliche Beitrag zur Bildung der normalen E-Schicht von einer langwelligen Röntgenstrahlung der Sonnenkorona stammt, wird die Intensitätsverteilung dieser Strahlung über die emittierende Flache für die ungestörte Korona unter Berücksichtigung der Selbstabsorption der Linien untersucht. Am Rand ergibt sich eine Aufhellung. Deshalb ist der Wert von $R = \Delta J/J$ vom Verhältnis η des scheinbaren Mondradius zum Sonnenradius abhängig, kann also bei den einzelnen Finsternissen merklich verscheidene Werte haben. Infolge der Abplattung der Korona kommt die Strahlung hauptsächlich aus der Äquatorgegend. Für die Reststrahlung R verwendet man das Wahrmeiersche Modell der Dichte verteilung der Elektronen, so findet man für mit $\eta = 1{,}02$ (gültig für die Finsternisse von 1952 und 1954) etwa 17 bis 22%, mit $\eta = 1{,}06$ (Finsternis von 1955) etwa 10 bis 12%. Diese Ergebnisse ermöglichen eine Deutung der ionosphärischen Beobachtungen, wobei gegebenenfalls noch die Beiträge lokaler Quellen zu berücksichtigen sind.

Abstract—In the interpretation of the time changes of the electron density in the E-layer during total eclipses, it has usually been assumed that the intensity of the ionizing radiation is proportional to the area of the optically visible solar disk. Recently, however, it was found that a residual amount ΔJ of the intensity J remains. It is probable that the formation of the E-layer is mainly due to a long-wave X-ray radiation of the corona. The distribution of that radiation over the emitting area of the undisturbed corona is studied in this paper, taking into account the self-absorption of these lines. A brightening near the edge is found. Therefore the value of $R = \Delta J/J$ depends on the ratio η of the apparent lunar radius to the solar radius, which may differ appreciably from one eclipse to the other. Because of the ellipticity of the corona, the radiation comes mainly from the equatorial region. Using Wahrmeier's model for the density distribution of the electrons, for the residual radiation R one finds, with $\eta = 1{\cdot}02$ (valid for the eclipses of 1952 and 1954), about 17–22 per cent, with $\eta = 1{\cdot}06$ (eclipse of 1955) about 10–12 per cent. These results may be used for an interpretation of the ionospheric observations; if necessary, the contributions of local sources will have to be taken into account also.

BEI Sonnenfinsternissen ändert sich bekanntlich die Elektronendichte der ionosphärischen Schichten, da das Gleichgewicht von Ionisation und Rekombination durch die Änderung der Intensität der ionisierenden Strahlung gestört wird. Die zeitliche Änderung der Elektronendichte ist abhängig von der Rekombinationsgeschwindigkeit, deshalb ist die Untersuchung des Ablaufs dieses Vorgangs von Wichtigkeit für die empirische Bestimmung des Rekombinationskoeffizienten. Dabei nimmt man gewöhnlich an, dass die Intensität J der ionisierenden Strahlung proportional zur Fläche der optisch sichtbaren Sonnenscheibe ist, indem man voraussetzt, dass diese Strahlung aus der Photosphäre oder Chromosphäre stammt. Erst neuerdings hat sich durch Untersuchungen von MINNIS (1955); PIGGOTT (1952); BIBL and DELOBEAU (1956) u.a. herausgestellt, dass bei der Totalität noch ein Restbetrag der Intensität ΔJ übrig bleibt. Nach theoretischen Untersuchungen (ELWERT, 1952) wie Messungen der extraterrestrischen Strahlung mit Raketen (siehe HULBURT, 1955) ist es andererseits in den letzten Jahren wahrscheinlich geworden, dass der wesentliche Beitrag zur Bildung der normalen ionosphärischen E-Schicht durch eine langwellige Röntgenstrahlung der Sonnenkorona geliefert

wird. Dadurch ergibt sich die Möglichkeit der Erklärung einer Reststrahlung, da die Sonnenkorona bei totalen Sonnenfinsternissen nicht vollständig abgedeckt wird. Es entsteht nun die Frage, ob ihr Betrag auf Grund der bisherigen Kenntnisse der Ausstrahlung der Korona im Röntgengebiet zu verstehen ist. In der vorliegenden Untersuchung soll daher die theoretische Verteilung der Röntgenintensität der ungestörten Korona über die emittierende Fläche untersucht werden. Aus ihr ist dann die auf die Normalintensität J bezogene Restintensität bei der Totalität ΔJ in Abhängigkeit vom Verhältnis des scheinbaren Mondradius zum Sonnenradius zu gewinnen.

1. RANDAUFHELLUNG UND BEDECKUNGSGRAD

Die Röntgenstrahlung der ungestörten Korona wurde in einer früheren Arbeit des Verfassers (ELWERT, 1952) ausführlich untersucht. Sie kommt im wesentlichen zustande durch Linienemission der Ionen nach Stossanregung durch Elektronen und zu einem unwesentlichen Teil durch Photorekombination der freien Elektronen mit hochionisierten Ionen und durch frei-frei-Übergänge der Elektronen. Die Zahl der Stossanregungen wie die der Rekombinationen und frei-frei-Übergänge pro cm³ ist proportional zur Ionen- und Elektronendichte. Bei konstanter Temperatur sind beide Dichten zueinander proportional. Also ist die Ausstrahlung je cm³ proportional zum Quadrat der Elektronendichte, wobei der Proportionalitätsfaktor nur die Temperatur und atomare Konstanten enthält. Wenn keine Absorption dieser Strahlung eintritt, erhält man den Intensitätsverlauf, indem man das Quadrat der Elektronendichte über den Sehstrahl integriert. Ist Absorption vorhanden, so erhält man auf diese Weise für jeden Sehstrahl obere Schranken der Strahlungsintensität. Das Integral über das Quadrat der Elektronendichte kommt auch in der Radioastronomie vor, da die Koronastrahlung bei Radiowellen durch frei-frei-Übergänge entsteht. Bei cm-Wellen ist die Korona optisch dünn und die Beiträge der einzelnen Volumenelemente überlagern sich ohne Schwächung. Man erhält deshalb ohne Absorption im Röntgengebiet denselben Verlauf der Helligkeit wie bei cm-Wellen. Wie früher gezeigt wurde (ELWERT, 1952), ist die Absorption der kontinuierlichen Strahlung vernachlässigbar; hingegen muss die Selbstabsorption der Linienstrahlung berücksichtigt werden.

Von der Radiostrahlung im cm- und dm-Gebiet ist bekannt, dass die Helligkeit am Sonnenrand am grössten ist. Die entsprechende Erscheinung ist also auch bei Röntgenstrahlung zu erwarten. Sie bleibt qualitativ bei Berücksichtigung der Absorption bestehen. Da sich das Verhältnis des scheinbaren Mondradius r_M zum Sonnenradius $r_\odot$ von Finsternis zu Finsternis ein wenig ändert, wird bei der Totalität ein mehr oder weniger grosser Teil der Intensitätsspitze am Rand abgeschnitten; die Restintensität bei der Totalität wird also auch bei gleicher radialer Intensitätsverteilung bei den einzelnen Finsternissen merklich verschieden sein können. Für die totalen Finsternisse der letzten Jahre ist $r_\odot$, r_M und das Verhältnis $\eta = r_M/r_\odot$ aus der folgenden Zusammenstellung zu ersehen.

	$r_\odot$	r_M	η
25. Febr. 1952	16′ 9,4″	16′ 29,2″	1,02
30. Juni 1954	16′ 43,9″	16′ 4,5″	1,02
20. Juni 1955	15′ 44,3″	16′ 39,7″	1,06

VOL. 12 1958

2. Kugelsymmetrisches Modell

(a) *Ohne Absorption*

Eine erste Näherung erhält man, wenn man für die Elektronendichte n_e die von Baumbach (1937) aufgestellte Formel verwendet. Sie ist gewonnen durch Mittelung der durch Streuung des Sonnenlichts an freien Elektronen entstehenden Koronahelligkeit über alle Positionswinkel, liefert also ein kugelsymmetrisches Modell der Korona. Es entspricht dem Zustand der Korona zur Zeit des Sonnenfleckenmaximums, bei dem die Korona ziemlich rund ist. Die Baumbachformel lautet

$$n_e = 10^8\left(\frac{1{,}55}{r^6} + \frac{2{,}99}{r^{16}}\right) \tag{1}$$

wobei r in Einheiten des Sonnenradius zu messen ist. Der Sehstrahl möge in der Richtung der x-Achse eines kartesischen Koordinatensystems verlaufen; die Ebene $x = 0$ gehe durch den Sonnenmittelpunkt. Das Integral über das Quadrat der Elektronendichte längs des Sehstrahls, ergibt

$$i(\rho) = \int_{-\infty}^{+\infty} \eta_e{}^2\, dx = 10^{16}[2{,}4J_{12} + 9J_{32} + 9{,}3J_{22}] \tag{2}$$

Die Länge der einzelnen Sehstrahlen ist dabei in Einheiten des Sonnenradius zu messen. Um den wahren Wert des Integrals über das Quadrat der Elektronendichte zu erhalten, ist (2) noch mit dem Sonnenradius $R_\odot = 7 \cdot 10^{10}$ cm zu multiplizieren. Im Aussengebiet ($\rho > 1$) gilt (Baumbach, 1937; Unsöld, 1955)

$$J_n = \int_{-\infty}^{+\infty} \frac{dx}{r^n} = \frac{2}{\rho^{n-1}} \int_0^{\pi/2} \cos^{n-2}\alpha\, d\alpha = \frac{1}{\rho^{n-1}} \frac{\Gamma\left(\frac{1}{2}\right)\Gamma\left(\frac{n-1}{2}\right)}{\Gamma\left(\frac{n}{2}\right)} \tag{3}$$

$\rho = r\cos\alpha$ bedeutet den Abstand des Sehstrahls vom Sonnenmittelpunkt, $\alpha = arctg(x/\rho)$ den Winkel zwischen der Meridianebene $x = 0$ und dem Radiusvektor zum Intergationspunkt. Damit ergibt sich

$$i(\rho) = 10^{16}(1{,}86\rho^{-11} + 4{,}07J\rho^{-31} + 5{,}12\rho^{-21}) \tag{4}$$

Das Integral im Innengebiet ($\rho < 1$) führt auf Integrale der Form $\int_{\alpha_0}^{\pi/2} \cos^{n-2}\alpha\, d\alpha$ mit $\cos\alpha_0 = \rho$, welche nicht geschlossen darstellbar sind, aber von Petri (1952) tabuliert wurden. Abgesehen von der nächsten Umgebung des Sonnenrandes erhält man eine ausreichende Näherung durch die für planparallele Schichten gültige Formel

$$i(\rho) = \frac{1}{\sin\alpha} \int_\rho^\infty n_e{}^2\, dr = \frac{9{,}4 \cdot 10^{15}}{\sin\alpha} \qquad (\rho \leq 0{,}9), \tag{5}$$

wobei $\int_\rho^\infty n_e{}^2\, dr$ das über einen radialen Sehstrahl genommene Integral von $n_e{}^2$ ist. Am Rand selbst tritt die bekannte Unstetigkeit auf; $i(\rho)$ ist auf der inneren Seite

halb so gross wie auf der äusseren. Der Funktionsverlauf von $i(\rho)$ ist in Abb. 1 als Kurve 1 wiedergegeben.

Bei der Berechnung der gesamten während der Totalität übrigbleibenden Strahlungsintensität benötigt man das Integral von n_e^2 über den Raum ausserhalb

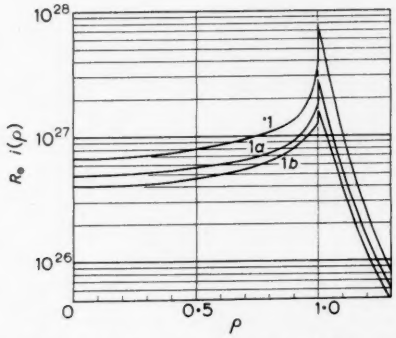

Abb. 1. Intensitätsverteilung der kugelsymmetrischen Korona Kurve 1 ohne Absorption Kurve 1*a* mit Absorption ($\tau_{00} = 0{,}5$) Kurve 1*b* mit Absorption ($\tau_{00} = 1$).

des Kreiszylinders mit dem Radius ρ. Es ist proportional zur Reststrahlung ΔJ. Da es beim Vergleich mit J nicht auf konstante Faktoren ankommt, werde dieses Integral selbst mit ΔJ bezeichnet. Es ergibt sich

$$\Delta J(\rho) = 2\pi \int_{\rho}^{\infty} i(\rho)\rho \, d\rho = 10^{16}(0{,}21\rho^{-9} + 0{,}27J\rho^{-19} + 0{,}14\rho^{-29}) \tag{6}$$

Numerisch folgt hieraus für

$\rho =$	1	1,02	1,06
$\Delta J(\rho) =$	3,9	2,7	$1{,}5 \cdot 10^{16}$

Zur Berechnung von J braucht man noch das entsprechende Integral über den Innenraum des Zylinders für $\rho = 1$ unter Ausschluss der von der Sonne eingenommenen Kugel mit dem Radius 1. Man berechnet es am einfachsten als Differenz des Integrals von n_e^2 über den gesamten äusseren Kugelraum J_{tot} und $\Delta J(1)$. Es ist

$$J_{\text{tot}} = 4\pi \int_{1}^{\infty} n_e^2 r^2 \, dr = 13{,}4 \cdot 10^{16} \tag{7}$$

Also wird

$$J_i = J_{\text{tot}} - \Delta J(1) = 9{,}5 \cdot 10^{16} \tag{8}$$

Für den vorderen und hinteren Teil des Zylinders ergibt sich also jeweils der Beitrag $J_i/2 = 4{,}8 \cdot 10^{16}$. Somit wird das Integral von n_e^2 über den gesamten sichtbaren Raum

$$J = \Delta J(1) + \tfrac{1}{2}J_i = 8{,}J \cdot 10^{16} \tag{9}$$

Für das Verhältnis $R = \Delta J/J$ der bei der Totalität übrigbleibenden Reststrahlung ΔJ zur Gesamtemission J folgt nun aus Gl. (6) und (9) die in Abb. 6 dargestellte

VOL. 12 1958

Kurve 1. Sie gilt für die kontinuierliche Strahlung, da bei ihr die Absorption vernachlässigbar ist, jedoch nicht für die Linienemission, welche nach B den Hauptbeitrag liefert.

(b) *Berücksichtigung der Absorption der Linienstrahlung*

Die über alle Frequenzen integrierte durchgelassene Intensität $\varphi(\tau_0)$ ist abhängig von der optischen Tiefe τ_0 in der Linienmitte und gegeben durch die Formel (ELWERT, 1952)

$$\varphi(\tau_0) = \frac{2}{\sqrt{\pi}} \int_0^\infty e^{-v^2 - \tau_0 e^{-v^2}} \, dv, \tag{10}$$

wobei die Gesamtintensität der Linie ohne Absorption gleich 1 gesetzt und der in Einheiten der Dopplerbreite gemessene Abstand der Kreisfrequenz von der Linienmitte

$$v = \frac{\Delta\omega}{\Delta\omega_D} \tag{11}$$

ist. Die Dopplerbreite ist gegeben durch

$$\Delta\omega_D = \frac{\omega}{c} \sqrt{\frac{2kT}{Am_H} + \xi_t^2} \tag{12}$$

Hierin bedeutet T die Koronatemperatur, A das Atomgewicht der absorbierenden Atome und ξ_t die mittlere Turbulenzgeschwindigkeit. Ferner ist die optische Tiefe in der Linienmitte gegeben durch

$$\tau_0 = Nf \, 2\pi^{3/2} \frac{cr_0}{\Delta\omega_D}. \tag{13}$$

$N = \int_{-\infty}^{x} n_i \, dx$ ist die Zahl der absorptionsfähigen Ionen längs des Sehstrahls, f die Oszillatorenstärke des betreffenden Übergangs und r_0 der klassische Elektronenradius. Bei konstanter Temperatur ist $N = (n_i/n_e)N_e$ proportional zum Integral über die Elektronendichte $N_e = \int_{-\infty}^{x} n_e \, dx$. Für den zentralen Strahl, der von $x_0 = 1{,}02$ ausgeht, wird $N_{e0} = N_e(1{,}02) = 4 \cdot 10^7$. Misst man die Länge des Sehstrahls in cm, so erhält man hierfür durch Multiplikation mit dem Sonnenradius den Wert $3 \cdot 10^{18}$. Da die hochionisierten Ionen wasserstoffähnlich sind, werden die Werte von f für Wasserstoff eine ordentliche Näherung liefern. Es geht jedoch an dieser Stelle eine gewisse Unsicherheit in die Rechnung ein.

Im Prinzip wäre nun die Berechnung der Ausstrahlung unter Berücksichtigung der Absorption für jede Linie mit dem für sie gültigen Absorptionskoeffizienten durchzuführen. Für einige wesentliche Linien sind die optischen Tiefen τ_{00} für den zentralen von dem Niveau x_0 ausgehenden Sehstrahl in der folgenden Tabelle angegeben. Dabei wurden die schon von ELWERT (1952) verwendeten Temperaturen $7 \cdot 10^5$ und 10^6 °K betrachtet. Die Grössen Y_{zi} sind zur Linienintensität proportional

und in Gl. (60) der angegebenen Arbeit des Verfassers definiert. Die Werte von Y_{zi} sind aus Tabelle 5 dieser Arbeit entnommen.

	λ_A°	Y_{zi}	τ_{00}	Y_{zi}	τ_{00}
Ne	95	2	0,2		
	85	7	1	7	0,5
Fe	88	5	1		
	73	4	1	3	0,3
	65			4	0,8
	62			2	0,4

τ_{00} nimmt also für die wesentlichen Linien Werte zwischen etwa 0,5 und 1 an; bei einigen Linien, welche nur einen unwesentlichen Beitrag liefern, kommen auch kleinere und grössere Werte von τ_{00} vor. Um zu übersehen, wie $R = \frac{\Delta \mathcal{F}}{\mathcal{F}}$ von τ_{00} abhängt, wurden deshalb die Rechnungen für $\tau_{00} = 0{,}5$ und 1 durchgeführt.

Es ist nun das Integral

$$i^*(\rho) = \int n_e^2 \varphi[\tau_0(N_e)]\, dx \tag{14}$$

über den Sehstrahl zu ermitteln. N_e ist in Abhängigkeit von α für verschiedene Entfernungen ρ von der Sonnenmitte in Abb. 2 dargestellt. Auf der Ordinate der rechten Seite dieser Abbildung sind zwei Skalen für τ_0 gezeichnet, für welche τ_{00}

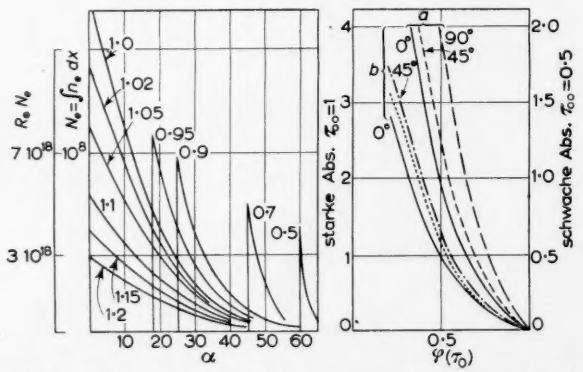

Abb. 2. Linke Seite: Integral N_e der Elektronendichte längs des Sehstrahls in Abhängigkeit von α für verschiedene ρ ordinate: rechte Seite: optische Tiefe τ_0 in der Linienmitte. Abszisse: Absorptionskoeffizient $\psi(\tau_0)$ Für die Nähe des Sonnenrandes Kurven a für schwache Absorption ($\tau_{00} = 0{,}5$) Kurven b fur strake Absorption ($\tau_{00} = 1$) Die angegebenen Zahlen geben den Wert des Winkels ψ . . . . . $\rho = 0{,}9$, $\psi = 90°$.

die Werte 0,5 und 1 annimmt. Ferner ist auf der rechten Seite $\varphi(\tau_0)$ als Funktion von τ_0 nach ELWERT (1952) Abb. 5(a) dargestellt (Kurven a und b für 0°). Das Integral (14) ist nun in Abhängigkeit von ρ numerisch zu berechnen, indem man N_e bei festgehaltenem ρ als Funktion von α betrachtet und für das betreffende ρ die Höhe der Ordinate entnimmt, welche einerseits auf der linken Seite N_e als Funktion von α, andererseits auf der rechten Seite τ_0 liefert. Auf der Abszisse der rechten Seite ist dann

sogleich $\varphi(\tau_0)$ abzulesen. Bildet man nun den Quotienten von $i^*(\rho)$ und $i(\rho)$, so erhält man die in Abb. 3 dargestellte Schwächungskurven der Intensität a und b für 0° in Abhängigkeit von ρ. Wie von vornherein zu erwarten ist, sit die Absorption dort am grössten, wo der Sehstrahl am längsten ist, also dicht ausserhalb des Sonnenrandes. Infolgedessen erhält man eine stärkere Verkleinerung der Strahlung

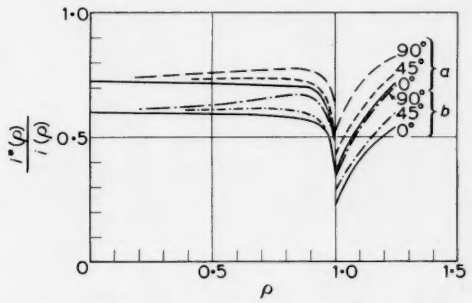

Abb. 3. Schwächungskurven $i^*(\rho)/i(\rho)$ a für $\tau_{00} = 0{,}5$, b für $\tau_{00} = 1$ Die angegebenen Zahlen bedeuten die Werte des Winkels ψ.

des Ringes als des bei der Totalität abgedeckten Teiles der Sonne. Die Intensitätsverteilung selbst ist für die beiden betrachteten Fälle $\tau_{00} = 0{,}5$ und 1 in Abb. 1 als Kurve 1a und 1b dargestellt. Berechnet man schliesslich durch Integration über die strahlende Fläche die Reststrahlung R bei der Totalität, so erhält man infolge der stärkeren Absorption in dem nicht abgedeckten Teil der Korona etwas kleinere Werte als ohne Absorption. R ist in Abb. 6 für die beiden betrachteten Werte von τ_{00} als Kurve 1a and 1b dargestellt.

3. Rotationssymmetrisches Modell

(a) *Ohne Absorption*

Das bisher verwendete kugelsymmetrische Modell der Korona liefert nur eine Näherung. Wie namentlich Beobachtungen zur Zeit des Fleckenminimums zeigen, ist die Korona an den Polen abgeplattet, die äquatoriale Elektronendichte n_{eA} ist also grösser als die polare Dichte n_{eP}. Nach Waldmeier (1955) gilt

$$n_{eA} = 10^8\left(\frac{3{,}00}{r^{16}} + \frac{1{,}42}{r^6} + \frac{0{,}034}{r^{2.5}}\right) \tag{15}$$

und

$$n_{eP} = 10^8\left(\frac{1{,}16}{r^{16}} + \frac{1{,}15}{r^8} + \frac{0{,}027}{r^4}\right) \tag{16}$$

In der inneren Korona, welche in der vorliegenden Untersuchung allein interessiert, sind die letzten Glieder vernachlässigbar. Zwischen Pol und Äquator kann die mittlere Elektronendichte durch Interpolation dargestellt werden. Der beobachtete Helligkeitsverlauf der Korona am Sonnenrand führt Waldmeier zu der Formel für das Quadrat der Elektronendichte in der Breite b

$$n_e^2(r,b) = n_{eP}^2 + \cos^3 b(n_{eA}^2 - n_{eP}^2) \tag{17}$$

Das Integral über n_e^2 wurde von ihm für verschiedene zur Äquatorebene parallele Sehstrahlen berechnet. Es ist eine Funktion von ρ und dem Winkel ψ zwischen dem radialen Strahl senkrecht zum Sehstrahl und der Äquatorebene. Dabei wurde $\psi = 0,\ 22{,}5°,\ 45°,\ 67{,}5°$ und $90°$ gewählt. Das Ergebnis ist in Abb. 4 für 3 Werte

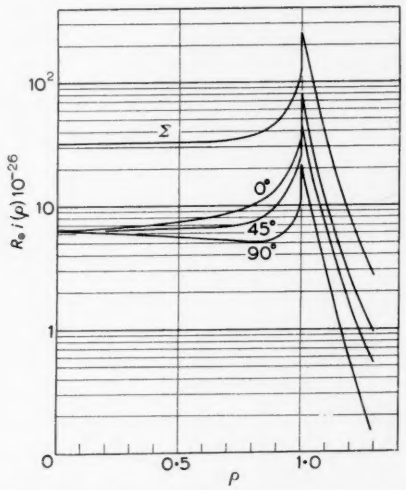

Abb. 4(a). Intensitätsverteilung der rotationssymmetrischen abgeplatteten Korona ohne Absorption. Die Zahlen bedeuten die Werte des Winkels ψ.

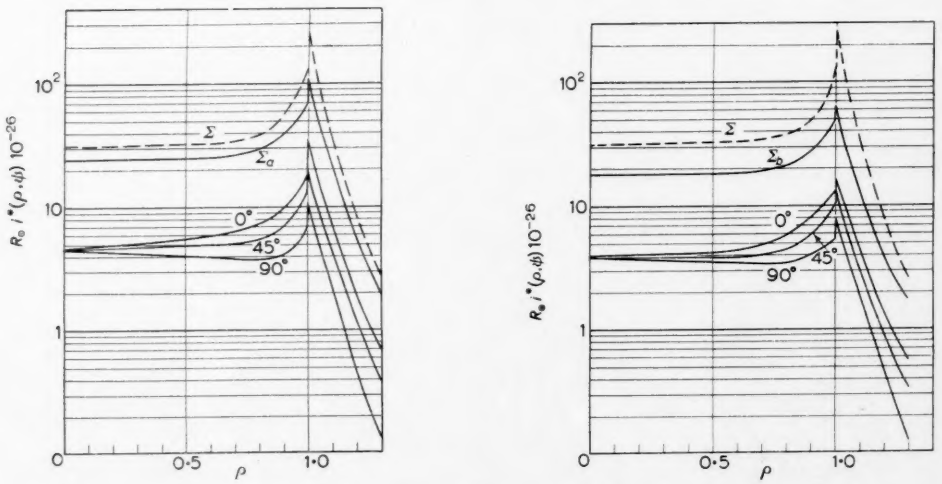

Abb. 4. Intensitätsverteilung der abgeplatteten Korona mit Absorption (b) $\tau_{00} \ldots 0{,}5$ (c) $\tau_{00} = 1$ Die angebebenen Zahlen bedeuten die Werte des Winkels ψ und $\Sigma_a\ \Sigma_b$ die jeweilige Summenkurve.

von ψ wiedergegeben. Den Verlauf der über alle ψ integrierten Intensitätsverteilung erhält man durch Addition der 5 Verteilungen für die angegebenen Werte

VOL. 12 1958

von ψ. Die Summenkurve ist ebenfalls in Abb. 4 als Kurve Σ dargestellt. Für die Restintensität bei der Totalität findet man damit Kurve 2 in Abb. 6.

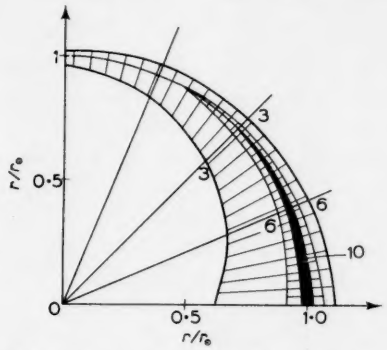

Abb. 5. Isophoten der Intensitätsverteilung der abgeplatteten rotationssymetrischen Korona mit $\tau_{00} = 1$.

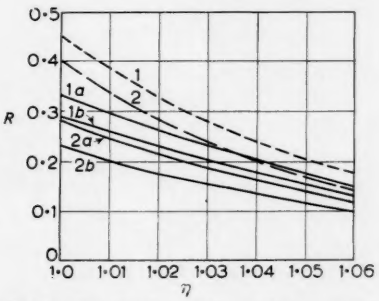

Abb. 6. Restintensität R bei der Totalität in Abhängigkeit vom Bedeckungsgrad $\eta = r_M/r_\odot$
Kugelsymmetrische Korona 1 ohne Absorption 1*a* mit $\tau_{00} = 0{,}5$
1*b* mit $\tau_{00} \dots 1$
2*a* mit $\tau_{00} \dots 0{,}5$
2*b* mit $\tau_{00} = 1$
Rotationssymmetrische abgeplatteten Korona 2 ohne Absorption

(b) *Berücksichtigung der Absorption*

Um die Absorption in Rechnung zu stellen, ist es nötig, die Elektronendichte zu kennen. Sie kann als Funktion von ρ, ψ und x nach der aus Gl. (17) folgenden Formel

$$n_e = n_{rA}\sqrt{1 - \left(1 - \frac{n_{eP}}{n_{eA}}\right)\left[1 - \left(\frac{x^2 + \rho^2\cos^2\psi}{x^2 + \rho^2}\right)^{3/2}\right]} \tag{18}$$

berechnet werden. Der Faktor $1 - n_{eP}^2/n_{eA}^2$ ist eine Funktion von r; es zeigt sich jedoch, dass er sich in dem interessierenden Bereich von $r = \sqrt{\rho^2 + x^2}$, der den wesentlichen Beitrag zur Absorption liefert, nur um etwa $\pm 5\%$ ändert. Bei festgehaltenem Winkel ψ ist das Verhältnis n_e/n_{eA} eine Funktion von ρ und x. Es ergibt sich aber weiter, dass die Abhängigkeit von diesen Parametern in dem hauptsächlich interessierenden Gebiet zwischen $\rho = 0{,}9$ und $1{,}3$ so gering ist, dass dieses Verhältnis dort durch einen konstanten Wert ersetzt werden kann. Er ist

etwa gleich der Wurzel aus dem Verhältnis $W = \int n_e^2\, dx / \int n_{eA}^2\, dx$ und hat folgende Werte

$\psi =$	22,5°	45°	67,5°	90°
$W =$	0,94	0,77	0,63	0,50

Da n_{eA} nach Gl. (15) mit der Elektronendichte der Baumbach-Formel (1) praktisch übereinstimmt, sind die optischen Tiefen τ_0 mit diesen Faktoren W zu multiplizieren. Die entsprechenden Funktionen $\varphi(\tau_0)$ sind in Abb. 2 für $\psi = 45°$ und 90° sowie $\tau_{00} = 0{,}5$ bzw. 1 (Kurven a bzw. b) eingetragen. Durch Integration über den Sehstrahl findet man dann die in Abb. 3 wiedergegebenen Schwächungskurven für die angegebenen Werte von ψ. Die Kurven für $\psi = 0$ gelten zugleich für das kugelsymmetrische Modell. Ferner ergeben sich die in Abb. 4(b) und (c) dargestellten relativen Intensitätsverteilungen als Funktion von ρ. Entsprechende Rechnungen wurden für die von Waldmeier betrachteten Zwischenwerte von ψ durchgeführt. Durch Addition der Intensitäten findet man wieder die über alle Polarwinkel ψ integrierten Intensitätsverteilungen. Sie sind ebenfalls in Abb. 4(b) und (c) als Σ_a und Σ_b dargestellt. Ein noch übersichtlicheres Bild der Intensitätsverteilung erhält man durch Darstellung der Isophoten. Sie sind in Abb. 5 für den Fall $\tau_{00} = 1$ gezeichnet. Für die Restintensität R folgen schliesslich die Kurven $2a$ und $2b$ in Abb. 6 für $\tau_{00} = 0{,}5$ und 1.

Es ist beachtenswert, dass am Sonnenrand auch bei Absorption ein Intensitätsmaximum bestehen bleibt, obwohl die optische Tiefe für randnahe Strahlen in den beiden betrachteten Fällen sogar etwa 2 bezw. 4 beträgt. Dies steht im Gegensatz zur Radiostrahlung der Sonne, bei der die Strahlungsintensität für optische Tiefen $\gg 1$ gleich der eines schwarzen Körpers wird, dessen Temperatur gleich der Elektronentemperatur der Korona ist. Der Fall $\tau \gg 1$ tritt im Gebiet der m-Wellen ein; es ist dann kein heller Rand vorhanden. Der Unterschied rührt daher, dass im Gebiet der Radiowellen der Kirchhoffsche Satz anwendbar ist, bei Röntgenstrahlen hingegen nicht. Indem man in die Formel für die emittierte Strahlungsintensität (ε_ν Emissions koeffizient)

$$J_\nu = \int \varepsilon_\nu\, e^{-\int_0^x k_\nu dx}\, dx \tag{19}$$

in bekannter Weise die optische Tiefe $\tau_\nu = \int_0^x k_\nu\, dx$ einführt, erhält man

$$J_\nu = \int \frac{\varepsilon_\nu}{k_\nu}\, e^{-\tau_\nu}\, d\tau_\nu \tag{19a}$$

Wenn die Bedingung thermodynamischen Gleichgewichts wenigstens nähdrungsweise erfüllt ist, kann man statt des Quotienten ε_ν/k_ν die Kirchhoff-Planck-Funktion B_ν einführen; dann geht J_ν für $\tau_\nu \gg 1$ in B_ν über. Bei Röntgenstrahlung aber ist diese Bedingung nicht erfüllt, da die Zahl der emittierten Photonen keineswegs gleich der Zahl der absorbierten ist. Die Anregung und damit die Emission erfolgt in der ungestörten Korona wie die Ionisation durch Elektronenstösse und ist damit proportional zu $n_i n_e$, *d.h.* $\varepsilon_\nu \sim n_e^2$. Hingegen ist die Zahl der Absorptionen proportional zu n_i und damit zu n_e, d.h. $k_\nu \sim n_e$. Durch Integration über alle Frequenzen folgt dann eben aus Gl. (19) die frühere Gl. (14) mit (10).

VOL. 12 1958

Die folgende Abschätzung zeigt, dass die Strahlungsintensität der Linien um viele Grössenordnungen kleiner ist, als der thermischen Strahlung eines innerhalb der Linien schwarzen Körpers entsprechen würde. Nach dem Planckschen Gesetz ergibt sich für $T = 7 \cdot 10^5$°K und das Wellenlängen-Intervall 1 cm $J_\lambda \approx 10^{25}$ erg/cm³ sec. Da die Breite der Röntgenlinien (ELWERT, 1952) etwa 10^{-2} Å $= 10^{-10}$ cm beträgt, ist die Strahlungsintensität einer schwarzen Linie etwa 10^{15} erg/cm² sec. Vernachlässigt man die Randaufhellung der Strahlung und nimmt konstante Intensität über die Sonnenscheibe an, so erhält man in Erdentfernung r durch Multiplikation mit $\pi(R_\odot/r)^2 = 6 \cdot 10^{-5}$ eine Strahlungsintensität von etwa 10^{11} erg/cm² sec. Die Intensität der stärksten Linie ist in Erdentfernung von der Grössenordnung 10^{-2} erg/cm² sec, also um ungefähr 13 Grössenordnungen kleiner als bei schwarzer Strahlung.

Nach Abschnitt 4 der genanten Arbeit des Verfassers enthält die Linienstrahlung unterhalb von etwa 100 Å wesentlich mehr Intensität als die kontinuierliche Strahlung. Die Energie der Linien ist etwa 3 mal grösser als die der gesamten kontinuierlichen Emission unterhalb von 900 Å, welche aber hauptsächlich Beiträge zur Bildung der F-Schicht liefern wird. Bezeichnet man die gesamte Restintensität bei der Totalität mit R^*, so gilt für die bei der Bildung der E-Schicht wirksame Röntgenstrahlung

$$R^* \leqq R_L\left(1 + \frac{1}{4}\frac{R_K - R_L}{R_L}\right), \tag{20}$$

wobei R_L die Restintensität für die Linienstrahlung unter Berücksichtigung der Absorption und R_K die Restintensität für die kontinuierliche Strahlung bedeutet. Da nach Abb. 5 $(R_K - R_L)/R_L < 0{,}5$ ist, sind die Werte von R^* bei $\eta = 1{,}06$ maximal etwa um 1–2%, bei $\eta = 1$ maximal um etwa 3% höher als die von R_K; die Restintensität R^* wird also gegenüber R_L praktisch kaum geändert. Da der effektive Wert von τ_{00} nicht genau bekannt ist, bleibt noch eine gewisse Unsicherheit. Wie schon in Abschnitt 2b bemerkt wurde, liegt er aber wahrscheinlich zwischen 0,5 und 1. Man erhält dann für das rotationssymmetrische Modell $R^* \approx 17\%$ bis 22% bei $\eta = 1{,}02$ und $R^* \approx 10\%$ bis 12% bei $\eta = 1{,}06$.

Es ist jedoch zu beachten, dass dieses Ergebnis wesentlich die Gültigkeit des Waldmeierschen Modells der Dichteverteilung der Elektronen voraussetzt. Im Gebiet der Radiostrahlung der Korona bestehen noch Unterschiede zwischen der nach diesem Modell für 20 cm Wellenlänge berechneten Interferometerbeobachtungen von CHRISTIANSEN und WARBURTON (1955) für 21 cm Wellenlänge abgeleiteten Verteilung. Ob sie durch die Antennenkorrektur allein bedingt sind, ist noch nicht entschieden. Es ist deshalb auch möglich, dass die Restintensität etwas kleiner ist, als die oben angegebenen Werte. Ausserdem ist zu bemerken, dass die Elektronendichte der Modelle den mittleren Zustand der Korona beschreibt, von dem im Einzelfall Abweichungen auftreten können. Insbesodere können sich Zentren erhöhter Strahlungsintensität bilden. Solche lokale Quellen wurden in Radiofrequenzgebiet bei Sonnenfinsternissen und mit Interferometern beobachtet; sie werden koronalen Kondensationen zugeschrieben. Wie vom

Verfasser (ELWERT, 1955) gezeigt wurde, sind koronale Kondensationen auch lokale Quellen erhöhter Röntgenemission.

4. VERGLEICH MIT DEN BEOBACHTUNGEN

Verschiedene Autoren beobachteten den zeitlichen Verlauf der Elektronendichte in der E-Schicht während totaler Sonnenfinsternisse und schlossen aus diesen Beobachtungen auf die Restintensität der ionisierenden Strahlung während der Totalität und lokale Strahlungsquellen. Bei der Finsternis im Jahre 1952 fand MINNIS (1955, 1956) dass nur etwa 64% der Strahlung einer gleichförmig emittierenden Fläche zugeschrieben werden kann, während 25% von einer schmalen ringförmigen hellen Fläche in der Nähe des Westrandes der Sonnenscheibe stammt. Etwa 8% wurden von einem Gebiet in der Nähe des Ostrandes und 3% von einer randnahen Quelle zwischen dem Pol und dem Westrand ausgestrahlt. Zu ähnlichen Resultaten kam PIGGOTT (1952) bei derselben Finsternis. Nach ihm stammten 67% von der Scheibe, 25% von einem schameln Emissionsgebiet am Westrand und 8% von einer Quelle in der Nähe des Ostrandes. Die Restintensität bei der Totalität wird also etwas unterhalb von 25% liegen. Während die Sonnenaktivität im Jahre 1952 noch ziemlich gross war, fiel die Finsternis im Jahre 1954 in eine Zeit geringer Aktivität. Nach MINNIS wurde die beste Deutung der Beobachtungen unter der Annahme einer Aufhellung am West- und Ostrand und einer Verdunkelung in der Nähe der Pole erzielt; nach seinen Angaben ist von einer gleichförmig hellen Scheibe mit 92% der Gesamtintensität an den Polen insgesamt 6% abzuziehen, so dass bei der Totalität 86% der Strahlung abgedeckt sind und 14% übrig bleiben, die vom Ost- und Westrand geliefert werden.

Die Sonnenfinsternis von 1955 fällt ebenfalls in das Sonnenfleckenminimum. Nach MINNIS ist zu vermuten, dass mindestens etwa 13% der ionisierenden Strahlung von anderen Quellen als der Sonnenscheibe stammen. BIBL und DELOBEAU (1956) finden ebenfalls, dass es zur Deutung der Phänomene bei totalen Sonnenfinsternissen nötig ist, eine wirksame Fläche der Reststrahlung anzunehmen; sie vermuten eine Vergrösserung der Sonnenscheibe um etwa 8% gegenüber der sichtbaren Scheibe. Zusammenfassend kam RATCLIFFE (1956) bei dem Symposium über *Solar Eclipses and the Ionosphere* zu dem Schluss, dass eine Deutung der meisten Beobachtungen unter der Annahme möglich ist, dass 10 bis 15% der ionisierenden Strahlung bei der Totalität übrigbleiben.

Die vorliegende Untersuchung zeigt, dass während der Totalität eine Restintensität der Röntgenstrahlung der ungestörten Korona existiert, welche gerade etwa von der Grösse ist, auf welche die Beobachtungen in noch nicht sehr genauer Weise schliessen lassen. Im Einzelfall kommt es jedoch auf das Verhältnis des Mondradius zum Sonnenradius an. Sind lokale Quellen vorhanden, so sind sie natürlich bei der Berechnung der Reststrahlung zu berücksichtigen. Da die Quellen i.a. vom Mond abgedeckt werden, wird die bei der Totalität übrigbleibende prozentuale Intensität verkleinert. Liefern sie p% der Normalintensität, so ist die Restintensität $(1 - p)R^*$.

Infolge der Tatsache, dass der Zustand der Korona sich dauernd ändert und die Modelle eine mittlere Korona beschreiben, kann eine Übereinstimmung zwischen Beobachtung und Theorie nur bei Mittelung über mehrere Beobachtungen erwartet

VOL. 12 1958

werden. Es zeigt sich aber, dass bei den beiden Finsternissen, bei denen $\eta = 1{,}02$ ist, der theoretische Wert von etwa 20% zwischen dem aus den Beobachtungen gewonnenen von nahezu 25% im Jahre 1952 und 14% im Jahre 1954 liegt. Bei der Finsternis von 1955 ist $\eta = 1{,}06$; der theoretische Wert von 10% bis 12% stimmt mit dem experimentellen von etwa 13% fast überein. Ausserdem liefert die Theorie die mehrfach beobachtete Aufhellung des Ost- und Westrandes.

References

Baumbach S.	1937	*Astr. Nachrichten* **263,** 121.
Bibl K. und F. Delobeau	1956	*Z. Geophys.* **21,** 215.
Christiansen W. N. und Warburton F. A.	1955	*Amst. J. Phys.* **8,** 474.
Elwert G.	1952	*Z. Naturf.* **7a,** 432.
Elwert G.	1955	*Z. Astrophys.* **38,** 143.
Hulburt O. E.	1955	*Naval Research Laboratory Report* 4600.
Minnis C. M.	1955	*J. Atmosph. Terr. Phys.* **6,** 91; *Rep. Ionosph. Res. Japan* **4,** 53.
Minnis C. M., in Beynon W. J. G., und Brown G. M.	1956	*Solar Eclipses and the Ionosphere* p. 306, London.
Petri W.	1952	*Forschungsberichte d. Kommission Obs. Wendelstein* p. 2. München.
Piggott W. R.	1952	*Proc. Mixed Comm. Ionosph.* p. 42.
Ratcliffe J. A.	1956	*Solar Eclipses and the Ionosphere.* London.
Unsöld A.	1955	*Physik der Sternatmosphären* Springer, Berlin–Göttinger–Heidelberg.
Waldmeier M.	1955	*Z. Astrophys.* **38,** 143.
Wallis G.	1957	*Z. Naturf.* **12a,** 337.

Journal of Atmospheric and Terrestrial Physics, 1958, Vol. 12, pp. 200 to 205. Pergamon Press Ltd., London

Interpretation of rotational temperatures of auroral N_2^+ bands—I

Proton impact at intermediate energies*

F. L. Roesler,† C. Y. Fan‡ and J. W. Chamberlain
Yerkes Observatory, University of Chicago, Williams Bay, Wisconsin

(*Received* 29 *November* 1957)

Abstract—Laboratory experiments have been performed to find the rotational temperature of the first negative bands of N_2^+ when nitrogen is excited by proton collisions at energies between 10 and 30 keV. In this range there is little difference between the gas temperatures and the apparent (rotational) temperatures obtained by proton excitation. The question of the correspondence between auroral N_2^+ temperatures and the gas temperatures in the high atmosphere is reviewed. In spite of the agreement reported here, the matter is still not definitely settled. For a confident interpretation of auroral N_2^+ band structure, further experimental work is required.

1. Introduction

Potentially, spectroscopic temperatures are a powerful tool for studying the upper atmosphere. Practically, however, many of these temperature determinations have been a great disappointment, with difficulties of two types hampering their usefulness. Firstly, there are purely observational and instrumental obstacles. For the most part, the dispersion used has been insufficient to resolve rotational structure, and exposures have been so long that there is an uncertainty in the heights and auroral forms that have been observed. However, for the first negative bands, at least, these difficulties are now being overcome by careful observing techniques and modern instrumentation.

Secondly, there has been the difficult problem of interpreting the spectroscopic temperatures in terms of the kinetic temperature of the gas. With the relative transition probabilities known or assumed, the observed intensities give immediately the relative populations of the upper levels producing the lines or bands. The problem is this: With a particular kinetic temperature and excitation mechanism, what will these relative populations be? Ordinarily for emission spectra it is not permissible to assume that these populations are given by the Boltzmann distribution for the temperature of the gas. For permitted bands the populations of the upper levels are not likely to be redistributed before emission occurs. One must then inquire into the mechanism of excitation to ascertain what the effect is on the populations of rotational levels (Oldenberg, 1934).

We have conducted experiments with proton beams fired in air; the energy range used was between 10 and 30 keV. At higher energies than these the protons are travelling much faster than the orbital electrons, so that a proton will ionize an N_2 molecule in the same fashion that a fast electron would—by ejecting the orbital electron from the molecule. But in the energy range considered, charge

* The research reported in this paper has been supported in part by the Geophysical Research Directorate of the Air Force Cambridge Research Center, Air Research and Development Command, under Contract AF 19(122)-480 with the University of Chicago.

† Present address: University of Wisconsin, Madison, Wisconsin.

‡ Present address: University of Arkansas, Fayetteville, Arkansas.

VOL. 12 1958

transfer is likely to be the most important process for nitrogen ionization, with a bare proton capturing an orbital electron to form N_2^+ and H. A transfer of angular momentum during the collision would seem quite possible (CHAMBERLAIN and MEINEL, 1954; FAN, 1956a) with a resulting increase in the observed temperatures. Our experiments were therefore planned to detect any such anomalous rotational temperature arising from collisions in this intermediate energy range.

2. EXPERIMENTAL

The proton accelerator has been described by FAN (1956b). It is a low-energy, linear accelerator of a simplified Cockroft–Walton type. Hydrogen gas is ionized by a radio-frequency power supply, and the protons are accelerated into the adjustable field of a permanent magnet, which deflects the beam through 15° into the absorption chamber. Proton energies between 10 keV and 30 keV were used exclusively. The gas pressure in the absorption chamber was maintained by differential pumping between 0·5 and 5·0 μ (Hg), which is comparable to the atmospheric pressure around 85 to 100 km. The beam was viewed almost end on from an off-centre window in the end of the chamber. An off-centre window keeps the beam from striking the glass (which would cause the window to fluoresce), but still allows the spectrograph to look down the length of the beam for maximum brightness.

The light from the beam was focused on the slit of the spectrograph. The spectrograph has a grating with 600 lines per millimetre and an $F/0{\cdot}8$ flat-field Schmidt camera with an objective lens 23 cm in diameter, which was designed by A. B. MEINEL. This instrument has been used extensively at Yerkes Observatory in auroral and airglow observations. It was adjusted to record the rotational bands of the $\Delta v = 0, -1, -2$, sequences of the first negative system of N_2^+ (band heads for $v' = 0$ at 3914 Å, 4278 Å, and 4709 Å, respectively) in the third order, where the dispersion is about 23 Å/mm. Most of the photometric analysis has been performed on λ4278 (0–1 band), which was both well resolved and close enough to the blazed wavelength of the grating that there was no appreciable change of intensity across the band from instrumental effects. These bands were photographed on Eastman Kodak 103*a*-0 plates with the usual precautions necessary in photographic photometry. Plates for intensity calibrations were exposed in front of a fast (70 rev/sec) rotating sector.

The intensity distribution of the rotational lines of the R-branch when N_2^+ is excited without any change in rotational angular momentum, is (HERZBERG, 1950, pp. 126, 207; BRANSCOMB, 1950)

$$I_K = C(K+1)\exp\left[\frac{-B_{v''}(K+1)(K+2)hc}{kT_{\text{rot}}}\right]. \qquad (1)$$

Here C is a constant, K is the rotational quantum number of the lower level of the optical transition, and $B_{v''}$ is the rotational constant of the ground state of N_2 (on the assumption that excitation occurs from the ground state of N_2 and not that of N_2^+). This formula differs slightly from the Boltzmann distribution for the *populations* in that the relative transition probabilities are included. We have plotted $\log_{10}[I_K/(K+1)]$ against $(K+1)(K+2)$ and fitted the points

to a straight line, with slope $-0{\cdot}625B_{v''}/T_{\mathrm{rot}}$, by a least-squares analysis. The rotational temperature obtained in this manner has been compared with the kinetic temperature of the gas. Fig. 1 is a typical tracing of the λ4278 band, which was used in the analysis.

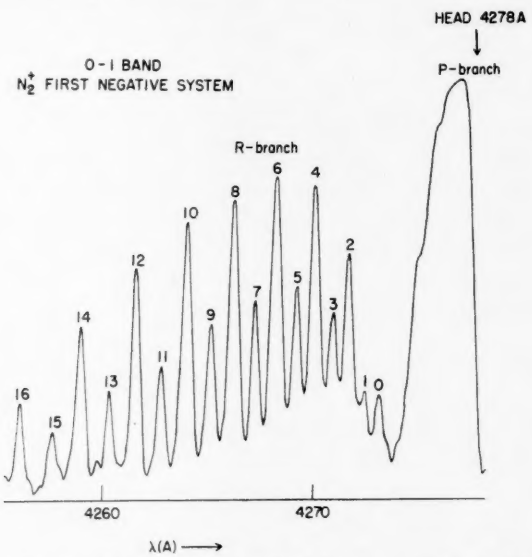

Fig. 1. Microphotometer tracings of λ4278, the (0–1) first negative band of N_2^+, as excited by proton impact. The K quantum numbers indicated in the figure refer to the lower state of the optical transition.

We found that within the 10–30 keV range of the experiments, the rotational temperature does not depend noticeably on the speed of the protons but does correspond closely to the kinetic temperature of the gas. The probable errors in the individual temperatures, derived from the least-squares analysis, were usually less than 10°K, but systematic errors are also likely to be this important. From the four best plates made at room temperature (296°K), T_{rot} was computed separately for the even and odd rotational lines. The mean value of these eight temperature determinations was $T_{\mathrm{rot}} = 305 \pm 8$°K; hence there was no significant difference between the spectroscopic and kinetic temperatures.

Fig. 2 shows some of the points used in the derivation of the rotational temperature for 10 keV protons. The lines with odd and even K values should have an intensity ratio of 1 : 2, other factors being the same (Herzberg, 1950; p. 210). The ratio in Fig. 2 is very nearly this value, which is some indication of the reliability of the photometry.

In order to substantiate the fact that the derived rotational temperature corresponded to the kinetic temperature and was not just accidentally so for a temperature around 300°K, the experiment was repeated twice under different conditions. In the first repetition, the proton beam was fired into air that had been cooled by packing the absorption chamber and inlet tube with dry ice. In the second, the chamber and inlet tube were heated by placing a jacket around

VOL. 12 1958

them and forcing steam through the jacket. In both these cases the derived temperature agreed, to within the experimental uncertainty, with the expected kinetic temperature of the gas inside the chamber.

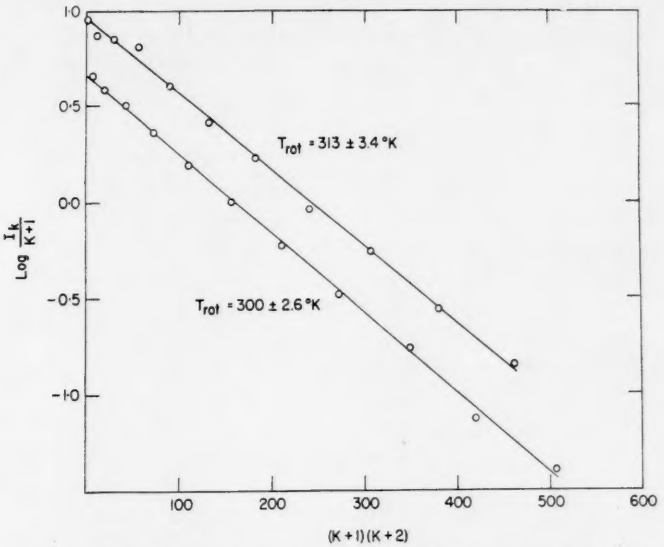

Fig. 2. Relative intensities of lines in the λ4278 band of N_2^+ for 10 keV proton excitation. Upper line, even K values; lower line, odd K values (see Fig. 1). The straight lines give the theoretical relative intensities for the indicated temperatures.

3. Discussion

Rotational temperatures of auroral N_2^+ bands observed by Vegard *et al.*, 1951; Vegard, 1956, have invariably been low (~225°K) and constant for all types and heights of aurorae. The results of various observations in Canada (Petrie, 1953; Vallance Jones and Harrison, 1955; Shepherd and Hunten, 1955; Montalbetti, 1957) have generally indicated a temperature variation with height not inconsistent with that derived from rocket studies. Vegard (1955) has maintained that the high temperatures found at Saskatoon were not indicative of high kinetic temperatures, but rather resulted from proton excitation, which seems to be more important at low than high latitudes. The recent agreement of Montalbetti's results at Churchill with those from Saskatoon cast doubt on any dependence of rotational temperature on the latitude or amount of proton influx. Nevertheless, there still remains the question of just how closely the rotational temperature coincides with kinetic temperature.

A number of experiments have been performed with this question in mind. It is often supposed that electron impact will produce little or no change in the rotation of a molecule (Massey and Burhop, 1952, p. 276) and that in a discharge at low current and low density the rotational temperature should correspond to the gas temperature, providing the rotational constant of the ground state is used in the temperature formula (Herzberg, 1950, p. 207). Indeed, the experiments of Vegard (1932) and his collaborators with cathode rays indicated that

the rotation is an accurate measurement of the gas temperature. On the other hand, discharges often indicate high rotational temperatures (e.g. see Ornstein and Van Wijk, 1928, for N_2^+ measurements), and it may be either that the gas temperature in the tube is increased by the discharge or that the rotational levels in the ground state of N_2 are excited by electron impacts (Anderson and Goldstein, 1956; Gerjouy and Stein, 1955). In the latter case, the rotational temperature would be governed by the energy of the discharge electrons and would not correctly indicate the gas temperature.

Duffendack, Revans and Roy (1934) concluded that N_2^+ bands excited by electrons in a low-voltage ($\sim$100 eV) arc had rotational temperatures governed by the energy of the electrons, and that the rotational temperature was no indication of kinetic temperature. They suggested that with simultaneous excitation and ionization, a small portion of the electron energy could go into molecular rotation. They rejected the possibility that the rotational levels of N_2 might be raised by successive electron collisions before ionization; but even if that were the case, there would still be disagreement between gas-kinetic and rotational temperatures.

The situation regarding excitation by heavy ions is almost as confusing. Vegard (1934) found that the rotational temperature exceeded the gas temperature by about 85°K when nitrogen was excited by canal rays (which consist of the positive ions and neutral particles that emerge behind the perforated cathode of a discharge) with several (less than 29) keV energy.* Branscomb, Shalek and Bonner (1954) estimated rotational temperatures between 700 and 1000°K at relatively high proton energies (100 keV).

VOL.
12
1958

And finally, this work (performed between 10 and 30 keV) and that of Carleton (1957) at low energies (3 keV) found agreement between the gas and rotational temperatures. Presumably the protons in Carleton's and our experiments excited nitrogen by charge-transfer collisions, as well as by ionizing collisions.

In the aurora if protons are important in producing ionization, they may enter the atmosphere with energies up to 500 keV. Thus, to interpret auroral measurements properly, further laboratory work seems to be required on proton excitation in the energy range 30 to 500 keV, in which accurate measurements of rotational temperatures are made. Electron excitation should also be investigated in more detail, especially at the higher energies, which may be appropriate for incident, primary electrons. We hope to report on some further experiments of this nature at a later date.

References

Anderson J. M. and Goldstein L.	1956	*Phys. Rev.* **102,** 388.
Branscomb L. M.	1950	*Phys. Rev.* **79,** 619.
Branscomb L. M., Shalek R. J. and Bonner T. W.	1954	*Trans. Amer. Geophys. Un.* **35,** 107.
Carleton N. P.	1957	*Phys. Rev.* **107,** 110.
Chamberlain J. W. and Meinel A. B.	1954	*The Earth as a Planet* (Edited by Kuiper. G. P.) p. 537. University of Chicago Press.

* The experiments of Smyth and Arnott (1930) also indicated an increased rotational temperature.

Duffendack O. S., Revans R. W. and Roy A. S.	1934	*Phys. Rev.* **45,** 807.
Fan C. Y.	1956a	*The Airglow and the Aurorae.* (Edited by Armstrong E. and Dalgarno A.) Pergamon Press, London.
Fan C. Y.	1956b	*Phys. Rev.* **103,** 1740.
Gerjouy E. and Stein S.	1955	*Phys. Rev.* **97,** 1671.
Herzberg G.	1950	*Spectra of Diatomic Molecules.* (2nd Ed.). Van Nostrand, New York, Toronto, and London
Massey H. S. W. and Burhop E. H. S.	1952	*Electronic and Ionic Impact Phenomena.* Clarendon Press, Oxford.
Montalbetti R.	1957	*Canad. J. Phys.* **35,** 831.
Oldenberg O.	1934	*Phys. Rev.* **46,** 210.
Ornstein L. S. and Van Wijk W. R.	1928	*Z. Phys.* **49,** 315.
Petrie W.	1953	*J. Atmosph. Terr. Phys.* **4,** 5.
Shepherd G. G. and Hunten D. M.	1955	*J. Atmosph. Terr. Phys.* **6,** 328.
Smyth H. D. and Arnott G. F.	1930	*Phys. Rev.* **36,** 1023.
Vallance Jones A. and Harrison A. W.	1955	*J. Atmosph. Terr. Phys.* **6,** 336.
Vegard L.	1932	*Geofys. Publ.* **9,** No. 11.
	1934	*Det Norske Ved. Akad., Avh. I, Matematisk-Naturvidenskapelig Kl.,* No. 12.
	1955	*Geofys. Publ.* **19,** No. 4.
	1956	*Geofys. Publ.* **19,** No. 9.
Vegard L., Tönsberg E. and Kvifte G.	1951	*Geofys. Publ.* **18,** No. 4.

OL.
12
958

Journal of Atmospheric and Terrestrial Physics, 1958, Vol. 12, pp. 206 to 210. Pergamon Press Ltd., London

The double field-mill

M. SMIDDY and J. A. CHALMERS
Physics Department, Durham Colleges in the University of Durham

(*Received* 16 *August* 1957)

Abstract—A double field-mill is described which is automatically brought to the potential of its surroundings and also registers the potential gradient at a point above ground level.

1. INTRODUCTION

THE traditional method of measuring the potential gradient in the earth's atmosphere has been to use a radioactive, or other, potential equalizer to obtain the potential at a known distance from the earth's surface. It has been shown, e.g. MÜHLEISEN (1951), that this method has grave disadvantages, and it can clearly at best do no more than give the mean potential gradient over a certain height.

For some purposes, e.g. for the determination of space charge, it is necessary to measure the potential gradient, neither at the earth's surface nor the mean value over a height from the surface up, but the actual values at definite heights; to achieve this, SCRASE (1935) used a pair of collectors at a fixed separation in height and has altered the mean height of the pair.

Modern practice in the measurement of the potential gradient near the earth's surface has tended towards the use of instruments of the "field machine" type which, when placed in the plane of the earth's surface, give the potential gradient at the surface. Such an instrument if placed above the earth's surface would distort the field and so not give an accurate value of the potential gradient.

The present work is concerned with the development of a double field machine which can automatically reach the potential of its surroundings, thus avoiding field distortion, and at the same time giving a measure of the potential gradient at a single level.

2. GENERAL THEORY

Consider a thin disk of area A placed with its surfaces horizontal. If the disk carries no resultant charge and is placed where there is a vertical potential gradient F, the upper surface of the disk will carry a charge $-Q = -\varepsilon_0 FA$ and the lower surface a charge $+Q$. ε_0 is the space permittivity of $8{\cdot}854 \times 10^{-12}$ F/m if m.k.s. units are used and must be replaced by $1/4\pi$ if c.g.s.e.s.u. are used.

If, on the other hand, the disk is situated in a region with no external field and carries a total charge of $+2q$, then each surface carries a charge of $+q$.

Electrostatic theory shows that, if the disk is situated in a field and carries a resultant charge, then it is possible to add the two results above. Thus the upper surface carries a charge $X = -Q + q$ and the lower surface a charge $Y = +Q + q$. The measurement of $Y - X$ thus gives $2Q$, irrespective of the value of q. This is the principle of the method used by GUNN (1948), GISH and WAIT (1950) and others

VOL. 12 1958

to obtain the potential gradient by measurements with two field-mills on an aircraft; DEMON (1953) has also used this method close to the ground.

Although the measurement of $Y - X$ gives the value of Q, and hence of F independent of q, this does not fulfil the requirements, since, unless q is zero, the field is distorted and space charges will not be in their normal positions. Fig. 1 illustrates the distortion of the lines of force when $q = \pm Q$.

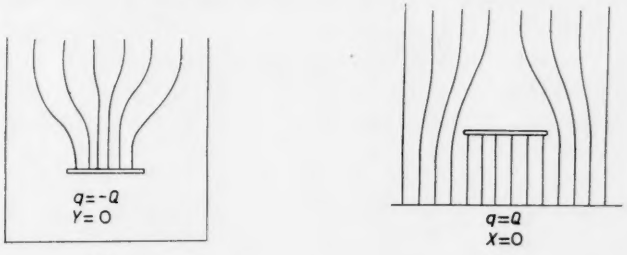

(a) (b)

Fig. 1

Since $X + Y = 2q$, it is necessary to arrange that this becomes zero, in which case the distortion of the field becomes reduced as far as possible. If $X + Y$ is positive, there must be a reduction of q, i.e. a reduction of the potential of the disk relative to earth, and an increase if $X + Y$ is negative.

Provided that the sign of F is known, it is not necessary to know the signs of X and Y. It is easy to see that, if F and so Q is positive, then when q is positive, whether greater or less than Q, $|X| < |Y|$, and when q is negative, $|X| > |Y|$, so that the potential of the disk can be regulated by the relative values of $|X|$ and $|Y|$. On the other hand, when F and Q are negative, then with q positive, $|X| > |Y|$ and with q negative $|X| < |Y|$; so, when F changes sign, the regulating potential must also change sign.

3. APPARATUS

The field-mill used is shown in Fig. 2. It is of the "sector" type described by MAPLESON and WHITLOCK (1955), but there are two sets of vanes on the same shaft. The vanes were made of stainless steel to avoid variations in contact potential, and the vane shaft was "earthed" to the mill case by carbon brushes bearing on to brass bushes.

The rotating vanes are driven externally by a belt-drive; the inclusion of a motor in the mill itself would have posed a difficult problem in regard to the insulation of the motor and its leads from the rest of the mill structure, as well as increasing the vertical size of the mill. When assembled, the mill has horizontal dimensions of 22 × 22 cm, with 20 cm between the rotating vanes.

The mill is attached to the centre of a metal girder 9 m long. The girder is fixed at each end to "Tufnol" bars, attached to wooden posts. It is hoped that the wood will be neither so good a conductor as to provide an artificial earth, nor so good an insulator as to retain electrostatic charges; either extreme would give rise to distortion of the field. The girder is at the same potential as the mill and, when the apparatus functions as desired, this is the potential of the surroundings

and so there is no field distortion. The belt-drive runs horizontally close to the girder and so would not be expected to carry any charge; a small effect on the mill, attributable to the belt, was removed by a metal shield round the belt close to the mill. Fig. 3 shows the mill in position.

Each end of the mill gives an a.c. output which is taken along the girder to a junction box where this output, at the mill potential, is converted into an output at earth potential by a blocking condenser (0·001 μF) and fed to the input impedance of $10^8\ \Omega$ and 200 pF. This junction box is carried on the "Tufnol" bars at the end of the girder. The signal is next taken to a cathode follower, situated half-way up the wooden post and then inside the laboratory, where it is amplified by a two-stage resistance-capacitance coupled amplifier, with negative feedback, having an overall amplification of 86·3.

The signal from each end of the mill is fed into a similar amplifier, these being matched to have the same linear amplification over a range of inputs of 0–1·0 V. Since the sensitivity of the mill is about 100 μV for 1 V/m, the amplifiers work linearly for potential gradients up to 10,000 V/m.

As discussed in Section 2, it is not necessary to know the signs of the mill outputs; this is very convenient, as it would be difficult, because of insulation problems, to rectify the amplified output by mechanical commutation on the mill, nor would a reference generator, as used by Mapleson and Whitlock (1955), be easy to incorporate.

The signals from the two ends of the mills are rectified and their difference is applied to a Honeywell–Brown continuous balance-recording potentiometer, adapted for the purpose by replacing the standard low-resistance slidewire by a 1 MΩ slidewire, well insulated from the rest of the apparatus. A high potential can be applied across the slidewire and a lead from the operating point taken direct to the girder and mill. The record then shows the position on the slidewire and hence the potential applied to the mill to give balance. As is shown by the theory of Section 2, this will function while the potential gradient remains positive, but not if it changes sign. It is therefore necessary to reverse the potential across the slidewire when the atmospheric potential gradient changes sign; at present this has to be carried out manually, but it is hoped to arrange automatic operation for this.

When the mill potential is correctly set, then the output from one end of the mill gives a measure of the potential gradient, so that this can be measured independently.

In operation, care is necessary to ensure that the time constants of the various parts of the apparatus shall be correctly related, otherwise there may be either instability or "hunting". To avoid this, theoretical calculations and "trial and error" tests were used to find suitable resistance–capacitance combinations to insert across the recorder input and from the mill to earth. Fig. 4 shows the general "flow diagram" and Figs. 5 and 6 the circuit details.

4. Results

Fig. 7 shows a trace of the balancing potential applied to the mill at a height of 1 m, during conditions of rain of moderate intensity. The second trace is that from a field-mill situated in the plane of the earth's surface about 10 m away.

VOL. 12 1958

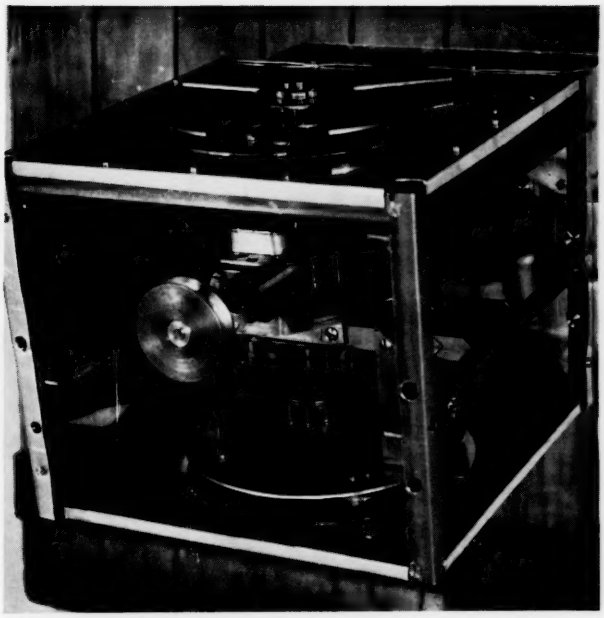

Fig. 2

Fig. 3

VOL.
12
1958

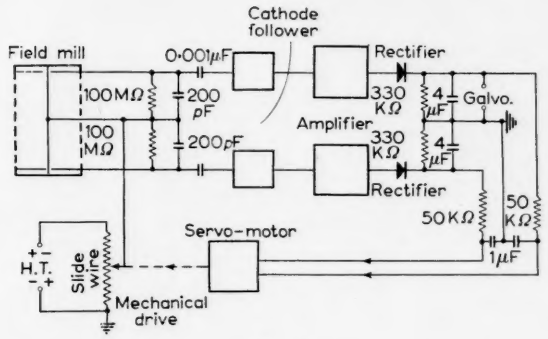

Fig. 4.

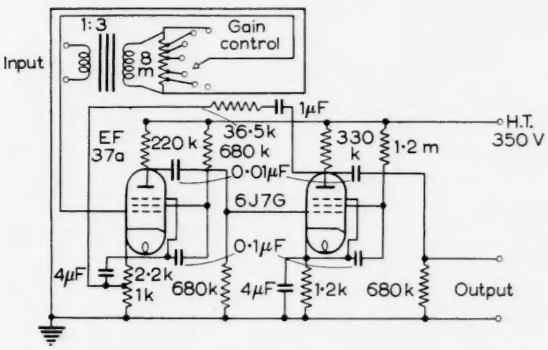

Fig. 5.

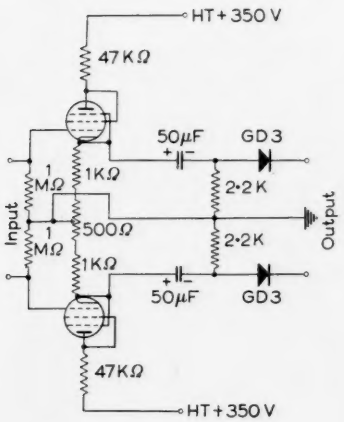

Fig. 6.

As can be seen, the double field-mill follows the changes very satisfactory, and a detailed comparison of two such records over a period of one hour shows no discrepancies beyond those depending on a difference in response times.

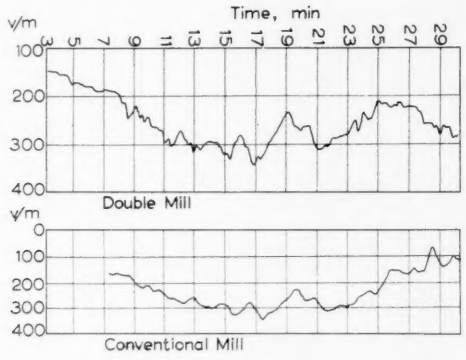

Fig. 7.

Acknowledgements—The work here reported has been sponsored by the Geophysics Research Directorate of the Air Force Cambridge Research Center, Air Research and Development Command, U.S.A.F., under Contract AF61 (514)–891, through the European Office, ARDC.

The authors wish to thank Mr. C. MACLEAN for help in the construction of the apparatus and Mr. M. W. RAMSAY, B.Sc., for help in the comparison records.

VOL.
12
1958

REFERENCES

DEMON L.	1953	*J. Res. C.N.R.S.* **24,** 126–127.
GISH O. H. and WAIT G. R.	1950	*J. Geophys. Res.* **55,** 473–484.
GUNN R.	1948	*J. Appl. Phys.* **19,** 481–484.
MAPLESON W. W. and WHITLOCK W. S.	1955	*J. Atmosph. Terr. Phys.* **7,** 61–72.
MÜHLEISEN R.	1951	*Z. Naturf.* **6,** 667–671.
SCRASE F. J.	1935	*Geophys. Mem., Lond.* **67**

Journal of Atmospheric and Terrestrial Physics, 1958, Vol. 12, pp. 211 to 215. Pergamon Press Ltd., London

RESEARCH NOTES

Relative vibrational transition probabilities and r-centroids for the Meinel ($A^2\Pi$—$X^2\Sigma$) band system of N_2^+

(*Received* 10 *December* 1957)

THE recent measurements of OMHOLT (1957) upon intensities $I_{v'v''}$ of the red and near infra-red auroral spectrum have provided valuable information from which may be derived smoothed relative vibrational transition probabilities $p_{v'v''}$ for the Meinel System ($A^2\Pi$—$X^2\Sigma$) of N_2^+ together with an indication of the dependence of electronic transition moment $R_e(r)$ with internuclear separation r for the system.

The purposes of this note are therefore (*a*) to provide a set of smoothed relative vibrational transition probabilities $p_{v'v''}$ and intensities at infinite temperature I_∞ (equal population $N_{v'}$ of upper levels v') for the strongest bands of the system, (*b*) to provide a set of r-centroids $\bar{r}_{v'v''}$ for the system and (*c*) to discuss the probable behaviour with internuclear separation r of the electronic transition moment $R_e(r)$.

The method has been used previously for other band systems, is described in detail elsewhere (NICHOLLS, 1956a,b, 1958) and is briefly as follows:

The integrated intensity $I_{v'v''}$ of a band in emission is given in equation (1)

$$I_{v'v''} = KN_{v'}E^4_{v'v''}R_e^2(\bar{r}_{v'v''})q_{v'v''}, \tag{1}$$

from which it is clear that plots of $(I_{v'v''}/q_{v'v''}E^4_{v'v''})^{\frac{1}{2}}$ vs. $\bar{r}_{v'v''}$ for each of the v'' progressions ($v' =$ constant) will delineate the variation of $R_e(r)$ with r. $q_{v'v''}$ is the Franck–Condon factor for the band and $E_{v'v''}$ is its energy quantum. By a rescaling procedure which employs factors derived from the quotients of areas under the segments which overlap in r of plots for adjacent progressions, all of the plots may be placed upon a common ordinate scale. The factors take account of the difference from progression to progression of $(N_{v'})^{\frac{1}{2}}$. An empirical curve, which can be fitted to this data by a least-squares criterion, provides an expression for $R_e(r)$ from which smoothed relative vibrational transition probabilities

$$p_{v'v''} = R_e^2(\bar{r}_{v'v''})q_{v'v''} \tag{2}$$

may be calculated. These are superior to probabilities ($I_{v'v''}/N_{v'}E^4_{v'v''}$ or $I_{v'v''}/E^4_{v'v''}$) derived from individual band intensities. The large variation of experimental error between data for intense and weak bands is substantially reduced by using equation (2) in which all of the measured intensities have played a part in the determination of the smoothed form of $R_e(r)$.

The basic data used are given in Table 1.

The integrated band intensities $I_{v'v''}$ were measured by photographic photometry of auroral spectra by OMHOLT, the r-centroids $\bar{r}_{v'v''}$ have been calculated by the "quadratic equation" method of NICHOLLS and JARMAIN (1956) using the molecular constants of DOUGLAS (1953) for the $A^2\Pi$ state and from HERZBERG (1950) for the $X^2\Sigma$ state. The band wavelengths $\lambda_{v'v''}$ are the average of the values for the R_2 and Q_1 heads given by DOUGLAS

Table 1. Basic data for the Meinel ($A^2\Pi$—$X^2\Sigma$) system of N_2^+

v' \ v''	0	1	2	3	4	5
	—	—	—	—	—	—
	11,085	14,608	—	—	—	—
0	$1{\cdot}15_1$	$1{\cdot}19_1$	$1{\cdot}23_8$	$1{\cdot}29_3$	$1{\cdot}35_2$	$1{\cdot}47_4$
	$0{\cdot}39_2$	$0{\cdot}40_0$	$0{\cdot}16_6$	$0{\cdot}03_6$	$0{\cdot}00_5$	$0{\cdot}00_0$
	—	—	—	—	—	—
1	9179	11,468	15,206	—	—	—
	$1{\cdot}12_2$	$1{\cdot}15_6$	$1{\cdot}19_9$	$1{\cdot}24_6$	$1{\cdot}30_2$	$1{\cdot}36_8$
	$0{\cdot}33_1$	$0{\cdot}00_2$	$0{\cdot}26_6$	$0{\cdot}28_0$	$0{\cdot}10_2$	$0{\cdot}01_8$
	78	—	—	—	—	—
2	7850	9467	11,875	15,848	—	—
	$1{\cdot}09_3$	$1{\cdot}12_6$	$1{\cdot}16_3$	$1{\cdot}20_6$	$1{\cdot}25_4$	$1{\cdot}31_2$
	$0{\cdot}17_0$	$0{\cdot}15_3$	$0{\cdot}07_5$	$0{\cdot}08_6$	$0{\cdot}29_2$	—
	11	38	—	—	—	—
3	6872	8080	9771	12,309	16,815	—
	$1{\cdot}06_7$	$1{\cdot}09_7$	$1{\cdot}13_2$	$1{\cdot}17_0$	$1{\cdot}12_3$	$1{\cdot}26_4$
	$0{\cdot}06_9$	$0{\cdot}19_6$	$0{\cdot}01_9$	$0{\cdot}15_5$	—	—
	—	10·3	12	—	—	—
4	6121	7059	8321	10,093	12,934	17,582
	$1{\cdot}04_4$	$1{\cdot}07_2$	$1{\cdot}10_4$	$1{\cdot}13_9$	$1{\cdot}17_8$	$1{\cdot}22_2$
	$0{\cdot}02_5$	$0{\cdot}13_3$	$0{\cdot}12_1$	—	—	—
	—	—	—	—	—	—
5	5528	6283	7261	8575	10,543	13,438
	$1{\cdot}02_3$	$1{\cdot}04_9$	$1{\cdot}07_9$	$1{\cdot}11_1$	$1{\cdot}14_7$	$1{\cdot}18_6$
	$0{\cdot}00_8$	$0{\cdot}06_7$	$0{\cdot}14_1$	—	—	—

v' \ v''

$I_{v'v''}$ (arbitrary units)
$\lambda_{v'v''}$(A)
$\bar{r}_{v'v''}$(A)
$q_{v'v''}$

(1953) and the Franck–Condon factors $q_{v'v''}$ are those of FRASER, JARMAIN and NICHOLLS (1954) computed upon a Morse model. Dr. FRASER has also kindly computed $q_{5,2}$, which was not previously available.

Plots were made for the $v' = 2$, 3, 4 progressions of $(I_{v'v''}\lambda^4_{v'v''}/q_{v'v''})^{\frac{1}{2}}$ vs. $\bar{r}_{v'v''}$, which resulted in two almost parallel straight lines ($v' = 3$, 4) and an isolated point ($v' = 2$).

A factor of 0·634 was used to scale the (2, 0) point on to the $v' = 3$ line and a factor of 1·44 (derived as described above) was used to scale the $v' = 4$ line on to the $v' = 3$ line. These scaling factors are equivalent to relative populations $N_2 : N_3 : N_4 = 1 : 0{\cdot}4 : 0{\cdot}2$. The fact that a semilogarithmic plot of these populations vs. vibrational energy results in a straight line whose slope is consistent with an excitation "temperature" in the $A^2\Pi$ state of 7300°K, is one justification of the scaling procedure for the isolated point (2, 0).

VOL. 12 1958

The "temperature" is of the same magnitude as those reported for other auroral band systems (CHAMBERLAIN and MEINEL, 1954).

The resulting points after scaling, lie with negligible scatter upon the least-squares line (in "standard" form, NICHOLLS, 1956b)

$$R_e(r) = \text{const}\ (-1 + 0{\cdot}987r)$$

$$1{\cdot}067\ \text{Å} < r < 1{\cdot}104\ \text{Å}$$

Thus over the above range of r (which corresponds to 6800 Å $< \lambda_{v'v''} <$ 8350 Å) there is a significant variation of the electronic transition moment with internuclear separation.

Table 2. Smoothed relative vibrational transition probabilities $p_{v'v''}$ and intensities at infinite temperature $I_{\infty v'v''}$ for the Meinel ($A^2\Pi$—$X^2\Sigma$) system of N_2^+

v' \ v''	0	1	2
2	786 882 7850		
3	146 279 6872	1000 1000 8080	
4	17 53 6121	335 575 7059	725 644 8321
5		8 21 6283	444 680 7261

v'	v''
	$p_{v'v''}$ (arbitrary units)
	$I_{\infty v'v''}$ (arbitrary units)
	$\lambda_{v'v''}$(A)

Smoothed relative vibrational transition probabilities $p_{v'v''}$ have been calculated (normalized to $p_{31} = 1000$) from equations (2) and (3) and are presented in Table 2 for bands which lie in the region 6120 Å $< \lambda_{v'v''} <$ 8320 Å. A reasonable extrapolation has been made for the (40) and (51) bands, of equation (3) as far as $r = 1{\cdot}044$ Å, $\lambda = 6121{\cdot}3$ Å. Table 2 also includes the intensities at infinite temperature $I_{\infty v'v''} = p_{v'v''}/\lambda^4_{v'v''}$ (equal population in all v') normalized to $I_{\infty 31} = 1000$)

BAGARIAZKY and FEDOROVA (1956) have recently reported observations upon the Meinel system of N_2^+ in the auroral spectrum, using infra-red image converter techniques. Their failure to observe the (0, 0) band at about 1·1 μ led them to suggest that the original vibrational assignment of the $A^2\Pi$ levels by MEINEL (1950, 1951a) should be reconsidered and that his (MEINEL, 1951b) and DOUGLAS's (1953) later assignments, which place $\lambda_{0,0}$ at about 1·1 μ should be treated with caution.

This raises the possibility that v' should perhaps be decreased by one unit. However the

existence of a strong H_2O absorption band at 1·11 μ (GOLDBERG, 1954) may explain the apparent absence of the (0, 0) band in auroral spectra.

Further observations, including intensity measurements, upon more bands of the Meinel system in the laboratory are clearly needed and are in progress. The author would like to acknowledge valuable correspondence with Dr. OMHOLT.

R. W. NICHOLLS

Department of Physics
University of Western Ontario
London, Canada

REFERENCES

BAGARIASKY B. A. and FEDOROVA N. I.	1956	*The Airglow and Aurorae* (Edited by E. ARMSTRONG and A. DALGARNO) p. 174. Pergamon Press, London.
CHAMBERLAIN J. W. and MEINEL A.B.	1954	*The Earth as a Planet* (Edited by G. KUIPER) p. 514. University of Chicago Press.
DOUGLAS A. E.	1953	*Astrophys. J.* **117,** 380.
FRASER P. A., JARMAIN W. R. and NICHOLLS R. W.	1954	*Astrophys. J.* **119,** 286.
GOLDBERG L.	1954	*The Earth as a Planet* (Edited by G. KUIPER) p. 434. University of Chicago Press.
HERZBERG G.	1950	*The Spectra of Diatomic Molecules* (2nd. Ed.) Van Nostrand, New York.
MEINEL A. R.	1950	*Astrophys. J.* **112,** 562.
	1951(a)	*Astrophys. J.* **113,** 583.
	1951(b)	*Astrophys. J.* **114,** 431.
NICHOLLS R. W.	1956(a)	*The Airglow and Aurorae* (Edited by E. ARMSTRONG and A. DALGARNO) p. 302. Pergamon Press, London.
	1956(b)	*Proc. Phys. Soc.* A **69,** 741.
	1958	*Ann. Geophys.* In press.
NICHOLLS R. W. and JARMAIN W. R.	1956	*Proc. Phys. Soc.* A **69,** 253.
OMOLT A.	1957	*J. Atmosph. Terr. Phys.* **10,** 320.

VOL. 12 1958

Magnetic activity following a solar flare

(*Received* 6 *November* 1957)

IN a recent analysis, WATSON (1957) has investigated the time intervals between the occurrence of solar flare effects (crochets) and the sudden commencements of marked geomagnetic disturbances following within three days. Since the time intervals give a random distribution, he concludes that either there is no increase of magnetic activity due to a solar flare or that the increase is a very rare event.

This result is not unexpected in view of the material used; for no account has been taken of the magnitude of the solar flare or of its position on the solar disk. When both these factors are considered, it may be shown that WATSON's findings are not inconsistent with the positive statistical result obtained by NEWTON (1943, 1944) working from very different data.

NEWTON (1943) examined the percentage association between *observed* flares of the highest intensity (3+) and magnetic storms occurring within 2 days. Following 37 such flares, magnetic storms began within 2 days in no fewer than 27 cases. When the flare was located in the central region of the solar disk (0°–45° longitude from the C.M.) the degree of association was even higher, viz. over 80 per cent (thus giving strong support to the hypothesis of particle ejection from the flare in a cone-shaped beam round the vertical). Great storms and great flares both being rare events, one would have expected only 1 chance coincidence within the 2 day interval. In fact, 17 coincidences were found. NEWTON (1944) next carried out a similar analysis by the superposed epoch method for 77 Class 3 flares and for 332 Class 2 fares, all visually observed. The percentage association of storms following Class 3 flares dropped to 31 per cent and for the Class 2 flares it was not significantly in excess of that expected by pure chance.

Now, the solar flare effect (crochet) by itself is undoubted evidence that a flare has occurred, but it provides (a) no evidence of the location of the flare on the sun's disk, (b) little indication of the intensity of the flare, except only that crochets are not usually caused by minor flares of Class 1. During the period covered by WATSON's analysis (1949–54), which were years of declining solar activity, there were at most 8 observed flares in the 3+ category (6 in 1949 and 2 in 1950). It seems, therefore, that of the 185 crochets included by WATSON, the majority will have been caused by the much more numerous flares of Classes 3 and 2, for which, as NEWTON showed, there is little correlation with subsequent magnetic activity for flares 3 and none for flares 2. The increasing numerical preponderance of these lesser flares may be illustrated by the numbers actually observed in the year 1949, namely Class 3(7), Class 2(150), Class 1(1053). Consequently, the introduction of Class 2 flares into the analysis, which is inherent in the use of crochets (without discrimination as to size, distance from the sub-solar point, etc.), will effectively dilute the positive statistical relationship which NEWTON showed to exist between 3+ flares and magnetic storms.

Lastly, the observational recognition of solar flares (denoting special activity in sunspots) has supported and amplified the relationships found between the largest sunspots within the central region of the sun's disk, and the greatest geomagnetic storms, and vice versa (MAUNDER, 1904; GREAVES and NEWTON, 1928). This relationship of geomagnetic storms with the central meridian passage of sunspots (with a *statistical* time lag of 1 to 2 days) becomes increasingly obscure as we proceed to the smaller storms and the smaller sunspots. Indeed, as GREAVES and NEWTON have themselves shown, there is a class of small magnetic storm (the recurrent *M*-storm) which shows an inverse correlation with sunspots. Again, because of the considerable numerical preponderance of the smaller sunspots over the larger and of the small magnetic storms over the great storms, if all the data were lumped together without discrimination for analysis a result of little or no statistical significance would emerge.

Royal Observatory
Edinburgh, 9

M. A. ELLISON

REFERENCES

WATSON R. A.	1957	*J. Atmosph. Terr. Phys.* **11,** 59.
NEWTON H. W.	1943	*Mon. Not. R. Astr. Soc.* **103,** 244.
	1944	*Mon. Not. R. Astr. Soc.* **104,** 4.
GREAVES W. M. H. and NEWTON H. W.	1928	*Mon. Not. R. Astr. Soc.* **89,** 84, 641.

Control of the ionosphere by means of radio waves

(*Received* 10 *January* 1958)

When a radio wave traverses an ionized gas it imparts energy to the electrons and thus increases their mean energy of random motion. The effect on the much heavier ions is much less and so may usually be neglected. Thus the corresponding "temperature" of the electron gas is raised by the wave above that of the other constituents of the medium, the ions and molecules.

It is also well known that in the absence of a source of ionizing energy, which tends to maintain it, a gaseous plasma* will decay by disappearance of the free electrons.

The different processes which cause the free electrons to disappear depend on, and may vary rapidly with, the "temperature" of the electron-gas in the gaseous plasma. These processes include the diffusion of the electrons, the attachment of electrons to certain neutral molecules or atoms in the gas and the direct recombination of electrons with positive ions.

In a nearly isothermal gaseous plasma at relatively low temperatures (250–300°K), such as that produced in any region of the ionosphere by ionizing solar radiations (or other agencies), radio waves of sufficient intensity can appreciably affect all such electron-removing processes. Thus, by local irradiation of such an ionospheric region with radio waves of appropriate frequency and amplitude the temperature and the number-density of the free electrons which normally exist in it can be controlled in some measure by day or by night.

An example of such control of a localized region of the ionosphere is provided by the interaction of radio waves (Bailey, 1956); this phenomenon has been investigated also under selected laboratory conditions (Goldstein *et al.*, 1953a; 1955). The wave-interaction arises through the disturbing wave raising the temperature of the electron-gas and so altering the absorbing power of the medium for the other radio waves. But another important effect of this temperature rise is to change the rates of those processes (diffusion, attachment and recombination) (Goldstein *et al.*, 1953b) which help to determine the free electron density at every point in the ionospheric region concerned.

Simple calculations show that an appreciable control of this kind can be exercised by means of radio stations on the ground and most easily so when the controlling waves have their frequencies near the gyro-frequency of electrons in the ionospheric region concerned (Bailey, 1937; Goldstein, 1956; 1958). The powers required for this kind of control are very much less than those which would suffice to produce an artificial air-glow or "aurora" (Bailey, 1938) by means of ionization by collision.

In addition to its scientific interest such control of ionospheric conditions may have practical applications in radio-communication.

Research Professor,
University of Sydney,
Australia.

V. A. Bailey

Professor of Electrical Engineering,
University of Illinois, U.S.A.

L. Goldstein

References

Bailey V. A. 1937 *Phil. Mag.* **23,** 929.
Bailey V. A. 1938 *Phil. Mag.* **26,** 425.

* i.e., a macroscopically neutral portion of ionized gas.

VOL. 12 1958

Bailey V. A.	1956	*Nuovo Cimento, Supplement to* **4,** *Series X* 1430.
Goldstein L., Anderson J. M. and Clarke G. L.	1953a	*Phys. Rev.* **90,** 151.
Goldstein L. Anderson J. M. and Clarke G. L.	1953b	*Phys. Rev.* **90,** 485.
Goldstein L., Anderson J. M. and Clarke G. L.	1955	*Phys. Rev.* **100,** 1037.
Goldstein L.	1956	*International Symposium on Wave Propagation* Paris, September 1956
Goldstein L.	1958	*I.R.E. Transactions on Microwave Theory and Techniques* January 1958.

A radar record of an aurora at Adelaide

(*Received* 14 *January* 1958)

On the evening of 13 September 1957 an aurora was widely visible throughout Australia. This aurora was also detected during routine operation at Adelaide of the 67 mc/s meteor survey equipment, described below. The large distance of this station from the south geomagnetic pole imparts unusual interest to this record.

Transmitter power is 50 kW, pulse length 20 μsec and pulse repetition frequency 95/sec. The axis of the aerial beam is directed to azimuth $35\frac{1}{2}^\circ$ S of E at elevation 9°. Half-power points are $\pm 2\frac{1}{2}^\circ$ in azimuth and $\pm 4\frac{1}{2}^\circ$ in elevation, and nulls in the azimuthal polar diagram are 16° apart. Echoes are presented on an intensity-modulated cathode-ray screen and photographed on continuously-moving film (12 cm/hr). The maximum slant range recorded is 900 km. Because of the low pulse repetition rate it is unlikely that the ranges recorded for auroral echoes are ambiguous. During September the equipment was not operated at full sensitivity; the sporadic meteor echo rate was about 300 per day.

Auroral echoes were present from 1655 to 1927 LT. The aurora was first detected at the limiting slant range of 900 km but from the manner of the cut-off echoes at still greater ranges were present. The mean range shortened until 1750. From 1750 to 1900 echoes were confined within the ranges 400–800 km, with the exception of a few centres extending out to beyond 900 km; over this period the mean range was constant at about 600 km. From 1900 onwards the range lengthened again, and reflections finally ceased with weak echoes at 1927 at 700 km range.

With the exception of a few minutes of discrete echoes near 1830, the echoes are all diffuse, the apparent thickness of the centres ranging from 50 to 200 km. Except near the beginning and end of the record, multiple centres are present, with up to 5 centres active simultaneously. The average lifetime of the individual centres is from 5 to 10 min. The regions responsible for the discrete echoes are not much thicker than the resolvable limit of 10 km set by spot size. Discrete echoes show the same range drifts as diffuse echoes received at the same time, and in fact appear to "grow out" of diffuse echoes as if the reflecting region had decreased in thickness.

Individual centres exhibit range drifts of from 0·3 to 1·2 km/sec, with a few stationary centres as well. Without exception the drift of the centres is towards the station; this is true even whilst the mean range is increasing, towards the end of the record.

If one accepts the picture of diffuse echoes proceeding from over-dense "blobs" of electrons, whose motion across the aerial beam produces the range drifts, it is possible to deduce the direction of motion of the blobs at those times when the upper and lower limits of echo range, corresponding to nulls in the aerial pattern, are sharply defined. Two such measurements give $9\frac{1}{2}^\circ$ S of E and 2° N of E for the directions of motion of the reflecting centres; these are to be compared with the direction, $4\frac{1}{2}^\circ$ S of E, of parallels of geomagnetic latitude near Adelaide. The main reflecting belt lies 550 km from Adelaide, near geomagnetic latitudes 47–48° S.

The true drift of the centres is to the west, i.e. in the same direction as found for northern hemisphere aurorae at similar local times (evening sequence). The average drift speed of $\frac{1}{2}$km/sec is also of the same order as that found for northern aurorae, which are observed a good deal closer to the geomagnetic pole.

Harang and Landmark (1954) have noticed motion of the centre of the activity, coupled with amplitude changes, similar to that found in the present case. Echoes first appear with small amplitude at maximum range; the amplitude increases until the range reaches a minimum value and thereafter decreases again as the range increases. This behaviour has been interpreted by Kaiser (1956) as a geometrical effect, with minimum range and maximum amplitude occurring when the reflecting centre lies on the same magnetic meridian as the observer. This explanation obviously cannot apply to the Adelaide record, as the aerial is fixed and the nearest illuminated point is at least 350 km from the magnetic meridian of Adelaide. Either changes in height of a non-uniform horizontal reflecting sheet, or changes in horizontal distance of reflecting centres aligned along magnetic arcs, or perhaps both, must be involved.

Division of Radiophysics, C.S.I.R.O. A. A. Weiss
Department of Physics, J. W. Smith
University of Adelaide

VOL. 12 1958

References

Harang L. and Landmark B. 1954 *J. Atmosph. Terr. Phys.* **4**, 322
Kaiser T. R. 1956 *The Airglow and the Aurorae* Section III, p. 156. Pergamon Press, London

Journal of Atmospheric and Terrestrial Physics, 1958, Vol. 12, pp. 219 to 221. Pergamon Press Ltd., London

LETTERS TO THE EDITOR

Ambipolar diffusion in the *F2*-layer

(*Received* 25 *October* 1957)

In 1954, Bates drew attention to the fact that according to Ferraro (1945) diffusion of the free charges in the *F2*-layer would be unacceptably rapid at the neutral particle concentration indicated by rocket measurements (cf. LaGow, 1954; Kallman, White and Newell, 1956; Horowitz and LaGow, 1957) and more recent discussions of diffusion (Martyn, 1955; Yonezawa, 1955; Ratcliffe, Schmerling, Setty and Thomas, 1956; Dungey, 1956) have all agreed that the densities appear to be too small by a factor of at least 4 or 5.

The diffusion coefficient D is an important parameter in these discussions. For an ion of mass M_1 in a gas composed of particles of mass M_2 it is given to a close approximation (cf. Chapman and Cowling, 1939) by

$$D = \frac{3\pi^{\frac{1}{2}}}{16 n_2}\left(\frac{2kT}{\mu}\right)^{\frac{1}{2}} P^{-1} \tag{1}$$

where k is Boltzmann's constant, T is the absolute temperature, μ is the reduced mass $M_1M_2/(M_1 + M_2)$, n_2 is the gas number density and P is an average effective diffusion cross-section. Ferraro (1945) calculated P by applying Sutherland's model (1909) to air and obtained

$$P = 3{\cdot}85 \times 10^{-15}\left(\frac{T + 187}{T}\right) \text{cm}^2 \tag{2}$$

whilst Cowling (1945) assumed that

$$P = 1{\cdot}89 \times 10^{-13}\, T^{-\frac{1}{2}} \text{ cm}^2 \tag{3}$$

a formula suggested by measurements of the mobility of ions in N_2 (cf. Tyndall, 1938) which he supposed referred to N_2^+. Taking $2M_1 = M_2 = 25$, Ferraro has computed the values of Dn_2, reproduced in Table 1, which includes also values corresponding to (3). All discussions of diffusion appear to be based upon these two sets of values.

Table 1. Values of $(Dn_2 \times 10^{-18})$ cm^{-1} sec^{-1}

T°K	300	400	500	700	1000
Ferraro	4	5	6	8	10
Cowling	2	3	4	5.5	8
Dalgarno	1.1	1.3	1.5	1.9	2.3

Although neither expression (2) nor (3) for P has much justification (in particular, the ions in N_2 were almost certainly N_4^+ (Varney, 1953)), the values of D are probably adequate for application to conductivity in the lower ionosphere (cf. Cowling, 1945; Bates and Massey, 1951) and to the diffusion of meteor trails (Kaiser, 1953; Greenhew and Neufeld, 1955; Weiss, 1955), the diffusion coefficient at temperatures near 300°K of an ion in a mixture of O_2 and N_2 usually being insensitive to the nature of the ion and to the gas composition (cf. Tyndall, 1938; Dalgarno, McDowell and Williams, 1957). However, the values are not appropriate to the *F2*-region, for there diffusion probably depends primarily on the diffusion coefficient of O^+ in O, and as was pointed out by Massey and Mohr (1934) the case of an ion moving in its parent gas requires special considerations. Dalgarno (1957) has recently analysed the experimental data on the mobilities of ions in their parent gases and has, using a rough interpolation

procedure, predicted the mobility of O^+ in O at various temperatures. Values of D may readily be obtained from these calculations, and they are given in the table.

At the temperatures believed to prevail in the $F2$-region, D for O^+ in O is seen to be about four times smaller than the values usually adopted for D in the $F2$-region. However, the data may well be in error by a factor as large as 2 and an attempt is being made to obtain results of greater precision. A more complete examination of the implications of diffusion theory should then be worthwhile.

Geophysics Research Directorate
ARDC, Bedford, Mass., U.S.A.

A. Dalgarno*

References

Bates D. R.	1954	*Rocket Exploration of the Upper Atmosphere* (Edited by R. L. F. Boyd and M. J. Seaton) Pergamon Press, London.
Chapman S. and Cowling T. G.	1939	*The Mathematical Theory of Non-uniform Gases.* Cambridge University Press.
Cowling T. G.	1945	*Proc. Roy. Soc.* A**183,** 453.
Dalgarno A.	1957	*Phil. Trans.* In press.
Dalgarno A., McDowell M. R. C. and Williams A.	1957	*Phil. Trans.* In press.
Dungey J. W.	1956	*J. Atmosph. Terr. Phys.* **9,** 90.
Ferraro V. C. A.	1945	*Terr. Mag. Atmos. Elec.* **50,** 215.
Horowitz R. and LaGow H. E.	1957	*J. Geophys. Res.* **62,** 57.
Kallman H. K., White W. B. and Newell H. E.	1956	*J. Geophys. Res.* **61,** 520.
LaGow H. E.	1954	*Rocket Exploration of the Upper Atmosphere* (Edited by R. L. F. Boyd and M. J. Seaton) Pergamon Press, London
Massey H. S. W. and Mohr C. B. O.	1934	*Proc. Roy. Soc.* A**144,** 188.
Martyn D. F.	1955	*The Physics of the Ionosphere.* Physical Society, London.
Ratcliffe J. A., Schmerling E. R., Setty C. S. G. K. and Thomas J. O.	1956	*Phil. Trans.* A**48,** 621.
Sutherland G. B. M.	1909	*Phil. Mag.* **18,** 341.
Tyndall A. M.	1938	*The Mobility of Positive Ions in Gases.* Cambridge University Press.
Varney R. W.	1953	*Phys. Rev.* **89,** 708.
Weiss A. A.	1955	*Aus. J. Phys.* **8,** 279.
Yonezawa T.	1955	*J. Rad. Res. Lab. Tokyo* **2,** No. 8.

VOL. 12 1958

Diffraction microscope and the ionosphere: use of a satellite

(*Received* 24 *October* 1957)

In a recent issue of *J. Atmosph. Terr. Phys.* (**10,** 332) a sober estimate of the value of diffraction microscopy in ionosphere studies was given, and it appeared, with the techniques then available, that the use was likely to be limited. The demonstration of a satellite capable of carrying a continuously emitting transmitter completely changes the prognosis, and the possibility of using diffraction microscopy in ionosphere studies now appears to be good, for the following reasons:

* On leave from Department of Applied Mathematics, The Queen's University of Belfast.

(a) The use of a transmitter beyond the E- and F-regions, or between them, means we can now get a transmitted diffraction pattern, closely analogous to that of the original Gabor method, without having to rely on a problematical "quiet" period in the ionosphere to secure sufficiently specular reflection.

(b) The speed of the satellite is high, and may be determined accurately, as can its height and the height of the layers being studied. This means that ionosphere drift is relatively unimportant, and a substantially "instantaneous" image may be obtained. While the method will give no information about ionospheric movement, it may give information about ionospheric structure.

The value of V_g required for the formula in paragraph 4 of the above paper, is to a first approximation the velocity of the satellite as projected through a point in the layer studied. This can be measured *before* interpreting the diffraction pattern and does not have to be determined later. Thus f_2 is readily calculated (within limits) and the position on the optical bench where the reconstructed image of the ionosphere will appear determined in advance: this greatly simplifies the search for it. A single aerial now gives a one-dimensional picture. Moreover, the value of the scale factor, p, is now much greater, and the problems of working near the limits of photographic reproduction are less acute. On the other hand the radio record must reproduce changes up to 100 c/s.

(c) The direction of the satellite's motion is known in advance. Two-dimensional recording with a transverse system of aerials becomes much easier, as the base-line direction can be chosen beforehand. Moreover, at shorter wavelengths, the total span of aerials is much reduced. For $\lambda = 4$ m transmissions, for instance, 101 aerials spaced 50 m apart would suffice for the E-region, rather wider spacings or shorter wavelengths being required for the F-region. Since the "speed of scan" is also known, the production of a photographic plate which represents the ground diffraction pattern in two dimensions with the same scale transverse to the path as along it, is much simplified: the main optical problem is thus overcome. Any small errors remaining will be easily dealt with by angling the plate to the beam in reconstruction.

(d) If it should prove possible to use very small wavelengths in the millimetre region, the diffraction effects would be so small that the pattern produced could be regarded as a direct projected image, without any need for reconstruction. Against this, the contrast of the ionosphere to waves in this region is probably very low.

(e) Opportunity is taken to point out that the very high speed of the satellite provides us with a body with $v/c \simeq 2{\cdot}5 \times 10^{-5}$, and a value of $\sqrt{1 - v^2/c^2}$ differing from 1 by about 3 parts in 10^{10}. This should be within the accuracy attainable with a caesium atomic clock. There will be considerable difficulty, both in principle and in practice, in comparing the satellite clock with an earth clock, and a study of these difficulties will throw further light on the concept we give the name of "time", and underline Einstein's essential wisdom in asserting that space-time is a continuum, and any attempt to divide time out of it is an illusion. One possible approach is indicated briefly below.

(f) A couple of caesium atomic clocks, one on earth and one on a satellite, the latter controlling the phase of the satellite transmitter, could be used to provide a "coherent background" for the Gabor and Goss method. It is only necessary to hold them in phase for the period of 10–15 sec during a single transit, so the relativistic correction is here unimportant. It should be noted, in passing, that the longitudinal Doppler shift will produce beats on the record, which correspond to the outer zones of a Newton's ring system passing over the ground aerial. The phase of the centre of this system should give information as to the phase of the two oscillators, local and satellite, as the latter passes overhead, provided the distance of the satellite can be measured to a fraction of a wavelength. By comparing this with the phase obtained at next transit, it might be possible to "rate" the satellite clock, but many observations would be necessary before a result could be obtained sensibly independent of random sources of error. For instance, there will be undetermined phase-paths in the ionosphere, unless we can use a wavelength short enough to avoid ionosphere absorption, yet long enough to enable the distance in wavelengths to be determined accurately.

College of Technology
Gosta Green
Birmingham, 4

G. L. Rogers

Journal of Atmospheric and Terrestrial Physics, 1958, Vol. 12, pp. 222 to 223. Pergamon Press, Ltd., London

Book reviews

H. SPENCER-GREGORY and E. ROURKE: **Hygrometry.** Crosby, Lockwood and Son, London, 1957. 254 pp., 36s.

THE measurement of humidity has become important in modern industrial processes only during the present century, and the authors of this book (the first of whom died shortly after its publication) begin with a brief historical résumé which is followed by a summary of the available methods of humidity measurement. A chapter on the vapour-pressure of water follows and leads up to the Frost Point hygrometer with its application to low-temperature hygrometry. The method of obtaining the Frost Point given on p. 76 as the mean of the temperatures at which the deposit slowly increases and decreases is by no means universally accepted, and it requires considerable manipulative skill to keep the difference between the two temperatures small.

Chapter III deals with the vapour-pressure of solutions in which the published values of vapour-pressures of sulphuric acid–water mixtures are discussed and compared with values obtained from theoretical considerations. This is followed by a chapter on the theory of moisture content of highly compressed gases, which is treated largely along the lines of the work of VAN LAAR.

The theory of the wet and dry bulb thermometers is developed and the authors extend this to an instrument of their own design for which they claim a much simplified theory.

The theory and characteristics of hair diffusion gravimetric and electrolytic hygrometers are treated similarly. There is a notable omission, however, in that no mention is made of the infra-red hygrometer, which is of interest theoretically and for its absolute measurement of humidity.

The book concludes with a chapter on the lag of Assmann and electrolytic hygrometers in relation to air-flow but without any real consideration, in the case of the latter instrument, of the effects of low ambient temperature upon the lag.

In general, there is much useful information for the reader, but the undoubted appeal is to the student and those interested in a theoretical treatment. Probably the most dissatisfied will be the meteorologist, who is dismissed in the opening sentences of the first chapter, and those requiring a hygrometer for a specific purpose who will wish to know which type is best suited to their needs and its limitations. Most of the information can be obtained from the text, but a chapter dealing with the practical problem would have been invaluable to engineers.

C. HINKEL

Artificial Stimulation of Rain. Edited by HELMUT WEICKMANN and WALDO SMITH, Pergamon Press, London, 1957. pp. 427. £5.5.0. $15.

A CONFERENCE entitled "The Physics of Cloud and Precipitation Particles" was held at Woods Hole Oceanographic Institution, Massachusetts in September 1955. The papers presented there together with the ensuing discussions have been collected and published in full under the title "The Artificial Stimulation of Rain". The delegates attending the meeting were almost exclusively from the U.S.A. and from Canada, so that the collection has historical interest as an account of researches being carried out two years ago on the North American Continent. The papers, I find, are of varied length and quality—the best generally provoking the liveliest discussions—and contain much stimulating material.

VOL. 12 1958

The book is lavishly produced on art paper with the accuracy, pleasing type and clean line diagrams which we have come to expect of the publishers and which cannot fail to give the reader pleasure. However, for the reviewer a not unmixed pleasure. Clearly the care and attention lavished on the volume is reflected in its cost (£5. 5. 0). Since a large number of the papers in this volume have been published in contract reports or in current meteorological literature, libraries—particularly those with small budgets—may consider it not indispensible.

Papers in the first section of the book are concerned with atmospheric aerosol; with techniques of measurement and problems of origin, chemical nature and geographical disposition. Notable contributions are made by JUNGE and SAGALYN and FAUCHER.

This is followed by a section devoted to the processes of droplet growth by condensation and coalescence, in which the unresolved problems of collection efficiency are emphasized (KINZER and COBB, SCHOTLAND) and in which an account of the development of precipitation in convective cloud is put forward (EAST).

The growth of crystals by condensation and aggregation and their melting to form raindrops is considered in the third section. An account is given (WEXLER) of the bright melting band familiar to radar meteorologists. And who can fail to be fascinated by the description (BLANCHARD) of the freezing and melting of giant raindrops?

Two papers on the electrification of the atmosphere are also commended; the first a (likely) theory of thunderstorm charge generation (WORKMAN), and the other describing measurements of space charge density (VONNEGUT *et al.*).

In the last major section are grouped together papers describing laboratory and field studies of ice-crystal nucleation, a topic on which the reviewer is not competent to comment.

In conclusion, we come to two papers describing experiments seeking to influence rainfall. In the first series carried out in Punjab, Pakistan (FOURNIER D'ALBE *et al.*) powdered salt was dispersed from the ground: no other conclusion than that "the results justified a repetition" could be drawn. In the other experiments in the United States (BRAHAM and SIEVERS) dry-ice was dispersed from an aircraft: as with all trials in which a small number of experiments have been performed the results are also inconclusive.

The outcome of these trials is not, however, expected to deter newcomers entering this difficult field: all are aware of its economic and sociological importance.

P. M. SAUNDERS

KARK RAWER: **The Ionosphere.** Frederick Ungar Publishing Company, New York, 1957. 254 pp., $7.50.

A TRANSLATION, from German into English, of Dr. K. RAWER's well-known book *The Ionosphere* is most welcome, and should now greatly extend the reading of it by students and research workers. Written five years ago, by one who himself has made many distinguished contributions to radiophysics, Dr. RAWER's work has served as a model introduction to the study of the ionosphere; for it provides a happy blend of material of scientific interest and of practical radiocommunication utility. It is not a long book—the present translation occupies less than 200 pages of eminently readable type—but it contains the essential material, expounded with both lucidity and economy. No one but a complete master of the subject could have written it.

In the case of such a rapidly developing subject such as the ionosphere it must be difficult to ensure that any edition is abreast with modern progress. For example, the present treatment of radio propagation by ionospheric "forward scatter" needs substantial extension, while the diagram of the atmospheric current system on magnetic storm days is now known to be incorrect.

E. V. APPLETON

Papers to be published in future issues

ROBERT E. HOUSTON JR: The effects of certain solar radiations on the lower ionosphere

R. B. BANERJI: Method of measuring ionospheric winds by fading at spaced receivers

GERARD A. FAUCHER: A study of air-flow in a large-ion chamber

D. LAL, P. K. MALHOTRA and B. PETERS: On the production of radioisotopes in the atmosphere by cosmic radiation and their application to meteorology

M. SRIRAMA RAO and B. RAMACHANDRA RAO: Investigation of magneto-ionic fading in oblique incidence medium-wave transmissions

C. M. MINNIS: Non-uniformity in the brightness of the sun's disk during the eclipse of 30 June 1954

V. VOLLAND and J. TAUBENHEIM: On the ionospheric current system of the geomagnetic solar flare effect

C. M. MINNIS: The interpretation of changes in the *E*- and *F*1-layers during solar eclipses

JOHN C. BRANDT and JOSEPH W. CHAMBERLAIN: Resonance scattering by atmospheric sodium—V. Theory of the day airglow

GERALD J. ROMICK and C. T. ELVEY: Variations in the intensity of the hydrogen emission line $H\beta$ during auroral activity

K. ENDRESEN, T. HAGFORS, B. LANDMARK and J. RÖDSRUD: Observations of angle of arrival of meteor echoes in VHF forward scatter propagation

HERMANN POEVERLEIN: Low frequency reflection in the ionosphere

E. HARNISCHMACHER and K. RAWER: Drift observations evaluated by the method of "similar fades"

J. E. TITHERIDGE: Variations in the direction of arrival of high frequency radio waves

M. W. CHIPLONKAR and V. N. ATHAVALE: Simultaneous recording of atmospherics on four different frequency bands in the low frequency region

R. SATYANARAYANA, K. BAKHRU and S. R. KHASTGIR: Triple-splitting of the F-echoes

B. A. P. TANTRY and R. S. SRIVASTAVA: Waveforms of atmospherics with superimposed pulses recorded with an automatic atmospherics recorder

N. C. GERSON: Very long distance ionospheric propagation

J. C. BHATTACHARYYA: Non-uniformity in the brightness of the sun's disk at sunspot minimum

A. VALLANCE JONES and A. W. HARRISON: $^1\Delta g - {}^3\Sigma\bar{g}O_2$ infrared emission band in the twilight airglow spectrum

G. R. ELLIS: The trapping of cosmic radio waves beneath the ionosphere

H. A. WHALE and L. M. DELVES: Some relations between the bearing and amplitude of a fading radio wave

---

Publisher's Notice

Please note that the Polar Atmosphere Symposium has been supplied to all 1957 subscribers in place of Volume 12. During 1958 we shall publish and supply Volumes 12, 13 and 14 (and not Volumes 13, 14 and 15 as listed in our Price List).

VOL.
12
1958

Journal of Atmospheric and Terrestrial Physics, 1958, Vol. 12, pp. 225 to 235. Pergamon Press Ltd., London

The effect of certain solar radiations on the lower ionosphere*

R. E. HOUSTON, JR. †
Ionosphere Research Laboratory, The Pennsylvania State University,
University Park, Pennsylvania

(*Received* 26 *August* 1957)

Abstract—An electron density distribution in the D and E regions of the ionosphere is computed. Lyman alpha, Lyman beta, the Lyman continuum and X-radiations are considered. The resulting electron distribution is used to compute parameters which may then be compared with data from rocket and long wave radio experiments. In general, there is good agreement between experimental results and the values predicted by the model.

1. INTRODUCTION

IN RECENT YEARS, measurements on various ionospheric parameters have indicated the necessity for a reappraisal of the ionizing radiations and atmospheric constituents contributing to the electron production and distribution in the lower ionosphere. It is the purpose of this paper to present the results of calculations based on recent relevant rocket and laboratory measurements. The resulting electron density distribution model is then compared, primarily, with experimental values obtained from pulsed long wave radio data, but also with other rocket data.

The initial explanation for the formation of layers of ionization in the earth's atmosphere was made by CHAPMAN (1931a), who proposed the theory which remains today as the basis for further considerations of this problem. Subsequent to the first CHAPMAN paper, many contributions to our knowledge of physical processes in the atmosphere have been made. The results for the lower ionosphere may be summarized in the following manner.

If the production function, q, is known and vertical motions are neglected, the equation governing the ionization distribution at a particular point may be written

$$\frac{dN_e}{dt} = q - \alpha N_e^2 \tag{1}$$

where N_e is the density of electrons and α is the effective recombination coefficient. No analytic solution to equation (1) is known, but to first order the approximate solution is given by

$$N_e = \sqrt{q/\alpha} \tag{2}$$

Assumption of quasi-equilibrium conditions, i.e. $dN_e/dt = 0$, leads to the same result. Equation (2) is used to compute the electron densities reported in this paper.

* The research reported in this paper has been sponsored by the Geophysics Research Directorate of the Air Force Cambridge Research Center, Air Research and Development Command, under Contract No. AF19(604)-1304.

† Now at the University of New Hampshire.

2. The Production Function

The production function has been deduced by Nicolet and Bossy (1949) and may be given in the form

$$q = NK_I Q_\infty \exp\left[-K_A f(\chi)\int_z^\infty N\,dz\right] \tag{3}$$

where q is the production of ion pairs due to a particular radiation, N is the number of absorbing particles, molecular or atomic, K_I is the absorption coefficient for processes producing ionization involving the particular radiation and absorbing particles, Q_∞ is the number of photons of the particular radiation incident at the top of the earth's atmosphere, K_A is the total absorption coefficient for the radiation, $f(\chi)$ is the Chapman angle of radiation function in which χ represents the solar zenith distance, and z represents the height of some arbitrary reference level.

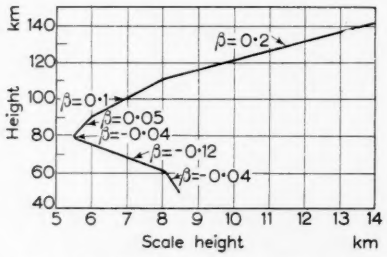

Fig. 1. Scale height as a function of height.

When the solar zenith distance is not greater than 70° the assumption of horizontally stratified layers in the atmosphere is adequate. However for high solar zenith distance sec χ must be replaced by the function $f(\chi, R)$ Chapman (1931b). Here R is a parameter involving the radius of the earth, the scale height, and the height of the layer in question. For D and E layer heights and the scale height model of Fig. 1, $R \approx 800$ and hence $f(\chi, R)$ may be written as $f(\chi)$ only. Values of $f(\chi)$ for various values of R are given by Chapman (1931b).

The scale height model of Fig. 1 was derived by Nicolet (1954a). It is formed from linear segments according to the relation

$$H = H_0 + \beta(z - z_0) \tag{4}$$

where $\beta = dH/dz$, the scale height gradient, and H_0 is the scale height at some fixed altitude z_0, $z > z_0$. This model is based on pressure and temperature measurements from rocket data and the value of the scale height for any particular height may be read directly from the curve.

The distribution of constituents used in these computations is shown in Fig. 2. The total number of air molecules cm^{-3} $N(M)$, is obtained from values given by Nicolet (1954a) as deduced from rocket pressure measurements. It is presumed that the minor constituents represent such a small proportion of the atmosphere that, to a high degree of approximation, molecular nitrogen comprises four-fifths of the total atmosphere. It is also assumed that dissociation of molecular nitrogen is negligibly small at these altitudes.

VOL. 12 1958

However, such is not the case with oxygen. Both atomic and molecular oxygen play a significant role in the formation of ions in the atmosphere and the region of transition where $N(O) > N(O_2)$ is of great interest and importance. NICOLET (1954b) has considered the problem of oxygen dissociation in terms of recombination, photoequilibrium, mixing, and diffusion. The resulting distribution, shown in Fig. 2, agrees rather well with the molecular oxygen distribution

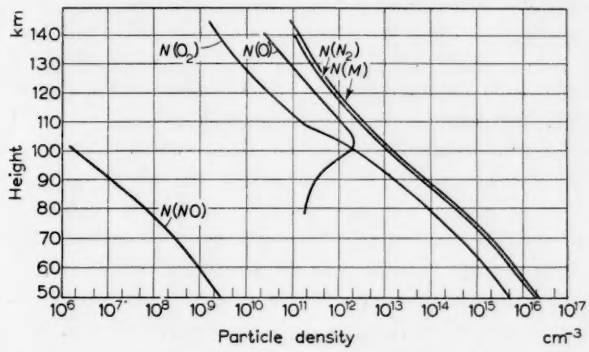

Fig. 2. Constituent distribution.

deduced by BYRAM *et al.* (1953) from certain rocket data. In this distribution, the transition region begins at about 95 km and extends to 105 km or so.

It should be pointed out here that the linear segmented scale height distribution of Fig. 1 results in a constituent distribution of the form

$$N = N_0 \left(\frac{H}{H_0}\right)^{-1+\beta/\beta} \tag{5}$$

as was shown by NICOLET and BOSSY (1949). Hence, in general,

$$\int_z^\infty N\, dz = NH\,. \tag{6}$$

However, in the case of molecular oxygen, NICOLET (1954b) has shown that

$$\int_z^\infty N(O_2)\, dz = \frac{N(O_2)H}{X(1+\beta) - \beta} \tag{7}$$

where the parameter X is determined by the type of process controlling the constituent distribution. If $X = 1{\cdot}00$, mixing is predominant, but for $X = 1{\cdot}28$, it is primarily diffusion which controls the vertical distribution of O_2. A sudden change in the value of X would create a discontinuity in the electron density curves. To avoid this, the value of $X = 1{\cdot}00$ at 96 km was gradually increased to $X = 1{\cdot}28$ at 106 km with the consequent prevention of any such discontinuity.

Since NICOLET (1945) first proposed the photo-ionization of nitric oxide by Lyman alpha radiation (1215·68 Å) as the source of D-layer ionization, the distribution of this constituent has been under much investigation. Because mixing is the predominant process below 95 km it is assumed that the distribution of NO will follow that of the main atmosphere. The absolute density at any altitude

remains undetermined as yet. On the basis of the absorption cross-section of NO for Lyman alpha, NICOLET estimates that $N(NO)$ is about one millionth that of the main atmosphere. BATES and SEATON (1950) give values slightly higher than this, although they agree the distribution probably follows that of the main atmosphere. The value chosen here yields a maximum electron density for the D region which is less than the electron density required to reflect 75 kc/s radio waves, a result in conformity with experiment.

Two absorption coefficients are used in computing the production function. The exponential factor determines the decrease in intensity of the incident energy and hence this absorption coefficient, K_A, is the sum of the coefficients of every process which removes energy from the incident flux. On the other hand, only a certain number of the absorptions result in ionization, and this is reflected either in the ionization efficiency of the particular process or a different absorption coefficient, K_I.

WATANABE *et al.* (1953) have recently made measurements of the absorption coefficients at Lyman alpha. The pertinent results yield $K_A(N_2) < 3{\cdot}0 \times 10^{-22}$ cm^2, $K_A(O_2) = 1{\cdot}0 \times 10^{-20}$ cm^2, and $K_A(NO) = 2{\cdot}5 \times 10^{-10}$ cm^2. In their measurements, WATANABE *et al.* also found that at Lyman alpha, photo-ionization accounted for approximately 50 per cent of the total absorption in NO. Because the cross-section for N_2 is so small, this constituent plays only a slight role in the absorption of Lyman alpha and it is primarily molecular oxygen which absorbs this radiation. Consequently, this constituent plays a major part in determining the shape and height of the D-layer.

The fact that Lyman alpha is observed as a strong radiation from the sun suggests the existence of other Lyman radiations. In this regard, WATANABE *et al.* (1955) have investigated absorption by O_2 and N_2 in the range from 850 to 1100 Å. The resulting absorption curve for O_2 is rather complicated but certain features are evident. At Lyman beta (1025·7 Å) the total cross-section is $1{\cdot}54 \times 10^{-18}$ cm^2 and photo-ionization accounts for 58 per cent of the total absorption. Toward the shorter wavelengths the cross-section increases to about 10^{-17} cm^2. These investigators also measured the first ionization potential of O_2 and found it to be $12{\cdot}07 \pm 0{\cdot}01$ eV. This corresponds to a wavelength of 1027 Å and, hence, a photon of Lyman beta is sufficiently energetic to photo-ionize O_2.

The results for N_2 showed that very little absorption occurs in the 995–1050 Å region with the cross-sections being less than 10^{-20} cm^2. Specifically, at Lyman beta, the cross-section was 4×10^{-21} cm^2. Below 995 Å there are strong absorbing bands as well as deep windows in which the cross-section ranges from 3×10^{-17} cm^2 to 2×10^{-20} cm^2.

It is also necessary to know the absorption cross-section in the 30–100 Å region. HAVENS *et al.* (1955) have used values of the order of 10^{-18} cm^2, which were obtained primarily from COMPTON and ALLISON (1954). Because these were obtained directly from X-ray measurements and agree rather well with the values given by other authors, 1×10^{-18} cm^2 was adopted for the computations reported here.

The final quantities needed to calculate the production function are the incident energies. Prior to the results of rocket flights, no direct measurements

VOL. 12 1958

of incoming radiation were obtainable. NICOLET (1952a) made some remarkably accurate estimates of the number of photons, and hence the energy, that would be present for a particular wavelength. These values agree well with the energy of Lyman alpha from the rocket data of FRIEDMAN (1955) and the energy of Lyman beta from TOUSEY (private communication), which yield $1{\cdot}2 \times 10^{10}$ photons cm^{-2} sec^{-1} and $3{\cdot}75 \times 10^{8}$ photons cm^{-2} sec^{-1}, respectively. The value

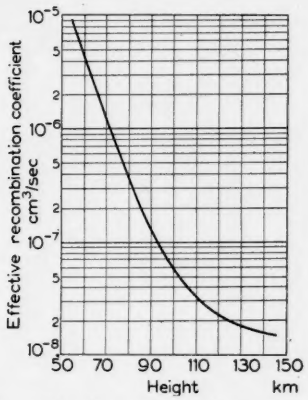

Fig. 3. Recombination coefficient as a function of height.

given by TOUSEY is reduced by a factor of four in the numerical studies of this paper since, on the same rocket flight, a measurement of the Lyman alpha radiation showed it to be four times greater than the quiet sum value of FRIEDMAN (1955). In another rocket experiment, BYRAM *et al.* (1956) obtain the value of 0·1 ergs cm^{-2} sec^{-1} for the X-radiation between 44 and 100 Å. This converts to 5×10^{8} photons cm^{-2} sec^{-1} at 100 Å.

Recent chromospheric models of OSTER (1956) and ATHAY and THOMAS (1956) are in accord with the proposals of NICOLET (1952a). These models predict Lyman alpha and Lyman beta energies rather well, and as a consequence, their value for the energy in the Lyman continuum has been adopted. This leads to a flux of 5×10^{9} photons cm^{-2} sec^{-1} at the top of the earth's atmosphere.

All quantities necessary to compute the production function have been discussed. The effective recombination coefficient must be determined so that the electron density distribution may be found. Using a variety of experimental and theoretical results, MITRA and JONES (1954) have determined a daytime recombination model in which the effective coefficient varies with height. This is shown in Fig. 3.

3. The Electron Distribution in the Lower Ionosphere

It is now possible to assemble the quantities of the preceding sections to calculate the various contributions to the electron density distribution in the lower ionosphere. The net result is shown in Fig. 4. The lowest layer, hereafter referred to as the *D*-layer, is due solely to Lyman alpha radiation photo-ionizing *NO*, as no other radiation considered penetrates to such a depth. The maximum

of this contribution for midsummer noon ($\chi = 17°22'$) at University Park has an electron density of 1260 electrons cm^{-3} at an altitude of about 83 km.

The upper layer, hereafter referred to as the *E*-layer, is a result of the combined effects of Lyman beta ionizing O_2 as well as X-radiation and the Lyman continuum. These latter radiations act in a rather complicated manner on the atmospheric constituents at the relevant heights.

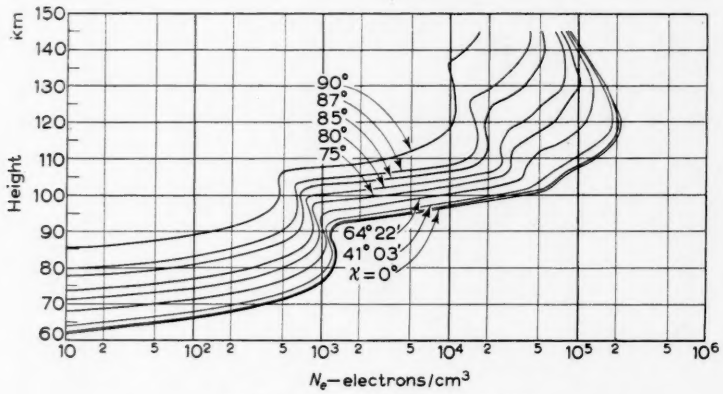

Fig. 4. The total lower ionosphere.

The lower portion of the *E*-layer is due entirely to the ionization of O_2 by Lyman beta. None of the other *E*-layer producing radiations are of sufficient intensity at this level to contribute appreciably to the electron density. Thus, long-wave radio experiments which have a frequency of sufficient magnitude to penetrate the *D*-layer are incident upon that part of the *E*-layer which is produced by the monochromatic Lyman beta line. The 75 and 150 kc/s long-wave radio experiments to be discussed later fall in this category.

The most dense portion of the *E*-layer for midsummer noon at University Park is $2{\cdot}08 \times 10^5$ electrons cm^{-3} and is due, in some measure, to all of the above mentioned radiations with the exception of Lyman alpha. In this region, the recombination coefficient of oxygen was assumed to be that given by Mitra and Jones (1954). However, Massey (1954) has indicated that molecular nitrogen recombines more rapidly and in these computations $\alpha N \approx 10^{-6}$ cm^3 sec^{-1}. The X-ray contribution reported here differs from the calculations of Friedman (1954) or Elwert (1953), who used a constant recombination coefficient throughout the entire *E*-region. Also, the X-ray contribution computed here is at variance with the results of Rawer and Argence (1954), who use a particle density much greater than present rocket data permit. They also use an extremely high pair production efficiency, i.e. 15·8 eV/ion pair as compared to the 30 eV/ion pair used here and by both Friedman and Elwert.

In the Lyman continuum the computations become very involved due to the presence of N_2 windows and the competition between atomic and molecular oxygen in the absorption of this radiation. An ionization efficiency of 60 per cent and the absorption coefficients of Watanabe *et al.* (1955) were used to complete these computations.

VOL. 12 1958

4. Discussion

It is important to note that these computations are based on Q_∞ values established for a quiet sun. The change in energy over a solar cycle will be reflected primarily in the density of the maxima of the various contributions at their respective heights. Due to the distribution of constituents and the recombination coefficient model used, the effect of the solar cycle on the lower edge of the layers

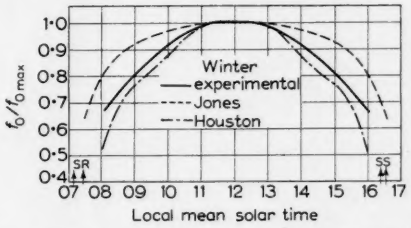

Fig. 5. Experimental and theoretical critical frequency.

is slight. If solar conditions change from minimum to maximum activity, the reflection height of long radio waves change only by a kilometre or two. Of course, the maximum of the electron density will vary as the square root of the ratio of the prevailing solar activity to quiet solar conditions at the minimum of solar activity.

No experimental evidence is available locating the maximum of the *D*-layer, but Straker (1955) gives the reflection height of 16 kc/s waves as 69 $\pm$ 0·25 km. The reflection height predicted for this frequency by the above model is 69 km. Straker's value agrees well with that obtained by several other observers. The diurnal variation reported by Straker also agrees reasonably well with the diurnal variations predicted by the above model.

Using *CRPL-F* bulletins,* it is possible to obtain critical frequency measurements for Washington, D.C. Correcting these for latitude, the critical electron density for winter at University Park is $1{\cdot}2 \times 10^5$ electrons cm^{-3}. On the model given here, the winter-time critical electron density is $1{\cdot}3 \times 10^5$ electrons cm^{-3}. The normalized diurnal variation in the critical frequency for December at University Park is shown in Fig. 5, as obtained from the *CRPL* reports. This is compared with the diurnal variations predicted by the model of Jones (1955) and the model of Fig. 4. Once again, there is rather good agreement between theory and experiment.

To this point, a great many rocket data have been utilized to determine the value of certain quantities in these calculations. During several rocket flights an actual measurement of the electron density versus height, over most of the height range of interest, has been made. An average of four of these which occurred at about the same time of day and relatively close to the equinoxes is shown in Fig. 6. The so-called "composite" curve is the average of the rocket results of Jackson (1954) and Seddon *et al.* (1954) for values of N_e greater than 10^4. This is

* U.S. Department of Commerce, National Bureau of Standards, Central Radio Propagation Laboratory *CRPL-F Reports*. Boulder, Colorado.

combined with the D-layer of GARDNER and PAWSEY (1953) for values of N_e less than 500. From an electron density of about 400 electrons cm^{-3} to approximately 2×10^4 electrons cm^{-3} along this composite curve, the density is in reality unknown. The other distributions in this figure are due to JONES (1955), PFISTER (1954) and the result of this work. The models proposed by PFISTER and in this work are in fair agreement with one another, but PFISTER's model is, in general, in better agreement with the rocket results.

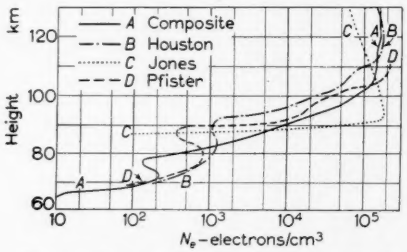

Fig. 6. Comparison of electron distributions.

The Ionosphere Research Laboratory of The Pennsylvania State University has obtained various vertical incidence data at 75 and 150 kc/s over a period of years. Group height, absorption, and change in phase height records on these frequencies are rather extensive. While comparisons of experiment with theory have been made using the data on both frequencies, only the 75 kc/s results will be reported here. Midday winter-time group height records of ROSS (private communication) show that 75 kc/s waves are reflected at 93 km while the Lyman beta calculations presented here indicate group reflection at 96 km.

Absorption measurements at 75 kc/s give a midsummer value slightly in excess of 5 nepers (SCHMERLING, private communication). Using the model of curve B in Fig. 6 and the collision frequency curve of NICOLET (1952b) a value of about 10 nepers is obtained. Such a value is much too large. From the shape of the absorption versus collision frequency curves, it is apparent that the electrons in the 80–90 km region contribute a disproportionate amount to the total absorption. If the electron density for the above model is reduced to a value of 600 electrons cm^{-3} at 90 km, the calculated absorption would agree with the experimentally obtained value. Other possibilities for the removal of this discrepancy include a different distribution of constituents in this particular region, a change in the collision frequency model or both.

Computations of the change in phase height for 75 kc/s waves suffer in a manner similar to the absorption results. However, the diurnal variation in phase height predicted by the variation in Lyman beta intensity for 75 kc/s is in quite good agreement with experimental data (HOUSTON, 1957) obtained at the same frequency. This is shown in Fig. 7.

There are certain features of this figure relative to the 75 kc/s phase height variations which should be emphasized. The first is that in each case, the shape of the theoretical and experimental curve is, in general, quite similar. In the summer portion of the diagram it was necessary to use April data since no later

VOL. 12 1958

summer months records were complete enough to obtain a trustworthy average. Hence, sunrise and sunset are closer to noon than they would be in a true summer month. In turn, this implies that in every case the theoretical curve should lie inside the experimental curve. On this basis it might be concluded that the transition region, where oxygen changes from molecular to atomic form, may be slightly sharper than given by the curve in Fig. 2. The reason for this is that as

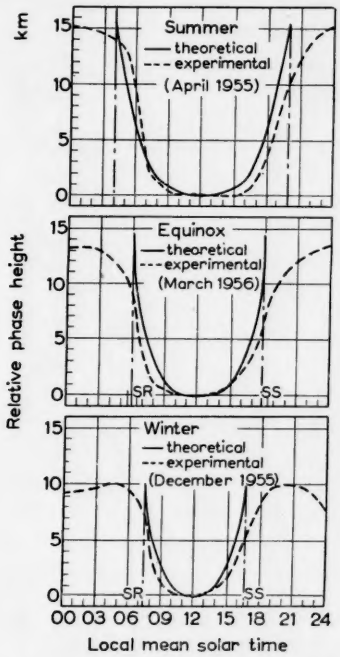

Fig. 7. Experimental vs. theoretical phase height.

the O_2 to O transition becomes sharper, the phase height diurnal variation curve becomes flatter in the period around local noon.

Secondly, while the theoretical curves are symmetrical, it is obvious that the experimental curves are not. This may be the result of different values of polarization due to a phase change between the ordinary and extraordinary mode during the course of the day, the assumption of equilibrium conditions, or some other explanation which is, as yet, unknown.

It should also be pointed out that night-time production may affect the electron distribution for $\chi > 85°$ and hence the diurnal variation predicted by the above model will be somewhat altered.

5. Conclusions

The computations leading to the electron density distribution shown in Fig. 4 are based on rocket measurements obtained independently of the rocket-borne electron density and long-wave radio experiments which are used to verify the theoretical results. This independence lends greater credence to the results

obtained. However, such a model cannot be considered final, since any change in the measured values of incident energy or constituent distributions will alter the electron distribution. A change in the effective recombination coefficient will also affect the electron distribution markedly.

The effect of the helium radiations at about 300 and 500 Å has not been considered, due to a lack of direct experimental measurements on their respective energies. Calculations based on their absorption coefficients, however, indicate that the peaks of absorption should occur at about 120 and 145 km, respectively. This would cause the electron distribution curve to rise almost vertically above 120 km and hence be in closer agreement with the electron distribution curves obtained by rockets.

The overall agreement between values predicted by this model and those obtained experimentally suggest that the predicted electron density distribution is not without merit. The need for more complete and accurate knowledge of the physical processes and numerical values of certain quantities in the region from 85 to 100 km is indicated.

Acknowledgements—The author would like to express his appreciation to Drs. M. Nicolet, J. J. Gibbons and A. H. Waynick, who gave many helpful suggestions and valuable criticisms during the course of this work.

VOL.
12
1958

References

Athay R. G. and Thomas R. N.	1956	*Astrophys. J.* **124,** 586.
Bates D. R. and Seaton M. J.	1950	*Proc. Phys. Soc.* B**63,** 129.
Byram E. T., Chubb T. A. and Friedman H.	1953	*Phys. Rev.* **92,** 1066.
	1956	*J. Geophys. Res.* **61,** 251.
Chapman S.	1931a	*Proc. Phys. Soc.* **43,** 26.
	1931b	*Ibid.* **43,** 484.
Compton A. H. and Allison S. K.	1954	*X-Rays in Theory and Experiment* p. 524. Van Nostrand, New York.
Elwert G.	1953	*J. Atmosph. Terr. Phys.* **4,** 68.
Friedman H.	1954	Conseil International des Unions Scientifiques. *Huitieme Rapport de la Commision pour l'Etude des Relations entre le Phenomenes Solaries et Terrestres* p. 59 Paris.
	1955	*Ann. Geophys.* **11,** 174.
Gardner F. F. and Pawsey J. L.	1953	*J. Atmosph. Terr. Phys.* **3,** 321.
Havens R. J., Friedman H. and Hulbert E. O.	1955	The Ionospheric F_2 Region. *Cambridge Meeting of the Physical Society on the Physics of the Ionosphere* p. 237. The Physical Society, London.
Houston R. E., Jr.	1957	*Scientific Report No.* 93. Ionosphere Research Laboratory, University Park, Pa.
Jackson J. E.	1954	*J. Geophys. Res.* **59,** 377.
Jones R. E.	1955	*J. Atmosph. Terr. Phys.* **6,** 1.
Massey H. W. S.	1954	Mixed Commission on the Ionosphere. *Proceedings of the Fourth Meeting* p. 32. Brussels.
Mitra A. P. and Jones R. E.	1954	*J. Geophys. Res.* **59,** 391.

Nicolet M.	1945	*Mem. Roy. Met. Inst., Belgium* **19,** 1.
	1952a	*Physics and Medicine of the Upper Atmosphere* p. 207. University of New Mexico Press, Albuquerque.
	1952b	*Scientific Report No.* 32. Ionosphere Research Laboratory, The Penn State University.
	1954a	*Scientific Report No.* 61. Ionosphere Research Laboratory, University Park, Pa.
	1954b	*J. Atmosph. Terr. Phys.* **5,** 132.
Nicolet M. and Bossy L.	1949	*Ann. Geophys.* **5,** 275.
Oster L.	1956	*Z. Astrophys.* **40,** 28.
Pfister W.	1954	Report to the National Research Council. *U.S.A. National Committee of URSI on the* XI *General Assembly of URSI* pp. 3–11
Rawer K. and Argence E.	1954	*Phys. Rev.* **94,** 253.
Seddon J. C., Pickar A. D. and Jackson J. E.	1954	*J. Geophys. Res.* **59,** 513.
Straker T. W.	1955	*Monograph No.* 114. Inst. Elec. Engrs., London.
Watanabe K., Marmo F. and Inn E. C. Y.	1953	*Phys. Rev.* **90,** 115.
Watanabe K., Marmo F. and Inn E. C. Y.	1955	*J. Geophys. Res.* **60,** 513.

L.
2
58

Journal of Atmospheric and Terrestrial Physics, 1958, Vol. 12, pp. 236 to 247. Pergamon Press Ltd., London

Low-frequency reflection in the ionosphere—II*

HERMANN POEVERLEIN
Propagation Laboratory, Electronics Research Directorate, Air Force Cambridge Research Center, Air Research and Development Command, Bedford, Massachusetts

(*Received* 25 *January* 1958)

Abstract—The first part of the paper dealt with a theory for ionospheric reflection of low frequencies, i.e. of wavelengths comparable to or great compared to the layer thickness. In the present second part various ranges of data are specified and their reflection characteristics are investigated. Metallic-type reflection is found at high electron concentration and dielectric-type reflection at medium electron concentration above a certain frequency limit. In this latter case, the currents in the ionospheric layer have the direction of the terrestrial magnetic field and the propagation in the layer is very peculiar.

Some consequences of the theory are discussed with references to observations where possible. Among them there are statements about phase, sign, and Brewster case and possibilities of transmission through a layer.

The final section brings some remarks on the theory, mainly on the field-strength quantities introduced. These quantities allow an interpretation which points at a close relationship to Budden's theory.

1. TYPES OF REFLECTION UNDER VARIOUS CONDITIONS

THE theory of low-frequency reflection, on which this paper is based, was developed in Part I of the paper (POEVERLEIN, 1958, referred to as I). For wavelengths long compared to the thickness of the reflecting layer, simple formulations were obtained by considering the layer as an entirety or, in other words, as a thin sheet in comparison to the wavelength. For somewhat shorter wavelengths differential sublayers were assumed to be the reflectors. The combination of all partial reflections from these sublayers represent the actual reflection. The currents or current densities in the sublayers are the reflecting agents. The relationship between the current density and the electric-field strength determines the characteristics of reflection.

The studies in Part I were quite general. In this first section of Part II various typical cases shall be distinguished corresponding to various possible ranges of data. Each of them is characterized by a certain simple approximation for the current density as a function of field strength. Strictly speaking, it is not the field strength that appears as the independent variable, but the components E_x, E_y, D_z. The vertical component of the displacement vector replaces the vertical field-strength component as it did in the formulations of I.

Real cases surely do not always coincide with one of the typical cases. They may sometimes lie at a boundary between them or embrace two typical cases in the reflecting height interval.

1.1. *High collision frequency*

The first case considered is that of high collision frequency, high as compared to the (angular) gyro-frequency (which may be taken positive disregarding the negative sign of the electron charge)

$$\nu \gg \omega_H. \tag{1}$$

* See Erratum page 352.

VOL. 12 1958

This case corresponds to the lowest region of the ionosphere, where the air density is high.

Inequality (1) means that the terrestrial magnetic field is negligible. The equations for the current density components given in I [equations (39)] yield then

$$\left.\begin{aligned} J_x &= \frac{{\omega_0}^2}{\nu}\,\varepsilon_0 E_x \\ J_y &= \frac{{\omega_0}^2}{\nu}\,\varepsilon_0 E_y \\ J_z &= \frac{{\omega_0}^2}{\nu - i\,\dfrac{{\omega_0}^2}{\omega}}\,D_z \end{aligned}\right\} \tag{2}$$

with the dielectric constant of vacuum ε_0 (denoted by ε in I). It was tacitly supposed that ν is also great compared to ω.

From the differential equations of the up-going and down-going wave [I, equations (43)] it follows that this current density in a thin layer can produce remarkable reflection only when

$$\frac{{\omega_0}^2}{\omega} \gg \nu. \tag{3}$$

Under this condition, vice versa, good reflection is actually obtained if the layer is sufficiently thick (but still thin compared to the wavelength).

An estimation based on inequality (3) shows that J_z in a thin layer is negligible (the estimation requires also an estimation of D_z). The reflection, thus, is of the thin-sheet type discussed in I (Section 2) and consequently of the metallic type, except perhaps in the case of poor reflection at grazing incidence.

1.2. *High electron concentration*

The collision frequency shall now be of any magnitude. From the differential equations (43) in I together with the equations for the current density (39) in I it can be seen that good reflection from a thin layer implies the two inequalities

$$\left.\begin{aligned} \frac{{\omega_0}^2}{\omega} &\gg |\nu + i\omega| \\ \frac{{\omega_0}^2}{\omega} &\gg \omega_H. \end{aligned}\right\} \tag{4}$$

With all quantities but ω_0 given they demand a sufficiently high ω_0, i.e. a sufficiently high electron concentration. Decreasing frequency leads to their fulfilment in any case.

Approximations for the current density components under conditions (4) can again be derived from equations (39) in I. For the horizontal current density components the same expressions are obtained as in the thin-sheet reflection theory [I, equations (22)]. The vertical current density component is in general negligible. The fact that now only horizontal current density components have to be considered

and that they depend only on the horizontal field-strength components [see I, equations (22)] should simplify the study of the present case.

In case of a thin layer, inequalities (4) lead to the thin-sheet reflection theory of I (Section 2.3). The reflection is then of the metallic type. In a thicker layer, the partial reflections under conditions (4) are still of the metallic type, but their

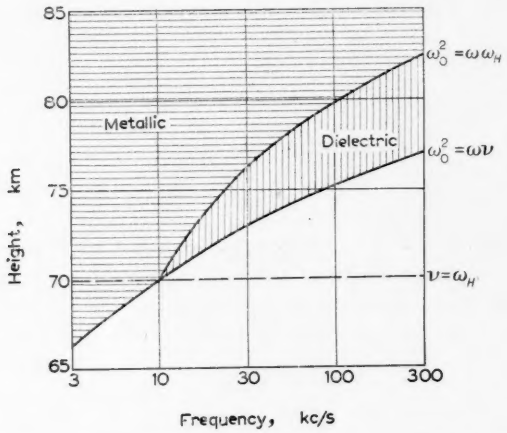

Fig. 1. Conditions for metallic and dielectric reflection at day-time.

superposition with varied phases may entail complications (cf. Section 2.4).

Good reflection from a thicker layer is possible even without fulfilment of inequalities (4), as the subsequent section will show.

1.3. *Intermediate electron concentration*

The case of medium electron concentration corresponding to

$$|\nu + i\omega| \ll \frac{{\omega_0}^2}{\omega} \ll \omega_H \tag{5}$$

offers some interesting aspects.

Fig. 1 shows in a rough sketch the boundaries of this and the other cases in dependence on frequency (for day-time).* An electron concentration increasing monotonically with height and a collision frequency decreasing with height were assumed, using approximately data given by WAYNICK (1957) and NICOLET (1952). The vertically shaded area of Fig. 1 refers to the present case; the horizontally shaded area to the preceding case (Section 1.2). The area below $\nu = \omega_H$ corresponds to Section 1.1 with inequality (1). Only the horizontally shaded part of this area is essential to reflection [inequality (3)]. The notation "dielectric" for the present case will be justified later. It is seen that the present case is encountered in some part of the lower ionosphere, but only for frequencies above a certain limit. Inequalities (5) imply, of course, that $\nu \ll \omega_H$.

* In the boundaries ω in $|\nu + i\omega|$ was neglected.

VOL. 12 1958

The approximative formulas for the current density components derived from I, equations (39), for the present conditions are

$$\left.\begin{aligned} J_x &= i\,\frac{\varepsilon_0\omega}{\omega_z^2}\,\omega_x\left(\omega_x E_x + \omega_y E_y + \omega_z \frac{D_z}{\varepsilon_0}\right) \\ J_y &= i\,\frac{\varepsilon_0\omega}{\omega_z^2}\,\omega_y\left(\omega_x E_x + \omega_y E_y + \omega_z \frac{D_z}{\varepsilon_0}\right) \\ J_z &= i\,\frac{\varepsilon_0\omega}{\omega_z^2}\,\omega_z\left(\omega_x E_x + \omega_y E_y + \omega_z \frac{D_z}{\varepsilon_0}\right). \end{aligned}\right\} \tag{6}$$

As in the first part of the paper ω_x, ω_y, ω_z are the components of the gyro-frequency $\boldsymbol{\omega}_H$ which is considered as a vector. An arbitrary direction of the terrestrial magnetic field with ω_z not disappearing has been assumed.

Equations (6) are somewhat surprising. First they are very symmetrical. Secondly they do not contain ω_0, the quantity expressing the electron concentration; hence the differential equations [I, equations (43)] with equations (6) result in reflection characteristics which are independent of the electron concentration. Another striking fact is that the differential equations with equations (6) allow an easy integration; the solutions for the field-strength components are sums of exponential functions.

The question arises for the actual meaning of equations (6). They represent a current density in the direction of the gyro-frequency vector $\boldsymbol{\omega}_H$ or of the terrestrial magnetic field. Any motion of the electrons perpendicular to the magnetic field is, under the present conditions, apparently suppressed by the magnetic field.

The motion of the electrons along the magnetic force lines is practically free. Collisions could confine it, but they are negligible in consequence of the left-hand inequality (5). The polarization produced will then be so strong as to make the electric-field strength component parallel to the magnetic force lines disappear, whence

$$\omega_x E_x + \omega_y E_y + \omega_z E_z = 0. \tag{7}$$

This equation, after introduction of D_z/ε_0 from I, equation (34), is identical with the third one of equations (6). Thus, our idea proves to be correct.

The polarization is negligible perpendicular to the terrestrial magnetic field and is perfect parallel to it. Perfect polarization means disappearance of the electric-field strength component, but not of the current density component in that direction. It was found that the current density has just the direction of the terrestrial magnetic field. The two facts—**J** being parallel to and **E** being perpendicular to the terrestrial magnetic field—determine the characteristics of the medium regardless of the underlying mechanism and of the electron concentration, provided the electron concentration stays within the limits of inequalities (5).

A further conclusion is: Since the electron concentration has no influence, the ionospheric layer appears as a homogeneous medium for wave propagation. That is the reason why the differential equations are now easily integrable.

A study of the reflection characteristics could be based either on the present theory or on the concept of a homogeneous medium with the limits of inequalities (5) as boundaries. Poor definition of the boundaries could make the latter method fail.

The various current density components in equations (6) are of comparable magnitude. Therefore, all the remarks in Section 3.2 of I about influence of horizontal and vertical current density components apply to the present case. The reflection for **E** parallel to the plane of incidence is consequently of the type obtained from a dielectric. At steep incidence the horizontal component of **E** is reversed, while at shallow incidence the vertical component is. Between, there is a Brewster angle with minimum or zero reflection (see Section 2.3). This type of reflection, in general, is neither close to perfect nor poor. It is due to the terrestrial magnetic field, as the above explanations show.

A detailed study of the present case will not be given now; however one fact may still be mentioned. **E** was seen to lie in a plane perpendicular to the terrestrial magnetic field. If the magnetic field of the wave lies also in that plane, the Poynting vector or the ray has the direction of the terrestrial magnetic field and will probably over longer paths follow changes of it. This guided propagation recalls the type of propagation considered to be responsible for the audio-frequency whistlers, but it yields no dispersion, which would produce the typical whistler sound as originating from pulses. Whistler propagation in general is explained from assumptions corresponding to those of the foregoing section (Section 1.2) and is thought of as occurring in thick, gradually varying layers, which are not considered here.

VOL. 12 1958

2. CONSEQUENCES

The consequences of the theory shall be discussed with a view to phenomena observed or possibly observable in low-frequency propagation. It has to be noticed, however, that previous theories (YOKOYAMA and NAMBA, 1932; BUDDEN, 1951; WAIT and PERRY, 1957; WAIT and MURPHY, 1957), in which a sharp boundary of an otherwise more or less realistic ionosphere was assumed, could already account for some of the observed effects.

Absorption will not be discussed. In any case of imperfect reflection there are actually the two possibilities—absorption or transparency—which might also occur simultaneously.

2.1. *Metallic and dielectric type of reflection*

For **E** perpendicular to the plane of incidence, **E** was found to be reversed in reflection. For **E** parallel to the plane of incidence, the horizontal **E** component in steep incidence is also reversed. The case commonly met with in practical propagation is shallow incidence with **E** parallel to the plane of incidence. Just in that case there are two types of behaviour possible: reversal of the horizontal **E** component as corresponding to metallic reflection and reversal of the vertical **E** component as corresponding to dielectric reflection. The metallic type is obtained under condition (4) and the dielectric type under condition (5).

The height intervals and frequency intervals for the two types at day-time were represented in Fig. 1, but the figure is simplified in that it gives sharp boundaries

($\gg$ sign interpreted as $>$). Actually there is a transition area between metallic and dielectric area, where one type or the other might be found depending on the angle of incidence and on the direction of the terrestrial magnetic field. Also a more complicated transitional behaviour is possible and it can happen that the entire dielectric-type interval is transition area.

A rigorous definition of the boundaries is hardly possible. Any little deviation from the idealized conditions for metallic type will show up at almost grazing incidence and will lead there to a Brewster angle with inversion of sign.

It has to be kept in mind that the reflection takes place not in one definite level, but in a wider height interval (starting at the bottom of the shaded area in Fig. 1). The dielectric type of reflection, as being in general imperfect, is accompanied by some metallic-type reflection from higher levels.

The distinction between the two types of reflection loses its meaning at higher frequencies, at which the phase change in propagation within the layer becomes remarkable. That may be the case in shallow incidence at frequencies above 100 kc/s and in steep incidence at even lower frequencies.

Fig. 1 showed exclusively metallic-type reflection at frequencies below roughly 10 kc/s. That was for day-time only. For night-time the boundaries are shifted towards greater heights and the frequency limit of 10 kc/s consequently towards lower frequencies.

Wide-band observations of atmospherics (100 kc/s cut-off) made by Philip T. Hirt* occasionally exhibit very short peaks which appear twice, the second time with reversed sign. Only night-time observations of this kind were available. The two received pulses seem to be propagated by ground wave and ionospheric wave. The reversed sign of the second pulse indicates dielectric type of ionospheric reflection for the observed vertical **E**.

2.2. *Received phase, reflection height*

The phase of received waves quite generally can be considered as depending on the reflection height, on the phase change in the reflection process, and on the propagation characteristics in the part of the ionosphere below the reflection level.

In the present theory the propagation of the partial waves is always vacuum propagation. The phase of the received wave appears to be determined by the superposition of partial waves with two types of phase behaviour in reflection, with various reflection levels, and with certain phase relationships between them.

Propagation experiments at 16 kc/s (Bracewell *et al.*, 1951; Pierce, 1955, 1957; Straker, 1955) show a very regular diurnal variation of the received phase. The phase changes rapidly around sunrise and sunset, but it stays rather constant at other times (at least in propagation over longer distances). For a complete understanding, especially of the constancy, it may be necessary to consider both the variation of reflection height and the transition from one type of phase behaviour in reflection to the other type. There is the possibility that the two effects on the received phase cancel each other, either partly or completely (Pierce, 1957, p.801).

The present theory permits a relatively simple study of the resulting phase if

* Measurement made for the Air Force Cambridge Research Center. I have to thank Dr. E. Lewis and Mr. L. C. Humphrey for directing my attention to these observations, which are not published yet.

only one type of partial reflection is encountered or, in other words, if the vertical current density components in the reflecting layer are negligible. That is the case, for example, at vertical incidence without terrestrial magnetic field or generally at sufficiently low frequencies (Section 2 of I and Section 1.2 of this paper).

At the lowest frequencies, the entire layer contributes to the reflection. This may be seen from the thin-sheet theory in I (Section 2) or from the differential equations for the up-going and down-going wave [I, equations (43)] after discarding the term with $\pm ik_z$. Since at the lowest frequencies all partial waves have the same phase behaviour in reflection, the resulting wave must also show this phase behaviour, i.e. reversal of the horizontal **E** component. The apparent reflection level of the resulting wave is then near the centre of all partial reflection levels, i.e. somewhere in the middle of the layer.

At much higher frequencies than those under consideration now, geometric optics is valid. The higher frequencies there have a reflection level high up in the layer and the lower frequencies near the bottom of the layer (in its so-called lower tail). In approaching geometric-optical conditions from lower frequencies, therefore, the reflection level must fall. It must reach a minimum in transition to geometric-optical conditions, after which the rise follows.

Ionospheric sounding records at low frequencies (WATTS, 1957) show a slight minimum of one trace around 200 kc/s.* Another trace has no minimum within the recorded frequency range (down to almost 50 kc/s). It seems possible that the two traces represent the two magneto-ionic modes, one of which might have its minimum in the observed frequency range, the other one below. Definite statements, however, shall not be made before any computation. The recorded reflection heights are apparent group reflection heights, whereas the theoretical discussions above were concerned with the phase reflection heights, but the qualitative behaviour of the two is presumably the same.

VOL. 12 1958

2.3. *Brewster case*

Two types of reflection were distinguished with regard to the sign of the (total) reflected electric-field strength, one with reversed horizontal **E** component, the other with reversed vertical **E** component. Which type is encountered, depends on the electron concentration, the angle of incidence, and the frequency of the wave. Lower ionization (at night), shallower angles, and higher frequencies favour reflection with reversed vertical **E** component, i.e. the type corresponding to shallow incidence on a dielectric. There may be a more or less gradual phase transition between the two types.

As mentioned in I (Section 3.2) the partial waves during the transition have different sign behaviour leading to a diminished resulting field strength or, in other words, to minimum or zero reflection. Minimum reflection in combination with phase transition is in optics known as Brewster case, the angle of incidence, at which it is observed, as Brewster angle.

Field-strength minimum and phase transition have been observed for many

* I gratefully acknowledge that Dr. JAMES W. WATTS gave me the opportunity of having a look at the records before publication. The small published reproductions hardly exhibit the minimum.

years. At 17–60 kc/s a minimum in propagation over longer distances appears regularly around sunset (GROSSKOPF, 1941; BRACEWELL *et al.*, 1951; VILBIG, 1953). This minimum was already previously attributed to a presumable transition from metallic to dielectric reflection.

Various authors observed at roughly 16 kc/s a transition with increasing distance, which consists in a change of phase, reflection coefficient and polarization (WEEKES, 1950; BRACEWELL *et al.*, 1951; STRAKER, 1955; HERITAGE *et al.*, 1957). This transition might also be the Brewster case. Some authors (WEEKES, 1950; BRACEWELL *et al.*, 1951) found only a rapid change of the reflection coefficient in the transition, some others (HERITAGE *et al.*, 1957) indication of a minimum. Most observations are made during the day, a few are made at night (BRACEWELL *et al.*, 1951).

The cited observations seem to indicate two types of reflection with a transition between them, but it is not always clear with which type to co-ordinate any observation. It has to be recalled that mode propagation between earth and ionosphere with the superposition of different modes is another reason for field-strength minima.

2.4. *Polarization of the reflected wave*

The reflection of the partial waves in the present theory is a reflection with unchanged polarization. The only variable characteristic of the partial waves is the sign of the field strength after reflection. However, there are in general partial waves with different direction of **E** (in both the incident and the reflected part). Their superposition with certain phase differences may lead to a peculiar polarization of the resulting wave.

In the case of high electron concentration (Section 1.2) it is possible to derive two independent wave equations, which are attributed to two different characteristic polarizations. Thus, two components of a wave are obtained, which correspond to the magneto-ionic modes at high frequencies. At the lowest frequencies, however, any phase difference between these two modes disappears and they are then no longer separable in the downcoming reflected wave. Under this condition the reflection must be of the metallic type as previously stated.

The publications referred to in the preceding section report different polarization of the received waves in the various cases distinguished. An explanation of the observed polarization might follow from an elaboration of the outlines given right now.

2.5. *Possible transparency of a layer*

Several cases have been found, in which the reflection is poor or disappears: for instance, the Brewster case discussed in Section 2.3 or grazing incidence of very-low frequencies with vertical **E** (Sections 2.2 and 2.3 of I). In all these cases the wave passes through the layer unless it is suppressed by absorption. Whilster propagation is an example of waves passing through the thick $F2$ layer. In addition to these singular cases there is a more general transparency possible at the lowest frequencies.

HINES (1957) pointed out that at the lowest frequencies ions have a strong influence on propagation. Therefore, they must also affect the reflection at these frequencies. A look at the current densities should prove that.

The electron current density at sufficiently low frequencies is given by equations (22) in I, which are an approximation applicable under the conditions (4) of Section 1.2. If

$$|\nu + i\omega| \ll \omega_z \tag{8}$$

is assumed, the expressions for the electron-current density are further simplified into

$$\left.\begin{aligned} J_x &= \varepsilon_0 \frac{{\omega_0}^2}{\omega_z} E_y \\ J_y &= -\varepsilon_0 \frac{{\omega_0}^2}{\omega_z} E_x \\ J_z &= 0 \end{aligned}\right\} \tag{9}$$

The contribution of the ions is taken into account by adding the ion-current density to this electron-current density. It may now be supposed that inequalities (4) and (8) are equally valid for ions, i.e. with the quantities ω_0, ω_H, ω_z and ν taken for ions. (That requires, first of all, a frequency well below the gyro-frequency for ions, which is in the order of 30 c/s.) The ion-current density is then also given by the approximation (9), but with ω_0 and ω_z for ions. The only individual factor in equations (9), ${\omega_0}^2/\omega_z$, is independent of the mass of the particles. Its magnitude, therefore, is equal for electrons and for ions of the same concentration, but its sign is different for negative and positive charges. Consequently, the resulting current density as the sum of the two contributions vanishes. This is fortunately not exactly correct, since equations (9) are only approximations.

The correct conclusion is that the remaining current density is much smaller than derived for electrons only, but is still large enough to provide good, though somewhat impaired, reflection. A weak transparency of the layer will be the consequence of the deficiency in reflection. A closer study of this expected transparency may be deferred to another paper.

VILBIG (1953) has suspected a transparency for the lowest frequencies, since the ratio of layer thickness to wavelength becomes there arbitrarily small. On the other hand, formulae of the refractive index as due to electrons indicate an increase of the efficiency of a layer towards lower frequencies, which could nullify this suspected transparency. Ion currents, according to the above explanations, and perhaps other factors which must be taken into consideration support a transparency of an ionospheric layer at the lowest frequencies.

2.6. *Mode theory*

Various studies of mode theory, which assume a sharp boundary of a homogeneous ionosphere, are capable of explaining observed effects (BUDDEN, 1957; SCHUMANN, 1954, 1955; WAIT, 1957; some more references are given by these authors). A few other papers take a stratified layer with simplifying assumptions into consideration (RYDBECK, 1944; SHMOYS, 1956). How the mode theory is influenced by the above reflection theory has not been investigated as yet. One conclusion,

VOL. 12 1958

however, may be drawn for the zero-order mode. In the common meaning this is the mode with **E** being vertical and independent of height, which represents a wave travelling horizontally between two perfect conductors as limiting walls. The ionospheric reflection for exactly grazing incidence was found to disappear at the lower frequencies and to be of the dielectric type at the higher frequencies. The zero-order mode, thus, must be badly affected. WAIT (1957) deduced a heavy attenuation of this mode at frequencies above 3 kc/s.

3. THE FIELD QUANTITIES **F** AND **G**

Any splitting of the field into an up-going and a down-going wave is to some extent arbitrary within the layer. In I the partial-wave concept leads to such a splitting. The vectors **F** and **G** were introduced as representing the two waves. They were derived from the horizontal components of the electric-field strength together with the vertical component of the displacement vector. That is another fact which looks arbitrary. The following explanations, however, may make the two field quantities **F** and **G** more plausible.

3.1. *Characteristics of* **F, G** *and the partial waves*

The partial waves show some simple characteristics. They are propagated with vacuum velocity (propagation constant is vacuum k) and they appear to be transverse plane waves [see equations (33) and (42) in I]. The only characteristic that distinguishes them from vacuum waves is their reflection.

The vector **F** represents the combination of all the ascending halves of the partial waves and **G** that of all the descending halves. Therefore both vectors correspond also to transverse waves [I, equation (42)]. Their differential equations [I, equations (43)] express the vacuum propagation and the simultaneous gradual change with height due to the continuous reflection process. In vacuum, i.e. below and above the layer, **F** and **G** are the electric fields of the actual waves proceeding in the upward and downward direction (directions of incident and reflected wave), as was already mentioned in I.

3.2. *Various interpretations*

The quantities **F** and **G** in any level within the layer contain the partial waves reflected above that level and the wave passing through the layer. They are consequently not affected by the current densities below. That permits some statement. The field in the ionospheric layer is assumed to be given by **F** and **G** as functions of height. If then a lower part of the layer up to a certain level is removed, the quantities **F** and **G** as given are still the solution in the remaining upper part of the layer, provided the wave leaving the layer at the top is unchanged. At the cut-off level the vectors **F** and **G** are to be continued steadily into the vacuum space below. Therefore, they represent in this level the incident and reflected wave. Briefly, **F** and **G** in any level of a layer are the field strengths which would be incident and reflected, if the part of the layer below were cut off and everything above were kept unchanged.

From this interpretation the following one can be inferred: The vectors **F** and **G** at any place are the electric fields of the up-going and down-going wave which

would be obtained in a narrow horizontal gap introduced at that place. A sufficiently narrow gap would have no influence on **F** and **G**. It would therefore be a vacuum space below some part of the layer with the field in this upper part kept unchanged. The statement of the last paragraph applies then to the gap and leads to the present interpretation of **F** and **G**.

3.3. *Budden's reflection coefficient*

BUDDEN (1955) in his second method defines a reflection coefficient R not only for the bottom of the layer, but also for each level inside. This reflection coefficient is conceived as a matrix with four components corresponding to the various incident and reflected horizontal field-strength components. BUDDEN'S reflection coefficient in any level represents the reflection which would be obtained after removing the part of the ionosphere below.

From this interpretation it becomes evident that the components of BUDDEN'S R are just the ratios between our horizontal **G** and **F** components. Only the signs are chosen differently. In a test, BUDDEN's differential equations for R in the isotropic case were easily obtained from the differential equations for **F** and **G** [I, equations (43)] together with equation (44) of I and equations (2) of this paper, which relate to the isotropic case.

3.4. *Comparison with geometric optics*

The present theory is not limited to low frequencies. At frequencies adequate to geometric optics, however, it does not offer as simple a consideration.

In a homogeneous medium the vectors **F** and **G** do not describe the waves in the geometric-optical sense; either one combines wave functions of both an up-going and a down-going geometric-optical wave. That becomes not immediately clear from the integral representation of **F** and **G** in I. The necessary exponential functions are included in the amplitudes under the integrals.

These statements apply also to a slowly varying medium, i.e. to any case in which geometric optics is valid. The whole area, in which geometric-optical propagation takes place, is the reflecting area in terms of our theory. The individual contributions to the total field, however, run through all possible phases and must in superposition lead to the geometric-optical solution.

Coupling between the two magneto-ionic modes as a correctional effect of the geometric-optical theory has not been studied here. The statement in Section 2.4 that two independent differential equations are derivable under the conditions of Section 1.2 (high electron concentration or low frequency) points out disappearance of coupling also in the limit case of the lowest frequencies.

3.5. *Additional remarks*

The picture of a partial wave reflected in a plane is not in accordance with the common concept of radiation or re-radiation from a plane. Under radiation from a plane one might understand a radiation leaving the plane with equal intensity both upward and downward. From this type of radiation, however, the partial wave is easily obtained by adding a wave which travels continuously upward and has just the amplitude and phase as to cancel the wave radiated upward. A combination of

VOL. 12 1958

the re-radiations from all horizontal planes would require the assumption of an additional proceeding wave, which is different from that of the partial-wave concept and which actually represents the incident wave. Taking these re-radiations rather than the partial waves as basis of a theory would entail the occurrence of multiple reflections or higher-order re-radiations and is therefore not advisable.

The integral representations in I recall methods of solving differential equations by means of Green functions. However, these methods seem not to suggest the introduction of the vertical **D** component, which is essential to our theory.

It could be thought that the theory will be helpful in computation. Whether the differential equations (43) of I stated for **F** and **G** are more appropriate to computer work than existing formulations, which have already been used, is not decided yet.

Acknowledgements—I owe thanks for stimulating discussions to Mr. Rodney A. Brooks, Mr. Leonard C. Humphrey, Dr. Edward A. Lewis and Dr. Friedrich Vilbig; for aid in preparing the manuscript to Miss Olive Denniston and Mr. Frank Pivarunas.

References

Bracewell R. N., Budden K. G., Ratcliffe J. A., Straker T. W. and Weekes K.	1951	*Proc. Inst. Elect. Engrs* Part III, **98,** 221.
Budden K. G.	1951	*Phil. Mag.* **42,** 833.
Budden K. G.	1955	*Proc. Roy. Soc.* **A 227,** 516.
Budden K. G.	1957	*Proc. Inst. Radio Engrs* **45,** 772.
Grosskopf J.	1941	*Fortschritte der Hochfrequenztechnik* (Edited by Vilbig F. and Zenneck J.) Vol. 1, p. 95. Akademische Verlags gesellschaft, Leipzig.
Heritage J. L., Weisbrod S. and Bickel J. E.	1957	*Symposium on the Prop. of VLF Radio waves*, Vol. 4, p. 77. National Bereau of Standards, Boulder, Colo.
Hines C. O.	1957	*J. Atmosph. Terr. Phys.* **11,** 36.
Nicolet M.	1952	*Ionospheric Research Scient. Rep., Penn. State College, University Park, Penn.*, No. 32.
Pierce J. A.	1955	*Proc. Inst. Radio Engrs* **43,** 584.
Pierce J. A.	1957	*Proc. Inst. Radio Engrs* **45,** 794.
Poeverlein H.	1958	*J. Atmosph. Terr. Phys.* **12,** In press.
Rydbeck O. E. H.	1944	*Chalmers tek. Högsk. Handl.* No. 34.
Schumann W. O.	1954	*Z. Angew. Phys.* **6,** 225, 267, 3461.
Schumann W. O.	1955	*Z. Angew. Phys.* **7,** 284.
Shmoys J.	1956	*Proc. Inst. Radio Engrs* **44,** 163.
Straker T. W.	1955	*Proc. Inst. Elect. Engrs* **102B,** 396.
		pp. 558, 776. Akademische Verlags-gesellschaft, Leipzig.
Vilbig F.	1953	*Lehrbuch der Hochfrequenztechnik*, Vol. 1, pp. 558, 776.
Weekes K.	1950	*Proc. Inst. Elect. Engrs* Part III, **97,** 100.
Wait J. R.	1957	*Proc. Inst. Radio Engrs* **45,** 760, 768.
Wait J. R. and Murphy A.	1957	*Proc. Inst. Radio Engrs* **45,** 754.
Wait J. R. and Perry L. B.	1957	*J. Geophys. Res.* **62,** 43.
Watts J. M.	1957	*J. Geophys. Res.* **62,** 484.
Waynick A. H.	1957	*Proc. Inst. Radio Engrs* **45,** 741.
Yokoyama E. and Namba S.	1932	*Rep. Radio Res. Japan* **2,** 131.

Journal of Atmospheric and Terrestrial Physics, 1958, Vol. 12, pp. 248 to 257. Pergamon Press Ltd., London

Method of measuring ionospheric winds by fading at spaced receivers

R. B. BANERJI *
Indian Statistical Institute, Calcutta

(*Received* 22 *August* 1957)

Abstract—The different statistical methods developed for the measurement of ionospheric drifts by spaced receivers have been reviewed and the essential unity of the basic model brought out. The geometrical method of PÜTTER and the probability-distribution method of the Cambridge School have been merged into a single method which promises to be less laborious than the autocorrelation methods but of comparable accuracy.

1. INTRODUCTION

THE method of measuring winds in the ionosphere by spaced receivers is based on the theory of random fading originally proposed by RATCLIFFE (1948) and developed by BOOKER, RATCLIFFE and SHINN (1950). According to this theory, the fading of a singly reflected sky wave (when only one of the magnetoionic modes exists) is caused by diffraction at an irregular ionosphere. This phenomenon gives rise to a random diffraction pattern of signal strength at the ground. The fading is caused by the drift of this random diffraction pattern across the ground as well as by irregular changes in the pattern.

This pattern can be represented by contours of equal signal strength on the ground and can be imagined to have a general form similar to that shown in Fig 1. Since the mapping of the pattern from instant to instant is not practically feasible, we have to be satisfied with the specification of certain statistical properties of the pattern which can be deduced from the fading at some isolated points. The arrangement universally used at present for this purpose is a set of three receivers placed at three corners of an approximate isosceles right-angled triangle, such a geometry being very convenient though not essential for drift measurement.

In the next section we shall develop the statistics of the random diffraction pattern and its relationship to the fadings at three points.

2. STATISTICAL MODEL OF THE RANDOM DIFFRACTION PATTERN

The basis of all methods of drift measurement lies in the space correlation, time correlation and cross-correlation of the amplitude.

The space correlation between two points separated by a distance ξ in the X-direction is defined by

$$\rho(\xi) = \frac{\overline{R(x)R(x+\xi)} - \overline{R(x)}^2}{\overline{R(x)^2} - \overline{R(x)}^2} \tag{1}$$

where R is the amplitude at x and the bars denote average values, either over all x at one instant or, more practically, over time at two locations x and $x + \xi$. Under constant conditions they lead to identical values. From the formula it can be seen that the maximum possible value of this quantity is 1 and is attained at $\xi = 0$.

* Now at Operations Research Group, Case Institute of Technology, Cleveland 6, Ohio, U.S.A.

VOL. 12 1958

The correlation in another direction can be defined similarly. The time correlation at a single point is defined by

$$\zeta(\tau) = \frac{\overline{R(t)R(t+\tau)} - \overline{R(t)}^2}{\overline{R(t)^2} - \overline{R(t)}^2} \tag{2}$$

All these quantities, however, are derivable from the general function known as cross-correlation, which is the correlation between the amplitude at (x, y) at time t and at $(x + \xi, y + \eta)$ at time $t + \tau$. It is thus written as

$$\rho(\chi,\eta,\xi) = \frac{\overline{R(x, y, t)R(x + \xi, y + \eta, t + \tau)} - \overline{R(x, y, t)}^2}{\overline{R(x, y, t)^2} - \overline{R(x, y, t)}^2} \tag{3}$$

We will now study the properties of this function in some detail and correlate the results obtained by YERG (1955) and BRIGGS, PHILLIPS and SHINN (1950), who developed their methods independently and from somewhat different points of view.

It is clear how $\rho(0, 0, 0) = 1$ and attains its maximum value at this point. It is also symmetrical about this point, so that the function can be approximated by a quadratic function of the variables up to a considerable distance from the origin.

To understand the physical significance of the different terms of this expression, let us first take up an unchanging diffraction pattern. Here the correlation function will be a function of space only, so that we can write

$$1 - \rho = A\xi^2 + B\eta^2 + 2C\xi\eta \tag{4}$$

which shows that the average shape of the diffraction contours is elliptical.

When there is a random change of the pattern going on, a quadratic term in τ is added, yielding

$$1 - \rho = A\xi^2 + B\eta^2 + 2C\xi\eta + D\tau^2 \tag{5}$$

In the absence of anisotropy this can be written as

$$1 - \rho = A(\xi^2 + \eta^2 + V_c^2\,\tau^2) \tag{6}$$

Where V_c is a fictitious velocity (named by BRIGGS, PHILLIPS and SHINN, the characteristic velocity) which is a measure of the random change of the pattern and may be defined as the "speed at which the stationary pattern would have to drift to get the same average rate of change of amplitude that is occurring in the absence of drift, by random changes alone".

In the anisotropic case we can rotate the co-ordinate axes so that the correlation function is given by

$$1 - \rho = (\xi A'^2 + K\eta^2 + V_c^2\tau^2) \tag{7}$$

where $K < 1$; in this case V_c^2 is defined in terms of drift along the major axis of the correlation ellipse.

Let us now consider the effect of drift. To do this we imagine a system of co-ordinates (ξ', η') moving with the drift. With respect to this system, the pattern can still be considered as one with only random changes and in this system the correlation is still given by equations (5), with a uniquely defined V_c. On

transforming to the co-ordinates fixed with respect to the ground, the equation changes to

$$1 - \rho = A\xi^2 + B\eta^2 + 2C\xi\eta + D'\tau^2 + 2E'\xi\tau + 2F'\eta\tau \tag{8}$$

where A, B, C corresponds to the stationary pattern and

$$\left.\begin{aligned} D' &= D + 2V^2C \sin\theta \cos\theta \\ E' &= -CV \sin\theta - AV \cos\theta \\ F' &= -CV \cos\theta - AV \sin\theta \end{aligned}\right\} \tag{9}$$

(V, θ) being the magnitude and direction of the velocity of drift.

Now let the co-ordinates at the ground have one of the receivers at the origin, one at a distance ξ_0 along the x-axis and the other at a distance η_0 along the y-axis. Then by evaluating the correlations between the various receivers we can obtain $\zeta(\xi_0, 0, 0)$, $\zeta(0, \eta_0, 0)$, $\zeta(-\xi_0, \eta_0, 0)$, $\zeta(0, 0, \tau_i)$, $\zeta(\xi_0, 0, \tau_i)$, $\zeta(0, \eta_0, \tau_i)$, the first three being space correlations, the next, the time correlation, and the last two, cross-correlations. From these, the general expression for ρ and hence the co-efficients of the quadratic expression in equation (8) may be calculated.

From the values of the coefficients the values of V, θ and $D(AV_c^2)$ can be deduced easily as

$$\left.\begin{aligned} V \sin\theta &= -\frac{CE' - AF'}{C^2 - AB} \\ V \cos\theta &= -\frac{CF' - BE'}{C^2 - AB} \\ D &= D' + \frac{AF'^2 + BE'^2 - 2CE'F'}{C^2 - AB} \end{aligned}\right\} \tag{10}$$

The above formulae, deduced by YERG, is a direct extension of BRIGGS, PHILLIPS and SHINN's formula to the anisotropic case. However, BRIGGS, PHILLIPS and SHINN derived their formula from a different point of view. They started by defining "apparent drift velocities" V_x' and V_y' as follows.

"If two receivers are separated by a distance ξ_0 in the x direction, then the lag τ_{0x} for which the correlation between two receivers is a maximum is given by

$$\xi_0 = V_x'\tau_{0x} \tag{11}$$

and similarly for V_y'".

In the isotropic case, our analysis as applied to their point of view leads to the equations

$$V_x'V \cos\theta = V_y'V \sin\theta = V_c'^2 \tag{12}$$

$$V_c^2 = V_c'^2 - V^2 \tag{13}$$

where $V_c'^2 = D'/A$. This will be clear if we find V_x' from our value of ρ and use equation (10). In BRIGGS, PHILLIPS and SHINN's paper (where these coefficients are not discussed) V_c' is obtained by noting the value of τ for which

$$\rho(\xi_0, 0) = \rho(0, \tau)$$

and defining

$$V_c' = \frac{\xi_0}{\tau}$$

VOL. 12 1958

It must be remembered, however, that though BRIGGS, PHILLIPS and SHINN's formulae are derivable from our approximation to the shape of the autocorrelogram, they are somewhat more generally deducible. Specifically, instead of taking $1 - \rho$ to be a homogenous linear expression in $\xi^2 + \eta^2 + V_c^2\tau^2$, we can take it to be any single valued monotonic function of $\xi^2 + \eta^2 + V_c^2\tau^2$ to derive the same results.

It is clear how the property of the non-drifting pattern, as depicted in equation (5), leads to the results of YERG (1955) and of BRIGGS, PHILLIPS and SHINN (1950). Let us now look at the pattern from another point of view.

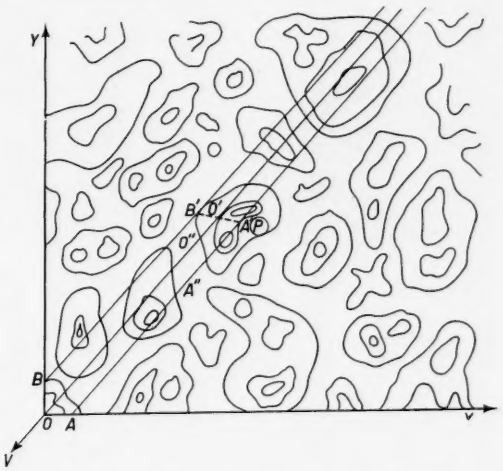

Fig. 1. A typical diffraction pattern on the ground.

3. THE BASIS FOR THE METHOD OF SIMILAR FADES

Let us once more look at Fig. 1, assumed devoid of random changes. Let this pattern now move in the direction OV so that the three observing stations appear to move across the pattern along OO' AA' and BB'. Let us consider the fading caused by the "blob" P. From the shape of the contours we can see that the signal strength at the receiver B goes through a maximum when B' (the point of tangency of BB' to the contour) goes through B. Similarly, the signal at O and A will go through maxima when O' and A' go through them. In other words, maxima are encountered on the records when the lines like $A'B'$, passing through the points of tangency of the line of velocity to the contours, pass through the receiving stations. We shall call these the lines of maxima. The fundamental problem in the determination of velocities by the method of similar fades is the determination of the distribution of the inclination of these lines and its relationship to the autocorrelation ellipse. Let us, however, initially consider the relationship between the inclination of the line of maxima $B'O'A'$, the lags between the maxima in the three receivers and the magnitude and direction of the drift.

In Fig. 2, let a certain line of maxima cross the receiver at O at time $t = 0$ and the receiver at A time $t = t_1$. Let V be the velocity of drift and θ the angle between its direction and the x-axis; and let the inclination of the line of maxima

to the perpendicular to the direction of drift be ψ. Let OA, the separation between the receivers, be ξ_0; then we have

$$t_1 = \frac{\xi_0}{V \cos \psi} \cos (\psi + \theta) \tag{14}$$

and similarly if η_0 be the separation between O and B and t_2 the time of passage of the same line of maxima through B, we have

$$t_2 = \frac{\eta_0}{V \cos \psi} \sin (\psi + \theta) \tag{15}$$

obtaining

$$\left.\begin{aligned} \frac{t_2/\eta_0}{t_1/\xi_0} &= \tan (\psi + \theta) \\ \text{and} \quad (t_2/\eta_0{}^2) + (t_1/\xi_0)^2 &= \frac{1}{V^2 \cos^2 \psi} \end{aligned}\right\} \tag{16}$$

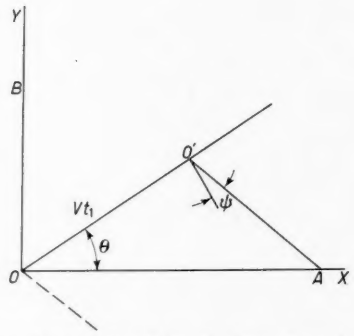

Fig. 2. The drift of a line of maxima.

Mitra (1949) and Kraütkramer (1950) based their analysis on the tacit assumption that $\psi = 0$; i.e. that the line of maxima will always be perpendicular to the line of motion, and obtained somewhat simpler formulæ which allowed an estimation of V and θ from t_1 and t_2. As can be gathered immediately, this method of analysis would lead to different values of the velocity vector for different sets of maxima, depending on the value of ψ. However, Pütter (1955) pointed out that in the absence of random velocities, all time-lag pairs obtained would be related to one another. This can be obtained by eliminating ψ between equations (14) and (15) to yield

$$\frac{t_1}{\xi_0} \cos \theta + \frac{t_2}{\xi_0} \sin \theta = \frac{1}{V} \tag{17}$$

That is, in the absence of random velocities, the plots on the (t_1, t_2) plane corresponding to different maxima would lie on a straight line perpendicular to a line through the origin and with a slope λ, given by

$$\tan \lambda = \frac{\xi_0}{\eta_0} \tan \theta \tag{18}$$

VOL. 12 1958

from which the value of θ can be found. Now, if we draw another line with equation

$$\frac{t_2}{t_1} = \frac{\eta_0}{\xi_0} \tan \theta \tag{19}$$

it intersects our line of plot at a point

$$\bar{t}_1 = \frac{\xi_0 \cos \theta}{V} \tag{20}$$

$$\bar{t}_2 = \frac{\eta_0 \sin \theta}{V} \tag{21}$$

which will be found to be identical with MITRA's expression for t_1 and t_2, the "unique" lags corresponding to this velocity for $\psi = 0$.

It will be noted that PÜTTER's analysis does not in any way depend on the statistical distribution of the points corresponding to the different maxima. It is the relative orientation of the points rather than their actual positions which is important. If absence of random motions can be assumed, therefore, the method is the least laborious and involves the use of very few maxima—which is an advantage over the previous methods. However, PÜTTER's methods does not indicate how the results would be modified in the presence of random motions. One purpose of this paper will be to extend PÜTTER's method to include the effect of random motions. To do this, however, we shall have to take into account the actual statistical distribution of t_1 and t_2 (instead of the simple geometrical relationship between the two.). The problem was first taken up by RATCLIFFE (1954). In the following we shall present RATCLIFFE's analysis as improved and developed by BRIGGS and SPENCER (1955) and then develop the work further as an extension of PÜTTER's geometrical approach.

4. Analysis of Time Lags Between Maxima in the Presence of Random Changes

Let us once more consider the system of co-ordinates drifting with the diffraction pattern, as in Section 2. The receivers then drift along this pattern along the lines OO', AA' and BB', as in Fig. 1. The resulting fluctuations in the signal strength at two receivers are correlated. In other words, knowing the signal strength at O'', the probability distribution of the signal strength at A'' can be calculated. This distribution changes with the position of A'' relative to O'', but does not depend on the actual position of any of them.

Let us initially consider random changes to be absent. In the isotropic case, the correlation between the signals depends only on the distance between them, being greatest when A'' is at the foot of the perpendicular from O'' on AA'. The value of the correlation is given by the parameters of the correlation ellipse. The point of interest to us is "Given that there is a maximum of signal strength at O'', what is the probability that there is a maximum at A'', when A'' is at a given distance x from the foot of the perpendicular?"

BRIGGS and PAGE (1955) approached the problem empirically by constructing artificial time series with different correlations between them and found that, if

the autocorrelation in space of a stationary pattern were isotropic and Gaussian, the angle $\psi = \tan^{-1} x/d$ (where d is the length of the perpendicular) had a distribution given by

$$P(\psi)\, d\psi \propto e^{\tan^2 \psi / 0{\cdot}74}$$

It is to be noted that this angle is the inclination of the line of maximum to the perpendicular.

This idea of BRIGGS and PAGE can be directly extended to the case of superposed random changes if we remember that their experimental analysis pertains to two

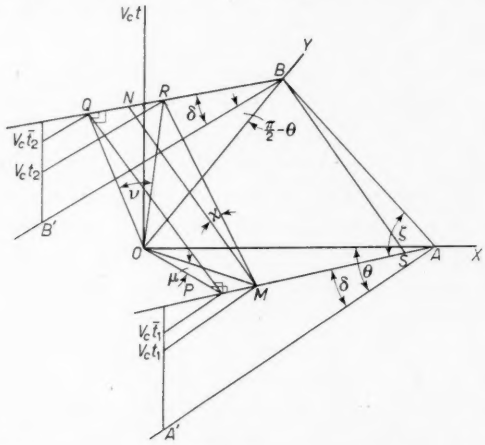

Fig. 3. Geometry of the diffraction pattern in space and time.

time series and bears no relation to the dimensionality of the diffraction pattern. BRIGGS and SPENCER, therefore, applied their analysis to the three-dimensional contour of the signal strength in space and time.

Fig. 3 shows a co-ordinate system drifting with the pattern as before. If we now introduce a co-ordinate $V_c t$ perpendicular to the (x, y) plane, the contours of equal signal strength will form a three-dimensional pattern. Since the auto-correlation is a symmetric function of x, y and $V_c t$, this three-dimensional pattern will be isotropic.

The signal strength at the receiver A at time t is given by the value of the contour at the point $(\xi_0 - Vt \cos\theta, \eta_0 - Vt \sin\theta, V_c t)$ and similarly for receivers O and B. Now, if there is a maximum at the receiver O at time $t = 0$, the probability of there being a maximum at the receivers A and B will be greatest at time t_1 and t_2, corresponding to P and Q, the feet of the perpendicular from O on AP and BQ. The direction cosines of these lines is $(-\cos\theta, -\sin\theta, \cos\delta)$ where

$$\delta = \tan^{-1} \frac{V_c}{V}$$

According to BRIGGS and PAGE's analysis, the probability of there being a maximum at receiver A_1 at time t_1 when there is one at O at time $t = 0$ is given by

$$P(t_1) \propto e^{-\tan^2 \mu / 0{\cdot}74} \qquad (22)$$

VOL. 12 1958

and similarly for t_2. BRIGGS and SPENCER's distribution follows from this if we substitute the value of μ in terms of space and time, to obtain

$$P(t_1) \propto \exp\left[-\frac{(t_1 - \bar{t}_1)^2}{0{\cdot}74\{\xi_0/(V^2 + V_c^2) - \bar{t}_1^2\}}\right] \tag{23}$$

$$\bar{t}_1 = \frac{\xi_0 V}{V^2 + V_c^2}\cos\theta \tag{24}$$

and similarly for $P(t_2)$ from the angle ν.

5. Extension of Pütter's Method to the Case of Random Changes

The work of the Cambridge School, as described in the last section, deals with the individual distribution of the time lags observed between individual pairs of receivers. It is our purpose in this section to examine the relationship of the lags $t_1$and t_2 observed in the two pairs of receivers. In the case of pure drift, PÜTTER has shown how t_1 and t_2 are connected linearly. Evidently, this exact relationship will break down in the presence of random motion. *A* correlation, however, is still expected to remain. To investigate this correlation, let us first investigate the joint distribution of t_1 and t_2. It will be seen that the angle χ in Fig. 3 is related to $t_1 - t_2$ just as μ and ν are related to t_1 and t_2. Knowing χ to be normally distributed, we obtain

$$P(t_2 - t_1) \propto \exp\left[-\frac{\{(t_2 - \bar{t}_2) - (t_1 - \bar{t}_1)\}^2}{0{\cdot}74\left\{\frac{\xi_0^2 + \eta_0^2}{V^2 + V_c^2} - (\bar{t}_1 - \bar{t}_2)^2\right\}}\right] \tag{25}$$

Now, any two normally distributed variables with a correlation ρ between them have a joint distribution

$$P(x, y) \propto \exp\left[-\frac{1}{2(1-\rho^2)}\left\{\frac{x^2}{\sigma_x^2} - 2\rho\frac{xy}{\sigma_x\sigma_y} + \frac{y^2}{\sigma_y^2}\right\}\right] \tag{26}$$

which leads to the distribution of their difference

$$P(x - y) \propto \exp\left[-\frac{(x-y)^2}{2(\sigma_x^2 - 2\rho\sigma_x\sigma_y + \sigma_y^2}\right] \tag{27}$$

which, when compared to equation (25), yields for the value of the correlation between t_1 and t_2 as

$$\rho = -\frac{0{\cdot}74}{2}\frac{\bar{t}_1\bar{t}_2}{\sigma_{t_1}\sigma_t} \tag{28}$$

Thus we obtain the joint distribution of t_1 and t_2, being given their individual distribution as also their correlation. The lines of equal probability on the (t_1, t_2) diagram, are ellipses. When $\xi_0 \approx \eta_0$ the major axes of these ellipses lie perpendicular to the direction λ where

$$\tan\lambda = \frac{\xi_0}{\eta_0}\tan\theta$$

i.e. the direction is the same as that corresponding to the PÜTTER straight line in the absence of random motions. However, the intersection of this line with

$t_2/t_1 = \eta_0/\xi_0 \tan\theta$ does not yield the magnitude of the velocity but leads to a "velocity"

$$\frac{V^2 + V_c^2}{V} \tag{29}$$

as indicated by equation (23). However, the spread of the points about the major axis is an independent indication of the magnitude of V_c. It can be shown that ρ is connected to V and V_c by the relation

$$\frac{2}{V^2 + V_c^2} = \left(\frac{\bar{t}_1^2}{\xi_0^2} + \frac{\bar{t}_2^2}{\eta_0^2}\right) + \left[\left(\frac{\bar{t}_1^2}{\xi_0^2} - \frac{\bar{t}_2^2}{\eta_0^2}\right)^2 + 4\,\frac{\bar{t}_1^2\bar{t}_2^2}{\xi_0^2\eta_0^2}\cdot\frac{1}{\rho^2}\right] \tag{30}$$

Thus V can be determined unambiguously. A procedure for this is described below.

The analysis starts with a plot on the (t_1, t_2) diagram of all the points obtained from a single record by measuring the lags between corresponding maxima on the three receivers.

Having obtained the plots, the first task would be to find the major axis of the ellipse over which they are distributed. Denoting the (t_1, t_2) pairs by (x_i, y_i), the inclination ϵ of this major axis to the $x(t_1)$–axis can be shewn to be obtainable by the formula:

$$\tan 2\epsilon = \frac{2\sum_i (x_i - \bar{x})(y_i - \bar{y})}{\sum_i (x_i - \bar{x})^2 - \sum_i (y_i - \bar{y})^2} \tag{31}$$

The perpendicular to this major axis thus has an angle $\lambda = \epsilon + \pi/2$. From this we can find θ, the direction of drift, as well as $V/(V^2 + V_c^2)$. The correlation coefficient being obtained by the usual formula, $V^2 + V_c^2$ can be determined also. Thus V, θ, V_c can be determined.

VOL. 12 1958

6. Concluding Remarks

In conclusion, a short comparison of the different known methods of wind measurement is attempted.

In MITRA's method, no indication of the velocity can be obtained from a small number of observations, as no provision is made for the elimination of ψ, the angle between the line of maximum and the perpendicular to the line of motion, which differs from one set of maxima to another. However, in the case of isotropic patterns, ψ is symmetrically distributed about zero, and if t_1 and t_2 are averaged over a large number of maxima, the mean values can be taken to satisfy MITRA's formula for the velocity. It can be seen from a study of the geometry of the pattern, however, that in the anisotropic case, this would again lead to a wrong value of the velocity (BANERJI, 1956) and direction. It is also clear from what has gone before, that even in the isotropic case the presence of random motions will indicate a larger value of the velocity with this method, though the direction will be correctly determined.

The method of PÜTTER gets rid of the effect of ψ by a simple geometrical method, so that the velocity is obtainable from a smaller number of maxima in the absence of random motions. The method is also independent of any effect of anisotropy.

There is thus a double advantage in using the PÜTTER method in the case of pure drift. The extension of PÜTTER'S method made here, as well as the method

of BRIGGS and SPENCER, shows that in the presence of superposed random motion both fail to evaluate the wind velocity without a large number of observations. As to whether the presence of anisotropy affects the extended PÜTTER method also still remains to be seen.

The autocorrelation method of BRIGGS, PHILLIPS and SHINN and that of YERG are identical in principle, except that YERG has explicitly worked out the effects of anisotropy. From the point of view of computational labour, however, YERG's method presents a distinct advantage, involving the computation of only six correlation coefficients. A quick method for computing autocorrelation curves has, however, been suggested by BOWHILL (1956).

One point that needs detailed investigation is the accuracy of estimation afforded by the different methods. We can look at the problem of wind determination as one of statistical estimation of parameters and different methods have different "efficiencies" in the statistical sense. In this connection it would also be of value to estimate the amount of information obtainable from a given length of fading record and to find means of utilizing the whole of this information. Some results of studies in these directions will be reported in the near future.

Acknowledgements—The work described in this paper was carried out at the Pennsylvania State University and sponsored by the Geophysics Research Directorate of the Air Force Cambridge Research Center, Air Research and Development Command.

Thanks are due to Dr. A. H. WAYNICK of the Pennsylvania State University and Prof. S. K. MITRA of the University of Calcutta for their unstinted help during the work and during the preparation of the paper. The helpful discussions with Dr. W. PFISTER are acknowledged gratefully.

REFERENCES

BANERJI R. B.	1956	Scientific Report No. 81; Ionosphere Research Laboratory, The Pennsylvania State University.
BOOKER H. G., RATCLIFFE J. A. and SHINN D. H.	1950	*Phil. Trans. Roy Soc.* A **242,** 579.
BOWHILL S. A.	1956	*J. Atmosph. Terr. Phys.* **8,** 129.
BRIGGS B. H. and PAGE E. S.	1955	Phys. Soc. Report on 1955 Cambridge Conference on Physics of Ionosphere, p. 119.
BRIGGS B. H., PHILLIPS G. J. and SHINN D. H.	1950	*Proc. Phys. Soc.* B **58,** 106.
BRIGGS B. H. and SPENCER M.	1955	Phys. Soc. Report on 1955 Cambridge Conference on Physics of Ionosphere, p. 123.
KRAÜTKRAMER J.	1950	*Arch. Elect. Übertrag.* **4,** 133.
MITRA S. N.	1949	*Proc. Inst. Elect. Engrs* III, **96,** 517.
PÜTTER Von P. St.	1955	Phys. Soc. Report on 1955 Cambridge Conference on Physics of Ionosphere, p. 191.
RATCLIFFE J. A.	1948	*Nature, Lond.* **162,** 886.
RATCLIFFE J. A.	1954	*J. Atmosph. Terr. Phys.* **5,** 173.
YERG D. G.	1955	*J. Geophys. Res.* **60,** 173.

Journal of Atmospheric and Terrestrial Physics, 1958, Vol. 12, pp. 258 to 265. Pergamon Press Ltd., London

On the ionospheric current system of the geomagnetic solar flare effect (s.f.e.)

H. VOLLAND and J. TAUBENHEIM
Heinrich-Hertz-Institut der Deutschen Akademie der Wissenschaften zu Berlin, Berlin-Adlershof

(*Received* 3 *January* 1958)

Abstract—A synoptical chart of the horizontal vectors of a geomagnetic s.f.e. and a comparison of the s.f.e. vectors of a number of selected effects at Niemegk shows, that the s.f.e. current system is not a simple enhancement of the S_q current system. The s.f.e. current system is an independent system having a phase difference between 15 and 30 deg. with respect to S_q system, and flowing in a level different from the S_q current level. A correlation between the respective intensities of geomagnetic s.f.e., sudden ionospheric disturbance, and E-layer effect, suggests that both the E-layer and the D-layer contribute to the geomagnetic s.f.e. From a number of selected effects the respective contributions of D- and E-layer are estimated as nearly equal.

1. INTRODUCTION

SINCE MCNISH's investigations (MCNISH, 1937) on the geomagnetic solar flare effect (s.f.e.) the opinion exists, that the s.f.e. is generated by a short time enhancement of the ionospheric S_q current during the flare. After TAUBENHEIM (1957) has quantitatively examined the enhancement of the E-layer critical frequency during solar flares, and on the other hand the E-layer is regarded as contributing the main part to the S_q current, it has become possible to examine MCNISH's idea.

The following data have been used for the investigation described below:

(a) Copies of magnetograms from 21 European and African observatories at 30 and 31 May 1956.

(b) Copies of magnetograms from the Geomagnetic Observatory, Niemegk, from January 1951 to June 1957, inclusively.

(c) The critical frequency measurements of the E-layer at Lindau/Harz, from April 1951 to May 1957, inclusively.

(d) The Mögel–Dellinger effects (S.I.D.) reported by the Max-Planck-Institute, Lindau/Harz, published monthly by Dieminger, in *Nachrtech. Z.* (formerly, *Fernmeldetech. Z.*), and observations of S.I.D. by the Heinrich-Hertz-Institute, Neustrelitz.

2. THE SOLAR FLARE EFFECT ON 31 MAY 1956, 0750 GMT

The s.f.e. at 31 May 1956, beginning on 0750 GMT, is outstanding by its distinctness. It showed the typical form of s.f.e. (i.e. quick increase and slow decrease) and was not superposed by non-periodic perturbations. The geomagnetic field on 31 May 1956, was relatively quiet (K-indices between 1 and 3) and had a clearly pronounced S_q variation. Simultaneously with the occurrence of the

VOL. 12 1958

s.f.e., a Mögel–Dellinger effect (S.I.D.) an effect in atmospherics (S.E.A.), and a solar radio burst were reported. The horizontal vector of the departure from the S_q variation at the maximum time of the s.f.e. (0800 GMT) was determined from the magnetograms of 20 European and 1 African geomagnetic observatories. This value was compared with the horizontal vector of the S_q variation. For the zero level of the S_q variation the mean of the 4 night hr of the preceding night was used.

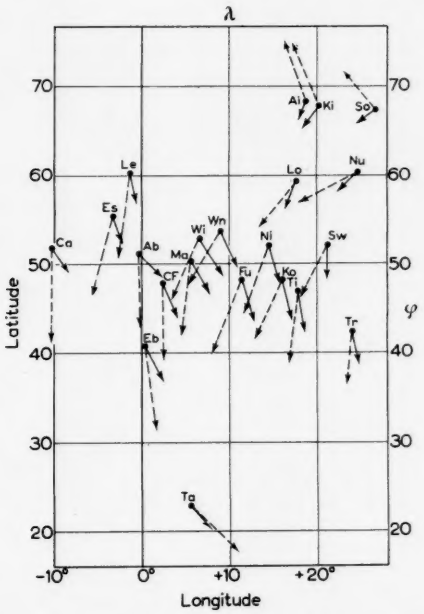

Fig. 1. Synoptical chart of vectors of the S_q current (broken lines) and the s.f.e. current (full lines) determined from the geomagnetic s.f.e. on 31 May 1956, 0800 GMT. (For names of the observatories see *Acknowledgements* at the end of the paper.)

In the case of Niemegk this base and the S_q-vector are not essentially different from the comparable data determined from the hourly means of the five international quiet days of May 1956 (see Fig. 4). Other variations (L, S_D and non-periodic perturbations) which superpose the S_q-vector so determined are therefore believed to be so small that they need not be considered.

A consideration of the induced field in the earth's interior was not necessary, since RIKITAKE (1951) has shown that the ratio of the internal and external parts of the s.f.e. practically equals the corresponding ratio of the S_q variation.

In Fig. 1 the horizontal vectors $\Delta \boldsymbol{H}$ of the s.f.e. (full lines) and of the S_q variation $\Delta \boldsymbol{H}_0$ (broken lines) from all observatories are drawn, each turned clockwise by 90°, so that the direction of the arrows is now identical with the direction of the equivalent ionospheric currents. The S_q current system is clearly visible, which is an evidence for the admissibility of the zero level determination used. At the three northern stations the geomagnetic conditions during the night were disturbed, therefore the zero level determination of these stations is questionable.

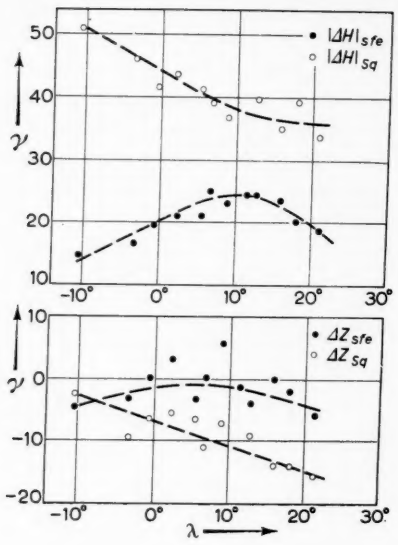

Fig. 2. ΔH and ΔZ vs. longitude, of geomagnetic S_q and s.f.e. vectors from 12 stations between 47 and 55 deg. geographical latitude (cf. Fig. 1).

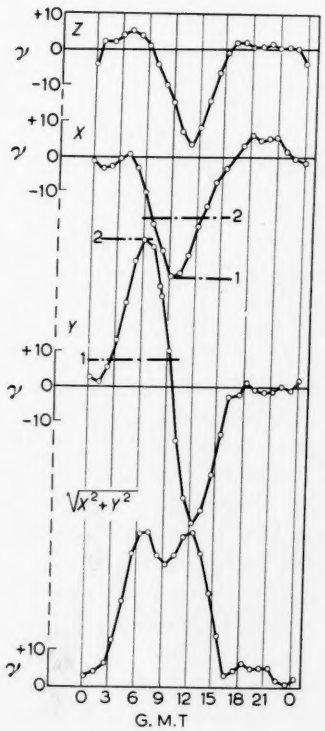

Fig. 3. S_q variation for May 1956 of the Niemegk observatory, determined from the 5 international quiet days.

VOL. 12 1958

The directions of the s.f.e. vectors at all stations show a distinct positive difference from the S_q vectors. Only the most southern station, Tamanrasset, shows an exception.

Since most of the observatories are situated between 47 and 55 deg. of northern latitude, their S_q variations are approximately comparable with each other. For this comparison, the absolute values of ΔH and ΔH_0, and ΔZ and ΔZ_0 are represented in Fig. 2 as functions of geographic longitude. Whilst ΔH_0 and ΔZ_0 tend to a relative minimum with increasing eastern longitude, ΔH and ΔZ reach a maximum at about 10°E. For comparison, Fig. 3 gives the diurnal variation of the absolute value of the S_q horizontal vector, and the X-, Y-, and Z-components of S_q at Potsdam–Niemegk for May 1956. These curves are determined from the hourly means of the five international quiet days of May 1956.

Comparing the Figs. 1, 2 and 3, the facts may be simply explained as follows. The s.f.e. of 31 May 1956, is not produced by a simple enhancement of the S_q current, but by an independent s.f.e. current system generated by the flare. The centre of this s.f.e. current must be situated in a level different from the S_q current centre. (It will be shown below, that the s.f.e. current flows likely below the S_q current within the E- and D-regions.) The mechanism generating the s.f.e. current corresponds to that of the S_q current and can be explained by the dynamo theory. Therefore the s.f.e. current is qualitatively similar to the S_q current, the daytime current eddy on the north hemisphere, however, lags behind the S_q eddy by about 15–30 deg. This is a consequence of the phase difference of the wind systems in the corresponding levels. At Tamanrasset, south of the midday centre of the S_q eddy, the horizontal vector of S_q moves counter-clockwise, in contrast to Niemegk, north of the eddy centre. Following our model, the departure in direction of the s.f.e. vector from the S_q vector must be negative at Tamanrasset. This is to be seen on Fig. 1.

In order to prove that the angle differences on Fig. 1 are not a consequence of the arbitrariness of the zero level determination, in Fig. 3 there are drawn two zero lines respectively, for ΔX and ΔY. These zero lines had to be used, if the angle differences on Fig. 1 should be vanishing. It may be seen that a distinct angle difference between S_q and s.f.e. currents remains even in the case, that the daily mean is used as zero level for S_q.

3. Investigation of Selected Solar Flare Effects at Niemegk

In order to clear up, whether the behaviour of the s.f.e. of 31 May 1956, is generally valid for all solar flare effects, 16 effects from the magnetograms of Potsdam–Niemegk, occurring between January 1951 and May 1957, were analysed in the same manner as described in Section 2. The S_q-vectors were determined from the five international quiet days of the corresponding months. These effects occurred simultaneously with clear sudden ionospheric disturbances, and only very distinct magnetic effects without influences of perturbations were selected. The result is shown in Fig. 4. It supports the opinion, that a particular s.f.e. current system is generated at all seasons and times of day.

Fig. 5 shows the angle difference between S_q and s.f.e. versus time of day for these 16 cases. Moreover, in Fig. 5 the angle between two horizontal vectors of

S_q, different by one hour, from Fig. 3, is drawn as a function of time of day. This curve, varying with season and solar activity, is only a qualitative illustration but it shows, that the angle difference between the s.f.e. and S_q currents has a

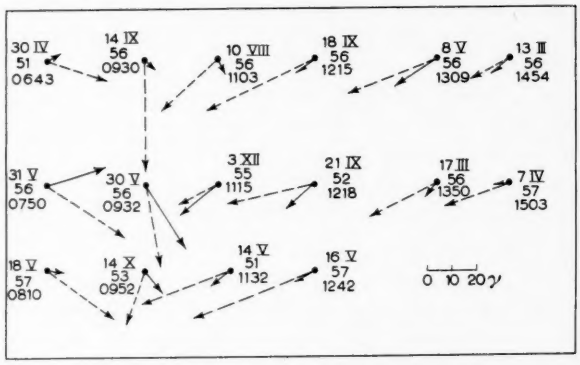

Fig. 4. Geomagnetic S_q (broken lines) and s.f.e. (full lines) horizontal vectors of 16 selected s.f.e. at Niemegk (time of the beginning of the s.f.e. in GMT).

maximum at about 1100 hr local time and decreases strongly both towards sunrise and sunset. A similar behaviour of the angle difference can be seen in Fig. 5.

VOL. 12 1958

4. Statistical Results on the Connexion between Ionospheric and Geomagnetic Solar Flare Effects

During the time from April 1 1951 to May 31 1957, 350 sudden ionospheric disturbances were recorded. Of these, 76 effects must be excluded because of too high geomagnetic activity, which made the detection of solar flare effects impossible. Among the remaining 274 effects only 7 cases were found, which

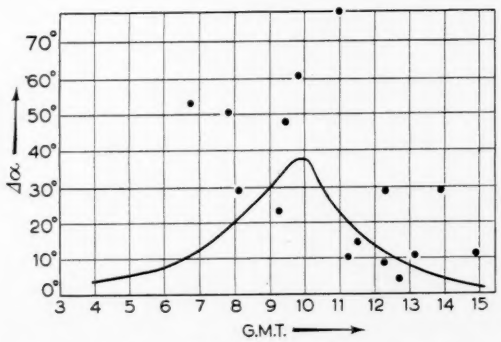

Fig. 5. Angle difference between S_q horizontal vectors, different by 1 hr, of Niemegk, for May 1956 (full curve) (see Fig. 3), and angle difference between S_q and s.f.e. from Fig. 4 (dots).

showed no measurable geomagnetic s.f.e. at the time of the S.I.D. In all other cases, geomagnetic effects were observable and, at least approximately, measurable. This suggests that sudden ionospheric disturbances are at least much more frequently accompanied by geomagnetic effects, than it was hitherto supposed.

If we take into consideration the solar flare effects in the E-layer (TAUBENHEIM, 1957), we find, that of the 7 cases without geomagnetic effect 6 cases show no E-layer effect, too. This suggests a correlation test between the ionospheric and geomagnetic solar flare effects, in order to determine the ionospheric regions responsible for the geomagnetic s.f.e. For 120 cases the amplitude of the geomagnetic s.f.e. can be numerical given. Among these, there are 29 cases for which both the amplitude of the S.I.D. and the amplitude of the E-layer effect are measurable. In all other cases, one of the amplitudes is uncertain. The following values were correlated:

x = Intensity of the sudden ionospheric disturbance, expressed in decibels.
y = Maximum enhancement of E-layer electron density, determined from the ionograms at Lindau/Harz, expressed in per cent of normal electron density ($\Delta N_E/N_{0E}$).
z = Maximum horizontal vector of the geomagnetic s.f.e. from the magnetograms of Niemegk, expressed in per cent of the S_q horizontal vector (after BARTELS, 1952) for the same time of day ($\Delta H/\Delta H_0$).

The maximum enhancement of the E-layer electron density was extrapolated from the half-hourly critical frequency measurements according to an exponential decrease of the ionizing radiation (TAUBENHEIM, 1957).

For the 29 cases mentioned above, the following correlation coefficients were found:

$$r_{xz} = 0{\cdot}60; \qquad r_{yz} = 0{\cdot}52; \qquad r_{xy} = 0{\cdot}34.$$

Because of the small number of data involved, only the coefficients r_{xz} and r_{yz} are statistically significant. But if a number of additional cases is taken into account, for which only the values x and y are given, we get a statistically significant coefficient r_{xy} which differs not significantly from the value given above, so that the above value of r_{xy} is usable.

A mutual influence of the three correlations can be eliminated by partial correlation after R. A. FISHER. The partial correlation coefficient between magnetic s.f.e. and S.I.D. eliminating the influence of the E-layer effect, is

$$r_{xz.y} = 0{\cdot}52$$

The partial correlation coefficient between E-layer effect and magnetic s.f.e., eliminating the influence of the D-layer (S.I.D.), is

$$r_{yz.x} = 0{\cdot}42$$

This result may be interpreted as an evidence, that generally the D-layer (responsible for the anomalous S.I.D. absorption) and the E-layer are to nearly equal amounts responsible for the resulting geomagnetic solar flare effect.

5. Estimate of the Respective Contributions of D- and E-layer to the Geomagnetic s.f.e.

By the following simple consideration we can get an estimate of the relative portions of the s.f.e. current flowing in the E-layer and in the remaining layers (presumably the D-region), respectively.

The S_q current i_0 is composed by a portion i_{0E} flowing in the maximum level of the E region, and a remaining portion i_{0R} flowing in other regions. Thus

$$i_0 = i_{0E} + i_{0R} \qquad (S_q \text{ current}) \tag{1}$$

In the same manner, the additional current i of the geomagnetic s.f.e. is composed by a portion i_E in the E-region maximum, and a portion i_D in other regions, so that

$$i = i_E + i_D \qquad (\text{s.f.e. current}) \tag{2}$$

The whole current flowing during the s.f.e. is then

$$i_0 + i = i_{0E} + i_E + i_{0R} + i_D \tag{3}$$

or

$$i_0 \left(1 + \frac{i}{i_0}\right) = i_{0E} \left(1 + \frac{i_E}{i_{0E}}\right) + i_{0R} + i_D \tag{4}$$

Since the magnetic horizontal intensity is proportional to the current, we have

$$\frac{i}{i_0} = \frac{\Delta H}{\Delta H_0} \tag{5}$$

Moreover, the E-layer current is approximately proportional to the E-layer maximum electron density, so that

$$\frac{i_E}{i_{0E}} = \frac{\Delta N_E}{N_{0E}} \tag{6}$$

Both $\Delta H/\Delta H_0$ and $\Delta N_E/N_{0E}$ are given for a number of s.f.e. If we presume, that the S_q current is flowing only in the E-region, so that $i_{0E} \equiv i_0$, then for a number of cases a negative current i_D follows from equation (4). The assumption $i_{0E} \equiv i_0$, therefore, will not be correct. Negative values of i_D, however, can be avoided, if we approximately assume that within the E-region about one half of the S_q current is flowing, so that

$$i_{0E} \approx i_{0R} \approx \tfrac{1}{2}\, i_0 \tag{7}$$

Then after equation (4)

$$\frac{i_D}{i_E} = 2\, \frac{\Delta H/\Delta H_0}{\Delta N_E/N_{0E}} - 1 \tag{8}$$

The evaluation of 23 selected effects yields as a mean value

$$\frac{i_D}{i_E} \approx 1{\cdot}1$$

Thus the respective contributions of the E-region and the remaining regions (presumably the D-region) to the s.f.e. current may be regarded as nearly equal.

6. Conclusions

Both the synoptical chart of the horizontal vectors of the s.f.e. field on 31 May 1956 (Fig. 1), and the comparison of the s.f.e. vectors of 16 additional effects at Niemegk show that the current system of the geomagnetic s.f.e. cannot be

VOL. 12 1958

identical with the S_q current system. The phase difference between the two current systems, being 15–30 deg., may be regarded as an evidence that the current systems are situated in different levels. The correlation analysis of the intensities of geomagnetic s.f.e., sudden ionospheric disturbance (D-region), and E-layer effect suggests contributions of both the D- and the E-region to the magnetic s.f.e., while according to other authors (LUCAS, 1954) the centre of the S_q current system is above the E-layer. Thus the s.f.e. current system must be situated below the S_q system. This result agrees well with the conclusions of APPLETON and PIGGOTT (1954) from absorption measurements. Similarly MITRA and JONES (1953) suggest that the s.f.e. current system flows either in or below the E-layer. There is also some agreement with ELLISON (1950), who showed that the s.f.e. current level is not identical with the S_q current level, though we disagree with his conclusion that the s.f.e. current is confined to the D-layer. An estimation from a number of selected effects shows that the D- and E-regions contribute nearly equal parts to the s.f.e. current.

Acknowledgements—The authors are indebted to the geomagnetic observatories of Abisko (Ai), Kiruna (Ki), Sodankylä (So), Nurmijärvi (Nu), Lerwick (Le), Lovö (Lo), Eskdalemuir (Es) Wingst (Wn), Witteveen (Wi), Swider (Sw), Niemegk (Ni), Cahirciveen (Ca), Abinger (Ab), Manhay (Ma), Wien–Kobenzl (Ko), Furstenfeldbruck (Fü), Chambon-la-Forêt (CF), Tihany (Ti) Trojan (Tr), Ebro (Eb), and Tamanrasset (Ta), for sending magnetograms.

REFERENCES

APPLETON E. V. and PIGGOTT W. R.	1954	*J. Atmosph. Terr. Phys.* **4,** 141.
BARTELS J.	1952	*Landolt-Börnstein, Zahlenwerte u. Funktionen* (6th Ed.) Vol. III. Springer Verlag, Berlin, Göttingen, Heidelberg.
ELLISON M. A.	1950	cited after FERRARO (1955) in *Nature, Lond.* **175,** 242.
LUCAS I.	1954	*Arch. Elektr. Ubertr.* **8,** 123.
MCNISH A. G.	1937	*Terr. Mag.* **42,** 108.
MITRA A. P. and JONES R. E.	1953	*J. Atmosph. Terr. Phys.* **4,** 141.
RIKITAKE T.	1951	*Bull. Earthq. Res. Inst. Tokyo* **28,** 219.
TAUBENHEIM J.	1957	*J. Atmosph. Terr. Phys.* **11,** 14.

Journal of Atmospheric and Terrestrial Physics, 1958, Vol. 12, pp. 266 to 271. Pergamon Press Ltd., London

Non-uniformity in the brightness of the sun's disk during the eclipse of 30 June 1954*

C. M. MINNIS
D.S.I.R. Radio Research Station, Ditton Park, Slough

(*Received* 14 *December* 1957)

Abstract—Previously published Norwegian and British ionospheric measurements, made during the eclipse of June 1954, showed that the solar ionizing radiation was not emitted uniformly from the whole disk. Although the brightness distributions derived from the Norwegian and British data appeared to be dissimilar, it is shown that the difference is superficial and that the underlying similarity is very close. Quantitative data for the most probable distribution are given and the results are compared with the distribution calculated from observations of solar noise radiation at 10·7 cm during the eclipse.

1. INTRODUCTION

THE total eclipse of the sun on 30 June 1954 occurred during an extended period of very low solar activity and optical observations made on the day of the eclipse confirmed the almost complete absence of any local sources of activity on the disk. It was expected, therefore, that this would be one of the rare eclipses during which the sun's disk could be regarded as a uniformly bright source of ionizing radiation and that the ionospheric changes accompanying the eclipse would conform to this simple model. In the event, the ionospheric data showed that the brightness distribution was not quite uniform. Attempts have been made to deduce the actual distribution by LANDMARK *et al.* (1956) from Norwegian data and by MINNIS (1956a) using measurements made in Great Britain; in both cases the results refer to the ionizing radiation responsible for the *F1*-layer.

The resulting Norwegian and British distributions have been presented in different forms and this fact obscures the underlying similarity between them. Further, in computing the distributions, different values have been used for the effective recombination coefficient and the published results are not, for this reason, immediately comparable. The purpose of this note is to reduce the two sets of results to a form which allows them to be compared directly and to derive the best estimate of the brightness distribution making use of the results from all five of the observatories concerned.

2. THE EFFECTIVE RECOMBINATION COEFFICIENT

At one of the three Norwegian observatories (Tromøya) and also at Ekenäs in Sweden (STOFFREGEN 1956), the eclipse was total at the height of the *F1*-layer. At both places, assuming that the ionizing radiation was completely cut off at second contact, the effective recombination coefficient in this layer (α'_{F1}) was found to be $1{\cdot}7 \times 10^{-8}$ cm^3 sec^{-1}. This value is higher than expected but it is consistent with ionospheric measurements which were made at the same time by

* Official communication from D.S.I.R. Radio Research Station, Ditton Park, Slough.

VOL. 12 1958

Bibl and Delobeau (1956) near Bergen and by Minnis (1956b) at Inverness; at these places the maximum areas obscured were 98 per cent and 91 per cent respectively and, in consequence, only lower limits for α'_{F1} could be obtained.

In the derivation of the brightness distribution at the Norwegian observatories, the measured value, $\alpha'_{F1} = 1{\cdot}7 \times 10^{-8}$ cm^3 sec^{-1}, was used. At the British observatories, since the eclipse was partial and no measured value could be obtained, an assumed value, $\alpha'_{F1} = 1{\cdot}0 \times 10^{-8}$ cm^3 sec^{-1}, was used in the original calculations. The British distributions have now been revised using the measured value for α'_{F1} and it is these amended distributions which are compared in Section 4 with the Norwegian results.

3. The Location of the Bright Sources

After making certain assumptions, the changes in the intensity of the ionizing radiation during an eclipse can be expressed in terms of the electron density of the *E* or the *F1* layer and its rate of change with time. The instantaneous intensity, $J(t)$, as derived in this way would be proportional to the unobscured area, $A(t)$, of the disk if the ionizing radiation were emitted uniformly from the whole disk. The $J(A)$ plots for the 1954 eclipse at Inverness and Slough (Minnis 1956c) show that, to a first approximation, the disk was, in fact, uniformly bright. However, a more careful analysis showed that, to explain the rapid changes in electron density near first and last contacts, it was necessary to postulate the existence of small additional bright sources near the East and West limbs. Up to this point the Norwegian and British interpretations of the eclipse data are the same.

At Inverness and Slough small discrepancies still remained after allowing for the East and West limb sources. To account for these it was necessary to assume a slight darkening of the disk near the North and South Poles. A geometrically acceptable system of brightness contours which would represent this combination of equatorial brightening and polar darkening is shown in Fig. 1a. Unfortunately the accuracy of the ionospheric measurements is not good enough to allow the exact positions and shapes of these contours to be established and the idealized model shown in Fig. 1b. was used in subsequent quantitative work.

Instead of assuming that the disk brightness decreased towards the poles, the Norwegian workers postulated the existence of an additional bright line source near the centre of the disk (Fig. 1c). The authors say, however, that this is not intended to represent an actual localized source and that it "may cover the greater part of the sun's disk." If this source is expanded into an elliptical area to cover the disk except at the polar regions, the Norwegian model reduces essentially to the British one. Since there is no evidence for the existence of a local source of radiation near the centre of the disk during the eclipse, the British model seems more likely to represent the actual brightness distribution.

4. The Intensities of the Bright Sources

Both the Norwegian and the British conclusions can thus be interpreted in terms of the following component sources of the total radiation:

(a) a uniformly bright disk;
(b) east and west limb sources;
(c) an elliptical central source.

The contribution of each source to the total has been computed for each of the five observatories using the same value for α'_{FI} and the resulting mean values are

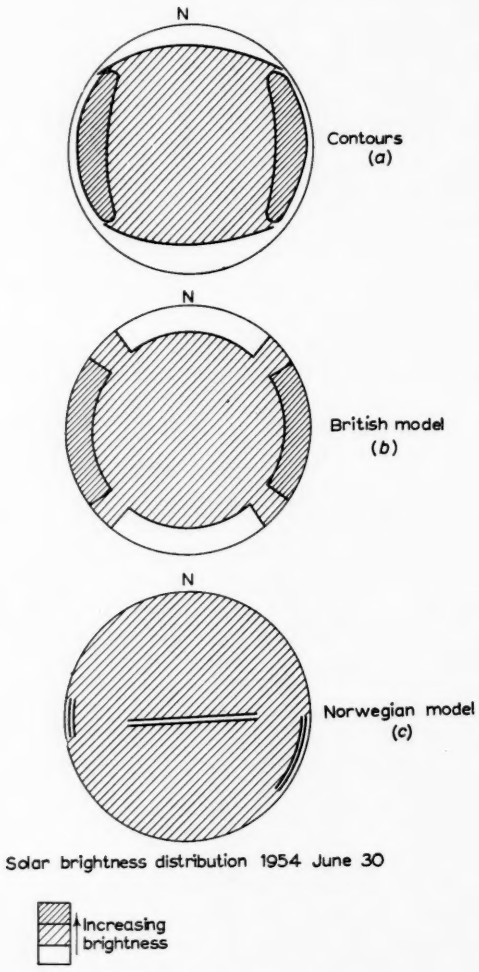

Fig. 1

given in Table 1. The consistency of the results obtained at the individual observatories can be judged from Table 2 in which the differences between the observed and mean intensities are shown.

It is estimated that a difference of about ± 2 per cent in the intensity of any component would not significantly worsen the fit between the observed $J(t)$ curves and those derived from the model. Bearing in mind that the sum $(J_C + J_D)$ is the quantity which is measured directly, and that it is more difficult to separate the two components, the values of ΔJ given in Table 2 are of the expected order of magnitude.

VOL. 12 1958

5. The Surface Brightness

In Table 1 the best estimate of the fractional contribution of each source to the total intensity has been given. It is probably more useful, when considering the physical implications of the observations, to convert these data into corresponding values of the brightness of the disk (flux per unit area) and to do this it is necessary

Table 1. Intensities of sources of ionizing radiation. 1954 June 30
($F1$-layer; $\alpha'_{F1} = 1{\cdot}7 \times 10^{-8}$ cm^3 sec^{-1})

Source	Mean Intensity (per cent)
Uniform disk	72 (J_D)
Central area*	10 (J_C)
East limb	5 (J_E)
West limb	13 (J_W)
Total	100

* This area does not extend to the poles.

Table 2. Differences between observed and mean intensities
ΔJ (per cent of total) = (observed − mean)

Observatory	Maximum obscuration (area per cent)	$\Delta(J_C + J_D)$	ΔJ_D	ΔJ_C	ΔJ_E	ΔJ_W
Tromøya	100	−2	−8	+6	−1	+3
Kjeller	99	−1	0	−1	0	+1
Inverness	91	+2	+4	−2	−1	−1
Tromsø	75	+1	+3	−2	−1	0
Slough	72	−1	−1	0	+3	−2

to know the areas of the bright and dark annular regions shown in Fig. 1b. These areas cannot be obtained accurately from the ionospheric data but the British results suggest that their radial extent does not exceed 0·2 R

Since it is not possible to define these areas precisely, the brightness has been calculated for a number of possible radial and angular dimensions. The results are given in Tables 3 and 4 in which the brightness of the centre of the disk is represented by unity. As mentioned earlier, the error of measurement of the intensity of each source is estimated to be ±2 per cent of the total radiation. This leads to possible errors of only ±3 per cent in the brightness of the polar regions (Table 3) but, for the east limb area (Table 4), the error varies from ±16 per cent (90°, 0·2) to ±35 per cent (30°, 0·05).

If the west limb source is assumed to extend over the whole of the corresponding annular area, the brightness of this area would be about $2\frac{1}{2}$ times that of

the east limb area (Table 4). The British results suggested the possible existence of a small bright spot near the west limb and, if such a spot did exist, the multiplying factor just quoted would be smaller.

Table 3. Relative brightness of polar regions referred to centre of disk

θ	r/R	
	0·05	0·2
30°	0·88	0·87
90°	0·87	0·86

Table 4. Relative brightness of east limb source referred to centre of disk

θ	r/R		
	0·05	0·1	0·2
30°	8·5	4·8	2·9
60°	4·7	2·9	2·0
90°	3·5	2·3	1·7

Table 5. Relative brightness of east limb source and polar regions referred to centre of disk

	East limb	Poles
Ionosphere (*F1*-layer)	1·8	0·86
Radio noise (10·7 cm)	1·5	0·91

It is interesting to note that there is some similarity between the relative brightness values quoted in Tables 3 and 4 and those determined by Covington *et al.* (1955) who made solar radio noise intensity measurements at 2800 Mc/s during the same eclipse. This is illustrated in Table 5 in which the data of Tables 3 and 4 have been adjusted to fit the geometry of Covington's model which differs slightly from that of Fig. 1b.

Covington's model extends slightly beyond the visible disk but only the brightness contours on the disk have been considered in deriving the figures in Table 5.

6. Conclusions

The changes in the *F1*-layer which occurred during the 1954 eclipse at three Norwegian and two British observatories have already been used to show that, even at sunspot minimum, the ionizing radiation is not uniformly distributed over the sun's disk.

VOL. 12 1958

Although the resulting Norwegian and British distributions are superficially different, it is shown here that they are essentially the same. Further, when the Norwegian measured value for the effective recombination coefficient is used in conjunction with the British data, very satisfactory quantitative agreement is obtained between the results obtained at all the observatories.

The brightness at the poles is found to be about 87 per cent of that at the centre of the disk. For the east limb, the figure depends on the area from which the additional radiation is emitted but the brightness is probably between two and five times that at the centre of the disk. The west limb appears to be even brighter than this but this may be due to the presence of an additional small bright source.

These results bear some resemblance to the brightness distribution derived from measurements of solar radio noise on 2800 Mc/s which were made in Canada during the same eclipse.

Acknowledgements—The work described above was carried out as part of the programme of the Radio Research Board. This paper is published by permission of the Director of Radio Research of the Department of Scientific and Industrial Research.

References

Bibl K. and Delobeau F.	1956	*Z. Geophys.* **21,** 215
Covington A. E., Medd W. J., Harvey G. A. and Broten N. W.	1955	*J. Roy. Astr. Soc. Canad.* **59,** 235.
Landmark B., Lied F., Orhaug T. and Skribeland S.	1956	*Geofys. Publ.* **19,** 1.
Minnis C. M.	1956a	*J. Atmosph. Terr. Phys.* **9,** 201.
Minnis C. M.	1956b	*Solar Eclipses and the Ionosphere* p. 204 Pergamon Press, London.
Minnis C. M.	1956c	*Solar Eclipses and the Ionosphere* p. 158. Pergamon Press, London.
Stoffregen W.	1956	*Solar Eclipses and the Ionosphere* p. 57. Pergamon Press, London.

Journal of Atmospheric and Terrestrial Physics, 1958, Vol. 12, pp. 272 to 282. Pergamon Press Ltd., London

The interpretation of changes in the *E*- and *F1*-layers during solar eclipses

C. M. MINNIS
D.S.I.R. Radio Research Station, Slough

(*Received* 3 *January* 1958)

Abstract—Recent eclipse measurements have been explained in terms of the response of a Chapman layer to the obscuration of a solar disk on which localized sources of ionizing radiation are superposed on a uniformly bright background. This interpretation is supported by several features of the results obtained during a series of eclipses.

An alternative interpretation postulates a complex layer containing two different species of ion but assumes only a uniformly bright solar disk. This hypothesis has been examined but calculations based on it result in expected changes in the layer, during an eclipse, which are not in accord with certain characteristics of the experimental data.

A suggestion has been made that the layer tilts which occur during an eclipse may give rise to errors in the interpretation of the data. Experimental results are quoted which suggest that such errors are probably not important.

1. INTRODUCTION

1.1. *The simple theory*

PROVIDING that certain initial assumptions are made, the calculation of the changes in the peak electron density (N) of the E- or the $F1$-layer during a solar eclipse is quite straightforward. The assumptions on which such calculations are usually based are as follows:

(a) The layer behaves as a simple Chapman layer;

(b) The changes in N during an eclipse can be represented by the relation:

$$\frac{dN}{dt} = q - \alpha' N^2 \tag{1}$$

which is strictly applicable only to a fixed height;

(c) The effective recombination coefficient (α') is of the order 10^{-8} cm^3 sec^{-1};

(d) The solar ionizing radiation is emitted uniformly from the whole of a disk having the same diameter as the visible disk.

The shape of the resulting ideal $N(t)$ curve is well-known: apart from its smooth V-shaped form, its principal characteristics are (i) the slow rate of change of N at the beginning and end of the eclipse and (ii) a lag (Δt) of several minutes in $N_{\min}$, the minimum value of N, which always occurs after the maximum phase of the eclipse.

1.2. *The experimental data*

The ideal $N(t)$ curve described above generally provides only a rough first approximation to the changes which are actually observed during eclipses. Typical characteristics of the observed $N(t)$ curves, which differentiate them from the ideal one, are as follows:

(a) The presence of fairly abrupt changes in slope;

(b) The rate of change of N at the beginning and end of the eclipse is frequently much greater than the theoretical one;

VOL. 12 1958

(c) Δt may be either positive or negative;

(d) The observed values of $N_{\min}$ and Δt at a given station are often inconsistent with any single value of α'.

In any attempt to account for these differences it is necessary to ask whether all the assumptions made in Section 1.1. are true.

If a layer does, in fact, behave as a Chapman layer, it seems unlikely that, during an eclipse, the inapplicability of 1.1(b) could give rise to discrepancies of the kind and magnitude observed. Also, the choice of a value of α' different from that given in 1.1(c) could not alone account for the characteristics in 1.2(a)–1.2(d). This leaves the assumptions in 1.1(a) and 1.1(d) under suspicion and it seems probable that they must be jointly or individually responsible for most of the differences between the ideal and the experimental $N(t)$ curves. These possibilities are discussed in the following sections in the light of theoretical work and eclipse observations carried out during recent years.

2. The Sun's Disk

2.1. *Early eclipse observations*

The existence of sudden changes in the slope of the observed $N(t)$ curves has often been used as evidence for the existence of isolated bright sources of ionizing radiation superposed on the uniform disk referred to in 1.1(d). Attempts have sometimes been made to relate these changes, in a qualitative way, with the obscuration and subsequent emergence of visible active areas on the sun, but the results are not convincing.

For the eclipse of January 1940, Higgs (1942) made a quantitative estimate of the relative contributions to the total ionizing radiation of the uniform disk and of four other sources which were assumed to coincide with four calcium plages; he concluded that the whole of the radiation came from the plages and also that the solar brightness distributions for the *E*- and *F1*-layers were quite different from each other. These conclusions are difficult to accept and may be criticised on the grounds that the analysis began by assuming that the sources of the ionizing radiation were located in the visible plages.

Since Higgs' observations, the results of a recent sequence of carefully observed eclipses have become available and in some cases these allow the hypothesis of non-uniformity in the brightness of the disk to be examined more closely than has hitherto been possible.

2.2. *Recent work*

The key to the technique usually adopted for dealing with the *E*-and *F1*-layer measurements made during eclipses is to rewrite Chapman's equation in the form

$$\left(N^2 + \frac{1}{\alpha'}\frac{dN}{dt}\right)\sec^n \chi = A'\left(\frac{q_0}{\alpha'}\right) = J \qquad (2)$$

Equation (2) defines the parameter J and A' represents the fraction of the ionizing radiation remaining unobscured; the other symbols have their usual meanings. If the relation $N^2 \propto \cos \chi$ is not valid on the control days, the index n in equation

(2) differs from unity and it must be given the appropriate value which will allow the diurnal component of the changes in N to be eliminated. If q_0/α' remains constant, J will be proportional to the changes in the intensity of the incident ionizing radiation during the eclipse. For any given value of α', the changes in J can be evaluated using the measured values of N and dN/dt.

Having obtained an observed $J(t)$ curve in this way, it is possible to compare it with the curve calculated assuming a uniformly bright disk. The component of an observed $J(t)$ curve which is attributable to any elementary bright point source must obviously be a rectangular pulse, the amplitude and width of which

Table 1. Consistency of ionospheric eclipse data with a model brightness distribution

Eclipse	Number of stations		Reference
	Consistent	Inconsistent	
January 1940	?		HIGGS (1942)
July 1945	1 (a)		RYDBECK (1946)
February 1952	2		MINNIS (1955)
June 1954	3 (b)		LANDMARK *et al.* (1956)
June 1954	2 (b)		MINNIS (1956a)
December 1954	1		SZENDREI and MCELHINNY (1956)
June 1955	1		MINNIS (1957)
December 1955		1 (c)	MINNIS (1958a)

(a) The curve for $\alpha' = 1{\cdot}2 \times 10^{-8}$ cm^3 sec^{-1} given by RYDBECK in his Fig. 13 can be shown to be consistent with a solar model.

(b) Superficially different models have been published to explain the Norwegian and British results but it has since been shown that a common model can be used for all five stations. (MINNIS, 1958b).

(c) The inconsistency is thought to be due to vertical movements in the E-layer and the consequent inapplicability of equations (1) and (2).

VOL. 12 1958

will be determined by the intensity and latitude of the source. It is not possible to interpret an observed $J(t)$ curve in terms of a non-uniform disk unless the component attributed to sources other than the uniformly bright background can be obtained by integrating a number of such pulses. The $J(t)$ curves which have been observed usually can be interpreted in this way and, in consequence, it does not seem unreasonable to accept the existence of additional bright sources as a tentative explanation of the departures of the observed from the theoretical curves. Only in one out of eleven actual $J(t)$ curves which were suitable for examination is there a lack of consistency between the $J(t)$ curve and some acceptable model of the brightness distribution.

For the eclipses of February 1952 and June 1954, this consistency for individual observing stations is supplemented by the fact that, for each eclipse, a single model results from the $J(t)$ curves made at several stations. The measurements on which these conclusions are based are given in Table 1.

If the existence of a localized bright source is postulated to explain ionospheric results obtained during an eclipse then, if the source is real, there should be a fall in the electron density in the layer when the source eventually disappears round the West limb of the sun. To explain the results of the February 1952 and June 1955 eclipses, it was necessary to postulate the existence of intense bright sources

in the Western Hemisphere. Examinations of the day-to-day changes in ionization in the *E*-layer during the control days for these eclipses have been made and in both cases the magnitude and timing of the fall in ionization which occurred several days after the eclipse was found to be consistent with the disappearance of the sources at the West limb. (MINNIS, 1956b, 1957)

For some of the eclipses which have been mentioned, the locations of the bright sources which were postulated entirely on ionospheric evidence have been

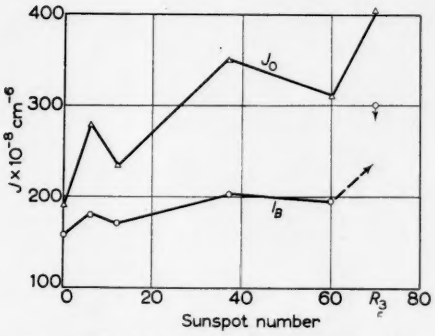

Fig. 1. The total solar ionizing radiation (J_0) and the uniform background component (J_B) plotted against the 3 day mean sunspot number for six eclipses.

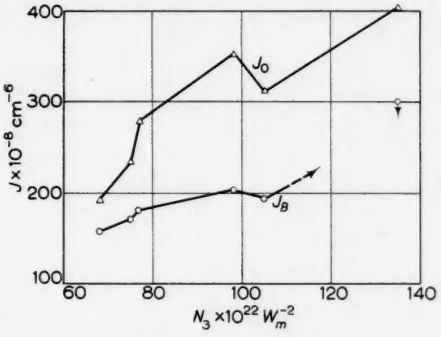

Fig. 2. The total solar ionizing radiation (J_0) and the uniform background component (J_B) plotted against the 3 day mean solar noise flux (2800 Mc/s) for six eclipses.

found to coincide with coronal condensations or other visible feature of the sun's disk. (LANDMARK *et al.*, 1956; MINNIS, 1955, 1957; WALDMEIER, 1947). This also tends to confirm the reality of these sources of ionizing radiation.

3. VARIATIONS IN THE BACKGROUND RADIATION

By analysing ionospheric data using the method described in Section 2.2, it has been possible to divide the value of J for the unobscured disk (J_0) into two components: that due to the uniformly distributed background radiation (J_B) and the residue due to local bright sources. In Fig. 1, the absolute values of J_0 and J_B for $\chi = 0$ have been plotted against the mean value (R_3) of the daily sunspot number for the three days centred on each of several recent eclipses. In Fig. 2 the same J values have been plotted against an alternative index of solar activity: the intensity of the solar noise flux on 2800 Mc/s measured in Ottawa (I.A.U., current). In calculating the values of J_0 and J_B in these figures, a correction, given by ALLEN (1948), for the effect of latitude on the *E*-layer electron density has been included to make the data homogeneous.

The rapid increase in J_0 which accompanies increasing solar activity is clearly visible in both figures and there appears also to be evidence for a corresponding slow increase in J_B. These conclusions are similar to those reached by COVINGTON and MEDD (1954) and by WALDMEIER (1955) concerning the solar-cycle changes in the analagous components of the solar noise flux on 2800 Mc/s.

The consistency of the trend of J_B in Figs. 1 and 2 and the similarity between

this trend and that deduced from direct measurements of the solar-noise flux lend further support to the validity of the interpretation of the ionospheric data in terms of non-uniformity in the solar brightness distribution.

4. THE EFFECTIVE RECOMBINATION COEFFICIENT

4.1. *Measurements at a single station*

Expressions have been given by RYDBECK and WILHELMSSON (1954) from which it is possible to find α' from the measured values of either $N_{\min}$ or Δt. In practice, these alternatives usually give conflicting results and, since the expressions are based on the assumption that the sun's disk is uniformly bright, this disagreement could be due to the presence of local bright sources of radiation on the disk during the eclipse. Thus it is dangerous to place any reliance on determinations of α' which are based on $N_{\min}$ or Δt if the possibility of a non-uniform disk is admitted.

Since the $J(t)$ curves discussed in Section 2.2 must be calculated using either a measured or an assumed value for α', it is evident that the brightness distributions derived from ionospheric results must depend, to some extent, on the value of α' adopted in computing J. Conversely, unless some initial assumptions are made about the brightness distribution, it is not generally possible to use ionospheric eclipse data to determine α'. This follows from the expression for α' [equation (3)] which is obtained by rearranging the terms in equation (2) but which cannot be evaluated unless A' is known.

$$\alpha' = (dN/dt)/[(q_0/\alpha')\, A' \cos^n \chi - N^2] \tag{3}$$

Even if A' is known, it is also evident from equation (3) that, unless dN/dt is large, it is not possible to make any reliable inferences about the magnitude of α'. In consequence, any determinations of α' made from eclipse data must be heavily weighted in favour of the value which obtains near the maximum phase of the eclipse when dN/dt may reach 50–100 $\text{cm}^{-3}\,\text{sec}^{-1}$ in the *E*- and *F1*-layers. RATCLIFFE (1956) has suggested that evidence should be sought, in ionospheric eclipse data, for any change in α' which may occur during eclipses but, in view of what has been said above, it seems unlikely that reliable information of this kind could be obtained in practice.

An alternative but controversial method of finding α' during a total eclipse is to assume that the ionizing radiation is completely cut off at second contact. Equation (3) then reduces to

$$\alpha' = -(dN/dt)/N^2 \tag{4}$$

Since dN/dt is large at second contact, this expression can often be evaluated with an accuracy which is quite high. Unfortunately the maximum height at which the ionizing radiation originates in the sun's atmosphere is not known and it is not possible, therefore, to be sure that there is no residual ionization during totality. For the present, therefore, estimates of α' based on equation (4) ought to be regarded as minimum values.

VOL. 12 1958

4.2. *Measurements at two stations*

As a result of the considerations of Section 4.1, it is difficult to see how it is possible to use ionospheric eclipse data from a single station to derive a value for α' which is not open to serious objections. An alternative method is to make use of data obtained at two different stations during the same eclipse. This allows the fraction (J_s/J_0) of the total ionizing radiation attributable to a particular source (S) to be expressed in the form $J_s/J_0 = a + b/\alpha'$ in which the coefficients a and b are determined independently at the two stations. Equating the two

Table 2. Determination of α'_E. February 1952 (unit 10^{-8} cm^3 sec^{-1})

Assumption made	Two stations		Single station
	$\alpha'_k = \alpha'_i$	$\alpha'_k \neq \alpha'_i$	$A' = 0$ [equation (4)]
Khartoum	1·2	1·2	1·5
Ibadan	1·2	1·4	—

expressions for J_s/J_0 gives a value for α', and, if more than one source can be identified, it is possible to solve a set of simultaneous equations from which independent values of α' at the two stations can be derived.

For the eclipse of February 1952, it was possible to derive expressions for J_s/J_0 for three component sources of the ionizing radiation and to determine α' separately for Khartoum and Ibadan (MINNIS, 1956b). The values obtained by this method are given in Table 2 and it is interesting to note that they are in good agreement with the value obtained from the Khartoum data alone by assuming that there was no residual radiation during totality and applying equation (4).

5. A COMPLEX RECOMBINATION PROCESS

5.1. *Theory*

It has been assumed throughout that changes in the *E*- and *F1*-layers can be represented by Chapman's equation; but the high value of α' which is necessary to explain both the diurnal changes and those due to eclipses shows that α' cannot be a radiative recombination coefficient. BATES and MASSEY (1948) have suggested that it may represent a dissociative recombination coefficient and recent determinations of such coefficients for typical ions show that suitably high values are possible (BATES, 1956).

However, it has also been pointed out by BATES and MASSEY that, in the ionosphere, several species of ion having very different recombination coefficients may be present together and that changes in electron density will be controlled mainly by the species having the smaller α. In consequence, it might be expected that any estimates of the rate of electron production (q) which are based on the relation $q = \alpha' N^2$, and in which values of α' determined by radio sounding methods are inserted, would lead to an underestimate of the flux of ionizing radiation. The best estimates of this flux do, in fact, lead to values several times greater

than those implied by the values of α' quoted in Table 2 and this tends to support the suggestion that a second ion, having a higher α, may also be present.

If this suggestion is correct, it is conceivable that during eclipses the presence of the second ion might be detected owing to its influence on the shape of the $N(t)$ curve. This possibility has been investigated by BATES and MCDOWELL (1957) who have computed a series of $N(t)$ curves for various pairs of values of α and two different relative concentrations of the ions. The calculations have been made assuming the total eclipse of a uniformly bright disk. The outstanding feature of the resulting curves is that although, as a result of the addition of the ion with a high α, the time lag Δt is smaller than would be expected on the simple theory, $N_{\min}$ does not fall much below the levels normally associated with typical eclipses and with the α' values of Table 2. Thus the shape of the modified $N(t)$ curves of BATES and MCDOWELL (1957) bears some resemblance to that often observed during eclipses even though no additional sources of ionizing radiation have been postulated in computing them. At first sight, therefore, it seems possible that the assumption of the presence of a second ion having a high α might allow actual ionospheric eclipse results to be explained in terms of a uniformly bright disk.

5.2. *Comparison with experimental results*

It is not practicable to use the two-ion hypothesis to recalculate the $N(t)$ curves for the actual eclipses discussed earlier. A useful alternative approach is to assume that the curves published by BATES and MCDOWELL represent actual eclipse measurements and to try to interpret them, using the methods outlined in Section 2.2, in terms of equation (2) and a uniform disk on which additional bright sources have been superposed.

This has been done for the curves marked (*d*) in Figs. 1 and 2 of the paper by BATES and MCDOWELL. Since the authors assumed a total eclipse in their calculations, α' has been determined by inserting the appropriate parameters for second contact in equation (4). The resulting J values are shown in Figs. 3 and 4; they have been plotted against the geometrical area (A) of the disk remaining unobscured since this allows easy comparison between the "observed" $J(A)$ curves and the broken straight line representing the $J(A)$ relation for a uniformly bright disk.

It is obvious that, in both the early and final stages of these hypothetical eclipses, the $J(A)$ curves remain very close to the line representing a uniform disk. Near totality, on the other hand, the curves depart from this line in a sense which would be interpreted as indicating the presence, near the west limb, of a bright source which contributes about 10 per cent of the total radiation. Thus the sections of the curves corresponding to large and small values of A would lead to conflicting conclusions regarding the brighness distribution. Hence the $J(A)$ curves derived from the $N(t)$ curves given by BATES and MCDOWELL cannot be interpreted in terms of a model brightness distribution; they are inconsistent in the sense used in Section 2.2 and Table 1.

It appears, therefore, that although the hypothesis used by BATES and MCDOWELL is capable of accounting for a reduction in Δt without the need for

VOL. 12 1958

postulating bright sources on the sun, it does not, in its present form, explain the rapid changes in N which often occur near the beginning and end of actual eclipses. These changes are at least as important as those which occur near the maximum phase because the evidence which they provide about the intensity of the bright sources near the limbs during actual eclipses is affected to only a very small extent by the value of α' used in the analysis of the results.

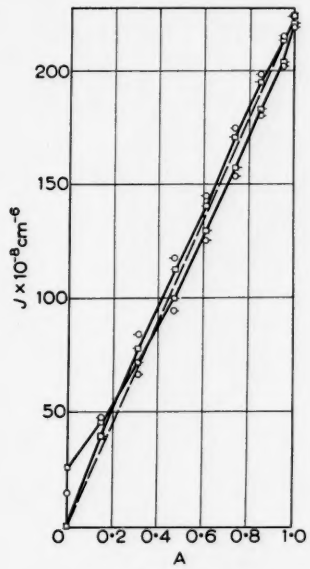

Fig. 3. Full line: $J(A)$ curve derived from curve (*d*). (Fig. 1 of BATES and MCDOWELL.) Broken line: $J(A)$ curve for uniformly bright disk.
□ □ $\alpha' = 5{\cdot}9 \times 10^{-8}$ cm³ sec⁻¹
○ ○ $\alpha' = \infty$

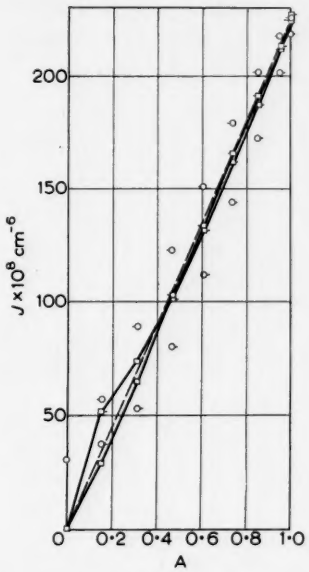

Fig. 4. Full line: $J(A)$ curve derived from curve (*d*) Fig. 2 of BATES and MCDOWELL. Broken line: $J(A)$ curve for uniformly bright disk.
□ □ $\alpha' = 1{\cdot}4 \times 10^{-8}$ cm³ sec⁻¹
○ ○ $\alpha' = \infty$

6. Errors Due to Tilted Layers

6.1. *Theory*

MUNRO and HEISLER (1956) have suggested that, when interpreting $N(t)$ curves obtained during eclipses, the effects of tilts in the reflecting surfaces ought to be considered. Their argument is summarized in the paragraph which follows.

Owing to the existence of horizontal electron density gradients in the ionosphere during an eclipse, the surfaces of constant density cease to be horizontal. In consequence, the reflexions received on the ground "at vertical incidence" from an ionosonde will come from a point which has been displaced from the zenith in the direction of increasing critical frequency. Further, near the maximum phase of an eclipse, these surfaces will be concave as seen from the ground and it is possible that the point of reflexion may travel so rapidly across the concavity that the chance of receiving a reflexion from the central point may be very small. Both these effects would tend to introduce a positive error into the values of N

read from the measured $N(t)$ curve. The error would be greatest near the maximum phase of an eclipse and it is suggested that the unexpectedly high values of $N_{\min}$ for the 1952 eclipse at Khartoum may be due to this cause.

The constant density surfaces visualized by MUNRO and HEISLER are related to the changes in height at which reflexion takes place at a fixed frequency. For the critical frequency, however, the final reflexion comes from the height of maximum density which is practically constant. In the presence of a horizontal gradient, the reflecting surface, on simple ray theory, is vertical at frequencies

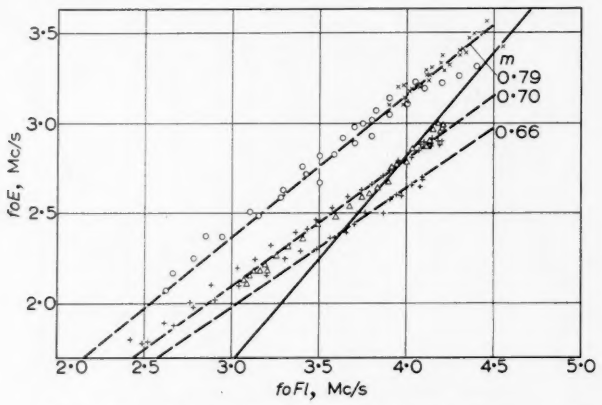

Fig. 5. The relation $f_0E/f_0F1 = m$ during four solar eclipses.

× × ×	Singapore	20 June 1955
○ ○ ○ ○	Khartoum	25 February 1952
△ △ △	Slough	30 June 1954
+ + +	Inverness	30 June 1954
———	Approximate diurnal variation.	

just below the critical frequency, but the validity of ray theory in these circumstances is doubtful and any detailed investigation of actual ray paths hardly seems justified. Although the possibility of errors due to displacement of the reflexion point during eclipses must be admitted on theoretical grounds, some experimental data are discussed in Section 6.2 which seem to imply that the magnitude of any such errors is small.

6.2. *Experimental results*

The changes in the tilt of constant density surfaces during partial eclipse conditions in 1954 have been measured by BRAMLEY (1956) who found a maximum tilt of 5°. The corresponding displacements of the reflexion points in the *E*- and *F1*-layers for vertical incidence soundings would be equivalent to errors in timing of about $\frac{1}{4}$ and $\frac{1}{2}$ min respectively and neither of these is large enough to lead to serious misinterpretation of the data.

At the critical frequency, however, particularly during total eclipses, the errors might be more serious since deviative effects would then be greatest. It would be expected that any displacement of the reflexion point would increase with increasing thickness as well as increasing height of a layer and that, as a

VOL. 12 1958

result, it would be greater in the *F1*- than in the *E*-layer. The errors in f_0F1 would, therefore, be proportionately greater than those in f_0E and during the eclipse this would lead to changes in the ratio f_0E/f_0F1 which would be most marked near the maximum phase.

In Fig. 5, the relations between simultaneously measured values of f_0E and f_0F1 are shown for four eclipses for which reliable data are available. In no case is there any significant departure from a linear relation and the ratio f_0E/f_0F1 remained constant even during the total eclipse at Khartoum. The difference in the ratios derived from the Singapore–Khartoum and Inverness–Slough relations is due to the influence of latitude on the *E*- and *F1*-layers and is not an eclipse effect. The ratios obtained are in good agreement with estimates of the latitude effect made by ALLEN (1948) using the normal diurnal and seasonal variations of these layers. The much smaller ratio which applies to part of the Inverness data is due to obscuration of the true f_0E cusp by sporadic-*E* ionization in the later stages of the eclipse.

In view of these considerations, it is concluded that any displacement of the point of reflection away from the zenith is too small to lead to misinterpretation of eclipse data.

7. CONCLUSIONS

In recent years it has been usual to explain eclipse changes in the *E* and *F1*-layers in terms of simple Chapman theory and a non-uniform distribution of the sources of solar ionizing radiation. This explanation is supported by several observations:

(a) The internal consistency of the changes in electron density in ten out of eleven sets of eclipse data which have been examined;

(b) For two eclipses, the same distribution of brightness follows from measurements made at more than one station;

(c) The long-term trend of the background component of the ionizing radiation, calculated from eclipse data, is consistent with the trends both of solar activity and of the background component of solar noise flux.

The value of the effective recombination coefficient (α') which results from *E*-layer measurements during eclipses leads to a value for the ionizing radiation flux which is too small. This suggests that a second ion species with a much higher α may be present and the changes which would occur in a layer during an eclipse if this were so have been examined. It is concluded that this hypothesis, in its present form, does not account for the type of change which frequently occurs in practice, to explain which it still appears to be necessary to assume the existence of localized bright sources of ionizing radiation.

The possible effects of a tilted layer on the displacement of the point of reflection for vertical incidence soundings during eclipses has been considered. It is concluded that the experimental data show that no serious misinterpretation of the data results from this effect.

Acknowledgements—The work described above was carried out as part of the programme of the Radio Research Board. The paper is published by permission of the Director of Radio Research of the Department of Scientific and Industrial Research.

REFERENCES

ALLEN C. W.	1948	*Terr. Mag. Atmos. Elect.* **53,** 433.
BATES D. R.	1956	*Solar Eclipses and the Ionosphere* pp.191–197. Pergamon Press, London.
BATES D. R. and MASSEY H. S. W.	1948	*Proc. Roy. Soc.* **192,** 1.
BATES D. R. and MCDOWELL M. R. C.	1957	*J. Atmos. Terr. Phys.* **10,** 96.
BRAMLEY E. N.	1956	*J. Atmos. Terr. Phys.* **8,** 98.
COVINGTON A. E. and MEDD W. J.	1954	*Canad. J. R. Astr. Soc.* **48,** 136.
HIGGS A. J.	1942	*Geofys. Publ.* **19,** 1.
I. A. U.	current	*Quarterly Bulletin on Solar Activity.* Zurich.
LANDMARK B., LIED F., ORHAUG T. and SKRIBELAND S.	1956	*Geofys. Publ.* **19,** 1.
MINNIS C. M.	1955	*J. Atmos. Terr. Phys.* **6,** 91.
MINNIS C. M.	1956a	*J. Atmos. Terr. Phys.* **9,** 201.
MINNIS C. M.	1956b	*J. Atmos. Terr. Phys.* **9,** 36.
MINNIS C. M.	1957	*J. Atmos. Terr. Phys.* **10,** 229.
MINNIS C. M.	1958a	*J. Atmos. Terr. Phys.* In press.
MINNIS C. M.	1958b	*J. Atmos. Terr. Phys.* In press.
MUNRO G. H. and HEISLER L. H.	1956	*Aust. J. Phys.* **9,** 343
RATCLIFFE J. A.	1956	*Solar Eclipses and the Ionosphere* p.219. Pergamon Press, London.
RYDBECK O. E. H.	1946	Chalmers Solar Eclipse Ionospheric Expedition 1945. *Trans. Chalmers Univ. Tech. Gothenburg, Sweden No.* 53.
RYDBECK O. E. H. and WILHEMSSON H.	1954	A Theoretical Investigation of the Ionospheric Electron Density Variation during a Solar Eclipse. *Trans. Chalmers Univ. Tech. Sweden* No. 149.
SZENDREI M. E. and MCELHINNY M. W.	1956	*Solar Eclipses and the Ionosphere* pp.74–80. Pergamon Press, London.
WALDMEIER M.	1947	*Terr. Mag. Atmosph. Elect.* **52,** 333
WALDMEIER M.	1955	*Z. Astrophys.* **36,** 181

VOL. 12 1958

Journal of Atmospheric and Terrestrial Physics, 1958, Vol. 12, pp. 283 to 287. Pergamon Press Ltd., London

Variations in the intensity of the hydrogen emission line H_β during auroral activity

G. J. Romick and C. T. Elvey
Geophysical Institute, University of Alaska, College, Alaska

(*Received* 14 *January* 1958)

Abstract—Through the qualitative analysis of the auroral spectrum incident from the magnetic zenith, the variation of the estimated intensity with time has been obtained for H_β (4863 Å) and the 4709 Å line of N_2^+. The results show that the peak in intensity of H_β preceeds that of the 4709 Å line by 1–4 hr, and that the period in which the intensity of H_β peaks occurs when quiet forms of the aurora are present. This same period is associated with low amplitude low frequency fluctuations of N–S earth potential. The overall earth potential fluctuation is highly correlated with the intensity variations of the 4709 Å line of N_2^+ and with the type of aurora present at the zenith.

Introduction

In the past few years many investigators have worked on the establishment of the role of the proton in the excitation of the auroral spectrum. Most of the work has been directed towards determining the presence or absence of the hydrogen emission lines in specific auroral forms and their intensity variations relative to those of the other auroral emissions (Chamberlain, 1954; Fan and Schulte, 1954). Other work has delved into the variation of intensity with latitude and altitude (Montalbetti and Jones, 1957; Vegard and Kuifte, 1954; Vegard, 1955). This investigation proposed to study the time variations of the hydrogen emission for a fixed position in the sky, the magnetic zenith. It is generally considered that the hydrogen lines are present in the quiet auroral forms, mainly the homogeneous arc (Chamberlain, 1954; Fan and Schulte, 1954) and that at the time of the break-up of the auroral arc into rays and other rapidly moving forms, the hydrogen lines disappear. Since the break-up of the quiet arc system behaves similar to the defocussing of a beam of particles, it was thought possible that the hydrogen lines might then be dispersed over the sky. Hence we believed that time-resolved spectra at the magnetic zenith would be able to solve this question. Observations were obtained on all nights regardless of clouds. On clear nights the spectra were from a fixed part of the sky, while on cloudy nights the spectra were integrated light from a large portion of the sky. If the hydrogen lines were dispersed over the sky as are the auroral forms at the time of break-up, then one would expect to see a less marked decrease of intensity of the hydrogen lines on cloudy nights.

Experimental Procedure

The basic instrument is a HUET C-1 flint glass prism spectrograph with an effective speed of $f/0{\cdot}7$. The only modification made was to enable the plate holder to move in a direction perpendicular to the dispersion of the instrument. The combination of a short slit and the speed of motion gave an effective exposure equivalent to one hour over a time-resolved spectrum. The instrument was mounted so that the field of view (11°) was approximately centred on the magnetic zenith,

and the instrument operated in an enclosed room through a hemispherical dome or through an open window. The photographic plates used for this study were Eastman spectroscopic plates type 103a-F.

For the preliminary analysis of the plates it was decided to study the differences between the intensity variations of H_β and the 4709 Å line of N_2^+, the pair being free of appreciable overlap by other emissions. The 4709 Å line is a representative spectrum line for the normal visible aurora and is believed to be primarily produced by electron excitation. Another more basic reason for its selection is its spectral nearness to H_β, which means a greater reliability in the comparison of the two intensities, as both the spectrograph and the photographic emulsion have fairly uniform response over such a short spectral range (less than 200 Å). In this region the dispersion combined with the slit width produced integrated lines each of approximately 50 Å width. Also 4709 Å was never so intense as to make its intensity variation indiscernable with our exposure time.

The qualitative method used in obtaining the intensities is basically one of visually estimating the variation in density produced on the photographic emulsion by using a convenient scale of 10 for the range from a line just detectable to the brightest observed for 4709 Å (all exposures equivalent to 1 hr). While the numbers of this scale are only roughly proportional to the logarithm of the average intensity over 1 hr, they are quite adequate for our primary purpose, that of showing line variations with time.

During the period from September 1956 through April 1957, 200 photographic plates were obtained of the sky spectral emissions at College, Alaska. Of this total, only 75 were selected for analysis, the others being classified as unusable for this study because of moonlight contamination, lack of aurora, or too short a time period recorded with respect to the exposure length to observe a time variation of the intensity. Of these 75 plates, only 19 were obtained on clear nights; the remainder were taken on partly cloudy or completely overcast nights.

VOL. 12 1958

Results

For clear nights the study of the intensity variation with time is possible on only 16 of these plates, the three others having such faint spectral lines that by visual methods it is difficult to pick out variations in intensity. On 15 of the 16 plates the plot of intensity vs. time shows a peak in H_β preceding the peak in the 4709 Å line by more than 1 hr and as much as four (Fig. 1). The 16th plate shows the variation in the intensity of H_β to be the same as that of the 4709 Å line. However, for this plate the entire observation period contained active aurora and the time resolution of the plate is not sufficient for deciphering the rapid changes within long active periods.

A comparison between the type and position of the auroral form with the variations of H_β and the 4709 Å line can be made by use of the photographs made with the all-sky camera at College. The 15 sec exposures taken every minute provide a very good record as to the type of aurora present. Continuous all-sky camera photographs are available for four of the 15 clear nights previously mentioned and the comparison between the spectrographic plates and the film shows that the peak in the intensity of H_β at the zenith occurs when the only visible auroral forms

present are quiet arcs in the far north, or when no aurora is visible at all. When active aurora appears at the zenith in the all-sky camera record a large peak in the 4709 Å line occurs. The passage of arcs or rays through the zenith is associated with smaller peaks in the intensity of the 4709 Å line.

From these four sets of data we have the relation that a peak in the intensity of H_β preceding a peak in the intensity of the 4709 Å line indicates quiet forms of the aurora with no visible aurora in the field of view of the instrument. Peaks and variations in the intensity of the 4709 Å line indicate the passage of aurora through

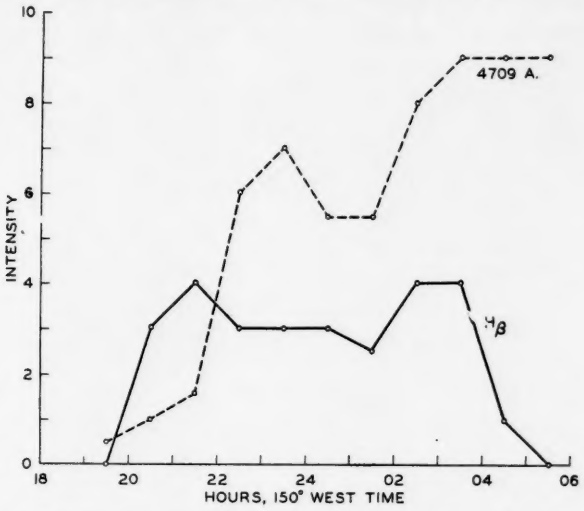

Fig. 1. Plot of the average hourly intensity with time for H_β and the 4709 Å line of N_2^+.

the zenith with the intensity of the line indicating the general degree of activity and type of aurora passing through the zenith.

In investigating the very complete N–S earth potential records* obtained at College by Dr. V. P. Hessler for the same four nights, it was found that the amplitude and frequency fluctuation of this trace could be highly correlated with the variations in the zenith intensity of the 4709 Å line and with the type of aurora present. For example, at the time when an auroral break-up occurs as seen on the all-sky camera film, a large amplitude high frequency variation appears on the earth potential trace and an increase in the intensity of the 4709 Å line is seen on the plate. Arcs across the zenith produce a small peak in the 4709 Å line intensity and moderate to low amplitude variations of the earth potential.

Invariably the peak in the intensity of H_β occurs during the period when the earth potential trace has very low amplitude and low frequency fluctuations. When the high frequency appears on the trace, the intensity of H_β decreases and the 4709 Å line reaches its maximum intensity (example Fig. 2).

* Earth potentials have been found to be a very convenient monitor of local auroral activity, the records agreeing well with those of magnetic fluctuations in regard to times of disturbance. However the earth potential fluctuations can differ from the magnetic fluctuations in amplitude, frequency and phase.

On one of the four plates previously mentioned as well as on many others, the intensity of H_β after being present at the beginning of the large peak in 4709 Å of several hours duration, dropped to zero intensity 2 hr before any lessening of the intensity in the 4709 Å line. Associated with this period in which H_β was not present is a very high frequency fluctuation of the earth potential which indicates active aurora at the zenith. At times after an auroral break-up anomalous ionospheric absorption appears which is tentatively correlated with pulsating aurora (Little and Leinbach, 1958). This occurs during the high frequency fluctuations of the earth potential mentioned above. The decrease in hydrogen emission during periods of pulsating aurora is not inconsistent with observations by other investigators (Omholt, 1957).

By using the correlations between the earth potential trace fluctuations and the general auroral forms corresponding thereto, the 46 plates obtained on partly cloudy or completely overcast nights were analysed. The correlations between the intensity variations of the 4709 Å line and the earth potential trace fluctuations continued. On those plates which showed a peak in the intensity of H_β preceding a peak in the intensity of the 4709 Å line there was always a period of low amplitude low frequency fluctuation on the earth potential trace which indicates the presence of the quiet auroral forms. On two plates the peak in intensity of H_β occurs during a period in which the earth potential trace is flat and the intensity on the plate of the 4709 Å line is nil. There seems to be no indication of any type of hydrogen dispersal over the sky during auroral break-up. The decrease in the intensity of the hydrogen lines on cloudy nights seems to fall off with the onset of an auroral break-up in the same manner as on clear nights.

VOL.
12
1958

Conclusions

In summary this study, routinely covering all available nights of the 1956–1957 seasons, indicates that the intensity of H_β at the zenith is not dependent on the amount of visual aurora present there. Certainly it is not correlated to the more active and intense forms of aurora which occur mainly at the zenith.

Furthermore H_β appears to peak at the zenith when only quiet forms such as arcs or possibly glows are present lower in the sky. (Whether these are only in the north cannot be stated definitely due to the lack of all-sky camera film showing arcs in the southern sky for the spectroscopic plates available.) Whether or not a greater intensity in H_β is more localized towards the quiet form is not known from this study. When H_β is weak near active forms at the zenith, the possibility exists that it may be more intense towards the south, as might be the result of a southerly motion of the bombarding stream leaving in its wake the more active forms. This would seem unlikely, however, because of the long time delays of one to four hours observed between the peaks in the intensities of $H\beta$ and 4709 Å at the zenith. Also the similar delays obtained with the integrated spectra on cloudy nights would suggest that the north–south motion of the bombarding stream is not directly correlated with active forms at the zenith. Further measurements with greater resolution in time as well as position will be quite valuable for this consideration.

From a general visual examination of the plates the intensity of no other

GEOPHYS. RES. 63, 1958

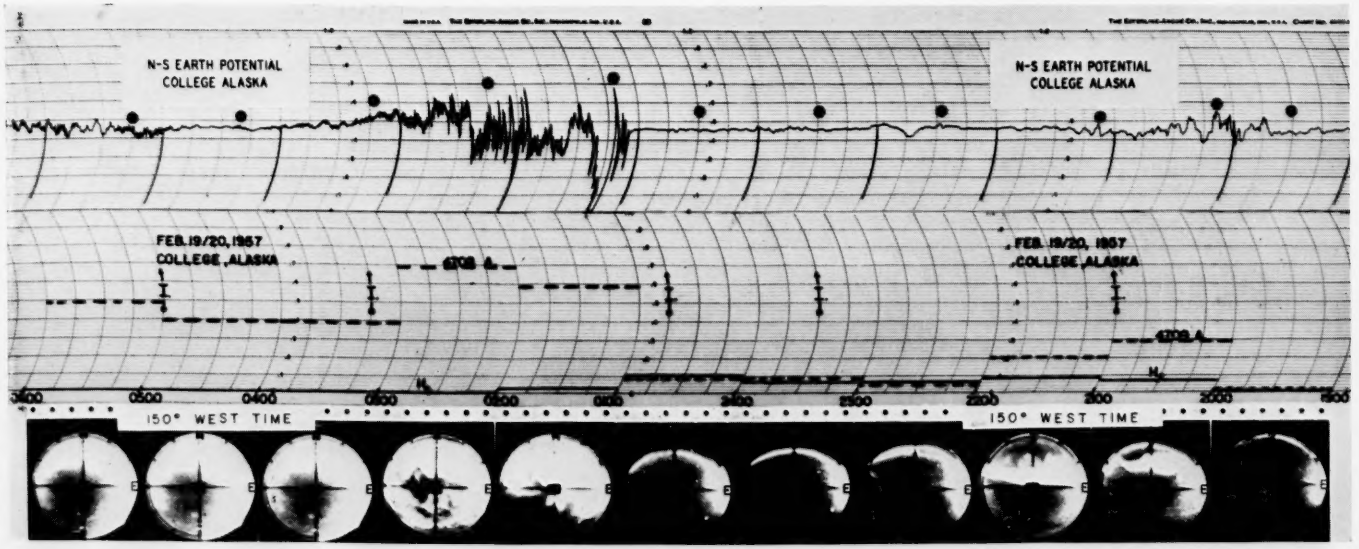

Fig. 2. Variation with time of the earth potential fluctuation (top trace), hourly average intensity of H_β and the 4709 Å line of N_2^+ (middle trace) and the hourly representative picture of the aurora by use of the all-sky cameras. The dots on the earth potential trace indicate the actual time at which the all-sky photograph was obtained.

VOL.
12
1958

spectral line seems to follow the variations in intensity of the hydrogen lines. Somewhat close correlations are evident with the 5200 Å line of atomic nitrogen and with the two red lines (6300 and 6364 Å) of atomic oxygen, both of which are high altitude emissions. However, a closer study of this correlation remains to be made before any definite relationships can be postulated.

This work has been partially supported by a grant from the Office of Naval Research, Contract No. Nonr-1289(00).

References

Chamberlain J. W.	1954	*Astrophys. J.* **120,** 566.
Fan C. Y. and Schulte D. H.	1954	*Astrophys.* **120,** 563.
Little, C. G. and Leinbach, H.	1958	*Proc. Inst. Radio Engrs* **46,** 334–348.
Omholt, A.	1957	*Astrophys. J.* **126,** 461.
Montalbetti R. and Jones A. V.	1957	*J. Atmos. Terr. Phys.* **11.** 43.
Vegard L.	1955	*Geofys. Publ.* **19,** No. 4 9.
Vegard L. and Kuifte G.	1954	*Geofys. Publ.* **19,** No. 2 10.

DL.
2
958

Journal of Atmospheric and Terrestrial Physics, 1958, Vol. 12, pp. 288 to 292. Pergamon Press Ltd., London

A study of air flow in a large-ion chamber

G. A. FAUCHER
Geophysics Research Directorate, Air Force Cambridge Research Center,
Air Research and Development Command, Bedford, Massachusetts, U.S.A.

(*Received* 17 *September* 1957)

Abstract—Turbulence in a large-ion chamber has an influence on the measured ion mobility distribution. A technique was developed to investigate the flow in a large-ion chamber with titanium tetrachloride smoke. Many sources creating turbulence in the chamber were revealed. The entire set-up consisted of Pyrex glass, and the complete flow of smoke was recorded on cine film. These smoke experiments made it possible to re-design the chamber with laminar flow at air velocities up to 3 l./sec

INTRODUCTION

THE work of ISRAËL (1931) and WAIT (1905) has shown that turbulence in a large-ion chamber results in an error in the measured ion mobility distribution. A series of experiments was carried out in the laboratory to determine the current-voltage characteristic of the large-ion chamber as a function of air-flow. It was found that the computed ion content values obtained from the high air-flow system were low by a factor of $3{\cdot}4 \pm 0{\cdot}5$; the limiting mobility was high by a factor of $7{\cdot}5 \pm 0{\cdot}5$. The effect of high air-flow was to shift the distribution toward higher mobility values. This indicates that a significant number of ions are removed from the stream by adsorption and diffusion to the walls under the mixing action of turbulence. The large-ion chamber is designed to be operated with laminar air-flow. Since very low flow rates, guaranteeing laminar flow in the instrument, are difficult to achieve in aircraft measurements, the experiments under discussion were carried out to investigate and eliminate sources of turbulence in the large-ion chamber in the flow range 0·5 l./sec to 3·0 l./sec. The theory and method of measurement, which are carried out in aircraft with this large-ion chamber for measuring and recording the concentration and mobility distribution of charged particles, have been described previously (SAGALYN and FAUCHER, 1954).

VOL. 12 1958

AIR-FLOW—SMOKE

The flow of titanium tetrachloride smoke through a glass model of the large-ion chamber provided a method of locating sources creating turbulent flow. Surfaces of discontinuity created by an abrupt change of velocity or density within the chamber are the origins of turbulence. For example, we found that a source of disturbance to the smoke-flow in the glass model was caused by a leakage in the form of small jets. These smoke experiments made it possible to redesign the chamber so that laminar flow occurs with air velocities up to at least 3·0 l./sec

Forecasting the flow pattern in our large-ion chamber with present theories would have been very difficult. For this reason it was decided to determine the flow pattern of air as it goes through the chamber by observing the behaviour of

a smoke introduced into the air stream. The technique of using smoke for examining flow patterns depends very much on the particular problem under investigation. It is not easy to make the smoke visible in a useful manner under all conditions, and the difficulty increases rapidly with increasing air-flow velocity. Many smoke-producing devices are not suitable because they introduce additional disturbances in the flow path which are not present normally. At low air currents, for example, flow patterns have been examined in the past with the aid of cigarette smoke introduced into the stream. In these experiments a more elaborate technique was required because of the larger volume of air. The smoke generated by titanium tetrachloride on exposure to air was suitable.

Titanium tetrachloride smoke has its disadvantages as well as its advantages. A few remarks on its use may help anyone who might want to make use of it in a similar way. Titanium tetrachloride, a liquid at room temperature, combines chemically with the moisture present in the air to form a dense white smoke containing the oxide of the salt, hydrochloric acid, and water. A solid deposit is left by the smoke after evaporation. The fact that the smoke contains hydrochloric acid is a disadvantage, but by avoiding the use of metal in the construction, the system will not suffer damage due to corrosion. Care must also be taken to clean everything after each application to remove the solid deposit left, as its presence may cause eddies and change the measured air-flow. The smoke is heavier than air and, unless allowance is made for the motion due to gravity, observations at low rates of flow may be misleading; but at higher speeds, when the rate of descent is small compared with the air speed, this source of error is reduced. The great ease with which one can produce a large quantity of smoke of high optical density made titanium tetrachloride smoke especially useful in these experiments. A continuous stream of smoke lasting for several minutes was obtained by dipping a glass rod into the liquid and then introducing it into the system. The use of a small glass rod as the source of the smoke was also a great advantage in this experiment.

Apparatus

Fig. 1 is a schematic diagram of the experimental arrangement used for studying the air-flow through the glass model of the large-ion chamber. The flow maintained by a blower speed-rheostat was varied from 0·5 l./sec through 3·0 l./sec. A calibrated Hastings precision thermal anemometer probe, mounted and inserted identically as the glass rod shown in the diagram, was used for measuring the flow prior to introducing the smoke. Except for the central probe in the glass model of the large-ion chamber, the entire set-up consisted of Pyrex brand "Double Tough" glass pipe and fittings manufactured by Corning Glass Works, Corning, New York. Its transparency permitted constant visual inspection of the smoke pattern throughout the set-up. The very smooth surface of the glass made cleaning after each experiment easy. The pipe and fittings are made from heavy wall tubing which is machine-drawn to assure uniformity. The flanges are accurately pressed and ground flat. Tight joints were easily made with the metal flanges, which are cushioned from the glass by moulded asbestos inserts. An interface gasket of Teflon is gripped between the pipe ends when the flange bolts are

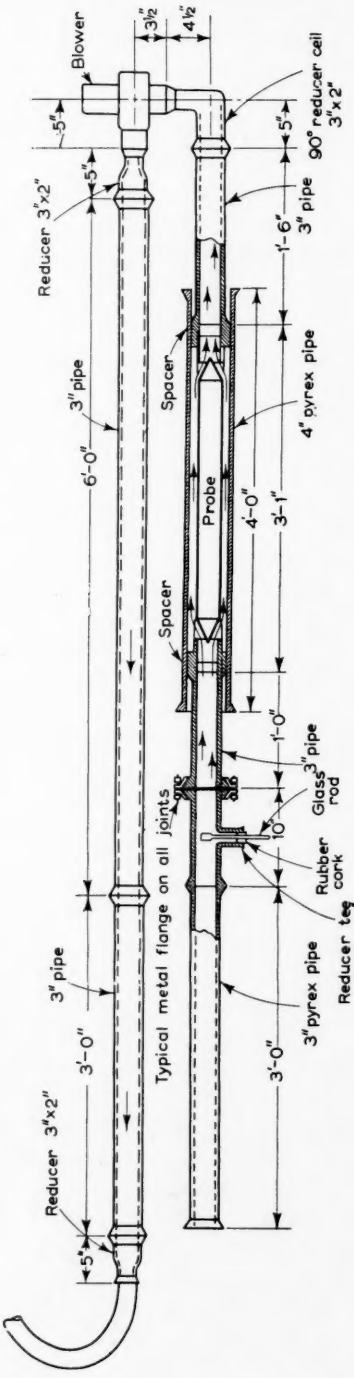

Fig. 1. Schematic diagram of the experimental arrangement for smoke experiment.

VOL. 12 1958

tightened. There is no contact between the metal flanges and the smoke which is conveyed. The length of Pyrex pipe at the entrance and exit of the glass model was to ensure the steadiest condition in the model. A previous measurement showed a disturbing backwash of 12 in. caused by the blower at the highest speed of this experiment. At the slower speed the backwash was less than the

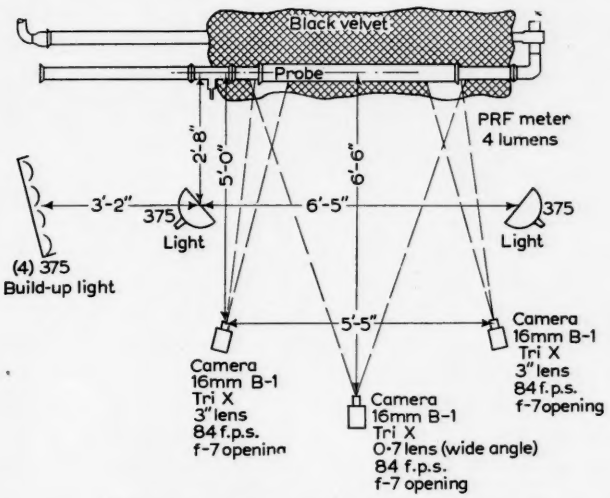

Fig. 2. Arrangement of apparatus for smoke photography.

12 in. It was also found desirable not to exhaust this smoke out of doors, because the differences of pressure involved caused disturbances. The 9 ft of Pyrex tubing followed by a rubber hose was tied to the exit of the blower to evacuate the objectionable smoke out of the room into the hallway.

Smoke photography

While much valuable information can be obtained by observing smoke, it is very difficult, by inspection alone, to detect the fine details of eddying motion. Photography was an invaluable aid in these experiments by providing permanent records which could be examined at leisure. By careful attention to background and direction of lighting, we were able to obtain close-ups of the entrance and the exit and a complete view of the entire glass model of the large-ion chamber simultaneously. The central cylinder was painted black and the surrounding walls of the room were covered with black velvet so that the white smoke was always viewed against a dark background. In order to eliminate all undesired reflection from the glass tubing, it was necessary to perform these experiments in a dark room where all the sources of light could be controlled. Fig. 2 is an outline of the arrangements of the various photofloods and cameras we used for this experiment. The two single-bulb photofloods on each side of the glass model were 2 ft higher than the glass model at a 45 deg. angle to the model. The other bank of photofloods was 4 ft higher than the glass model and was used as an auxiliary illumination for better rendering for background separation. Two 16 mm

B-1 cine cameras with the 3 in. lens were used for a close view of the entrance and exit where the most disturbed regions were found. A similar camera with a wide-angle lens was used to record the flow through the entire glass model of the large-ion chamber. All three cameras were driven by the same motor at 84 frames/sec. After each injection of the glass rod containing a few drops of $TiCl_4$, it was possible to obtain several minutes of cine film at the lower speed of 0·5 l./sec to approximately 1 min of film at the maximum speed of 3·0 l./sec. A measurement of the air-flow was made before and after each injection of the smoke and it was found that the deposits left from the smoke of a few drops of the liquid did not effect the flow velocity. The tubing was cleaned after each operation to prevent the accumulation of any deposits which might alter the air-flow and obscure the view of the smoke passing through the glass tubing.

RESULTS

Examples of the kind of photograph obtained with a still camera are illustrated in Figs. 3 and 4. Fig. 3 shows the smoke patterns in the glass model of the original design at a flow of 1·0 l./sec. Fig. 4 illustrates the smoke patterns in the glass model of the newly designed chamber at the same flow for purposes of comparison. These photographs were taken with a Rolleiflex camera having a Tessar lens (f—75 mm). The two most serious sources of disturbances as revealed by the smoke were at the entrance and exit of the chamber as designed by TORRESON and WAIT (1934). They had designed the entrance to their chamber to guard against any field by which the ions might be driven away. The entrance and exit of their design, for purposes of describing the flow disturbances, can be pictured as regularly spaced bars placed across a stream of air. Each bar introduces eddies in the flow. These eddies disappeared some way downstream. The distance downstream that the eddies disappeared depended on the speed of the flow. At 1·0 l./sec, as shown in Fig. 3, the eddies extended to 8 in. At 2 l./sec, the eddies extended to 12 in. At faster flows the films showed turbulence throughout the chamber. The smoke-flow at the exit also showed serious disturbances in the flow similar to those at the entrance. In the new design of the centre probe, the exit and entrance were fitted with fins which will prevent swirl. The function of the fins is to maintain the direction of flow parallel to the axis of the chamber and also to break up any occasional large eddies which may reach the intake. As shown in the photograph of Fig. 4, the smoke patterns in this model are very smooth. This same smooth flow was obtained up to the maximum velocity of our blower, which was 3 l./sec. The flow of the smoke was a little disturbed before reaching the intake but was straightened out by the fins.

Acknowledgements—The author thanks Mrs. R. C. SAGALYN for initiating this experiment and for her many helpful suggestions; also Mr. L. WILSON for the fine photography.

REFERENCES

ISRAËL H.	1931	*Beitr. Geophysik* **31,** 193.
SAGALYN R. C. and FAUCHER G. A.	1954	*J. Atmosph. Terr. Phys.* **5,** 253
TORRESON O. W. and WAIT G. R.	1934	*Terr. Mag.* **39,** 47.
WAIT G. R.	1905	*C.R. Acad. Sci. Paris* **140,** 232.

VOL. 12 1958

Fig. 3. Smoke flow at 1·0 l./sec in original design.

OL.
12
958

Fig. 4. Smoke flow at 1·0 l./sec in new design.

VOL.
12
1958

Journal of Atmospheric and Terrestrial Physics, 1958, Vol. 12. pp. 293 to 305. Pergamon Press Ltd., London

Investigation of magneto-ionic fading in oblique incidence medium-wave transmissions

M. Srirama Rao* and B. Ramachandra Rao
Ionospheric Research Laboratories, Physics Department,
Andhra University, Visakhapatnam 3, India

(*Received* 23 *November* 1957)

Abstract—Periodic fading of magneto-ionic origin observed in oblique incidence medium-wave records is interpreted theoretically by calculating the phase paths by a graphical integration method assuming Chapman and parabolic ion distribution. Analytical expressions have also been derived for phase paths of both magneto-ionic components by an approximate method involving the use of an empirical formula for q–x curves. The theoretical values of fading periods compared very well with the experimental data, the agreement being particularly good for the case of Chapman distribution.

1. Introduction

Fading of radio waves can be broadly classified into two types, namely (1) periodic and (2) random fading. Interference of the two magneto-ionically split components of a radio wave traversing the ionosphere in the presence of the earth's magnetic field gives a type of periodic fading known as magneto-ionic fading. This type of fading was first observed by Appleton and Beynon (1947) in the signal strength records of continuous wave transmissions from Oslo on 9·53 Mc/sec received at Slough. While studying the signal strength variations of medium-wave transmissions from distant stations, Tantry and Khastgir (1951) have observed slow-period fading of the order of 5 min which they attributed to magneto-ionic origin. Later Satyanarayana and Dharrambir Rai (1954) confirmed experimentally that this observed fading on medium-wave transmissions is of magneto-ionic origin. Using transmissions on 760 kc/s and circularly polarized aerials, they recorded separately the two magneto-ionic components with opposite senses of rotation and showed that the slow-period fading recorded in the composite signal was absent in the records of each component. Similar periodic fading of magneto-ionic origin was observed by the authors in the signal strength records of medium-wave transmissions from Madras on 1·42 Mc/s received at Waltair. The present investigation was undertaken with a view to giving a quantitative interpretation of the periodicities observed in such records by a theoretical calculation of the phase paths of the two magneto-ionic components in the ionosphere.

As Satyanarayana and Dharambir Rai have shown by polarized aerials that this type of fading is magneto-ionic, we have made no attempt in this investigation to confirm the magneto-ionic origin of the observed fading experimentally. However, there is considerable evidence, both theoretical and experimental, for attributing the observed fading to interference of magneto-ionic components. The possibility that this type of fading might be due to $1E$- and $2E$-interference is ruled out by the fact that the expected period calculated from

* At present working in National Research Council Laboratories, Ottawa, Canada.

known values of vertical velocity of the layer comes out to be of the order of 1 min whereas the observed period of fading is much higher, being in the range of 6–9 min. Further, the quick-period fading due to $1E$ and $2E$ is noticed sometimes in the earlier part of some of the fading records.

It has also been shown by theoretical calculation that the extraordinary wave will be returned from E-region during the hours of recording with sufficient signal strength so as to cause periodic fading. Using certain approximate formulae as given by Mitra (1952) and employing graphical methods of computation, the ratios of extraordinary to ordinary absorption have been calculated for the case of longitudinal propagation. The results showed that the ratio of extraordinary to ordinary absorption for the deviative case is of the order of 1·5, while for the non-deviative case the ratio is about 10. The actual ratio of total absorption will lie between these two values depending upon the relative order of magnitude of deviative and non-deviative absorption. In the morning hours of recording, as the critical frequency of the E-layer increases, the deviative absorption decreases, while the non-deviative absorption increases due to the enhanced ionization in D-layer. This accounts for the rapid increase of the absorption ratio of extra-ordinary to ordinary in all the records from 0700 to 0800 hr. The observed ratio of extraordinary to ordinary absorption in all the records falls in the range of 3–12, and this range agrees approximately with the theoretically calculated ratios. Thus the extraordinary ray is actually present till 0800 hr with sufficient strength.

VOL. 12 1958

2. Experimental Technique and Results

In the earlier part of the investigation, a photographic method of recording signal strength variations is employed, using a drum type of camera. This was replaced later by an Esterline–Angus pen recorder driven by a d.c. amplifier. A Hallicrafters Model SX42 communication receiver was used for the reception of C.W. transmissions from distant All-India radio transmitting stations. The d.c. amplifier is connected across the a.v.c. voltage and it is found by calibration with a standard signal generator that the deflection varies linearly with the input voltage over the range of signal strengths observed in this investigation. Using this equipment, signal strength records of medium-wave transmissions from Madras on 1·42 Mc/s were taken regularly during the morning hours of 0700 to 0800 hr I.S.T, these hours being particularly convenient as the single-hop reflection from the E-region is most prominent during this period. Three typical records taken on 14 May 1954, 27 January and 1 March 1955 are reproduced in Fig. 1 to illustrate the various features of magneto-ionic fading in oblique incidence medium-wave transmissions. As can be easily seen from Fig. 1, one of the records was taken by using the earlier photographic recording equipment. The smooth long-period fading observed in these records is attributed to the interference between the lower trajectory ordinary and extraordinary rays. Besides this long-period magneto-ionic fading, a quick-period fading of small amplitude due to interference of multiple reflections is occasionally observed as in record shown in Fig. 1(a). The fading period in almost all the records is found to vary with time. In most of the records the fading period is low in the early half of the record and gradually increases during the latter part of the record. It can be shown that this non-uniformity in

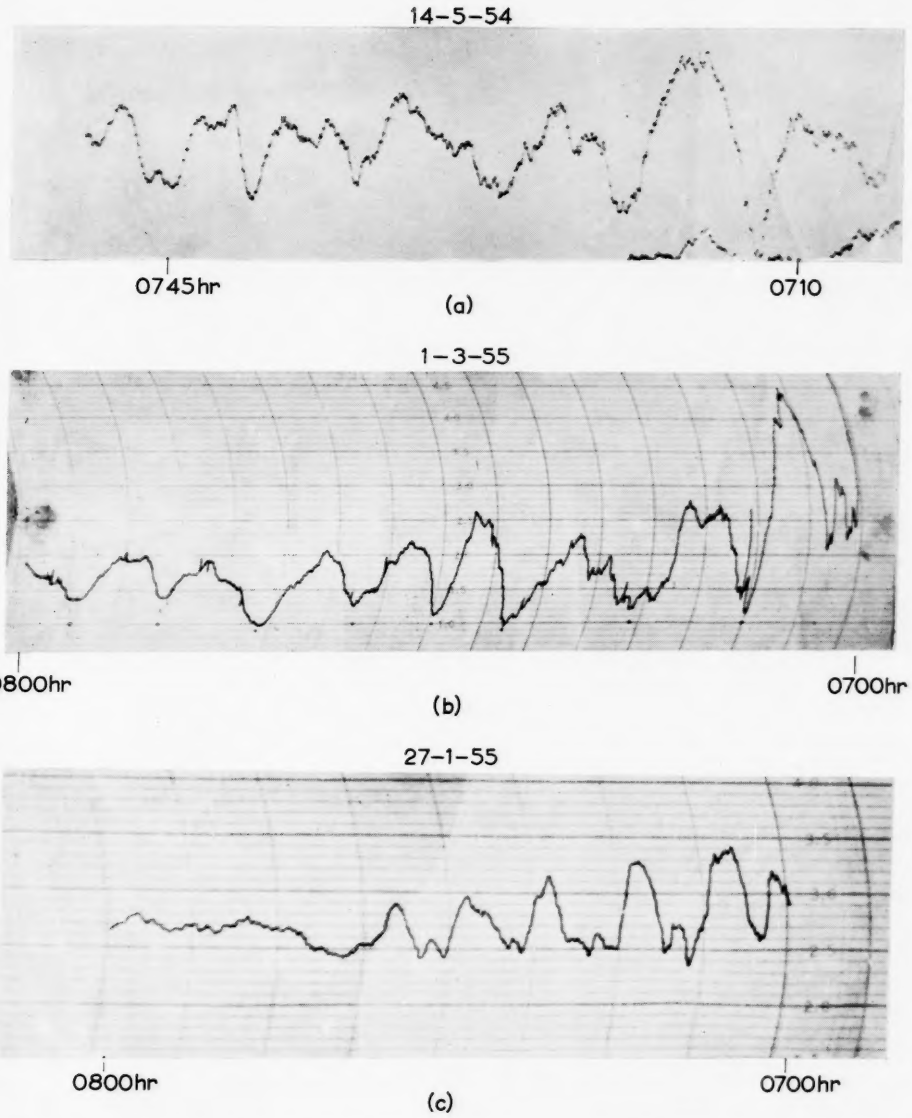

Fig. 1. Magneto-ionic fading records of medium-wave transmissions for three typical days.

VOL.
12
1958

fading period is due to more rapid change of critical frequency in the early portion of the record when compared to the later part. An interesting feature of all these records is the prominent and rapid decrease of the amplitude of fading with time in all the records. For instance, the amplitude of fading falls to nearly one-third from the beginning to the end of records shown in Figs. 1(b) and (c). It will be noticed that this fall of amplitude is not due to the general decrease of signal strength with time but due to the relatively high attenuation of the extraordinary ray with time of day. The average time periods of fading for each fading record taken in the months of May 1954, January and March 1955, are determined in the usual manner and the results are presented in Table 1.

Table 1. Experimentally observed magneto-ionic fading periods

Date	Fading period (min)	Date	Fading period (min)
9 May 1954	6·3	11 January 1955	8·6
13 May 1954	6·8	12 January 1955	9·4
14 May 1954	7·0	13 January 1955	7·9
16 May 1954	6·9	19 January 1955	9·3
17 May 1954	6·8	20 January 1955	9·3
		21 January 1955	6·9
Mean period for May 1954	6·76	22 January 1955	3·5*
		25 January 1955	9·6
1 March 1955	6·5	27 January 1955	8·3
		Mean period for January 1955	8·65

* This value is not considered in taking averages.

It will be noticed from these observations that the period of fading does not vary widely from day to day in any particular month. The period of fading in the summer month of May is, however, lower than that in the winter month of January and this may be attributed to the more rapid rate of change of ionization density in the *E*-region in the summer time.

3. Outline of the Graphical Method of Calculation of Phase Paths

The phase path P of each of the magneto-ionic components inside the ionosphere can be calculated by using the well-known relation

$$P = \int \mu \, ds \tag{1}$$

where ds is an infinitesimal element along the path of the wave at any point and μ is the refractive index at the same point for propagation along the direction ds. The integration is carried over the entire path in the ionosphere. Following Booker's notation (1949), if ψ is taken to be the angle of refraction at this particular point in the path, we can write the usual relations

$$\mu \cos \psi = q \tag{2}$$

and

$$\mu \sin \psi = \sin i = S \tag{3}$$

where i is the angle of incidence and q is known as the "phase propagation vector". Using relations (2) and (3) in (1), we can now write the phase path as

$$P = \int \mu \frac{dh}{\cos \psi} = \int \frac{\mu^2}{q} dh = \int \frac{q^2 + S^2}{q} dh \tag{4}$$

where dh is the vertical component of the element ds. Differentiating (4), we can write

$$\frac{\delta P}{\delta h} = q + \frac{S^2}{q} \tag{5}$$

To calculate $\delta P/\delta h$ at every point in the path of the ray, it is necessary to first evaluate q over the entire path of the trajectory. This is done by following the treatment of Booker outlined below.

Assuming that the ionosphere is stratified horizontally in planes parallel to a plane earth and following the ray treatment, Booker (1938) has generalized the magneto-ionic theory for the case of oblique incidence propagation of radio waves in the ionosphere. Choosing a right handed co-ordinate system with axis 3 in vertical direction and axes 1 and 2 in the horizontal plane and having the origin at the point of incidence of radio wave on ionosphere, he has first deduced a quartic equation for q which was later transformed into a simpler cubic equation (Booker, 1949) in $x\ [= Ne^2/(\pi m f^2)]$ given by

$$x^3 + Ax^2 + Bx + \Gamma = 0 \tag{6}$$

Neglecting the collision term, the constants in this equation are given by the following relations

$$A = -[1 + 2(c^2 - q^2)] \tag{7}$$

$$B = (c^2 - q^2)[(2 - y^2) + (S_1 y_1 + S_2 y_2 + q y_3)^2 + (C^2 - q^2)] \tag{8}$$

$$\Gamma = -(1 - y^2)(C^2 - q^2)^2 \tag{9}$$

where y_1, y_2 and y_3 are the components of $y\ (= f_H/f)$ along the 1, 2 and 3 axes, and S_1, S_2 and C are direction cosines of the direction of propagation along the 1, 2 and 3 axes respectively. Using relations (7) to (9), the cubic equation (6) for x can be solved numerically and the three solutions of x can be obtained for any numerical value of q. One of the three roots is discarded, as it is not of any practical importance. The other two roots correspond to the lower trajectory ordinary and extraordinary rays. The q–x curves for the ordinary and extraordinary rays can thus be drawn by numerically solving the cubic equation for various values of q.

In order to use the relation (4) for obtaining the phase path by integration, it is necessary to calculate the height h in the ionosphere corresponding to each value of x obtained by solving equation (6). As this calculation involves a knowledge of the ion density distribution, it is necessary to assume a plausible ionospheric model for making the phase height calculations. In the present investigation these calculations are carried out for the E-region assuming Chapman and parabolic

VOL. 12 1958

distributions. The CHAPMAN electron density distribution is given by the well-known relation (CHAPMAN, 1931):

$$N = N_{\max} \sec^{1/2} \chi \exp \tfrac{1}{2}[1 - Z - \sec \chi e^{-z}] \tag{10}$$

where $Z = (h - h_0)/H$ (Z is negative for lower trajectory rays)

and $H = KT/mg$

This equation gives the electron density N at any height h measured from ground as a function of Z, χ being the zenith angle. $N_{\max}$ is the maximum density in the region and h_0 is the height at which maximum rate of ion production takes place for $\chi = 0$. This equation can be rewritten as

$$x = \frac{f_0^2}{f^2} \sec^{1/2} \chi \exp \tfrac{1}{2}[1 - Z - \sec \chi e^{-z}] \tag{11}$$

where f_0 is the critical frequency of the region and f is the wave frequency. Knowing the value of f_0 and the sun's zenith angle at the time of recording, this relation can be utilized for the calculation of Z corresponding to each value of x. A graph is thus drawn showing the variation of $\partial p/\partial z$ against Z for both the up-going and down-coming waves and the total phase path for each magneto-ionic component is obtained by graphical integration of the curve between the limits Z_0 and Z_r, where Z_0 is lower limit given by $Z_0 = -2{\cdot}5$ and Z_r is the value corresponding to the level of reflection. The value of $Z_0 = -2{\cdot}5$ is taken as the lower limit of the layer, following CHAPMAN, as the value of $\partial p/\partial Z$ becomes constant for lower values of Z.

The Chapman distribution reduces to the following parabolic form for values of $\cos \chi = 1$ and for small values of Z.

$$x = \frac{f_0^2}{f^2}\left\{1 - \frac{(h_m - h)^2}{h_m^2}\right\}$$

This relation can be written as

$$x = \alpha h - \beta h^2 \tag{12}$$

where $\alpha = \dfrac{2f_0^2}{f^2 h_m}$, $\beta = \dfrac{f_0^2}{f^2 h_m^2}$ and $\dfrac{\alpha}{2\beta} = h_m$

h_m is the semi-thickness of the layer and h is the height measured from the bottom of the layer. Solving this equation, we obtain

$$h = h_m - \sqrt{h_m^2 - x/\beta} \tag{13}$$

or $$h = h_m [1 - \sqrt{1 - f^2 x/f_0^2}],$$

discarding the other solution for h which is greater than h_m. Using this relation, the values of h corresponding to each value of x can be calculated and the phase paths obtained in the usual manner by graphical integration after plotting $\partial p/\partial h$ against h.

4. Development of an Approximate Formula for the Calculation of Phase Paths of Both the Magneto-ionic Components

As the general and exact method of phase path calculations outlined in the previous section is quite involved and laborious, an attempt has been made to derive a simple formula for readily calculating the phase paths sufficiently accurately. Calculations of q–x values by using Booker's formula given in the previous section have shown that, for the particular case of medium-wave transmission from long distances, the q–x curves are very nearly parabolic in shape. This suggested the possibility that a linear relation between q^2 and x would give a close fit with the actual q–x curves. The following empirical relations are then tried and are found to give close agreement with the actual q–x values for both the magneto-ionic components.

$$q^2 = C^2 - \Delta x \tag{14}$$

where $\Delta = C/^2x_r$ and x_r is the value of x for the reflection level (i.e. at $q = 0$) and differs for the two magneto-ionic components. The constants in this relation are determined to satisfy the limiting values of q and x. This empirical relation, which is an approximation for the quartic and cubic equations given by Booker, is found to hold good fairly accurately for the case of medium-wave transmissions incident at high oblique incidence in the equatorial zone.

Assuming the validity of this empirical relation for the particular transmission from Madras, a simple formula can now be derived for the phase paths of either of the magneto-ionic components for the case of parabolic distribution of ionization in the E-region. As the q–x curves for this relation are truly parabolic, we shall take the upper limit of phase integral h_r as the values corresponding to $q = 0$ and write the phase path integral as

$$P = 2\int_0^{h_r}\left(q + \frac{S^2}{q}\right) dh \tag{15}$$

$$= 2\int_0^{h_r} \frac{1 - x\Delta}{\sqrt{C^2 - x\Delta}}\, dh,$$

since $c^2 + S^2 = 1$.

Using relation (12) of the parabolic layer for substituting for x and changing the variables, we have the integral

$$P = -2\sqrt{\beta\Delta}\int_{z_0}^{z_r} \frac{R^2 - b^2}{\sqrt{R^2 - a^2}}\, dR \tag{16}$$

where

$$R = \frac{\alpha}{2\beta} - h \quad = (h_m - h).$$

$$a^2 = \frac{\alpha^2}{4\beta^2} - \frac{C^2}{\beta\Delta} = {h_m}^2 - \frac{C^2}{\beta\Delta}.$$

$$b^2 = \frac{\alpha^2}{4\beta^2} - \frac{1}{\beta\Delta} = {h_m}^2 - \frac{1}{\beta\Delta}.$$

$$R_0 = \frac{\alpha}{2\beta}.$$

$$R_r = \frac{\alpha}{2\beta} - h_r.$$

VOL. 12 1958

On integrating (16), we obtain

$$P = -2\sqrt{\beta\Delta}\left\{\frac{R}{2}\sqrt{R^2 - a^2} + \left(\frac{a^2}{2} - b^2\right)\ln\frac{R + \sqrt{R^2 - a^2}}{a}\right\} \tag{16a}$$

It can be easily shown that

$$R_r^2 - a^2 = 0, \qquad R_0 = \frac{\alpha}{2\beta} = h_m$$

$$R_0^2 - a^2 = \frac{C^2}{\beta\Delta} = \frac{x_r}{\beta};$$

so that equation (16a) can now be written as

$$P = 2\sqrt{\beta\Delta}\left\{\frac{h_m}{2}\sqrt{\frac{x_r}{\beta}} + \left(\frac{a^2}{2} - b^2\right)\ln\frac{h_m + \sqrt{\frac{x_r}{\beta}}}{Z_r}\right\} \tag{16b}$$

since
$$b^2 - \frac{a^2}{2} = \frac{h_m^2}{2} - \frac{1}{\beta\Delta}\left(1 - \frac{C^2}{2}\right)$$

$$Z_r^2 = (h_m - h_r)^2 = h_m^2 - \frac{x_r}{\beta}$$

$$\sqrt{\beta\Delta} = \frac{f_0}{h_m f}\cdot\frac{C}{\sqrt{x_r}} = \frac{C}{h_m D}$$

and
$$\sqrt{\frac{x_r}{\beta}} = \frac{h_m f}{f_0}\cdot\sqrt{x_r} = h_m D$$

where
$$D = \frac{f\sqrt{x_r}}{f_0} \tag{17}$$

We can simplify the relation (16b) and write it in the final form as

$$P = h_m C - \tfrac{1}{2}h_m C\left\{\frac{1}{D} - D\left(\frac{2 - C^2}{C^2}\right)\right\}\ln\frac{1 + D}{1 - D} \tag{18}$$

This relation is in a simple form to calculate the phase paths of both the magneto-ionic components if we know the values of critical frequencies at the time of recording and x_r values for both the magneto-ionic components. The x_r values for both the magneto-ionic components are calculated by solving relation (6) for $q = 0$. Though this does not correspond exactly to the maximum levels of reflection, it is quite close enough to this level for this particular case of medium waves propagated at high oblique incidence near low latitudes. For the case under consideration x_r occurs at value of $q = -0{\cdot}01$ for ordinary ray and $q = 0{\cdot}01$ for extraordinary ray.

5. Results of Phase Path Calculations

In this investigation the phase paths of the two magneto-ionic components of medium wave transmissions from Madras (600 km) received at Waltair on a frequency of 1·42 Mc/sec are calculated theoretically by following the procedures

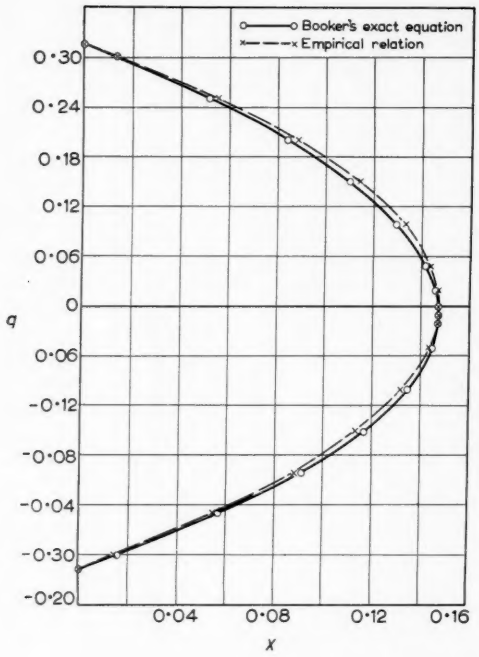

Fig. 2. q–x curves for the ordinary wave obtained by using Booker's equation and the empirical formula of the authors.

VOL. 12 1958

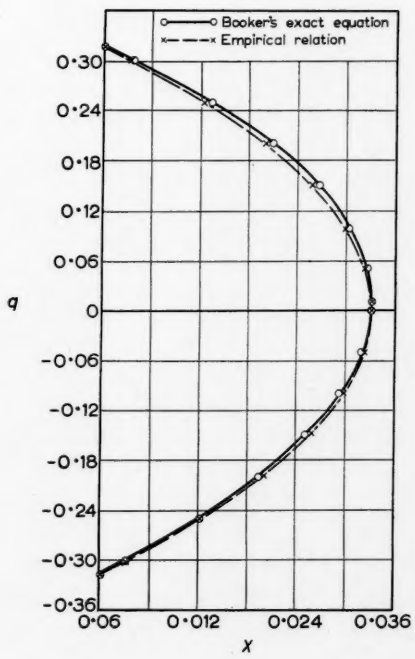

Fig. 3. q–x curves for the extraordinary wave obtained by using Booker's equation and the empirical formula of the authors.

outlined in the previous sections. We shall first give the calculations based on the accurate method involving graphical integrations. The q–x curves are first drawn by solving the cubic equation (6) after assuming the following data for the constants involved. Assuming 100 km as the height of reflection from the E-region, the angle of incidence is calculated from simple geometry and the value is 71° 34′. As several previous investigators have shown that the magnetic field at the E-region level is about 5 per cent less than the ground value, the total magnetic field H at the reflection point is taken as equal to 0·3605 gauss, the ground value being 0·3795 gauss. To simplify the calculations, the 2–3 plane is chosen to be in the plane of propagation, so that $S_1 = 0$ and $S_2 = S$. The magnetic meridian makes an angle of 34° with the plane of propagation and the dip angle is +15·5°. The following numerical data are then finally used for the constants involved in solving the cubic equation (6) for x by taking various values for q ranging from $+C$ to $-C$, as these are the limiting values that q can take during the entire traverse of the wave inside the ionosphere:

$$f_H = \frac{He}{2\pi mc} = 1{\cdot}008 \text{ Mc/s} \qquad \frac{f_H}{f} = y = 0{\cdot}7099$$

$$y_1 = 0{\cdot}3826 \qquad y_2 = -0{\cdot}5671$$

$$y_3 = 0{\cdot}1897 \qquad S_2 y_2 = -0{\cdot}5380$$

y_1, y_2 and y_3 are the components of y along the 1, 2, 3 axes.

The resulting q–x curves thus obtained are shown in Figs. 2 and 3. The maximum value of x gives the ionization density corresponding to the level of reflection. For the ordinary ray this occurs at $q = -0{\cdot}01$ and for the extraordinary at $q = +0{\cdot}01$. Though $\partial p/\partial h$ becomes infinite at $q = 0$, this gives only the level where the phase wave is directed horizontally and does not correspond to reflection level. The graphical integration in (4) should be done between the limits corresponding to the lower boundary of the layer and the level of reflection for both the up-going and down-coming waves as the two paths will not be, in general, the same.

The phase paths are calculated for a few particular days in the months of May 1954, January and March 1955 for the hours 0700 and 0800 I.S.T. for the case of both Chapman and parabolic distributions. The critical frequency values required for the calculations are taken from Ahmedabad or Calcutta data according to availability after correcting for local mean time difference, and these values are shown in Table 2.

Fig. 4 shows the curves for $\partial p/\partial h$ vs. Z obtained for 14 May 1954, assuming Chapman distribution. The curves on the positive side of the ordinates are for the up-going and the negative side are for the down-coming rays. The curves for the times 0700 and 0800 hr are shown in a single figure for convenience. The limiting values of integration are shown as ordinates in the graphs. Results of graphical integration by a planimeter or by counting squares gives the values of phase paths p_0 for the ordinary ray and p_e for the extraordinary ray after multiplying

Table 2. Zenith angles and the corresponding critical frequencies used in phase-path calculations

Date	0700 hr I.S.T. f_0E		0800 hr I.S.T. f_0E	
14 May 1954	2·26 Mc/s	69° 5′	2·64 Mc/s	55° 7′
27 January 1955	2·04 Mc/s	73° 21′	2·32 Mc/s	59° 26′
22 January 1955	2·04 Mc/s	—	2·62 Mc/s	—
1 March 1955	2·14 Mc/s	76° 6′	2·62 Mc/s	61° 49½′

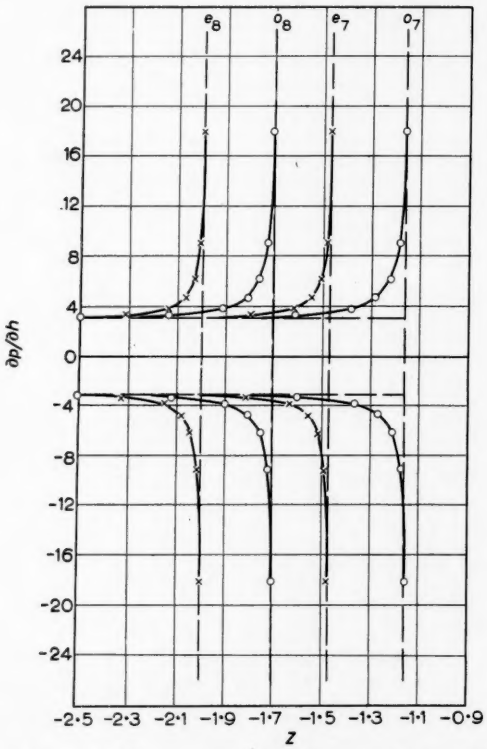

Fig. 4. Graph of $\delta P/\delta h$ vs. Z for the ordinary and extraordinary rays at 0700 and 0800 I.S.T.

the areas by H. Chapman (1931), Mitra (1952) Guha (1949) and others have taken a value of 10 km for the scale height H, but recent rocket data (Rocket Panel, 1952) has shown that for the 100 km level a value of 8 km is a reasonably good value. Following this latter evidence, H is taken as equal to 8 km in these calculations. Similar calculations were made for records taken on other days, and all the results are presented in Table 3.

δP in this table refers to the difference between the ordinary and extraordinary

VOL. 12 1958

phase paths. The expected time periods of magneto-ionic fading for all the three records are shown at the bottom of the table. Calculations of phase paths for the same records by assuming parabolic distribution are done in a similar way and the results obtained are presented in Table 4.

Table 3. Phase paths and time periods of fading for the case of Chapman distribution

Description	Time	Phase paths (km)		
		14 May 54	27 January 1955	1 March 1955
P_0	0700 hr	81·81	99·48	104·00
P_e	0700 hr	61·37	79·20	82·61
δP	0700 hr	20·44	20·28	21·39
P_0	0800 hr	51·95	64·71	63·65
P_e	0800 hr	33·20	45·88	44·43
δP	0800 hr	18·75	18·83	19·22
Change in δP from 0700 hr to 0800 hr		1·69	1·45	2·17
Calculated period (min)		7·49	8·74	5·84
Observed value		7·00	8·30	6·50

Table 4. Phase paths and time periods of fading for the case of parabolic distribution

Description	Time	Phase paths (km)		
		14 May 1954	27 January 1955	1 March 1955
P_0	0700 hr	7·06	8·59	7·82
P_e	0700 hr	1·54	1·84	1·63
δP	0700 hr	5·52	6·75	6·19
P_0	0800 hr	5·10	6·59	5·12
P_e	0800 hr	1·11	1·53	1·18
δP	0800 hr	3·99	5·06	3·95
Change in δP from 0700 hr to 0800 hr		1·53	1·69	2·24
Calculated period (min)		8·29	7·51	5·72
Observed value		7·00	8·30	6·50

The semi-thickness of the layer is taken to be 20 km in these calculations.

The empirical formula derived in the previous section is then used to calculate analytically the phase paths for the records taken on the same dates and the results are presented in Table 5.

Table 5. Phase paths and time periods of fading as calculated from empirical formula

Description	Time	Phase paths (km)		
		14 May 1954	27 January 1955	1 March 1955
P_0	0700 hr	6·99	8·62	7·82
P_e	0700 hr	1·55	1·89	1·73
δP	0700 hr	5·44	6·73	6·09
P_0	0800 hr	5·10	6·63	5·18
P_e	0800 hr	1·13	1·47	1·15
δP	0800 hr	3·79	5·16	4·03
Change in δP from 0700 hr to 0800 hr		1·47	1·57	2·06
Calculated period (min)		8·61	8·05	6·15
Observed value		7·00	8·30	6·50

6. Comparison with Experimental Results and Discussion

With a view to comparing the values of the periodicities obtained experimentally with the values obtained for all the three cases theoretically, the final values of the time periods are tabulated and presented in Table 6.

VOL. 12 1958

Table 6. Comparison of the theoretical and experimental values of fading periods

Description	Fading period (min)			
	14 May 1954	27 January 1955	1 March 1955	22 January 1955
Experimental	7·00	8·30	6·50	3·5
By graphical method assuming Chapman layer	7·49	8·74	5·84	—
By graphical method assuming parabolic layer	8·29	7·51	5·72	—
By empirical formula	8·61	8·05	6·15	4·68

This table includes also the values obtained by empirical formula for the special case of record taken on 22 January 1955, as it is an exceptional case having a low value for the period.

It will be seen from this table that the agreement between the experimental values and theoretical values of periodicity calculated by graphical method is fairly good if we assume Chapman distribution for the E-region. The agreement is particularly good for the month of January 1955. The periodicities calculated theoretically by the graphical method for both the Chapman and parabolic

distributions agree within 10 per cent. Though there is a reasonable agreement in these periodicities, it is interesting to note that the actual values of δP for both cases differ widely, the values being of the order of 20 km for CHAPMAN layer and 5–7 km for the parabolic layer. This discrepancy in the value of the path differences is due to the fact that these medium radio waves at oblique incidence traverse more path in a CHAPMAN layer than a parabolic one, as the gradient of ionization is very low in the former for these levels of reflection. It is interesting to note that in spite of this large difference in δP values, the time periods of fading work out to be of the right order for both cases.

Now, comparing the graphical method and the analytical method by using the empirical formula, it may be noticed from a comparison of the actual paths given in Tables 4 and 5 that the paths obtained by empirical formula agree fairly well with those by the graphical integration method. The agreement is better for the ordinary ray, the difference being 1 per cent for the ordinary and 6 per cent for the extraordinary ray. If we compare the time periods obtained by both methods, it will be seen that the empirical formula gives values which are slightly greater than the values obtained by the graphical method. The maximum error involved in using the empirical formula is about 8 per cent. Thus it may be said that the simple method of calculating periodicity of fading by using empirical formula gives reasonably good values. Considering the simplicity of the method and the ease of calculations involved, the method is definitely advantageous in such phase path calculations involving long-distance medium-wave transmissions at equatorial latitudes.

The record taken on 22 January 1955 shows an unusually low fading period, and with a view to seeing whether the method applies for such a case, calculations were made for this particular record by using the empirical formula and taking the f_0E data on the particular day from Haringhata Ionospheric Research Station. The theoretical value of 4·7 min is in reasonable agreement with the actual value, considering the fact that only approximate values are used for the f_0E values at the actual region of reflection.

In conclusion, it may be said that this investigation gives a quantitative interpretation for the periodic fading of magneto-ionic origin in oblique incidence medium-wave transmissions. It is also found that the lower E-region conforms more closely to the CHAPMAN distribution compared to the parabolic form.

Acknowledgement—The authors are indebted to the Council of Scientific and Industrial Research for financial support of this research scheme.

REFERENCES

APPLETON E. V. and BEYNON W. J. G.	1947	*Proc. Phys. Soc.* **59,** 58.
BOOKER H. G.	1938	*Phil. Trans. Roy. Soc.* A **237,** 411.
	1949	*J. Geophys. Res.* **54,** 243.
CHAPMAN S.	1931	*Proc. Phys. Soc.* **43,** 483.
GUHA U. C.	1949	*J. Geophys. Res.* **54,** 355.
MITRA S. K.	1952	*Upper Atmosphere.* The Asiatic Society
ROCKET PANEL	1952	*Phys. Rev.* **88,** 1029.
SATYNARAYANA R. and DHARAMBIR RAI	1954	*J. Sci. Indust. Res.* **13,** 66.
TANTRY B. A. P. and KHASTAGIR S. R.	1951	*Indian J. Phys.* **25,** 217.

Journal of Atmospheric and Terrestrial Physics, 1958, Vol. 12, pp. 306 to 328. Pergamon Press Ltd., London

On the production of radioisotopes in the atmosphere by cosmic radiation and their application to meteorology

D. Lal, P. K. Malhotra and B. Peters
Tata Institute of Fundamental Research, Bombay

(*Received* 13 *November* 1957)

Abstract—Cosmic radiation produces, in the atmosphere, various radioisotopes which are efficiently collected during the condensation of moisture and can be detected in rain-water. The production rates of various radioisotopes, mainly those whose half-lives make them suitable for studying meteorological phenomena, have been calculated for all parts of the atmosphere, and are presented in graphical form.

For the isotope, ^{10}Be, whose half-life is long compared to the characteristic time of mixing between the stratosphere and the troposphere, the fall-out rate agrees with the calculated production rate.

For the isotopes, ^{7}Be, ^{33}P, and ^{32}P, whose half-lives are short compared to the characteristic time of mixing between the stratosphere and the troposphere, the measured fall-out rates agree with the calculations, provided one assumes that,

(a) only the activity produced in the troposphere appears in rain-water and contributions from air irradiated in the stratosphere are comparatively rare,

(b) the mean period, between successive removals of radioisotopes from air masses, is about 1 month.

Tentative measurements on the fall-out of ^{35}S activity indicate an appreciably higher rate than calculated.

It is shown that the *relative* concentrations of any two radioisotopes with appreciably different half-lives, in a *particular* rain, do not depend on the local meteorological conditions, but only on the latitude and altitude at which the air mass was irradiated and can therefore be used as labels to trace the history of air-masses. The study of such *isotope ratios* in individual precipitations can, therefore, lead to useful meteorological information.

VOL. 12 1958

Introduction

The discovery in rain-water of various short-lived isotopes which are produced by cosmic radiation opens up the possibility of using radioactivity measurements for determining the over-all features of large-scale atmospheric circulation. This possibility arises mainly because of two important properties of these activities. On the one hand, the relative concentrations of different isotopes in rain-water will be directly related to the corresponding ratio in which they are present in the air from which the condensation took place. On the other hand, cosmic radiation intensity differs appreciably in various parts of the atmosphere, and if the half-lives of these isotopes are widely different, the ratio of their concentrations in a given mass of air must depend strongly on the history of the air-mass; more precisely it will depend on the time spent by the air at different altitudes and latitudes since it was last cleansed of radioactive products by condensation and precipitation.

A first prerequisite for using cosmic-ray produced radioactivity for meteorological or allied purposes is an exact knowledge of the rate at which cosmic radiation produces these isotopes in various regions of the atmosphere.

This paper is devoted to constructing a chart giving the rate of production of the relevant isotopes per gramme of air at all latitudes and altitudes.

The cosmic-ray-produced isotopes discovered so far are listed in Table 1, in the order of decreasing half-lives. The radioisotopes ^{3}H and ^{14}C, whose presence was first demonstrated by Faltings and Harteck (1950) and Libby (1952),

respectively, have been known for some time. Five additional radioisotopes have been detected during the last 2 years. The isotopes ^{10}Be, ^{14}C, ^{3}H and ^{7}Be arise mainly in the interactions involving atmospheric nitrogen and oxygen nuclei, while the isotopes ^{35}S, ^{33}P and ^{32}P arise exclusively in the disintegrations of atmospheric argon nuclei.

Table 1

Radioisotope	Half-life	Disintegration product	Reference
^{10}Be	$2{\cdot}7 \times 10^6$ years	β^- −550 keV	Peters (1955), Arnold (1956), Goel *et al.* (1957)
^{14}C	5700 years	β^- −156 keV	Libby (1952)
^{3}H	12·5 years	β^- −18 keV	Faltings and Harteck (1950), Kaufman and Libby (1954)
^{35}S	87 days	β^- −167 keV	Goel (1956)
^{7}Be	53 days	γ −480 keV	Arnold and Al Salih (1955), Goel *et al.* (1956), Cruikshank *et al.* (1956)
^{33}P	25 days	β^- −250 keV	Lal *et al.* (1957)
^{32}P	14·3 days	β^- −1·7 MeV	Marquez and Costa (1955), Lal *et al.* (1957)

In this paper we shall discuss the production of all these isotopes except ^{14}C and ^{3}H. The production of ^{14}C has already been discussed extensively in the literature. Calculations on the production of ^{3}H and ^{7}Be have been reported by Currie *et al.* (1956), and by Benioff (1956) respectively. Our work differs from the previous calculations not only because it includes four newly discovered radioisotopes, but also because our approach to the calculations is somewhat different from that of previous authors. They have made extensive use of the nuclear cascade theory, whose validity is still subject to serious doubt. We have tried to avoid this difficulty by relying almost entirely on the experimental data from cosmic-ray and accelerator experiments. There is only one departure from this: We have made a limited use of Rudstam's semi-empirical spallation formula (Rudstam, 1955), not in order to calculate spallation probabilities, but solely for the purpose of obtaining isotope distribution among the spallation products of a given element. We believe that in the present state of our knowledge this phenomenological approach is likely to give the more accurate results.

In Section I, we discuss briefly the type of reactions responsible for the production of these isotopes.

In Section II, we construct a family of curves proportional to the rate of occurrence of low-energy nuclear disintegrations, defined in this paper as those events which are produced by nucleons with energies less than 400 MeV. These are the disintegrations which are responsible for most of the isotope production. We also give curves for all nuclear disintegrations regardless of energy. The curves are drawn for various latitudes at intervals of 10° and for all altitudes. The relative star production rates are then converted into an absolute star

production by using certain measurements on the frequency of cosmic-ray stars in cloud chambers filled with various gases.

In Section III, we deduce the yield per star of various isotopes as a function of energy. From this we obtain the average yields of the various isotopes in cosmic-ray stars produced in different regions of the atmosphere. The production rates of the various isotopes are then calculated, at all latitudes and altitudes, by multiplying the yields by the corresponding rate of star production obtained in Section II.

In Section IV, we have evaluated the global production rates of the various isotopes in the atmosphere as a function of latitude, separately for the troposphere and the stratosphere. The effect of time variations in cosmic-ray intensity on isotope production is also discussed. Our calculations of production rates of stars and of ^{7}Be are compared with those reported by other authors. We also compare our calculations with the measured yearly fall-out rates, wherever such measurements are available.

Finally in Section V, we discuss the usefulness of the radioisotopes ^{35}S, ^{7}Be ^{33}P and ^{32}P, as tracer elements in meteorological research.

Section I

The nature of nuclear reactions giving rise to particular isotopes

The nuclear interacting particles of the cosmic radiation include nucleons, π-mesons, and K-mesons. Neutrons and protons are responsible for almost all nuclear disintegrations in the atmosphere. π-mesons and K-mesons travel only short distances before they decay in one or two steps into weakly interacting particles. Therefore, they do not contribute appreciably to the nuclear disintegrations. γ-rays are responsible for a few per cent of the nuclear disintegrations occuring in the atmosphere. This contribution to isotope production is quite negligible, except for those isotopes which can be obtained from the nuclei of the air by (γ,n) and (γ,p) reactions. Neutrons and protons are produced in about equal numbers in the atmosphere as a result of the nucleonic cascade which is initiated near the top of the atmosphere by the energetic primaries of cosmic radiation. As the cascade develops and the number of nucleons increases, the average energy of the nucleonic component falls. We need to know the intensity and the energy spectrum of the nucleonic component, as well as the excitation function for the formation of a particular radio-nuclide. We will first discuss qualitatively the nature of the relevant nuclear reactions and the energy at which they can occur.

The production of ^{14}C occurs predominantly as a result of the capture of thermal neutrons by atmospheric nitrogen nuclei; its production rates have been studied both theoretically and experimentally, and will not be discussed in this paper.

The production of all isotopes listed in Table 1 (except ^{14}C and ^{3}H) require nucleons which have energies of at least 30–50 MeV. The production of the isotopes, ^{10}Be and ^{7}Be from N, O nuclei and the production of ^{35}S, ^{33}P and ^{32}P from argon nuclei, involve the emission of 2–4 protons and 1–5 neutrons from the target under conditions in which the residual nucleus remains intact. The

VOL. 12 1958

protons and neutrons are emitted either singly or in groups as deutrons, tritons, alphas or as heavier aggregates. The corresponding reactions appear as 1–4-pronged stars in cloud-chambers and photographic emulsions. Reactions of this type can be produced both by low-and by high-energy nucleons ; in the cosmic radiation, most of these reactions will be induced by low-energy nucleons for two reasons:

(a) The flux of low-energy nucleons is larger by at least an order of magnitude than the flux of high-energy nucleons, in all parts of the atmosphere except near the very top.

(b) The reactions which are responsible for radioisotope production involve the emission of a few nucleons only and require that most of the target be left intact. High-energy collisions will not in general leave a large undamaged nuclear residue except when they have the nature of glancing collisions. The excitation functions are, therefore, expected to fall off for higher energies.

The largest contribution to the isotope production comes, therefore, from low-energy interactions produced by nucleons with energies of 100–200 MeV.

At all energies, neutrons and protons are produced in about equal number. Above 500 MeV they play essentially identical roles, but at lower energies, protons, because they lose energy rapidly by ionization, are brought to rest before they can induce nuclear reactions; at 100 MeV protons are very rare in the atmosphere compared to neutrons. In all regions of the atmosphere except near the top the majority of radioisotopes are, therefore, produced by neutrons.

OL.
12
958

Section II

The rate of star production as a function of latitude and altitude

1. *Relevant experimental data on star production.* Direct measurements of star production rates due to cosmic radiation, in the upper regions of the atmosphere, at mountain altitudes and sea-level have been made by several investigators employing photographic emulsions and ionization chambers. Star production by cosmic rays in nitrogen- and argon-filled cloud chambers has been measured at mountain altitudes (W. W. Brown, 1954; Bullock, 1957), and at sea-level (W. W. Brown, 1954).

Because of the comparative ease with which photographic emulsions can be exposed at high altitude, the most extensive star production data in the upper regions of the atmosphere are derived from experiments employing photographic plates as detector. For various reasons, these data cannot be used directly to ascertain absolute disintegration rates.

(a) The composition of emulsions is very different from that of the atmosphere; approximately 65 per cent of all stars are produced in the silver and bromine nuclei and only 35 per cent of the stars are formed in the carbon, nitrogen and oxygen constituents. As a result, large corrections have to be applied to the data in order to get information on stars in light nuclei.

(b) We are primarily interested in small stars (1–4 prongs). Most of the data are confined to stars of 3 or more prongs. One- and two-pronged stars are usually left out because they cannot be easily distinguished from

proton recoils and scattering events respectively. In addition, there is usually a marked lack of efficiency in scanning for small stars, as can be seen by comparing data of different investigators on 3 and 4 prong stars.

The most detailed and careful measurements here have been reported by Lord (1951) at geomagnetic latitudes 28° and 54° at mountain altitudes and near the top of the atmosphere. Although the data are not satisfactory for ascertaining absolute star production rates, they are valuable for obtaining relative star production rates in the upper regions of the atmosphere, where no other measurements are available.

At atmospheric depths greater than 300 g. cm^{-2}, Simpson, Baldwin and Uretz (1951) have measured low-energy nuclear bursts in thin-walled ionization chambers filled with high-pressure argon. Results are available for several latitudes and altitudes. Even for thin walls, the proportion of stars formed in the wall of ionization chamber remains large compared to the number of stars formed in the gas. The data cannot, therefore, be used to determine absolute disintegration rates in argon, but are valuable for comparing low-energy star production rates in different regions of the atmosphere. Other data which are useful for studying the variation of the low-energy star production with altitude and latitude, are the flux of the neutron component (neutrons with energy less than 30 MeV). Extensive measurements at various latitudes and altitudes have been made by Simpson, and by Korff and their collaborators.

2. *Procedure and results.* Various experiments (Simpson *et al.*, 1951; Simpson, 1951; Yuan, 1951; Staker *et al.*, 1951; Soberman, 1956) show that there exists an equilibrium between low-energy stars and slow neutrons ($E < 30$ MeV) at all latitudes for depths, $x > 200$ g cm^{-2}. In regions close to the upper boundary of the atmosphere, where neutrons escape into space and in regions close to hydrogenous substances like lakes and clouds, where neutrons are slowed down more rapidly, the proportionality between low-energy stars and slow neutrons is destroyed.*

The altitude and latitude variation of slow neutrons is identical with that of protons of energy up to 400 MeV and, therefore, identical with the variation in the intensity of what we shall call "low-energy stars". For instance, the absorption of protons with $E \sim 420$ MeV between atmospheric pressure 231 g cm^{-2} and sea-level has been measured by Conversi (1950) and was found to correspond to an absorption mean free path of 150 g cm^{-2} at $\lambda = 50°$. The intensity ratio at 30,000 ft of protons in the same energy interval, between 60°N and equator has also been determined by Conversi and was found to be 3·2. Both the absorption mean free path and the latitude effect of 420 MeV protons agree well with the corresponding results on slow-neutron intensities (Conversi, 1950). It follows that measurements on slow neutrons ($E < 30$ MeV) for which extensive data are

* This is in agreement with the theory of slowing-down and capture processes of neutrons as given by Bethe *et al.* (1940). A small number of high-energy neutrons are carried into the atmosphere by the primary radiation, but within the first 100 g cm^{-2} of air, their number becomes negligible compared to that of the secondary neutrons, which are products as well as originators of a nucleon cascade in the atmosphere. Once the energy of neutrons has fallen to <1 BeV, most of the energy is absorbed in a single collision. The resulting stars give rise to neutrons with energies between 5 and 30 MeV which in turn are brought down to thermal energies by elastic scattering with air nuclei in mean distances ~90 g cm^{-2}. Thermal, epithermal and fast neutrons below 0·5 BeV are, therefore, in equilibrium.

VOL. 12 1958

available can be used to construct the latitude and altitude variation of the low-energy stars.

In the upper regions of the atmosphere ($x < 200$ g cm^{-2}), the neutron measurements cannot be used directly; one has to consider their escape probability

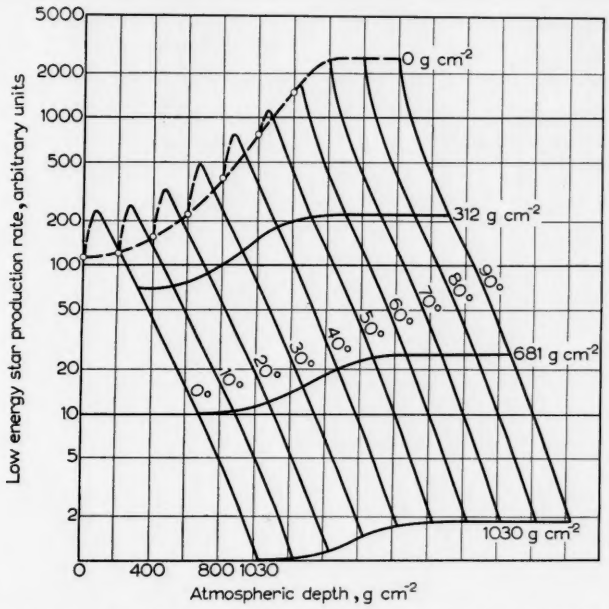

Fig. 1. The rate of production of stars due to nucleons of $E < 400$ MeV, is given (in arbitrary units) as a function of depth in the atmosphere for various latitudes at intervals of 10°. The curves for various latitudes have been successively displaced along the abscissa by 200 g cm^{-2}.

as a function of distance from the top of the atmosphere. However, the flux of the slow neutrons is still proportional to star production rate if we make a comparison for different latitudes at the same pressure. The method we have used is to obtain first the altitude variation of small stars for $x < 200$ g cm^{-2} from nuclear emulsion work at a particular latitude; then to extend the data to different latitudes with the help of neutron flux data.

A network of the relative production rates of low-energy stars at different altitudes and latitudes was established, using the neutron data (Simpson, 1951; Simpson and Fagot, 1953; Rose *et al.*, 1956; Soberman, 1956) and the observed altitude dependence of low-energy stars from the photographic emulsion work (Lord, 1951). The detailed procedure used for constructing the network from 0–1030 g cm^{-2} is discussed elsewhere (Lal, 1958). The resulting relative star production rates are shown in Fig. 1. The ordinate represents the intensity in arbitrary units and the abscissa represents the atmospheric depth in g cm^{-2}. For clarity's sake, the curves for various latitudes at 10° intervals have been displaced along the abscissa, with respect to each other. In the same figure we have also shown the latitude variation of slow neutrons at pressures of 312 g cm^{-2} (Simpson,

1951), 681 g cm^{-2} (Simpson and Fagot, 1953) and 1030 g cm^{-2} (Rose *et al.*, 1956) used for constructing the network.

The star production curves show a transition effect in the upper atmosphere between latitudes 0°–50°. The position of maxima is observed to shift to greater depths as one moves towards the equator. At the same time the height of the transition maximum increases towards the equator. This behaviour must be expected and arises from the increasing hardness of the primary radiation as one proceeds to lower latitudes. At latitudes greater than 60° the maxima vanish and the curves represent an initial exponential absorption of the star producing radiation with a mean absorption length of 70–80 g cm^{-2}, only slightly larger than the interaction mean free path of nucleons in air. The near equality of the absorption mean free path with the interaction mean free path shows that most of the primary nucleons, at $\lambda > 60°$, produce on the average only one interaction and do not contribute to the cascade development. Since the majority of nucleons at these latitudes have energies less than 500 MeV, such a behaviour is to be expected.

The general character of the curves which we have derived can, therefore, be understood in terms of the known energy distribution of primary cosmic-ray particles and present knowledge of high-energy nuclear processes. Thereby they give support to our method of obtaining the relative star production rates in the stratosphere.

VOL. 12 1958

The curves in Fig. 1 refer to a period of maximum sunspot activity, i.e. a period of low cosmic-ray intensity, since we have used the latitude effect at 312 g cm^{-2} as measured by Simpson (1948). The variations in the primary cosmic-ray flux with solar cycle and the corresponding contribution to star production are significant at high latitudes but affect the global production rates very little; they will be discussed in Section V.

The fraction of stars produced by high-energy nucleons ($E > 400$ MeV) in different regions of the atmosphere is obtained from the relative production frequency of small and large stars as observed in photographic emulsion. Data are available (Birnbaum *et al.*, 1952; Lal, 1958) both in the stratosphere and at mountain altitudes for latitudes between 3° and 54°. Total star production rates, still in arbitrary units, are then obtained by multiplying the ordinates of the curves in Fig. 1, by the appropriate factors. The resulting curves are shown in Fig. 2. The details of the procedure are given elsewhere (Lal, 1958).

It remains now to ascertain the *absolute* star production rates in the atmospheric nitrogen, oxygen, and argon. One might think that the relative star production rates could be normalized near the top of the atmosphere with the help of the available flux measurements on the primary cosmic-ray beam, using the inelastic cross-sections measured in the laboratory. This, however, cannot be done satisfactorily because at all altitudes there exist directions in space from which particles arrive after traversing a considerable thickness of atmosphere. At a height of 30 km, where the atmospheric pressure is 12 g cm^{-2}, 45 per cent of the available solid angle corresponds to directions of arrival in which a primary particle would have to traverse an atmospheric thickness of more than 30 g cm^{-2} and 12 per cent to a thickness of more than 300 g cm^{-2}. Even at 40 km (3·2 g cm^{-2}),

the corresponding fractions are 20 and 11 per cent respectively. The importance of secondary effects at great height is illustrated by the fact that more than 50 per cent of the stars observed at rocket (YAGODA, 1956) and at balloon (CAMERINI *et al.*, 1949; LORD, 1951; and MEI, 1952) altitudes are produced by neutral particles, although the primary radiation consists of charged particles only. Without an accurate knowledge of the composition of the secondary radiation at large zenith angles it is therefore not possible to convert stratosphere measurements into absolute disintegration rates by such a procedure.

It is equally unsatisfactory to calculate absolute star production rates from the observed omni-directional particle intensity at high altitudes, measured with ionization chambers or single counters, because the large number of secondary particles incident at large zenith angles contain an unknown fraction of electrons and μ-mesons which do not produce stars, and of fast neutrons which produce stars but are not registered by the detectors.

It seems to us that, for obtaining absolute disintegration rates, the most reliable experimental data involving least corrections are due to W. W. BROWN (1954) and BULLOCK (1957), who measured star production rates, employing high-pressure cloud chambers, in argon and nitrogen, and argon respectively at mountain altitudes. Their data need to be corrected for the inefficiency in the detection of small stars (1 and 2 prongs), which have been missed due to the instrumental bias used. The cloud chamber was triggered whenever the built-in ionization chamber recorded a pulse greater than that produced by a 5 MeV (BULLOCK) and 8 MeV (W. W. BROWN) α-particle. The loss factors in BULLOCK's experiment are, therefore, smaller than those in W. W. BROWN's experiment. The total amount of material in BULLOCK's experiment was, however, larger (114 g cm^{-2} Pb, 53 g cm^{-2} stainless steel), than in W. W. BROWN's experiment (10·6 g cm^{-2} brass, contributed by the chamber wall). Furthermore, W. W. BROWN has also determined corrections necessary for the absorption of the nucleonic component in the chamber wall.

The results of BULLOCK, therefore, are good for ascertaining the relative production rate of stars of different sizes, whereas W. W. BROWN's experiment yields absolute production rate of large stars. Combining these data, we can, therefore, obtain fairly well the absolute rate of star production in *argon*, at $\lambda = 50°$, 680 g cm^{-2} atmospheric depth, where measurements of W. W. BROWN were made.

For ascertaining absolute star production rate in nitrogen, we similarly make a comparison of the star size distribution as observed by BROWN with that obtained in the *unbiased* cloud chamber experiments of KELLOGG (1953), BØGGILD and TENNEY (1951), and FULLER (1954), who studied neutron-produced stars, in carbon by 90 MeV, in oxygen by 190 MeV, and in oxygen by 300 MeV, respectively. These experiments give correct relative production frequency of small stars, since they are necessarily free of instrumental bias and refer to an energy region where most of the star production occurs in the cosmic radiation.

The estimated correction factors are 1·85 and 2·15 for stars in argon and nitrogen respectively (LAL, 1958). The correction to nitrogen data is greater than that for the argon stars. This was also expected, since the instrumental

bias which depends on the ionization produced by an event will discriminate more against stars in nitrogen than in argon.

The absolute star production rates at latitude 50°, and atmospheric depth 680 g cm^{-2} are then found to be

16·4 stars/g atom/hr in argon

11·8 stars/g atom/hr in nitrogen

For obtaining star production rates in oxygen, we extrapolate from the rate in nitrogen, using a dependence of star production on the two-third power of the atomic number, we get

12·9 stars/g atom/hr in oxygen

One would have preferred to convert relative into absolute star intensity by using some measurements near the top of the atmosphere where star production is at its maximum, but no suitable experiments exist. However, it is possible to check the conversion from relative to absolute intensities in another way.

At geomagnetic latitude 50° and atmospheric pressure 680 g cm^{-2} the energy spectrum of vertically incident protons of $E > 20$ MeV is known (Filthuth, 1955, and references contained in Puppi and Dallaporta, 1952). The relative neutron-to-proton flux at the same place is known, as a function of energy, from measurements on the frequency of stars of different sizes produced by neutrons and protons in photographic emulsions (Barford and Davis, 1952, R. H. Brown *et al.*, 1949). Therefore we can derive the vertical neutron flux at $\lambda = 50°$, atmospheric depth 680 g cm^{-2}. With the help of the measured angular dependence of protons and neutrons (Conversi and Rothwell, 1954), and the known star production cross-sections of nucleons for average cosmic-ray energies in nitrogen and argon nuclei, we determine the absolute star production rate at a pressure of 680 g cm^{-2}, $\lambda = 50°$.

The two independent methods for determining *absolute* star production rates agree well. They differ by about 6 per cent for stars produced in nitrogen and by about 11 per cent for stars produced in argon.

The total rate of star production in the atmosphere (in nuclei/sec/g air) is shown in Fig. 2 as a function of altitude for all latitudes at intervals of 10°. In order to obtain the production rates separately in nitrogen, oxygen and argon nuclei the ordinate should be multiplied by 0·768, 0·225, and $6{\cdot}34 \times 10^{-3}$ respectively.

In our present state of knowledge on cosmic-ray phenomena, we consider this empirical approach to the problem of ascertaining absolute star production rate preferable to the commonly used approach involving nucleonic cascade theories. The theories of the nucleonic cascade are still subject to serious uncertainties; in particular, results depend critically on assumptions as to the degree of inelasticity in high-energy collision, which is not as yet well known in all relevant energy intervals.

Fig. 3 shows the total number of stars produced in the atmosphere per primary particle and per primary nucleon as a function of geomagnetic latitude. The primary flux for the different components of the cosmic-ray beam as a function

VOL. 12 1958

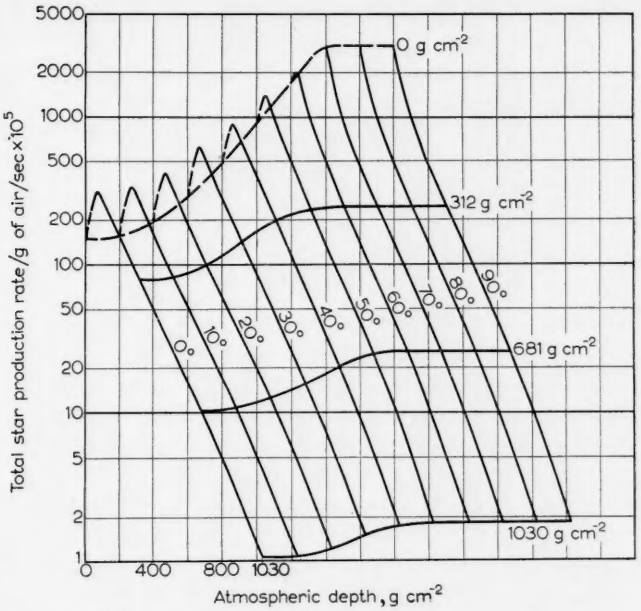

Fig. 2. Star production rate and production rates for ^{7}Be and ^{10}Be. The ordinate represents the rate of production for all stars/sec/g of air as a function of depth in the atmosphere for various latitudes at intervals of 10°. Curves for successive latitudes have been displaced along the abscissa. For obtaining the production rate of stars separately in nitrogen, oxygen and argon, the ordinate should be multiplied by 0·768, 0·225 and $6{\cdot}34 \times 10^{-3}$ respectively. To obtain the rates of production of ^{7}Be and ^{10}Be (atoms/sec/g of air) the ordinate should be multiplied by $4{\cdot}2 \times 10^{-2}$ and $4{\cdot}9 \times 10^{-2}$ respectively.

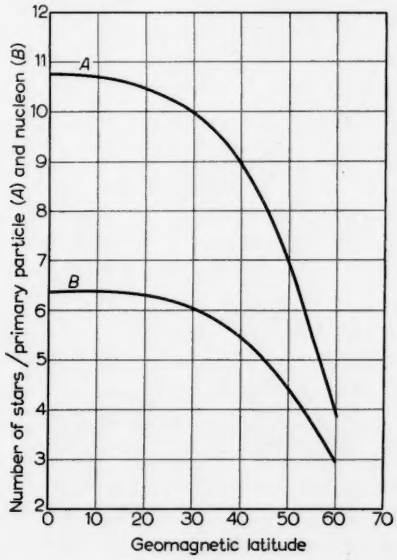

Fig. 3. Number of stars produced in the atmosphere per primary particle (a), and per primary nucleon (b), are given as a function of geomagnetic latitude.

of latitudes was obtained from the energy spectrum (Lal, 1953). The flatness of the graph representing stars per primary nucleon between latitude 30° and 0° indicates that the increase in energy per primary particle above ~3 BeV/nucleon is used up mainly in meson production and does not appear as additional energy in the nuclear cascade. The drop in the number of stars per primary at higher latitudes corresponds to the fact that the additional low-energy primaries admitted by the earth's magnetic field induce only small nuclear cascades and also lose a significant part of their energy by ionization before they can give rise to stars.

Section III

Yield of radioisotopes in cosmic-ray stars in the atmosphere

Having determined the star production rates in various regions of the atmosphere, we now proceed to evaluate the cross-section for the formation of the various radioisotopes. This requires a knowledge of the excitation function for the relevant nuclear reactions and of the energy spectrum of nuclear interacting particles, prevalent in different regions of the atmosphere.

The elements in which we are interested are produced in nuclear reactions involving the emission of a few neutrons and charged particles, most of which are singly and doubly charged. Sulphur and phosphorus are produced from argon in 1 or 2 and 2 or 3 pronged stars respectively, but so are chlorine, silicon and magnesium. Beryllium nuclei together with other elements are produced in 2 or 3 pronged stars in nitrogen and in 2, 3 or 4 pronged stars in oxygen. The yields of the various elements will be proportional to the cross-section for the formation of the particular stars from which they result. The size distribution of stars in argon at $\lambda = 50°$, 680 g cm^{-2} and in nuclei of photographic emulsions at several latitudes and altitudes are available (Section II). These data make it possible to obtain the size-frequency distribution of stars in N, O and A, and, therefore, furnish relative yields in different regions of the atmosphere.

For obtaining the absolute yields of the particular isotopes ^{35}S, ^{33}P and ^{32}P, we first obtain the total yields of the elements sulphur and phosphorus in argon stars. We make use of the fact that in heavy nuclei the ratio of singly charged to all charged particles emitted during evaporation is reasonably independent of star size and close to 0·8 (Hodgson, 1954, Grigorov and Soloveva, 1957; Bailey, 1956). The yield of the elements is calculated from the frequency of production of 1, 2 and 3 pronged stars and the probabilities of emission of singly and doubly charged particles in argon stars (Lal, 1958). It turns out that the result is not very sensitive to the exact ratio of singly to doubly charged particles emitted.

The proportion of ^{35}S amongst S nuclei, and of ^{32}P and ^{33}P amongst P nuclei is then estimated by using Rudstam's semi-empirical relation (Rudstam, 1955). This relation has been fitted by Rudstam from spallation studies in elements of mass number greater than 51. It also predicts correctly spallation in aluminium, and is therefore probably applicable to spallation in argon (Lal, 1958). Though the relation predicts the absolute yield of a particular isotope only within a factor of about 2, the relative yields of a particular isotope compared to others of the same element should be given fairly accurately, as evidenced by the generally

VOL. 12 1958

good agreement between theory and experiment wherever data for comparison are available (RUDSTAM, 1956). In the stratosphere and at low latitudes the energy spectrum of nucleons becomes harder; the production frequency of 1, 2 and 3 pronged stars in argon increases less rapidly than that of larger stars; this results in a drop of isotope yield. As expected, the drop is larger in the case of ^{35}S than in the case of ^{33}P or ^{32}P. The calculated yields are summarized in Table 2, for two selected regions in the atmosphere.

Table 2

Atmospheric region	Yield/star in argon		
	^{35}S	^{33}P	^{32}P
680 g cm^{-2}, $\lambda > 30°$	0·077	0·046	0·042
50 g cm^{-2}, $\lambda < 30°$	0·055	0·039	0·035

The variations in the yield per star are large and therefore cannot be neglected. We, therefore, have constructed a new family of curves which represent production rate of total stars (Fig. 2) multiplied by the corresponding yields of ^{35}S, ^{33}P and ^{32}P per star in argon.

The curves representing the ^{35}S production are given in Fig. 4, as a function of altitude for all latitudes at intervals of 10°. Similar families of curves are given for the rate of production of ^{33}P and ^{32}P in Fig. 5.

The absolute yields of ^{7}Be and ^{10}Be cannot be derived in a manner similar to that employed for sulphur and phosphorus isotopes. In light nuclei, the relative probability of emitting singly- or doubly-charged particles is observed to change with star size (KELLOGG, 1953; FULLER, 1954). To ascertain their yields, we therefore, have to make use of both the nucleon energy spectrum and the cross-sections for their formation.

The yield of ^{7}Be by protons on carbon (BENIOFF, 1956; MARQUEZ and PERLMAN, 1951; DICKSON and RANDLE, 1951) has been measured up to about 6 BeV energy. In addition, total cross-sections for the production of all isotopes of a given element by 90 MeV neutrons on carbon (KELLOGG, 1953) and 300 MeV neutrons on oxygen (FULLER, 1954) are available. Using these data and the nucleon energy spectrum derived at 680 g cm^{-2}, $\lambda = 50°$, we have obtained the yields of ^{7}Be and ^{10}Be from stars produced in nitrogen and oxygen nuclei. Now it remains to ascertain the variation of yield per star in different regions of the atmosphere.

The production of ^{7}Be and ^{10}Be mainly occurs in 2 and 3 pronged stars produced in nitrogen and oxygen. In these light nuclei, the fraction of small stars to the total number of stars does not depend strongly on energy and therefore does not vary appreciably in different regions of the atmosphere. Therefore, the

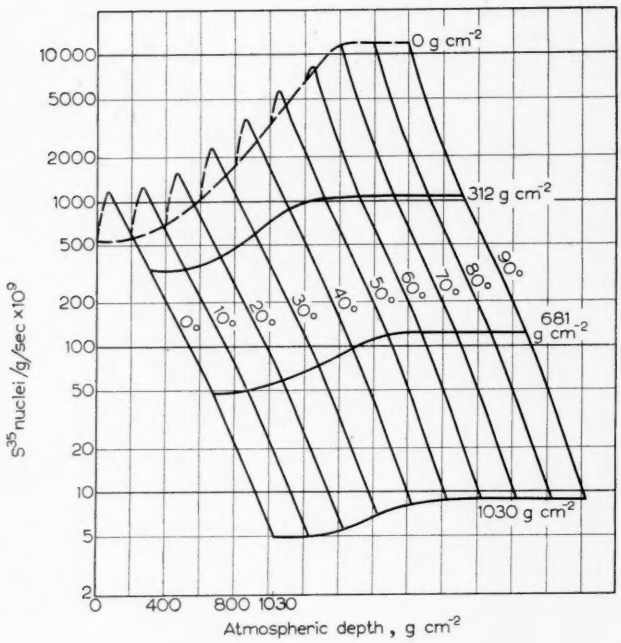

Fig. 4. The rate of production of ^{35}S atoms/sec/g of air is given as a function of depth in the atmosphere for various latitudes at intervals of 10°. Curves for successive latitudes have been displaced along the abscissa.

VOL. 12 1958

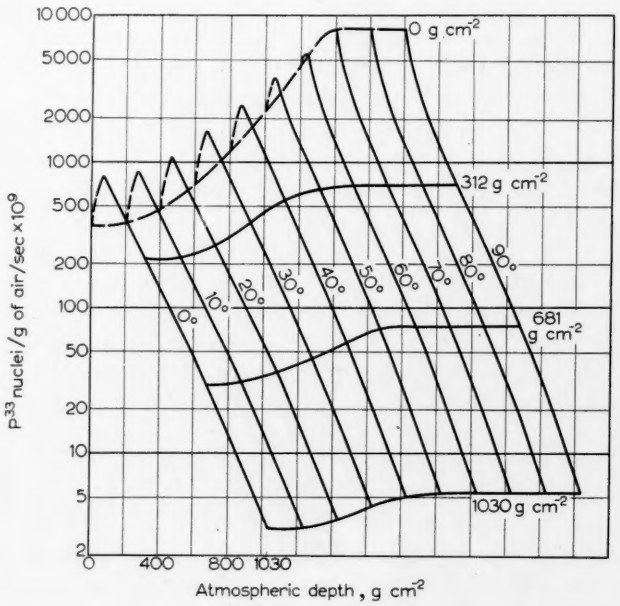

Fig. 5. ^{33}P and ^{32}P production rates. The rate of production of ^{33}P atoms/sec/g of air is given as a function of depth in the atmosphere for various latitudes at intervals of 10°. The curves for successive latitudes have been displaced along the abscissa. For obtaining the rate of production of ^{32}P (atoms/sec/g of air) the ordinate should be multiplied by 0·9.

yields found at 680 g cm^{-2}, $\lambda = 50°$ are valid over the entire range of latitudes and altitudes. The estimated yields (LAL, 1958) of ^{7}Be and ^{10}Be in stars produced in the atmospheric nuclei are listed in Table 3.

Table 3

Target	Average yield per star	
	^{7}Be	^{10}Be
Nitrogen	0·046	0·052
Oxygen	0·027	0·040
Air	0·042	0·049

The absolute production rates of ^{7}Be and ^{10}Be are, therefore, given by the curves in Fig. 2, which represent the total star production rate, if we multiply the ordinates by

$4{\cdot}2 \times 10^{-2}$ to obtain production rate of ^{7}Be/g of air/sec.

$4{\cdot}9 \times 10^{-2}$ to obtain production rate of ^{10}Be/g of air/sec.

SECTION IV

The global production of stars and cosmic-ray produced isotopes

(1) *Global production rates in the troposphere and stratosphere*

The star and isotope production rates as a function of altitude and latitude are given in Figs. 2, 4 and 5. Integrating these throughout a column of atmosphere of 1 cm^2 cross-section, we obtain the variation of isotope production with latitude (Figs. 6, 7 and 8), which show the production rates of stars of ^{7}Be and ^{10}Be (Fig. 6), ^{35}S (Fig. 7), and ^{32}P, ^{33}P (Fig. 8) in the entire atmosphere, as well as the fraction produced below the tropopause.

The troposphere production rate stays remarkably constant over all latitudes. The effect of higher production rates at higher latitudes is compensated by the decrease in the height of the tropopause.

The global average production rate of stars and of various isotopes in a column of atmosphere with 1 cm^2 cross-section are listed in Table 4.

Averaged over the globe, the production in the troposphere amounts to 30 per cent of the total production.

(2) *The effect of time variations in cosmic-ray intensity on isotope production*

The major intensity changes in cosmic-ray flux are of two types: short-lived increases and decreases associated with solar flares and sunspots respectively and variations arising from changes in the low-energy cut-off with a period corresponding to the 11 year sunspot cycle (FORBUSH, 1954; NEHER, 1956). Solar flares producing substantial increases in cosmic-ray intensity occur rarely

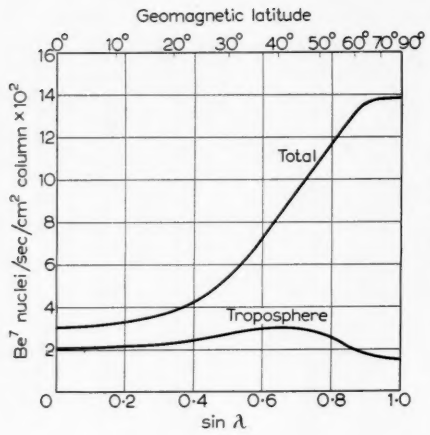

Fig. 6. Total ^{7}Be, ^{10}Be and star production rates. The rate of production of ^{7}Be (atoms/sec/cm^2 column) is given as a function of latitude for the entire atmosphere as well as for the troposphere only. In order to obtain the rate of production of ^{10}Be and of stars (per sec/cm^2 column) the ordinate should be multiplied by 1·17 and 23·8 respectively.

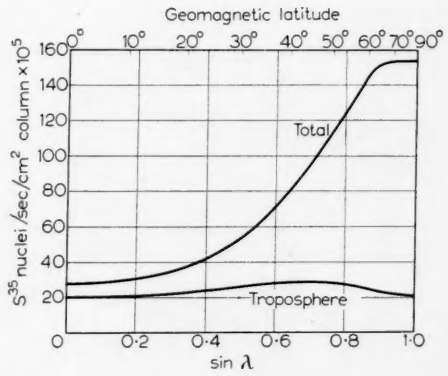

Fig. 7. The total rate of production of ^{35}S (atoms/sec/cm^2 column) is given as a function of latitude λ for the entire atmosphere as well as for the troposphere only.

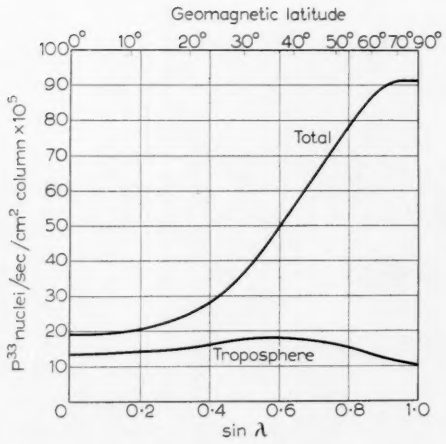

Fig. 8. The total rate of production of ^{33}P (atoms/sec/cm^2 column) is given as a function of latitude λ for the entire atmosphere and for the troposphere only. In order to obtain the rate of production of ^{32}P, the ordinate should be multiplied by 0·9.

VOL. 12 1958

(on the average less than 1/year). They last for a few hours only and therefore cannot affect average isotope production rates. Variations with the solar sunspot cycle are confined to high latitude and are appreciable only above $\lambda = 58°$. NEHER showed that during 1954, when the sun activity was at a minimum, primaries with energies as low as 150 MeV entered the atmosphere in the polar region, while in years of great solar activity the observed minimum energy lies in the neighbourhood of 800–1000 MeV. The total ionization produced at the top of the atmosphere was higher by a factor of 2·4 between the maximum and

Table 4

	Global average production rate per cm^2 column per year		
	Troposphere	Stratosphere	Total
Stars	$1{\cdot}8 \times 10^7$	$3{\cdot}6 \times 10^7$	$5{\cdot}4 \times 10^7$
^{10}Be	$9{\cdot}0 \times 10^5$	$1{\cdot}7 \times 10^6$	$2{\cdot}6 \times 10^6$
^{7}Be	$7{\cdot}5 \times 10^5$	$1{\cdot}5 \times 10^6$	$2{\cdot}2 \times 10^6$
^{35}S	$8{\cdot}1 \times 10^3$	$1{\cdot}5 \times 10^4$	$2{\cdot}3 \times 10^4$
^{33}P	$4{\cdot}8 \times 10^3$	$9{\cdot}8 \times 10^3$	$1{\cdot}5 \times 10^4$
^{32}P	$4{\cdot}4 \times 10^3$	$8{\cdot}8 \times 10^3$	$1{\cdot}3 \times 10^4$

minimum of solar activity. Almost the entire increase is due to particles with energies below 300 MeV, and these are brought to rest by ionization before they have an appreciable chance to contribute to nuclear collisions. Yet their effect on star production is not entirely negligible. This is shown by the fact that the neutron intensity at 312 g cm^{-2} in 1954 was 13 per cent higher than in 1948, at latitude $\lambda = 50°$.

The production rates in Fig. 1 have been calculated for 1948, a year of maximum sunspot activity and minimum cosmic-ray intensity. We estimate that the average increase in isotope production between the maximum and minimum of the solar cycle amounts to 20 per cent above $\lambda = 58°$ and is negligible at lower latitudes. This corresponds to a 3 per cent change in global production rates between sunspot maxima and minima.

(3) *Comparison of our results with other calculations and with experimental data.*

(a) *Star production rates.* The total star production rates in 1 cm^2 column at three latitudes 51°, 31° and 0° have been reported by VERNOV and GRIGOROV (1956), and at $\lambda = 50°$ by PUPPI and DALLAPORTA (1952). A comparison of their results with ours is made in Table 5.

The agreement between the various results is seen to be fairly good.

(b) *Isotope production rates.* The production rate of ^{7}Be has recently been calculated by BENIOFF (1956). His value for the global production, $3{\cdot}3 \times 10^6$–^{7}Be atoms/cm^2/year should be compared with our value of $2{\cdot}2 \times 10^6$. While the total production rates do not differ much, the altitude dependence of the production

of ^{7}Be differs by factors of up to 3. This discrepancy arises because of the entirely different procedures adopted; Benioff has made use of the cascade theory to ascertain the variation in the nucleon flux with altitude, whereas our results are based on an experimentally observed altitude dependence.

Table 5

Stars/sec/cm^2 column			Reference
51°	31°	0°	
2·7	1·3	0·7	Present work
3·5	1·4	0·8	Vernov and Grigorov (1956)
2·0	—	—	Puppi and Dallaporta (1952)

In case of the isotope ^{10}Be, whose half-life is very long compared to the time scales involved in atmospheric circulation processes, the average radioactivity per cm^2 of earth's surface should be a measure of the global production rates. Its deposition has recently been measured in Pacific sediments and constitutes a check on our calculations. The relation between its concentrations and the production rate has already been discussed by one of us (Peters, 1957). The most probable value for the global production was found to be $2{\cdot}5 \times 10^6$ — ^{10}Be atoms/cm^2/year. The present calculations yield the same figure.

VOL. 12 1958

Table 6

	^{7}Be atoms/cm^2 year at latitudes			Global average
	1°	10°	54°	
Experimentally observed deposition rate	$5{\cdot}1 \times 10^5$	$4{\cdot}5 \times 10^5$	$5{\cdot}3 \times 10^5$	5×10^5 (estimated)
Calculated value for the troposphere	$6{\cdot}6 \times 10^5$	$7{\cdot}0 \times 10^5$	$7{\cdot}8 \times 10^5$	$7{\cdot}5 \times 10^5$
Calculated value for the entire atmosphere	$9{\cdot}5 \times 10^5$	$10{\cdot}1 \times 10^5$	$3{\cdot}8 \times 10^6$	$2{\cdot}2 \times 10^6$

The concentration of ^{7}Be in rain-water (atoms/cc) has been determined for a period of about one year at Kodaikanal ($\lambda = 1°$, 7600 ft) and Bombay ($\lambda = 10°$, sea-level) by Rama and Zutshi (1957) and at Chicago ($\lambda = 54°$) by Arnold and Al-Salih (1955). The yearly deposition rates of ^{7}Be can then be estimated at these latitudes by multiplying the observed average yearly ^{7}Be concentrations with the total yearly rain fall (cm) in the corresponding zonal belt. The calculated deposition rates of ^{7}Be for the three latitudes* are given in Table 6. In the same

* The latitudes listed are actually geomagnetic rather than geographic latitudes, but because of strong zonal circulation the distinction is probably of no importance in meteorological problems.

table we have also shown the calculated production of ^{7}Be in 1 cm^2 column extending through the entire atmosphere and the production per cm^2 in the troposphere only.

The experimentally determined deposition rates of ^{7}Be agree well with its calculated production in the troposphere only, and disagree with the calculated value for the *entire atmosphere*, both on the absolute values and the latitude variation. This, therefore, shows that the ^{7}Be activity in rains mainly derives from production in the troposphere. This must be expected because mixing between tropospheric and stratospheric air masses is a slow process. The study of radioactive fall-out from bombs indicates that the mean life of air in the stratosphere is larger than 5 years (LIBBY, 1956). Stratospheric contribution to the ^{7}Be activity in rain-water should therefore, be negligible.

Closer agreement between the calculated production and observed precipitation is obtained if one takes into account the amount of ^{7}Be which has decayed during the time interval between its production and removal. We define removal time in the troposphere by the diffusion equation:

$$\frac{dN}{dt} = R - \frac{N}{\tau} - \frac{N}{\tau_f} \tag{1}$$

where R is the production rate of ^{7}Be in the troposphere; τ and τ_f are the average decay and the fall-out times of ^{7}Be, respectively. The equilibrium concentration of ^{7}Be in the troposphere is then given by setting, $dN/dt = 0$. Using for R the calculated annual global production of ^{7}Be in the troposphere, $R = 7{\cdot}5 \times 10^5$ atoms/cm^2/year and taking $\tau_f = 22$ days, which is the value obtained by STEWART *et al.* (1957), from a study of the fission activity produced by thermonuclear weapons, we calculate $N/\tau_f = 5{\cdot}8 \times 10^5$ atoms/cm^2/year. Our measured value (Table 6), is $N/\tau_f = 5 \times 10^5$ atoms/cm^2 year.

The concentrations of ^{33}P, ^{32}P and ^{35}S isotopes in rains have recently been measured for about 1 year at Kodai–Kanal ($\lambda = 1°$, 7600 ft), Bombay ($\lambda = 10°$ sea-level), Shillong ($\lambda = 16°$, 5000 ft) and Mussoorie ($\lambda = 20°$, 6900 ft). From these measurements one can estimate their deposition rates. The analyses are yet incomplete, and it is hoped a comparison of their deposition rates with calculations can be made in the near future. The results obtained so far by GOEL *et al.* (1958) indicate that there exists a close agreement between the calculated and observed values for ^{33}P and ^{32}P activities, but there is a considerable excess of ^{35}S activity in rains over and above that calculated.

SECTION V

Meteorological information from the studies of short-lived isotopes

The production rates of the various isotopes are strongly latitude- and altitude-dependent (Figs. 2, 4 and 5).

Their concentration in an air mass depends therefore on the past history of its motion. The short-lived isotopes ^{35}S, ^{7}Be, ^{33}P and ^{32}P whose half-lives range from about a fortnight to 3 months, should be suitable tracers for studying meteorological processes.

Rain forms a very convenient method for studying the cosmic-ray-produced isotopes, since air-masses lose their radioactivity chiefly through wet precipitations. It removes bomb-produced radioactivity from the atmosphere very effectively. The results of STEWART *et al.* (1957) show that less than 5 per cent of the activity is brought down by dry deposition. The approximate agreement between our calculated and observed deposition by rain-water indicates that rain is equally effective in removing cosmic-ray-produced radioactivity from the atmosphere, which at least initially is not associated with dust.

The isotope concentrations in rain-water show the large fluctuations which must arise from variations in the amounts of moisture condensed from a given air-mass. Nevertheless, it is possible to obtain detailed information on non-local meteorological phenomena from the study in *individual rains*, if one measures the ratio of at least two of the short-lived isotopes. These ratios depend only on the past radiation history of the air-mass. This statement is strictly true only in the case of the two isotopes ^{33}P and ^{32}P, which are chemically identical and necessarily have identical precipitation mechanisms. But it applies to other isotopes as well if they are efficiently removed by the condensation of water-vapour.

In order to show that the ratio of two isotopes with different half-lives are quite different for an air-mass which has descended from the stratosphere and another air-mass which since the last precipitation has remained in the troposphere, we have calculated the ratio of the expected concentration of ^{7}Be and ^{32}P in air-masses for a few simple hypothetical trajectories. These calculations are not meant to describe actual situations, but are given simply to illustrate the sensitivity of the proposed method.

VOL. 12 1958

The equation of growth of a radioisotope in an air-mass can be written as:

$$\frac{dn}{dt} = -\frac{n}{\tau} + S(t) \qquad (2)$$

where τ is the average life of the isotope and n represents the number of atoms of the particular isotope per gramme of air; $S(t)$ is its production rate as a function of time and therefore as a function of its sojourn at various altitudes and latitudes.

We shall assume that the isotopes collect on dust or moisture and are effectively removed when condensation of moisture and precipitation takes place. After a rain, the air-mass is supposed to be completely free of isotopes. Equation (2) must therefore be solved for the boundary condition $n = 0$ for $t = 0$.

We shall further assume that there is a good vertical mixing in the troposphere and a much slower mixing within the stratosphere, but that there is little exchange between the two regions. Good mixing in the troposphere seems to be in accord with meteorological evidence; it arises from the large negative temperature gradients. In the stratosphere, which signifies a nearly isothermal region, the configuration is inherently stable, and vertical mixing must be a slow phenomena. However, at a given latitude, the production rates of the various isotopes within the stratosphere do not differ by more than a factor of 2, except at very high latitudes (see Figs. 2, 4 and 5). We therefore can replace $S(t)$ by two average values $\overline{S_S}$ and $\overline{S_T}$ which represent the isotope production rates in the stratosphere and troposphere respectively.

We now solve equation (2) for three different histories of the air-mass:

(1) The air spends the time between successive rains exclusively within the troposphere;

(2) The air first spends a period in the stratosphere which is long compared to the half-life of the isotopes and then descends to the troposphere, where

(a) it spends its time at various altitudes so that it receives the average tropospheric irradiation;

or (b) it remains confined to the lower regions of the troposphere, where cosmic radiation and therefore the isotope production rates are negligibly small.

The solution of equation (2) (with the boundary condition $n = 0$, $t = 0$), is:

$$n(t) = e^{-t/\tau} \cdot \int_0^t e^{t/\tau} \cdot S(t)\, dt \tag{3}$$

The concentration $C(t)$, number of atoms/cc, will be proportional to $n(t)$, the concentration of the isotope in the air from which it was condensed.

$$C(t) = \alpha n(t) \tag{4}$$

For case (1) we obtain

$$C(t) = \alpha\tau\bar{S}_T(1 - e^{-t/\tau}) \tag{5}$$

For cases 2(a) and 2(b) we obtain

$$C(t) = \alpha\tau[\bar{S}_T + (\bar{S}_S - \bar{S}_T)e^{-t/\tau}] \tag{6}$$

$$C(t) = \alpha\tau\bar{S}_S e^{-t/\tau} \tag{7}$$

respectively, where t is the time since the air-mass descended from the stratosphere into the troposphere. The ratios of concentration for two different isotopes are independent of α.

We have calculated variations in the ratio $^7Be/^{32}P$ with time t, for the particular case when a polar air-mass descends from the stratosphere and settles in the troposphere at intermediate latitudes. In this case $\bar{S}_S = 11\bar{S}_T$. This can be obtained from Fig. 6 or 7, and from the well-known curves giving the height of the tropopause at different latitudes. The calculated ratio of concentration $^7Be/^{32}P$ is plotted in Fig. 9 as a function of time t for the three cases 1, 2(a) and 2(b). The numbers alongside the curves represent the number of Be^7 atoms per gramme of air.

For the case (1), when the air-mass spends its time entirely in the troposphere, the ratio R, ($^7Be/^{32}P$), increases slowly from about 170 to 650, reaching this limiting value after several months. The air-mass which had remained in the stratosphere for a long time also contains ^7Be to ^{32}P in the ratio 650 : 1. Suppose such an air-mass enters the troposphere. In case 2(a) the ratio reaches a maximum value of 2300 after about 3 months, it then falls and slowly returns to its equilibrium value, $R = 650$. In case 2(b), when the air after descent from the stratosphere spends most of its time in the lower regions of the troposphere, where the production rates are small, the ratio R increases more rapidly with time and continues to increase.

R behaves very differently in the three cases and stratosphere air remains distinguishable from troposphere air by its radioactivity until removed by precipitation.

Since four isotopes with half-lives ranging from a fortnight to 3 months are available, one can study simultaneously three independent concentration ratios. The assumed history of the air-mass may, therefore, contain several free parameters which can be determined in a single rain.

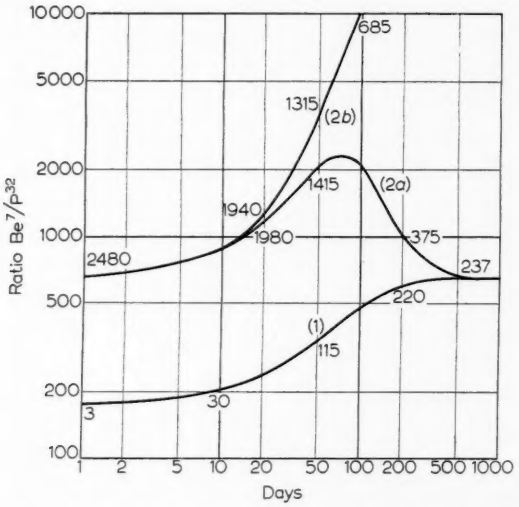

Fig. 9. The calculated ratio, $R = {}^7Be/{}^{32}P$ for three hypothetical trajectories of air-mass are shown as a function of the time spent in the troposphere. Curve (1) refers to the case when the air-mass spends its time exclusively within the troposphere at middle latitudes; curves 2(a) and 2(b) show the variation in R for air-masses which descend from the polar stratosphere to the troposphere at middle latitudes and spend time, 2(a) uniformly at various altitudes in the troposphere and 2(b), only in the lower regions of the troposphere. Numbers adjacent to the curves represent the concentration of ^7Be (atoms/g of air) as a function of time.

Apart from the ratio of isotope concentrations which gives information on the trajectory of an air-mass, the absolute concentration of individual isotopes may be useful for obtaining information on the moisture content of the air and the fraction of moisture which was condensed.

CONCLUSIONS

The rates of production of the radioisotopes ^{10}Be, ^7Be, ^{35}S, ^{33}P and ^{32}P by cosmic radiation are calculated as a function of depth in the atmosphere and of latitude. The global average production rates in the entire atmosphere are given separately for the troposphere and the stratosphere (Table 4).

The calculated global production rates of ^{10}Be, ^7Be, ^{35}S, ^{33}P and ^{32}P are compared with the experimental determinations on their fall-out rates. The agreement is satisfactory in the case of all isotopes except for ^{35}S, where the calculated production rates are lower than the available (provisional) measurements.

The application of the short-lived isotopes ^{35}S, ^7Be, ^{33}P, and ^{32}P to problems

VOL.
12
1958

of meteorology is discussed. It is suggested that the ratio of the activities of two or more isotopes can provide detailed meteorological information. Some examples are given as illustration.

Acknowledgements—We are grateful to Mr. S. Basu, and Dr. S. Mull, Director General and Deputy Director General, Indian Meteorological Department, for their co-operation in establishing rain-collecting stations in different parts of India. Our special thanks are due to Mr. T. S. G. Shastry and Mr. S. R. Kane, of the Physical Research Laboratory, Ahmedabad, for assisting in the analyses of rains at Kodai Kanal.

We also express our thanks to Dr. S. A. Korff for making available to us some unpublished neutron flux data.

References

Arnold J. R. and Al-Salih H.	1955	*Science* **121,** 451.
Arnold J. R.	1956	*Science* **124,** 584.
Bailey L. E.	1956	Angle and energy distributions of charged particles from the high-energy nuclear bombardment of various elements. Thesis, UCRL–3334.
Barford N. C. and Davis G.	1952	*Proc. Roy. Soc.* A **214,** 225.
Benioff P. A.	1956	*Phys. Rev.* **104,** 1122.
Bethe H. A., Korff S. A. and Placzek G.	1940	*Phys. Rev.* **57,** 573.
Birnbaum M., Shapiro M. M., Stiller B. and O'Dell F. W.	1952	*Phys. Rev.* **86,** 86
Bøggild J. K. and Tenney F. H.	1951	*Phys. Rev.* **84,** 1070.
Brown W. W.	1954	*Phys. Rev.* **93,** 528.
Brown R. H., Camerini U., Fowler P. H., Heitler H., King D. T. and Powell C. F.	1949	*Phil. Mag.* **40,** 862.
Bullock F. W.	1957	*Proc. Phys. Soc.* A **70,** 134.
Camerini U., Coor T., Davies J.H. Fowler P. H., Lock W. O., Muirhead H. and Tobin N.	1949	*Phil Mag.* **40,** 1073.
Conversi M.	1950	*Phys. Rev.* **79,** 749.
Conversi M. and Rothwell P.	1954	*Nuovo Cim.* **12,** 191.
Cruikshank A. J., Cowper G. and Grumitt W. E.	1956	*Canad. J. Chem.* **34,** 214.
Currie L. A., Libby W. F. and Wolfgang R. L.	1956	*Phys. Rev.* **101,** 1557.
Dickson J. M. and Randle T. C.	1951	*Proc. Phys. Soc.* A **64,** 902.
Faltings V. and Harteck P.	1950	*Z. Naturforsch.* **5a,** 438
Filthuth H.	1955	*Z. Naturforsch.* **10a,** 219.
Forbush S. E.	1954	*J. Geophys. Res.* **59,** 525.
Fuller M. O.	1954	Thesis, UCRL–2699.
Goel P. S., Jha S., Lal D., Radhakrishna P. and Rama Thor	1956	*Nucl. Phys.* **1,** 196.
Goel P. S.	1956	*Nature, Lond.* **178,** 1458.
Goel P. S., Kharkar D. P., Lal D., Narasappaya N., Peters B. and Yatirajam V.	1956	*Deep-Sea Res.* **4,** 202.
Goel P. S., Narsappaya N., Rama Thor and Zutshi P. K.		(To be published)
Grigor'ev E. L. and Solov'eva L. P.	1957	*Sov. Phys.* JETP **4,** 801.

Hodgson P. E.	1954	*Phil. Mag.* **45,** 190.
Kaufmann S. and Libby W. F.	1954	*Phys. Res.* **93,** 1337.
Kellogg D. A.	1953	*Phys. Rev.* **90,** 224.
Lal D.	1953	*Proc. Ind. Acad. Sci.* **38,** 93.
Lal D., Narsappaya N. and Zutshi P. K.	1957	*Nucl. Phys.* **3,** 69.
Lal D.	1958	(Thesis to be published.)
Libby W. F.	1952	*Radio-carbon dating.* University of Chicago Press.
Libby W. F.	1956	*Proc. Nat. Acad. Sci.* **42,** 365.
Lord J. J.	1951	*Phys. Rev.* **81,** 901.
Marquez L. and Costa N. L.	1955	*Nuovo Cim.* **2,** 1038.
Marquez L. and Perlman I.	1951	*Phys. Rev.* **81,** 953.
Mei J. Y.	1952	*Canad. J. Phys.* **30,** 453.
Neher H. V.	1956	*Phys. Rev.* **103,** 228.
Peters B.	1955	*Proc. Ind. Acad. Sci.* **41,** 67.
Peters B.	1957	*Z. für. Phys.* **148,** 93.
Puppi G. and Dallaporta N.	1952	*Progress in Cosmic-Ray Physics* Vol. 1. 315.
Rama Thor and Zutshi P. K.	1957	(In press).
Rose D. C., Fenton K. B., Katzman J. and Simpson J. A.	1956	*Canad. J. Phys.* **34,** 968.
Rudstam G.	1955	*Phil. Mag.* **46,** 344.
Rudstam G.	1956	*Spallation of Medium Weight Elements.* Gustaf Werner Institute for Nuclear Chemistry, University of Uppsala.
Simpson J. A.	1951	*Phys. Rev.* **83,** 1175.
Simpson J. A., Baldwin H. W. and Uretz R. B.	1951	*Phys. Rev.* **84,** 332.
Simpson J. A. and Fagot W. C.	1953	*Phys. Rev.* **90,** 1068.
Soberman R. K.	1956	*Phys. Rev.* **102,** 1399.
Staker W. P., Pavalow M. and Korff S. A.	1951	*Phys. Rev.* **81,** 889.
Stewart N. G., Crooks R. N., Fisher E. M. R.	1957	*A.E.R.E. Report No.* HP/R 2017.
Vernov S. N. and Grigorov N. L.	1956	*Nuovo Cim. Supp.* **4,** No. 2, 879.
Yagoda H.	1956	*Canad. J. Phys.* **39,** 122.
Yuan L. C. L.	1951	*Phys. Rev.* **81,** 175.

VOL.
12
1958

Journal of Atmospheric and Terrestrial Physics, 1958, Vol. 12, pp. 329 to 334. Pergamon Press Ltd., London

Observations of angle of arrival of meteor echoes in v.h.f. forward scatter propagation

K. Endresen, T. Hagfors, B. Landmark and J. Rödsrud
Norwegian Defence Research Establishment, Kjeller, Norway

(*Received* 18 *January* 1958)

Abstract—Observations of the azimuth angle of arrival of meteor reflections in forward scattering are presented. The properties of background meteor as well as shower meteor reflections are studied. The diurnal variation of the angle of arrival of the meteoric reflections is in good agreement with present theories.

1. Introduction

At an early stage it became apparent that reflections from meteor trails play an important part in v.h.f. ionospheric forward scattering (Bailey *et al.*, 1952). When it was realized that the meteoric signal bursts might be of some value in practical point to point communication, the properties of the meteoric signal component became the subject of extensive theoretical and experimental studies (Eshleman, 1952; Forsyth, 1954).

This paper describes some observations of the azimuth angle of arrival of meteor echoes over an 1150 km path in Norway at 46·8 Mc/s. A brief outline is given of the physical principles governing the directional properties of meteor reflections, the measuring method is explained, and some results are presented for background as well as for shower meteors. The results are discussed and compared with predictions according to existing theories.

2. General Considerations

Meteoric particles entering the earth's atmosphere are heated by collisions with individual gas molecules. Evaporated atoms from the meteoric particles give up their kinetic energy in collisions with surrounding gas molecules, thereby providing a straight trail of ionization in the wake of the meteor. At great heights the collisions between the meteors and the gas molecules are too infrequent for appreciable evaporation, while at low heights most meteors are "burnt out". It is thus evident that meteoric ionization must be confined to a limited height range, usually taken to extend between 80 and 120 km.

Theory predicts that the ionization line density caused by a meteoric particle is proportional to $\cos \chi$, where χ is the angle between the vertical and the direction of the trail (Herlofson, 1948).

Since the trails are straight, the reflections are specular. The reflection point is found to be the point of tangency between the trail and one or other of a family of ellipsoids of revolution with the transmitter and receiver as common foci. In addition, the point of reflection must lie within the appropriate height range. In practice the aerial systems are most sensitive to reflections in the area not too far removed from the midpoint of the transmitter–receiver (TR) path. Hence reflections near the TR path must be due to nearly horizontal trails. On account of the $\cos \chi$-factor these trails give very weak reflections, and thus it can be expected

that the number of observed reflections will be a minimum near the TR direction.

From areas at large distances at either side of the TR path, few reflections are observable for at least three reasons: (i) the path length becomes very long and hence the received signal weak, (ii) practical aerial polar diagrams are not very sensitive at great off-path angles and, finally, (iii) in the case of horizontal polarization reflection at certain off-path angles will be suppressed. A detailed account is given by Hines and Pugh (1956).

For isotropic incidence probability it can thus be expected that there will be a maximum number of meteoric reflections at either side of the TR path and a minimum in-between (Eshleman and Manning, 1954). A better approximation to the actual conditions is obtained by assuming the meteoric particles to be travelling with equal probability in all directions in a heliocentric co-ordinate system. As the earth on its way round the sun is moving through this system, the meteors will appear to be concentrated in the direction of the apex of the earth's way. For a N–S path in northern temperature latitudes, which is of particular interest, the meteor reflections therefore appear to be distributed symmetrically about the TR axis at 6 a.m. and 6 p.m. only. In the daytime more reflections occur at the east side and by night more at the west side. Some complications arise because the path considered below is not exactly in the N–S direction, and also because the midpoint is so far to the north. An account of the directional properties of meteoric reflections is given by Eshleman (1957).

So far only background meteors have been considered. The effect of a meteor shower can most easily be understood as follows: Again consider a N–S path, and imagine a radiant not too far from the celestial equator. As the radiant is rising above the horizon in the east, the shower meteors are travelling nearly horizontally and giving reflections at the west side of the TR path, quite close to it. With the ascent of the radiant the points of reflections move out towards the west. Near the time of upper culmination of the radiant, there is practically no effect of the shower at all. Some time after upper culmination reflections from shower meteors again become observable, but now far towards the east side of the path. With further descent of the radiant the reflections move towards the TR path, disappearing when the radiant goes below the horizon.

Calculations have been made of the azimuth angle of the reflection point for the Geminid shower at the vertical plane bisecting the TR axis, assuming the reflections to occur at 100 km. This provides a rough idea of the expected variation of the azimuth angle of arrival of the reflections from Geminid meteor trails. The results are given in Fig. 1 and are compared with observations and discussed in Sections 4 and 5.

3. Measuring Equipment

The transmitter, which generates a 46·8 Mc/s unmodulated carrier, is situated near Tromsö (70°N, 19°E). Five kilowatts are fed into a rhombic aerial, the polar diagram of which has a width of 15·5 degrees between half power points, and which gives a maximum radiation at an elevation of 5·6 deg.

At the receiver, which is located near Kjeller (60°N, 11°E) two 6 element yagi aerials with 66 deg. between half power points and with about the same beam

VOL. 12 1958

elevation as at the transmitter are used. The two aerials are at a spacing of two wavelengths, and the baseline is perpendicular to the TR axis. This aerial arrangement allows azimuth angles of up to 15 deg. to be measured at either side of the TR path, without ambiguity.

The signals from the two yagi aerials (see Fig. 2) are fed through separate cascade pre-amplifiers (PA1 and PA2), separate receivers (RX1 and RX2) with

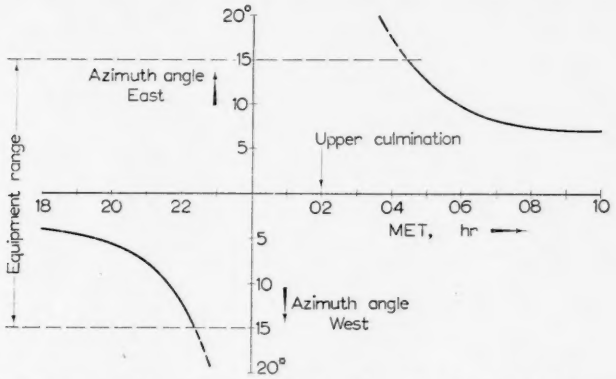

Fig. 1. Calculated variation with time of azimuth angle of arrival of Geminid shower meteor echoes.

common local oscillators (OSC), and the two resulting 10 kc/s signals are fed to a direct reading phase meter (PM). A d.c. signal proportional to the phase difference between the two 10 kc/s signals is fed through an amplifier to one of the channels of a pen recorder. The other channel is used to record the field strength from one of the receivers (here from RX2). Calibration of the phase channel was done readily by comparing the pen recorder readings with the readings of the phase

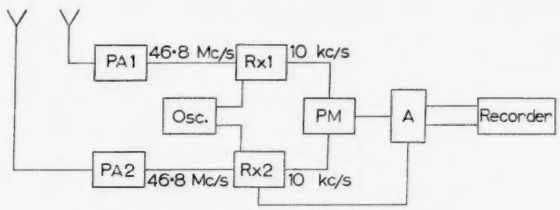

Fig. 2. Block diagram of receiving equipment.

meter, which was calibrated from −180 to +180 deg. The zero of the whole system was checked by using a test transmitter at a distance of 2 km in front of the aerial system, and this arrangement was again checked by aeroplane measurements. A sample of a typical record is shown in Fig. 3.

4. Observational Results

The observations presented here were made during November and December 1957. Half hour records were taken and analysed, the transmitter only being in operation during half an hour every hour. Fifty-three such records were analysed.

In addition to these a considerable number of records were made which could not be analysed due to strong Rayleigh-fading background signals. The properties of the background meteors were tested at four times during the day, round midnight, 06 a.m., noon and 06 p.m. MET. Observations of the Geminid shower meteors were made before and after upper transit of the radiant point during the days 12–14 December.

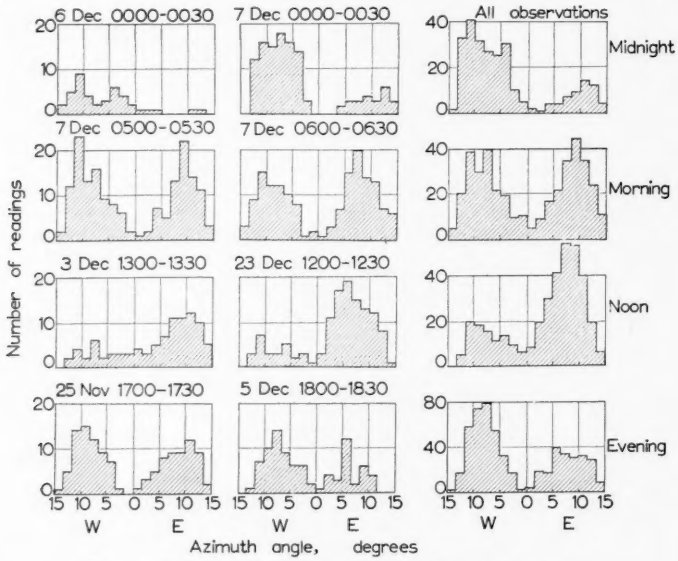

Fig. 4. Observed distributions for background meteors.

Background meteors

As shown in Fig. 3 both amplitude and phase difference were measured simultaneously. From the amplitude record the bursts which could be attributed to meteors with certainty were selected and the phase differences were grouped in 20 deg. intervals, and were plotted as shown in Fig. 4 for each half hour record. The variation in the total number of readings is not only due to variable meteoric incidence rate, but also due to variable intensity of the background signal masking the meteoric burst component. The angular distributions of all background meteor records are shown at the right in Fig. 4 for the four different times of day examined. A discussion of the results is given in Section 5.

Shower meteors

On the day of predicted maximum shower intensity upper culmination of the radiant point of the Geminid shower occurred at 2 a.m. at the midpoint of the path. Observations were made a few hours before and a few hours after the time of upper transit.

In order to separate the shower meteors from the background meteors measurements were made some days before the appearance of the shower at the appropriate times of day, and these results were compared with the results obtained

VOL. 12 1958

TEL.
2
58

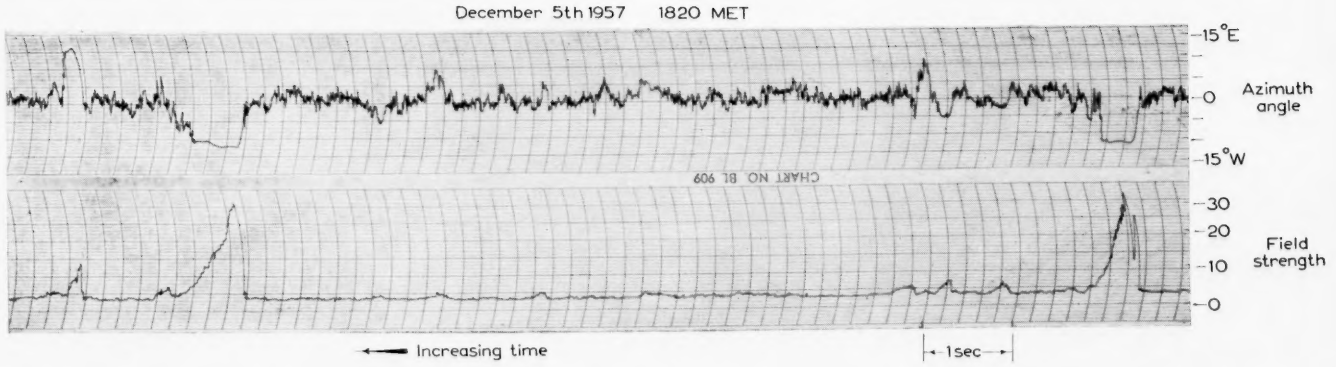

Fig. 3. A typical record sample.

VOL.
12
1958

during the shower in the following way: the angular distributions during the test period were normalized to give as good a fit as possible to the corresponding shower results in the angular regions in which the shower meteors were not expected to be of importance. These normalized distributions were then subtracted from the distributions observed during the shower. The results are shown in Fig. 5. Arrows indicate the expected angle of arrival of the shower meteor echoes. (See Fig. 1.)

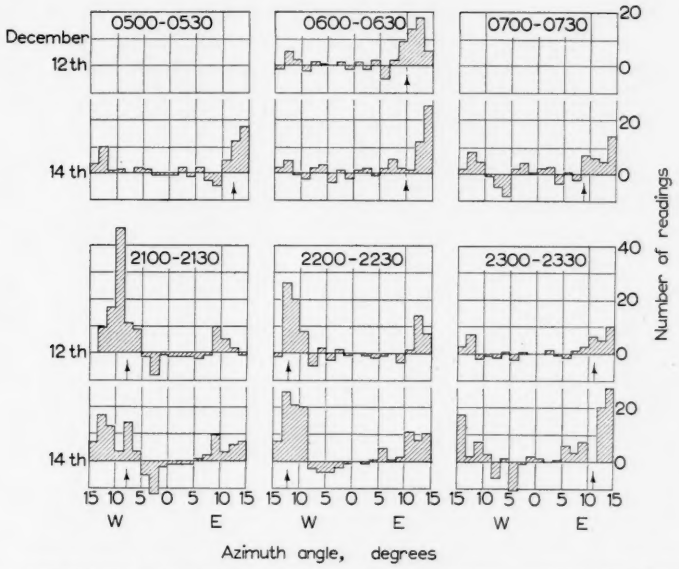

Fig. 5. Distributions for shower meteors when background meteors are subtracted.

5. Discussion of Results

All distributions show a distinct minimum in the direction of the great circle path towards the transmitter indicating that the cos χ-law for the ionization of a meteor trail is valid.

Regarding the midnight and noon distributions of angle of arrival of meteor bursts, good qualitative agreement with the assumption of isotropic meteor velocities in a heliocentric co-ordinate system is obtained. Round 6 a.m., on the same assumption one would expect slightly more meteoral echoes from the west than from the east, whereas the observed distribution is very nearly symmetrical. At 6 p.m. one would expect a somewhat greater number of bursts from the east, contrary to the observed result. It therefore appears that meteors are not moving with random directions in a heliocentric co-ordinate system. It appears that a distribution of radiants of sporadic meteors as measured by Davies (1957) would in particular fit our evening distribution much better.

Fair agreement is found between predicted and observed azimuth angle of arrival during shower conditions. The observed large angular extent of the region of the shower meteor echoes is evidently due to variable height of the different reflections, and also to the fact that the reflections take place in zones elongated

in the path direction. The tendency of the shower meteor echoes to arrive from larger angles than predicted can be ascribed to the transmitter polar diagram being narrower than that of the receiver. This tends to enhance reflections occurring nearer the receiver.

6. Conclusion

The present work shows that there is good agreement between theory and observations of meteor trail reflections in forward scattering. It is also indicated that the assumption of isotropic distribution of the direction of background meteor velocities in a heliocentric co-ordinate system is a fair approximation for most practical purposes. A more refined model of meteoric motion would be necessary, however, to describe certain details such as the times at which the maximum of meteoric reflection rate changes from one side of the path to the other.

Acknowledgement—The above work is part of a research project sponsored by the Mutual Weapons Development Programme.

References

Bailey D. K. *et al.*	1952	*Phys. Rev.* **86,** 141.
Davies J. G.	1957	*Advances in Electronics and Electron Physics* Vol. 9, p. 119. Academic Press. New York.
Eshleman V. R.	1952	*Techn. Rep.* 49, Elec. Res. Lab. Stanford Univ.
Eshleman V. R.	1957	*AGARDograph* **26,** 15.
Eshleman V. R. and Manning L. A.	1954	*Proc. Inst. Radio Engrs* **42,** 530.
Forsyth P. A.	1954	Radio Physics Lab. Project *Report* 12-1-5.
Herlofson N.	1948	*Phys. Soc. Rep. Progr. Phys.* **11,** 444.
Hines C. O. and Pugh R. E.	1956	*Canad. J. Phys.* **34,** 1005.

VOL.
12
1958

RESEARCH NOTES

On the interpretation of the Doppler effect from senders in an artificial satellite

(*Received* 13 *January* 1958)

1. Introduction

In 1929 Mirick and Hentschel observed beats in the signal strength of radio waves from an aircraft at a fixed receiver. They interpreted these beats as interference effects between a direct ray and a ray reflected from the ionosphere and deduced a height for the effective reflecting layer.

Appleton (1930) compared this method of estimating the height of the ionosphere with those previously used. He showed that the beat could be regarded as a Doppler beat between the rays arriving by the two paths and that, as the height of the aircraft was negligible compared to that of the ionosphere, the experiment measured directly sin i where i is the angle of incidence of the ray on the reflecting layer.

This problem is very similar to that of the observation of the Doppler effect from a sender in an artificial satellite and it is of interest to enquire whether the Doppler shift depends simply on sin i in this case when the sender is in the ionized medium and the distances are such that allowance must be made for the curvature of the earth.

2. Calculation of the Doppler effect

Let us assume that the satellite is travelling with velocity V in an orbit which passes over the observing site, and that the ionosphere is horizontally stratified. The apparent frequency of the sender is measured by the rate of change of phase of the wave at the receiver, this phase is given by

$$\Phi = \omega t - 2\pi P/\lambda$$

where P is the phase path along the ray from sender to receiver and ω is the apparent frequency of the sender, as observed by an observer stationary with respect to the receiver and under a Lorentz transformation it is related to the frequency ω_0; observed by an observer in the satellite by the relation

$$\omega = \omega_0 \Big/ \left(1 - \frac{V^2}{c^2}\right)^{1/2}$$

The apparent frequency at the receiver is then:

$$\frac{\mathrm{d}\Phi}{\mathrm{d}t} = \omega - \frac{\omega}{c}\frac{\mathrm{d}P}{\mathrm{d}t}$$

and the Doppler shift may be written

$$c\,\frac{\Delta f}{f} = \frac{-\mathrm{d}P}{\mathrm{d}t}$$

We shall suppose that the frequencies in use (20 and 40 Mc/s in the U.S.S.R. satellites) are

so high compared with the gyro-frequency of electrons in the earth's magnetic field that at any level there exists a unique value of the refractive index μ independent of the direction of the ray relative to the geomagnetic field. Then it is possible to apply Snell's law and if ψ be the angle of incidence at a height r, at which the refractive index is μ, above the centre of the earth, then:

$$\mu r \sin \psi = r_0 \sin i$$

or

$$q \sin \psi = \sin i \tag{1}$$

where

$$q = \frac{r}{r_0}\,\mu \tag{2}$$

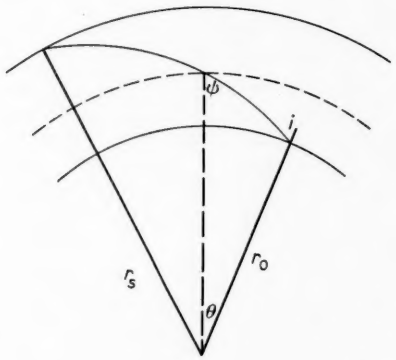

Fig. 1

To calculate the Doppler shift we wish to determine the phase path along a ray from the point (r_s, θ_s) in Fig. 1 to the receiver $(r_0, 0)$ arriving at an angle of incidence i.

Now $$r\,\mathrm{d}\theta = \tan \psi\,\mathrm{d}r$$

and hence $$\theta_s = \int_{r_0}^{r_s} \tan \psi\,\mathrm{d}r/r$$

or from (1) $$\theta_s^r = \int_{r_0}^{r_s} \frac{\sin i}{(q^2 - \sin^2 i)^{1/2}}\,\frac{\mathrm{d}r}{r} \tag{3}$$

Also $$P = \int \mu\,\mathrm{d}s = \int_{r_0}^{r_s} \mu \sec \psi\,\mathrm{d}r = \int_{r_0}^{r_s} \frac{q^2 r_0}{(q^2 - \sin^2 i)^{1/2}}\,\frac{\mathrm{d}r}{r} \tag{4}$$

Hence from (3)

$$\dot{\theta}_s = \int_{r_0}^{r_s} \frac{1}{r}\,\frac{q^2 \cos i}{(q^2 - \sin^2 i)^{3/2}}\,\mathrm{d}t\,\frac{\mathrm{d}i}{\mathrm{d}t}\,\mathrm{d}r + \frac{1}{r_s}\,\frac{\sin i}{(q_s^2 - \sin^2 i)^{1/2}}\,\dot{r}_s \tag{5}$$

and from (4)

$$c\,\frac{\Delta f}{f} = -\int_{r_0}^{r_s} \frac{r_0}{r}\,q^2\,\frac{\sin i \cos i}{(q^2 - \sin^2 i)^{3/2}}\,\frac{\mathrm{d}i}{\mathrm{d}t}\,\mathrm{d}r - \frac{r_0}{r_s}\,\frac{q_s^2}{(q_s^2 - \sin^2 i)^{1/2}}\,\dot{r}_s$$

$$= -r_0 \sin i\left(\dot{\theta}_s - \frac{1}{r_s}\,\frac{\sin i}{(q_s^2 - \sin^2 i)^{1/2}}\,\dot{r}_s\right) - \frac{r_0}{r_s}\,\frac{q_s^2}{(q_s^2 - \sin^2 i)^{1/2}}\,\dot{r}_s$$

$$= -r_0 \dot{\theta}_s \sin i - \frac{r_0}{r_s}\,(q^2 - \sin^2 i)^{1/2}\,\dot{r}_s \tag{6}$$

VOL. 12 1958

For the case of a satellite in a circular orbit $\dot{r}_s = 0$ and it is clear from (6) that the Doppler shift depends on the angle of incidence of the wave arriving at the receiver, for in this case

$$c\frac{\Delta f}{f} = -\frac{r_0}{r_s}\sin i\,(\dot{r}_s\dot{\theta}_s) = -\frac{r_0}{r_s}\sin i\; V$$

More exactly the shift measures the angle of incidence at the satellite orbit of the straight line leaving the receiver at angle i.

For the case of a sender moving vertically (6) reduces to the familiar expression which Seddon has used in interpreting rocket observations and the effect depends only on the refractive index at the satellite.

If the orbit of the satellite does not pass over the receiver the velocity associated with $\dot{\theta}_s$ in (5) is the component of its horizontal velocity in the plane of incidence. This may be written $V_0 \sin\phi$ where ϕ is the angle between the plane of incidence and the vertical plane through the receiver perpendicular to the plane of the orbit. If the ionosphere is horizontally stratified rotation of the plane of incidence will not produce any change of phase path.

3. Approximation for a flat earth and sufficiently high frequencies

Suppose actual angle of incidence at the ground is i and the angle of incidence of the straight line to the satellite is i_0. Then the horizontal distance to the satellite is $x = h\tan i_0$

By tracing the ray we deduce that

$$x = \sin i \int_0^h \frac{\mathrm{d}h}{(\mu^2 - \sin^2 i)^{1/2}}$$

and

$$\mu^2 = 1 - \frac{Ne^2}{\varepsilon_0 \pi m f^2}$$

$$x = \tan i \int_0^h \frac{\mathrm{d}h}{\left(1 - \dfrac{e^2}{\varepsilon_0 \pi m f^2 \cos^2 i}\, N\right)^{1/2}}$$

and for sufficiently high frequencies

$$x = \tan i \int_0^h \left(1 + \frac{e^2}{2\varepsilon_0 \pi m f^2 \cos^2 i}\, N\right) \mathrm{d}h$$

$$= \tan i \left\{h + \frac{e^2 \sec^2 i}{2\varepsilon_0 \pi m f^2} \int N\,\mathrm{d}h\right\}$$

and we may write $\tan i_0 = \tan i \left\{1 + \dfrac{e^2 \sec^2 i}{2\varepsilon_0 \pi m f^2} \int N\,\mathrm{d}h\right\}$

Hence $\sin i_0 = \sin i \left\{1 + \dfrac{e^2}{2\varepsilon_0 \pi m f^2} \int N\,\mathrm{d}h\right\}$

Thus for this case the Doppler effect may be seen to give a measure of $\int N\,\mathrm{d}h$ as has been stated by various authors.

For the case of a curved earth the effect even at high frequencies was not reduced to such a simple expression.

4. Conclusions

In the U.S.S.R. satellites the vertical velocity has been only a small fraction of the horizontal velocity so that the analysis of the Doppler effect given here shows that the Doppler curves enable us to determine $\sin i$, which is exactly the quantity determined by the refraction type of experiment.

If the effect of the earth's magnetic field is included the expression for μ is altered, and differently for the two magneto-ionic components. The expressions corresponding to (3) and (4) are no longer simple, but could be computed for any given model ionosphere. The Doppler shifts of the two components would differ from each other, and from that given by equation (6). It would follow that, in this case, the Doppler shifts were not related so simply to the angles of arrival. Moreover the different Doppler shifts of the two magneto-ionic components would result in their beating together and it is this beating which produces the "Faraday rotation". It seems that a proper calculation of these phenomena requires an investigation of the paths of the two magneto-ionic rays even for the deduction of approximate numerical values.

K. WEEKES

Cavendish Laboratories
Cambridge

References

APPLETON 1930 *Proc. Phys. Soc.* **42**, 321.
MIRICK and HENTSCHEL 1929 *Proc. Inst. Radio Engrs* **17**, 1034.

The effect of the ionosphere on the Doppler shift of radio signals from an artificial satellite

(*Received* 13 *January* 1958)

IT IS of interest to examine the effect of the ionosphere on the Doppler shift in the frequency of a radio signal, emitted from an artificial earth satellite travelling in the ionosphere, when observed at a fixed point on the ground.

We consider the satellite at any instant during its travel and the ray from satellite to receiver at this instant. The refractive index of the medium at the satellite is denoted by μ_s, the velocity of the satellite relative to the observer by V, and the component of this velocity, in the direction of the above ray as it leaves the satellite, by v. No Doppler shift arises from the velocity component perpendicular to v. If f_0 is the frequency of the emitter and c the velocity of radiation in free space, the frequency of the radiation along the ray specified, and adjacent to the emitter, is known from elementary considerations to be

$$f = f_0\left(1 + \frac{v}{\text{phase velocity in medium}}\right)$$
$$= f_0\left(1 + \frac{\mu_s v}{c}\right) \qquad (1)$$

The radiation travels on through the intervening medium to the observer with frequency f.

For the instant considered we take the position of the satellite as origin 0 and take axes as follows (Fig. 1):

Ox lies in the plane of incidence at the receiver and is perpendicular to the radial direction from the centre of the earth to the satellite;

Oy is the outward radial direction;

Oz is perpendicular to Ox and Oy.

VOL. 12 1958

The direction cosines of V, referred to the above axes, are denoted by $\cos\alpha$, $\cos\beta$, $\cos\gamma$. The component v, of the velocity V, in the direction of the observed ray as it leaves the satellite is easily shown to be

$$v = V(\cos\mu \sin\psi_s - \cos\beta \cos\psi_s) \tag{2}$$

where ψ_s is the angle at the satellite between the ray and the inward radial direction — Oy.

Substituting this expression for v into (1) yields

$$f - f_0 = \frac{Vf_0\mu_s}{c}(\cos\alpha \sin\psi_s - \cos\beta \cos\psi_s) \tag{3}$$

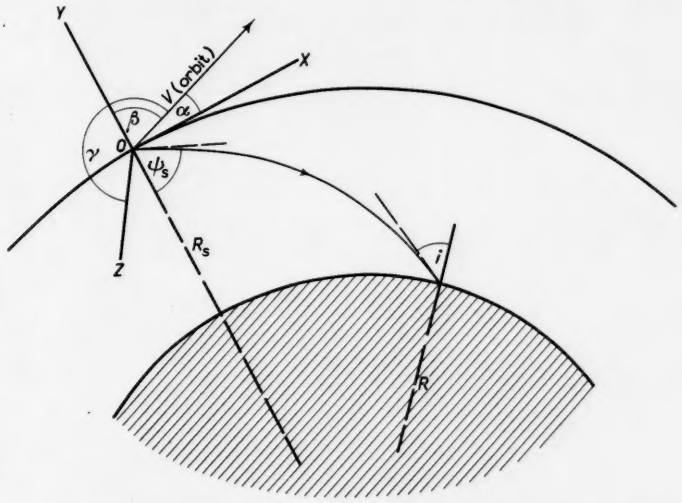

Fig. 1

For a spherically stratified ionosphere and spherical earth, the Doppler shift may readily be related to the angle of arrival i of the ray at the receiver. Application of Snell's law to a ray passing through a spherically stratified ionosphere to the receiver on the ground leads immediately to the relation

$$\mu_s R_s \sin\psi_s = R \sin i \tag{4}$$

where R and R_s are the respective distances of the ground and satellite from the centre of the earth. On combining (4) with (3) we obtain

$$f - f_0 = \frac{Vf_0}{c}\left[\frac{R}{R_s}\cos\alpha \sin i - \cos\beta\left\{\mu_s^2 - \left(\frac{R}{R_s}\right)^2 \sin^2 i\right\}^{1/2}\right] \tag{5}$$

The angle of arrival i differs from the value it would have if the ionosphere were absent and the ray followed a straight-line path from satellite to receiver. This difference is due to refraction and depends on the distribution of electron density between satellite and receiver.

Some simple cases of equation (5)

(a) Circular orbit ($\beta = \pi/2$)

$$f - f_0 = \frac{Vf_0}{c}\frac{R}{R_s}\sin i$$

(b) Circular orbit with observing point in the plane of the orbit ($\beta = \pi/2$, $\alpha = 0$)

$$f - f_0 = \frac{Vf_0}{c}\frac{R}{R_s}\sin i$$

(c) Flat earth and "satellite" travelling horizontally overhead

$$f - f_0 = \frac{Vf_0}{c}\sin i$$

(d) "Satellite" travelling vertically upwards (i.e. a rocket), directly above observer

$$f - f_0 = -\frac{\mu_s Vf_0}{c}$$

Acknowledgement—This note was written during the tenure of a British Council Scholarship, which is gratefully acknowledged.

F. H. HIBBERD*

Cavendish Laboratory
Cambridge

* On leave from the University of New England, Armidale, Australia

VOL. 12 1958

Preliminary results of studies of the angular distribution of a VHF ionospheric forward scatter signal

(*Received* 25 *November* 1957)

THE signals received by forward scattering from the ionosphere at VHF have been the subject of extensive investigations during the last few years (BAILEY *et al.*, 1955). There still is, however, a considerable uncertainty as to the exact mechanism of this kind of radio wave propagation (BRAY *et al.*, 1956). Valuable information about the physical principles involved can be obtained by a study of the angle of arrival of the scatter signals. The angular spectrum of the received waves may be determined either by measuring the correlation over the wavefront (RATCLIFFE, 1956), or by simple scanning with a pencil beam aerial. The former line of attack was chosen by us.

In order to find the correlation over the wavefront four yagi aerials were erected along a line perpendicular to the great circle path joining the transmitter and the receiver, the spacing between the aerials being 2, 3 and 4 wavelengths. Pairs of these aerials were combined in phase and in antiphase simultaneously to give azimuth (power) polar diagrams as shown in Fig 1. A determination of the ratio between the power received by the two aerial combinations is sufficient for the evaluation of the correlation between the fields at the two aerials provided the angular spectrum is symmetrical about the direction of the receiver-transmitter great circle path (i.e. $\Theta = 0$).

Examples of some of the first successful recordings obtained at 46·8 Mc/s over an 1150

km North South path are shown in Fig. 2. The records are seen to provide valuable information on the angular spectrum of the background signal. However, another very interesting feature of the total signal is revealed by these records: The number of strong meteor bursts is higher in the Δ than in the Σ combination. The background signal, on the other hand, is practically absent in the Δ-records, particularly at small aerial spacings.

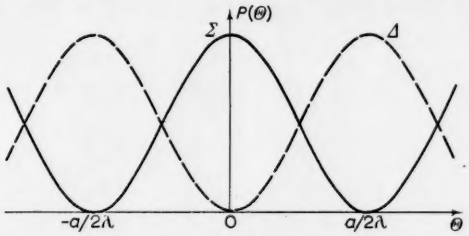

Fig. 2. Examples of records obtained with aerial polar diagrams as shown in Fig. 1 for three different aerial spacings (a) Frequency 46·8 Mc/s, distance 1150 km, approximate north-south path. Records obtained 28/10, 1320 Local time, 1957.

As the distribution of echo amplitudes is believed to be virtually independent of the aerial polar diagrams, this indicates very strongly that the Rayleigh-fading noiselike background signal component is not due to the overlapping of very large numbers of small meteoric echoes.

Further studies of the directional properties of the background signal are being undertaken, and the results will be published later.

Acknowledgements—The work reported in this Note has been sponsored by the Mutual Weapons Development Program. The author is indebted to his colleagues at the NDRE for helpful cooperation.

REFERENCES

BAILEY D. K., BATEMAN R., and KIRBY R. C.	1955	*Proc. Inst. Radio Engrs* **10,** 1181.
BRAY W. T., SAXTON J. A., WHITE R. W. and LOSCOMBE G. W.	1956	*Proc. Inst. Radio Engrs* B **103,** 236.
RATCLIFFE J. A.	1956	*Rep. Prog. Phys.* **19,** 211.

Norwegian Defence Research Establishment
Kjeller, Norway.

TOR HAGFORS

The fading of long duration meteor bursts in forward scatter propagation

(*Received* 25 *November* 1957)

MANNING (1957) has developed a theory of the fading of enduring meteor echoes on the assumption that the trail is distorted by a wind profile having the statistical properties of Gaussian noise. A study of the cross correlation between the observed signal envelopes in two points with variable spacing showed that the correlation was a function of the product of the spacing and time after formation of the echo. This means that the effective length of the trail also increases linearly with time. MANNING also showed how important parameters, like the rms value of the random wind velocities, the sizes of the irregularities and

the height differential necessary to cause zero correlation in wind velocity could be determined.

It is the purpose of this note to show that MANNING's method may be used in order to study seasonal variations of the wind sheer in the actual height range, i.e. the lower *E*-layer.

The signal envelopes were recorded in two points with a spacing ξ-wavelengths, the wavelength being 6·4 m. Values of ξ between 4 and 10 were used. Each pair of bursts was divided into equal periods determined as the mean distance between successive maxima of envelope of the first few fading cycles, and the cross correlation was determined for each period. For each value of ξ, the mean value of the correlation coefficients was determined

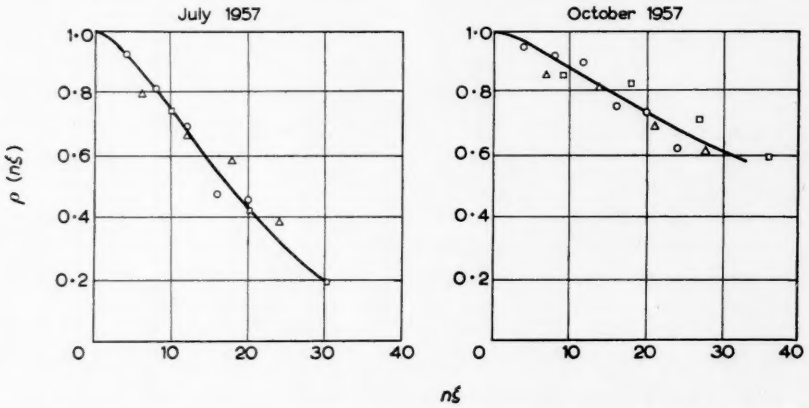

Fig. 1. Observed cross-correlation against $n\xi$, where n is number of fading cycle and ξ-spacing in wavelengths.

for each fading cycle number n, and plotted as a function of ξn. It was found, in accordance with the results of MANNING, that the points found for the different values of ξ, fell on the same curve, and that the shape of this was approximately Gaussian.

In Fig. 1 the results for the months July and October 1957 are shown. We see that the shape of the observed curves are markedly different for the two months, in that the correlation falls off more rapidly in July than in October. This must mean that the rms value of the random wind velocities is higher in July than in October. Only in these two months a sufficient number of observations were made so that the curve could be established, but the few bursts which were observed in other months indicate that in March and April the curve is similar to the October one, while in the Winter and Summer months the curve is more like the July one.

A more detailed study of the fading of the long duration meteor bursts has been started, and the results will be published later.

Acknowledgements—The work reported in this Note has been sponsored by the Mutual Weapons Development Program. The author has been assisted by Mr. O. HOLT in analysing the records.

REFERENCES

MANNING L. A. 1957 Paper read at the XII General URSI Assembly, Boulder, Colorado.

Norwegian Defence Research Establishment
Kjeller, Norway

B. LANDMARK

VOL. 12 1958

OL.
12
958

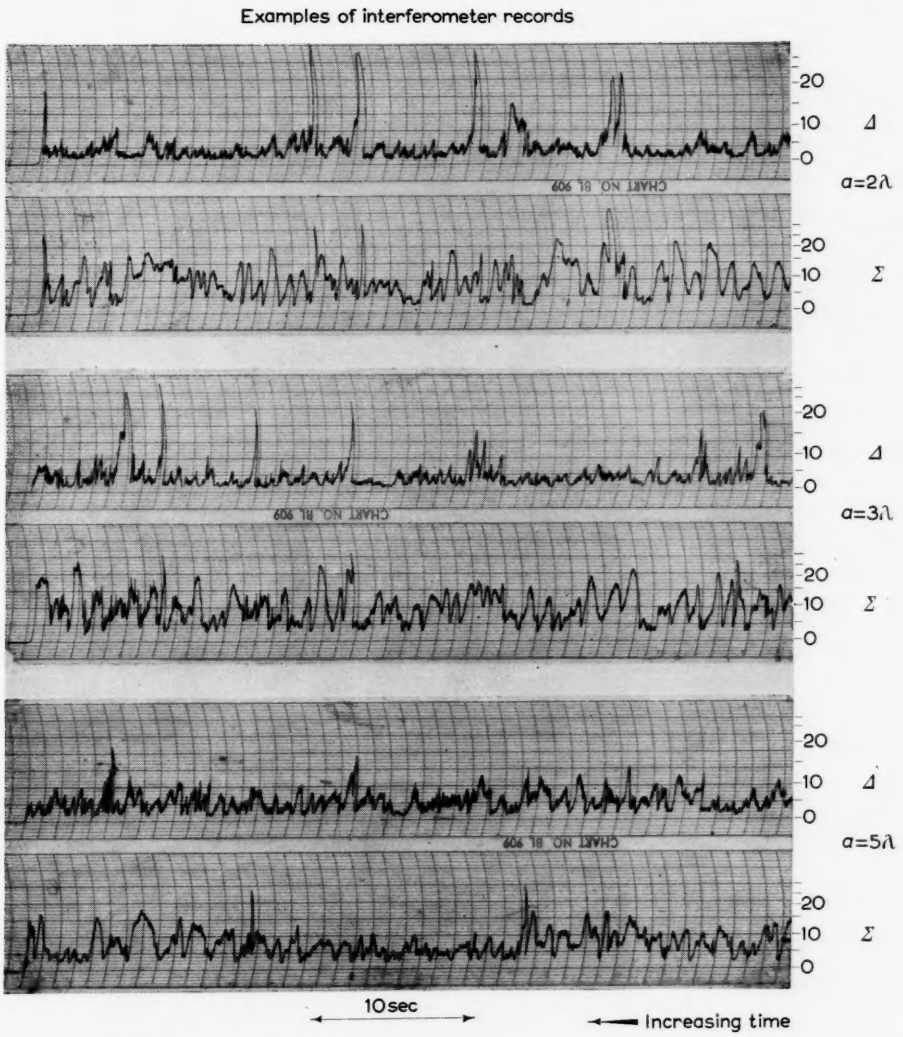

Fig. 1. Relative power polar diagram $P(\Theta)$ plotted against azimuth angle Θ measured from the transmitter–receiver great circle path. Σ: in phase diagram; Δ: out of phase diagram; a: aerial spacing

VOL.
12
1958

Journal of Atmospheric and Terrestrial Physics, 1958, Vol. 12, pp. 343 to 345. Pergamon Press Ltd., London

Indices of geomagnetic activity

of the Observatories HARTLAND (*Ha*), ESKDALEMUIR (*Es*) and LERWICK (*Le*)

December 1957

The figures given on pages 343 to 345 represent the K-indices for three-hour intervals, beginning with 00–03 hrs for the first and ending with 21–24 hrs for the eighth figure.

December 1957

Day	*Ha* Range for $K = 9 : 500\gamma$			*Es* Range for $K = 9 : 750\gamma$			*Le* Range for $K = 9 : 1000\gamma$			*Day*
	K-Indices		*Sum*	*K-Indices*		*Sum*	*K-Indices*		*Sum*	
1	5544	3324	30	4433	2224	24	4432	2114	21	1
2	3333	3222	21	3223	3222	19	3322	3221	18	2
3	2133	3223	19	1122	3323	17	1122	2224	16	3
4	3132	2213	17	3122	2213	16	3122	1103	13	4
5	4332	3344	26	4332	2344	25	5332	2366	30	5
6	4423	3343	26	3423	3332	23	6433	3444	31	6
7	3233	3232	21	2233	3223	20	3233	3223	21	7
8	3222	2122	16	3222	2122	16	3222	1112	14	8
9	3223	3325	23	3223	3324	22	3222	3314	20	9
10	3312	3444	24	3322	2444	24	3422	3545	28	10
11	4543	4345	32	3444	4345	31	4443	3356	32	11
12	4433	3444	29	4343	2343	26	4333	2344	26	12
13	3234	3432	24	2224	2421	19	3223	2422	20	13
14	2222	2112	14	2222	2112	14	2211	1112	11	14
15	2224	5431	23	2224	4421	21	2123	3431	19	15
16	3222	2234	20	3222	2234	20	3222	2233	19	16
17	3432	2333	23	3332	2333	22	3331	1234	20	17
18	3222	2202	15	3222	2212	16	3122	2202	14	18
19	2223	3254	23	2223	3344	23	2123	2244	20	19
20	3433	2233	23	3322	2233	20	4422	2233	22	20
21	2332	2112	16	2332	2122	17	2332	1122	16	21
22	2211	1100	8	2211	2110	10	2211	1100	8	22
23	1111	0101	6	1112	1101	8	1211	1011	8	23
24	1103	2132	13	1102	2122	11	1012	1121	9	24
25	1333	3243	22	1233	3233	20	1222	2244	19	25
26	2333	4331	22	2332	3331	20	2332	3241	20	26
27	2112	2123	14	2112	2223	15	1111	2123	12	27
28	1111	1122	10	1100	1121	7	1000	1111	5	28
29	0001	2103	7	0002	2123	10	0001	2123	9	29
30	3333	3101	17	3233	3112	18	3223	3111	16	30
31	3443	3555	32	3443	3555	32	3544	4577	39	31

January 1958

Day	*Ha* Range for $K = 9 : 500\gamma$			*Es* Range for $K = 9 : 750\gamma$			*Le* Range for $K = 9 : 1000\gamma$			*Day*
	K-Indices		*Sum*	*K-Indices*		*Sum*	*K-Indices*		*Sum*	
1	5543	3353	31	5543	3353	31	6543	3465	36	1
2	4323	3222	21	4333	3221	21	5333	3213	23	2
3	2102	2111	10	2101	1100	6	2112	1001	8	3
4	1102	2002	8	1000	1112	6	1000	1111	5	4
5	3202	2100	10	3111	2110	10	3201	1110	9	5
6	1112	3211	12	1212	2211	12	1111	2111	9	6
7	2212	2011	11	1111	2111	9	2111	1011	8	7
8	1011	3211	10	1111	2210	9	1111	1210	8	8
9	1112	3243	17	1112	2243	16	1012	3343	17	9
10	4112	3212	16	3112	2111	12	4212	2111	14	10
11	3213	3342	21	3212	2242	18	3212	2243	19	11
12	2323	3223	20	3322	2222	18	3322	2222	18	12
13	3323	2244	23	3321	2243	20	2221	2344	20	13
14	1123	2335	20	1112	2234	16	1022	2224	15	14
15	1133	3233	19	1232	3233	19	1233	3222	18	15
16	0222	3233	17	1122	2333	17	0112	2233	14	16
17	2333	3434	25	2332	3334	23	2333	2344	24	17
18	4444	4342	29	4333	3333	25	4433	3333	26	18
19	3222	2232	18	2211	3232	16	3112	3232	17	19
20	1123	3335	21	1012	3335	18	1122	3335	20	20
21	5534	2221	24	5523	2222	23	5643	2222	26	21
22	2234	4232	22	2223	4222	19	2223	4132	19	22
23	3333	3333	24	3322	3333	22	3333	3333	24	23
24	0113	3312	14	1113	3211	13	1112	2211	11	24
25	2223	4432	22	2223	3431	20	2213	3542	22	25
26	2422	1333	20	2421	1223	17	2441	1323	20	26
27	2111	0124	12	2110	0124	11	2111	1114	12	27
28	1023	2212	13	1022	1211	10	1021	1211	9	28
29	2432	2333	22	2432	1232	19	2431	1233	19	29
30	1223	2222	16	1222	2211	13	1111	1122	10	30
31	2012	2123	13	2111	1123	12	3111	1123	13	31

February 1958

1	3022	2113	14	2112	2112	12	2011	2112	10	1
2	3122	2111	13	2122	2010	10	3112	1011	10	2
3	0102	3112	10	1011	2122	10	0110	2122	9	3
4	3002	3353	19	2002	3354	19	3012	2253	18	4
5	3433	4355	30	3333	4344	27	3423	3355	28	5
6	3334	4424	27	3333	3424	25	4333	3435	28	6
7	3333	3444	27	3333	2343	24	3223	2344	23	7
8	3443	3344	28	3332	3343	24	3433	3344	27	8
9	3222	3443	23	3222	2343	21	3312	2353	22	9
10	4323	2544	27	4312	2554	26	4321	2664	28	10
11	9787	7445	51	9787	8455	53	9888	7476	57	11

VOL. 12 1958

February 1958 (*continued*)

Day	*Ha* Range for $K = 9 : 500\gamma$		*Es* Range for $K = 9 : 750\gamma$		*Le* Range for $K = 9 : 1000\gamma$		*Day*
	K-Indices	*Sum*	*K-Indices*	*Sum*	*K-Indices*	*Sum*	
12	5454 3463	34	4553 3453	32	5544 3463	34	12
13	3123 4343	23	3123 3232	19	3123 3333	21	13
14	4432 3423	25	4432 3423	25	4432 3433	26	14
15	1023 2324	17	1011 2324	14	1111 2223	13	15
16	3013 3433	20	3113 2333	19	2113 2322	16	16
17	3332 4443	26	3333 4343	26	2333 4343	25	17
18	3433 3343	26	3333 3353	26	4433 3264	29	18
19	4333 3244	26	3333 3333	24	5332 2243	24	19
20	3333 4254	27	3323 3345	26	3223 3356	27	20
21	3333 4245	27	3233 3345	26	3432 3365	29	21
22	3334 3244	26	3333 3344	26	5332 2344	26	22
23	4333 3333	25	3323 3333	23	4432 2343	25	23
24	2212 2221	14	2211 2121	12	2212 2220	13	24
25	0232 2000	9	1121 1111	9	1122 1111	10	25
26	2223 2210	14	2122 2111	12	2112 1011	9	26
27	3112 2234	18	2111 2234	16	2011 1234	14	27
28	2233 3221	18	2223 3222	18	1222 3222	16	28

OL.
12
958

Journal of Atmospheric and Terrestrial Physics, 1958, Vol. 12, pp. 346 to 350. Pergamon Press Ltd., London

Book reviews

Polar Atmosphere Symposium: Part II Ionospheric Section (Published for and on behalf of the Advisory Group for Aeronautical Research and Development, North Atlantic Treaty Organisation.) Pergamon Press, London, 1957. 212 pp., 60s.

IT is a great pity that this volume must be classed as professional writing for professional reading. Otherwise it could be used to demonstrate to the layman something of the fraternal spirit which is such an attractive feature of the scientific life. During the period 2–8 July 1956, a Symposium was held in Oslo, under the auspices of one of the scientific sections of a Defence Agency, the North Atlantic Treaty Organisation. The choice of the theme of the Symposium, the Polar Atmosphere, followed from a suggestion made by a distinguished Norwegian geophysicist, Dr. L. HARANG; and, as a tribute both to Dr. HARANG and to Norway's outstanding contributions to polar studies, the meeting was held in the Norwegian capital.

But this record of the papers presented at the Conference, and of the ensuing discussions, shows no signs of being restricted by military requirements. Evidently this international gathering appreciated the valuable precept that, in science, the most effective application derives from the deepest understanding.

The scientific papers included in the volume fall into three sections. In the first section are grouped papers dealing with ionospheric movement which is such a striking characteristic of the polar ionosphere. This is followed by a section, with a more utilitarian gloss, dealing with the influence of the polar ionosphere on practical radio communication in high latitudes; while the third section deals with the recently developed method of communication by way of ionospheric scattering, in which advantage is taken of the fact that the ionosphere is itself an irregular medium. The papers in each section are followed by an admirable record of the succeeding full and free discussion, due to Dr. K. WEEKES who is the editor of the volume as well as the author of one of the most thoughtful papers in it.

E. V. APPLETON

R. HANBURY BROWN and A. C. B. LOVELL: **The Exploration of Space.** Chapman and Hall, London, 1957. 207 pp., 35s.

THIS volume will appeal to a wide range of readers. In the first place it deals with one of the most progressive and fertile fields of physical science, the radio examination of the universe around us. In the second place it comes from the now famous Manchester University School of radio-astronomy; while in the third place it is admirably written. However, a postscript should be added to these general remarks. Although the authors naturally treat fully the results of the developments with which they have themselves been specially associated, such as the radio detection of meteors and the design of the Jodrell Bank giant radio-telescope, they give ample consideration to the researches of other workers in the same field, in Cambridge (England), Australia, Holland, Canada and the United States. The scientific reader will find much to engage his professional interest in the two chapters dealing with the experimental background and techniques of the subject; but the general or astronomical reader can skip these and read the remaining nine chapters as a continuous narrative. These chapters provide a notably lucid account of what has been discovered about solar, galactic and extra-galactic phenomena, using both the radio echo techniques employing artificially produced electric waves, as well as simple receiving techniques for detecting the natural radiations from outer space.

VOL.
12
1958

Perhaps many readers will find most stimulating of all the last two chapters, dealing respectively with echoes from the moon and the Jodrell Bank radio-telescope; and it is exciting to learn that an attempt to get echoes from a second planet, Venus, is to have a high priority in the research schedule when the giant radio-telescope is in full operation.

Unfortunately the volume seems to have been in the press before the Russian and American earth satellites were successfully launched; so it does not contain an account of the striking success achieved, using the Jodrell Bank telescope in detecting artificial satellites by radar. Let us hope that a new edition will soon be required so that this omission can be repaired.

E. V. APPLETON

B. J. MASON: **The Physics of Clouds** Oxford University Press, 1957. 481 pp., 70s.

RAINMAKING has long been a respected if risky occupation, but it is only recently that some scientific foundation has been established from which it may be possible in the first place to modify local weather and perhaps, in the long run, to adjust the climate of a given region.

Dr. MASON's book brings together practically all the relevant facts and theories concerning condensation and the small scale physics of clouds. An immense amount of material has been sifted with care and critical selection. The result is a comprehensive book which is immediately the textbook for those who are working on or close to the subject. However, the book will have a much wider appeal because any physicist interested in the methods of development of classical theory or in the art of elegant experimentation, will not fail to gain considerable satisfaction and pleasure from reading it.

After an introductory chapter (by Mr. F. H. LUDLAM) in which the large scale aspects and classification of clouds are discussed, Dr. MASON follows with eight chapters dealing with precipitation in one form or another. The treatment covers the process of condensation in clean air, upon charged ions, and upon atmospheric nuclei: the growth of droplets, the significance of ice crystallization lead to a discussion of the problems of the artificial seeding of clouds. The final chapters are comprehensive accounts of radar studies of cloud, rain and snow, and the electrical properties of clouds.

The important feature of the book lies not only in the fact that cloud physicists can now see the different parts of the subject in a realistic perspective, but also in that many physicists not previously interested in meteorology will (and should) have their attention drawn to this exciting field of work. For example in Chapter V the results of Dr. MASON's own work on the process of ice crystal growth in a diffusion cloud chamber cannot fail to interest all crystal physicists and chemists on the one hand and all cloud chamber workers on the other hand. Photographs of snow flakes have always been regarded as classical examples of the challenge and mysteries of nature, but Dr. MASON has shown that ice crystals can yield equal if not greater fascination—and difficulty of explanation.

The volume has been produced with great care and the quality of the diagrams and reproduction of photographs are excellent. It is well worth possessing and can be highly recommended.

J. R. ATKINSON

Proceedings of the Third Berkeley Symposium on Mathematical Statistics and Probability. Vol. III: Astronomy and Physics Edited by J. NEYMAN, University of California Press, Berkeley and Los Angeles, 1956. ix + 252 pp., $6.25

THIS is one of five volumes containing the papers presented at the Third Symposium organized by the Statistical Laboratory of the University of California, and in which problems of statistical theory and its applications to the most varied domains—ranging from astronomy to industrial research—are discussed. The present volume is devoted to astronomy (144 pages) and to the

statistical theory of matter (108 pages). All articles are of a very high quality and deserve the attention of the specialists; very few of them, however, have the synthetic character which one would wish for such an occasion as this symposium offered. The unfortunate result is that we have here just another repository of specialized work which only experts can appreciate; one cannot help feeling that its publication in the usual journals devoted to either of the two domains would have been more economical and serviceable than this hybrid volume. Apart from this criticism, which touches the vast and alarming problem of how to cope with the rising tide of technical reports on current research, it must be stressed that the printing and production of the book is of the highest standard.

L. ROSENFELD

Exploring the Atmosphere's First Mile. Edited by H. H. LETTAU and B. DAVIDSON. Pergamon Press, London, 1957. Volume 1: Instrumentation and data evaluation. xiv + 376 pp., 113 figures, 59 tables. Volume 2: Site description and data tabulation. v + 377–578 pp, mainly figures and tables, 140s, $20 per set.

OVER the last 10 years there has been a considerable growth of effort in studies which come under the title "micrometeorology", and which are concerned with the fine structure of the physical processes in the atmosphere, especially in the layers nearest the ground. On the one hand observational techniques with a precision approaching that of many laboratory measurements have been developed, while on the other hand there has been a growing recognition of the essentially statistical character of the properties under examination. Both of these features are apparent in the "Great Plains Turbulence Field Program", the history, operation and results of which are placed on record in these two volumes. The project was conceived by the Geophysics Research Directorate, Boston, Massachussetts, and was carried out cooperatively by fifteen university and government departments. Field operations were carried out near O'Neill, Nebraska, in August and September 1953. The main effort was concentrated in seven periods, averaging 24 hr in duration, in which a set programme of special observations was followed. Many of these observations were duplicated by independent teams.

The instruments, the techniques and some discussion of the results are covered in Volume 1 in a series of sixty-five separate papers, mostly very short, by thirty-four authors. Many of the contributions are concerned with the heat and moisture contents of the surface layer of soil, and with the mean vertical profiles of temperature, humidity and wind speed in the first few feet of the atmosphere. A substantial number are devoted to the rapidly developing studies of the turbulent fluctuations of temperature and wind speed. Other contributions deal with general weather, vertical profiles of ozone near the ground, radiation, surface drag and dew formation. Despite the title of the work only a small fraction of Volume 1 is directly concerned with properties at heights above about 50 ft. Tabular summaries of the data are given in Volume 2 for each of the seven main observation periods.

The difficulties of making observations in the field as compared with the laboratory are frequently underrated, and the range of activities and quantity of results described in the present volumes are a tribute to the organizing ability and technical skill invested in the project. As to the scientific advance thereby provided it is perhaps early to judge, for there is presumably much which has yet to be extracted from the material. It is however already admitted that some of the techniques were not entirely satisfactory and that anomalous features in the results on turbulent transport of heat require explanation. To the reviewer it has always appeared to be a debatable point as to whether observational effort of the present magnitude should be aimed at establishing a broad background or at clarifying particular features which are obscure. The full digestion of the results will no doubt provide valuable experience on this point.

The presentation of the work contains a few flaws, of which perhaps the most confusing is the interchanging of Figs. 7.54 and 7.55, but altogether they are of a relatively minor nature. In general the standard of production is high and the price is presumably inevitable for the detailed publication of such a specialized research.

F. PASQUILL

VOL. 12 1958

F. J. LUDLAM and R. S. SCORER: **Cloud Study: a Pictorial Guide.** John Murray, London. 1957. 80 pp., 7 Figs., 73 Plates, 12s. 6d.

THIS is a book that will be relished by the general reader and the meteorologist alike. The former will find in the dozen pages of the introduction as clear an exposition of the physical processes involved in the formation of clouds and of the factors that determine their constitution and shape as it can be possible to compose. The latter will applaud the skill with which this brief but remarkably comprehensive summary of the elements of cloud physics is presented. All will delight in the series of seventy-three fine cloud photographs that the authors have selected, mainly from the collections of the Royal Meteorological Society but also from their own and other collections.

Each photograph is described and fully analysed in the expert fashion that one expects from LUDLAM and SCORER, and the reader cannot fail to sense and to share their enthusiasm for cloud study.

This reviewer, having a special interest in the colour Plate 35 of a glory (its existence was brought to his notice by one of his students and the photographer prevailed upon to supply a copy to the Royal Meteorological Society) would beg the authors to extend its legend in the next edition to include a reference to its historic significance. The glory was photographed on the Tower Ridge of Ben Nevis precisely where C. T. R. WILSON, observing a similar glory during September 1894, was thereby inspired to begin the study of the optics of the phenomenon on his return to the Cavendish Laboratory. In his own words, as a result of his laboratory experiments to produce clouds: "Instead of pursuing the study of glories, I was led to design apparatus for subjecting a given volume of moist air to sudden expansions of known amount under conditions which excluded the possibility of any ordinary nuclei entering." So the ideas which culminated in the design of the Wilson cloud chamber were conceived at the very spot where the beautiful colour photograph of the glory which is Plate 35 was taken.

The cost is surprisingly low for a book so excellently produced and printed.

JAMES PATON

Advances in Geophysics. Vol. III. Edited by H. S. LANDSBERG. Academic Press, New York, 1956. 378 pp., 70s. 6d. $8.80

THE third volume in this series of review articles on geophysical topics contains articles of impressive authority. Perhaps the most important is one by BULLARD, MAXWELL and REVELLE, who discuss the measurement of the heat flow through the ocean floor. The difficulties which beset such measurements on the continents and the variability of the values obtained from place to place make it somewhat surprising at first sight that important conclusions have been reached from these measurements or indeed that it is possible to make them at all. The various factors involved in a successful determination of the temperature gradient in the sea floor are very carefully described and although the number of determinations is small, there can be no doubt that a rough equality of the heat flow through the ocean floor and through the continents has been demonstrated. It is less certain what consequences follow but it seems hard to believe that the flow is a result of conduction alone and when a full network of observations is obtained, important evidence on the existence of convection currents in the mantle should arise. The results may well be crucial for the further development of the physics of the earth's interior, of which Dr. JACOBS gives a very clear account including the earth's thermal history and magnetic field. This is a subject on which there have been many review articles written in the last few years but the problems are complicated and JACOBS' review will be helpful to all those interested in following the progress in this expanding field.

Professor BYERLY writes an extremely clear account of the inferences drawn from seismology on crustal structure. His account is historical in character and will be particularly

helpful to the young workers entering geophysics who wish to see the subject in perspective. Professor BYERLY's style of writing is characteristic and a refreshing change from the impersonal one typical of so many scientific papers.

Professor SINGER's description of the possible scientific uses of satellites will be of great help to all those who wish to follow the rapid progress in geophysics which will come from measurements in this field in the next few years.

Bore hole logging is a technique in applied geophysics which has been very widely used by exploration companies, but many will feel that a serious gap in the literature has been closed by the very informative article in this volume by JONES and SKIBITZKE. The polarization of sky light is one of the classical studies of physics but it is only in recent years that methods of measuring the polarization have been carefully developed, and DR. SEKERA in this volume shows clearly how valuable data on the upper atmosphere have been obtained. It is appropriate at the present time that there is an article by DR. A. P. CRARY on "arctic ice island research." He discusses the meteorological and gravitational observations and the flow of water and ice. This is presumably a subject in which we may expect considerable advances during the International Geophysical Year.

The whole volume is attractively produced and geologists and geophysicists will be grateful to the editor for the high standard of the articles.

S. K. RUNCORN

VOL.
12
1958

Papers to be published in future issues

J. C. Brandt and J. W. Chamberlain: Resonance scattering by atomospheric sodium—V. Theory of the day airglow

E. Harnischmacher and K. Rawer: Drift observations evaluated by the method of "similar fades"

J. E. Titheridge: Variations in the direction of arrival of high frequency radio waves

M. W. Chiplonkar and V. N. Athavale: Simultaneous recording of atmospherics on four different frequency bands in the low frequency region

R. Satyanarayana, K. Bakhru and S. R. Khastgir: Triple-splitting of the F-echoes

B. A. P. Tantry and R. S. Srivastava: Waveforms of atmospherics with superimposed pulses recorded with an automatic atmospherics recorder

N. C. Gerson: Very long distance ionospheric propagation

J. C. Bhattacharyya: Non-uniformity in the brightness of the sun's disk at sunspot minimum

A. Vallance Jones and A. W. Harrison: $\Delta_g{}^3\Sigma_g\, O_2$ infra-red emission band in the twilight airglow spectrum

G. R. Ellis: The trapping of cosmic radio waves beneath the ionosphere

H. A. Whale and L. M. Delves: Some relations between the bearing and amplitude of a fading radio wave

Sydney Chapman and Kenneth Davies: On the approximate daytime constancy of the absorption of radio waves in the lower ionosphere

John C. Brandt: Resonance scattering by atmospheric sodium—VI. The analytic solution for the twilight intensity

E. B. Armstrong: The temperature in the atmospheric region emitting nightglow OI 5577 line and in regions above faint auroral arcs

Vincente Marasigan, S.J.: Height-gradient of electron-loss in the F-region

R. W. Wright and N. J. Skinner: Lunar tides in the sporadic E-layer at Ibadan

F. E. Roach, E. Tandberg-Hanssen and L. R. Megill: Movements of airglow cells

F. E. Roach, E. Tandberg-Hanssen and L. R. Megill: The characteristic size of airglow cells

J. O. Thomas and Audrey Robbins: The electron distribution in the ionosphere over Slough—II. Disturbed days

F. Horner: The relationship between radio noise and lightning

J. L. Wolfe: Satellite tracking by H.F., D.F.

C. A. Onwumechilli: A study of the equatorial electrojet—I. An experimental study

C. A. Onwumechilli: A study of the equatorial electrojet—II. A model electrojet that fits H observations

H. A. Whale: The effects of ionospheric irregularities and the auroral zone on the bearings of short-wave radio signals

John C. Brandt and Joseph W. Chamberlain: Resonance scattering by atomospheric sodium—V. Theory of the day airglow

M. N. Rao and A. P. Mitra: Effects of vertical drifts on the nocturnal ionization of the lower ionosphere

A. W. Harrison and A. Vallance Jones: Observations of Meinel N_2 bands near $1{\cdot}5\,\mu$ in the auroral spectrum

Papers to be published in future issues

J. A. THOMAS and E. K. SMITH: A survey of the present knowledge of sporadic *E* ionization

W. R. FRENCH, JR. and R. L. CHASSON: Atmospheric effects on the hard component of cosmic radiation near sea level

C. COLLINS and P. A. FORSYTH: A bistatic investigation of radio-aurora

C. M. MINNIS: Ionospheric changes at Singapore during the solar eclipse of 14 December 1955

A. A. WEISS: The limitations of narrow-beam radio equipments in the detection of weak meteor showers

R. G. RASTOGI: Geomagnetic influence on the *F1* and *F2* regions of the ionosphere—Effect of solar activity

J. W. KING: Ionospheric self-demodulation and self-distortion of radio waves

J. E. TITHERIDGE: Ray paths in the ionosphere. Approximate calculations in the presence of the earth's magnetic field

G. C. REID and C. COLLINS: Observations of abnormal VHF radio wave absorption at medium and high latitudes

L. A. MANNING: Oblique echoes from over-dense meteor trails

B. RAMACHANDRA RAO and E. BHAGIRATHA RAO: Study of horizontal drifts in the *F1* and *F2* regions of the ionosphere at Waltair (17°43′N, 83°18′E, Mag. lat². 9°30′N)

L. HARANG and J. TRÖIM: Determination of the angle of arrival of auroral echoes

W. N. ABBOTT and S. CHAPMAN: On the aurora of 19 August 1950, photographed from Greece

VOL. 12 1958

ERRATUM

J. Atmosph. Terr. Phys. **12,** 126 (1958)

HERMANN POEVERLEIN: Low-frequency reflection in the ionosphere—I.

In equations (22) and (23) of Part I, $\nu^2 - \omega^2$ in the denominator should be replaced by $(\nu + i\omega)^2$. Actually, in many cases $i\omega$ is negligible compared to ν. I thank Dr. J. R. Wait for calling my attention to the error.

OL.
12
958